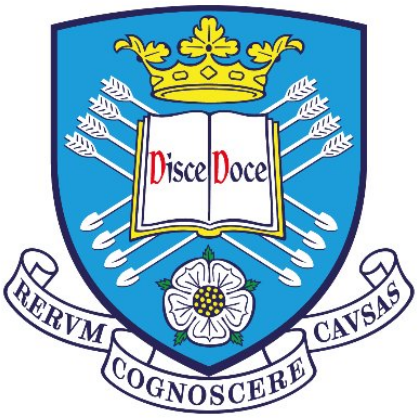

DEPARTMENT OF MECHANICAL ENGINEERING

THESIS SUBMITTED FOR THE DEGREE OF DOCTOR OF PHILOSOPHY

An assessment of railway freight axle corrosion damage, considering current conditions and predicted future development

PHILIP JAMES SHARPLES

August 2021

Abstract

Corrosion on rail axles can be a serious problem. Historically it has led to accidents that have resulted in extensive damage and fatalities, by causing crack initiation and propagation causing catastrophic component failure. To mitigate the risk, current UK maintenance standards set strict limits on permissible damage. These limits have resulted in a safe network, in terms of axle corrosion, with no failures in 20 years. However, anecdotal evidence suggested that this had been achieved through the unnecessary scrapping of many axles for minor corrosion damage. Over scrapping has a cost to industry financially, logistically and environmentally.

The scope of the problem was first established through consultation of industry data. Once it was shown that there was merit to the anecdotal reports, an axle survey was undertaken at a UK overhaul depot, the largest identified in literature. A new three dimensional survey technique was developed, improving on previous two dimensional surveys, and analysed using bespoke software based on image processing techniques to identify and separate corrosion pits. Pits identified through the survey were then analysed, using fracture mechanics techniques, to assess the risk of crack initiation they represented. It was found that no pits came close to current limits, in terms of depth, and presented a extremely small risk of crack initiation. This indicated that current limits and procedures were resulting in axles being scrapped with low levels of corrosion damage, suggesting improvements could be made.

To explore how corrosion damage changed over time, a series of novel experiments were performed. These experiments sought to replicate the rail axle environment during UK operations through the application of a representative corrosive medium to axle samples. The results of these experiments allowed an estimation to be made of the change in corrosion severity on rail axles under different starting conditions. The predicted changes were applied to the pits identified during the axle survey to assess the potential risk of changes to current corrosion maintenance practises.

By analysing the experimental results it was shown that removing the protective passivity layer to inspect axles resulted in significantly increased rates corrosion damage, compared to the case where the passivity layer was left in place. In some cases, this meant that correction of axles was required when it would not have been if no inspection were carried out.

Based on the results of the analysis, it was recommended that an extension inspection intervals be considered. This would reduce the scrapping of axles, without substantially increasing the risk of axle failure. This was due to the low level of damage observed on in service axles and the significantly slowed rate of corrosion if the passivity layer was left in tact.

Acknowledgements

I would like to thank the many people who have helped me during the past few years working on my thesis. Principally this includes Dr. Adam Beagles who offered me the project and guided me, with much patience, during the first few years. His help was invaluable and it was a real pleasure to have him as my supervisor.

Dr. Inna Gitman, who took me on after Adam moved on, also needs special thanks. Despite this work not being directly in her field, she has been a massive support and has helped keep me sane in some of the tougher times. Her skill in setting deadlines was exactly what was needed, despite protests at the time.

Without the laboratory technicians and machinists at the University this work would be been much more difficult. They have always been ready to help, with their time, experience and ability. In particular, I would like to thank Martyn Aspinall and Richard Kay, who have helped me enormously during this thesis, for letting me take advantage of their expertise and ideas when I was stuck, as well as letting me rant.

To all the staff and students at the University, particularly in the Mechanical Engineering department, it has been a great place to work due to the atmosphere that you created. It has been a pleasure studying here. Especially the people of RD14.

Finally, I would like to thank my parents. I hope I have made you proud.

Kirsty, sorry it took so long.

Contents

List of Figures

List of Tables

Chapter 1

Introduction

1.1 Statement of issue

Rail axles are a safety critical part of the rail network, where any failure could lead to significant damage and loss of life. To ensure that such outcomes do not occur, axles are subject to stringent safety standards and inspection regimes.

A major difficulty with defining safety standards and procedures is in setting the limits in such a way that failures are minimised or eliminated, but not setting them so severely that large numbers of safe components are rejected. The rejecting of otherwise safe components due to overly conservative standards is a source of inefficiency that comes with a financial, logistical and environmental cost.

Anecdotally, it had been suggested that rail axles exhibited over scrapping with regards to corrosion damage. This meant that large numbers of functional and safe axles were being scrapped due to either cosmetic damage or very minor damage that would not have a significant effect on safety.

Corrosion is the process that degrades materials, in this case metals, and converts them into a more stable state (an oxide for example) [1]. This degradation occurs when a susceptible component is exposed to a corrosive environment without protection [1], a process colloquially known as rusting. An example of this would be the formation of a red oxide of an iron component left outside and exposed to the environment. The corrosion process is an electrochemical one, requiring the presence of ions and an electrolyte to facilitate the process.

Corrosion damage occurs when a component undergoes corrosion. Due to the capture and removal of the metal atoms in the component to form the corrosion product (i.e. oxide), the surface of the component is changed. Over time the components surface may develop a roughness to it due to the loss of material. In some cases this may develop further, with some areas corroding more severely than others and forming deep craters on the surface, known as corrosion pits.

Corrosion pits are discontinuities in the surface of the component. When the component then undergoes stress, the stress level is increased around the corrosion pit due to the disruption of the stress flow in that area. If the stress is concentrated sufficiently, it may exceed the ability of the material to withstand the stress and a crack may initiate. These cracks may then propagate and lead to the catastrophic failure of the component. Catastrophic failure of a rail axle due to a crack propagating through the component is unacceptable, due to the high impact such a failure would have, as evidenced by historic examples.

This thesis investigates corrosion damage of rail axles in the UK to determine if over scrapping is a problem that the industry experiences and seeks to suggest possible changes to the current approach that could result in efficiency gains without risking the current safety record of the UK rail network.

Aim

The aim of the thesis was to inform current UK standards and procedures surrounding rail axle corrosion. By better understanding the realities of rail axle corrosion of the freight fleet, and focusing on the depot setting, changes could be suggested that could result in financial, logistical and environmental savings.

1.2 Thesis summary

This section brief summary of each Chapter. This information is for reference, with the justification for the selected approach detailed in Chapter 2.

Chapter 2

Chapter 2 contains the initial review of the work in the field and background information. Included is initial assessment of industry records surrounding the scrapping of axles, including both the numbers scrapped and specific information about the reasons for scrapping. The contents of this Chapter provides context for the problem and evidence of the industrial need for the work.

Chapter 3

Chapter 3 details the axle survey undertaken in an overhaul depot. The survey was conducted to ascertain the level of corrosion damage on UK rail freight axles by measuring the damage exhibited at overhaul. Within the Chapter the novel three dimensional technique used to collect the data is described and validated, then compared to previous techniques. After the data was collected, the techniques used to process the data and identify the pits is detailed. Finally the results of the analysis of the identified pits is presented.

Chapter 4

The work in Chapter 4 focused on assessing the pits identified in Chapter 3 in terms of the risk of crack initiation. This was achieved using a fracture mechanics concepts, based on two separate approaches; crack analogy and El Haddad. Initial work focused on assessing the different ways of defining an individual pit and the effect this would have on the calculated risk of crack initiation. The different definitions were then matched to previous approaches to measuring pits and potential sources of error assessed. Finally the pits were assessed for their Stress Intensity Factor compared to the threshold value of the material.

Chapter 5

Chapter 5 details the design of a novel experiment to replicate the rail axle environment and assess the changes in corrosion damage over time. This includes concept selection, justification of key parameters, the design process of critical components and the assembly process. During the experiment several setbacks took place, requiring significant changes to the initial experimental plan. The details of the setbacks are presented along with the changes that were undertaken to address them.

Chapter 6

The results of the experiment carried out in Chapter 5 are analysed in Chapter 6. This includes the collection of the data and separating of the pits using the approach developed in Chapter 3. Subsequently the separated pits were analysed using the techniques from Chapter 4, with adjustments made to account for the aim of assessing the changes in corrosion damage over time. The results of the analysis are then presented.

Chapter 7

The results of the two work streams (survey work and experimental work) were combined in Chapter 7. By combining the predicted changes in corrosion damage overtime, presented in Chapter 6, with the results of the axle survey, presented in Chapter 4. Through this combination, an assessment of the condition to rail axle corrosion was produced and recommendations of possible changes to procedure suggested.

The contents of the work and the connections between each section can be seen in Figure 1.1. This is to provide context to the project, with the reasoning behind the decisions detailed in Chapter 2.

1.3 Novelty and impact

The following section details the novelty of the work in this thesis by Chapter. These are summarised from the more detailed sections at the end of each Chapter.

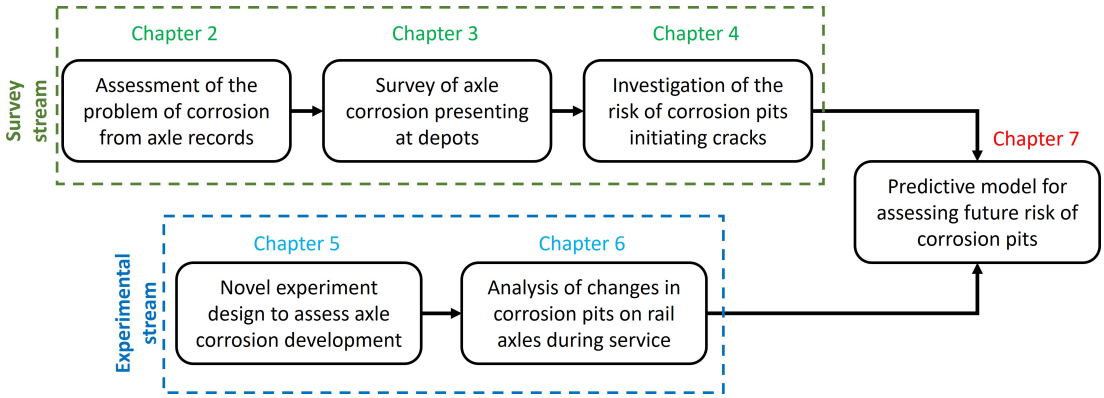

Figure 1.1: Workflow of the project connecting the Chapters

Chapter 2

Presentation of novel data from industry demonstrating the scale of the issue of rail axle corrosion in the freight industry and the most common types of damage, with locations. This provided concrete data that rail axle corrosion was an issue that, by improving outcomes, the work would provide tangible industrial benefit.

Chapter 3

Collection of a large, unique, real world data set of corrosion damage on UK rail freight axles that represents a large improvement on previous work, both in terms of scale and precision. This includes the validation of a novel collection and data processing procedure that could be applied in a depot setting, significantly improving capabilities of UK depots. The results of the work in this Chapter demonstrated the divergence of current standards and procedures from the real world presentation of corrosion on axles, and indicated the possible gains from further work in the field.

Chapter 4

Analysis of real world examples of corrosion pits demonstrated the lack of risk of crack initiation from any identified pits. This provided further evidence that significant improvements could be made to UK standards without significant impact on safety. It further demonstrated the suitability of the technique when applied to data collected in an industrial setting and could provide the basis of a commercially viable approach in future.

The work also evaluated the techniques used in previous work carried out in the field. It was able to demonstrate some of the weaknesses of other approaches and could help inform future investigations.

Chapter 5

A novel experimental approach was developed to assess the changes in corrosion pit morphology over time, under exposure to realistic accelerated corrosion conditions in a laboratory setting. The experiment made use of an existing corroded rail axle surface in a laboratory test to allow the use of a high fidelity starting point for corrosion pit development.

The rig not only filled a capability gap in the existing experimental repertoire, but also bridged a gap between large, expensive full scale testing and smaller bench testing. In combining the two ends of the spectrum, this concept allowed for faster, cheaper testing of a more specific rail axle environment, providing a platform for future work in this field.

Chapter 6

The results produced in Chapter 5 were used to analyse the development of corrosion pits in rail axles over time. Results suggested that the risk of crack initiation from corrosion pitting was very small and that the majority of the damage occurred within a short period of time before the passivity layer formed.

The inspection of rail axles has also been challenged. The inspection of rail axles produces an environment where pitting could develop much more rapidly than if it had been left in its previous, corroded, state. The inspection of the axles makes the correction of the damage a necessity. This suggested that the inspection interval of rail axles could be increased.

Chapter 7

The combination of the results of Chapter 4 and Chapter 6 resulted in an examination of the possibilities for changes to the maintenance and inspection procedures of rail freight axles in the UK. The outcome of the analysis was that there was scope for changes to inspection intervals without significantly increasing risk of crack initiation, possibly resulting in significant savings to industry. Other changes to the industry approach to corrosion were also suggested, although more work would be required to validate the outcomes.

Chapter 2

Industrial Practice and Practical Considerations

2.1 Introduction

Axles are an under-considered part of the rail industry. Although on the face of it they are a very simple component, merely used to keep the wheels in place and allow attachment of the power train systems, without them no rail system would be able to operate. An example of a rail axle in service can be seen in Figure 2.1, with other components marked.

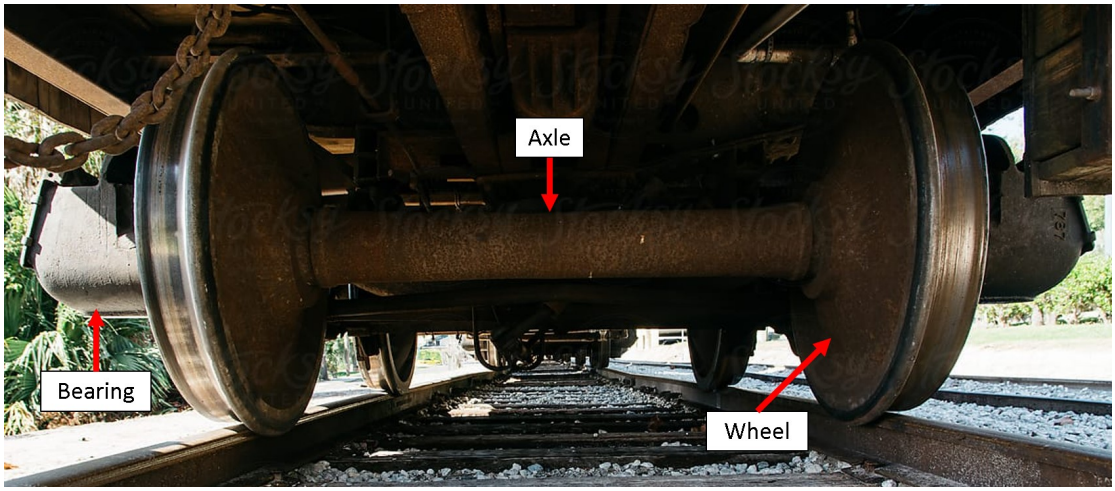

Figure 2.1: Illustration of a rail axle, with other components also marked

There are several historical examples of when axles have not performed correctly, leading to sometimes devastating accidents, all the way from the 1842 Versailles accident causing around 100 deaths [2] to the more recent example of a passenger train derailment in 2010 in Leicester [3] that resulted in damage to the vehicle and track. Naturally, after one of these accidents the industry returns to this safety critical component and improves on the previous work, with the aim of increasing the safety of axles, to prevent other tragedies.

All axle failures that result in these accidents are due to catastrophic fractures, when cracks suddenly propagate through the axle material. These cracks result in a sudden drop in strength of the component, below the level required for safe operation. Due to this, axle maintenance is dedicated to three main areas: the detection of cracks and damage that may lead to cracks; the correction of those identified; and the prevention of such damage happening again.

One of the types of damage that most commonly causes risk of failure to rail axles is corrosion induced fatigue failure [4]. Corrosion is the process by which metals, exposed to a corrosive environment, degrade through an electrochemical process [1], often colloquial referred to as rusting. Although the guidelines that have been put in place to mitigate corrosion in the UK are not a defined legal standard, they form the basis of industry practise. These guidelines define limits on corrosion in terms of size, colour, location and depth that lead to the axle being either returned to service, repaired or scrapped [5]. They also inform decisions about the types of inspections that are undertaken and the intervals between them.

There are two sources of inefficiency in the decision to scrap rail axles that must be balanced. One is not scrapping dangerous axles, the other is the scrapping of axles that could be safely returned to service. While it is not possible to define this perfectly, there is strong anecdotal and circumstantial evidence that the latter is the case. Reports of rail axle inspections have noted that some axles appeared to have been scrapped for cosmetic damage [6], while discussions with workers at overhaul depots suggests that between 15% and 25% of freight axles are scrapped at overhaul. This represents a potential annual cost to the UK industry of £9 million [7]. This represents a significant ongoing cost, however any savings made have to be balanced against the financial and moral costs of a higher probability of accidents.

Taking into account only the possible impact of fatalities or injuries, ignoring the cost of repair or replacement of vehicles and infrastructure, HM Treasury values human life using Value of Prevented Fatality (VPF) and Value of Statistical life year (SLY) [8]. In 2018 these values were set at £1.6m and £60,000 respectively, demonstrating how quickly a single serious accident could outstrip any savings made through changes to axle maintenance procedures. To make the economic case for changes, the increase in risk must be extremely small due to the large financial costs involved in any accidents.

The risk of corrosion for rail axles is from changes in the geometry of the affected surface that can lead to crack initiation, demonstrated in Figure 2.2, the formation of a crack, and propagation, the growth of a crack, resulting in ultimate failure. However, corrosion can also make detection of cracks difficult, as it is complex to differentiate cracking from corrosion damage (the geometric change of the surface due to the corrosion process) either visually, due the resulting rough surface, or using ultrasonic detection, the two main industry techniques for axle inspection [9]. This encourages very conservative limits on acceptable corrosion damage to avoid failures through the use of large factors of safety. The difficulty in defining an appropriate acceptable level of damage is that a certain level of surface roughness would be normal and acceptable on almost any component and the defining point at which the natural roughness of a surface could be defined as corrosion damage is subjective. However, this must be differentiated from more significant corrosion damage that may lead to cracking, with the division between these two conditions being difficult to define.

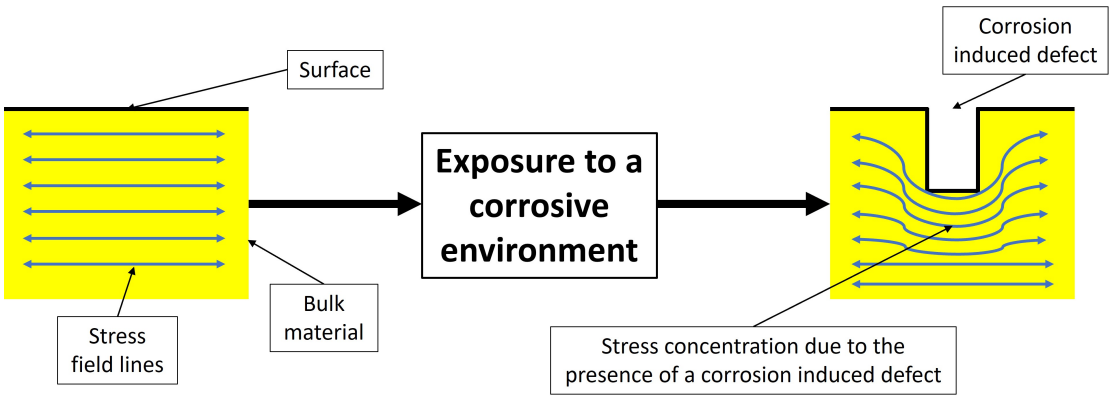

Figure 2.2: Demonstration of the process of crack initiation from surface defects caused by corrosion damage. The presence of an increased stress field near the surface defect increases the chance of a crack initiating from the defect.

The latest advice was produced after the 1996 Rickerscote accident [10] that resulted in a fatal derailment of a Royal Mail train due to a corrosion damage initiated fracture of an axle. The changes introduced increased the number of inspections and the widespread use of None Destructive Testing (NDT) techniques, as well as introducing stricter limits on the allowable corrosion damage. Since this advice was released in 1996, there have been only three axle failures leading to derailments due to corrosion in the UK, all within 6 years of the new guidance while it was still being implemented, as seen in Figure 2.3. This compares to 12 in the 13 years before the standard was introduced.

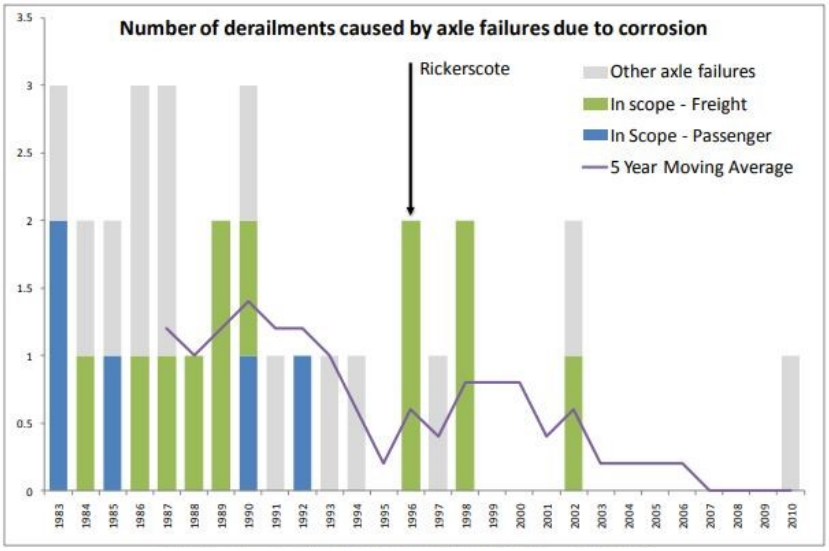

Figure 2.3: Derailments caused by axle failures by corrosion in the UK 1983-2010 [6]

The significant change in the prevalence of derailments due to axle failures from corrosion before and after the new limits suggests that the maintenance procedures are highly effective at preventing risky axles from remaining in service or going uncorrected. However, the lack of axles reaching catastrophic failure in recent years raises the question: are current requirements too strict?

If it was found that the current corrosion limits were too strict then this would lead to the conclusion that otherwise safe axles were being scrapped unnecessarily. The unnecessary scrapping of safe axles results in a financial, logistical and environmental cost to the industry. This cost affects the profitability of the industry and will ultimately be reflected in higher prices and lower levels of investment.

The aim of this work was to investigate if more appropriate corrosion thresholds and inspection intervals could be introduced without compromising safety. This was achieved by investigating the state of axle corrosion in the UK in the overhaul depot setting. The condition and risk of corrosion on in service axles was assessed and experiments were undertaken to investigate the progression of corrosion over time. All work was undertaken with the application to real world operations in mind.

2.2 Introduction to the scenario

2.2.1 What are rail axles?

When talking about rail axles, it is important to define what is being referred to. Rail axles are a large section of cylindrical material, most commonly steel, that connects the two wheels together. A simplified drawing of a rail axle with common terminology can be seen in Figure 2.4. This is simplified as it does not contain some other features that can be found on an axle, such as more seats for brake discs and drive train components or stress grooves and dust collars.

Axles in the UK are approximately of 2.2m long, weigh around 500kg and a plain solid freight axle costs roughly £2,000. These values are approximate and are meant to be indicative. Rail axles are designed to avoid failure in service, with a targeted service life of 40 years or around 10,000,000 km [11].

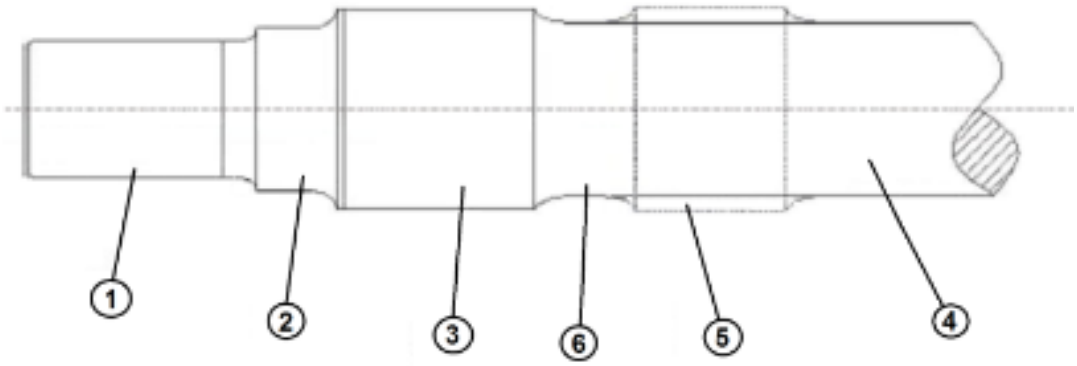

Figure 2.4: Simplified line drawing of a rail axle. 1) Journal 2) Abutment 3) Wheel seat 4) Axle body 5) Seat for brake disc, transmission or final drive 6) Transition zone between seats [12]

There are several types of rail axle variations, such as hollow or tapered axles but the most common form is a solid axle with a constant diameter within the body. These form the majority of rail freight axles [13].

Axles are most commonly referred to as part of the wheelset. This is the combination of the axle and wheels and other components, such as axle bearings. This larger assembly is treated as a single unit in many cases. A wheelset as defined by EN 15313 [12] can be seen in Figure 2.5 and Figure 2.6, with either case being referred to as a wheelset depending on context.

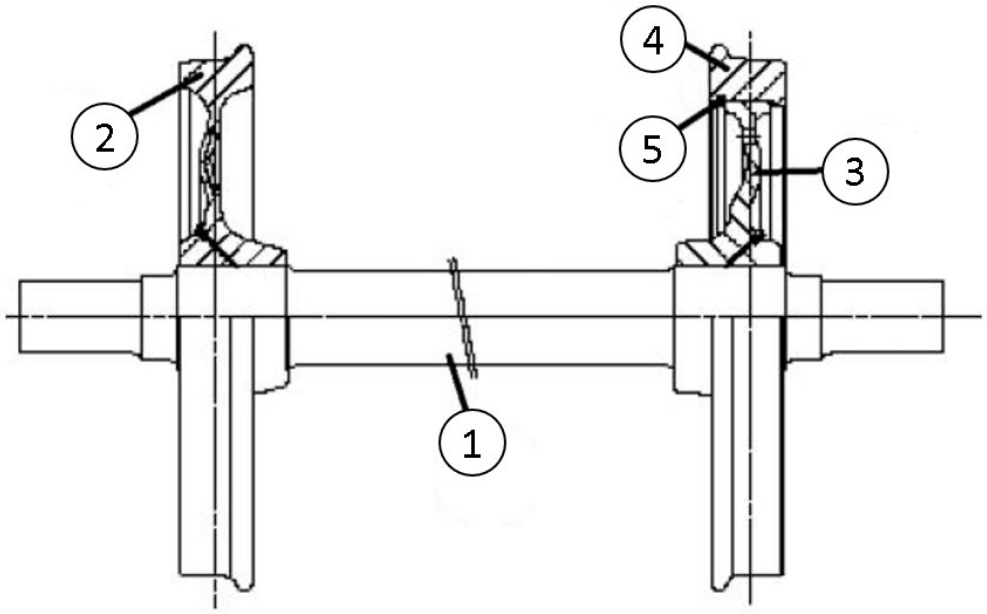

Figure 2.5: Principle components of a wheelset [12]. 1) Axle 2) Monobloc wheel 3) Wheel centre 4) Tyre 5) Retaining ring

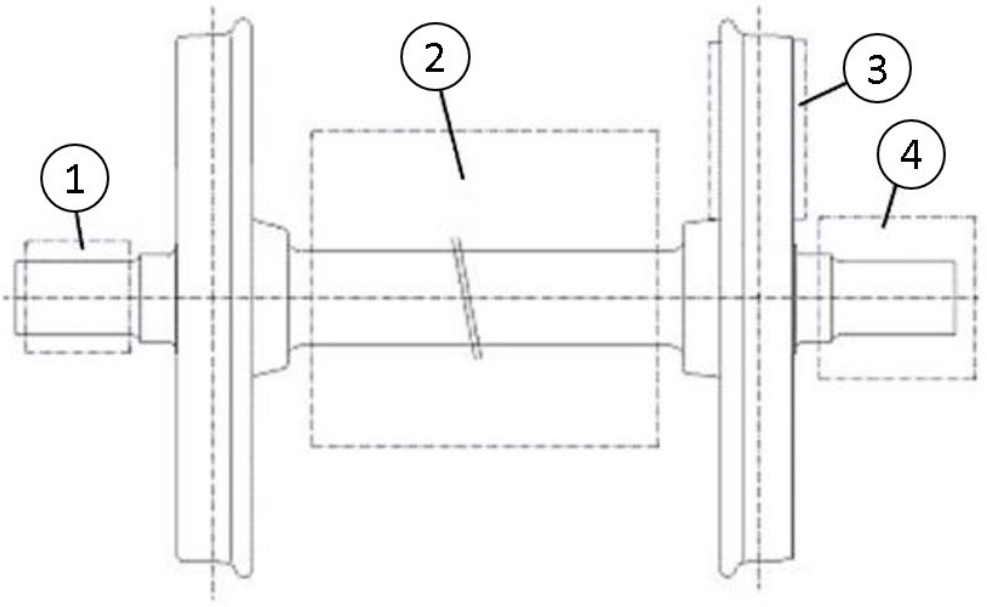

Figure 2.6: Secondary components of a wheelset [12]. 1) Bearings 2) Brake disc, transmission or final drive 3) Wheel-mounted brake disc 4) Axle box with bearings

There are no exact publicly available numbers for rail axles in the UK. This is mostly due to the fracturing and re-consolidating of companies over the years, particularly in the freight industry, that complicates the tracking of axles. By one estimate there are in excess of 144,000 [7] including both the passenger and freight fleet. Assuming a cost of approximately £2,000 per axle, there are at least £288 million of axles currently in the UK and this is likely a low estimate. Another value given for the number of axles is 170,000 [14], representing an 18.06% increase, and demonstrating the lack of information surrounding this field.

2.2.2 Rail axle design standards and methodology

In the UK, the design of rail axles is governed by three standards documents, BS EN 13103 [15], BS EN 13104 [16] and BS EN 13261 [17]. The first two of these specify the design methods used for non-powered and powered axles respectively and the final one is the product requirement. BS EN 13103 and BS EN 13104 are based on an infinite life design methodology [11], this means that if an axle remains within the limits of the standards it is designed to never fail in operation.

When designing an axle it is important to calculate the stresses that the axle experiences at different locations along the axle length. In BS EN 13103 [15] and BS EN 13104 [16] this is performed by calculating the bending moments produced from the load on the axle bearings, the forces acting at the wheel-rail contact points and the forces from any attached brakes or power train components.

As the exact loads from an axle in service are not known due to high levels of variation and complexity, a combination of the known loads are used to produce a representative critical case. This critical load case is then converted into stresses within the axle, which are then compared against the fatigue limit of the axle material (in the standards two steels are explicitly named, EA1N and EA4T) with a safety factor included to account for all variations and uncertainties between the service conditions and design assumptions. In these standards the safety factor (called the security factor) has a value of 1.2 for EA1N steel, meaning that the maximum permissible stress in the axle must follow Equation 2.1 [15]:.

$$\Delta\sigma < \Delta\sigma_{design} = \frac{\Delta\sigma_{lim}}{\eta} \tag{2.1}$$

$\Delta\sigma$ represents the range of stresses present in the axle, $\Delta\sigma_{design}$ is the range of stresses the axle is designed to withstand, $\Delta\sigma_{lim}$ is the limiting stress range that the material can withstand and η is the safety factor (security factor) defined in the standard. If a steel other than the ones mentioned is desired, then a simple equation linking the properties of the named steels and the new steel is given, to calculate the maximum permissible stress.

The calculation for the stress in a solid axle is given by Equation 2.2:

$$\sigma = \frac{K \times 32 \times MR}{\pi d^3} \tag{2.2}$$

This is fundamentally the four point bending equation for a cylindrical specimen, with added factors to account for the specifics of the rail axle. The diameter at the location being studied is given by d, the stress depends on K (a stress concentration factor used to account for the geometry changes between cylindrical parts - techniques to calculate this are given in the standards [15, 16]) and MR which is the resultant moment that accounts for bending components in the vertical and horizontal planes and the torsional components applied tangentially to the wheels. This torsional component also accounts for other unbalanced rotor issues, such as differences in wheel diameters.

While this design standard is effective it tends to be somewhat simplistic. Any issues that are unknown or subject to uncertainty, are dealt with by over engineering the part to remove or lessen the risk of failure. While a logical approach to take, given the complexity of the system and the development of the rail industry from a more technologically limited era, this will tend to lead to parts that benefit from layers of conservative estimation at each stage. This makes the component safe but potentially more expensive than necessary and with large margins for error resulting in a loss of efficiency and an increase in waste.

Part of the simplicity of the design process, was seen in relation to the experienced life of axles. The focus of this project was the corrosion damage of rail axles, which is not explicitly referred to in the design standards. This damage, along with any other damage to the axles, is dealt with the previously mentioned 1.2 safety factor [15, 16]. This implies that no expected corrosion damage on rail axle would cause a stress concentration factor of above 1.2, as this would raise the local stress above the fatigue limit of the material, risking failure when operating at the maximum allowable stress. All other damage to axles, such as ballast strikes and scoring, are dealt with in the same way.

Rail axle corrosion protection

While the design standard of the axles themselves do not deal directly with corrosion, there are other approaches used to prevent corrosion becoming an issue in the first place.

A common way to prevent corrosion damage in many applications, is to use a physical barrier (e.g. coating) between the metal and the environment. Examples of these coatings can be seen in the paint on cars or the plastic coating on copper wire. By separating the metal and the environment with an inert barrier, corrosion can be prevented from occurring. Rail axles use a similar approach of protective coatings, mostly in the form of a paint layer.

BS EN 13261 [17] gives details on protection from impacts and corrosion through protective coatings. There are 4 classes of protection mentioned in the document with different areas of the same axle being able to be in different classes.

- Class 1
  - Sections of axles that are subject to atmospheric corrosion and mechanical impacts
- Class 2
  - Sections of axles that are subject to the actions of specific corrosion products
- Class 3
  - Sections of axle that are subject to atmospheric corrosion
- Class 4
  - Axles that are subject to atmospheric corrosion when the stresses calculated according to EN 13103 and EN 13104 in the sections that are subject to atmospheric corrosion are less than 60% of the permissible stresses

The protective coatings minimum requirements of each class are given in Table 2.1. The specifics of the requirements for each category can be found, along with the tests required to prove that a level has been met, in the same document [17]. One issue with this approach is that each test is done independently of the others, so any interaction between different damage types to the protective coatings is not investigated. An example of this may be if cyclic mechanical stress had an impact on the coating adhesion and so increase the vulnerability to salt spraying and gritting.

As is stated in Table 2.1, there is a possibility for axles to be in service with some sections, or the entire axle, uncovered by any protective paint layer. However, this is extremely uncommon in the UK, most probably due to the low limit of maximum permissible stress in these sections limiting the uses of the axle without increased manufacturing cost and weight.

Table 2.1: Requirements of protective coatings for each corrosion protection class[17]

	Protective coating class level			
	Class 1	**Class 2**	**Class 3**	**Class 4**
Coating thickness	X	X	X	-
Coating adhesion	X	X	X	-
Resistance to impacts	X	-	-	-
Resistance to gritting	X	X	X	-
Resistance to salt spray	X	X	X	-
Resistance to specific corrosion products	-	X	-	-
Coating resistance to cyclic mechanical stresses	X	X	X	-

It is reported that in cases where the protective layer is correctly applied and remains undamaged, corrosion does not occur on the axle [6]. This means that for corrosion to occur, some previous action or mistake must have taken place to remove or damage the protective layer. An example of this can be seen later in the Chapter in Figure 2.9 with the corrosion developing in the area where the protective layer has been damaged.

2.3 Rail axle corrosion

2.3.1 Brief summary of corrosion with special reference to rail axles

Corrosion is a well understood field of study, with a long history behind it. As the focus of the project it is necessary to provide a brief introduction to the process of corrosion, although the topic is far too large for a thorough examination within this thesis. This section describes corrosion and corrosion processes that are especially relevant to the study of rail axles.

There are many different forms of corrosion. The simplest form is uniform corrosion, where the metal is affected uniformly across the entire surface [1]. It is the most common form as it will affect any metallic surface that is exposed to a reactive environment without protection. This type of corrosion is often easy to mitigate, as it is uniform and easy to predict so a corrosion allowance can be included in designs such as extra material to compensate for expected losses. An example is the security factor used in rail axle designs [15, 16]. On unpainted axles, corrosion is always found and is an unavoidable issue.

A type of corrosion that is often discussed as relevant to axles is pitting. This is specifically mentioned in the maintenance guidelines [5]. Pitting is a localised form of corrosion. A pit is defined as a corrosion feature where the material loss width is comparable to the depth [18]. Pits are sometimes isolated but can also be very close together so giving the combined appearance of a rough surface.

Pits are difficult to detect due to their small size (average of 300µm diameter on simulated rail axles [19]) and the fact that they are often covered in corrosion products [20]. It is an especially harsh form of corrosion as it is highly localised meaning that failures can occur extremely fast [18].

The shape of pits can also cause undercutting of the surface, meaning that inspection of the surface may not give a full account of the amount of material damage under the surface [21]. Examples of this process can be seen in Figure 2.7 [22]. This is particular difficult to detect in the case of visual inspections or other top-down inspection techniques.

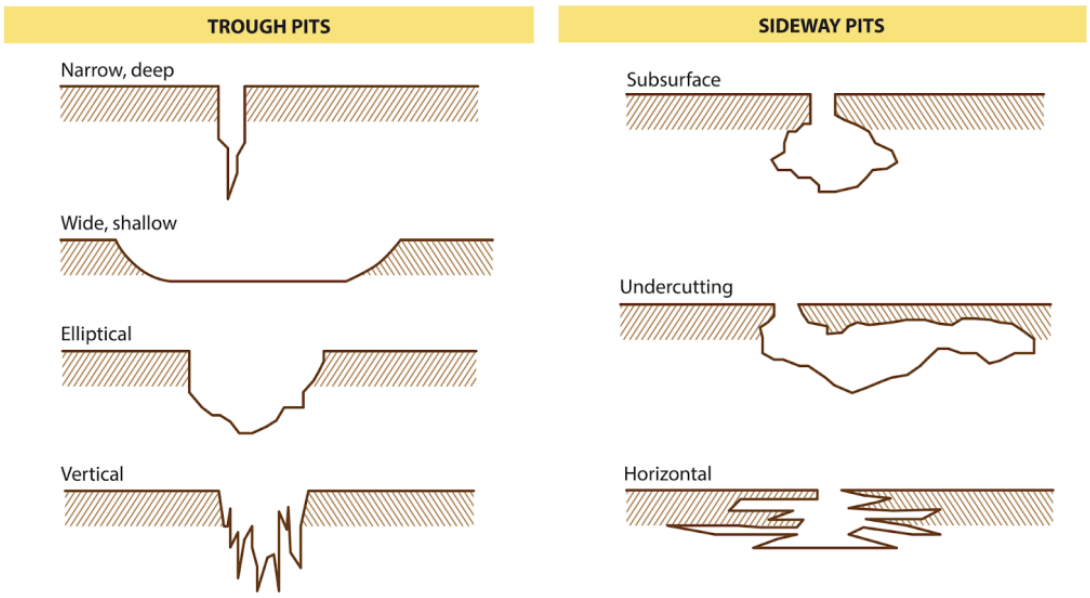

Figure 2.7: Examples of pitting corrosion undercutting [22]

Pits tend to penetrate metal at an increasing rate after the initial corrosion begins [1]. This is due to the auto catalytic nature of the process, i.e. the corrosion in a pit tends to stimulate the continuing activity in the pit.

Consider a metal, M, being pitted by an aerated sodium chloride solution, as in Figure 2.8. Rapid dissolution of the metal's positive ions occurs in the pit, which produces an excess of positive charge in this area, resulting in chloride ions migrating to the area to correct the imbalance. This means a high number of metal chloride and hydrogen ions the chemical breakdown of a compound due to reaction with water. Both the chloride and hydrogen ions encourage the dissolution of the metal and so the process accelerates with time. The cathodic reactions that occur outside the pit tend to suppress corrosion and so the area around the pit is cathodically protected [20], further increasing the pitting effect.

Pitting is often initiated by some sort of discontinuity in a surface allowing selective attack [18]. Examples include a surface scratch or other mechanically created break in a protective surface layer. This discontinuity will tend to form an area of locally high dissolution, causing the chloride ions to migrate to the area, beginning the pitting process.

Pits tend to grow in the direction of gravity [20], the auto-catalytic nature of pitting requires a concentration of dense solutions that is most stable in this direction. Pitting also tends to occur with a stationary electrolyte, as before a pit forms any flow can sweep away concentrations of the required ions to form one [18]. These last two points are of particular interest in reference to spinning railway axles, as this will change the relative direction that gravity acts within the pit, and may ensure a moving electrolyte.

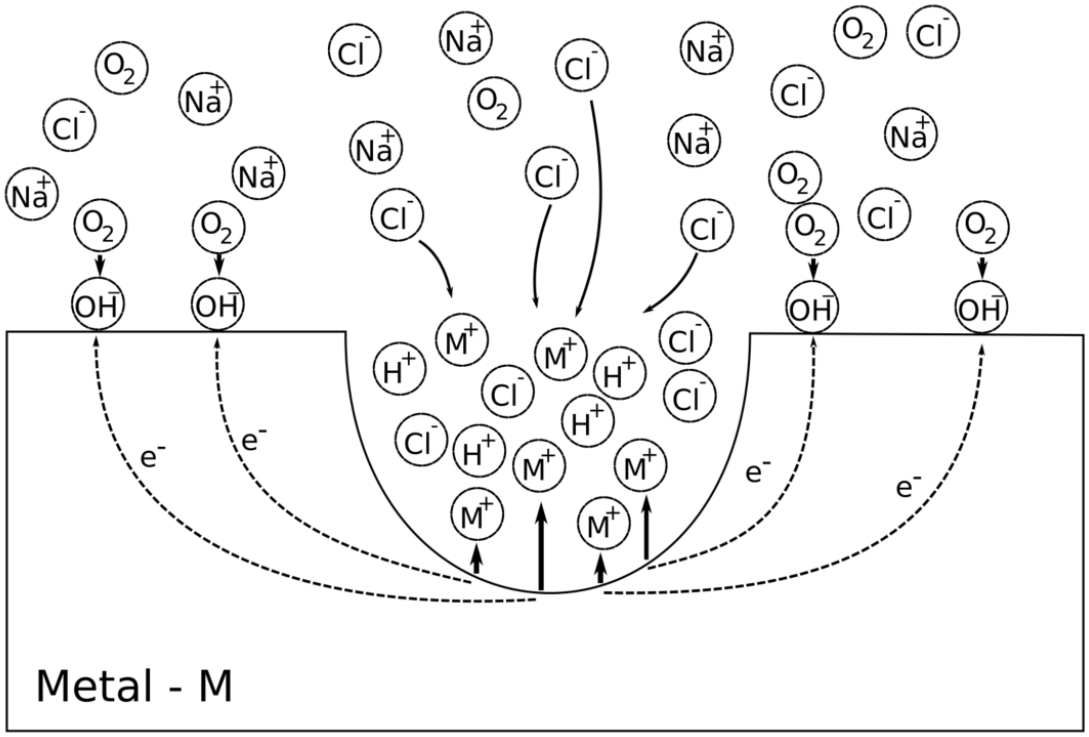

Figure 2.8: Autocatalytic processes in a corrosion pit

Most pitting failures are formed by chloride ions. Chlorides are present in most water solutions [21], particularly in marine atmospheres. Rail axles, due to the nature of their use, may regularly travel long distances and experience a wide range of different atmospheres.

2.3.2 Corrosion limits

Rail axle corrosion is the responsibility of the owners and operators of the axles with no explicit standards. However, current operations are heavily influenced by the guidance that is laid out by the RSSB, introduced after the Rickerscote accident. GM/RC2496 [5] recommends that "…axle corrosion be deemed unacceptable where it:

- Is located in any transition area
- Is concentrated at a particular point, that is a corrosion pit, particularly it has a ring of red/brown staining
- Is greater than 1 mm deep or longer than 30 mm circumferentially or 50 mm axially
- Cannot be removed by polishing up to 1 mm deep

If cracks are found in a corroded area it shall be dealt with by appropriate procedure or scrapped."

In the context of rail axles the transition area refers to the filleted areas at transitions between diameter, due mounting seats for wheels or other equipment, which can be seen in Figure 2.4. For context for some of the other recommendations, a rail axle has an approximate diameter of 200mm and an approximate length of 2m.

The recommendations of GM/RC2496 [5] are often used verbatim in wheelset operating procedures. The recommendations should be kept in mind going forward as they inform the current corrosion maintenance procedures that have resulted in the absence of axle failures for 20 years. However, there are questions around the suitability of these limits. Examples include issues with measuring corrosion depth in a depot setting, that will be discussed later, and the reasoning behind the area limits. Some of the limits also appear questionable, particularly the restriction on red/brown staining, which would always occur in the case of corrosion.

The reasoning behind the selection of the corrosion limits in GM/RC2496 [5] were not clear. No supporting documentation was identified to explain the values selected and based on enquiries put to industry it was not known by the people implementing them either. It is speculated that the values were selected to ensure very high factors of safety in the wake of the Rickerscote crash, rather than due to any specific calculation. However, this was not confirmed.

2.3.3 Corrosion pre-cursors

Corrosion protection is usually applied to rail axles. This is often in the form of a paint layer, as discussed in the previous section, designed to provide a barrier between the corrosive environment and the metal. These protective layers are highly effective and if undamaged could prevent all corrosion [23].

It has been observed in literature [24] and on depot visits as part of this project that almost all corrosion on protected axles occurs where there is a mechanical break in the protective layer. This can be caused by impacts on the axle that remove the paint layer such as axle scoring or dropping of objects onto the axle. It can also be caused by poor adhesion of the paint, either due to the properties of the paint or poor cleanliness during application [25].

An unexpected cause of damage to the paint layer can be when axles are dismantled for maintenance, with end caps, brake discs, etc. being removed. This can cause scratches on axles, from removing these parts, or from impacts from the tools used to remove them, which can promote fatigue and corrosion initiation [26].

Ballast strikes are a well-known example of a process which can cause breaks in the protective paint layer, as well as significant damage to the rest of the underside of the vehicle. The ballast is able to strike the underside of the locomotive, including the axles, due to the creation of aerodynamic lift by the locomotive passing above it, and potentially aided by ground based vibrations [27]. This phenomenon has become more of a problem as the speeds on tracks have increased [27]. One survey showed that around 30% of high speed train axles exhibit this damage, while only 5% of other axles do [28]. This 5% figure is supported by the depot visits carried out as part of this project. An example of how localised this can be can be seen in Figure 2.9. As expected by the source of the damage, ballast strikes can remove the protective paint layer from a very localised area on an otherwise well protected axle. This occurs mostly on the axle body as it makes up the largest exposed area of the axle.

Figure 2.9: Damage to the paint layer of an axle due to a ballast strike. Corrosion has already taken place in the unprotected areas

As observed on visits to inspect class 390 vehicles and other visits, areas where paint was removed always show signs of corrosion products. An example of this can be seen in Figure 2.10. Corrosion is only visible where the paint is removed and was always seen in these areas during depot visits. Based on conversations with inspectors, it was incredibly rare to find any corrosion damage on a section of the axle that was still visibly covered by the paint layer.

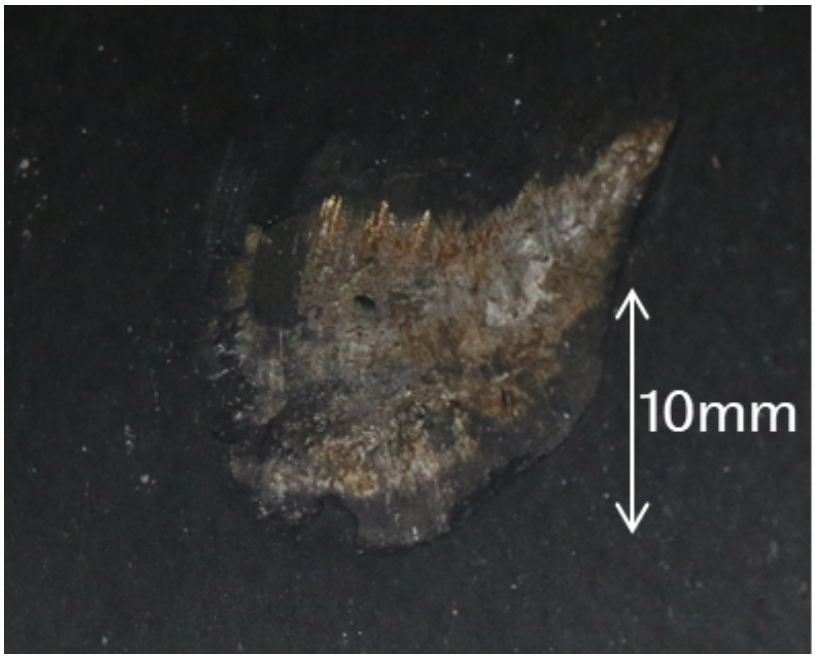

Figure 2.10: Corrosion on axle in an area with paint removed, likely by a ballast strike (note the scraping on the top edge)

The impacts from ballast flight can cause other problems beyond the removal of corrosion protection. As can be seen in Figure 2.11, it can also act as a crack initiator, as was the case in a 2006 derailment in Australia [29]. This is due to the denting of the axle, to depths of between 0.1 mm and 0.9 mm in this case, which concentrate the stresses making the area susceptible to fatigue crack initiation and growth. It is often the case that the impact damage caused by this sort of process, are deeper than those cause by corrosion [6].

Figure 2.11: Ballast impact as a potential crack initiator [29] (scale unknown)

2.3.4 Potential issues of rail axle corrosion

Rail axle standards are designed such that if the standards are met, no cracks will form on a smooth axle surface [30]. Therefore, for cracks to occur there must be an increase in local stresses at the surface, due to geometry change, resulting in a local stress above that which the material can withstand. There must also be a faster rate of growth of cracks than the rate of material loss due to processes such as corrosion. These competing rate effects are an area of interest of this research as it will have a significant impact on the chance of axle failure. It should be noted, however, that the crack would not have initiated without the corrosion damage, and any protection from the competition effect would only be temporary in many cases.

This increase in local stresses can be caused by the presence of surface defects or flaws such as corrosion damage, flying ballast allowing corrosion and causing indentation [29], fretting fatigue in press fitted areas [31], and non-metallic inclusions close to the surface [32]. These can all cause stress raisers that can results in crack initiation and growth due to changes in the surface geometry or other points of weakness.

Cracks can initiate from corrosion pits, which is the failure mode this project is interested in. There have been several different models produced to try and mathematically predict this initiation, but many are limited due to the variation in pit topology and service conditions.

Turnbull et al. reported that "the vast majority of cracks emanate just at or below the pit mouth" [33], in an alloy steel in a high stress corrosive environment, with the pit mouth being defined as the visible opening of the corrosion pit. Their suggestion is that the origin of a crack that extends beyond the pit is due to the coalescence of cracks that originate around the whole pit, having the overall effect of the crack extending beyond the pit base. The stress is localised in the bottom of the pit as expected, however the strain is localised near the pit mouth, as demonstrated by Figure 2.12.

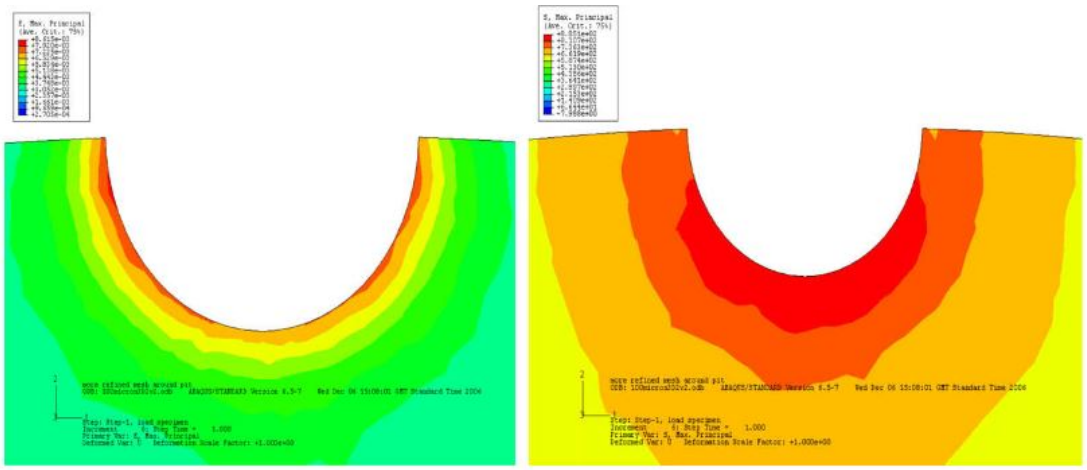

Figure 2.12: Maximum principal strain (left) and maximum principal stress (right) of 100µm pit [33]

This is further backed up by the work of Horner et al. [34] who also reported that the majority of cracks emanate at or just below the pit mouth, in turbine disc steels exposed to simulated steam-condensate, and FEA simulations of this situation.

Cerit et al. produced a finite element model to determine the stress concentration factors of potential corrosion pits [35]. This is given by Equation 2.3:

$$K = \frac{1 + 6.6(\frac{a}{2c})}{1 + 2(\frac{a}{2c})} \tag{2.3}$$

where K is the stress concentration factor, a is the crack depth and 2c is the crack width.

The maximum stress, according to this model, occurs slightly below the mouth of the pit or at the bottom of the pit depending on the aspect ratio, the ratio between the pit radius and pit depth. The aspect ratio appears to be the main parameter affecting stress concentration factor. There is also the potential of secondary pits within the primary pit. Once a secondary pit occurs the stress concentration factor is significantly higher than that due to a single primary pit, shifting the origin of cracking to the base. This work used perfectly symmetrical and smooth pit geometries, so questions could be raised as to the accuracy of this analysis.

Experiments performed by Berretta et al. [36] and Moretti et al. [19] suggest that the formation of cracks is trigged by a secondary pit at the bottom of the primary pit, at least in EA4T and EA1N steels. This appears to contradict the experimental observations of Turnbull, but is likely due to the relatively low stresses used in these experiments so plastic strains only develop at the mouths of secondary pits due to the high stress concentration factors at these points.

It appears that crack initiation is broadly accepted to be due to the occurrence of plastic strains at areas of high stress concentration. This can occur at different places based on the conditions. It is interesting that the papers that looked at rail axles found cracks from the bottom of the pits instead of the sides seen in other experiments. This can be compared to reports of an axle failing due to stress corrosion cracking on a salt hopper wagon in 1998 where surface cracking is clearly visible [37], shown in Figure 2.13. It should be noticed, however, this was under highly specific circumstances where a salt solution was trapped against the axle surface. This may restrict the applicability of applying this to the general axle population, as most axles would experience far less aggressive corrosive environments.

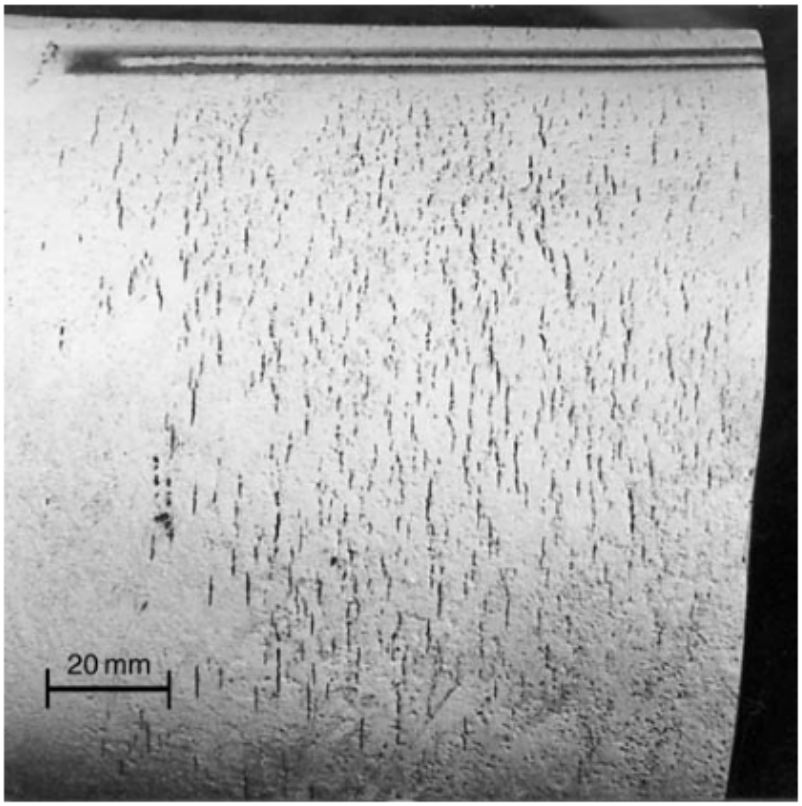

Figure 2.13: Multiple cracks on the surface of the axle involved in an accident at Shields Junction in 1989 [37]

2.3.5 Fatigue cracking in rail axles

The ultimate failure of axles is due to a crack propagating across the entire axle removing the ability of the component to support the required forces for operation. When talking about prevention of corrosion and other axle damage, this is done with the aim of preventing crack initiation points from forming. Once a crack has formed however, it will still take time to propagate until final failure.

One of the most common ways to determine the fatigue life of a material in high cycle applications is using S-N curves. These are empirically produced by testing standard samples of materials under repeated stress cycles. The number of cycles taken to fracture samples at different stress ranges is plotted, as shown in the example given in Figure 2.14 for EA4T steel.

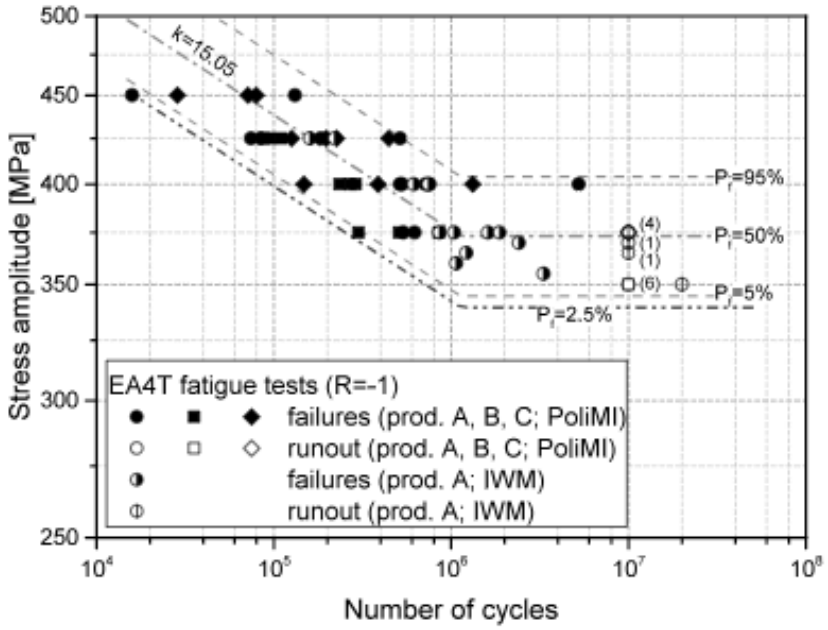

Figure 2.14: S-N curve of small specimens of EA4T steel often used in rail axles [38]

While these work well for comparing materials and are indicative of the number of cycles that a material may be expected to withstand, these results are highly dependent on the environment.

Significant changes can occur if there are variations in loading frequency, temperature, residual stresses, and with surface defects such as corrosion or impact damage. Corrosion damage can reduce the stress level at which a component would have an infinite life under cyclic loading, as reported by Beretta [39].

Cracks can be described in terms of a stress intensity factor (SIF) [11]. This is a term which describes the magnitude of the elastic stress field at the tip of a crack. This factor is given by Equation 2.4.

$$K = Y\sigma\sqrt{\pi a} \tag{2.4}$$

where K is the stress intensity factor, Y is a dimensional shape factor, σ is the nominal stress and a is the crack size.

This can be combined with the known stresses and material characteristics to estimate the development of a crack. The approach has also been successfully applied to stress corrosion cracking data [40].

Cracks tend to grow in three stages, as seen in Figure 2.15. ΔK is the stress intensity factor at the crack tip and ΔK_{TH} is the threshold SIF below which cracks do not propagate [40]. The final fracture occurs when the stress intensity factor equals the critical stress intensity factor within the fatigue stress cycle.

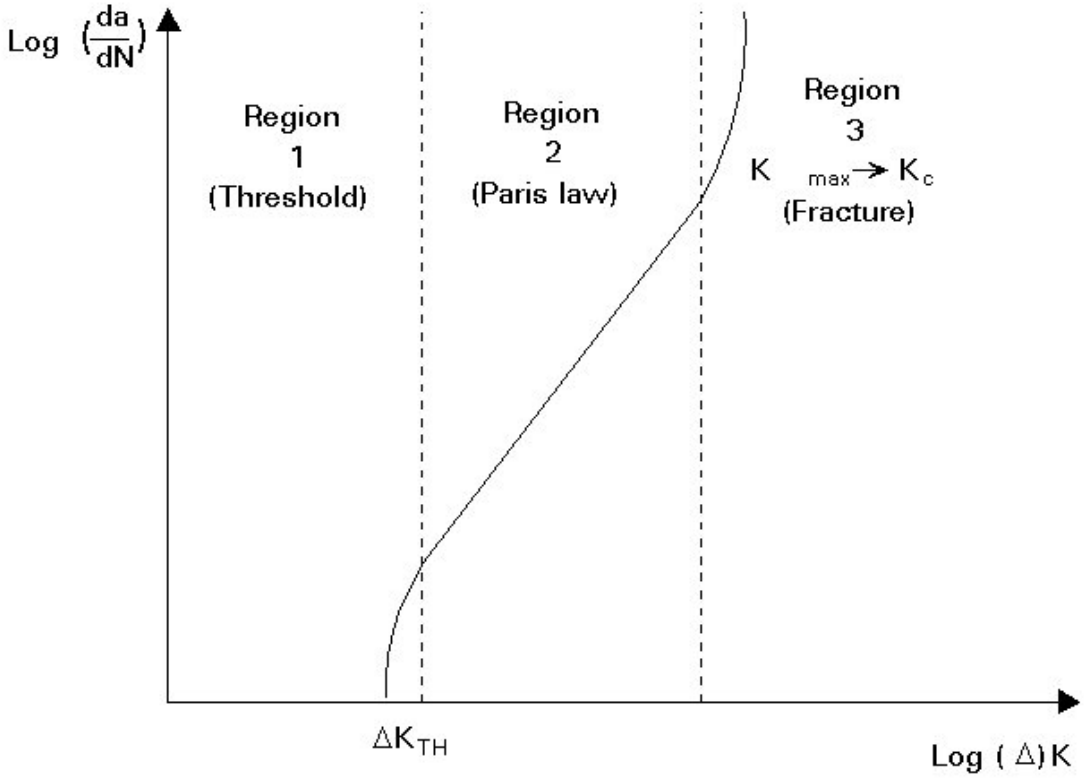

Figure 2.15: Typical fracture mechanics fatigue crack propagation behaviour [41]

As the crack develops into region 2, the stable region, it is described by the well-known Paris crack law, given in Equation 2.5.

$$\frac{da}{dN} = C(\Delta K)^m \tag{2.5}$$

where da/dN is the crack growth rate per cycle, C and m are material properties and ΔK is the stress intensity range.

2.4 Introduction to rail axle maintenance

2.4.1 Rail axle maintenance schedule

Rail axle maintenance takes place as part of the wheelset maintenance process.

Inspection intervals are the times between different inspections of components. There are different inspection intervals for different parts of the vehicle so there are many inspections focussing on different parts. There is currently no explicit legal requirement that covers the inspection intervals of railway axles and the responsibility for safety lies with the manufacturer and the maintainer to ensure safety.

The guidance for freight wheelset examination is given in RIS-2766-RST [4]. RIS-2766-RST gives two reasons for an inspection to take place. One is the normal time or mileage for an inspection to come due, the other is some event being reported that is separate to the usual operation of the axle, reported either by a driver or condition monitoring.

- Wheelsets shall be examined during service according to the maintenance plan
- In addition, wheelsets shall be examined in the event of:
  - Receipt of an incident report, for example rough riding, striking an object, unusual noise, wheel flats etc
  - Report of a wheel load impact detector exceedance
  - Activation of a hot box detector
  - Brake drag
  - Identification of other deficiencies associated with wheelsets, for example identified by High Risk Defect Reports, as set out in RIS-8250-RST
  - The vehicle having been stored for a period of time

The intervals for planned inspections (assuming no other reason is reported during operation) are calculated internally, checked by an independent assessor and then written into a maintenance plan and Wheelset Operating Procedures (WOPs) for use by depots. An example of the time between inspections of freight wagons can be seen, in the European VPI standard [42] as shown in Figure 2.16. As can be seen an inspection can be activated by mileage or time passed. These values would vary depending on the axle design.

Annual mileage		Inspection with NDT after	
		Max. mileage (km)	Max. service time [1) 2)] (years)
A	< 30,000 km/year	600,000	16
B	≥ 30,000 – < 50,000 km/year		12
C	≥ 50,000 – < 80,000 km/year		8

Figure 2.16: Inspection intervals for wheelsets with a diameter over 840 mm [42]

The intervals for passenger axles are significantly shorter than for freight axles. This is demonstrated in Figure 2.17 [43], where inspection intervals are between a tenth and a half of those for freight axles, depending on the type of inspection. This significantly longer inspection interval means that there is a significantly increased chance of corrosion to initiate and develop in the freight fleet compared to the passenger fleet. This is most likely due to the increased impact of an incident, in terms of injuries and fatalities, of passengers services compared to freight operations. Based on this the focus of the project was placed on freight axles.

Mileages (km)						
	High Speed Train	3.000 to 20.000	30.000 40.000	90.000 200.000	180.000 200.000	2.400.000[2] 1.600.000[3]
	Commuter Train	16.000	48.000	240.000		1.500.000
	Freight Wagon	50.000	100.000	200.000 to 600.000	200.000	1.500.000
Time (months)		Visual inspection	Instrumental Inspection (gauge, profile ...)	NDT inspection	Wheel tread re profiling	Wheel substitution[1]
	Freight Wagon	12	24	48 to 96	48	360
	Commuter Train	1	3	12		48
	High Speed Train	2 0.25	4 2.5	18 7.5	18 15	160[3] 150[2]

General wheelset review

[1] Target values (depends on material / freight wagons influenced by tread braked wheels)
[2] China HST
[3] EU HST

Figure 2.17: Example of inspection intervals for wheelsets under different use cases [43]

2.4.2 Rail axle maintenance procedure

The flow of an axle through the maintenance process is described in Figure 2.18. There are different levels of inspection for the axles, with many being visual to check for obvious faults. The techniques used for inspection will be discussed later. An inspection fail involves the damage on the axle being deemed too extensive for the axle to be reclaimed under the terms of the maintenance plan relevant to the axle type. If scrapped the axle is sold for recycling.

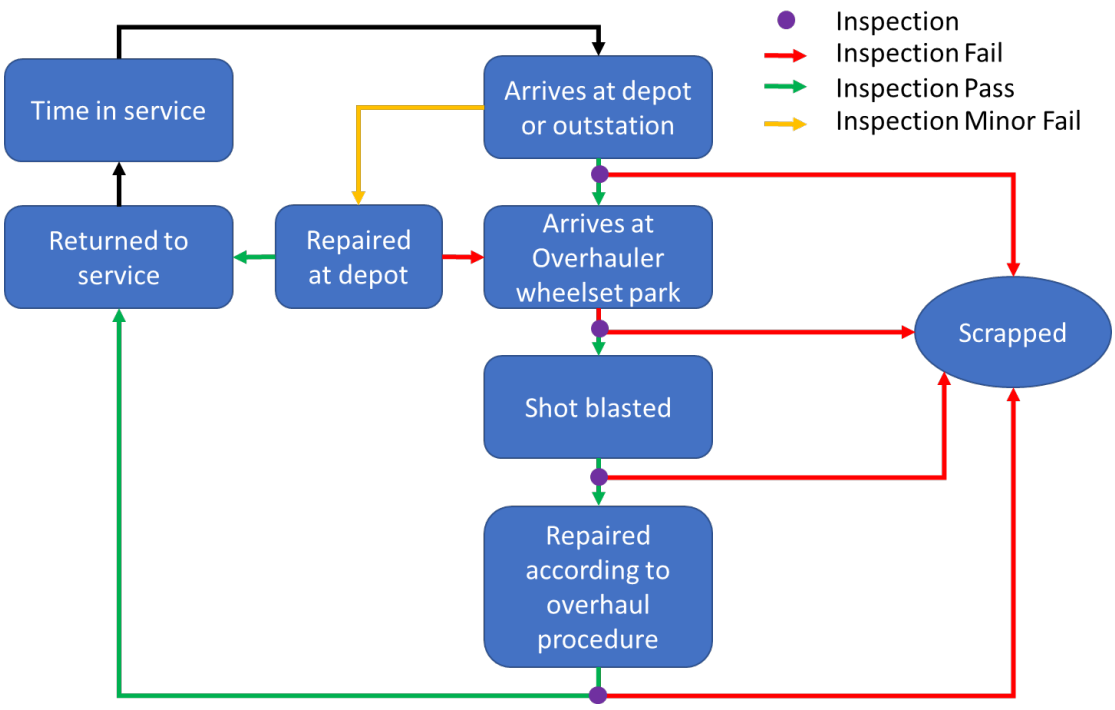

Figure 2.18: Graphic showing the flow of axles through the maintenance process

Axles undergo inspection at either depots or outstations, that identify any damage that requires the axle to go to overhaul, otherwise the axles are sent to overhaul based on a time frame, as described in the previous section. Overhaul is a type of inspection where the axle is removed from the vehicle and has the protective coating layer removed by shot blasting. This differentiates it from in-service maintenance that would occur while the axle remains in place without being removed, as might happen at a maintenance depot if minor damage was detected and different, more localised, techniques and procedures may be used. Axles can be sent for two types of overhaul depending on the requirements [12] of the maintenance plan.

- **Medium wheelset maintenance**

  Off-vehicle wheelset maintenance without change of wheels, combined with bearing overhaul

- **Heavy wheelset maintenance**

Off-vehicle wheelset maintenance with change of wheels, combined with bearing overhaul

An example of an overhaul depot can be seen in Figure 2.19. During an overhaul process, a wheelset is delivered and kept in a wheelset park until there is space available for it, as can be seen in Figure 2.19. At this stage the wheelsets are still whole, with any paint layer or corrosion products still present on the surface. An initial visual inspection takes place at this stage, and if there is evidence that an axle has no chance of being returned to service, due to extensive damage, it may be scrapped at this stage. Otherwise it continues into the maintenance sheds for further consideration.

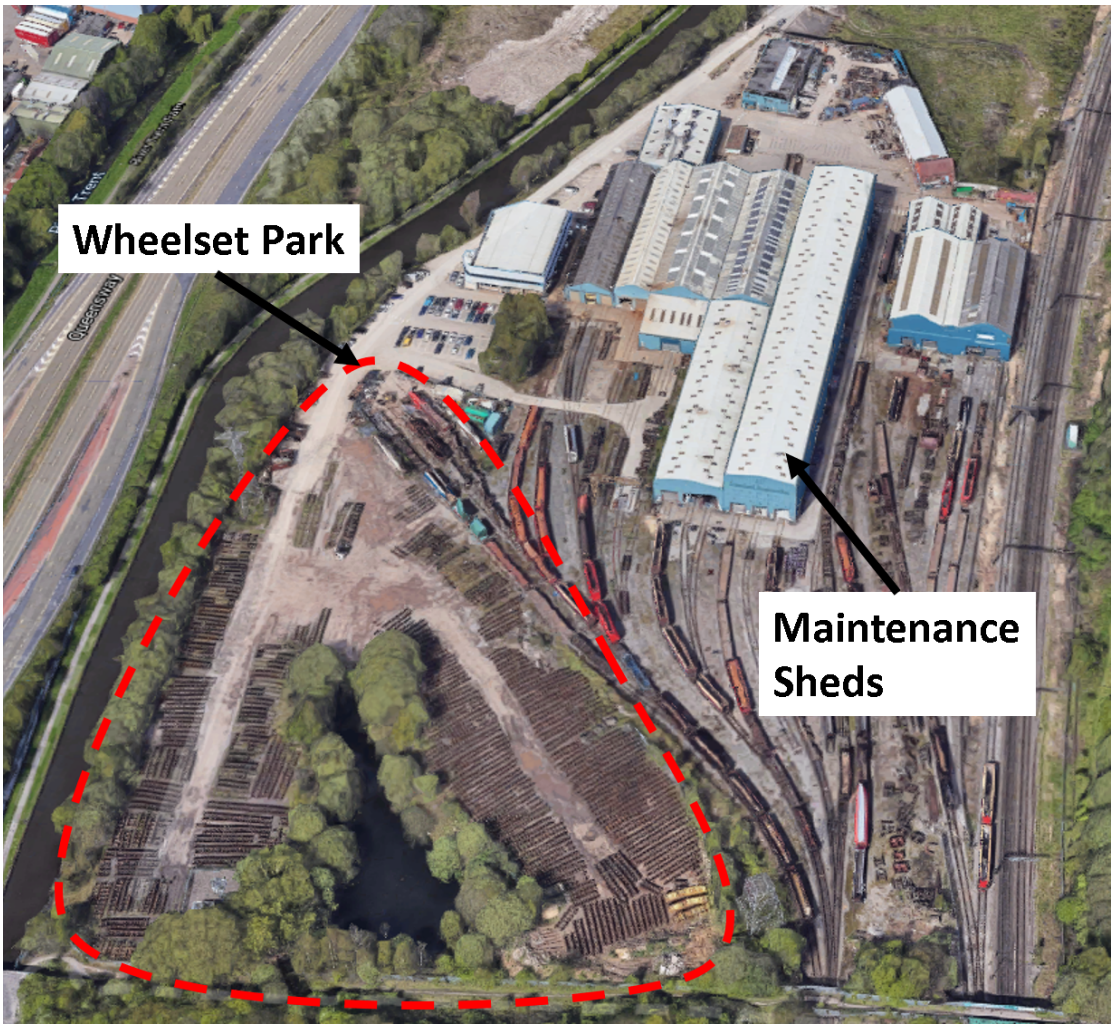

Figure 2.19: Example of an overhaul depot with wheelset park (Google Maps)

Once the axle has been deemed to be potentially recoverable by visual inspection in the wheelset park it enters the maintenance sheds and undergoes shot blasting to remove the paint layer and any corrosion products on the surface. The reason these are removed is to allow for a proper inspection of the axle surface that may be concealed if this layer was not removed.

Shot blasting is when fine, hard particles are blasted at a surface under high pressure, causing an abrasive process to remove unwanted surfaces. This blasting is done with small iron particles and an air pressure machine to accelerate the particles such that they have the energy to remove the unwanted surface products. An example of how shot blasting changes axles can be seen in Figure 2.20, the axles on the left of the image have been shot blasted while the painted axle can be seen on the right.

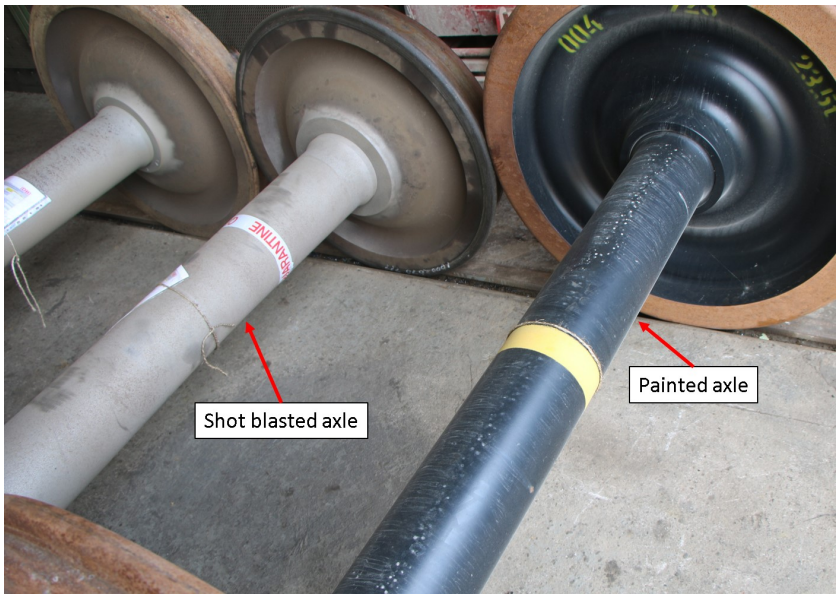

Figure 2.20: Examples of painted and shot blasted wheelsets. Shot blasted wheelsets can be seen on the left, with a non-blasted wheelset on the right with the paint layer still attached

This shot blasting does change the surface of the axle, as it is inevitable that the abrasive process has some effect on the base metal. This effect is minor and generally ignored by industry. An example of a surface that has undergone shot blasting, but has no corrosion damage, can be seen in Figure 2.21 (note the rough appearance of the axle surface).

Once the shot blasting has been completed, the axles are again inspected more thoroughly by an operator, visually for corrosion damage, and using ultrasonic techniques as well as magnetic particle inspection principally for crack detection. If the axle fails these inspections it is scrapped. If it is deemed to be recoverable, it moves on to the correction stage of the process, in an attempt to return the axle to an acceptable condition for it to be safely returned to service. This decision is made based on the condition of the axle, the maintenance plan and the likelihood of a successful recovery within the limits of the axle type.

Figure 2.21: Example of an axle that has undergone shot blasting, but exhibits no other surface damage

Inspection techniques

Inspection of axles is performed using NDT techniques to allow axle to be potentially reused after inspection. For cracks this is often done using magnetic particle inspection (MPI) and ultrasonic techniques [9, 32] as well as visual inspection, looking for corrosion damage, impact damage, scoring and cracks. Examples of ultrasonic and MPI inspections being undertaken in a depot setting can be seen in Figure 2.22.

Inspections are usually performed manually and are common across almost all depots in the UK and Europe [42]. It has been found that human factors, such as skill in interpreting equipment results, can be most significant for the capability of manual ultrasonic testing [44], and it is reasonable to assume there is similar variation in other inspection types that rely on a skilled operator. A report from 2006 [45] estimated the costs of inspecting an axle using ultrasonic inspection to be around £22 an axle. If axle end caps need to be removed and replaced this rises to £69 per axle.

(a) Ultrasonic inspection

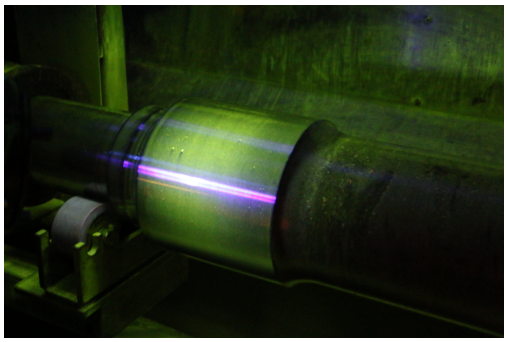

(b) Magnetic particle inspection

Figure 2.22: Inspection techniques being used in a depot setting, principally used for finding cracks

Based on observations during visits to multiple depots and literature, it can be seen that virtually all corrosion inspection is done visually [46]. Although this technique, is accurate at identifying damage [24], it is extremely difficult to determine depth visually, as required to fully implement the guidance [5].

There is currently no device to accurately collect quantitative corrosion data on site [2]. The WOLAXIM project has attempted to develop a system for detecting cracks caused by corrosion damage [25, 47]. However, there has been no indication of this equipment being used in depots visited. There are charts available to estimate pitting depth, such as in ASTM standard G46-94 [48], but there is no evidence of these being used in depots, either from visits or literature.

The inspections are performed by a depot technician whose main job is the return of safe axles as efficiently as possible back to the customer. They will not want to take on responsibility, legally or morally, for sending out an axle which may be unsafe. This means that if an axle is borderline then they are likely to scrap for safety. This is a worker dependent factor of safety on top of the other reasons factors of safety area applied. The randomness of this process was underlined by visits to a depot where some operators were anecdotally known to scrap many more axles than others. There can also be variation between depots which can affect where work is placed. This competition is one potential way that scrap rates are kept low.

Depot inspectors were not concerned with the collection of scientific data and measurements, as this is not their job. Inspectors are concerned with the pass/fail condition of the axle rather than the specifics of the failure. This was revealed when historic depot records were analysed, where highly non-specific terms were used, reducing the value of the data for scientific analysis. A common example of this in records analysed for the project was the term 'beyond limits' when referring to axles that were clearly not going to pass inspections, rather than quantifying the extent of the damage.

Correction

If an axle has moved into the correction stage it has been judged by the inspector to be possible to recover to a safe condition for continued use.

There are two major causes for an axle to not have recovery attempted. One is damage that is so large that it would be obvious that recovery was not possible, such as a large visual crack or extreme impact damage. The more common reason, especially in corrosions case, is that recovery is not possible 'within limits'.

'Within limits' means that each axle type has been designed with a large diameter initially, with each correction process removing material down to a limit where no more can be removed without the axle failing to meet the previously mentioned design standards. This means that in the case of an older axle, even relatively minor corrosion damage, that would normally be possible to remove would bring the axle close to or below this limit.

The judgement of rail depot operators, in deciding if recovery would be possible, is a source of possible inefficiency in the system, as demonstrated in Figure 2.23. The distributions used are not based on any data and are simply meant to demonstrate the locations of inefficiency within the maintenance system.

If axles are scrapped before recovery is attempted, as an operator judged there to be no way of correcting the damage, when there was sufficient material left for a successful recovery this results in a wasted axle. However, if there was not enough material left for a successful recovery, but one was attempted anyway, resulting in scrapping later, the time and expertise of the depot have been wasted. Both of these could be avoided if the nature of damage was quantitatively better known and did not rely on the judgement of depot operators.

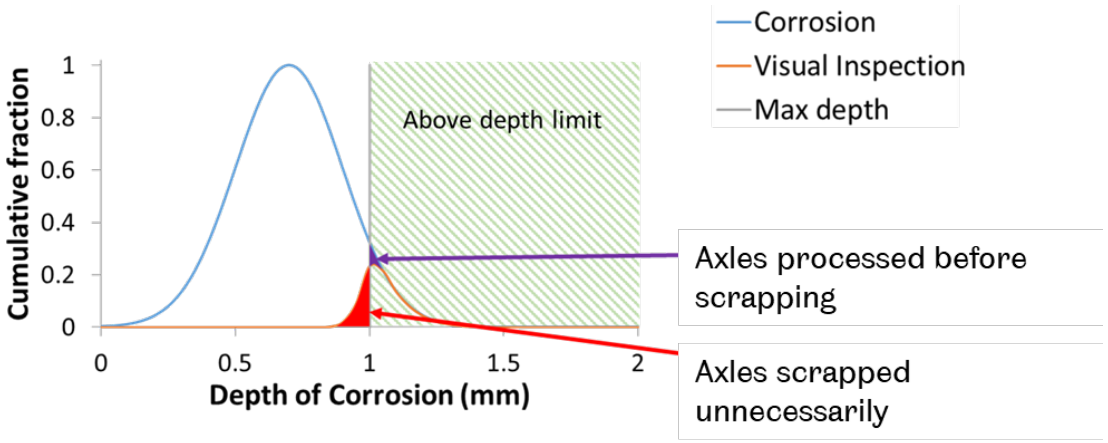

Figure 2.23: Graph of potential areas of inefficiency in the correction system of rail axles. Values are illustrative only

To correct recoverable damage on an axle, the shot blasted axle has its wheels removed (or has had them removed previously for inspection). It is then turned to remove small amounts of material over the entire length of the axle body. This then requires changes to be made to the transitions from any seats on the axles, to keep the radii consistent and prevent a change in stress concentration. The axle is potentially turned multiple times as it is not generally possible to know how deep the damage is, so many steps of material removal may be required to completely remove any damage.

Once this is completed to the satisfaction of the depot the axle can be re-painted, have the wheels and any other components reattached and be returned to service. At this point the axle could be considered ”as new” and has no other notes or restrictions placed on it. Due to the fracturing of the industry and poor record keeping over recent decades, many freight axles move through the maintenance process as ”new” axles each time. This is due to the design methodology of the axles that means that any axle that meets the standard is designed for infinite life as well as the loss of records between companies and the issues caused by the move to digital record keeping.

2.5 Axle records

It was identified at the beginning of the project that it was necessary to define the scope of current issues with railway axle corrosion. The first step was to build relationships within the rail industry, to gain access to the facilities and data required. This was done by contacting the Wheelset Management Group (WMG) of the RSSB and developing contacts to produce industry support for the project. The WMG consists of industry stakeholders for wheelsets and facilitates research and dissemination of best practise within the industry.

2.5.1 Results of axle records

Three overhauling depots scrap records were obtained from the Wheelset Management (WMG) group of the RSSB. The depots were widely separated geographically, represented three different companies, and a multitude of fleets. The data from all depots had been combined and was not able to be separated, however there was little reported difference between depots. It is worth noting that the vast majority of the axles dealt with at these depots were freight axles.

There were two types of records available to the project, axle returns and the scrap assessment record, although not all depots supplied both. The axle returns detailed the number of axles inspected and the number scrapped, but without reasons for the scrapping. The scrap assessment records give the reasons that a particular axle was scrapped, with the damage type (corrosion, indentation, scoring) and the location of the damage (body, transition zones, abutment/shoulder, wheelseat, other seats, bearing journal or all over).

The axle returns showed that 186 out of 1537 axles (where records were available) were scrapped, for various reasons at the depots in 2017. This represents around 12% of the axles, similar to the lower end of the anecdotal evidence. However, this headline figure disguises some significant variation in scrap rates between different fleets of axles, as can be seen in Table 2.2. No other information is available about the particular axles that were scrapped, and this is still a small part of the total number of axles in the UK so these values should be treated as merely indicative.

Table 2.2: Axle returns from available depot data

Axle type	Number of axles	Fails	Percentage fail
A	304	7	2.30%
B	259	0	0.00%
C	209	1	0.48%
D	190	1	0.53%
E	146	3	2.05%
F	141	10	7.09%
G	70	63	90.00%
H	44	17	38.64%
I	38	29	76.32%
J	31	0	0.00%
K	17	10	58.82%
L	16	14	87.50%
M	13	13	100.00%
N	13	13	100.00%
O	9	1	11.11%
P	8	0	0.00%
Q	8	0	0.00%
R	5	1	20.00%
S	4	0	0.00%
T	4	0	0.00%
U	3	1	33.33%
V	2	2	100.00%
W	2	0	0.00%
X	1	0	0.00%
Total	1537	186	12.10%

Table 2.3: Damage types found and reported on inspected axles

Axle contains	Number	Percentage
Scoring only	13	1.29%
Scoring and indentation	16	1.59%
Scoring and corrosion	139	13.80%
Scoring, indentation and corrosion	47	4.67%
Indentation only	50	4.97%
Indentation and corrosion	120	11.92%
Corrosion only	584	57.99%
None given	38	3.77%
Total	1007	100%

The scrap records were more detailed in the information they provided. These records were the paper forms that depot inspectors filled in when inspecting axles. The scrap records were available for 1007 axles inspected, and judged to be scrap worthy, between January 2015 and January 2018. It is worth noting that these do not represent the same dataset as the axle returns, although there may be some overlap.

The scrap records supply information on the location of the damage, the type of damage and sometimes more detailed information on the scale of the damage. This information can be seen in Figure 2.3, with corrosion being present in 91% of cases if blanks were excluded.

If the data is broken down by years the presence of corrosion is consistent in each year 2015: 82.9%, 2016: 90.8%, 2017: 91.5%. There appears to be little correlation between other forms of damage and corrosion, although the overwhelming number of corrosion cases may mask any patterns.

The locations of the corrosion reported can be seen in Table 2.4. These results demonstrate that corrosion was heavily focused on the axle body, with $\frac{2}{3}$ of reports of corrosion occurring in this location. The next most common areas for corrosion damage is the non-wheel seats, for things like brakes and traction devices. Based on conversations during depot visits these issues often were associated with trapped moisture problems beneath these components.

There were also 56 scrap records that also included information about the size of corrosion areas. From this limited sample the average size of the corrosion areas reported was 14,801mm^2 with a maximum size of 108,000mm^2 and a minimum 300mm^2. This does not include the large number of samples (441) that reported the corrosion as ”beyond limits” (50mm x 30mm). There is no information on the depth of the corrosion based on the lack any ability to measure the depth of corrosion in depots.

Table 2.4: Locations of corrosion damage reported on scrapped axles, with blanks excluded

Corrosion location	Number	Percentage (blanks excluded)
Axle body	656	65.14%
Seats for brakes, final drive and traction motors	243	24.13%
Transition zones between seats	19	1.89%
All over	7	0.70%
Abutment\Shoulder	5	0.50%
Bearing journal	3	0.30%
Wheelseat	0	0.00%
Hole for hollow axle	0	0.00%
Total	933	100.00%

It is worth noting that the data collected by the operators at the depots was never intended to be used for scientific research purposes. Due to this the exact veracity of the data cannot be confirmed. There are several scenarios that could be considered that may affect the results. One is if the operator finds severe damage early in the inspection, that would lead to scrapping, would they continue in their inspection? If not, not all of the data about the axle condition would be obtained. Another issue was that this data was lacking in any significant quantification of the results, with most of the recorded data being subject to the judgement of the individual depot worker. However, the procedure in many depots involves a senior worker verifying the scrapping decision, so a level of standardisation is enforced.

The 12% overall scrap rate matches the anecdotal information, which suggests this was within the correct range. Of the axles scrapped, 91% showed some corrosion and 65% of corrosion instances occurred on the axle bodies.

2.6 Approach summary

Based on the results of the axle survey, and the evidence of literature, the case for investigating corrosion was strongly supported. This project focused on the corrosion on the axle body, due to the decrease in complicating factors and majority of corrosion damage occurring there. The project worked with the freight fleet rather than the passenger fleet due to the availability of data and access as well as the larger inspection intervals that these axles undergo. The larger inspection intervals mean that there is an increased chance of corrosion damage developing.

It was decided that the work would be approached from two main directions. The workflow can be seen in Figure 2.24.

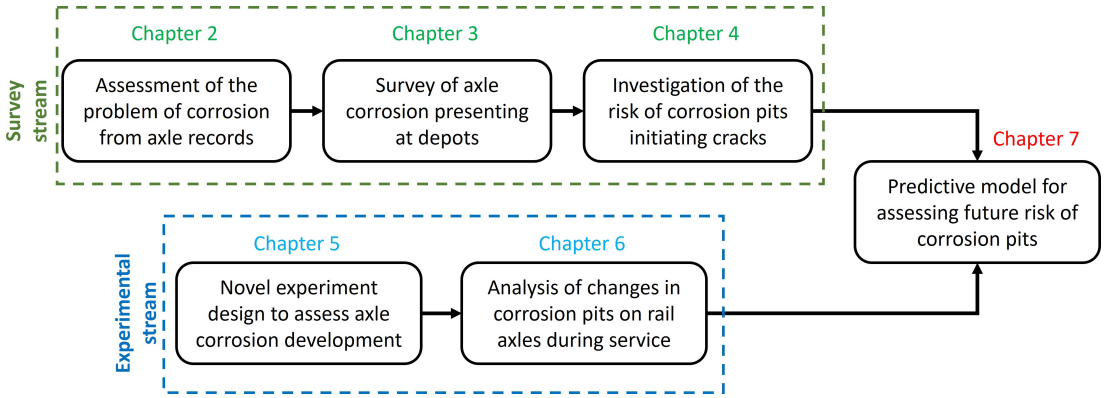

Figure 2.24: Workflow of the project, demonstrating the two separate streams

One workflow was a survey based approach, investigating the corrosion damage found on freight axle bodies in operation. Then assessing the risk that these pose to the axles. The second approach was to use experimentation to assess the changes to the corrosion pits over time when in operation.

By investigating the types of pits found in operation, and the risks associated with them, it was possible to draw conclusions on both the suitability of the current standards and their applicability to the real world maintenance setting.

Assessing the changes in pits overtime, allowed for conclusions to be drawn on the requirement of corrective work to be performed on axles. The potential of delaying correction of minor damage would have significant financial and logistical impacts on the industry.

Finally both these streams were to be bought together, to produce a predictive model that would assess the relative increase of risk from a pit over time if left uncorrected.

Chapter 3

Corrosion Pitting Observed in Depot Setting and the Programmatic Approach to Pit Identification and Separation

3.1 Introduction

Before examining corrosion damage to rail axles in great detail, it was necessary to define the problem. This required investigating what was already being found at maintenance depots. This meant surveying corrosion on rail axles in operation, to determine the extent and type of corrosion pits that were being observed.

Initially previous work in the area of rail axle corrosion surveys was considered. The results of the surveys were analysed as well as the strengths and limitations of the techniques and assumptions used. Based on these studies a new technique was proposed and discussed. The work undertaken to validate the approach is also presented.

An axle survey was undertaken at a UK overhaul depot using the technique developed as part of the thesis. Samples were taken of six corroded axles and one un-corroded axle for control purposes. The process for collection will be described and discussed.

After scanning the sample sites, the data was initially processed using filtering techniques before pit identification and separation using image processing techniques. This process, including the assumptions and techniques used, are discussed and evaluated.

The basic features of the identified pits were analysed and compared to previous studies. These results are discussed and the implications, in terms of the axle fleet, evaluated based on extreme value analysis. A flow diagram of the work carried out in this Chapter can be seen in Figure 3.1.

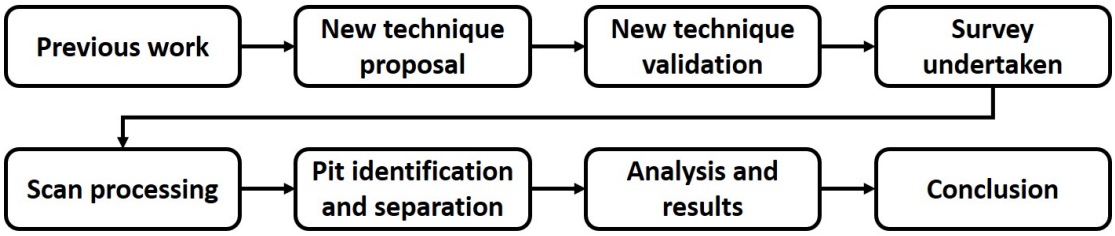

Figure 3.1: Work flow diagram for Chapter 2

3.2 Previous studies

A standard way of calculating the risk to axles that corrosion poses, would be to analyse the number of failures compared to the number of axles and the usage statistics. However, there have only been three freight axle failures due to corrosion since the new standard was introduced [6] and none since 2002. Comparing this to other statistics, such as the 305 million km travelled by freight trains between 2010 and 2017 [49], shows how small the number of failures had been compared to the scale of the rail freight industry in the UK. Any analysis that relied on these few cases to provide recommendations on the treatment of rail axles, risked misinterpretation due to the small number of failures.

To provide more relevant information on the appropriate actions to take with corroded rail axles, it would be necessary to investigate the corrosion damage that was being found at depots during maintenance.

While axles were regularly inspected in depots, there were several issues with this. These included the ability to collect information, and the willingness to do so, at a level sufficient for scientific evaluation. This meant that while axles were regularly inspected, there was not a large existing data set on the condition of rail axles. To this end, several surveys of rail axle corrosion have been performed in the literature in a more scientific manner.

3.2.1 Surveys by operators

In the depot setting, inspection of rail axle corrosion was limited to visual inspection and evaluation. The lack of any other form of evaluation was supported by the work of Rudlin [46, 50], Muller [51] and the T728 project [6] (a major survey of axle corrosion carried out for the RSSB. The main reports are restricted to RSSB companies).

The only more advanced technique used was Magnetic Particle Inspection (MPI), which enhanced the visual inspection, but does not represent a major step change in capability. Rudlin mentioned the use of a pit depth gauge at some depots, although when this was put to depot workers during visits, none reported having used one or having heard of them being used.

The limitation on inspection techniques and data gathering meant that there was no pit depth data available that had been systematically collected from the depots. This meant operator's judgements, or area restrictions in the standard, were used in practice to make decisions on axle scrapping. Due to the limitations on data collection in the maintenance setting, all detailed data for rail axle corrosion geometries has come from scientific surveys, carried out by external researchers.

3.2.2 Scientific survey techniques

There were two main technique types used in surveys of rail axle corrosion damage. Both of these were fundamentally two dimensional approaches to collection of rail axle corrosion data, which had follow on effects in the reported results.

The first technique was a cast based approach. Using a replicating compound, with high resolution, on the surface of the axle, it was possible to capture the geometries of the pits present on the surface with minimal distortion [52]. A British Railways Research report from 1972 [52] found that, using an epoxy resin as a replicating compound, a surface could be replicated effectively as long as the compound was used within a suitable temperature window.

The cast of the surface was then cut along its length and the internal profile was inspected optically, to assess the geometries of the pits that lay along the line, as shown in Figure 3.2. This was usually done using a camera and digital inspection software. This technique had been used in several different studies [24, 39].

An alternative approach was very similar, but involved fracturing the axle and then polishing the revealed surface to get the same effect, although this was a destructive process, making reuse of the axle impossible. Both of these processes were used by project T278 when inspecting axles [6]. The technique allowed for detailed inspection of the profiles of the corrosion pits along the line of the cut or fracture.

There were some problems with the exposed profile based technique. It required assumptions to be made about the pit shape, which are described in Figure 3.3. These assumptions stated that a pit could be described by extrapolating its two dimensional profile, assuming that all pits are either semi-circles or semi-ellipses. While the assumption may be correct, it did limit the accuracy of the collected data, as it would have the effect of smoothing pit shapes to conform to the assumption, removing small features in the pit particularly in three dimensions.

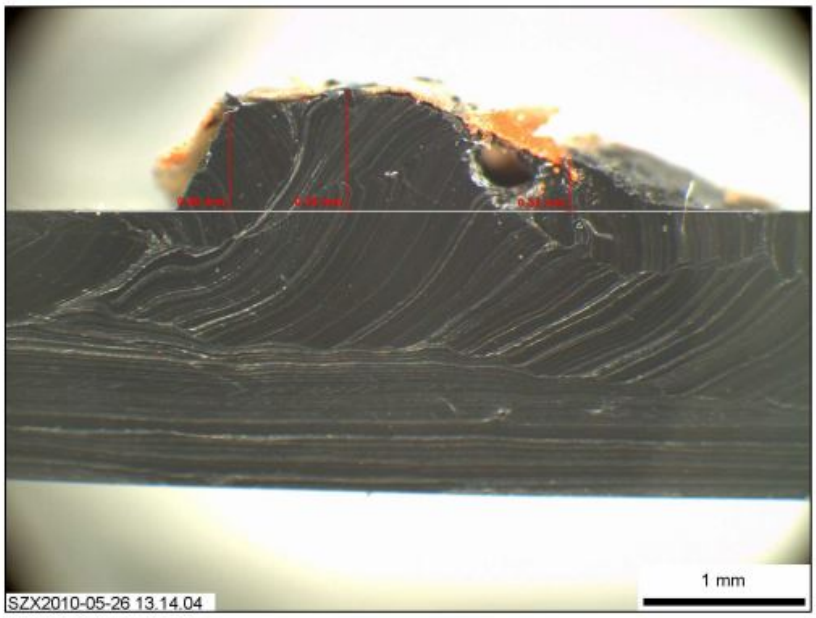

Figure 3.2: Example of cross sectioning technique [6]

Another issue was the limit on the area that could be investigated. While comparatively long lengths could be analysed, only a single plane could be assessed. Anything not lying on the inspected plane will not be assessed. This limited the ability to perform a systematic analysis of the entire component, as well as causing issues with later statistical extrapolation. This was addressed in project T728 by using the assumption shown in Figure 3.4. The observed profile of the pit in the plane, was extrapolated into three dimensions using the assumption that the pit was a hemi-sphere or hemi-ellipsoid. It was assumed that the three dimensional pit would have the same geometry as the two dimensional measured profile in the plane, if the profile were rotated around its centre perpendicular to the surface being inspected. The total width of the extrapolated three dimensional pit perpendicular to the inspection plane would represent the width of the analysed area. The assumed with would then be multiplied by the length of the plane would give the total area ”inspected”.

The extrapolation from two dimensions into three, with the approach demonstrated by Figure 3.4, was problematic. A large defect would expand the area that had been ’inspected’ significantly, increasing the width along the line of the exposed plane. However, smaller defects within the ’inspected’ area, but that did break the exposed plane, would be undetectable. Using this approach could lead to misleading results as to the distribution of corrosion damage, with small defects being less likely to be detected.

The final issue was the inherent over reporting of small defects. Using a single plane and making the shape assumption from Figure 3.4, meant that to fully capture a pit’s depth the cut must be placed exactly through the deepest point. This would not be possible to do with a longer cut that travelled through multiple pits.

Any deviation from the deepest point would result in a shallower result, which would then be extrapolated into a shallower and smaller pit than would actually be the case. This could again lead to misleading distributions of pit depths being reported.

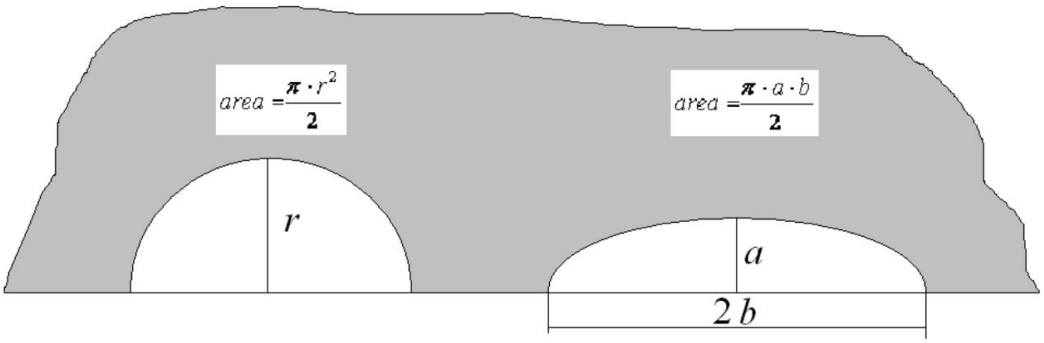

Figure 3.3: Assumption used in project T728 to relate the two dimensional data collected to three dimensional corrosion geometries [6]

$$A_{inspect} = L \cdot w$$

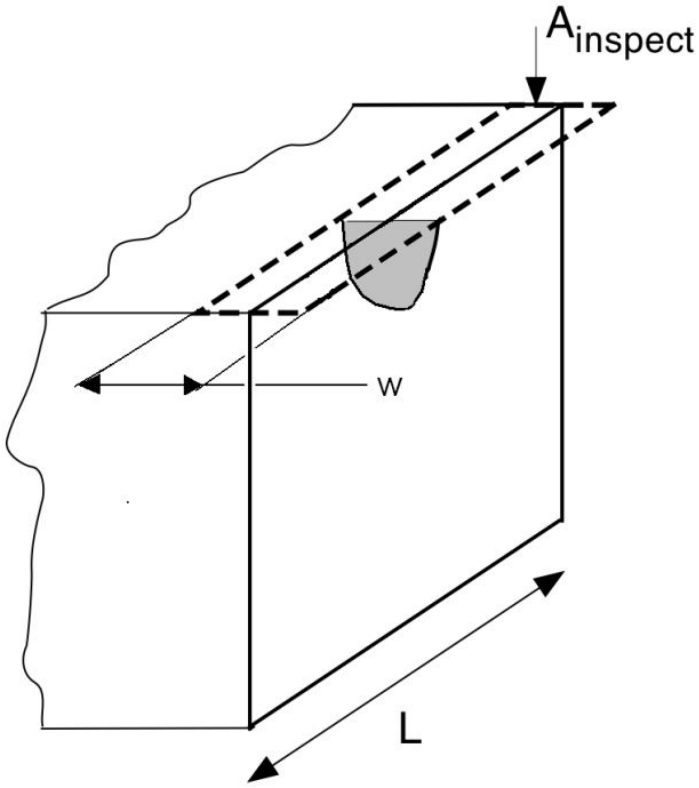

Figure 3.4: Assumption used in project T728 to relate the 2 dimensional data collected to a total area inspected [6]

Another technique to assess corrosion pits, used a camera to inspect a surface from above and identify the corrosion pit openings, shown in Figure 3.5. This was the technique used by Rudlin et al. [36, 50] in their work among others [36, 53, 54]. The benefits of this approach were that a large area was able to be covered, allowing for a larger survey of the component in question compared to the plane based inspection technique. It was also generally easy to identify surface corrosion defects and cracks, simplifying the exploration of corrosion damage and speeding up analysis.

Figure 3.5: Optical approach for assessing corrosion pits [36]

However, as the top down approach was a two dimensional approach, there was little information on the shape of the pit below the surface, due to the limited depth of focus of most optical techniques. This required assumptions to be made to link the appearance of the pit at the surface and the shape underneath. This often took the form of assuming that pits were a smooth hemi-spherical or hemi-elliptical shapes, calculated directly from their surface appearance. There were also some corrosion pit effects that could never be detected by this technique, such as undercutting caused by the pits, which would be covered by the surface above. This could result in corrosion damage being assessed as safe when in reality the represented a risk to the component.

There were three dimensional techniques that had been used in the analysis of corrosion pitting, however these had not been applied to rail axles in the literature.

The main use of three dimensional techniques in the rail industry focused on measuring the rail head profile or track bed, mostly using 3D laser profiling [55]. Any detection of corrosion damage using these techniques appeared to be of secondary interest and mostly performed by process of elimination of other damage types.

Corrosion had been investigated using three dimensional techniques in other fields in several ways. One way of analysing pits in three dimensions involved layering two dimensional readings [56]. This particular process could be cheap and effective, although it was also time consuming and destructive, as the corroded sample needed to be ground down or sectioned to assess the lower levels of corrosion features. This would make it unsuitable for use in industrial depot settings.

Non-destructive three dimensional inspection techniques used on corrosion pits came in several types. All of the types described directly scanned the surfaces of interest, using non-contact techniques, which may limit the use in a depot setting as any equipment would need to be in the same location as the axles. This makes the process of scanning complex due to issues with access, calibration and possible damage to equipment as well as potentially impacting on the day to day operation of an overhaul depot. All were also line of sight based, meaning that undercutting pits would not be detectable by any of these processes. Many of the pieces of equipment used were also highly specialised, making use of any particular type in this project dependent on availability.

One technique used three dimensional optical scanning [57, 58]. This technique involved the use of a laser scanner to digitise the surface of the object of interest, an example of this can be seen in Figure 3.6. The resolution achieved by this method was a maximum of 20µm, which would capture most pit geometries, but not pits with the smaller sizes reported in literature. The scanning process is highly susceptible to vibration and would be difficult to implement in a depot setting. It should be noted that in the studies that used this technique the three dimensional models were sectioned and analysed as two dimensional perimeter plots to identify corrosion pitting removing some of the advantages of the three dimensional data.

Another technique used was confocal scanning laser microscope [59, 60]. This equipment used a laser to scan a surface point by point to determine the depth at each location. It then constructed the three dimensional surface by collating the points to form a surface. This technique was capable of very fine resolutions, 10nm vertically and 120 nm laterally [61] although this was dependent on the confocal objective set. The limiting factor on use of this equipment was the size and weight of the samples it could accept [61]. In the afore mentioned studies, pits were identified initially using top-down image recognition. This was possible as samples used were initially clean and smooth, meaning that variations were easier to identify.

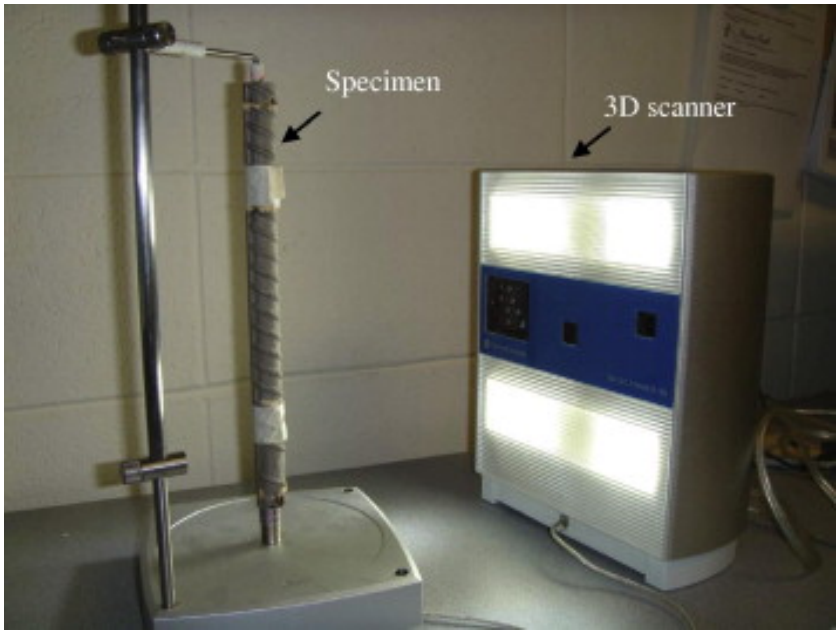

Figure 3.6: Three dimensional optical approach [57]

White light interferometry [62] was another technique used for three dimensional analysis of corrosion pits. This was conceptually very similar to the confocal scanning laser microscope, analysing the surface a point at time to determine the depth at each location. This technique had extremely good resolution as fine as 3nm vertically, however it struggled with analysis of sloped surfaces due to the lack of light returning to the sensor. This resulted in areas that had no data for them. An example of this can be seen in Figure 3.7, where the black areas represent areas with no data. In Figure 3.7 the difference between two resolutions was being compared, however the data loss in both is clear. While the data collected could be extremely high resolution, this came at the cost of large areas of missing data.

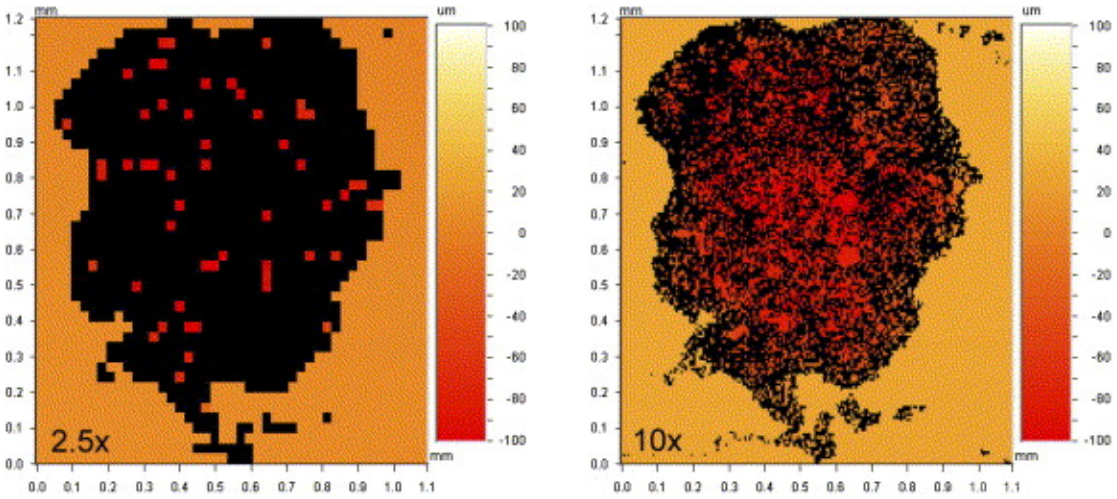

Figure 3.7: Example of missing data from white light interferometry [62]

White light axial chromaticism [63, 64] was the final technique considered in this project. This equipment can be seen in Figure 3.8, with horizontal and lateral resolutions of 280nm and 8µm respectively. This equipment could quickly analyse the surface, with a maximum speed of 1m/s, and was capable of being used over a large area. The depth of the point of interest was determined based on the different wavelengths of light, using a series of lenses to change the focal length of different frequency waves. Depending on the reflected colour from the surface back to the detector, the depth of the point on the surface could be determined. It should also be noted that, as with other techniques, white light axial chromaticism is a line of sight process, making it impossible to detect corrosion pit undercutting. The problem with the technique, in terms of this project, was that it required specialist equipment that was not available at the University.

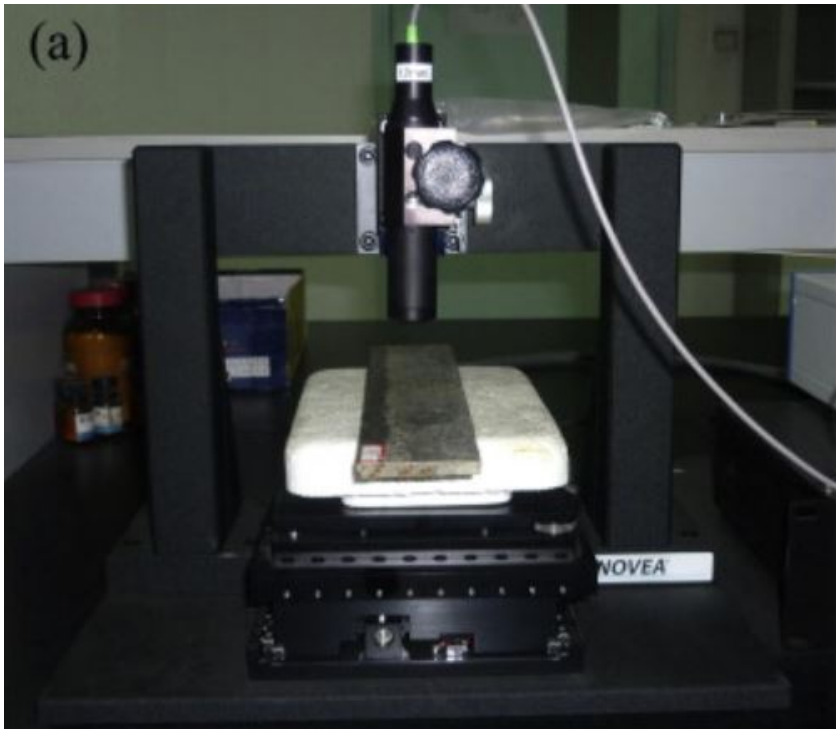

Figure 3.8: Equipment used for white light axial chromaticism [64]

The decision on which axles to inspect would have a significant bearing on the result of any investigation. While a separate issue to the details of the techniques used, it was still an important factor to consider. Selecting axles for the surveys was often a case of what has been donated by rail operators, or in the case of an inspection survey, what was in the depot on the day of the visit. There does not seem to be any increased planning beyond this in any of the surveys identified by this project. While this was an understandable real world limitation, it did mean that no systematic approach has been taken, for example tracking the same axle through its life.

3.2.3 Results of axle corrosion surveys

The T728 project survey [6] involved the analysis of 6 British axles donated to The Welding Institute (TWI) after being removed from service at overhaul, mainly due to corrosion damage. Four of these, axles 1-4, were from passenger trains, either powered Electric Multiple Units (EMUs) or a coach in the case of axle 4. Axles 5 and 6 were from freight wagons. The history of all the analysed axles was unknown beyond the industry they operated in. As previously discussed, the axle corrosion damage found on the passenger and freight sides of the industry were significantly different, with the freight industry being significantly more affected.

The surveying techniques used to inspect the rail axle corrosion pits, were a combination of metallic fracture and surface replication, discussed in the previous section. It should be remembered that these techniques used a plane based approach that over samples small pits. The results found that the maximum corrosion pit depth was 20µfor Axle 1, 40µm for Axle 2, 20µm for Axle 3, 50µm for Axle 4, 76µm for Axle 5 and 350µm for Axle 6, with no evidence of any cracks emanating from these pits [6]. All of these results were significantly below the 1000µm depth limit in the guidance document [5] although the freight axles reported significantly greater maximum values. It was also reported that the geometries were generally shallow and symmetrical, with smooth bottoms.

The raw data from these surveys was available and the data from the two freight axles, 5 and 6, was analysed. Three sections had been inspected, one on Axle 5 and two on Axle 6, with the pit depth and pit diameter being recorded. The number of pits identified in each section, with the maximum depth and width of pits can be seen in Table 3.1. The cumulative data can be seen in Figure 3.9. This demonstrated that the majority of the pits were found to be well below the approximately 350µm maximum reported in both sections of Axle 6. Axle 6 section 1, maximum depth was the largest reported across all axles surveyed, including the passenger axles.

Table 3.1: The number of pits detected on each freight section of the T728 survey [6], with the maximum depth and width of pits. Passenger axles have been removed.

Section	Number of pits	Maximum depth µm	Maximum width µm
Axle 5	72	75.74	782.67
Axle 6 - 1	153	346.23	1094.62
Axle 6 - 2	99	342.25	1123.21

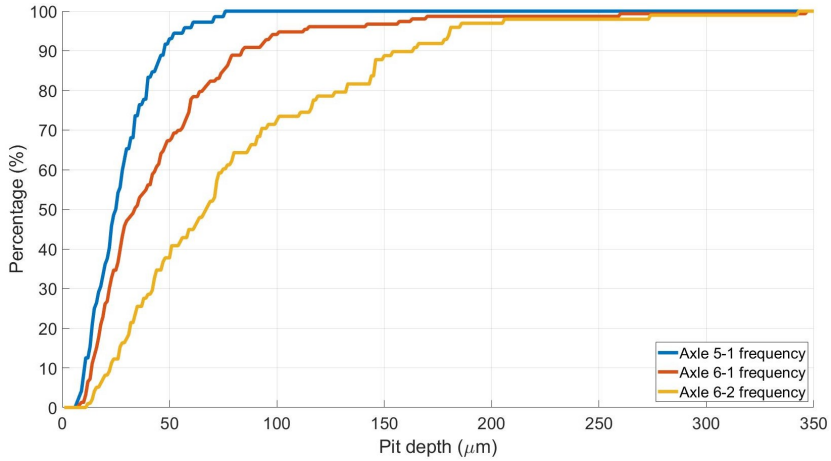

Figure 3.9: Cumulative distribution of rail axle corrosion pits from two freight axles surveyed in project T728 [6]. Plotted as part of this thesis from raw data collected as part of project T728.

Using the collected results for each inspected freight axle section, and extreme value analysis to assess the probability of events outside of the collected data, an assessment of the chance of corrosion occurring that would be deemed unacceptable was made. If the results were fitted to a Gumbel distribution, the same distribution used by Beretta et al. [24] to present similar data, shown in Figure 3.10, it can be seen that the chance of a pit having a depth at the limit of the maintenance guidance of 1000µm was small, almost negligible (with the highest probability density being for Axle 6 - 2 and having a value of 2.42×10^{-11}).

There was a significant variation between Axle 5 and both areas of Axle 6 which can also be seen in the results from Table 3.1. Axle 6 was in a more advanced state of corrosion than Axle 5, so the variation may give insight on how the corrosion pit depths changed with time, however there was no direct data to support this hypothesis. It could also be the case that the corrosion occurred over the same time frame but in different corrosive environments.

From the raw data from project T728 an analysis of the aspect ratios of the pits could be performed as part of this thesis. The results can be seen in Figure 3.11. It can be seen from this data that apart from a few outliers, the aspect ratios of the recorded pits tended to be low, with 98.8% of pits having a ratio below two and 94.7% having a ratio of below one.

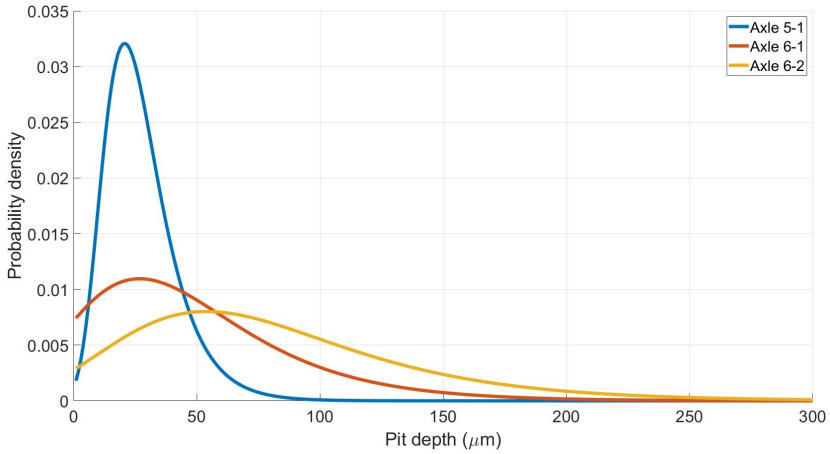

Figure 3.10: Gumbel distribution of rail axle corrosion pits from two freight axles surveyed in project T728 [6]

Some of the outliers in this data were improbable as an aspect ratio of 8.69, the highest reported value, would be extremely unusual, with no other literature on rail axle corrosion describing pits with such a high value. The pit in question was also the deepest pit recorded. While outliers were likely to be the ones that caused catastrophic failure, some of these results appeared unusually high. While there was no reason to discount any particular pit from the study, these outlying results may have been a by-product of the plane based technique used, removing surrounding geometry that may have provided a fuller picture of the circumstances in these cases.

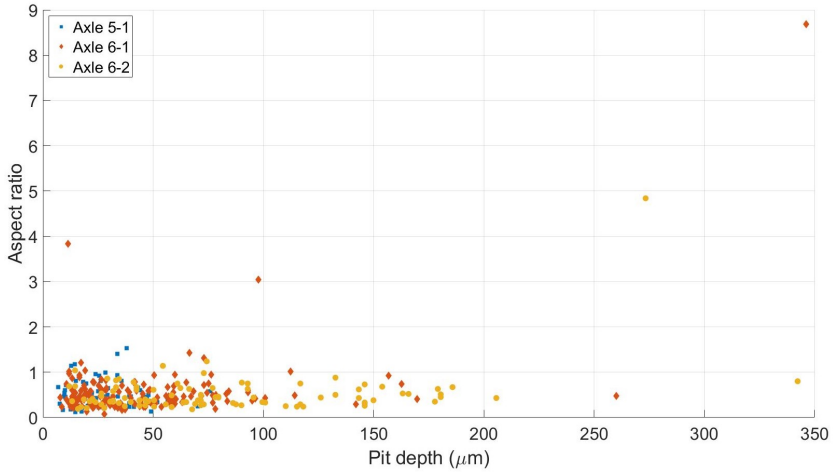

Figure 3.11: Aspect ratios of pits from two freight axles surveyed in project T728 compared with the depths of the pits [6]

Another survey was carried out by Beretta et al. from Politecnico di Milano [24]. Their study used three axles donated by Italian rail companies. Axles 1 and 2 were from freight trains and 3 was from a passenger service. This was relevant when comparing the results due to the different conditions and maintenance procedures between the freight and passenger axles.

This survey used the technique of fracturing the metal and observing the exposed profile. Gumbel distributions were developed that described the defect size of the corrosion pits identified, see Figure 3.12. Figure 3.12 demonstrated that the passenger axle, which will have received the most stringent maintenance, had a lower limit on corrosion pitting damage, whereas the freight axles had more severe issues. The values in Figure 3.12 represent the $\sqrt{Area}$ of the pits which was calculated using the semi-circle, semi-ellipse assumption shown in Figure 3.3. The distributions demonstrated the worse condition of freight axles compared to passenger services. This represented further supporting evidence that the most serious cases of corrosion damage were found on freight vehicles.

While the technique used tended to oversample smaller pits it was a reasonable conclusion, looking at Figure 3.12 and the similar Figure 3.10, that few if any of the pits identified came close to the 1000µm depth limit.

Another outcome of this work was that when the corrosion products were analysed there was no evidence of any factors that indicated anything more than atmospheric corrosion [24]. This agreed with the results from T728, with only standard pollutants being found in expected quantities. This means that there was no evidence of a unique corrosive environment for rail axles, due to location or function, compared to other components in the vicinity.

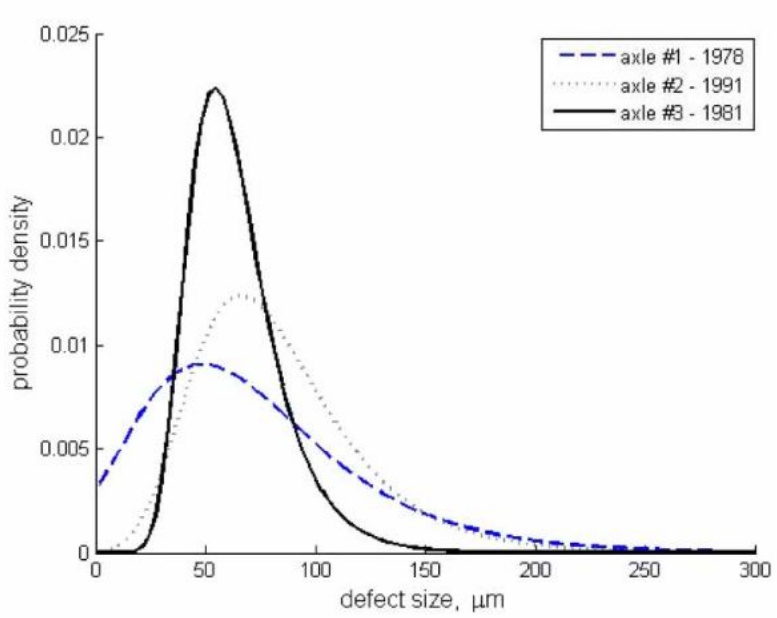

Figure 3.12: Gumbel Distributions of identified corrosion pit depths [24]. Axles 1 and 2 were from freight trains. Axle 3 was from a passenger service.

3.2.4 Outcome of previous surveys

- **No previous surveys identified any pits that approached the 1000µm limit**

None of the surveys, that have been identified, have pits close to the limit of the standard. This suggested that the current limit, at least in terms of depth, was not close to being reached and that it may have been set too high compared to current depot practise. Based on the extreme value distributions presented previously, the chance of a corrosion pit reaching the 1000µm limit for depth was vanishingly small. This did not mean that extreme events do not occur, as the sample size of the studies was small compared to the size of the axle fleet.

- **Aspect ratios of pits appeared to be generally low**

  The reported aspect ratios of pits tend to be around or below one. Based on the work of Cerit [35] aspect ratio was found to be the driving parameter in stress concentration for the idealised pits used. This suggested that corrosion pits on rail axles had a relatively low stress concentration effect. This would tend to support the data that there have been no rail axle failures in recent years. Some extremely high aspect ratio pits have been reported such as can be seen in Figure 3.11. However these were most likely from surveying errors rather than reflecting the conditions of rail axle corrosion pits.

- **There was no evidence of any corrosive influence apart from expected levels of atmospheric corrosion**

  Beretta's work and the results of T728 suggested that the rail axle operating environment did not have any special influence on the corrosive performance of the axle. This was as expected, with no other sources of corrosion being obviously apparent. In some specific cases the environment might have a more significant influence on the corrosion development of the axle, such as when the wagon is carrying salt as was seen on the fracture at South Shields [37]. In this particular instance some of the salt escaped the load and made the aqueous solution on the axle, a far more corrosive environment than would normally be expected. However, these instances did not represent the standard case.

- **Freight axles exhibited worse corrosion damage than their passenger counterparts**

  All of the data that had been found in the literature supported the assertion that the worst corrosion was found on freight axles rather than passenger axles. While this was understandable due to the increased risk, financially and morally, from failure on a passenger service, it suggested that while both types of axle were potentially over maintained in terms of corrosion damage, passenger axles had potentially the largest possible savings to be made. However, if the freight industry could reduce the limits and remain safe, this should still allow for the desired increased safety margins for the passenger fleet.

3.3 Proposed technique

After evaluating the techniques that previous studies used it was decided that a new technique would be preferable to avoid the issues with the shape assumptions and the limited scope of the two dimensional data collected. The requirements of the technique were defined, with the following points being identified as key parameters.

The technique must be capable of scanning larger areas

The standard that governs how rail axle corrosion damage is treated, used area as a characteristic of unacceptable corrosion [5]. It would be beneficial to be able to investigate areas of a similar scale to those that were laid out in the standard, in order to evaluate the influence the size of corrosion area may have on the risk of failure. It is also beneficial to capture larger areas of corrosion to get as full a picture of the condition of the axle surface as possible. This would allow increased confidence in the results due to increased sample size and number of pits detected.

The technique must be able to capture data in three dimensions

Previous studies have been limited to a two dimensional analysis of corrosion damage. The problem with this approach was that significant assumptions had to be made regarding the shape of the pits to investigate any three dimensional effects. While these assumptions may be broadly correct, they were not entirely accurate, and may miss small geometries within pits. Collecting the data in three dimensions directly would limit the assumptions made and increase the accuracy of the collected information.

Data captured by the technique must be of sufficient resolution to investigate the corrosion damage

A key requirement of any metrology process is that it is capable of capturing the information it is seeking to evaluate. With pits being of the order of 10µm in diameter, based on the smallest measured pits in project T728 [6], any measurements would have to have a resolution small enough to get accurate measurements of the internal shape of the pits. Using the same thought process as the Nyquist frequency in signal processing, the resolution would have to be at least half that of the smallest feature to express its general shape, although this represented the minimum value.

The limit for corrosion pit depth given by the RSSB guidelines [5] is 1000µm. Any selected resolution must be capable of fulfilling as much of the range of possible as practical, although previous literature suggested that it was unlikely that any pits of this size would be detected. This was a key requirement and referred to both the capturing of the data and any required transfer into digital form for analysis.

Technique must be suitable for use in a depot setting

As this study sought to investigate the corrosion found on rail axles in industry, and rail axles are too large and heavy to be easily transported, it stood to reason that at least part of any measurement process must be undertaken within a depot. This meant that any new technique must be suitable to be transported to and from a depot, not unduly inconvenience the operation of the facility and allow all involved to remain safe at all times.

Using the above requirements as a simple product design specification, it was decided that a cast based approach was the best solution, similar to that used in project T278 [6]. All the other solutions considered, such as direct scanning of the axles or the use of profilometers, suffered from either issues with moving and calibrating the equipment or from poorly fulfilling the specification.

The cast based approach involved a cast being taken of the surface, using a fast curing substance, which could then be returned to the laboratory for analysis. The cast would then be measured as a proxy for the true axle surface. This would negate the transportation and use of delicate metrological equipment, such as optical scanners or profilometers, and be unobtrusive enough to not significantly impact on the normal operation of the depot.

As part of the cast based approach, a replicating compound was required. The two part silicone replicating compound 101FF [65] produced by MICROSET was used. 101FF came in the form of a thick black liquid which is directed onto a surface by a nozzle and hardens to allow removal when cured. 101FF was chosen after initial tests of other similar fluids. These tests were done by drilling a series of small holes (0.1mm-1mm diameter) various depths into a section of scrap metal, shown in Figure 3.13. The aim was to produce difficult to capture, high aspect ratio geometries that were in excess of any expected corrosion damage. Different compounds were then used to try and take casts of the holes, with an example result using 101FF seen in Figure 3.14. The moulds were then analysed visually to assess the success in capturing the geometry.

Figure 3.13: Test sample for replicating compounds, with a series of micro holes drilled into a section of scrap metal

Figure 3.14: Example of a cast taken from the test sample using 101FF. Evidence of the air trapping issue can be seen at the tips of some of the columns

Problems that excluded these other fluids were that some were too viscous to properly penetrate deep, high aspect ratio features on corroded materials, so did not accurately capture the surface geometries. Others were liquid enough to penetrate all the features, however were so liquid that if applied to any surface that was not horizontal, they tended to flow off before curing. Another problem was that when some compounds cured, they became brittle so tended to crack and rip when attempting to remove them from the surface, meaning all the information they contained was lost.

101FF was capable of capturing the geometry of a surface to a resolution of 0.1µm and cured within 30 minutes, according to the manufacturer. This meant it was suitable to capture pit geometries, based on a resolution 100 times smaller the size of the smallest pits described in literature. It was also suitable for use in depots, as it cured within an acceptable time frame to allow several axles to be inspected within a single visit. Once removed it left no trace on the axle so would not damage or impair the owner's property.

While 101FF was found to be the best trade-off between these issues, it experienced problems penetrating the deepest features, as it tended to struggle to replace trapped air at the bottom of these features. It was possible to identify when this had occurred because, when the compound had not come into contact with a surface as it cured it produced a perfectly smooth, highly reflective, surface in contrast to areas that had taken on the geometries of the surface being inspected. An example of this can be seen in Figure 3.14. It was found that this problem could be effectively alleviated by using a silicone paint chisel to 'paint' the compound onto the surface when first applied. The 'painting' had the effect of forcing the compound deeper into features, replacing the air pockets, and fully replicating the surface. The success of this technique was judged by the lack of highly reflective areas that were seen previously.

Another key element to the use of the replicating compound, discovered through initial tests, was the vital importance of cleaning the surface before taking a cast. This was particularly evident when testing on corroded surfaces, as the cured samples, when removed, had a visible layer of corrosion product attached.

The corrosion product prevented the true surface from being measured, the true surface was prevented from coming into contact with the replicating compound, and was difficult to remove in post processing. Due to this problem, all surfaces that the product was used on required cleaning to remove extraneous material adhered to the surface. It was found that the method of cleaning depended on the condition of the surface that was being replicated. The key requirement was to achieve access to the bare metal without additional corrosion product or dust on the surface. This was not achieved at the expense of the surface that was being evaluated, with light acid baths or compressed air being the best solutions depending on the application.

The second stage required analysing the corrosion damage. To do this the Alicona SL [66] was selected due to its availability and suitability in terms of scanning area and resolution. This equipment can be seen in Figure 3.15.

The Alicona machine is a three dimensional optical scanner. By using a motorised camera with very fine focal lengths, the Alicona takes a series of pictures at different heights and analyses them to determine what is in focus in each image. By doing this over the entire height of the sample, a three dimensional point cloud is produced which can then be evaluated. This negated an issue with many optical techniques which have poor depth of focus making it difficult to determine the heights of scanned surfaces.

An issue with this approach was that it was a top down process, meaning that any undercutting in the pit geometries would be difficult to detect. While undercutting could not be analysed, it could be detected and discounted. In the event that an undercut was scanned, it would produce a significant vertical step in the data. This could be detected during analysis and these pits either discounted or evaluated in another way.

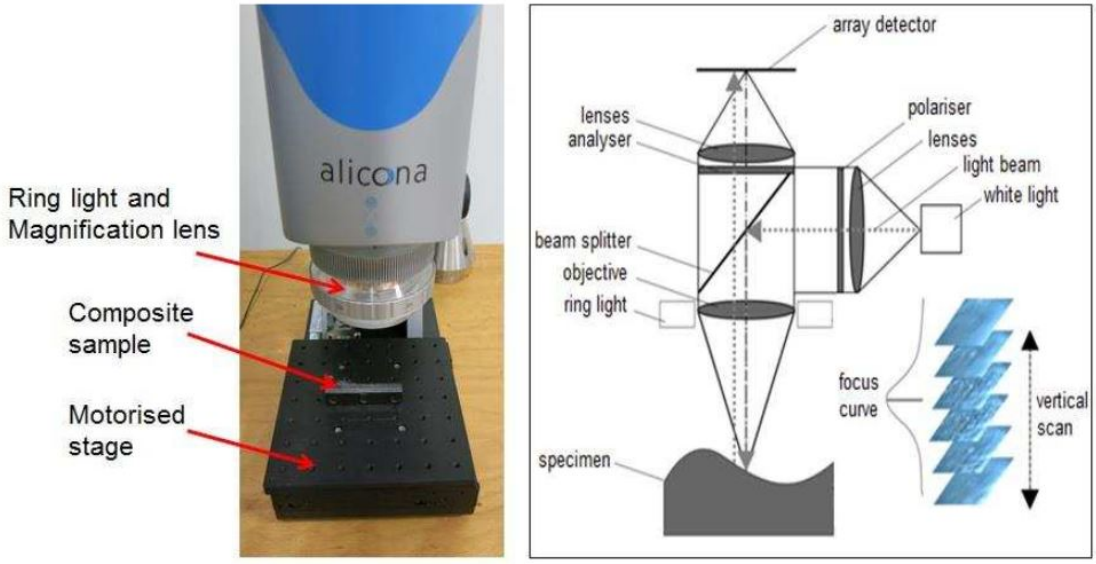

Figure 3.15: Image of Alicona machine and schematic diagram [67]

An initial decision that needed to be made was the resolution chosen to perform the scans. The Alicona has 3 lenses available, 5xAX, 10x and 20x magnification [66]. Each of these lenses had a different lateral measurement area with increasing magnification leading to decreasing lateral measurement area.

For this application the 5xAX lens was selected as its 3.61mm x 3.61mm lateral measurement unit area was the largest available with the vertical resolution set to the finest available of 460nm and the lateral resolution to 4500nm. A finer resolution could be used but would increase the time taken to scan the same area. This would limit the number of scans that could be taken as well as increasing the data density and significantly increasing analysis times, limiting use in a practical setting.

These values for the resolution represented a significant number of readings within all but the smallest pits using a similar thought process to the Nyquist frequency. The more data points within a pit, the better its geometry could be described.

Based on the order of magnitude of the largest expected pits of around 1000µm deep [5], the chosen resolutions would provide excellent insight of the geometries of corrosion pits, with significant numbers of readings.

The larger resolution that would struggle to deal with the very smallest pits reported in project T728 [6] was acceptable due to how the axles were shot blasted before measurement.

Shot blasting removed, damaged or masked any pits of a low order of magnitude (this is discussed later in the Chapter). If any information was required using a finer resolution, the Alicona was non-destructive, so other scans were still possible. The chosen scan resolutions were lower than the resolution of the casts, allowing more information to be extracted if required.

Other issues with the Alicona were that, as an optical scanner, it was not capable of measuring extremely reflective surfaces as the high light levels swamped the sensor. While this was a problem in some applications, it was not a significant issue here due to the types of surface under investigation in this study. The shot blasted and corroded surfaces being analysed produced sufficiently rough casts which were not too reflective.

The lack of reflection in correctly captured areas also meant that in the event of a trapped air problem, where the replicating compound did not fully penetrate a feature, the errors were easily identified. This was due to the highly reflective area that was produced in these cases, in contrast to the low reflection levels in other areas, allowing instances of trapped air to be discounted.

It was also vital to ensure that the casts were clean when scanned in the Alicona. It was not possible to differentiate between the surface and and dust or grit attached. To address this issue adhesive tape was used to remove any dust on the casts, immediately prior to scanning. This was demonstrated to be effective by using the microscope style viewer on the Alicona. No dust or grit was be detected during an inspection using this method.

In summary, the new technique proposed consisted of the combination use of a replicating compound to take casts and a 3D optical scanner to analyse the results. The proposed technique, as described, was capable of capturing data from an axle surface and analysing it with maximum vertical resolution of 460nm and lateral resolution of 4500nm.

3.4 Validation

Any novel technique requires validation before it can be used in industry. This ensures that the results can be trusted to a given degree of accuracy. Each individual part of this technique had been validated by its respective manufacture. A basic validation exercise was carried out to assess the techniques used in combination, particularly for heavily corroded surfaces.

Ideally a corroded rail axle surface would be used in the validation study, to best represent the survey that would be undertaken. However, rail axles are too large to be brought to the optical scanner and it was not feasible to scan axles in depots directly. Due to this a stand in sample, or proxy, was required to assess the technique.

The proxy needed to exhibit severe surface corrosion, to represent the worst case that could be expected to be found on rail axles. For the purposes of this study the main geometries that were of interest were those caused by corrosion damage, referred to from now on as the ”primary geometry”. At the scale of a single pit the axle surface could be treated as flat due to the relatively large curvature radius of an axle. However, for larger scans the curvature of the axle would need to be taken into account and will be referred to as the ”secondary geometry”.

The ”secondary geometry” was not of interest to the study but was still present and provided an extra complication that needed to be overcome, compared to using a perfectly flat sample. The proxy sample would need to exhibit a strong ”secondary geometry”, to represent the curvature of the rail axle. This would allow for checking for any issues arising from the presence of such a geometry during the survey.

The proxy used for this project was a section cut from a heavily corroded steel pipe shown in Figure 3.16a. It was not known what the use of the pipe was or the exact material it was made out of, however for this study it was sufficient for it to have a representative geometry of a heavily corroded metal component.

As can be seen in Figure3.16a, the pipe section was covered in corrosion product that would have impaired the accuracy of the casts taken. To mitigate this issue the proxy sample was subjected to a light phosphoric acid bath and light mechanical scrubbing to remove the corrosion product layer, without significantly effecting the underlying geometry. The result of this can be seen in Figure 3.16b.

(a) Before cleaning

(b) After cleaning

Figure 3.16: Pipe section used as a proxy in the validation study

The proxy had a cast taken, using the technique discussed earlier, which was then removed from the surface after curing. The cast was scanned in the Alicona, after which the pipe section was also scanned using the same settings. These two scans were flattened using a high pass filtering technique, discussed later in Section 3.6, to remove the secondary geometry of the pipe and to ensure that the corrosion damage was visible on the scans.

The filtering was necessary because when the proxy surface was scanned, the large curvature disguised the smaller variation caused by the corrosion damage, as shown in Figure 3.17. Another reason was that the cast became flat when removed, while the original scan was still curved. To compare them, both needed to be flattened to ensure like for like comparison. The final issue was due to the difficulties in using the replicating compound, as it was impossible to ensure a perfectly smooth layer was applied, particularly on a curved sample. This means that when it cured the cast had bumps where particular areas had more compound behind the surface of interest than others, lifting the surface artificially when it was placed in the Alicona. The filtering removed these distortions.

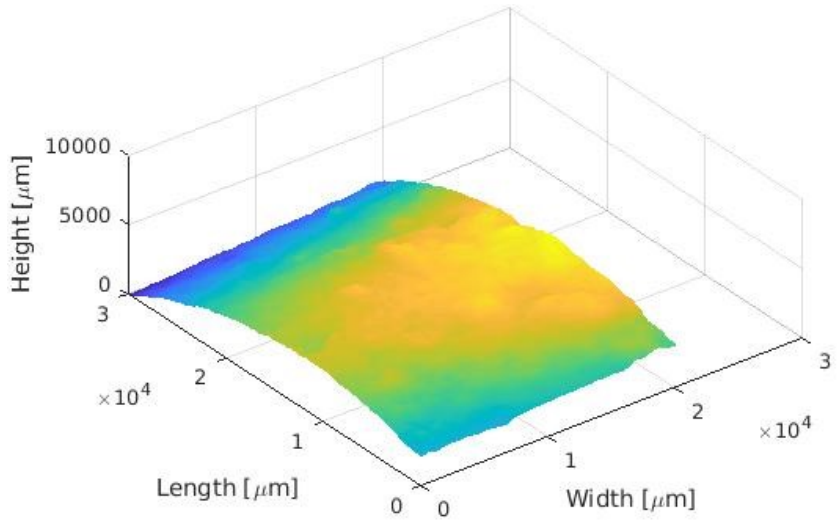

Figure 3.17: Scan of proxy demonstrating the difficulty identifying corrosion data within larger geometrical variation

Ten pits locations were identified and the same locations were found on both the replica surface (cast) and the original surface (proxy). This was done by identifying pits on both scans and then aligning them.

The identified pits were separated, as shown in Figure 3.18, and compared in terms of maximum depth and volume. These two criteria were selected due to their ease of calculation and, one represented an absolute scalar value while the other was a more complex value related to the shape of the pit. This allowed simple checking of the two types of information the survey was looking to extract.

While some distortion would have been caused by the filtering of the surfaces, this was calculated at a maximum of 1.1% from the original scan. The filter is discussed in more detail later in the Chapter.

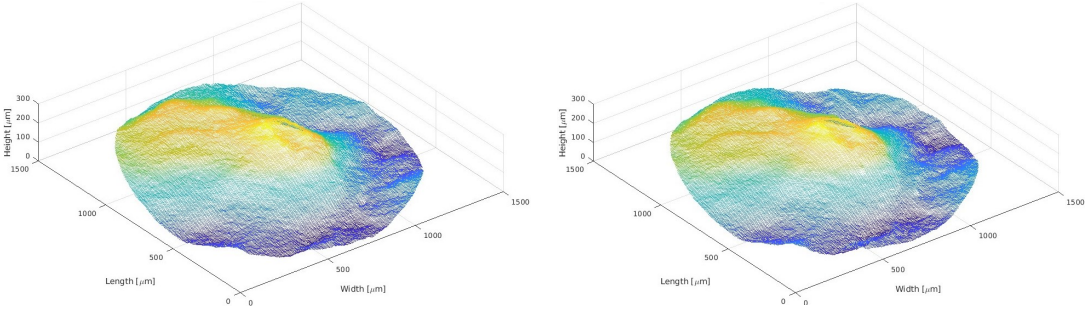

(a) Scan direct from proxy surface (b) Scan from cast of proxy surface

Figure 3.18: Examples of separated validation pits (Pit E)

The comparison of the ten separated pits can be seen in Figure 3.19. The variation of the maximum depth in the separated areas was within 6% and the volume within 10%. One of the reasons for the larger variation in volume than depth was that if the maximum depth point was in a slightly different location between the scans of the surface and the cast, this could mean a small area of significantly different depth value in the surrounding area were included. This was an issue as the deepest point was used as an alignment location between the two scans. Due to the small size of the separated pit regions, this could have a major impact on the calculated volume.

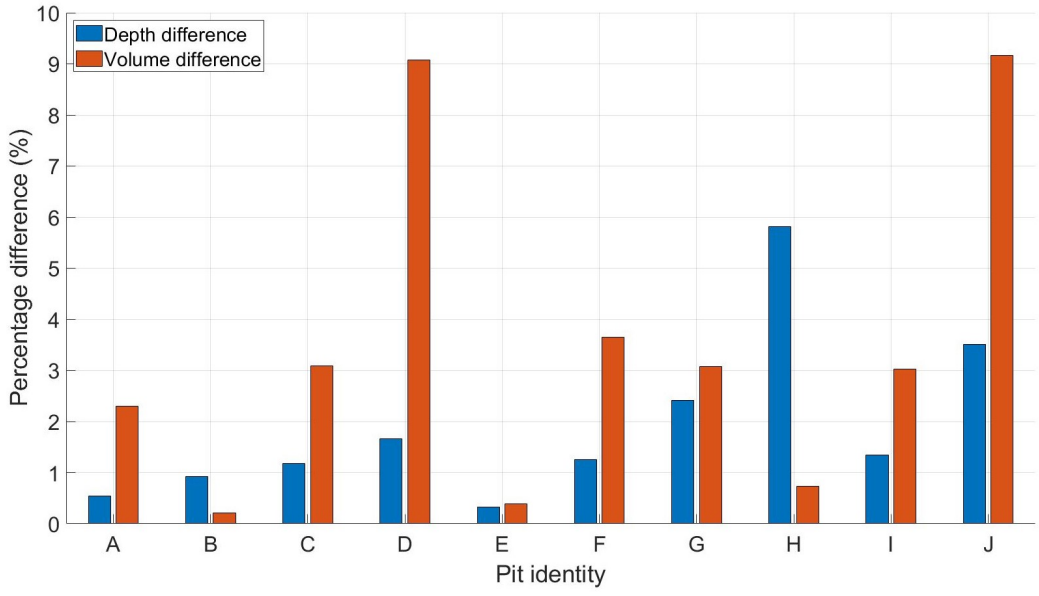

Figure 3.19: Comparison of separated pit features between direct surface scan and scan of surface cast

The variations reported by this validation study, <6% depth and <10% volume, were acceptable for the survey application. Given the shape approximations used in previous studies and the significant impact that those had on the depth and volume results, this variation represented a significant improvement on those techniques. The three dimensional data could be collected directly, without relying on extrapolating two dimensional results.

Using this study as validation, that scanning the casts was sufficiently similar to directly scanning the original sample, the survey was carried out using the technique as described.

3.5 Survey performed

The survey was carried out at an overhaul depot in the UK. The axles selected represented all of the freight axles in the depot that had passed the initial check in the wheel park and been deemed as having scope for being returned to service. They had then been shot blasted to remove the remaining paint and corrosion products on the surface, before being placed inside for secondary inspection. Freight axles were chosen as the target of the survey as the literature suggested that the most severe corrosion damage would be found on these axles.

The axles had undergone secondary inspection and had had areas of concern highlighted and marked with yellow pen. Some of this subgroup had failed the inspection and been deemed suitable for scrapping while others had been deemed worth attempting recovery by turning. The axles used for the study can be seen in Figure 3.20.

Wheelsets in this range of conditions were selected because they represented axles at the point at which the project was aiming to improve outcomes. The axles with no chance of recovery had been removed and the remaining population included the marginal axles that may be scrapped after shot blasting, which could be recovered if more was known about the risks of corrosion.

This point also represented the optimal juncture for taking the casts, as the paint and corrosion products had been removed, allowing the surface to be accessed free of any contaminants. The previous inspections by depot workers were also highly useful, as they ensured that areas that were a concern in the current maintenance process were examined.

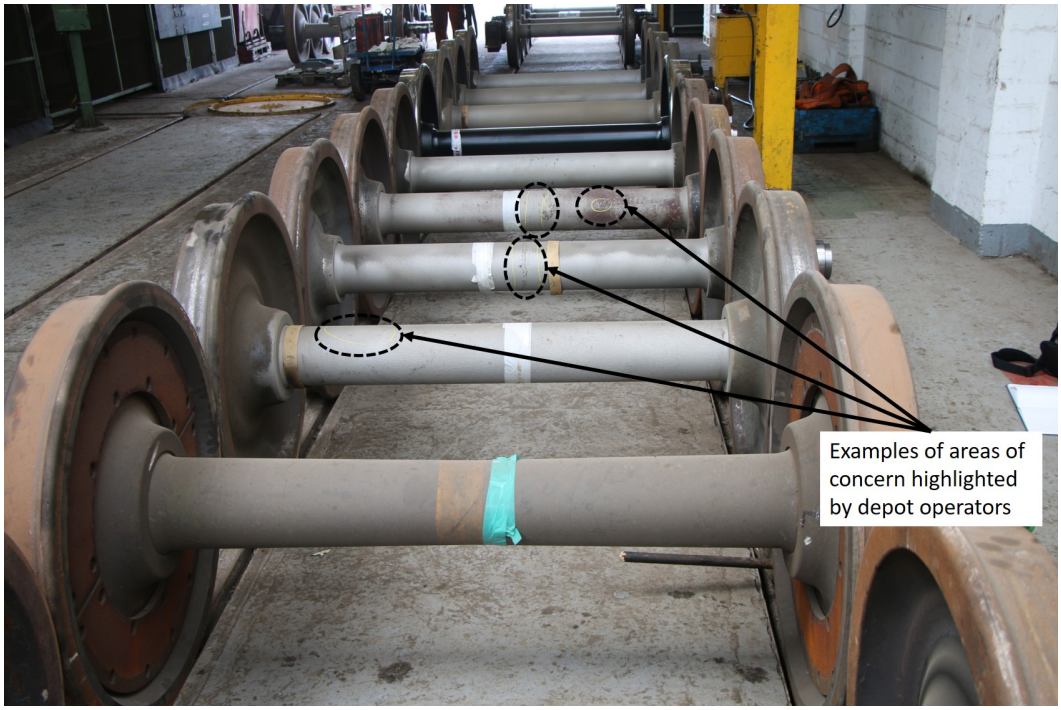

Figure 3.20: Image of wheelsets in the condition that the survey took place in (Not all axles part of the survey)

Seven axles were inspected in total, the process of inspecting the axle is detailed in Appendix A. 30 areas of the axles had casts taken of their surface, approximate locations are shown in Figure 3.21. 29 of these areas represented areas of corrosion and one (3-1) represented an area exhibiting no corrosion, only the damage from shot blasting, for control purposes. It was necessary to take a control sample as the shot blasting left a small amount of damage on the surface, that may be indistinguishable from low level corrosion. This needed to be controlled for when dealing with pit identification and separation from the larger scans.

The sites selected for inspection were the areas identified by depot operators as exhibiting problematic damage. The areas identified were first cleaned by compressed air, to remove any dust or metal filings from the shot blasting process, then the replicating compound was applied and left to cure. The backing papers of the samples were numbered to ensure correct record keeping and photographs were taken. While taking photographs, small stickers of known size where placed next to the areas of corrosion to provide a reference size when analysing photographs later. The casts were then removed and packaged for return to the laboratory, an example of a cast can be seen in Figure 3.22.

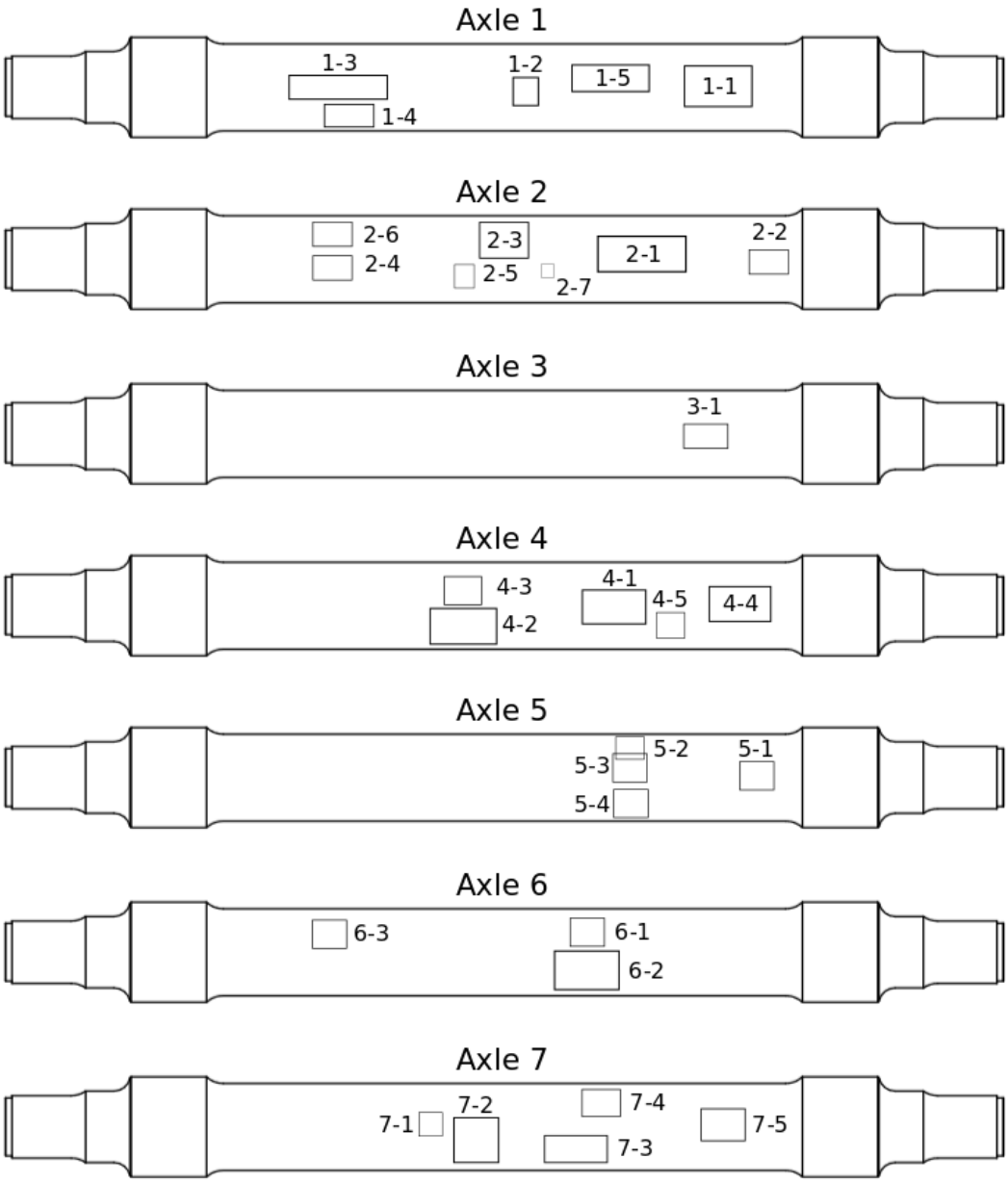

Figure 3.21: Approximate locations of samples taken from axles

On being returned to the laboratory the scans were analysed in the Alicona, using the settings defined previously. It was found that, due to the casts collected being far larger than the casts taken during validation, they tended to warp while on the scanner due to the malleable nature of the replicating compound. To address this problem the casts were fastened to pieces of wood to provide them with weight and rigidity to prevent them moving while being scanned, an example can be seen in Figure 3.23.

As the casts of the areas were large, some being up to 100mm long, it was not possible or practical to scan them in one go. To this end some of the casts were scanned multiple times in different, non-overlapping, locations.

Figure 3.22: Example of a cast of a region of corrosion from a rail axle

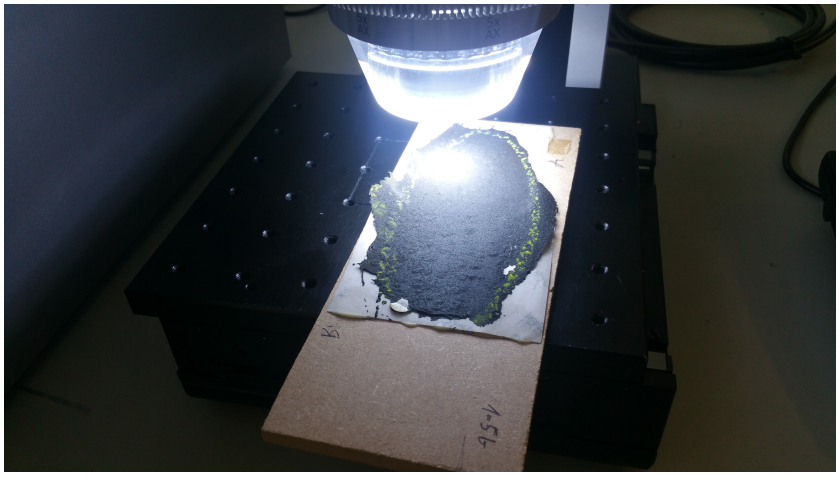

Figure 3.23: A cast being scanned in the optical scanner, after attachment to backing board.

The survey resulted in 51 scans of varying areas, including the 3-1 control scan. These can be seen in Table 3.2. The cumulative area investigated was 12874mm^2, representing the largest investigation of rail axle corrosion to date that the project was able to identify.

Table 3.2: All scans processed during the survey

Scan Name	Length (mm)	Width (mm)	Area (mm^2)	Scan Name	Length (mm)	Width (mm)	Area (mm^2)
1-1-A-1	10.15	10.15	102.95	4-4-p1	3.66	3.66	13.41
1-1-p1	23.21	16.66	386.68	4-4-p2	3.66	3.66	13.41
1-1-p2	29.70	19.90	591.19	4-4-p3	3.65	3.65	13.29
1-2	19.90	26.40	525.43	4-5-p1	16.66	13.40	223.25
1-3-A-1	10.15	10.15	102.95	4-5-p2	3.66	3.66	13.41
1-3-A-2	16.67	10.14	169.00	5-1	26.46	16.65	440.47
1-3-B-1	13.40	13.41	179.66	5-3-A	13.40	13.43	179.93
1-3-C-1	10.13	16.66	168.74	5-3-A-2	19.92	19.93	397.08
1-3-C-2	13.39	10.14	135.70	5-3-A-small	3.66	3.66	13.41
1-4	23.19	13.41	311.00	5-5-A	23.18	16.65	386.06
1-5b	26.45	20.46	541.19	5-5-AB	19.89	19.90	395.73
1-5-p2	29.69	19.90	590.95	5-5-C	23.16	16.62	385.01
2-2	19.94	13.40	267.25	6-1-p1	6.86	6.86	47.07
2-3-AB	23.19	26.46	613.70	6-1-p2	6.88	6.88	47.33
2-3-B	10.14	16.65	168.79	6-3-A	17.51	16.66	291.76
2-3-B-2	14.48	16.63	240.72	6-3-A-2	9.54	23.15	220.81
2-4	19.91	26.44	526.54	6-3-B	16.65	13.40	223.15
2-5-A	19.92	23.21	462.29	7-1a-1	10.15	10.15	102.97
2-7-A	26.46	19.93	527.30	7-2A	6.88	10.14	69.78
3-1	29.70	19.91	591.43	7-3A-A	13.41	13.41	179.87
4-1-p1	3.66	3.66	13.41	7-3A-B	19.94	16.66	332.25
4-1-p2	3.66	3.66	13.41	7-4-A-1	13.37	19.88	265.82
4-1-p3	3.66	3.66	13.41	7-4-A-2	19.92	23.19	461.84
4-1-p4	3.66	3.66	13.41	7-4-B	23.13	13.35	308.87
4-1-p5	3.66	3.66	13.41	7-5	26.45	13.38	353.91
4-1-p6	16.67	13.40	223.37				
					Total Area (mm^2)		12873.78

3.6 Pre-processing

Before beginning the identification and separation of pits from the larger scans to allow analysis of individual pits, it was necessary to correct issues with the scans taken from the casts. These issues were: incomplete data sets; removal of large geometrical abnormalities; and 'rogue' data points causing significant changes in the location of the datum.

The first issue was areas of missing data points. Occasionally during scanning, small areas would be missed leaving gaps in the data, the precise cause of this was unknown. These areas were identifiable as the scanner created points on a grid system and missing data points were easily observed, as demonstrated in Figure 3.24. The missing areas were generally of the order of tens of data points across and represented less than 0.5% of data points on the worst affected scans, with values on average of 0.05%. Despite the small impact it was necessary to fill in these areas to ensure a complete data set to allow further analysis.

Linear interpolation of the nearest data points in the X axis and then the Y axis was used to fill in the missing data points. These two values were then averaged using the mean, to produce an approximate value. Any interpolated data point was flagged to ensure it could be tracked through any later processes.

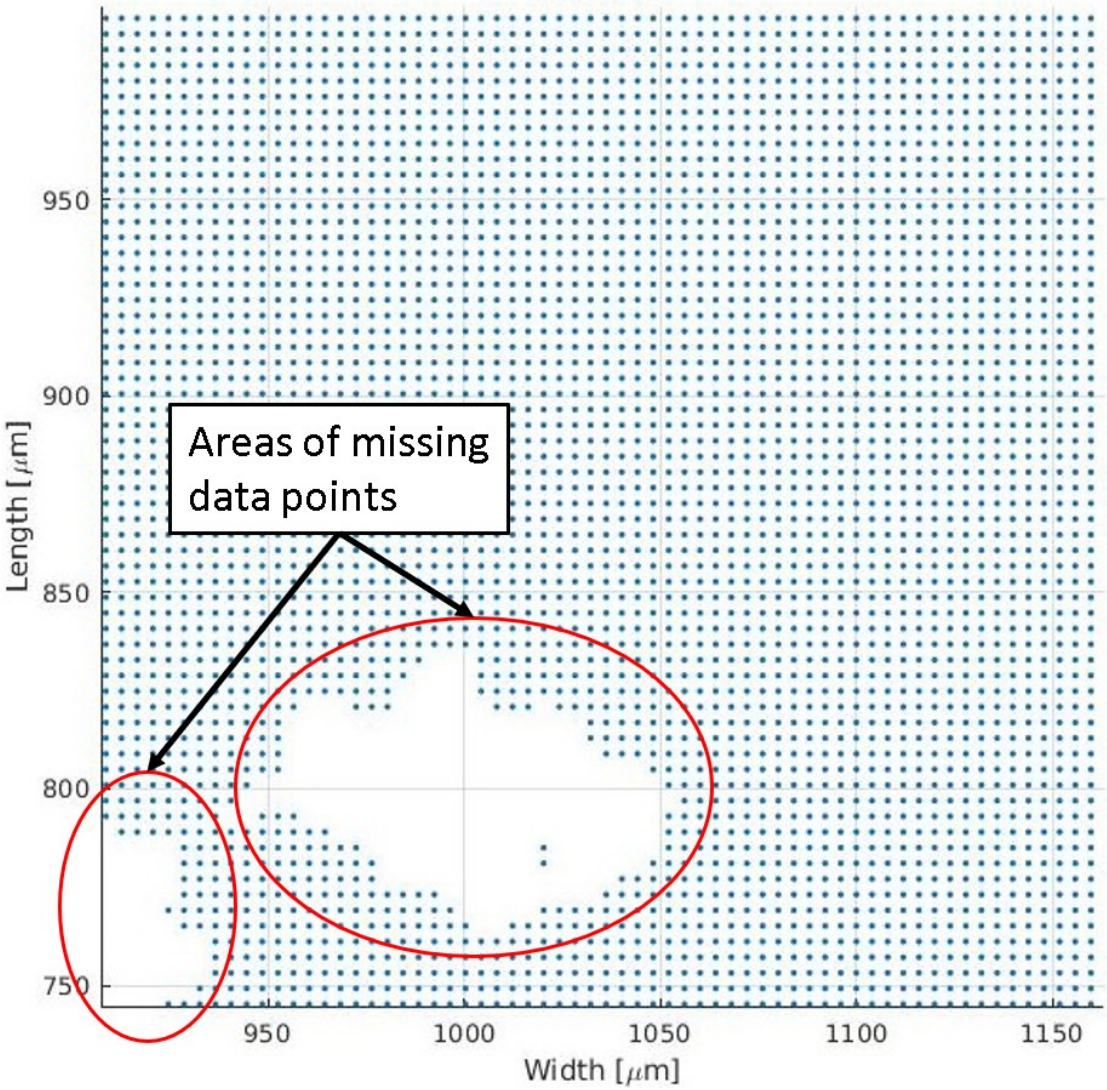

Figure 3.24: An example of an area of missing data in a scanned region. Note the regular grid of data in the X and Y axis

This technique was selected due to its computationally cheap implementation and the small distances being interpolated over, meaning that any error would be minimal. Any missing data points at the edges of the scanned areas resulted in the whole 'shell' of points being removed until the first whole rectangle of data points was achieved. Whilst this resulted in smaller scanned areas, the loss was minimal with below ten grid steps being lost. This represented a maximum lost distance of 0.045mm in the X and Y axes.

The next issue was the large scale secondary geometry variations in the samples. On larger samples these could be due to the curvature of the axle, more often it was due to issues with the collection process. Namely the issue of uneven application of the replicating compound resulting in variations in the sample thickness that distorted the results.

The problem was treated akin to a carrier wave containing a higher frequency signal wave that might be seen in Amplitude Modulation (AM) techniques. Most data sets contain some form of frequency component, and the collected data in this case is no different. Instead of being temporal as would be the case in communications system, it is spatial. By using a high-pass filter, the lower frequency carrier wave, which represented unwanted distortion in the scan, either due to the cast collection issues or the curvature of the axle, was removed. This left the high higher frequency distortions caused by the corrosion damage, that were of interest in this project.

The high-pass filter was designed using the inbuilt MATLAB filtering functions, which were developed for use on temporal data. By using the analogy that a second was equal to a micron, a frequency could be assigned to the various parts of the scan. The size of defect that the filter excluded was set at 5000µm . This was chosen as it was significantly larger than any expected corrosion damage and around the order of magnitude of observed variation in the samples due to errors in data collection. Based on this an equiripple high-pass filter was implemented with a passband frequency of 0.2mHz, a stop band frequency of 0.169mHz, stop band attenuation of 60dB and a passband ripple of 0.1dB. This left the scans flattened, with all large variations removed, but the corrosion damage remaining.

The use of filtering techniques will always cause some distortion in the original data in the region of interest. This was limited as the passband was set far in excess of the expected range for corrosion damage, meaning that it would not significantly affect the data. The passband ripple, at 0.1dB represented an approximate change in the signal of 1.1%.

The final part of the initial filtering process was the removal of outlier data points that significantly shifted the datum of the scans. As no information existed as to the original surface of the axle, it was assumed that the highest point in each scan, would represent the approximate location of the original axle surface. The corrosion depth was measured from that point.

In some cases the scanning process would produce a handful of points very significantly higher than all the others, which would appear to be outliers of the rest of the scan (this did not occur with unusual depth values). If these remained in the sample then all the depth readings would be shifted by a systematic error which in some cases represented over 100% of the apparent true value determined by visual inspection. It was presumed that the outliers were due to slight areas of reflection on the casts, not identifiable with manual visual inspection.

There were several approaches that were tried to remove these data points including various filters and averaging techniques. However, these tended to work for the initial testing scans but caused errors in others when applied to all scans, especially when applied to different scan sizes. Due to this a simplified approach was taken based on the 3σ principle.

Making the assumption that in any one scan area the data points would be scattered in a normal distribution, the lowest 0.3% of data points were removed, and linear interpolation technique was used to replace them. This worked well, as there tended to be a very small number of these points but a proportionally larger number in larger scans. If the removed points were not outliers the interpolation tended to replace the points in very similar positions, whereas the outliers were replaced by points that better represented the apparent surface. The entire sample was then moved to a new zero in the Z axis based on the highest point, and one of the corners was defined as the origin in X and Y.

3.7 Pit identification and separation

An issue with performing a three dimensional survey was the large amount of data that needed processing. This prevented a manual approach to pit identification, such as that carried out in T728 [6], as there was too much data to be easily processed and it would have been difficult to rigorously apply the same standards to every scan.

It was decided that a programmatic approach to pit identification was required, to process the data in a thorough and consistent way within a reasonable time frame. The development of bespoke software would also provide a starting point for later application in depots.

The first issue was how to define a pit. In two dimensions it was reasonably simplistic to define a pit, by using a defined line, representing an original surface. Any variation from that line over a threshold could be categorised as a pit. In three dimensions, while the same basic principle was applied it was far harder to define the edges of a pit, as they could be difficult to categorise.

Initial inspection of the scans after post processing suggested that the shape assumptions used in previous surveys, of hemi-elliptical or hemi-spherical pits, was broadly accurate although disguises smaller variations within each pit.

The correct thresholds for pits were also uncertain and subjective to the application, as there was a blurring of the line between a defect that could be defined as a pit and a surface defect that only contributed to surface roughness.

In this application a different parameter was used to define the smallest pit dimensions, due to the shot blasting process used to remove the paint layer and corrosion products. The 3-1 scan, shown in Figure 3.25, represented the shot blasted, but un-corroded surface of an axle, was used to determine the 'noise floor' of the samples. In this case the noise floor represented the damage by shot blasting. This can be compared to Figure 3.26, a scan that represented an area of corrosion, for reference. Anything that penetrated this floor was a candidate for being corrosion damage as it was additional to the damage caused by the shot blasting process.

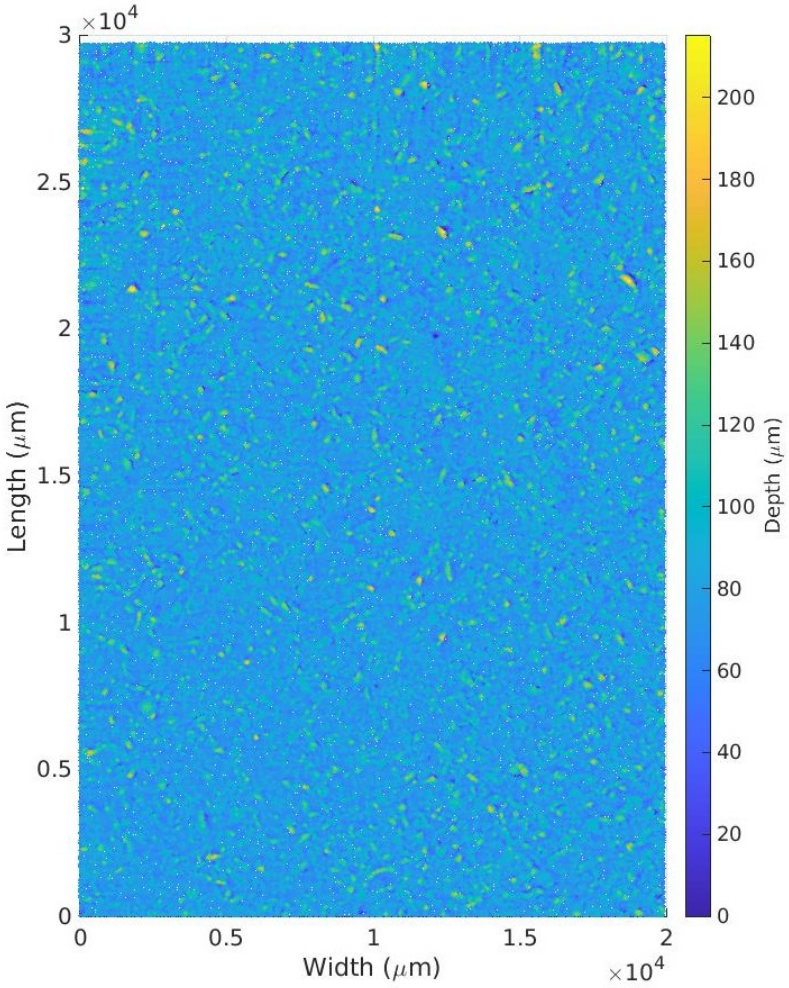

Figure 3.25: Scan 3-1 (control scan) after initial processing

Using the 3-1 sample it was found that the shot blasting process produced damage below 100µm in depth and presented small areas at the surface. Based on the control sample, it could be stated that damage with a depth less than 100µm could not be definitively defined as corrosion damage.

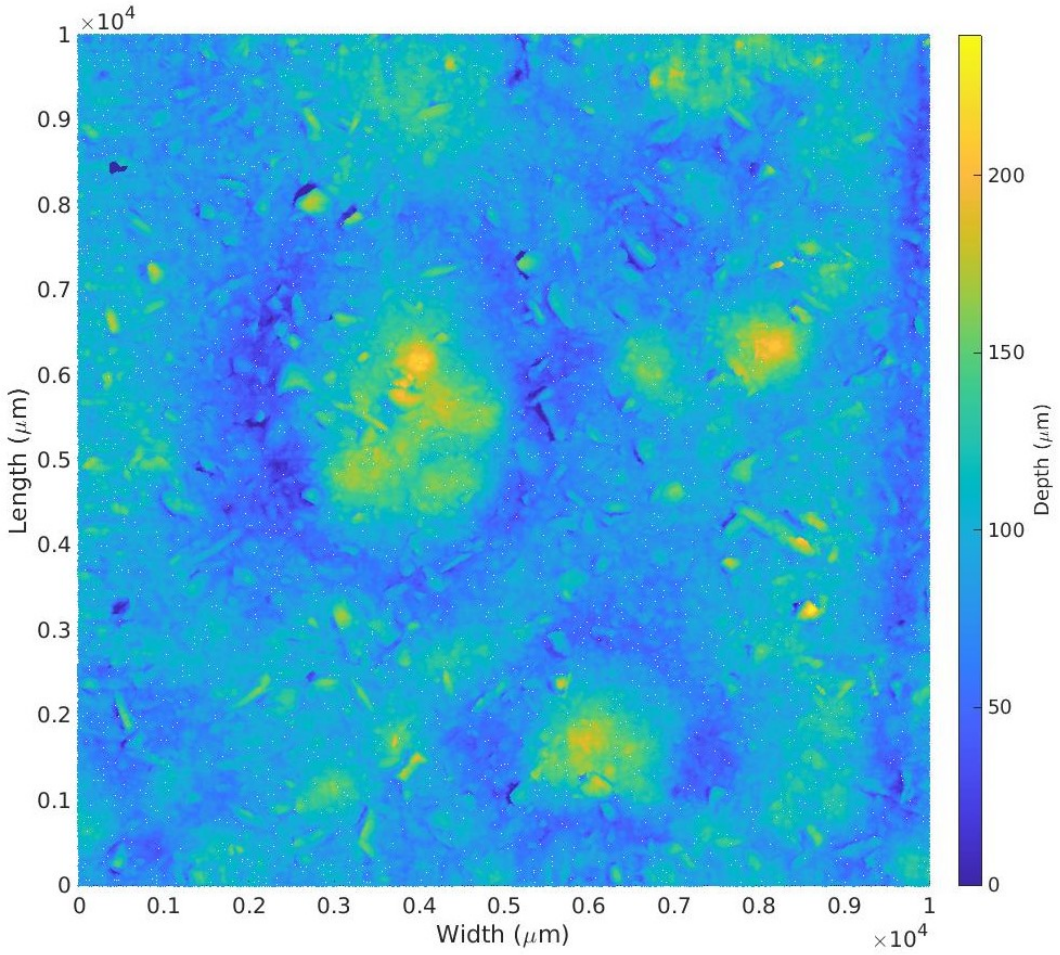

Figure 3.26: Scan 1-1-A-1 after initial processing

All data points with a depth less than 100µm were removed from scan 3-1. This removed 96.17% of the data in the control sample, leaving small areas of the very deepest shot blasting damage above the boundary. This was deliberate to ensure that the filter level was not set too high. Excluding all the data in the control sample would potentially mean excluding data that otherwise may have been due to identifiable corrosion damage.

The effects of this filter on the control scan can be seen in Figure 3.27 and compared to a scan which had undergone the same technique, but contained corrosion in Figure 3.28. The major difference between the two figures was the presence of far larger contiguous areas which exceed the noise floor in Figure 3.28, instead of the speckling visible in Figure 3.27.

To automatically collate the areas of corrosion, image processing techniques were used. Corrosion pits were defined as significant areas that broke through the 100µm threshold, while these can be easily identified visually it was difficult to separate them automatically.

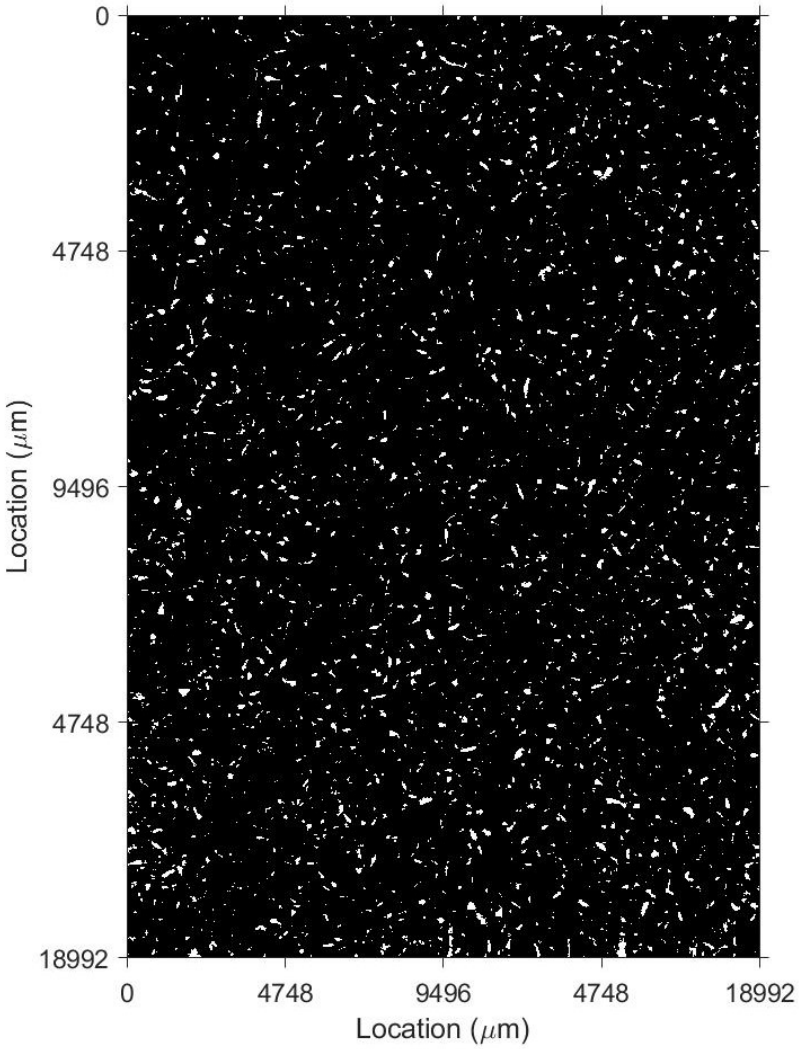

Figure 3.27: Scan 3-1 (control scan) after the 100 micron threshold had been applied (Binary image with white areas being above the threshold)

By producing binary representations of the scans, such that areas with a depth of below 100µm were set to zero and areas above 100µm were set to one, sharply defined images were produced. These images were then subject to feature detection processes to identify and separate the pixels that were part of each area.

Feature detection is a form of image processing that seeks to identify points or regions that satisfy certain conditions. They are often employed in applications such as automatic reading of scans of paper documents, where regions of high intensity (black text) may exist on a low intensity background (white paper). The letters can be separated, either by finding the edges or corners of the letters, or by extracting the whole region. This particular application is not dissimilar to the approach taken in this project.

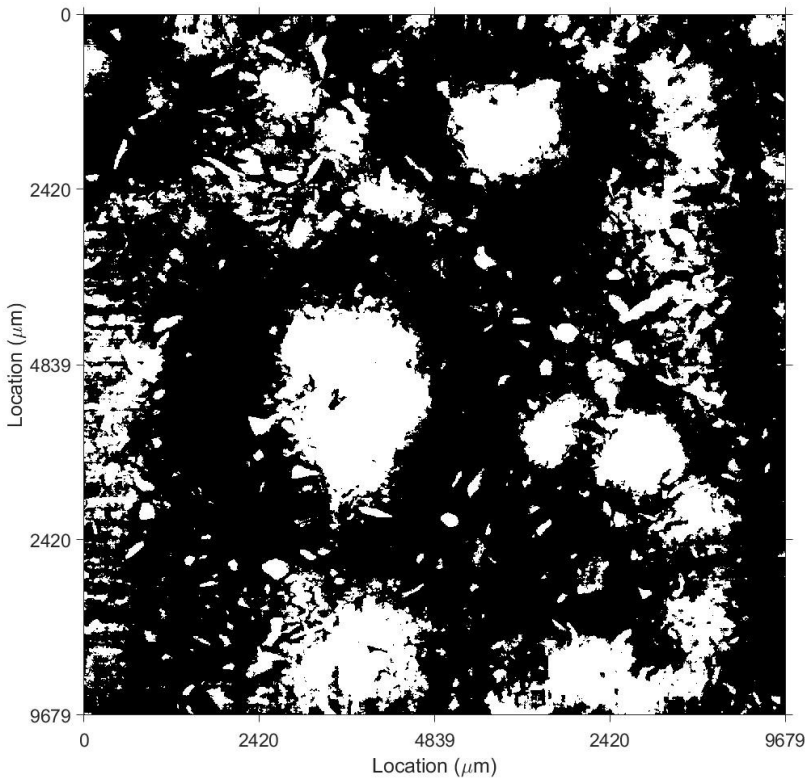

Figure 3.28: Scan 1-1-A-1 after the 100 micron threshold had been applied (Binary image with white areas being above the threshold)

The technique selected was Maximally Stable Extremal Regions (MSER). This approach was chosen in this case as the inbuilt Matlab function returned lists of pixels that were contained within each identified region. This allowed for overlap checking and easier production of separated pit files later in the extraction process.

To filter out the 'speckling' of extremely small areas that appear through the noise floor, and to prevent excessively large areas from being analysed, minimum and maximum areas were defined. This was to guide the function in its attempt to identify wanted regions, and ignore unwanted ones. If all areas that penetrated the noise floor were identified as possible pits, then the system would not only produce a large number of false positives but it would also substantially increase the computing cost of the program in terms of both time and storage.

Minimum and maximum areas were defined in pixels, however the values were chosen based on physical areas. The minimum value was set at 4,474 pixels, approximating to the area of a circle of diameter 300 microns. The maximum was set at 795,339 pixels, approximating to the area of a circle with diameter 4000 microns. These values were chosen based on the expected areas of corrosion pits reported in literature, as well as visual inspection. The limits were effective, based on observing the results, with the lower limit resulting in no detected pits in the control sample (3-1) and with no major features being missed in the other scans.

There was a secondary issue in using the MSER technique. Using a binary image to find the edges of the pit areas meant that if there were large areas of corrosion damage, consisting of several close pits, it was not always possible to separate the pits at the 100 micron filter level as the maximum area limit may be exceeded. To address this issue the filtering and feature detection algorithms were run over a series of levels, with a 25 micron interval. This technique can be seen in Figure 3.29 and with an example shown in Figure 3.30.

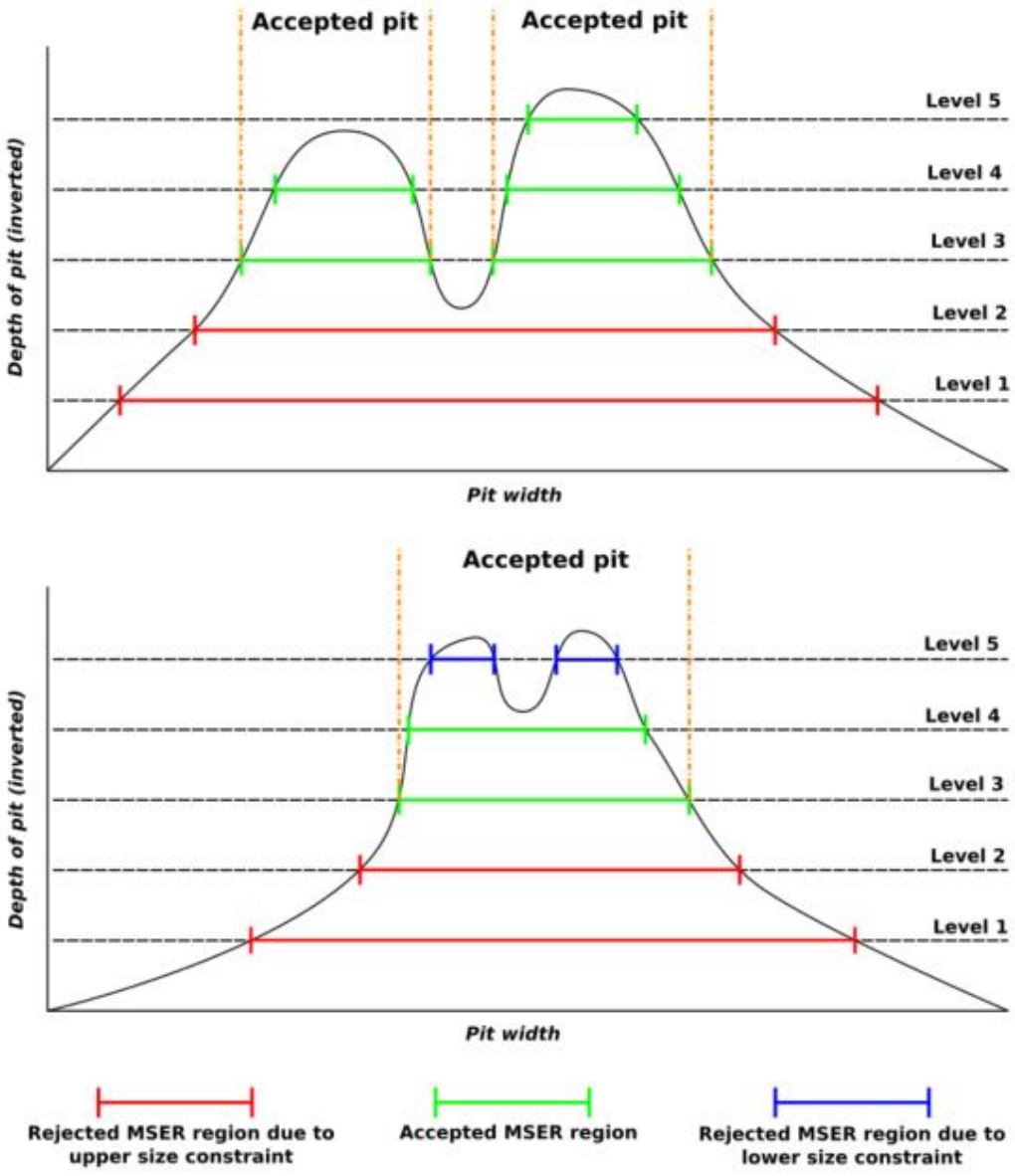

Figure 3.29: Demonstration of multilevel filtering technique

The purpose of the filtering levels was to ensure that the largest, most dominant features, were expressed. Any smaller feature that appeared within the larger features was categorised as a sub-feature and was not separated from the larger feature.

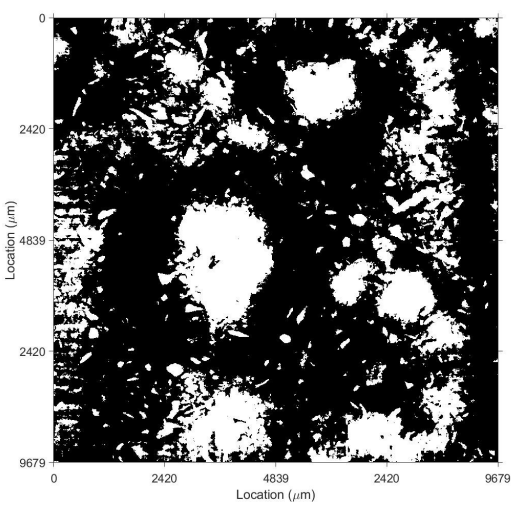

(a) Filter level 1 (100µm)

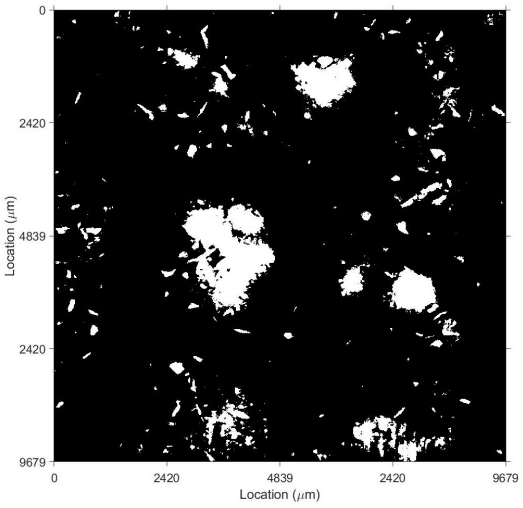

(b) Filter level 2 (125µm)

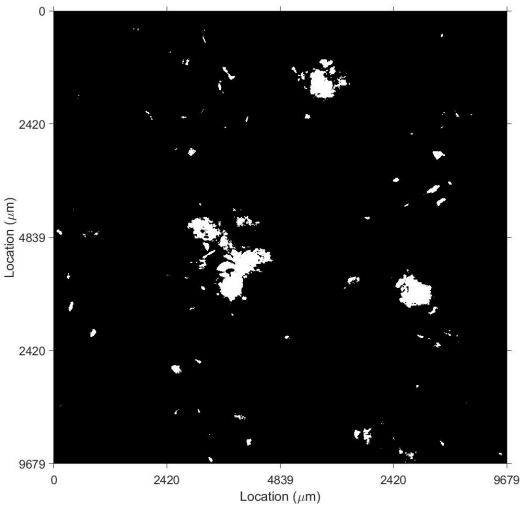

(c) Filter level 3 (150µm)

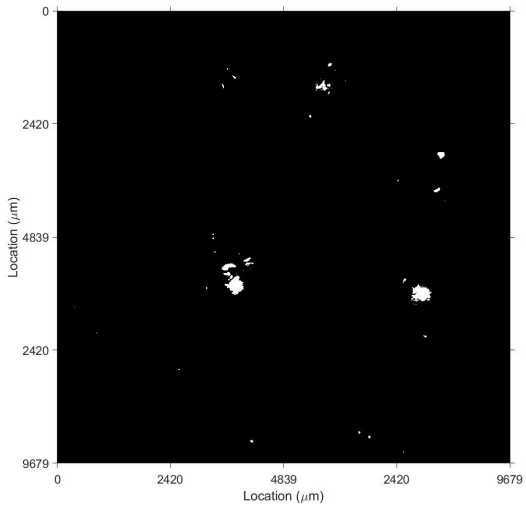

(d) Filter level 4 (175µm)

Figure 3.30: Demonstration of multilevel filtering of binary images, starting at 100 microns below the surface and increasing depth by 25 microns with each step

Extremely large variations were discounted and separated into their smaller features. An example of this being useful would be in the case of pit coalescence, where pits start to overlap but still consists of discrete features.

The levelled filtering approach resulted in fewer, larger, pits being identified than might have otherwise been the case. There were 11 levels of filtering, up to a total of 350 microns deep, although in most cases only a few of these levels were required.

Each level of filtering was processed with the MSER feature detection program. This produced different identified regions at each level, although these often overlapped with areas detected at previous levels. This can clearly be seen in a comparison of Figure 3.31 and Figure 3.32. Figure 3.31 indicates the pits identified at level 1 filtering (100µm), whereas Figure 3.32 shows all of the pits identified at every filtering level from one to 11. It can be seen that many concentric circles exist in some locations, centring on a single point. This represented the same pit being identified several times at different filter levels.

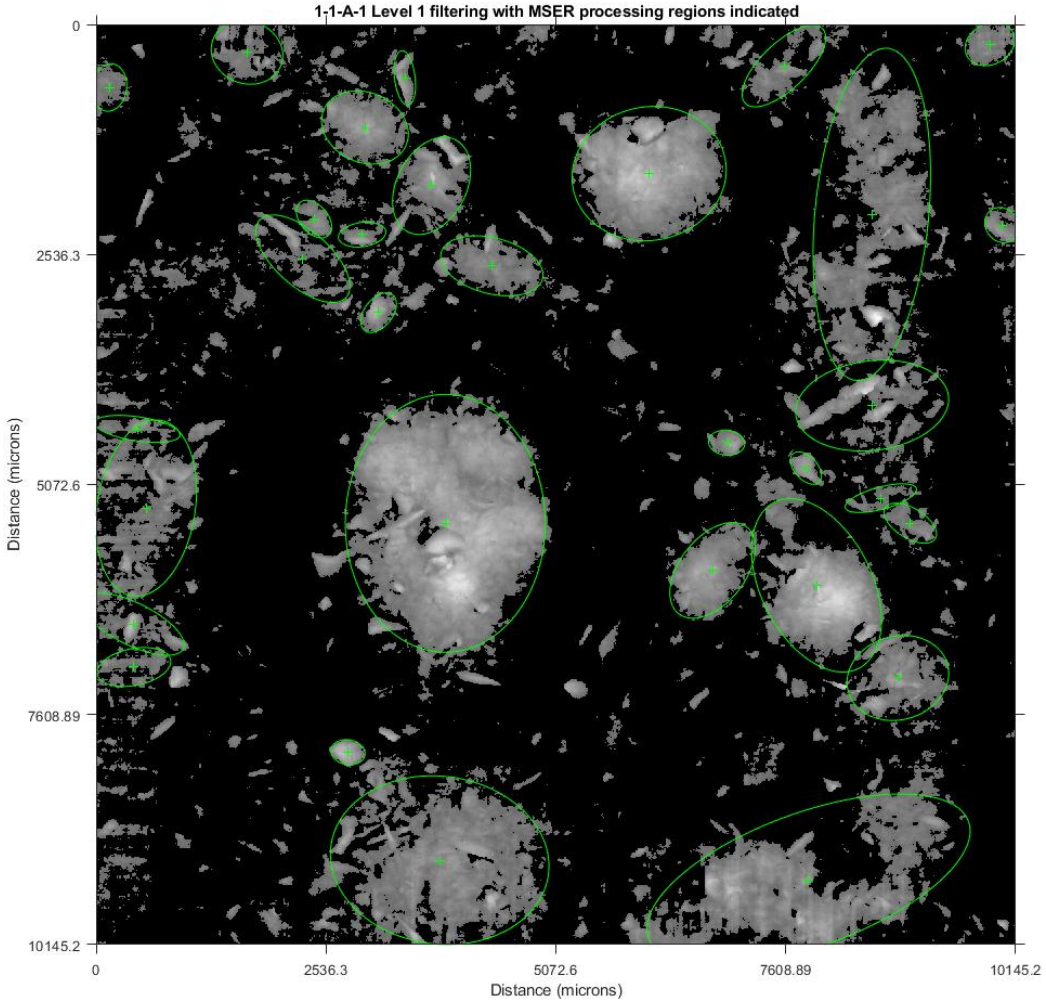

Figure 3.31: Filter level 1 (100 microns) with indications of identified regions at this filter level

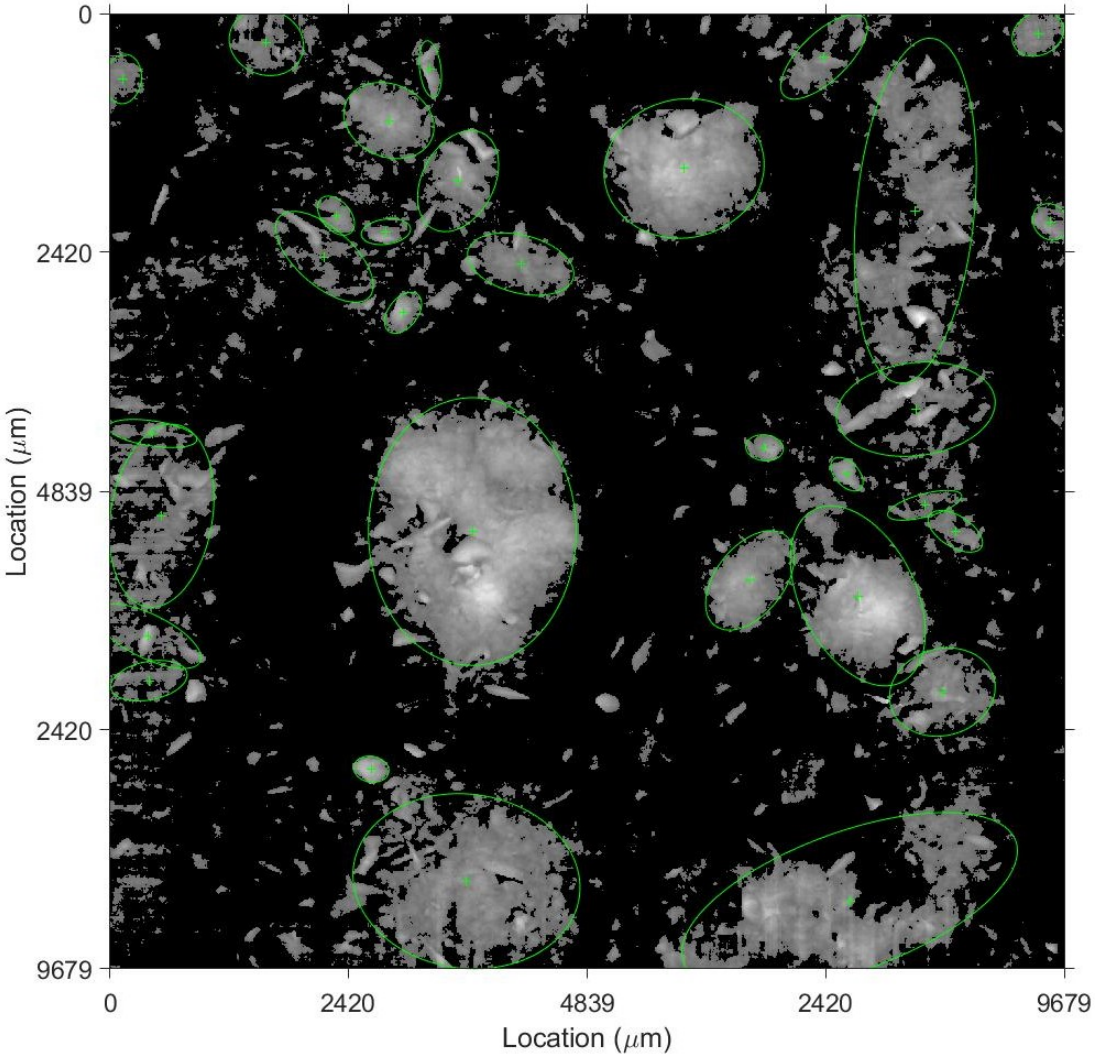

Figure 3.32: Filter level 1-11 (100 microns) with indications of identified regions at all filter levels

Once the regions were identified at every level, another set of processing was performed. MSER indicated any region of the same value band, this included areas that surround zero areas which only contain values with a depth below 100 microns. These regions were not of interest for this study, so were ignored. The other regions were analysed for levels of overlap.

Starting at level one, regions in following levels were analysed to see if they contained a significant percentage of the same pixles as other regions at different filter levels. If the higher filter level regions contained over 25% of the same data points as a lower level region, it was assumed to be a subset of the same pit and the lower filter level region was used. If it was found to be a new and independent pit, it was accepted and following filter levels were also checked to see if there was any overlap with the newly accepted pit.

Once the regions were identified they were separated with a 50 micron margin added on each edge. This represented an approximation of the required distance to find the edge of the pit, without making the scans larger than necessary. There were regions with some overlap within the areas identified as pits, however, this was decided to not have a significant effect, as the process for pit identification ensured that there was no direct overlap between the selected pixels. The results of the identification can be seen in Figure 3.33.

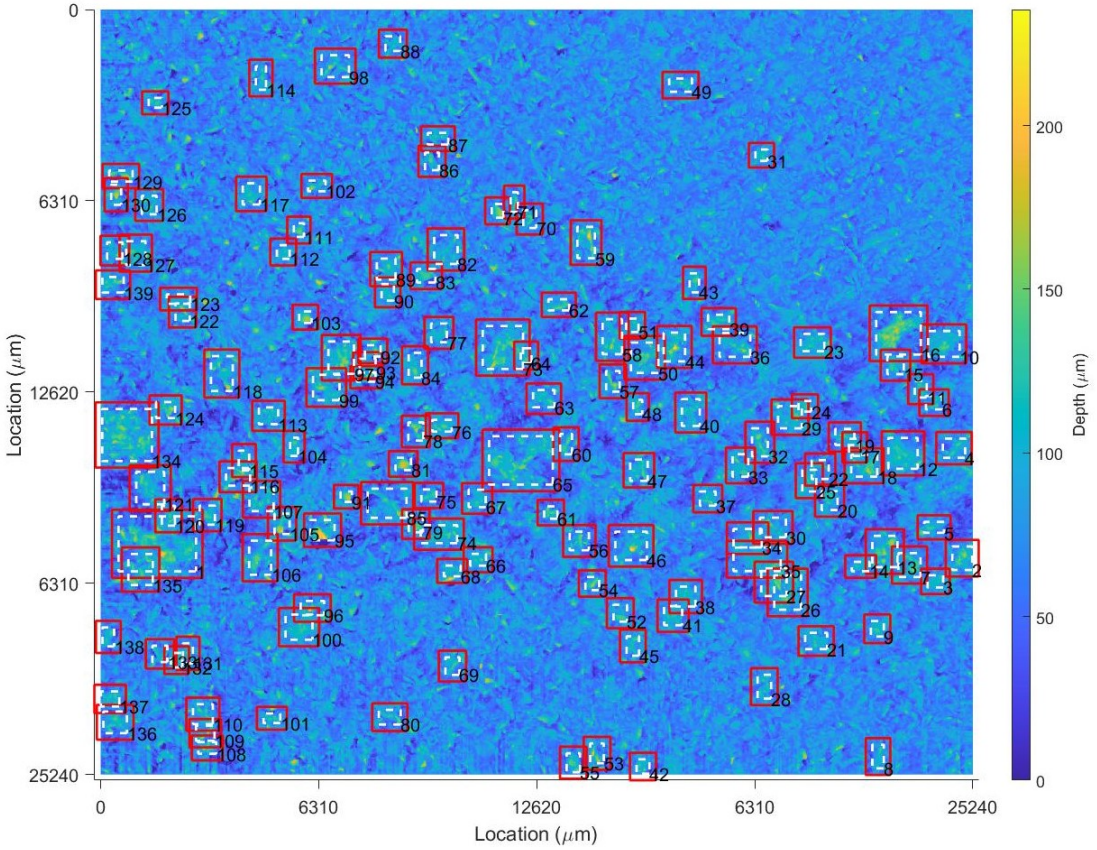

Figure 3.33: Scan 2-3-AB with pits identified as well as with margins applied

The separated pits varied in size and visual appearance, although they were generally a hemi-elliptical shape as would be expected from the literature. A few examples can be seen in Figure 3.34.

3.8 Results analysis

From the 51 scans performed, 4139 individual pits were identified. This was then reduced to 4126 after 13 pits were rejected due to problems with the data, such as rips in the data from a reflective part of the surface, or from detritus on the scan, such as the hair that can be seen in Figure 3.35. This demonstrated the necessity of cleaning the casts before scanning to ensure the removal of foreign object debris that could cause issues in the scanning.

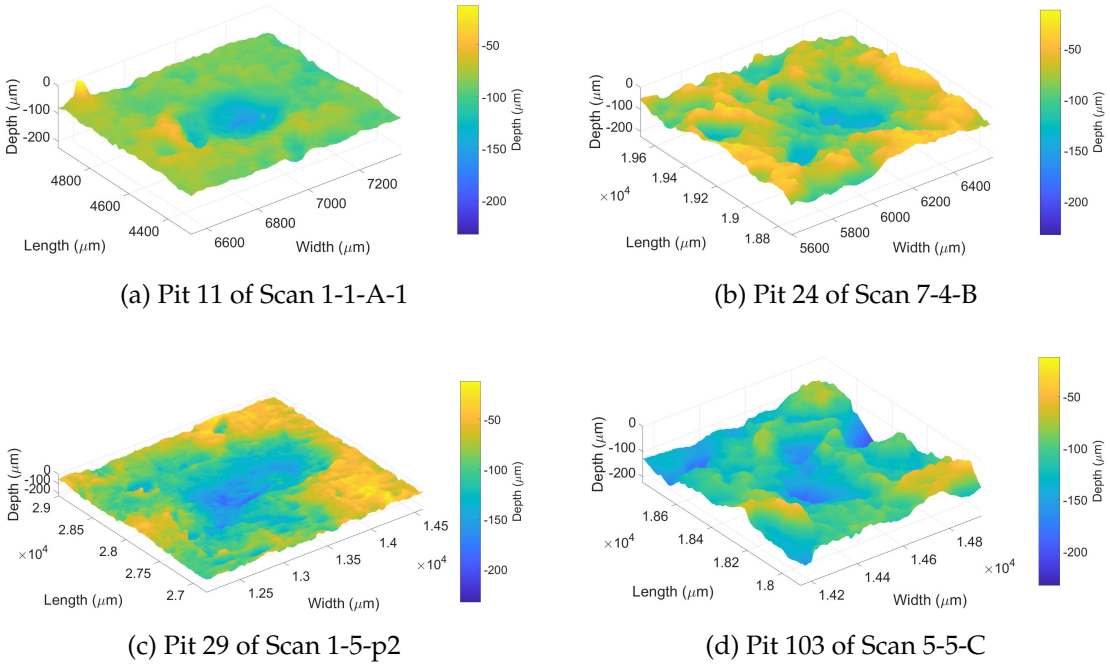

(a) Pit 11 of Scan 1-1-A-1

(b) Pit 24 of Scan 7-4-B

(c) Pit 29 of Scan 1-5-p2

(d) Pit 103 of Scan 5-5-C

Figure 3.34: Examples of pits identified and separated (Z axis inverted and colouring consistent across all pits)

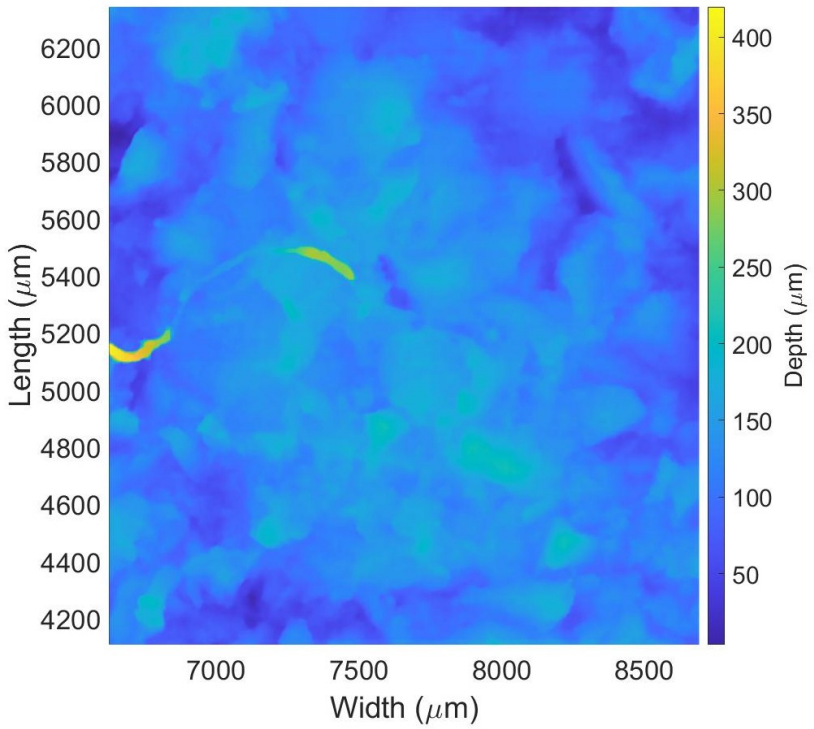

Figure 3.35: Scan 6-3-A-2 Pit 97 demonstrating issues with foreign object debris (Suspected hair on the centre left)

The 4126 remaining pits were initially assessed for three main characteristics, to allow comparison with previous studies. These were: the maximum depth; the width at the surface; and the aspect ratio. The maximum depth was determined by taking the lowest data point on each separated pit scan, using the pre determined zero point.

The widths were taken from the dimensions of the bounding rectangle of each scan, neglecting the additional margin. This was a crude measure of pit width due to the difficulty in defining boundaries of the pits on the three dimensional surfaces, and with the highly irregular shapes of some pits, it was decided that it was a good measurement of width despite the drawbacks. The surface ratio of the pits was the calculated ratio of these two values.

3.8.1 Pit depth data

The results of the survey in terms of depths can be seen in Figure 3.36. All values below 100µm had been excluded due to the definition of a pit used in this study. The maximum depth value recorded was 342.6µm with the maximum number of pits occurring in the 160µm to 170µm range.

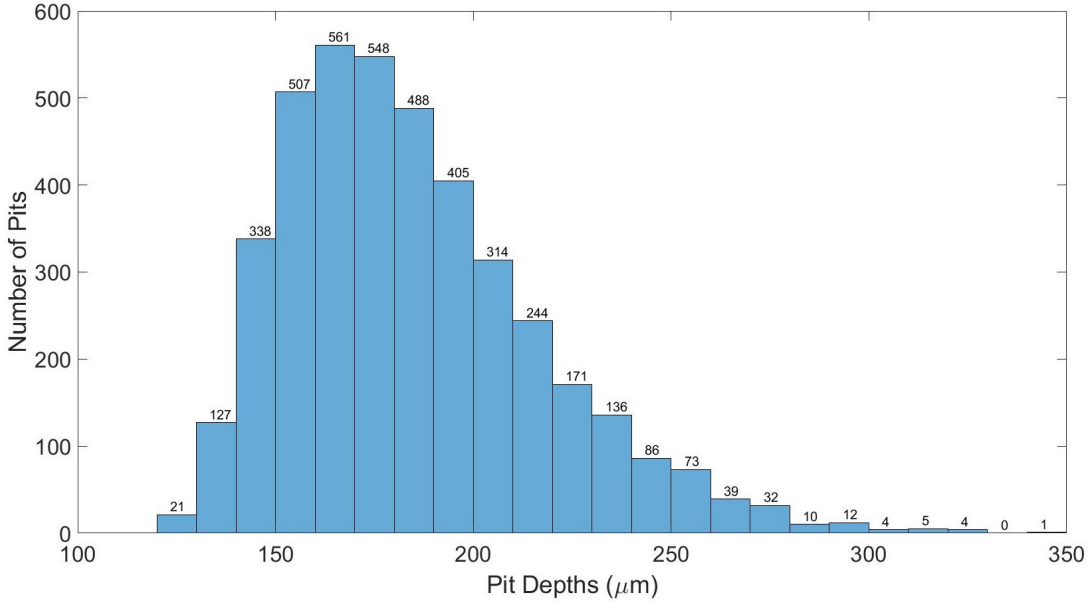

Figure 3.36: Histogram of pit depths from survey carried out

The mean, median and mode of the results were 184.7µm, 179.1µm and 171.6µm respectively. The relative closeness of these results suggested that there were few instances of outliers affecting the data.

The lack of pits in the region of 100µm to 120µm, was likely due to the minimum area definition used during pit identification, as any pit with a maximum depth of slightly greater than 100µm would be unlikely to be large enough to meet the requirement. This also meant that the pits detected were definitely pits and the speckling caused by shot blasting had been effectively mitigated.

The conclusion of the survey, in terms of pit depths, was that none of the axles identified had pits close to the 1000µm limit defined by the standard as unacceptable and requiring scrapping.

Based on the survey carried out as part of this thesis the deepest pit was around a third of this value and the average was closer to 20% of it. Given that the areas inspected as part of this survey had been identified as containing problematic levels of corrosion, the result suggested that it was highly unlikely that these axles contained above limits corrosion in terms of depth.

While these results were from a small sample size, it did suggest that the 1000µm limit was not relevant due to current procedures preventing axles developing corrosion of that depth. On the other hand it could be an indication the cautious approach of depots that are causing axles to be sent for scrap well before they would be required to do so by the guidance. This was possibly due to a lack of ability to quantify the depth of corrosion. However, based on the assessment of the axle records, it appeared that most axles scrapped for corrosion were due to the area of corrosion exceeding limits, suggesting that that restriction was the more onerous.

While it would not be possible to draw a definitive conclusion from a particular set of results, it suggested that there was a disconnect between the maintenance standards and the reality of corrosion observed in depots and its treatment.

3.8.2 Pit width data

Pit width data was calculated from the dimensions of the bounding rectangle used to identify the pits. While this rectangle was unlikely to perfectly represent the dimensions of the opening of the pit, it was judged to be sufficiently precise to achieve a good overall indication.

As there were two dimensions to the widths, which were not necessarily equal, comparison needed to be done between these two values. Initially the two values were compared to each other, to produce Figure 3.37. In Figure 3.37 the closer the values lay to the dotted line, the closer the aspect ratio of the pit bounding rectangle was to one. It could then be supposed, making a similar shape assumption of elliptical pits as previous studies, that these pits were closer to perfect circles, while the further from the line the result was, the more elliptical the pit.

The values in Figure 3.37 appeared to be approximately linear. To test this a linear line of best fit was calculated, and this can be seen in Figure 3.38. The R^2 value was calculated as 0.902 suggesting a good fit. The root mean squared error was 324.

The gradient value of 1.28 indicated that there may be some shape factor at work in the data. The hypothesis was that some factor, such as stress direction or the way the corrosive medium moved around the surface, may have influenced the direction that corrosion pits developed in. An example might be that an axle that was in constant use would have large axial stresses on the developing pit, which might encourage growth in a particular direction, as opposed to an axle used infrequently which would not experience the same bias.

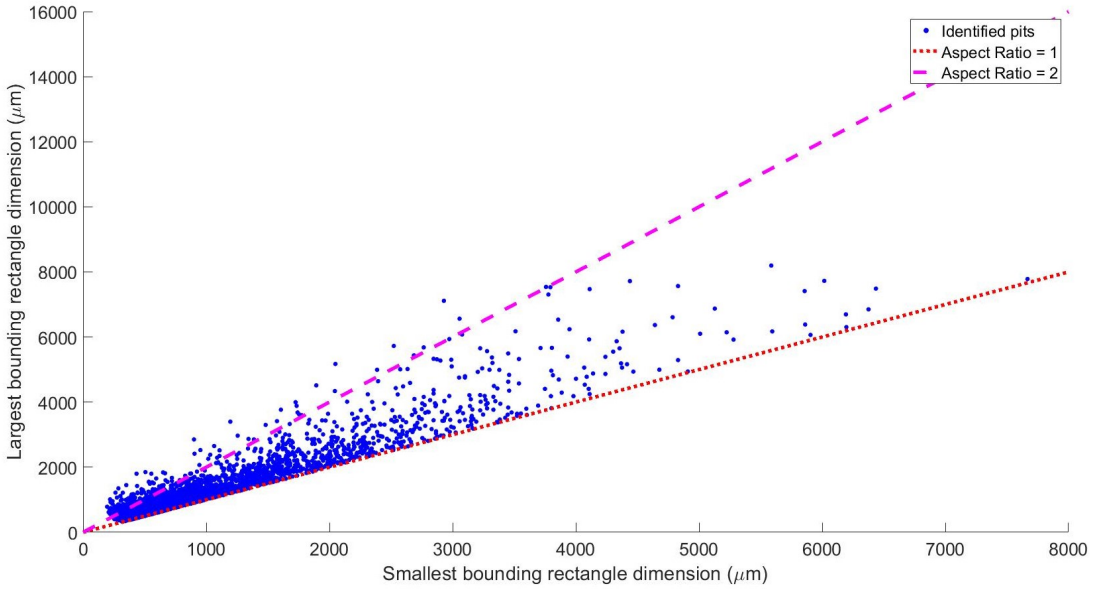

Figure 3.37: Comparison of the largest and smallest bounding rectangle dimensions of identified and separated pits

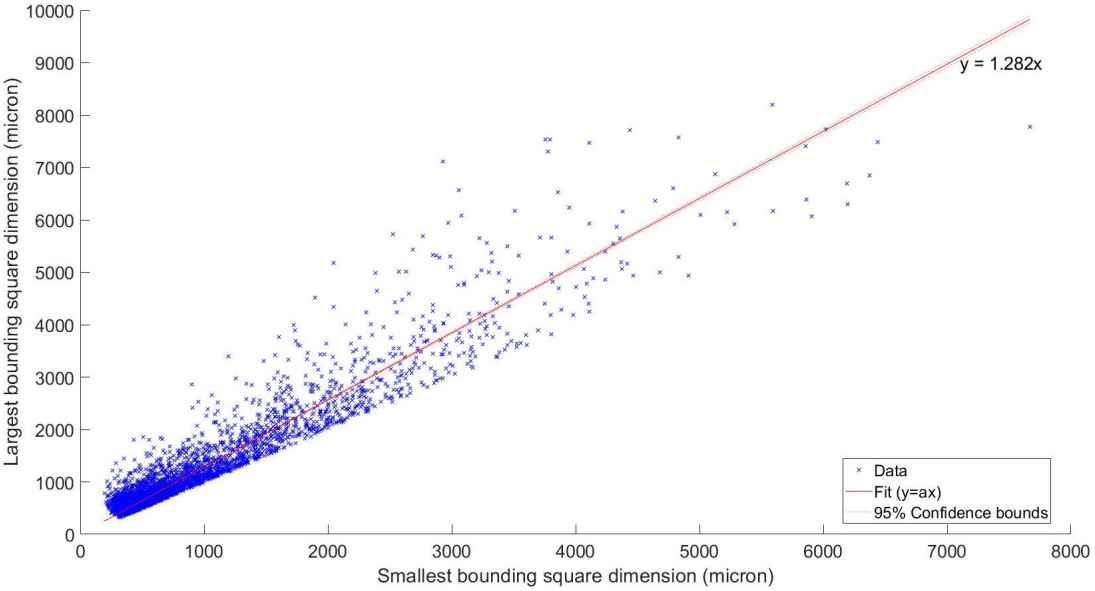

Figure 3.38: Linear line of best fit for comparing the smallest and largest bounding rectangle dimensions

To investigate if there was any influence in the shape of pit development, scans had their aspect ratios calculated in the X and Y directions compared. It was an oversight in the original survey that the axial direction of the scans was not recorded when using the Alicona machine. This meant that it was not possible to determine which orientation the corrosion pits were lying in relative to the axial direction of the axle. However, by examining the individual scans and comparing any bias in directional data it would be possible to demonstrate if this was an area worth further investigation.

Each scan was processed independently. Each pit had its X dimension divided by the Y dimension and then the mean of the ratios was found for each scan. If this value was less than one, the reciprocal was taken. The results of this can be seen in Figure 3.39. If there was no directional influence then the expected value would be 1 or near it, as the spread of dominant bounding rectangle dimension would be random, however these values appeared to be consistently above this, with a mean value of 1.12.

The p-value of the result against the expected mean of one was found to be vanishingly small (7.23×10^{-11}). The small p-value indicated a rejection of the null hypothesis, meaning the result deviated from the expected value by a statistically significant amount. This meant that the true mean of the collected data was not 1, as expected, indicating that the pit shape was being influenced by some unexplained factor.

There was no clear correlation with the number of pits detected in a scan, or the axle that the scans came from, with some significant variation within different scans of the same axle. This suggested that the operation and use of the axle did not have a significant influence on the directional development of the corrosion on the rail axle as a whole, although further work would be necessary to definitively rule out any influence.

If it could be shown that the corrosion pits tended to develop in a particular direction, this could improve the understanding of corrosion development on rail axles and potentially allow for a more granular approach to pitting damage on rail axles depending on prevailing conditions.

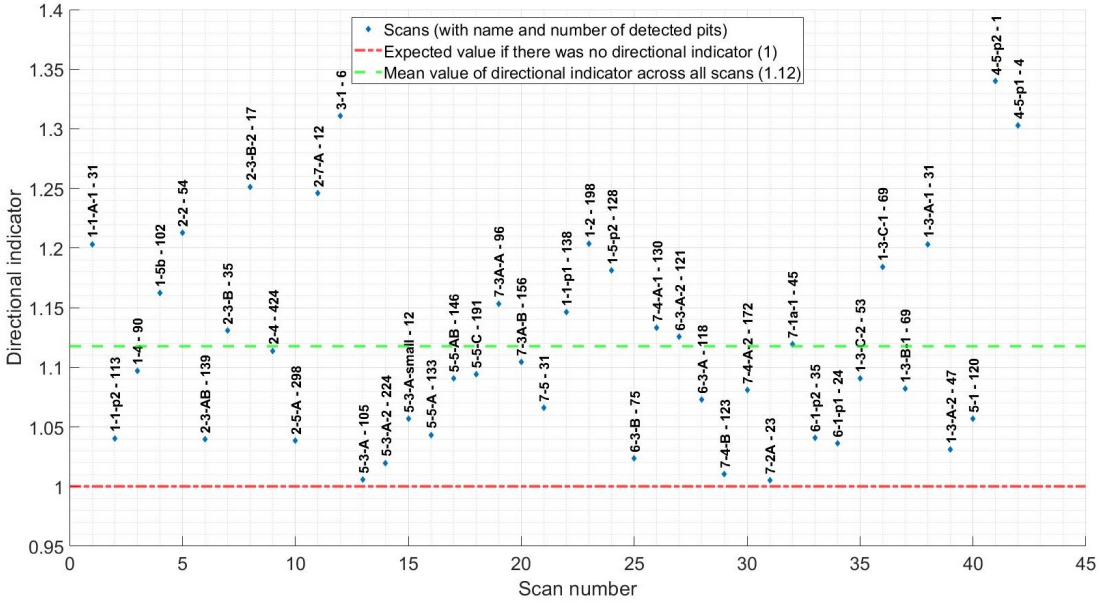

Figure 3.39: Investigation of directional influence in pit bounding rectangle dimensions

3.8.3 Aspect ratio of pits

The aspect ratios of the pits were also investigated. The ratio was defined as the comparison between half the surface diameter of a defect and its depth. The results can be seen in Figure 3.40.

When calculating the aspect ratio using the largest dimension, the highest value was 1.56 and when using the smallest dimension the highest value was 2.17. This suggested that extremely high aspect ratio features were not developing in the sample areas, which lowered the potential stress concentration factors as aspect ratios were the key parameter in the work performed by Cerit [35]. This conclusion was further supported by calculating the means of the two different aspect ratio values. Using the largest dimension the mean is 0.46, and 0.62 if the smallest is used, with 98.2% and 87.7% of all pits having an aspect ratio of less than one.

While normal corrosion damage does not regularly lead to catastrophic failure of axles, and it is the exceptional pits that are the problem, the finding of this survey suggests low values for aspect ratio with regards to depth. Based on Cerit's work the risk of this corrosion damage producing high stress concentrations and contributing to the failure of the component was low.

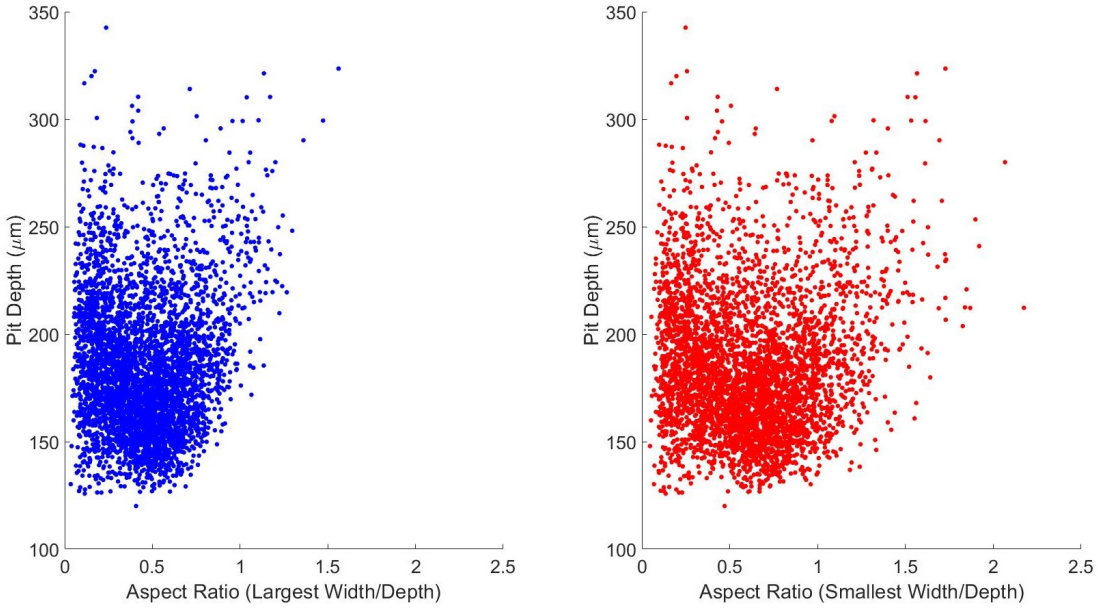

Figure 3.40: Aspect ratios of pits comparing the depths with the smallest and largest bounding rectangle dimensions

It was possible to compare two of the sets of data together. Namely the relationship between the surface ratio of the bounding rectangle dimensions, and the aspect ratio. This can be seen in Figure 3.41. As can be seen in this Figure the pits identified tended to have a ratio of near one at the surface and the vast majority had a depth aspect ratio of below one in both calculations of the depth aspect ratio.

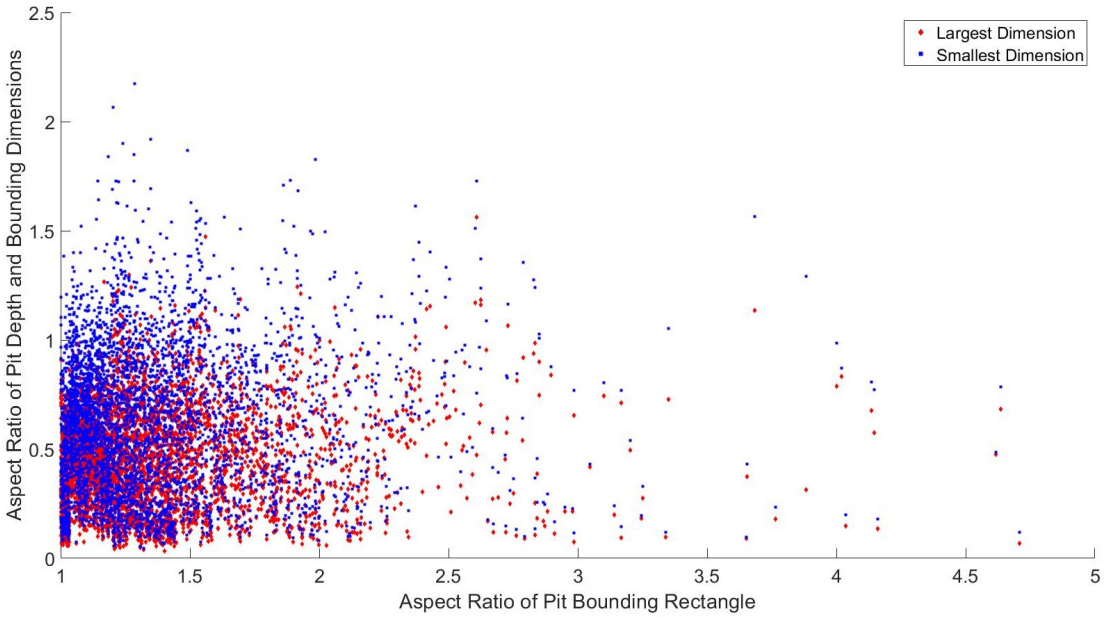

Figure 3.41: Comparison of the bounding rectangle aspect ratios and the depth aspect ratios

There was a noticeable tail of pits that were of a higher aspect ratio, approaching two, however these were almost exclusively points calculated using the smallest bounding rectangle dimension, so can be most probably excluded as a variance due to the method of calculating the depth aspect ratio.

There was also a tail of pits that had a large surface ratio, but a low depth aspect ratio. This area consisted of data points calculated using both the largest and smallest dimension, compared to the previous tail which consisted of only smallest dimension calculations. This was expected, as the change in calculation technique affected only the Y axis on the graph, and not the X axis. There were few pits that displayed high aspect ratios in terms of both the surface bounding square and the depth aspect ratios.

In conclusion, few pits had large aspect ratios in terms of their depth with the vast majority of them having aspect ratios below one and the maximum being below 2.5 when the most severe assumptions were used. This suggested that these pits represented a low risk of cracking based on Cerit's work. There was no obvious correlation between the ratio of the bounding rectangle and the aspect ratio of the pits, suggesting a decoupling of the surface appearance of the pits and the aspect ratio. This would suggest a weakness of top down optical identification approach using shape assumptions to model pit dimensions.

3.8.4 Statistical distributions of results

One of the aims of collecting this data was to evaluate the number of axles in the fleet that suffer from damage at the limits of the standard. As none of the pits identified in the study had any damage near the limit allowed by the standard (1000µm), a result outside of the collected data range needed to be estimated from available data.

Extreme Value Theory was used to estimate the chance of events outside of the experience of the data. This branch of statistics is commonly used in the insurance industry, and many other fields, to predict the chance of events that are far in excess of any previously observed events.

There are three types of extreme value distributions (EVD): Type 1 (Gumbel Distribution), Type 2 (Fréchet Distribution) and Type 3 (Weibull Distribution) [68]. There is then a generalised form called the Generalised Extreme Value distribution (GEV), which combines the other three types of distribution. Selecting the appropriate distribution for the observed and expected data was required to ensure accurate results.

Type 1 or Gumbel Distribution is the most common form of EVD [68]. There are two types, to model the maximum value or minimum value of a distribution. It is unbounded so can cover the entire range of real numbers. In this case the maximum form of the Gumbel Distribution would be appropriate.

The probability density function (PDF) of the maximum Gumbel distribution is given by Equation 3.1 [68]. The μ and β can be found from the mode and variance of the data set. The Gumbel PDF is governed by one unchanging shape while its location is defined by the parameter μ. The β is a scale factor which governs the width and height of the peak.

$$PDF = \frac{1}{\beta} e^{-\frac{x-\mu}{\beta} + e^{-\frac{x-\mu}{\beta}}} \tag{3.1}$$

Type 2 or Fréchet Distribution is used to model maximum values from a dataset [69]. The distribution is bounded on the lower side so is only suitable to assess the higher side. The Fréchet Distribution PDF is given by Equation 3.2 and shows how the distribution is governed by three parameters representing shape (α), scale (β) and location (μ).

$$PDF = \frac{\alpha}{s}\left(\frac{x-m}{s}\right)^{-1-\alpha} e^{-\frac{x-m}{s}^{-\alpha}} \tag{3.2}$$

Type 3 or Weibull distribution refers to a family of distributions that is often used when looking at product reliability and life time assessments [68]. There are two forms, two parameter Weibull and three parameter Weibull. In this study only the two parameter form is considered. The PDF for values of x greater than zero is shown in Equation 3.3.

$$PDF = \frac{k}{\lambda}(\frac{x}{\lambda})^{k-1}e^{-(\frac{x}{\lambda})^k} \tag{3.3}$$

The fourth type of extreme value distribution, Generalised Extreme Value Distribution, is a combination of the three other types [69]. It is often used in scenarios where the tail behaviour is not known, so it is not know which is the most appropriate model. The PDF is given in Equation 3.4 [69] and contains three parameters location (μ), scale (σ) and shape (ϵ). It is possible to determine which of the distributions is dominant in a particular distribution by the value of the shape parameter, if $\epsilon = 0$, it is a type 1 distribution, if $\epsilon > 0$ it is a type 2 distribution and it is type 3 is $\epsilon < 0$.

$$PDF = \frac{1}{\sigma}t(x)^{\epsilon+1}e^{-t(x)} \tag{3.4}$$

$$t(x) = \begin{cases} (1+\epsilon(\frac{x-\mu}{\sigma}))^{\frac{1}{\epsilon}} & \text{if } \epsilon \neq 0 \\ e^{-\frac{(x-\mu)}{\sigma}} & \text{if } \epsilon = 0 \end{cases} \tag{3.5}$$

In this project the exact tail behaviour was not known, however it could be estimated. The GEV was used as it allowed the combination of the different Extreme Value distributions and an evaluation of which was the most appropriate [69]. The parameters of the GEV distribution, were acquired using the maximum likelihood estimation method. Using the gathered data the parameters were calculated as shown in Table 3.3.

Table 3.3: Estimations of the parameter values of the Generalised Extreme Value Distribution fitted to pit depth data (Maximum Likelihood Estimation).

Parameter	Symbol	Value	95% confidence (Lower)	95% confidence higher
Shape	ϵ	0.0058	-0.0187	0.0304
Scale	σ	25.2766	24.6386	25.9311
Location	μ	169.8832	169.0049	170.7615

While the shape factor was above zero, indicating a Fréchet distribution, it was close to zero, and the 95% confidence values bracketed zero, which suggested the distribution was of type 1 or Gumbel distribution [68]. This was the same distribution as Beretta found fitted the data from the axle corrosion survey carried out in his study [24].

The GEV distribution was plotted against the histogram of pit depths as shown in Figure 3.42.

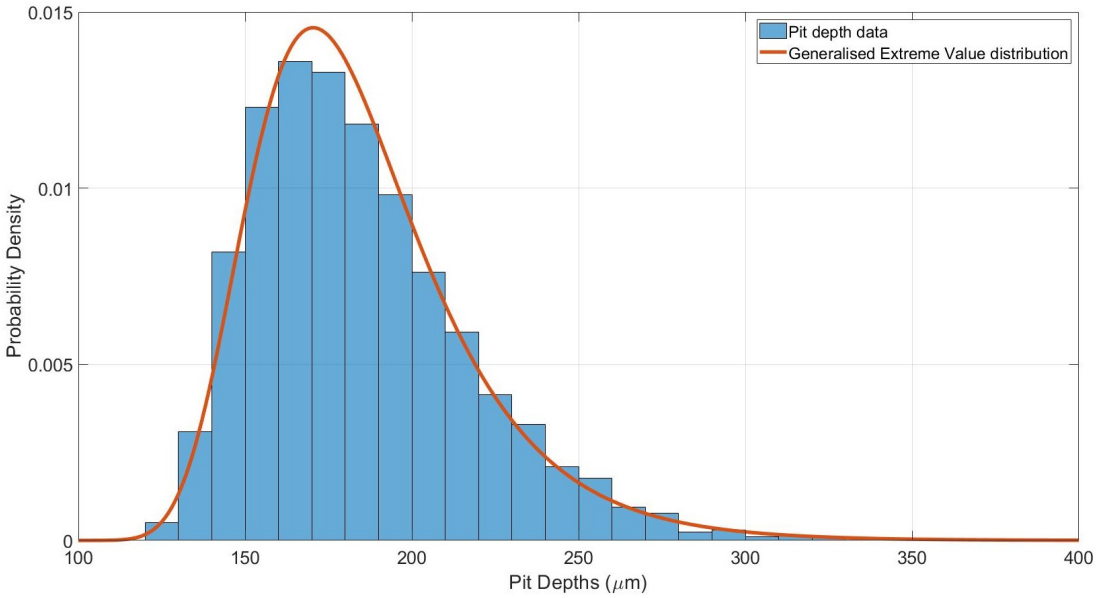

Figure 3.42: Probability density function of the GEV distribution and the normalised histogram of pit depths

Using the Gumbel distribution, as the extreme value distribution that most closely fitted the data, the distributions were calculated and plotted for each individual scan area and the combined pit depth data from the entire study. This can be seen in Figure 3.43. The individual scans can be seen to be closely clustered, with peaks between 140µm and 215µm. This demonstrated the lack of difference in pits that were identified over the six axles investigated, suggesting a level of consistency in the collected data.

While the different scan areas had differences in their shapes and tail behaviours, it should be noted that in all cases the PDF dropped to extremely low levels well before the depth limit. The variation in the distributions, especially with the sharper distributions, was due to smaller number of pits being identified in these scans. The single higher distribution seen in Figure 3.43 was due to to a scan area that contained a single pit resulting in an unusual distribution.

It should be remembered that due to the shot blasting of the axles and the definitions of a pit used in the processing of the survey data, that no pit could have a depth of below 100µm. This meant that the left hand side of the distribution had been affected by this and that pits below this level would be found on the axle before the shot blasting. However, the right hand side behaviours would be unaffected by this.

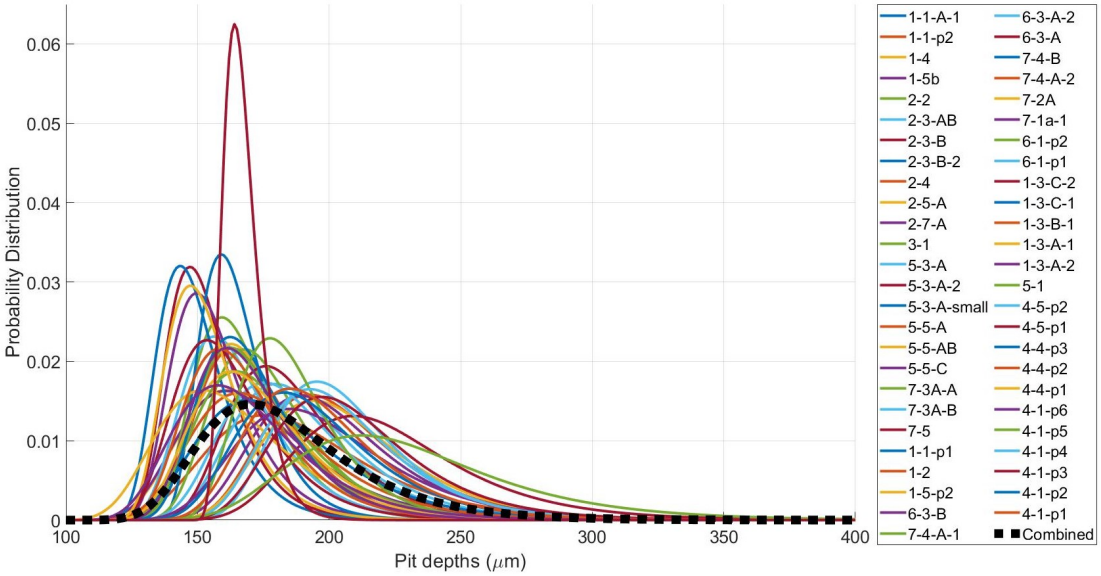

Figure 3.43: Gumbel distributions of pit depths of individual scans and the combined data

Estimate source	Number of wagons
R2 vehicle register	26,100
Industry best guess	17,000
PWF estimate	15,000

Table 3.4: Estimates of the number of freight wagons in the UK from three different sources (2020)

3.9 Application of statistical results to whole UK fleet

While the results of the scanned samples were interesting, the real value was in the implications for the whole fleet of freight rail axles in the UK. This would allow approximations of the severity of corrosion pitting in the UK, and an assessment of current regulations.

To perform such analysis, an estimate of the number of freight rail axles in the UK was required. This was not available in literature, possibly due to the fragmentation of the industry historically and the loss of data over time. To supply an estimate the Private Wagon Federation (PWF) was contacted. They are the trade association for companies with a particular interest in rail freight wagons in the UK.

The PWF were unable to supply a number of rail axles. However they were able to supply estimates of the number of wagons in the UK. These estimates can be seen in Table 3.4. The reasons for the differences in the estimates was put down to the number of idle and withdrawn wagons as well as EU wagons that were no longer in the UK.

In the UK both two and four axle wagons are used, and an estimate of the ratio in use was not available. However, based on discussions with members of the Wheelset Management Group, the consensus was that the majority of wagons in the UK were of the four axle configuration. Using the four axle assumption leads to a range of values of the number of rail axles in the UK between 104,400 and 60,000.

Based on the available information, it was more likely that the number of axles is closer to 60,000 than 104,400. For this reason it was decided to use the industry best guess as a middle ground, assuming all wagons had four axles, giving an estimate of 68,000 freight axles in service. This meant that the survey carried out represented 0.009% of the population.

Based on the collected data from the six axles a margin of error (MOE) was calculated. Due to the small sample size of six axles, Student's t-test approach was used with the t distribution. The first stage was to estimate the standard deviation of average pit depths on rail axles. This was done using Equation 3.6 which estimated the Standard deviation as 18.87. In this equation n is the number of samples, X_i is the variable being measured and $\bar{X}$ is the mean of the samples.

$$Std_{estimated} = \sqrt{\frac{1}{n-1}\sum_{i=1}^{n}(X_i - \bar{X})^2} \tag{3.6}$$

The confidence interval was initially set at 99%, resulting in a t-value with 5 degrees of freedom as 4.032. Equation 3.7 was then used to calculate the 99% confidence interval, where $\bar{X}$ is the sample mean, t is the t value of the distribution, s is the standard deviation of the sample values and n is the number of samples. Using these values the MOE was found to be $\pm$ 31.53µm from a mean of 181.9143µm, representing an MOE percentage of $\pm$ 17.07% at 99% confidence. This result meant that the mean of the distribution of pit depths lay between 150.85µm and 213.00µm to a 99% confidence level corresponding to location parameters of 155.29 and 184.47.

These values were inserted into the Gumbel Distributions to assess the chances of extreme value events. However, the changes at the limit for the standard were minimal, with tiny variations. These results can be seen in Figure 3.44, comparing the use of different mean estimations.

$$\left[\bar{X} - t_{n-1} \times \frac{s}{\sqrt{n}}, \bar{X} + t_{n-1} \times \frac{s}{\sqrt{n}}\right] \tag{3.7}$$

To apply the distributions found in the axle survey to the entire UK fleet required some assumptions to be made. The distributions were produced from a set of data collected from areas of corrosion from axles that had been in service long enough to need maintenance at an overhaul depot. The axles had then passed the initial test to see if there was any chance of returning the axle to service.

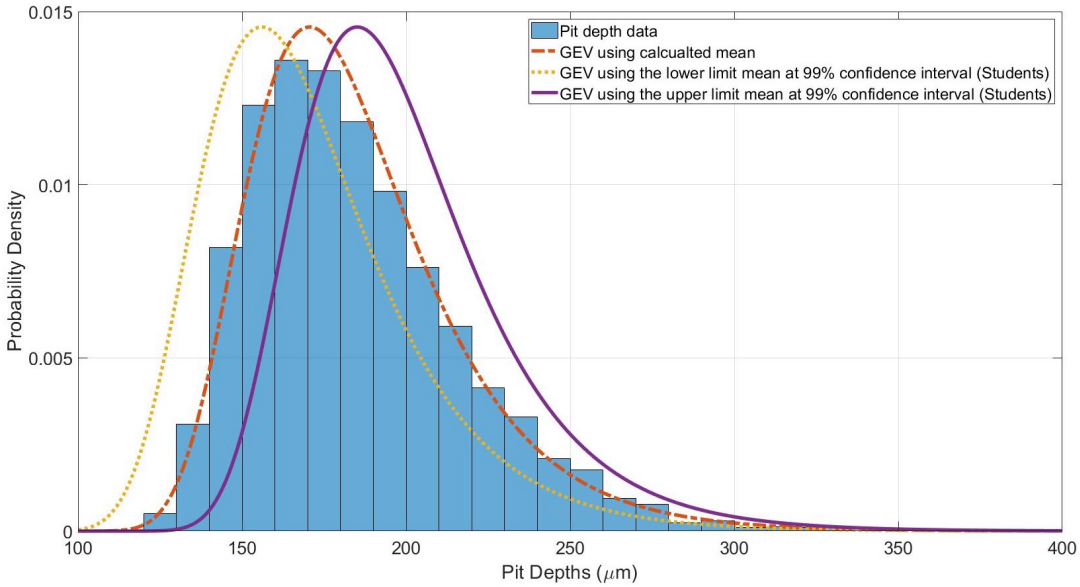

Figure 3.44: Impact of potential variations in mean values on GEV distributions due to small sample approximations at the 99% confidence level

Of the chosen axles only areas on the axle body that exhibited corrosion were investigated in this survey. The outcomes of these assumptions suggested that the results of any extrapolation represented a worst case scenario, as far as rail axle pitting was concerned. However, there are circumstances where more extreme conditions could occur, such as salt transportation, where a different distribution may be required.

Using the total area investigated, minus the control area, gave a total area investigated of 12541.45mm^2. Making the assumption that all the axle bodies of the UK freight axle fleet, consisted of 2m long, 0.2m diameter cylinders, this gave a total axle body area of the fleet of $8.545 \times 10^{10} mm^2$. This meant that this study could theoretically be run 6,813,512 times.

Using the Gumbel distribution of the pit depths calculated previously, this suggested that if all the axles in the UK fleet were in same condition as the six axles that were part of the study, the number of axles that would have corrosion pitting of over 1000μm in depth, the limit in the standard, would be 5.55×10^{-13}% or 3.781×10^{-6} axles. This was a vanishingly small number and was at least partly borne out by the lack of axle failures in the last 25 years.

Data from the work by Beretta et al. [24] calculated even lower chances of corrosion pitting below the depth limit. It has to be kept in mind, however, the extremely small sample sizes involved, both in terms of the number of axles surveyed and the area of each axle surveyed. This made large scale applications of these distributions to rail axles problematic.

The survey undertaken demonstrated, when taken with other surveys performed, that the 1000µm limit on rail axle corrosion, did not seem to be being reached or even approached on a regular basis, if at all. This begged the question as to why this limit had been imposed if it was irrelevant to the experience of rail axles? How was this value chosen in the first place? Would another limit be more applicable?

3.10 Conclusions

This Chapter detailed the process of designing, validating and carrying out the corrosion pitting survey. Then the post processing of the data and the automatic identification and separation of pits in the processed scans. Finally the results of the survey were presented and discussed, with comparisons with previous surveys carried out, and the compared to the current standards environment. The process undertaken to collect the required information and analyse it to extract useful conclusions is summarised in Figure 3.45.

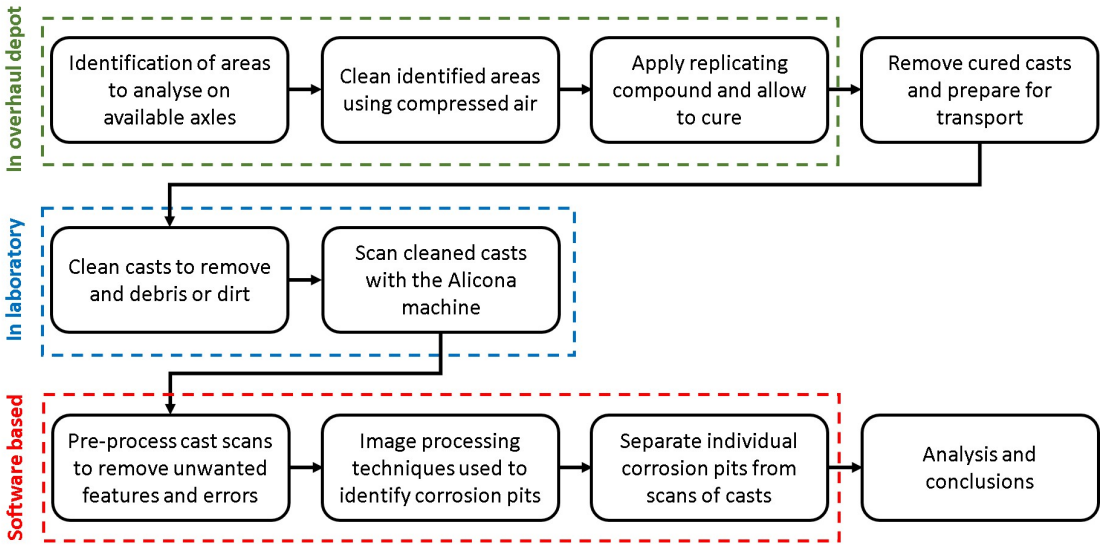

Figure 3.45: Summary of the approach taken to collect and analyse data in Chapter 3

The subject of the survey has been demonstrated to be of interest to the industry. This has been demonstrated by the previously mentioned axle audit, from Chapter 2, as well as the existence of previous, industry funded, studies and the support this project has attracted from a wide range of industry stakeholders.

The technique prosed by the project, using a combination of replicating compound and optical three dimensional scanner, had been shown to be effective at capturing and extracting the surface geometry of rail axles during the overhaul process without significant disruption. This technique allowed analysis of larger areas of interest, and in more dimensions, than previous studies and represented an improvement in the investigative capacity.

A method allowing the automatic processing of the scans had been developed. This was required due to the novel nature of the information collected and the specifics of the axle environment. This technique has been discussed and was capable of identifying pits with acceptable accuracy, based on visual verification of the scans. The overall process has been demonstrated to be suitable for use in a depot setting and has the capability to be used widely in the industry.

There were several conclusions that could be drawn from this work. One of the key ones was that there was no evidence of axle corrosion approaching the depth limit, either in previous work or this study. Combined with the fact that it was not currently possible for depots to collect this data, suggested that this guidance was either unnecessary, or more worryingly wrong.

If no axles were approaching the limiting level of corrosion then there was no proof that this limit would be safe. This had to be balanced against the very small sample sizes of the studies used, however the fact that the maximum depths recorded were around 350µm, suggested this represents a corrosion maximum depth value.

Another factor was assuming that the area restriction on axle corrosion was related to risk of a corrosion pit forming that approaches the limit for a single pit. This did not appear relevant based on extreme value statistical analysis.

The casts that were taken from the depots had been identified by operators, due to them breaching the area restrictions in the standard. Based on an increase in area creating an increased number of independent pits and the calculated statistical distribution of pit depths, the 50mm by 30mm restriction would not lead to a significant increase in the risk of a 1000µm pit developing.

These conclusions suggested that the limits on corrosion as currently defined in the standards were not relevant to the experience of rail freight axles, as the depth limits were not being approached and the chance of a pit reaching the limit with the prescribed area limits were statistically negligible. This suggested that there were potential savings to be made in industry through increasing the area requirement that was mainly used at depots. The depth requirement was harder to address as it was not being reached or even significantly approached according to all identified research.

While these conclusions were potentially important to the industry, the small sample size meant that more work should be done to ensure that these conclusions hold up to increased testing.

3.11 Novelty

3.11.1 Industrial

In this Chapter techniques have been applied in a novel way to address an industrial problem. The largest survey of rail axle corrosion has been undertaken to address an area that has not been studied extensively in recent years. The outcome of the work brings into question the current limits in the standards and highlights the disconnect between the reality of axle maintenance from the theory represented by the guidance documents. A case has been demonstrated that this is an area that merits further investigation.

The technique used has been shown to produce significantly improved inspection results compared to current methods and be capable of use within an industrial setting without disruption to business as usual operations.

Further work would be required before the technique could be used on a fully commercial scale. Principally this is due to the slower speed of inspection compared to current practises, despite the improved results. The slower inspection times come from three main sources, curing time for the compound, optical scanning and digital processing. These drawbacks would need to be addressed by future work to allow maximum value to be obtained for industry. Other lesser weaknesses include the fragility of the equipment and training operators would currently require.

It should be noted that due to the total process improvement that this technique represents, compared to current practises, a decision to implement the technique would not solely be focused on speed, but also the total value added to customers.

3.11.2 Scientific

The work in this Chapter has collected a large and detailed dataset of real world data, demonstrating the successful application of a two stage data collection technique. A multi-level programmatic approach to corrosion pit identification and separation within a damaged surface has been presented and demonstrated to be capable of producing results that can help inform further work. The results of the survey of rail axles provides much needed information, in three dimensions without major shape assumptions, as to the nature and extent of corrosion on rail axles in the UK, information that was not available before this work.

The information collected in this Chapter will be taken forward for further analysis and used to produce an assessment of the risks corrosion damage poses on the UK rail network.

Chapter 4

Investigation of crack initiation and propagation risks due to corrosion pitting damage

4.1 Introduction

The previous section detailed the survey of rail axles in an operational setting, to assess the extent and level of corrosion damage found on axles. It was demonstrated that the maximum depth of axle corrosion pitting was significantly below the allowable limits in UK standards.

Once the pits had been identified and separated, in Chapter 3, the next stage was to assess the risk that the pits represented. To achieve this, the failure condition for this work was defined as the point at which a pit would cause a crack to be initiated. Propagation and ultimate failure was beyond the scope of this work.

The approach used was based on fracture mechanics, using a combination of crack analogies for corrosion pitting as well as the El Haddad method [70] for assessing stress intensity factors under fatigue. This approach was chosen after an analysis of the state of the art approaches used in literature across a range of industries.

In this Chapter different definitions for collecting the input parameters to fracture mechanics equations from three dimensional datasets are explored, with implications on the accuracy of previous work in this field. The reasoning behind different approaches is discussed and analysed.

Using conservative estimates for input parameters, the risk of the pits identified in the survey initiating cracks are assessed. The likely crack initiation location for the surveyed pits was also investigated based on the fracture mechanics approach.

In summary, the aim of this Chapter is to evaluate the variations in the stress intensity factor produced by the pits identified in the previous survey of rail axle corrosion. These results can then be compared to the chance of crack initiation from the pit. The ultimate goal is to use these results to evaluate the current standards. The work in this Chapter is summarised in Figure 4.1.

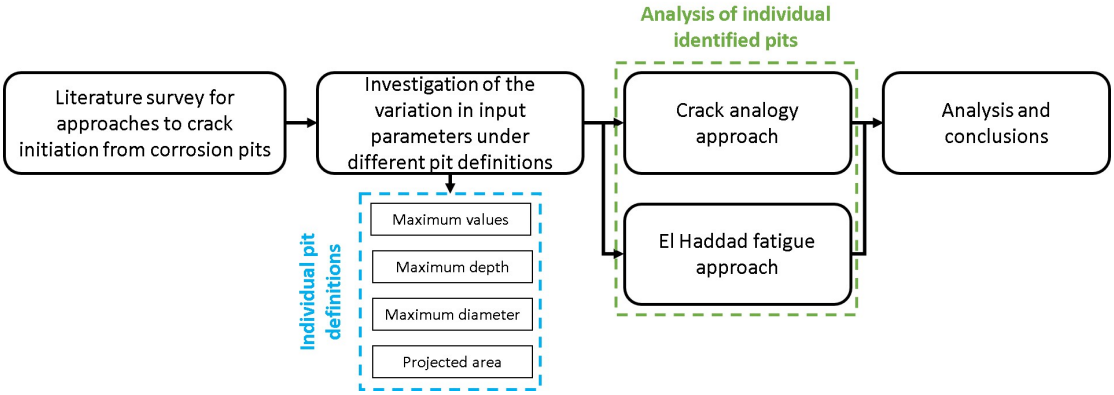

Figure 4.1: Work flow for Chapter 4

4.2 Approaches to predict crack initiation from corrosion pits

The problem with corrosion damage is often not the corrosion itself, rather the cracking that can be initiated from that corrosion. Cracks can, in some circumstances, propagate from corrosion pits to cause ultimate failure of the component. Attempting to predict the failure of components undergoing stress cycles in corrosive environments is a complex issue as there are many different, and sometimes competing, mechanisms at work, which will be time, material and environment dependent [18]. It should be remembered that corrosion is a system driven process, rather than simply a material property, [18], so adding stress or fatigue elements to the system would lead to an increasingly complicated scenario.

4.2.1 Initial proposed method

At the conception of the project it was intended that a Finite Element approach would be taken. As part of Chapter 3 three dimensional models had been produced of corroded axle surfaces and individual pits. One approach to determining the risk of crack initiation from an individual pit or a whole axle surface would be to use the collected data to produce Finite Element models.

A Finite Element approach would have several advantages. Surface conditions could be analysed directly and individually, without simplification, to assess the risk of crack initiation by inspecting the stress condition of a pit. This would be a significant improvement on current two dimensional approaches and could result in very detailed, individual, assessments of different pits. It would also allow study of the effects of different geometric variations within pits on crack initiation risk.

Issues arise, when implementing a Finite Element approach for the rail axle application, especially when considering use of the technique in industry. The data collected in Chapter 3 resulted in surface scans in the form of point surfaces. This meant that single measured locations were present at regular intervals, but with no information regarding the space between each point. This was due to the digitised method of data collection.

To convert the three dimensional point surfaces into complete surfaces that could be useful in a Finite Element study, some form of extrapolation would have to take place to connect the points to produce a contiguous surface. In three dimensions this could be done using a triangular facet approach, similar to that seen when using Standard Triangle Language (STL) files.

By definition the use of facets to produce a contiguous surface, would result in smooth geometries being replaced by sharper equivalents. At inflection points on the surface, such as at the bottom of a pit, the sharper geometry would lead to the formation of singularities. The singularities could occur at any location with an inflection point regardless of their location within the pit. If a finer mesh were applied to try and overcome the singularities, it would not only fail to address the underlying geometric issue, but also risk "creating" data by adding nodes onto faces between measured points. This would significantly negatively impact the reliability of any results.

These issues could be overcome to a degree by taking a higher resolution scan of the pit, smoothing out some of the areas around the singularities and allowing more stable analysis. This would have several issues especially when applied in a depot setting.

To increase the resolution to a degree that a Finite Element approach would yield useful results the amount of data being collected would have to increase significantly. This would lead to several detrimental factors for industrial application including increased scanning time and increased processing time, potentially disrupting operational throughput. Increased data density would also require more processing power, increasing costs and reducing the value gained from any savings.

The presence of singularities in the Finite Element models required a new approach to be taken. When analysing cracks, the issue of singularities is avoided by using the concepts of fracture mechanics. In particular the concept of the stress intensity factor (SIF) is a very powerful one, allowing assessment of the initiation and progression of cracks.

The stress intensity factor approach has been used extensively to define what is known as a critical pit, when a pit develops the the point that a crack would be capable of being initiated from it. However, this approach often requires simplifying corrosion pits into two dimensional cracks, due to the assumptions of linear elastic fracture mechanics and the problems of solving the required surface integrals for non-standard geometries.

In this application a stress intensity factor approach still represented a significant improvement on previous work and would be possible to implement consistently in a depot setting.

4.2.2 Stress intensity factor - Background

The stress intensity factor (SIF), denoted by K, describes the magnitude and proportionality of the elastic crack tip stress field. It can be used to describe crack growth and performance of materials during fracture as long as the crack tip remains predominately elastic [71]. It is assumed that if the SIF is greater than a critical value (fracture toughness) then the material will fracture and fail.

When considering the stresses at the crack tip, they can be broken into three basic types. These are described in Figure 4.2 and are referred to as mode I, K_I, mode II, K_{II}, and mode III, K_{III}. Mode I is an opening load, mode II is shearing and mode III is tearing.

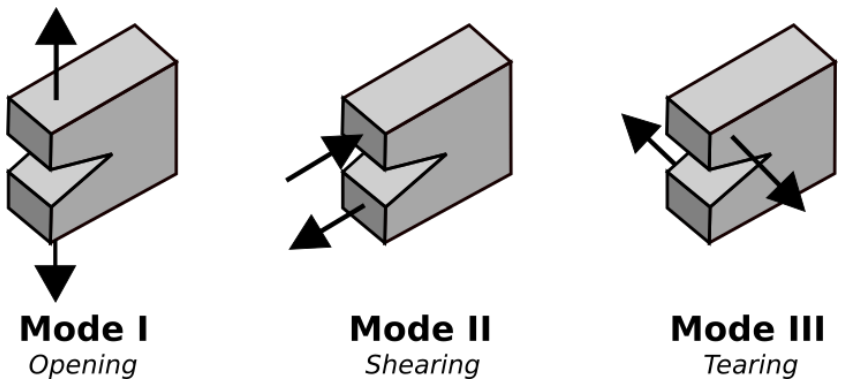

Figure 4.2: The three fracture modes for cracks [72]

The values of the stress intensity factor are derived from the common factor of the stress components around a crack tip, given a particular loading mode. For mode I this can be expressed in index notation as shown in Equation 4.1, where r is the distance from the crack tip of the location being considered and θ is the angle from the axis of the crack of the location being considered. This is demonstrated in Figure 4.3. The value of K_I changes based on the geometry of the crack being analysed, and the expression $f_{ij}(r, \theta)$ changes with different assumptions around the definition of the crack (for example if the crack is infinitely sharp or rounded).

$$\sigma_{ij} = K_I f_{ij}(r, \theta) \tag{4.1}$$

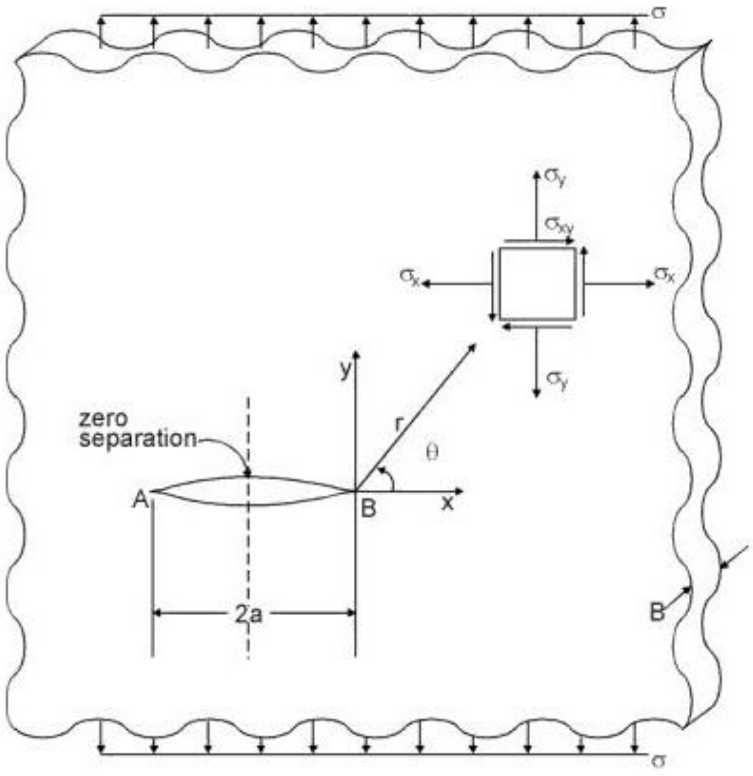

Figure 4.3: Definition of terms around stress intensity factors of cracks [73]

4.2.3 Predicting crack initiation from corrosion pits using fracture mechanics

Rail axles operate in under conditions of high cycle counts, fully reversed stress cycles and a corrosive environment. This falls under the category of corrosion fatigue, which is common in many industries but has been of particular focus in the oil and gas, nuclear and aviation sectors. While all of these sectors have investigated corrosion fatigue, they each have a different use cases to study. For example, the stress cycles in the nuclear sector tend to be relatively few in number and of consistent amplitude, whereas the aviation sector tends to experience unpredictable stress cycles, both in terms of amplitude and frequency. There are also variations in the corrosive environments due to different locations. These variations have led to work being carried out that tends to focus on particular scenarios and materials, producing models with little generality [74].

The life of a component that fails by corrosion fatigue, can be described by Equation 4.2. N_f is the number of cycles in the life of the product, N_i is the number of cycles to initiate a pit that can form a crack and N_p is the number of cycles for the crack to propagate to a size that cause the failure of the component. These terms will inform the thought process going forward in this thesis. However, the conceptual approach was limited in its application to rail axles due to the large variation in the experiences of a particular axle. Defining a number of cycles to failure may be misleading in the case of rail axles due to the variation in the cycles, long periods of storage or significant changes in environmental and protective conditions.

$$N_f = N_i + N_p \tag{4.2}$$

The case of corrosion pit induced failure compared to general corrosion failure can be seen in Figure 4.4. As shown in the Figure a key event in corrosion fatigue cracking is the initiation of a crack from a pit at the point ΔK_{thCF}. At the point at which a pit has developed enough to cause a crack to nucleate from it, it can be said to be a "critical pit". The definition of this critical pit varies by different models and is often affected by the material used, but can be summarised as the point at which a crack would initiate from a corrosion pit. Most models judge the point at which a pit has reached criticality based on the linear elastic fracture mechanics (LEFM) concept of threshold stress intensity factor (SIF). The issue with this approach is that the assumptions of LEFM do not hold for short cracks as would be expected at crack initiation [74].

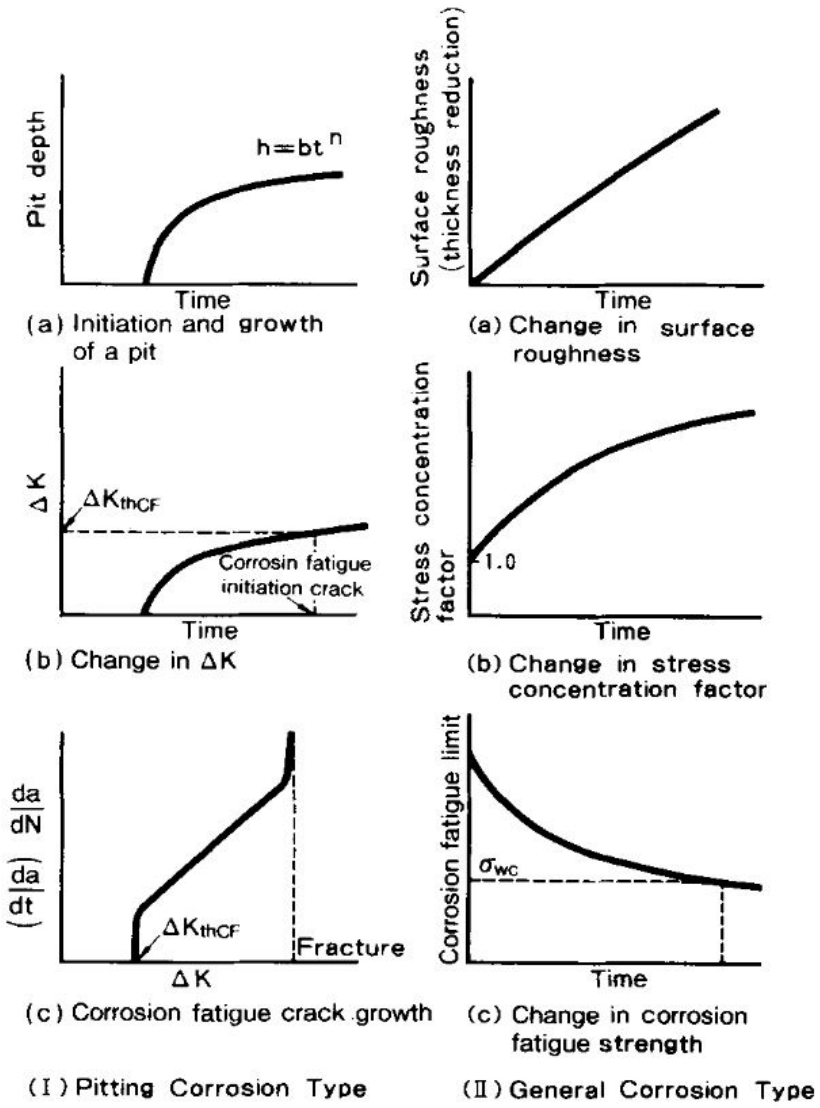

Figure 4.4: Basic concepts to estimate corrosion fatigue compared to general corrosion [75]

In most models of corrosion fatigue, the two terms in Equation 4.2 are treated as separate sequential processes. While a pit is growing, the corrosion process is considered and once a crack has nucleated the crack growth is considered independently of the corrosion process. There are some conceptual variations on this such as the 'competition model' proposed by Kondo [76], which states that a pit will only reach a critical point when a crack from the pit is able to propagate at a faster rate than the material can be corroded. If this is not the case the crack will be overcome by the corrosion and will disappear.

According to the stress intensity factor concept, a crack will not propagate below the threshold stress intensity factor ΔK_{th}. Once it has begun to propagate, the growth of the crack will be governed by different laws depending on the range of stress intensity ΔK [77]. This will also change over time, as the growth of the crack may move the crack from one stage to another as the geometry changes. The changing process is described by Figure 4.5.

The ΔK_{th} value in terms of corrosion pits would be the point known as the critical pit, when a crack initiates from a pit. When the pit is smaller than the critical pit, it does not induce a stress intensity range above ΔK_{th} and so not crack is initiated. Once the pit reaches, or exceeds, the ΔK_{th} value a crack will initiate. The crack will then propagate depending on the stage it is in on Figure 4.5.

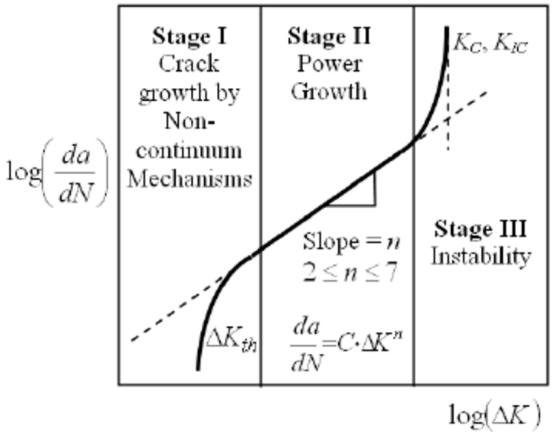

Figure 4.5: Fatigue crack propagation stages, showing the threshold stress intensity factor [78]

In this section three different concepts will be explored.

1. **Different approaches to predicting pit development to the critical pit**
2. **Differences in the definition of the critical pit**
3. **Different approaches to modelling crack growth from a critical pit until failure**

4.2.4 Pit growth models

There are two different ways of conceptualising the pit growth phase of corrosion fatigue. The first is to imagine that the overriding mechanism for pit growth is an electrochemical reaction. This allows the neglecting of any form of the stress element from the pit growth phase. The first model using this approach was published by Hoeppner [79], where he built on the earlier work of Godard [80] and Rowe [81] regarding his assumptions of pit development. The models of Godard and Rowe used in the model can be seen in Equation 4.3 and Equation 4.4:

$$d = C(t)^B \tag{4.3}$$

$$d = bA^2 \tag{4.4}$$

where d is the maximum pit depth, A the area of exposure, t being time and C and B are parameters that relate the material and environmental combination and are calculated experimentally. These equations are very general and would require testing to develop specific values for the parameters in question.

Equations 4.3 and 4.4 do not have any components representing either stress amplitude or stress cycle frequency, representing a complete decoupling of the corrosion and stress processes. This approach has been widely used in corrosion fatigue models [75, 82], with Kawai et al. stating that the B term is almost always in the range of 0.3-0.5 [75], with $\frac{1}{3}$ being commonly used [76]. These models can be used to estimate the time for a particular depth of corrosion pit to develop, allowing an estimation of the N_i term from Equation 4.2, based on a critical pit defined by pit depth. In models based on this type, it is assumed that a crack instantaneously initiates from a pit when it reaches the critical pit condition. The critical pit condition is when a corrosion pit has developed to a point where it induces a SIF greater than the threshold value of the material, thus initiating a crack.

Other models have been suggested that seek to couple the fatigue and corrosion mechanisms at work within pit growth. Some of these involve variations on the general Godard approach shown in Equation 4.3. An example of this is shown in the work of Ishihara et al. [83] where components relating to the stress amplitude and stress cycle frequency are included. In Equation 4.5, d is the maximum pit depth, $A(\sigma_a)$ is a function of the stress amplitude, t is time, f is the stress cyclic frequency and B and C are experimentally determined.

$$d = A(\sigma_a)t^B f^C \tag{4.5}$$

This can be expanded by using the location factor of the extreme value distribution, ν, of the corrosion pits measured experimentally rather than the pit depth d, and substituting the frequency component as the number of cycles divided by time. This led to Equation 4.6:

$$\nu = A'(\sigma_a)t^{B-C}N^C \tag{4.6}$$

In the worked example by Ishihara et al. the stress frequency was found to be small enough to be neglected, as C was found to be an order of magnitude smaller than B. This led to the final equation shown in Equation 4.7:

$$\nu = A'(\sigma_a)t^B \tag{4.7}$$

By substituting $N = ft$, and adjusting for critical parameters, an estimate of the N_i term, was given as shown in Equation 4.8:

$$N_i = \sqrt[B]{\frac{\nu_i f^b}{A'(\sigma_a)}} \tag{4.8}$$

As earlier mentioned an influential model, the 'competition model', was produced by Kondo [76]. Starting at the concept that the opening radius of a corrosion pit c could be expressed by Equation 4.9, where C_p is a correction factor, t is time, N is the number of cycles and f is the frequency. From this the pit growth rate $\frac{dc}{dN}$ can be expressed as shown in Equation 4.10:

$$c = C_p t^{\frac{1}{3}} = C_p \left(\frac{N}{f}\right)^{\frac{1}{3}} \tag{4.9}$$

$$\frac{dc}{dN} = \left(\frac{1}{3}\right) C_p f^{-\frac{1}{3}} N^{-\frac{2}{3}} = \left(\frac{1}{3}\right) C_p^3 f^{-1} c^{-2} \tag{4.10}$$

In his work Kondo gave the range of stress intensity factor (ΔK) as shown in Equation 4.11. . Equations 4.10 and 4.11 can be combined to produce a rate of pit growth relationship, given in Equation 4.12:

$$\Delta K = 2.24\sigma_a \sqrt{\pi c \frac{a}{Q}} \tag{4.11}$$

where σ_a is the stress amplitude, a is the aspect ratio and Q is a shape factor of the pit

$$\frac{dc}{dN} = \left(\frac{1}{3}\right) C_p^3 f^{-1} a^2 \pi^2 Q^{-2} (2.24\sigma_a)^4 \Delta K^{-4} \tag{4.12}$$

The outcome of this competition model is that the growth of corrosion pit slows as they develop, while the crack growth rate accelerates. At a critical point the corrosion is no longer able to outpace the crack growth and the pit initiates a crack. An implication of this is that a pit that does not grow would not initiate a crack.

A separate approach was proposed by Wang et al. [84]. This concept assumed that crack initiation was comprised of two stages: (i) Pit growth; (ii) Fatigue crack initiation.

Based on Wang's approach, the N_i term can be given as a combination of these two processes as shown in Equation 4.13. This accounts for the fact that cracks do not instantly appear when a pit reaches the critical pit condition.

$$\frac{1}{N_i} = \frac{1}{N_i^{fat}} + \frac{1}{N_i^{cor}} \tag{4.13}$$

where N_i^{fat} is the cycles to crack initiation, and N_i^{cor} is the number of cycles for corrosive pit growth.

The pit growth was estimated using an electrochemical approach, which shows that pit size varies with the cube root of time or frequency, as shown in Equation 4.14:

$$a_{pit} = Bt^{\frac{1}{3}} = B(\frac{N_i^{cor}}{f})^{\frac{1}{3}} \tag{4.14}$$

where a_{pit} is the radius of the pit, B is a constant that depends on the environment and material situation and f is the frequency of the stress cycle. The value of B can be given as shown in Equation 4.15 [85]:

$$B = \left(\frac{3MI_p}{2\pi nF\rho \exp^{\frac{\Delta H}{RT}}} \right) \tag{4.15}$$

where M is the molecular weight of the material, I_p is the pitting current coefficient, n is the valence, F is the Faraday's constant, ρ denotes the density, ΔH is the activation energy, R is the Universal gas constant and T is the absolute temperature. Equations 4.14 and 4.15 can then be combined and rearranged to produce an expression for N_i^{cor}, given in Equation 4.16.

$$N_i^{cor} = \frac{a^3 f 2\pi F\rho \exp^{\frac{\Delta H}{RT}}}{eMI_p} \tag{4.16}$$

The N_i^{fat} term must then be calculated. Wang et al. used a dislocation model suggested by Mura and Nakasone which is shown in Equation 4.17:

$$N_i^{fat} = \frac{AW_s}{(\Delta\tau - 2\tau_f)^2} \tag{4.17}$$

where W_s is the specific fracture energy, $\Delta\tau$ is the range of local shear stress, and τ_f is the friction stress that needs to be overcome to allow the dislocations to move. A is a function depending on the materials properties and the type of initial cracks.

A is different in different situations [86]. The different options are detailed in Equation 4.18:

$$A = \begin{cases} \frac{4G}{\pi(1-\nu)l} & \text{crack initiates along slip bands} \\ \frac{2G}{l} & \text{crack initiates along grain boundary} \\ \frac{4G(G+G_i)h^2}{G_i(h+l)^2 a_i} & \text{crack initiates along interface of inclusions (pitting)} \end{cases} \tag{4.18}$$

where G is the bulk shear modulus, G_i is the shear modulus of inclusion (pitting), l is the semi length of the slip band, h is the semi minor length of the elliptical slip band area and ν is the Poisson's ratio.

Two further assumptions were then made. First using the Mura and Nakasone approach that the frictional stress, τ_f, is half of the fatigue limit and second that the von Mises yield criteria applies.

Assuming that the frictional stress, τ_f, is half of the fatigue limit, means that no crack can initiate if the stress is lower than twice the frictional stress. The physical interpretation of the von Mises yeild criteria is that yielding occurs when the resolved shear stress on the octahedral plane exceeds the octahedral shear strength τ_0. These led to Equation 4.19 and Equation 4.20:

$$\Delta\tau = \left(\sqrt{\frac{2}{3}}\right)\Delta\sigma \tag{4.19}$$

$$\tau_f = 0.5\left(\sqrt{\frac{2}{3}}\right)\sigma_D^R \tag{4.20}$$

where σ_D^R is the fatigue limit of the material at a stress ratio R.

The fracture energy can be obtained using Equation 4.21:

$$W_s = \frac{\Delta K_{th}^2}{E} \tag{4.21}$$

These equations can then be combined to produce an expression for N_i^{fat}. By combining the expressions for N_i^{fat} and N_i^{cor} as shown in Equation 4.13, an expression for N_i can be produced. This is shown in Equation 4.22:

$$\frac{1}{N_i} = \frac{1}{N_i^{fat}} + \frac{1}{N_i^{cor}} = \frac{(\Delta\sigma - \Delta\sigma_D^R)^2 E G_i (h+l)^2 a_0}{18G\Delta K_{th}^2 (G+G_i)h^2} + \frac{3MI_p}{2\pi n f F \rho (a_i^3 - a_0^3)\exp^{\frac{\Delta H}{RT}}} \tag{4.22}$$

The complexity of Equation 4.22 demonstrates the challenges of modelling corrosion pit crack initiation. Equation 4.22 also represents only half the total process of predicting the failure of a component as the crack growth phase also needs to be considered. In many applications some of the terms in Equation 4.22 would be difficult if not impossible to define, limiting application in an industrial setting.

An alternative model for pit growth was later suggested by Sriraman [87], based on the corrosion approach of Wang et al. [84], although it does not include the fatigue element in the corrosion process. Based on the relationship defined by Kondo [76] and given in Equation 4.14, the value of B was calculated using Faraday's law, given in Equation 4.23. Where the pitting current I_p can be expressed as shown in Equation 4.24.

$$B = \left(\frac{3MI_p}{2\pi nF\rho}\right)^{\frac{1}{3}} \tag{4.23}$$

$$I_p = I_{p0} \exp^{\frac{-\Delta H}{RT}} \tag{4.24}$$

The next stage used the work of Ishihara et al. [83], who demonstrated that the pit depth was related to the stress amplitude by the equation $depth \propto K^{\sigma_a}$. The value of K was set at 1.01, as it must be greater than one to contribute to pit growth and was similar to the 1.014 found by Ishihara.

By incorporating this relationship into Kondos relationship between time and pit depth, Faraday's law and substituting time as number of cycles divided by the cycles frequency, an expression for the number of cycles required to reach a defined depth can be produced. This expression is given in Equation 4.25 where N is the number of cycles to a set pit size. It can be converted to the N_i term by using the critical pit depth parameter.

$$N = \frac{2\pi nF\rho}{3M}(f)(A_p^3)) \left(\frac{1}{I_p}\right) \left(\frac{1}{1.01^{\sigma_a}}\right)^3 \tag{4.25}$$

The models presented in this review were not directly applicable to the rail axle scenario that is being studied by this project. Many were calculated using empirical results for aluminium, as the main thrust behind this field appeared to be from the aerospace industry. However, they appear to demonstrate the cutting edge approaches to corrosion pit development over time, and seem more advanced than the current techniques being used in the rail industry.

4.2.5 Definitions of critical pits

The previous section dealt with the various proposed ways of modelling the initiation and growth of corrosion pits over time. The point at which the corrosion feature causes a crack to initiate can be said that the pit has become critical. This is defined based on the stress intensity factor from the pit, following various assumptions about appropriate ways to simplify its geometry and how to approach modelling them.

In the early work by Hoeppner [79] the pit was assumed to be a half penny crack with and aspect ratio of $\frac{a}{2c}$. This produces a definition of the critical pit shown in Equation 4.26, that would form a crack. In this model, it is assumed that the pit initiates instantly upon the pit reaching criticality.

$$\Delta K_{th} \geq K_{si} = 1.1\sigma_a\sqrt{\pi(\frac{a}{Q})} \tag{4.26}$$

where K_{si} is the stress intensity factor, σ_a is the applied stress, a is the size of the flaw and Q is a function linking the size of the pit and the tensile yield stress.

A later paper by Lindly [82] built upon this approach by suggesting a different critical pit, modelling the pit as a semi-elliptical crack in a semi-infinite plate, as shown in Figure 4.6 with the same $\frac{a}{2c}$ shape as Hoeppner. The equation is derived from Irwin's solution for an elliptical crack in an infinite plate and can be seen in Equation 4.27.

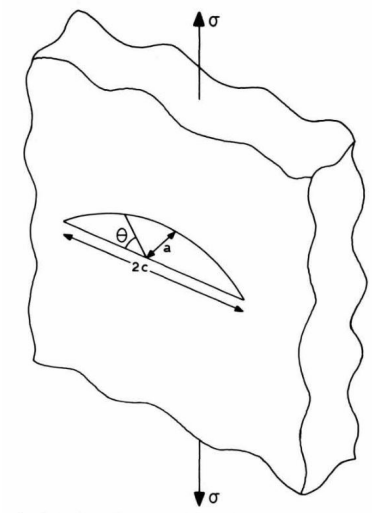

Figure 4.6: Assumptions of the critical pit geometry used by Lindley [82]

$$\Delta K_0 = \frac{\Delta\sigma_{lim}\sqrt{(\pi a)(1.13 - 0.07\left(\frac{a}{c}\right)^{\frac{1}{2}})}}{\left(1 + 1.47\left(\frac{a}{c}\right)^{1.64}\right)^{\frac{1}{2}}} \tag{4.27}$$

$\Delta\sigma_{lim}$ is the overall surface stress range at the fatigue limit. In the paper, it is stated that this could not be applied on pits 40µm deep or less, as the LEFM assumptions it relies on break down. Both of these equations were based on work with an aluminium alloy.

A set of critical pit criteria were suggested by Kawai and Kari [75] and can be seen in Equation 4.28. The pit was assumed to be a long crack that obeys standard crack laws.

$$\begin{cases} \Delta\sigma_{all} = \frac{\Delta K_{all}}{F\sqrt{\pi h_{max}}} & (R > 0) \\ \sigma_{max,all} = \frac{K_{all}}{F\sqrt{\pi h_{max}}} & (R \leq 0)) \end{cases} \tag{4.28}$$

where $\Delta\sigma_{all}$ is the allowable stress range for $R > 0$, ΔK_{all} is the threshold stress intensity factor range in corrosive environments for $R > 0$, F is a correction factor and h_{max} was the maximum pit depth. $\sigma_{max,all}$ is the allowable maximum stress for $R \leq 0$ and K_{all} was the allowable value of threshold stress intensity factor in corrosive environments for $R \leq 0$.

Several models, including Ishihara [83] used the $\sqrt{Area}$ parameter suggested by Murakami [88] to evaluate the stress intensity factor of a crack with an irregular shape. This is calculated by evaluating the 2D shadow of the irregular feature.

Ishihara assumed the pit could be modelled as a crack, with the experimental results produced by fracturing corroded surfaces and evaluating the area using image processing software. According to Murakami the critical stress intensity factor can be given by Equation 4.29 with $K_{p\to c}$ being the stress intensity factor for crack initiation and σ_a is the stress amplitude.

$$K_{p\to c} = 0.65\sigma_a\sqrt{\pi\sqrt{(Area)_{p\to c}}} \tag{4.29}$$

Other models [84, 87] assumed pits were hemi-spherical pits in a semi-infinite plate, using the same stress intensity factor approach. This critical pit criteria can be seen in Equation 4.30:

$$\Delta K = \left(\frac{2.2}{\pi}\right) K_t \Delta\sigma\sqrt{\pi a_p} \tag{4.30}$$

where $\Delta\sigma$ is the stress range and K_t is the stress concentration factor from a circular rivet hole.

Using the critical pit criteria and the pit depth expression shown in Equation 4.25, the critical depth of a pit for spontaneous initiation can be written as shown in Equation 4.31:

$$a_{pc} = \pi \left(\frac{\Delta K_{th}}{4.4 K_t \sigma_a} \right)^2 \tag{4.31}$$

A slightly different approach was used in the Electric Power Research Institute fatigue prediction methodology project [89, 90]. The same LEFM approach is taken, however the concept of intrinsic crack length suggested by El Haddad et al. was used [70]. This is useful to account for the short crack behaviours that would be present at the moment of crack initiation. The estimate for the threshold stress intensity factor for short cracks is given in Equation 4.32. With the value of the intrinsic crack calculated using Equation 4.33:

$$\Delta K_{th,pits} = \frac{\Delta K_{th}}{\sqrt{1 + \frac{c}{c_0}}} \tag{4.32}$$

$$c_0 = \frac{1}{\pi} \left(\frac{\Delta K_{th} Y}{\Delta \sigma_{FL}} \right)^2 \tag{4.33}$$

All of the models here used fundamentally the same approach, with the LEFM methodology used to produce an estimated critical pit criteria. Any variations are almost always due to variations in the assumptions used to simplify the pits.

4.2.6 Crack growth models

All of the models considered the crack propagation stage in the general terms of the Paris crack law, shown in Equation 4.34. This is a popular law that describes the rate of crack growth in a fatigue crack. It holds over the mid range of stress intensities and has been observed to be non-conservative for small cracks. Some models used this directly to approximate the number of cycles to failure [79].

$$\frac{da}{dN} = C \Delta K^m \tag{4.34}$$

The Paris law has been subject to some small variations with different models, many of which involve dividing the short and long crack behaviours of the initiated pit [84, 87, 91]. These models tended to be aware of the law being non-applicable for short cracks but use this approach due to its simplicity and long history of use.

Sriraman [87] used an approach built on the work of Wang et al. [84]. This approach worked by treating the pit as a semi-circular surface flaw until the crack reaches the long crack regime, where it is then treated as a through crack. Both conditions are governed by a stress intensity factor range given by Equation 4.35, where β is $\frac{2.2}{\pi}$ for the semi-circular surface flaw (β_1), and is 1 for the through crack assumption (β_2), $\Delta\sigma$ is the applied stress at the pit and a is the crack length.

$$\Delta K = \beta K_t \Delta\sigma \sqrt{\pi a} \tag{4.35}$$

The crack growth life (N_p) was then calculated by summing the cycles in the long and short crack regime (denoted by the subscript sc). This can be seen in Equation 4.36. Where the first term is the short crack regime and the second is the long crack regime, with the value a_{sc} can be considered the transitional length of the crack between the two:

$$N_p = \frac{a_{pit_{cr}}^{(1-n/2)} - a_{sc}^{(1-n/2)}}{C\Delta\sigma^n \beta_1^n K_t^n \pi^{n/2}(n/2-1)} + \frac{a_{sc}^{(1-n/2)} - a_f^{(1-n/2)}}{C\Delta\sigma^n \beta_2^n K_t^n \pi^{n/2}(n/2-1)} \tag{4.36}$$

Sriraman suggested an expression for the final critical crack length a_f that signifies failure when R=-1 which is given in Equation 4.37, based on the stress amplitude σ_a and the material fracture toughness K_c.

$$a_f = \frac{1}{\pi}\left(\frac{K_c}{1.12\sigma_a}\right)^2 \tag{4.37}$$

Fatigue approach

A separate approach, that uses a more general view of the stress intensity factors from a crack under fatigue, was based the work of El Haddad [70], following the approach to cracks of arbitrary dimensions produced by Murakami et al. [92, 93]. In this methodology the stress intensity factor of a crack was defined as being equal to Equation 4.38:

$$\Delta K = Y\sigma_a \sqrt{\pi\sqrt{Area_{eff}}} \tag{4.38}$$

where Y is 0.65 for surface defects and 0.5 for internal defects [94].

In this case the $\sqrt{Area_{eff}}$ is the square root of the projected area perpendicular to the loading direction, demonstrated in Figure 4.7. This approach, while producing a similar result to the other equations, is a more flexible and adaptable, although does implicitly smooth the geometry either by the use of the whole pit projection rather than a slice or the lack of any secondary geometrical parameters to govern the variations that are collapsed into a single area value.

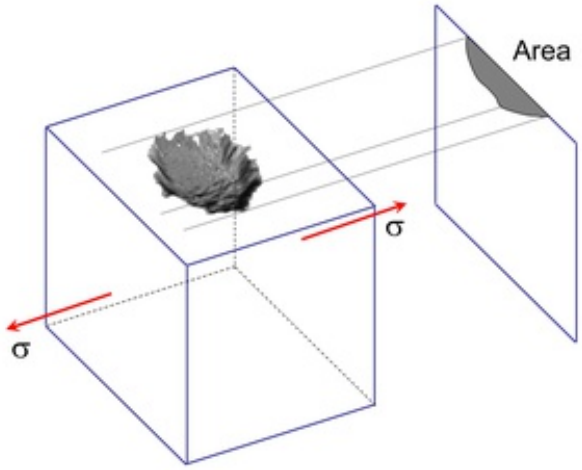

Figure 4.7: Definition of the $\sqrt{Area_{eff}}$ for Murakami approach [95]

4.2.7 Conclusions

The conclusion of the review of available literature was that this area is a highly complex one. Many different approaches and rationales had been used to try to predict the corrosion-to-failure process, but none seemed to have been accepted as a defining approach. This suggests that this area still requires work to fully define the very complex interplay of factors.

The focus of the stress intensity factor approach in the past has been on cracks, defined by their very thin width compared to their depth. Some works assume that cracks have infinitely sharp tips, while others assume rounded ends. There are also generalised equations for different shapes of cracks, for example semi-elliptical cracks. The aim is often to predict the growth behaviours of pre-existing cracks, rather than the conditions that initiate the cracks themselves.

The most popular method for assessing crack initiation from corrosion pits, the focus of this work, was a fracture mechanics approach based on the concept of the critical pit. This method often treated the pit as a semi-elliptical crack and calculated the threshold value at which this crack would propagate. This approach was taken forward by the following work, particularly informed by the work of Ishihara [83] and El Haddad [70] as well as the principles of Hoeppner [79].

The crack analogy approach did have its drawbacks. With combined models for corrosion fatigue, the corrosion pit was commonly assumed to act like a crack, as discussed in Section 4.2.5. This meant that when the pit (a three dimensional geometry) reached critical parameters for cracks (fundamentally two dimensional geometries), such as depth or $\sqrt{Area}$, that produced stress intensity values that would lead to crack propagation, it was assumed a crack is immediately initiated. This meant that the geometry had been collapsed from a three to two dimensional shape, with the increased cracking risk that this produced, and that any time required for a crack to initiate once the critical values have been met has been ignored.

To help address this problem, the separate El Haddad approach [70] was also taken forward. This approach was more heavily focused on the fatigue side of the problem and had been developed specifically for surface defects in three dimensions, such as corrosion pits, rather than applying work produced for two dimensional cracks to corrosion pits. However, by summarising a pit as a single numerical value, $\sqrt{Area}$, it arguably made larger assumptions about the shape of the pit than the multi-parameter crack analogy approach.

In summary, due to the strengths and weaknesses of the two analytical approaches found in literature; crack analogy and El Haddad, both were taken forward to analyse the identified pits. By using both, the results of each could be compared and contrasted to achieve as well rounded an analysis as possible to inform the final conclusions.

4.3 Stress intensity factors from observed pit geometries

Initially the rail axle needed to be assessed from a fracture mechanics mindset. This meant defining the loading scenario of the axles and the limitations of the material.

4.3.1 Fracture mechanics definition of the rail axle

Modes of loading

A rail axle body can be considered a cylindrical bar, which has no features, if any potential damage is excluded, and the area of interest is away from any transitional areas. An axle body was assumed to have an illustrative diameter of around 200mm.

The loading of a rail axle is complex, and will depend on many factors. In an axle, there will be a bending component and a torsional component to the stress. This will depend on many predictable factors that are covered in the design standard [15] , such as the loading of the axle, cornering and the effects of secondary attached components such as brakes or the power train. There will also be other, unpredictable factors such as the effect of any defects (polygonalised wheels for example) or generic track defects. These unpredictable factors, combined with unknown variations in predictable factors such as routes or loads, make the perfect expression of the rail axle loading condition problematic.

The axle loading in this section will be considered as fully reversed loading, with constant amplitude. This would be the equivalent of the axle running straight, in ideal conditions with a non-varying load. In this scenario the axle would undergo rotating bending under torsion that would influence how the stress intensity factors would be calculated. However, to simplify the problem and to lower the number of calculations required, this section will consider the loading to be fully reversed tensile loading of a pit in a plate.

The problem is suitable to be simplified in this way due to the difference in sizes between the pits being considered and axles they originate on. The maximum depth of a pit that has been found in the survey of axle corrosion in Chapter 3, was 342.6μm. When compared to the diameter of an axle at approximately 200,000μm, the ratio between the size of the defect and the axle is approximately 0.0017. Other papers that consider the effect of bending separate to reversed tensile loading cycles use ratio values around two orders of magnitude larger [96] suggesting that tensile cycles are an appropriate approximation in this context.

At this small scale, on the surface of the axle, the pit is effectively undergoing a tensile-compressive load, and the effect of the bending will be minimal, with most of the effects being captured by the axially applied stress. This is demonstrated in Figure4.8.

The difference in stress along the depth of the pit, due to bending, was also ignored as the pits were small compared the radius of the axle, that the variation is around 1% per mm depth. Given that even for the deepest pit the difference in stress would only be 0.34% it was decided that this would not have a significant effect on the result.

The approaches found in literature to define mode III (tearing) of a semi-elliptical crack seem to be performed numerically with finite element methods. This approach was not possible in this case due to the limitations of the data collection as discussed in an earlier section, with the presence of multiple singularities making it impossible to achieve reliable results. To this end, mode III was ignored in this study with the following justification.

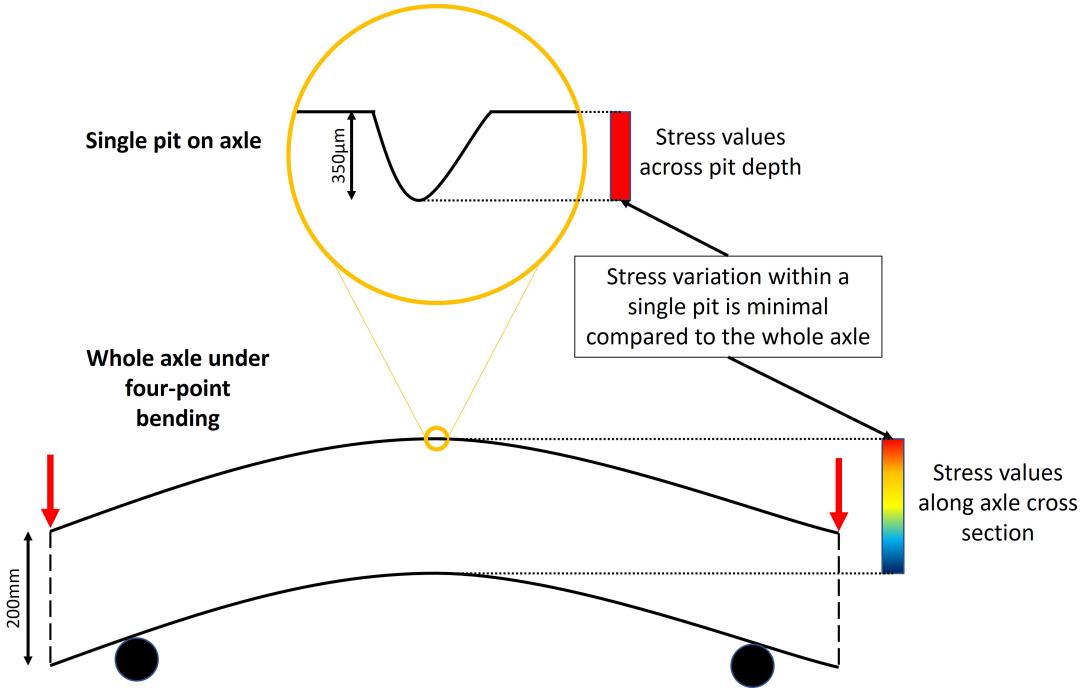

Figure 4.8: Schematic diagram demonstrating the justification of using tensile loading to replicate bending of rail axles with regards to corrosion pits

The different modes can be combined to produce an equivalent range of stress intensity factors, using the the addition of Irwin's energy release rate G. This is expressed in Equation 4.39 [96]:

$$\Delta K_{eq} = (G_{Total}E)^{\frac{1}{2}} = \left\{\Delta K_I^2 + \Delta K_{II}^2 + (1+\nu)\Delta K_{III}^2\right\}^{\frac{1}{2}} \tag{4.39}$$

The design standard [15], mentions that the torsional stress is an order of magnitude lower than that of the bending stress (this concurs with an example calculation carried out in Chapter 5). Making the assumption the value of ΔK_I and ΔK_{III} are both proportional to the stress that would cause each stress intensity value, then the rough assumption shown in Equation 4.40 is made.

$$\Delta K_{III} \approx 0.1\Delta K_I \tag{4.40}$$

This assumption, combined with a negligible mode II value and an approximate Poisson ratio of 0.3, applied to Equation 4.39 would lead to the following statement in Equation 4.41 and Equation 4.42. This demonstrates that the inclusion of the mode III value would have a small, approximately 0.6%, effect on the final value.

$$\Delta K_{eq} = \left\{\Delta K_I^2 + (1+0.3)(0.1\Delta K_I)^2\right\}^{\frac{1}{2}} \tag{4.41}$$

$$\Delta K_{eq} = 1.006 \Delta K_I \tag{4.42}$$

Based on this the final result will be calculated only accounting for the mode I results. Although it is acknowledged that other modes will be present and contribute to the risk of crack initiation. It is hoped that as the use of the crack assumption being an over estimate of the risk will mitigate the lack of the extra modes alongside the conservative assumptions made throughout.

Fracture mechanics limits of the material

A key parameter to define the chance of long cracks propagating under fatigue is the threshold stress intensity factor ΔK_{th} of the material. The general assumption is that below this factor, the crack will not propagate, or will propagate extremely slowly [71]. However, this value is dependent on the stress ratio R. A series of experiments was undertaken on the EA1N rail axle steel to determine the threshold value under different conditions [97], the results can be seen in Figure 4.9.

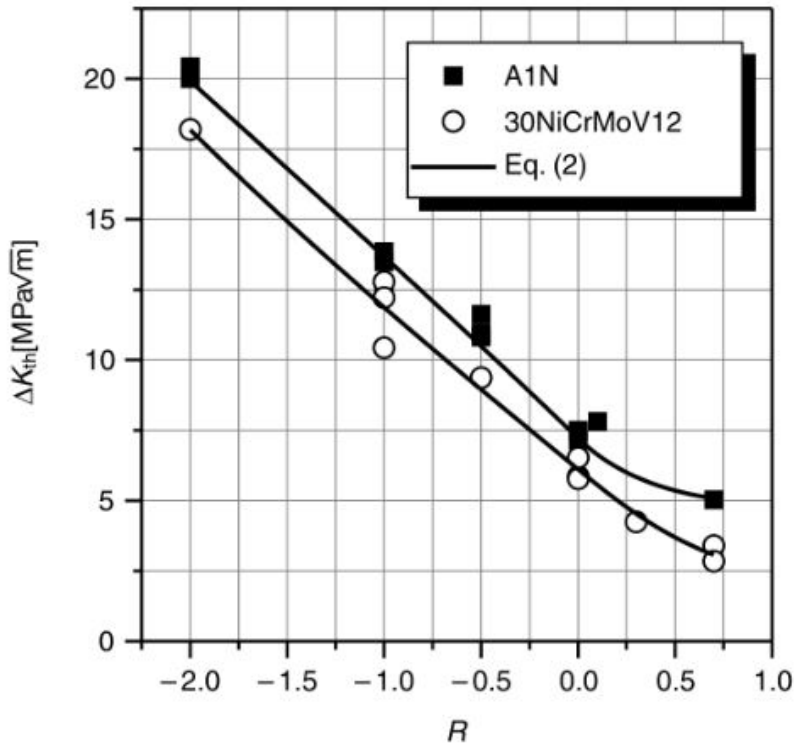

Figure 4.9: Experimental values for ΔK_{th} of EA1N steel for different R values [97]

The average of these values was found to be 7.23 $MPa\sqrt{m}$, which was used by Beretta and is similar to the values found in other papers. However, the stress ratio of a rail axle will be close to, if not exactly, R=-1. Based on Figure 4.9 this places the ΔK_{th} value at above 13 $MPa\sqrt{m}$.

4.3.2 Calculation approaches

Having consulted the literature, the best approximation of a corrosion pit to a crack was likely to be a semi-elliptical surface crack. The relationship to the pit geometry can be achieved by collapsing the dimensions from three to two in a similar way to that used in other studies, by assuming that the pit can be described sufficiently by using the diameter of the pit at the surface and the maximum depth.

While this was not ideal, as it still requires the simplification of a three dimensional shape to a two dimensional crack, it does still have advantages over other studies in the field. For example, in the analysis of the survey results presented in Chapter 3, each pit was given two diameters, based on the bounding rectangle identified. This allows for the two different cracks to be considered separately due to the different geometries.

Another advantage was that in collecting the whole surface, it was possible to be certain that the deepest point had been found. In previous studies, especially over those using sectioning techniques, it was not possible to ensure that the deepest point of each pit had been found.

After looking at the results of the survey carried out in Chapter 3, it could be seen that (depending on the definition of aspect ratio used) between 98.2% and 87.7% of all pits observed had an aspect ratio of below one. This meant that for the vast majority of the pits the analogous cracks could be considered shallow and expressed using equations that were limited to aspect ratios of below one.

While the following equations deal with the pit under static loading, this was necessary to calculate the range (from minimum to maximum) of stress concentration factors that the pit would undergo during the cycle.

Mode I

In this section the pit terms will be defined using the terms seen in Figure 4.10.

There were several equations to describe the mode I stress intensity factor of semi-elliptical, shallow, pits. One of these equations is given in Equation 4.43 [71], for a semi-elliptical crack in tension in a finite plate with an aspect ratio less than or equal to one:

$$K_I = C\frac{\sigma\sqrt{\pi a}}{\Phi}(sin^2\theta + \frac{a^2}{c^2}cos^2\theta)^{\frac{1}{4}} \tag{4.43}$$

where:

$$\Phi = \frac{3\pi}{8} + \frac{\pi}{8}\frac{a^2}{c^2} \tag{4.44}$$

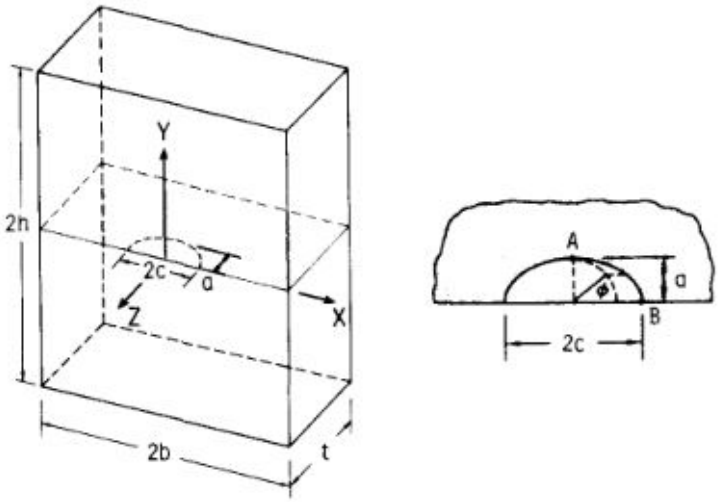

Figure 4.10: Terms regarding cracks used in this section [98]

$$C = 1.12 \ \textit{for shallow cracks} \tag{4.45}$$

This was a simple commonly used equation for small shallow cracks [71]. There are several other equations that also provide an estimate of the stress intensity factor of a semi-elliptical surface crack in tension [71, 77], however, there does not appear to be an equivalent simple equation for the case of a crack with an aspect ratio above one.

To achieve a consistent estimate of the simulated cracks, including both high and low aspect ratio cracks, the work of Newman and Raju was used [98]. Their work consists of a series of equations that describe the stress intensity factor of various cracks, based on fitting to empirical data from finite element analysis. These equations were laid out more clearly in a later paper that used their work [99]. For a surface crack, these equations hold for all the crack depths and aspect ratios between zero and two.

For both the high and low aspect ratio cases the stress intensity factor for a semi-elliptical surface crack uses the base equation seen in Equation 4.46, where Q is the shape factor for an ellipse, that can be defined differently for each case. These can be seen in Equation 4.47 and Equation 4.48:

$$K = \sigma \sqrt{\frac{\pi a}{Q}} F \tag{4.46}$$

For $0 \geq \frac{a}{c} \leq 1$:

$$Q = 1 + 1.464 \left(\frac{a}{c}\right)^{1.65} \tag{4.47}$$

For $1 < \frac{a}{c} \leq 2$:

$$Q = 1 + 1.464 \left(\frac{c}{a}\right)^{1.65} \tag{4.48}$$

The F term in Equation 4.46 is a function of the aspect ratio, relative crack depth compared to the thickness of the component and the position being inspected on the crack front. The F term can be described by Equation 4.49:

$$F = \left[M_1 + M_2 \left(\frac{a}{t}\right)^2 + M_3 \left(\frac{a}{t}\right)^4\right] g f_\phi \tag{4.49}$$

The parameters for this equation, M_1, M_2, M_3, g and f_ϕ, are calculated differently for each case.

For $0 \leq \frac{a}{c} \leq 1$:

$$M_1 = 1.13 - 0.09 \left(\frac{a}{c}\right) \tag{4.50}$$

$$M_2 = -0.54 + \frac{0.89}{0.2 + \left(\frac{a}{c}\right)} \tag{4.51}$$

$$M_3 = 0.5 - \frac{1}{0.65 + \left(\frac{a}{c}\right)} + 14 \left[1 - \left(\frac{a}{c}\right)\right]^{24} \tag{4.52}$$

$$g = 1 + \left[0.1 + 0.35 \left(\frac{a}{t}\right)^2\right] (1 - sin\phi)^2 \tag{4.53}$$

$$f_\phi = \left[\left(\frac{a}{c}\right)^2 cos^2\phi + sin^2\phi\right]^{\frac{1}{4}} \tag{4.54}$$

For $1 < \frac{a}{c} \leq 2$:

$$M_1 = \left(\frac{c}{a}\right)^{\frac{1}{2}} \left[1 + 0.04 \left(\frac{c}{a}\right)\right] \tag{4.55}$$

$$M_2 = 0.2 \left(\frac{c}{a}\right)^4 \tag{4.56}$$

$$M_3 = -0.11 \left(\frac{c}{a}\right)^4 \tag{4.57}$$

$$g = 1 + \left[0.1 + 0.35\left(\frac{c}{a}\right)\left(\frac{a}{t}\right)^2\right](1 - sin\phi)^2 \tag{4.58}$$

$$f_\phi = \left[\left(\frac{c}{a}\right)^2 sin^2\phi + cos^2\phi\right]^{\frac{1}{4}} \tag{4.59}$$

These equations were used to calculate the maximum stress intensity factors of the analogous cracks of pits, up to and including an aspect ratio of two. The accuracy in the case of a crack below an aspect ratio of one has been found to be better than 3% compared to the finite element results and in the case of an aspect ratio between one and two better than 2% [100].

It was not possible to find a convincing technique to analytically calculate the stress intensity factors of pits with a higher aspect ratio. Based on comments in other papers [101], and not finding any suitable equation in the literature, this is an area that is known to require more research.

One of the issues with all of these equations, was that they were designed for static calculation of the stress intensity factor of a crack under tension. When transferring this methodology to that of the fatigue scenario for a crack, the range between the maximum and the minimum can be taken, even when transferring into a compression state. This is because it can be assumed that a thin crack in compression is unlikely to propagate without any other external factors. This is a reasonable assumption for a crack, however is less likely to hold for a corrosion pit.

The corrosion pit is a three dimensional feature rather than a two dimensional feature. For a crack in compression the two faces of the crack would meet and then most of the movement would be stopped. However, this would not be the case in a corrosion pit, where there would be no similar crack closure. This requires an assessment of the risk from the mode I fracture load in compression. However, no suitable way of performing this has been identified. It appears that in most literature that the R value is set as positive, or the effect of the compressive part of the cycle is ignore and assumed to be significantly smaller than that during the tensile section.

4.3.3 Application of equations to collected data

For the identified equations there were several different approaches to generate the input terms. These may or may not have a significant impact on most pits, and mostly derive from the idealised nature of the initial derivation process.

For example, the two main terms in most equations are the depth of the pit and the radius or diameter at the surface. When using idealised pits or cracks to simplify corrosion pits, values for maximum depth and radius are easy to identify and lie, by definition, in the same plane as each other. This has not been an issue in previous attempts to apply this methodology to corrosion pits, as the inspection regimes have been viewing planes, or have assumed ideal "bowl shaped" pits. This leads to the deepest measured point and the measured radii to lie on the same plane making extraction of the parameters trivial.

Using the three dimensional data collected in the survey, presented in Chapter 3, this assumption does not necessarily hold. This can be demonstrated in Figure 4.11. As shown in this Figure the deepest point does not lie on the same plane as the maximum surface diameter in any orientation. This leads to different interpretations of the input parameters to the equations, that will change the value of the stress intensity values calculated and possibly lead to significantly different conclusions. The different interpretations can be seen in Figure 4.12.

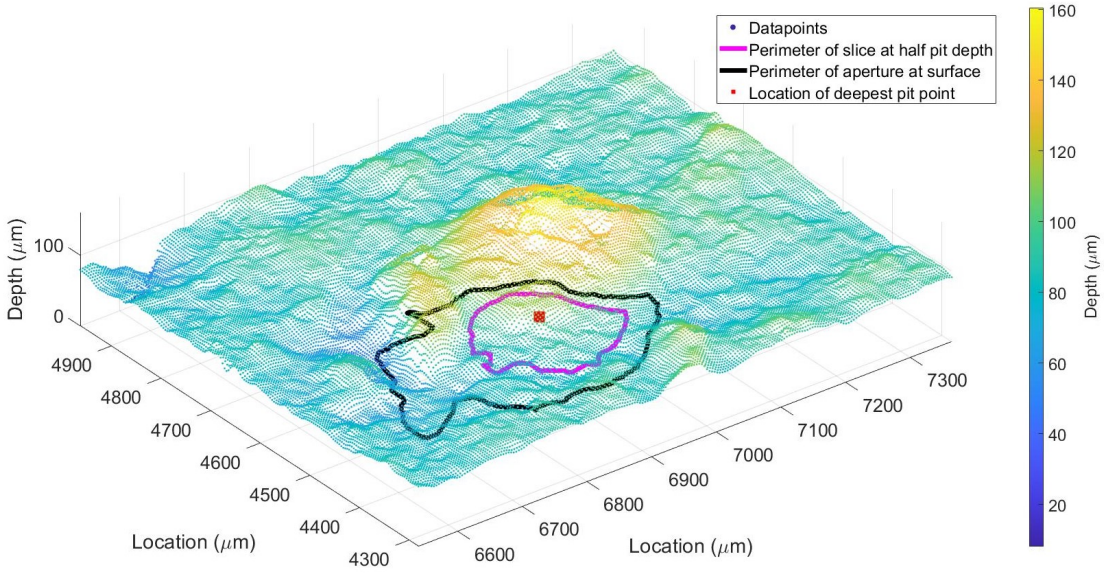

Figure 4.11: Scatter plot of Pit 11, showing the detected edge of the pit, the perimeter at half pit depth, and the deepest point, projected onto the XY plane

The first option was to take the maximum calculated values for each parameter, ignoring the alignment of points in question. This has the benefit of simplicity as the absolute values are easier to measure than the values by planer position. However, as the maximum depth is fixed, in many cases using the largest diameter will result in a lower aspect ratio, that will likely give a lower stress intensity factor and possibly non-conservative conclusions. This approach was used in Chapter 3 to produce the headline results of the survey. In some cases, due to irregular shapes of coalescing pits, extremely large values for the bounding diameter could be produced leading to unrealistic outcomes.

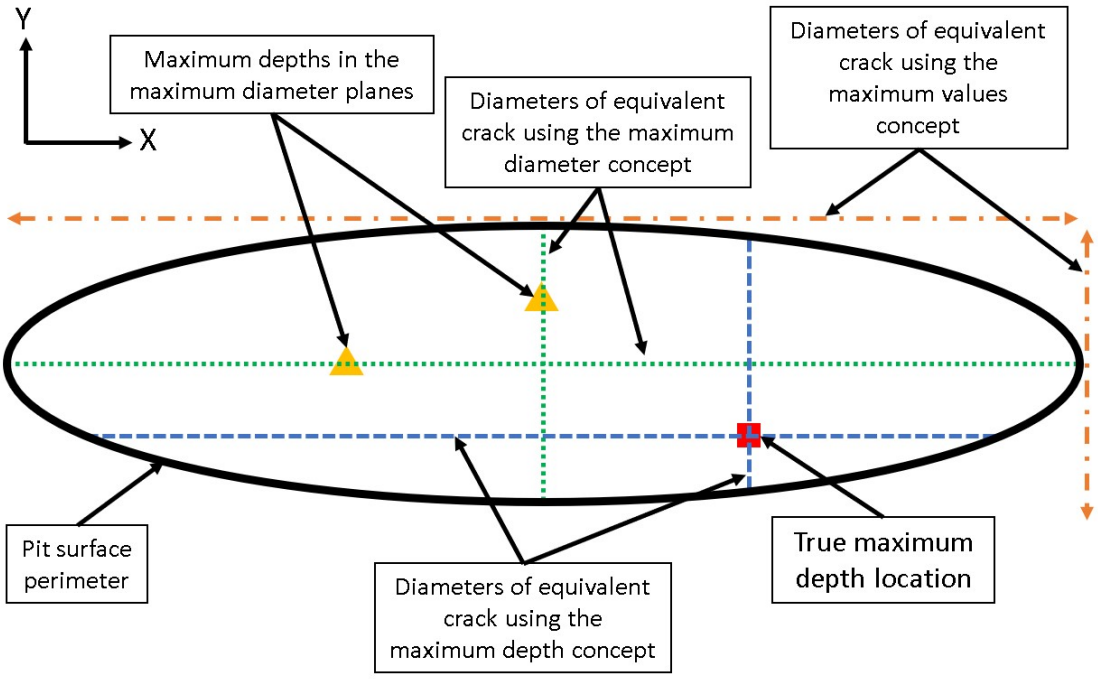

Concept used	Diameter used	Depth used	Aspect ratio
Maximum values	Maximum diameter	Maximum depth	Middle
Maximum depth	Diameter through maximum depth point	Maximum depth	Maximum
Maximum diameter	Maximum diameter	Maximum depth on maximum diameter plane	Minimum

Figure 4.12: Schematic diagram of the different parameter definitions for corrosion pits, with the implications on the reported aspect ratio of a pit

Another option was to draw a plane through the lowest point of the pit, perpendicular to the axis of loading, and take the diameter of the opening in this plane as the input radius. This would often give a smaller radius than the maximum measured, and so a thinner crack with a higher aspect ratio. This would result in higher values of the stress intensity factor than by using other techniques. This is likely to produce the most conservative values.

The final solution would be to use a plane through the maximum diameter of the pit, along a plane that lies perpendicular to the direction of loading, and use the deepest point in this plane. This would lead to low estimates of the stress intensity factors, as the pit would likely be of a significantly lower aspect ratio, than calculated by other measures. However this approach is often used by techniques that look at the surface aperture of pits.

In this study all of these techniques were used, to compare the values calculated from each. This produced a range of values and allowed the assessment of the accuracy of different sets of assumptions against the ability to use these techniques in a depot setting.

4.3.4 Parameter collection

To summarise, four different approaches were used to collect the input parameters for the stress intensity factor equations. The input parameters required were; pit depth, pit diameter and projected pit area. The exact values used for a single pit varied depending on the approach used.

It should be noted that as the samples were taken such that the scans were always either axial or radial to the axle but the direction for each sample was not recorded. This means that it was known that the direction perpendicular to loading was either in the X or Y direction, but not which it was. This meant that the calculation would have to be performed separately for each direction.

1. **Maximum Values** Using the maximum depth and diameter values of the pits. This was achieved by using the results observed in Chapter 3.
2. **Maximum depth plane** This required a slice to be taken in the X and Y planes through the deepest point of the pit. The diameter in these planes could then be easily measured.
3. **Maximum diameter plane** The maximum distance between the edges of the pit in the X and Y planes was identified. A slice was then produced from these planes and the deepest point on the plane measured. Note that the deepest point in the X or Y plane were highly likely to be different, potentially significantly.
4. **Projected area** The projected area in the X and Y direction was produced. This approach captured the whole projected profile, rather than a slice as was used in other methods.

The results were collected using MATLAB code to interrogate the results collected in the survey. It should be noted that the points included in these calculations were the ones initially identified through image processing. The boundary areas added later were not included.

An example pit can be seen in Figure 4.13, and will be used as an example for the process of extracting the input parameters in this section.

The first values to be calculated were using the maximum depth plane. These were easy to define, as it was known that the direction of tensile stress would be in either the X or Y directions. Once the location of the deepest point was defined the profile in the X and Y planes from this point were captured. This can be seen in Figure 4.14.

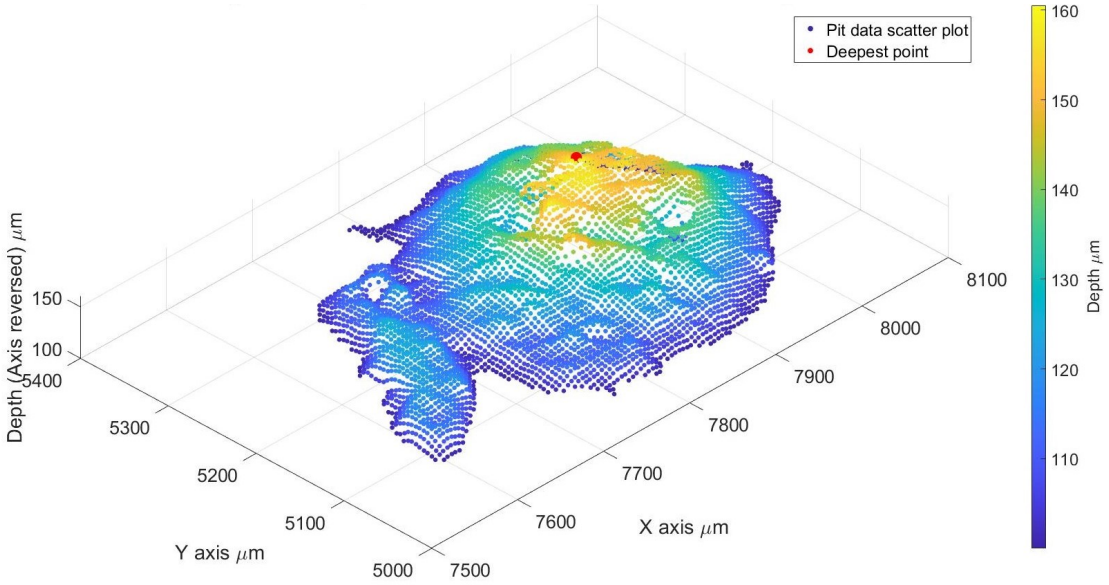

Figure 4.13: Scatter plot of the detected data points of pit 11 without additional boundary and with the deepest point marked

The deepest point is marked in all the plots and the locations of the profiles are marked on the scatter plot. The diameter of the pit through these planes can be calculated from the widths of the profiles in X and Y seen in Figure 4.15 and Figure 4.16.

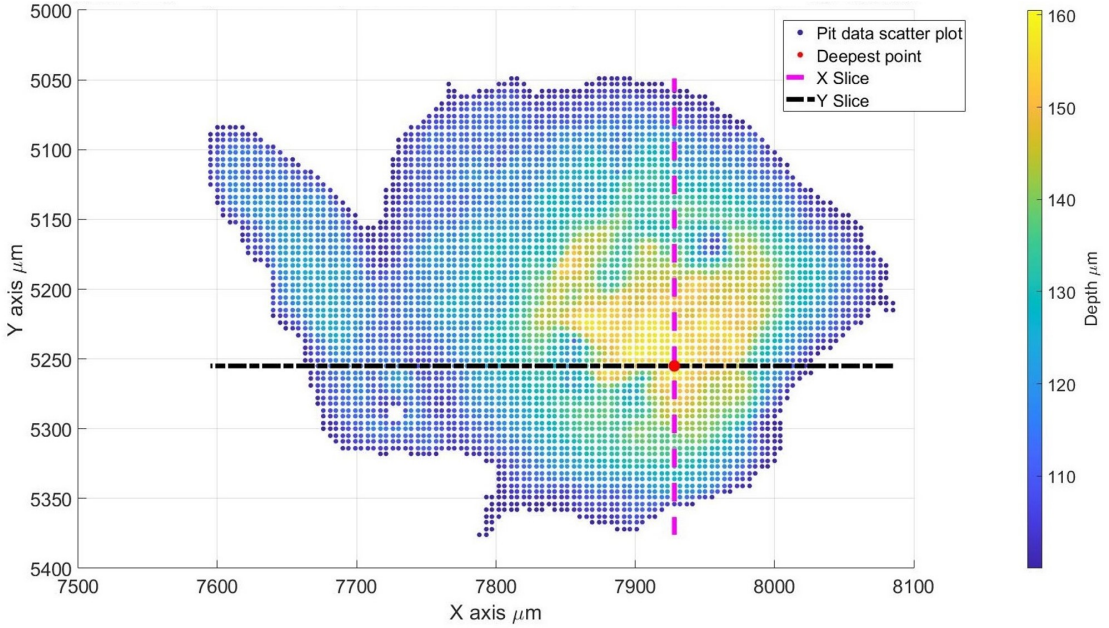

Figure 4.14: Scatter plot of pit 11 with the X and Y profiles of the pit through the deepest point of pit 11 for scan 1-1-A-1

As can be seen in Figure 4.14, the planes through the deepest point express the majority of the information of the pit with a little variation. It does not capture the off centre nature of the deepest point that would be assumed if these readings were produced using the previously used two dimensional techniques.

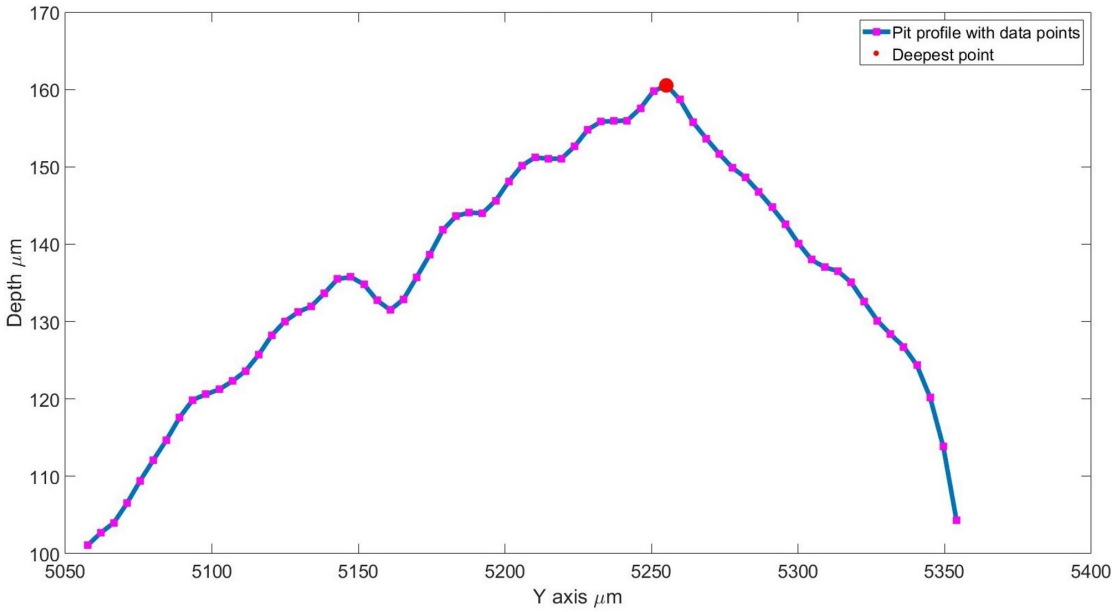

Figure 4.15: The X plane profile of the pit through the deepest point of pit 11 for scan 1-1-A-1

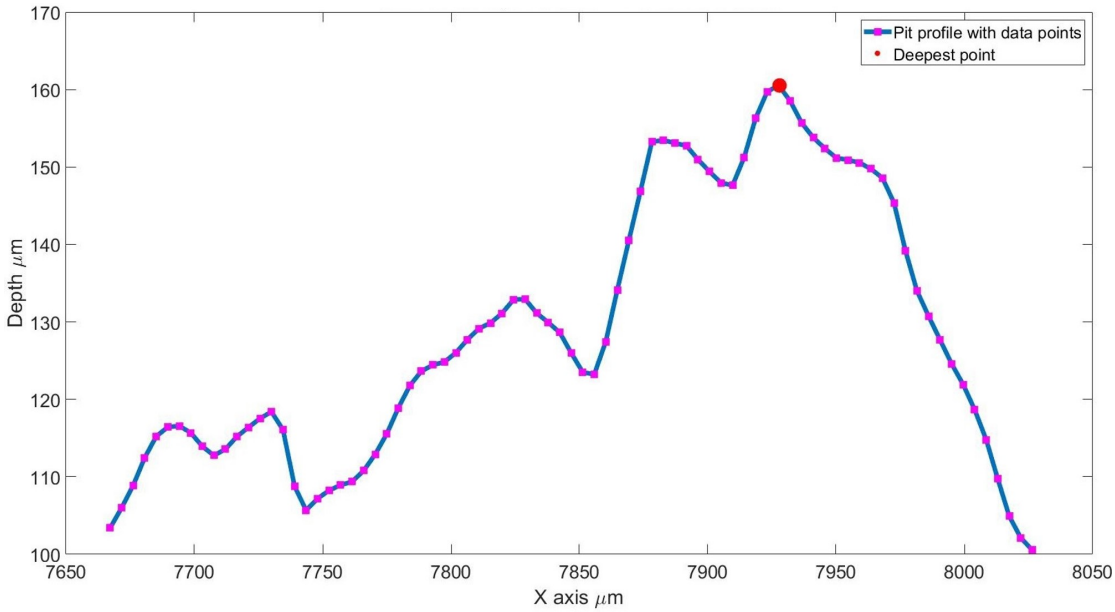

Figure 4.16: The Y plane profile of the pit through the deepest point of pit 11 for scan 1-1-A-1

It can also be seen in Figure 4.15 and Figure 4.16 that the shape of these profiles deviates somewhat from a semi-elliptical curve through the diameter of the pit and the deepest point. The profile appears more pointed and sharp than with previous smooth geometry assumptions [35, 102], with noticeable peaks at the deepest point. This may be partly due to the digitisation of the data, due to sampling, that caused issues when using Finite Element techniques.

The next technique used the maximum diameter plane. The value of profiles for each line in the X and Y planes were calculated and the ones with the largest diameter in each were selected. The maximum depth on each profile was then measured, which maybe at different locations for each plane. This can be seen in Figure 4.17, Figure 4.18 and Figure 4.19.

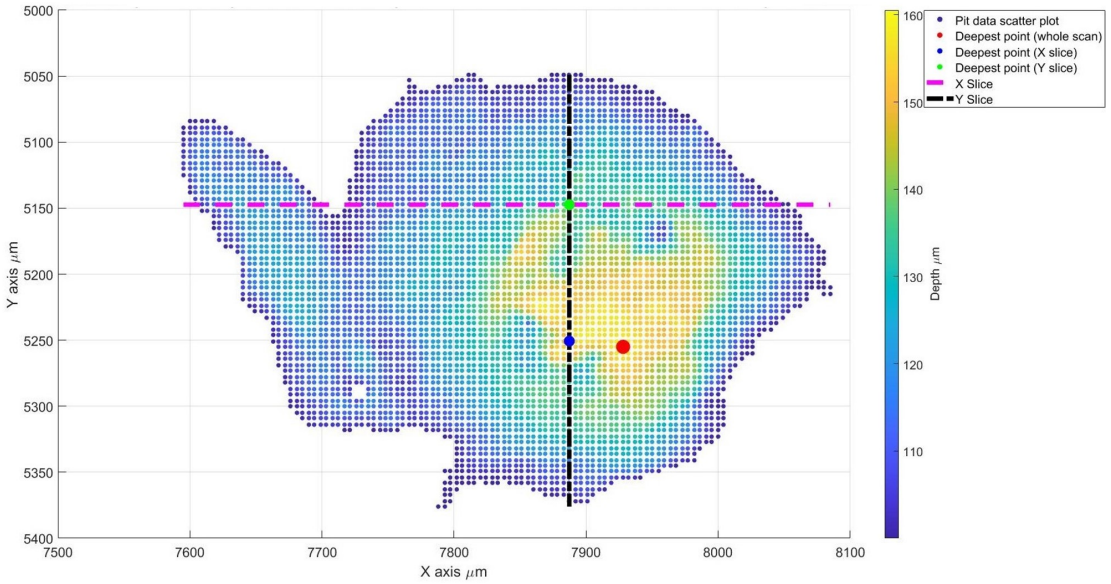

Figure 4.17: The X and Y profiles of the pit through the maximum diameter planes of pit 11 for scan 1-1-A-1, with the deepest points of each profile and the whole scan marked

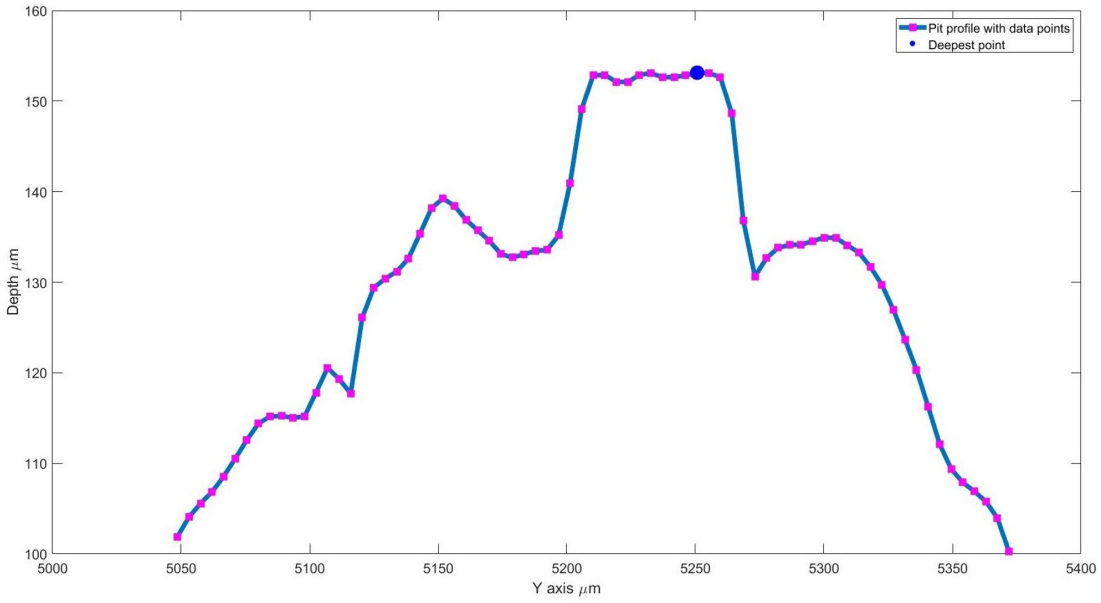

Figure 4.18: The X plane profile of the pit through the maximum diameter plane of pit 11 for scan 1-1-A-1

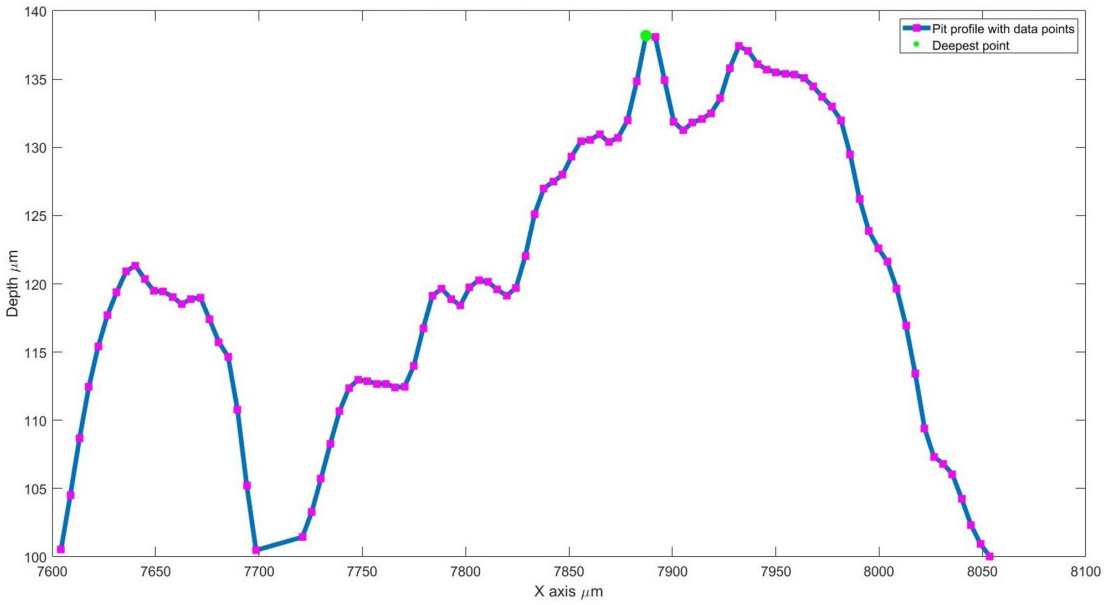

Figure 4.19: The Y plane profile of the pit through the maximum diameter plane of pit 11 for scan 1-1-A-1

As can be seen in Figure 4.17, the values of the maximum depth were different between each profile and both are lower than the actual maximum depth of the pit. This approach simulates the results that may be produced if a sectioning analysis was undertaken. If the assumption was made that the deepest point occurred on the plane of the largest diameter then one of these results would be achieved. This has obvious issues with underestimating the aspect ratio of the pit, as often the deepest point is somewhat offset from the geometric centre if a semi-elliptical assumption was used.

The variation in these approaches for pit 11 was quite significant in some cases, as can be seen in Figure 4.20. The difference in pit height varied by as much as 14% between the largest and the smallest values, with variations of 8% in the X diameter and 27% in the Y diameter.

The aspect ratio of the pit, a widely accepted key parameter in both crack and pit severity, varied by up to 12% in the X plane and 31% in the Y plane, depending on the technique employed. This would have very significant effects on the prediction of a crack initiation from a pit, with impacts on either excessive caution or, more worryingly, acceptance of dangerous damage.

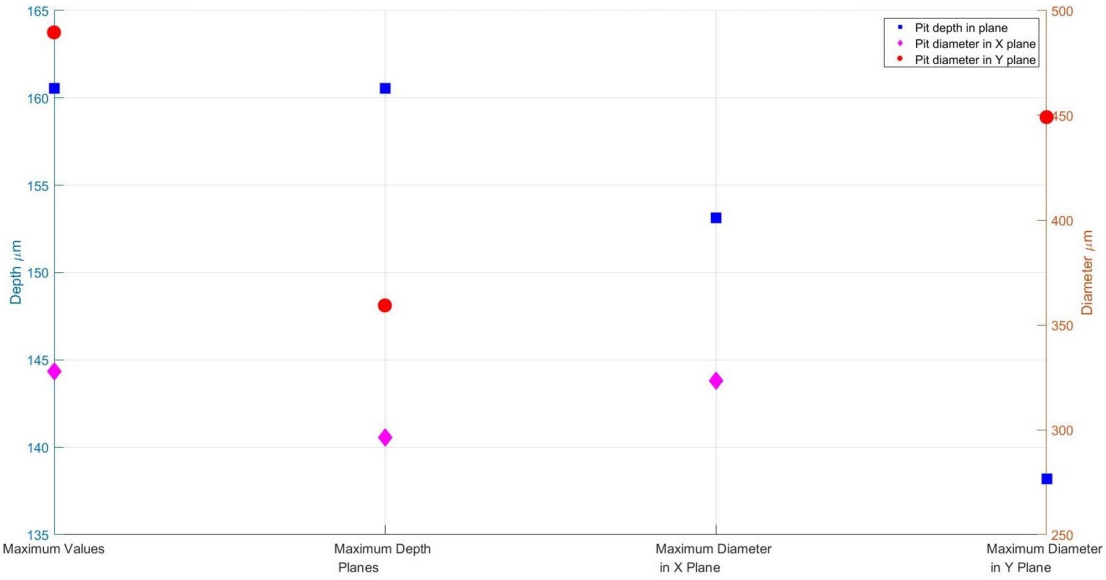

Figure 4.20: Variation in parameter values for pit 11 based on different assumptions used

While the absolute values for this single example pit were not especially enlightening, it served to demonstrate the variation that could occur within an inspection of corrosion damage. In particular some of the implications of these variations may have appeared in previous studies of rail axle corrosion that use pre-defined shape assumptions about pits. For example, a potential 31% error in measured aspect ratio if a surface only measurement approach was taken would result in significantly erroneous data. The variation will also have potential implications on the calculation of stress intensity factors, as the change in aspect ratio could mean that different equations become relevant for each pit as the values change.

The final calculation process was the projected area assumption, based on the work of El Haddad [70]. This was different to the other outcomes, as the aim was not to calculate the input parameters of diameter and maximum depth, but rather to calculate the area of the defect perpendicular to the plane of loading, as demonstrated in Figure 4.7. This was calculated by plotting a scatter plot of all of the data points in the pit in the X then Y planes. The results of this can be seen in Figure 4.21 and Figure 4.22, with the colouring of the projected areas resulting from a data points depth into the plane, however this has no impact of the calculation of the area result.

The boundary of the scatter plot was then computed using three different settings. First the convex hull was produced, this can be analogised as if a rubber band was placed around the shape, and is the shortest length of line to enclose all the points. This represents the largest possible area.

The next value used a shrink factor of 0.5, chosen as it was halfway between a convex hull and a compact boundary. This much more closely follows the perimeter of the shape, but omits some highly localised features such as sudden dips or ridges.

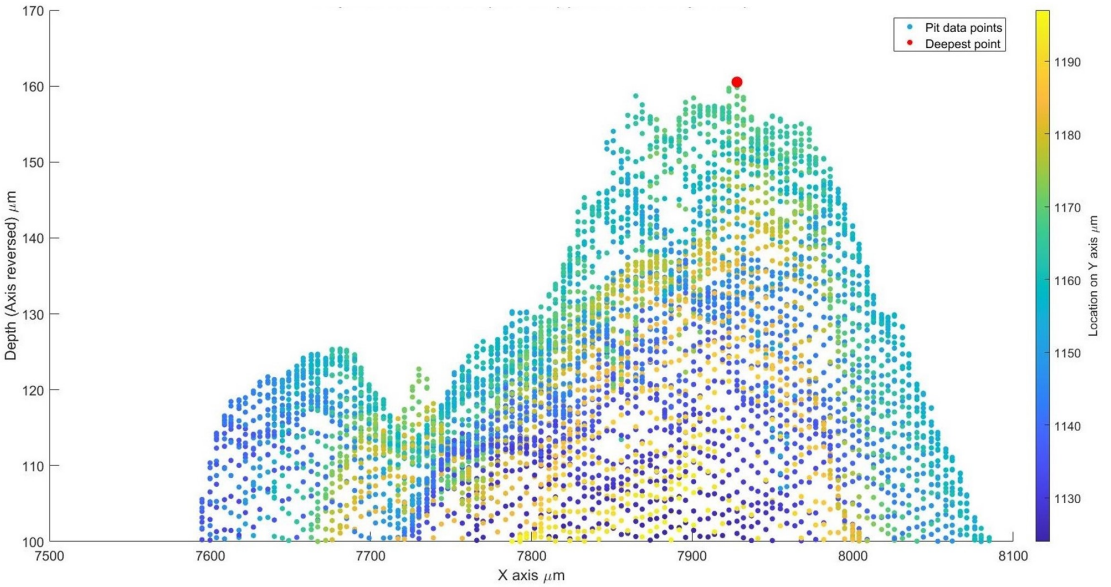

Figure 4.21: The X plane profiles of the pit of pit 11 for scan 1-1-A-1

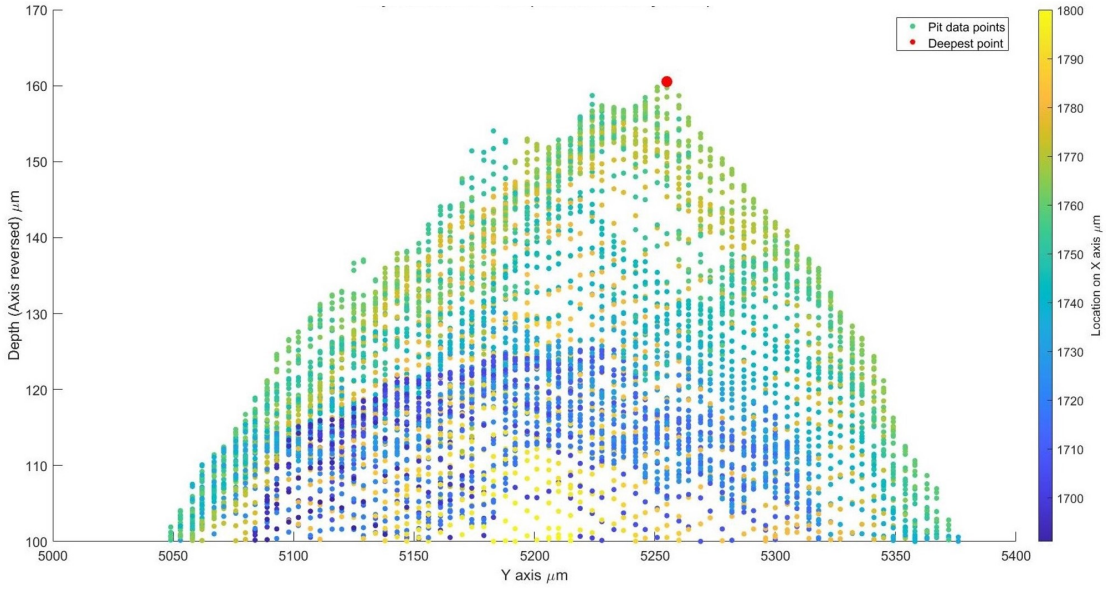

Figure 4.22: The Y plane profiles of the pit of pit 11 for scan 1-1-A-1

The final value represents the compact boundary of the projected area that faithfully follows the shape of the pit. This will likely have the smallest area, although this is not guaranteed.

The results of these can be seen for pit 11 in Figure 4.23 and Figure 4.24. The values for areas were significantly different in the case of the X plane, but far more similar in the Y plane. This was affected by the smoothness of the overall geometry, one that was very continuous with little variation or outcrops will be very similar with all three techniques, whereas a more irregular shape could have significant variation.

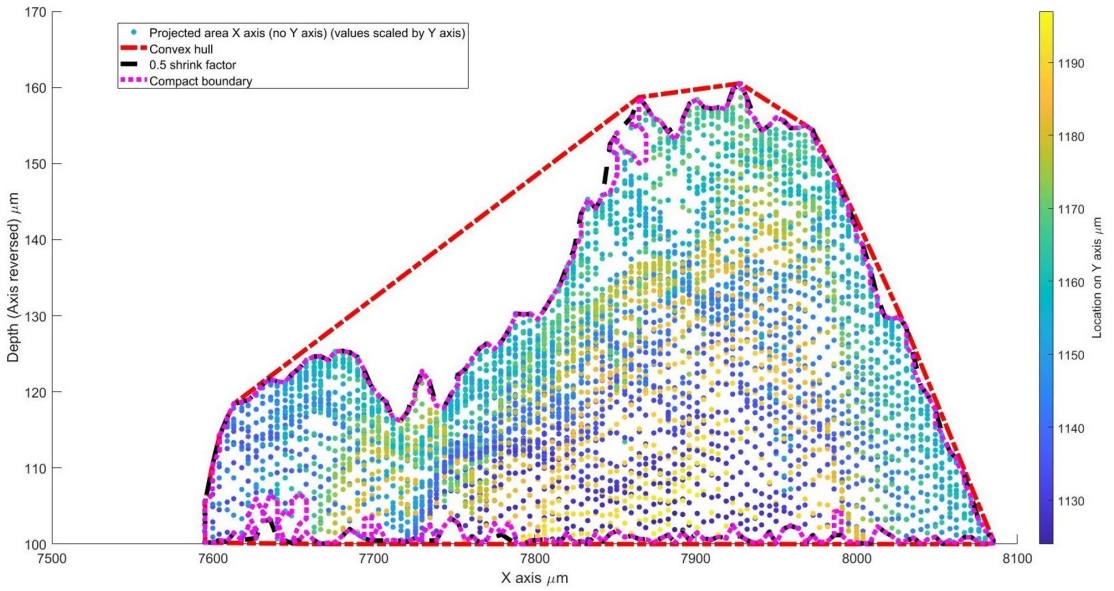

Figure 4.23: X plane projection of pit 11 area, with different definitions of the area of the pit

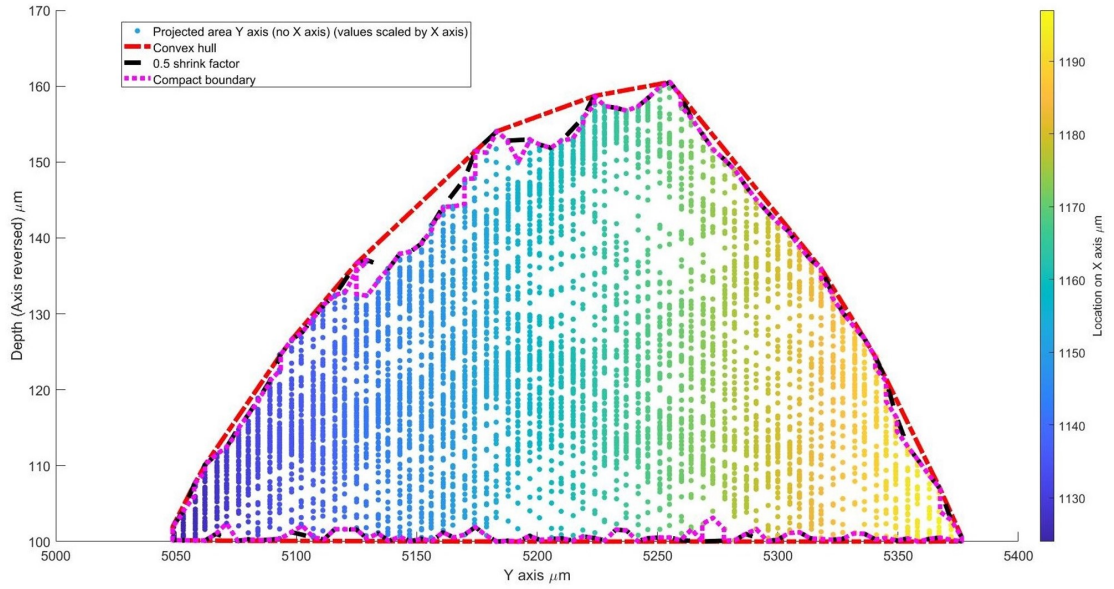

Figure 4.24: Y plane projection of pit 11 area, with different definitions of the area of the pit

The variations in the calculated area results can be seen in Table 4.1. As expected the variation for the Y plane was comparatively low, although the variation in the X plane was significant. While the impact of this variation, when applied to Equation 4.38, as the use of the $\sqrt{Area}$ minimises the percentage variation compared to the raw $Area$ values, it still represents a significant difference in the calculated risk of a crack forming from a particular pit.

Table 4.1: Variation in the projected area calculation of pit 11 in the X and Y plane

	X Plane Area	% change from convex hull	Y Plane Area	% change from convex hull
Convex Hull	19474	-	12553	-
0.5 Shrink Factor	16025	-17.7%	11897	-5.3%
Compact Boundary	15633	-19.7%	11707	-6.7%

4.4 Variation in input parameters

This section considers the variation in the input parameters, given the different approaches to defining a three dimensional pit as a two dimensional crack. These will have significant effects on the stress intensity factor range, demonstrating the weakness of some other data collection techniques and the limits of the crack assumption.

The results of each concept are presented together with the aspect ratios that result from the input parameters, as this is the main variable of most stress intensity factor equations.

Maximum values parameters

The values of maximum depth and the diameters of the bounding box are presented in Figure 4.25. Some of the diameter values are very large, the largest being around five times the maximum values produced in any other concept for defining the diameters. However, this effects only a few pits that exhibit coalescence, so have more sprawling geometries.

The percentage of pits that were over the maximum value detected using the maximum depth method was only 5.96% in the X plane and 6.23% in the Y plane. This suggests that less than 7% of pits have extremely high values, due to the inherent problems of the bounding box approach.

While the deepest point value will remain the same, the diameters in some cases will be very significantly larger. This would drive the aspect ratio down, and so lower the maximum stress intensity factor, lowering the perceived risk of a pit. While this does not necessarily mean these pits would be dangerous, it does suggest a certain percentage of pits were likely to have under reported crack initiation risk.

Maximum depth parameters

The values of maximum depth and the diameters of the pit through the maximum depth are presented in Figure 4.26. The values of maximum depth point are the same as for the maximum value concept, however the diameter values are lower in almost all cases. This leads to higher stress intensity factors and increased perceived risk from corrosion pits.

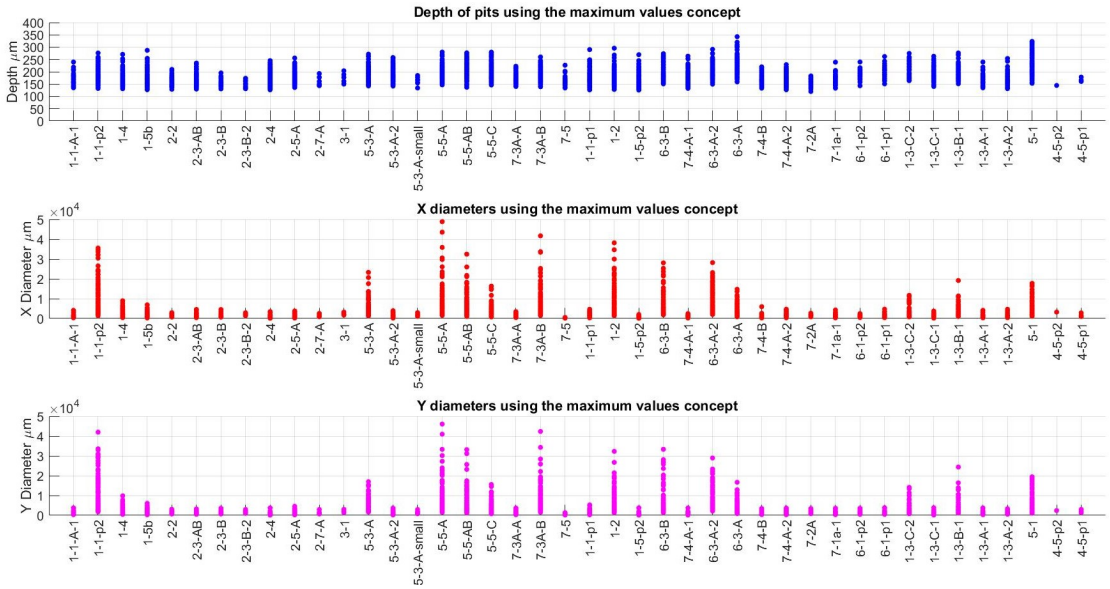

Figure 4.25: Collation of the values of depth, X plane diameter and Y plane diameter. These values were calculated using the maximum value concept

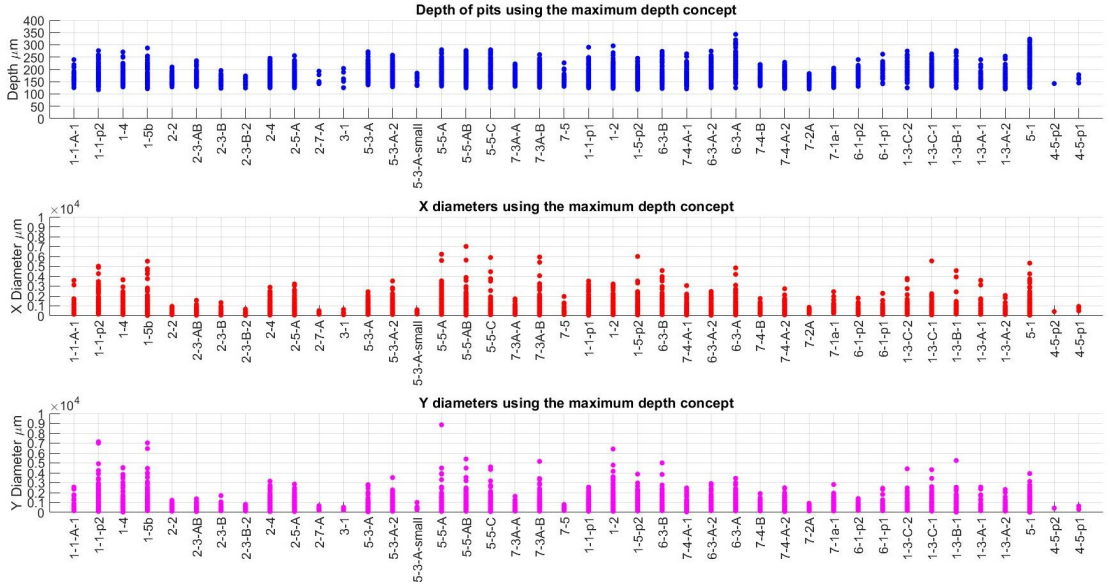

Figure 4.26: Collation of the values of depth, X plane diameter and Y plane diameter. These values were calculated using the maximum depth concept

This approach also benefited from a stronger theoretical basis for it's assumptions. In this approach the three dimensional pit is being treated as a two dimensional crack. It is a reasonable assumption that the deepest point of the pit will have a crucial role in the risk of crack initiation from that pit. From that logic, if a plane was to be picked to represent the pit as a crack, it should pass through the deepest point.

This still has issues, such as ignoring the effect of other features within the pit that may influence the mode I stress intensity factor or modes II and III. However, these are issues with the pits-as-cracks concept in general and the use of the deepest plane has a level of justifiability.

This approach does have its difficulties in application, as the depots (where this knowledge would be most important) currently have no ability to measure the depth of pits. This would make the measurement of a plane that passes through this point near impossible without the introduction of new technologies to the depot.

Maximum diameter parameters

The values of maximum depths and the diameters of the widest diameter planes are presented in Figure 4.27 and Figure 4.28. In these approaches the maximum depth in each plane will be different from both each other and the actual maximum measured depth in three dimensions.

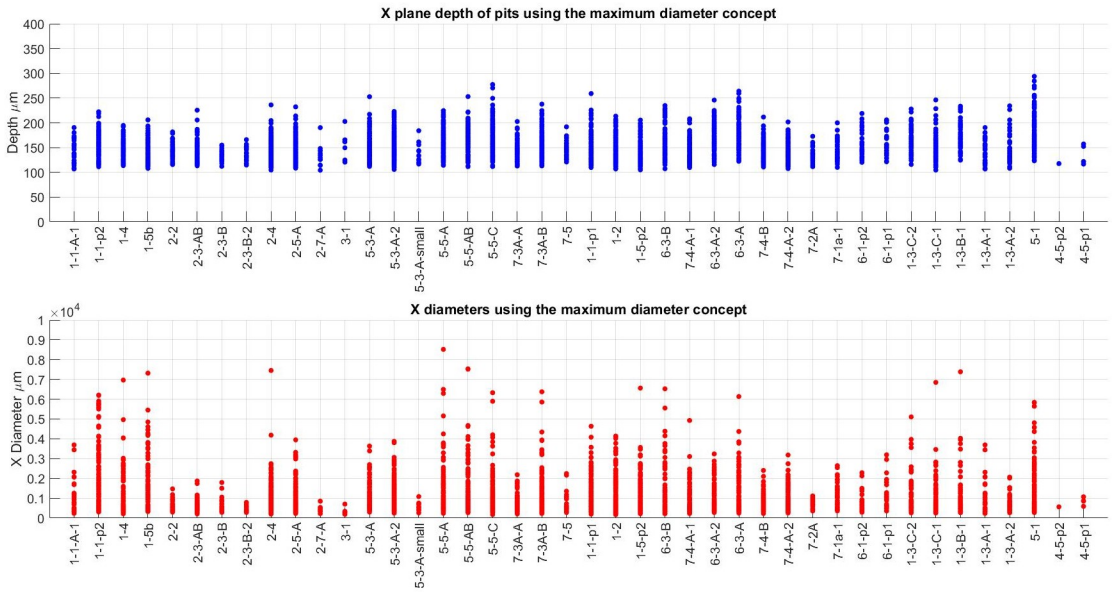

Figure 4.27: Collation of the values of depth, X plane diameter and Y plane diameter. These values were calculated using the maximum diameter concept in the X plane

As expected the maximum depths in both the X and Y planes was noticeably lower than that detected in the maximum values and maximum depth concepts.

This approach will almost certainly produce aspect ratios below those of the maximum depth values, lowering the perceived risk of the pit, as a large diameter value is compared to a lower than maximum depth value.

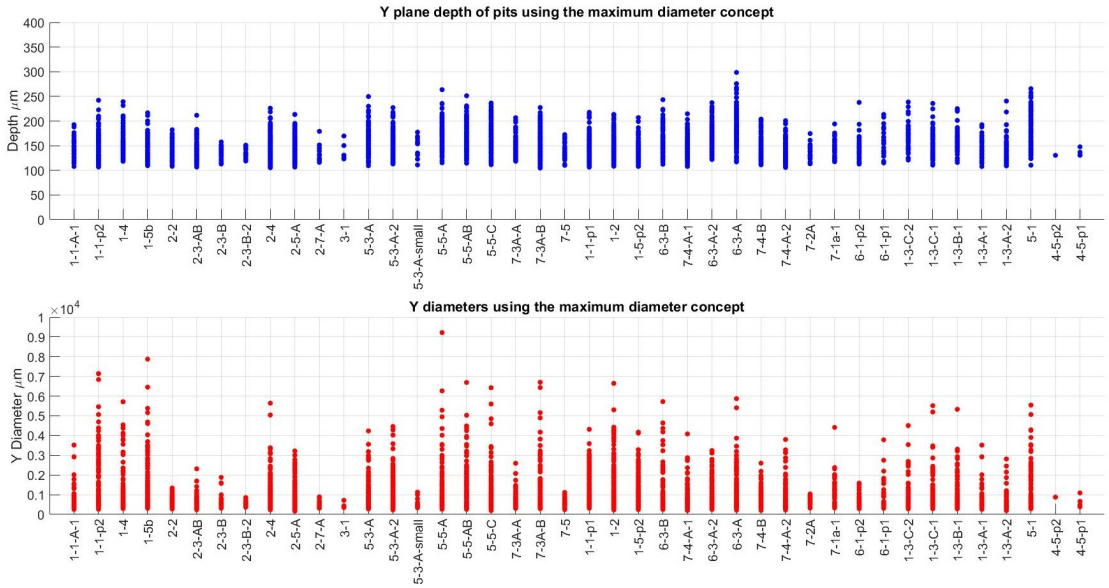

Figure 4.28: Collation of the values of depth, X plane diameter and Y plane diameter. These values were calculated using the maximum diameter concept in the Y plane

The maximum diameter approach represents the approach taken by surveys that seek to view the profile of the corroded survey, if a smooth shape for the pit was assumed. This assumption would conclude that the plane with the widest diameter in X and Y would contain the deepest point. This has been demonstrated not to be a strong assumption, as least in the case of rail axle corrosion damage. Using this assumption therefore could lead to erroneous results and potentially dangerous conclusions.

Comparison of results

The aspect ratios of each of the three techniques were calculated. This was defined by taking the depth of the pit divided by the radius in the relevant axis. The values calculated by the maximum values, maximum depth and maximum diameter concepts can be seen in Figure 4.29, Figure 4.30 and Figure 4.31 respectively.

A summary of the key parameters of the aspect rations for each technique can be seen in Table 4.2. As can be seen in the Table, the values are generally of a similar order of magnitude, apart from the maximum values for the maximum depth technique.

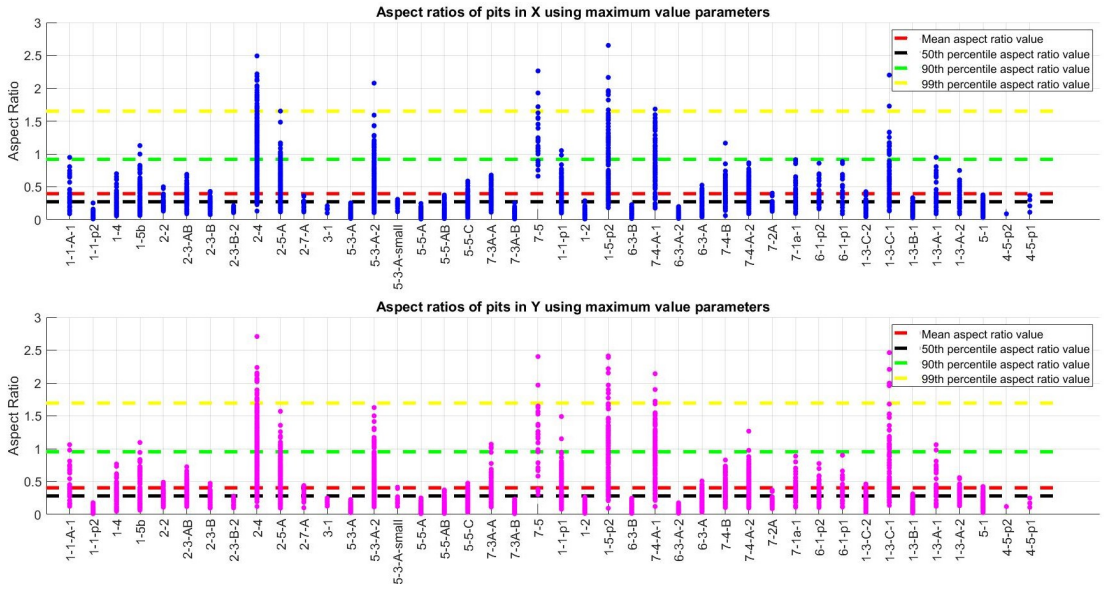

Figure 4.29: Aspect ratios of pits calculated using the maximum values concept

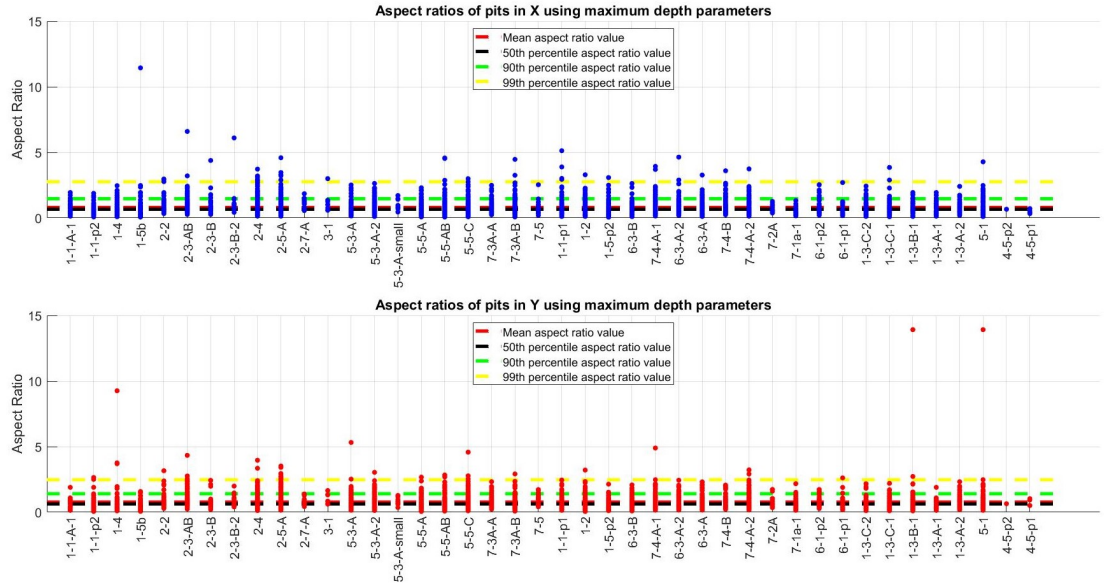

Figure 4.30: Aspect ratios of pits calculated using the maximum depth concept

Table 4.2: Comparison of the aspect ratios calculated for different pit-to-crack concepts

		Aspect Ratios				
	Plane	**Mean**	**50th Percentile**	**90th Percentile**	**99th Percentile**	**Maximum**
Maximum Values	**X**	0.396	0.273	0.919	1.651	2.652
	Y	0.405	0.284	0.953	1.695	2.707
Maximum Depth	**X**	0.800	0.668	1.469	2.760	11.44
	Y	0.769	0.6312	1.406	2.480	13.910
Maximum Diameters	**X**	0.450	0.420	0.776	1.145	1.590
	Y	0.442	0.410	0.771	1.152	1.982

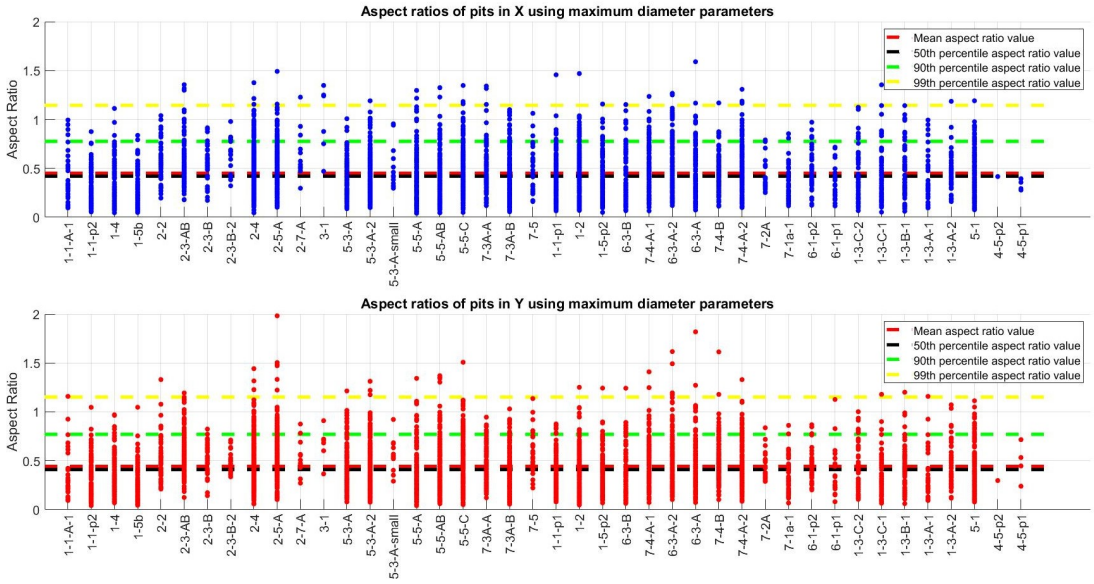

Figure 4.31: Aspect ratios of pits calculated using the maximum diameter concept

The higher values for the maximum depth were as expected and desired, producing more conservative and severe values for aspect ratio than the other techniques. By comparing the means, it is possible to say that the maximum depth technique was twice as severe on average compared to other values calculated by other techniques. There were some extreme outliers due to variations in geometry and the limitations of widespread application of an inflexible technique.

Using the maximum depth concept, the percentage of pits that had a calculated aspect ratio above one increased to 25.47% in the X plane and 23.65% in the Y plane. This can be compared to the values previously reported using the maximum values technique of 1.8% and 12.3% if the maximum or minimum bounding box dimension was used.

The maximum diameter concept produced the lowest values of aspect ratio for the pits with the highest aspect ratio values. This was despite having a mean that was very similar to the maximum values technique.

The variation in results suggested that while, on average, the maximum diameter concept was capable of producing similar aspect ratio results for the majority of pits, when the highest aspect ratio pits were considered, the approach could produce significantly lower values. These lower values could result in pits being reported as being safe when using the maximum diameter approach, while other approaches would flag the pit as potentially dangerous. The lower reported aspect values would result in a lower factor of safety in any assessment of axle safety.

Based on the more aggressive values, the maximum depth concept will be used to calculate the stress intensity factors going forward. Due to the safety critical nature of the components being assessed, a more conservative view of the risk increases the probability of over scrapping, compared to an increased risk of catastrophic failure.

$\sqrt{Area}$ parameters

The definition of stress intensity factor of pits using the El Haddad approach relies on the $\sqrt{Area}$ parameter.

In using the $\sqrt{Area}$ definition the variation between the different techniques for calculating the boundary, and therefore the area, can be seen in Figure 4.32 and Figure 4.33. These difference in areas have already been discussed in terms of the practical variations.

There are subtle changes in the $\sqrt{Area}$ of the pits. The average value for each different calculation techniques were 238.5μm, 206.3μm and 201.6μm in X and 236.9μm, 204.7μm and 200.0μm in the Y plane. This represents a maximum variation of 15.5% in the X plane and 15.6% in the Y plane, suggesting that on average the convex hull results in a larger $\sqrt{Area}$ value of around 16%.

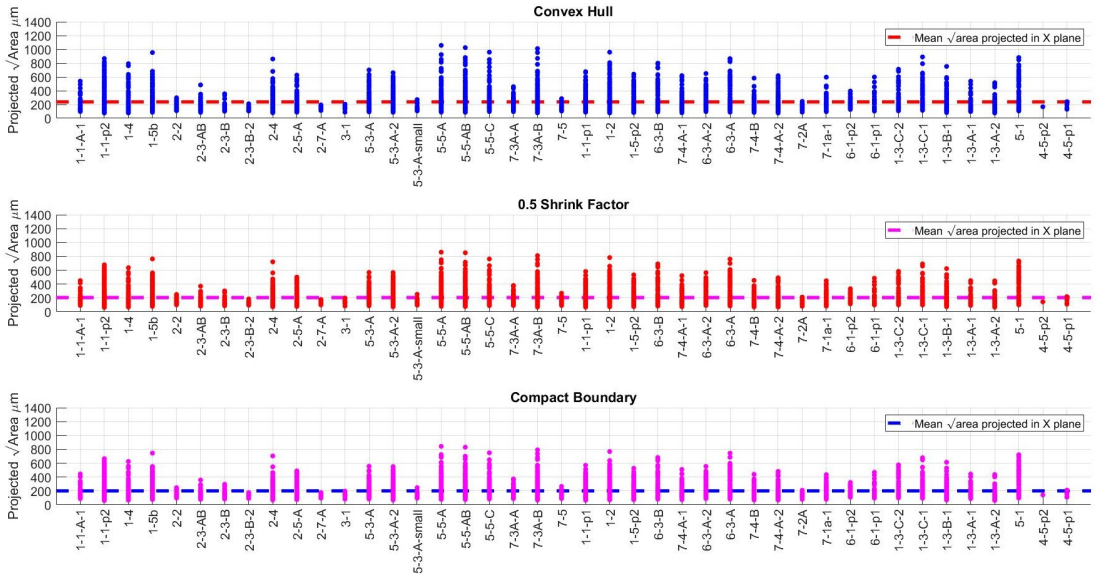

Figure 4.32: Comparison of the projected $\sqrt{Area}$ in the X plane of each pit (organised by scan) based on different definitions of area

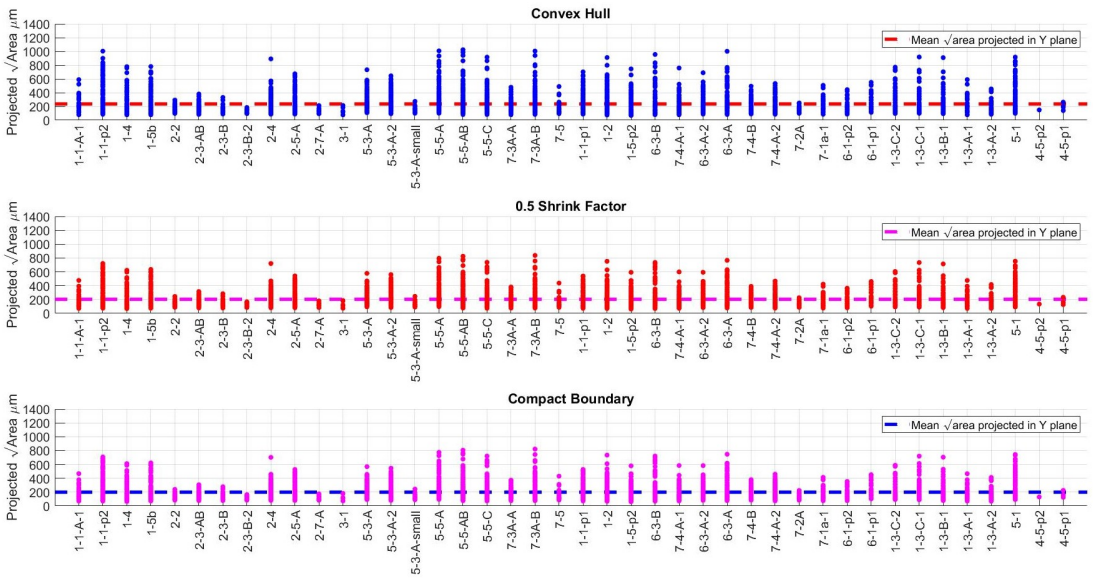

Figure 4.33: Comparison of the projected $\sqrt{Area}$ in the Y plane of each pit (organised by scan) based on different definitions of area

From these values it is suggested that the convex hull is the most reasonable definition of the $\sqrt{Area}$ of the projected area in the plane. This is due to the roughly 16% higher value, that would result in conservative estimates of the stress intensity factor, increasing the factor of safety of any decisions that arise from the outcome. The other is that the convex hull generalises that shape into a more regular one. This would smooth out some of the variations in the detected pits geometries due to the generalised nature of the pit detection methods. From now on the convex hull definition will be used to calculate the stress intensity factors.

4.5 Stress intensity factors from identified pits

4.5.1 Mode I stress intensity factors

Maximum depth approach

The stress intensity factors were calculated using the different forms of Equation 4.46, depending on the aspect ratio of the pit in each plane. This meant that if the aspect ratio was different between the X and Y plane then a different set of parameters would be used.

As previously mentioned, equations could only be found for cracks with aspect ratios up to two, this covers 96.3% in X Plane and 96.8% in the Y Plane. Despite this approach being able to calculate values for the vast majority of analogous cracks, the higher values were not able to be calculated. This was unfortunate, as it would be a reasonable assumption to make that the more extreme value cracks, would have a higher chance of failure. However, this cannot be overcome in this work and would be a focus of future work.

The results of the pits that were able to be determined, are presented in Figure 4.34 and Figure 4.35. These were calculated assuming the maximum stress amplitude of 166MPa [15], although almost all axles would usually experience values well below this [103], and a fully reversed cycle.

The maximum stress amplitude of 166MPa meant the tensile part of the cycle could produce a maximum stress of 166MPa. As can be seen, the maximum values of each pit change position, based on the aspect ratio of the pit, with the higher aspect ratio pits having the maximum at the mouth of the pit. This was as expected and agreed with other work in literature [35].

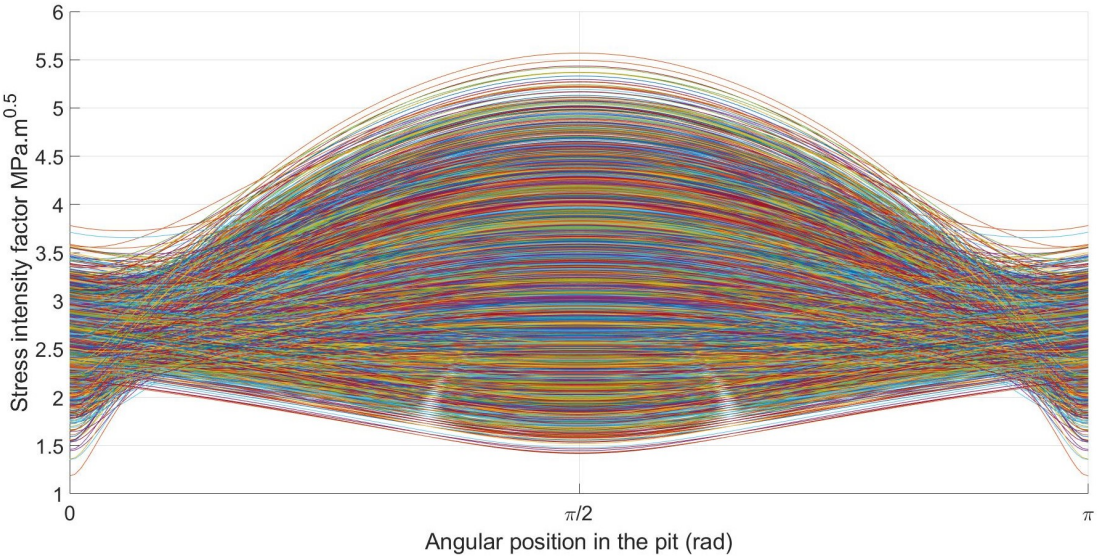

Figure 4.34: All stress intensity values in the X plane of the crack analogy of pits using the maximum depth concept based on the angular position in the pit (Only pits with an aspect ratio between 0 and 2)

The maximum values regardless of position can be seen in Figure 4.36 and Figure 4.37. None of the values approach the ΔK_{th} for EA1N steel mentioned earlier of 13 $MPa.m^{0.5}$ or even the averaged value of 7.23$MPa.m^{0.5}$. However, this section only included the tensile part of the cycle, as the compressive part was initially ignored.

It can be seen that the pits with the maximum values in the centre of the crack have generally higher values than the cracks with the maximum values at the surface of the crack.

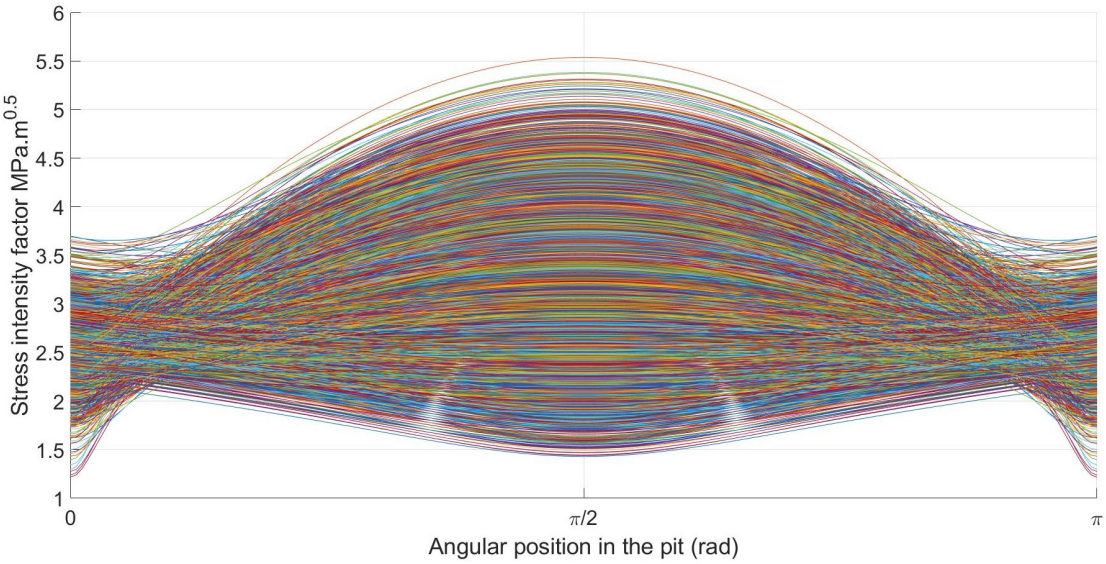

Figure 4.35: All stress intensity values in the Y plane of the crack analogy of pits using the maximum depth concept based on the angular position in the pit (Only pits with an aspect ratio between 0 and 2)

The conclusion of this work was that none of the pits identified were likely to result in a propagating crack, even if the value of SIF in the compressive cycle was assumed to be equal to the tensile part, resulting in the ΔK_{th} being double the maximum SIF values calculated.

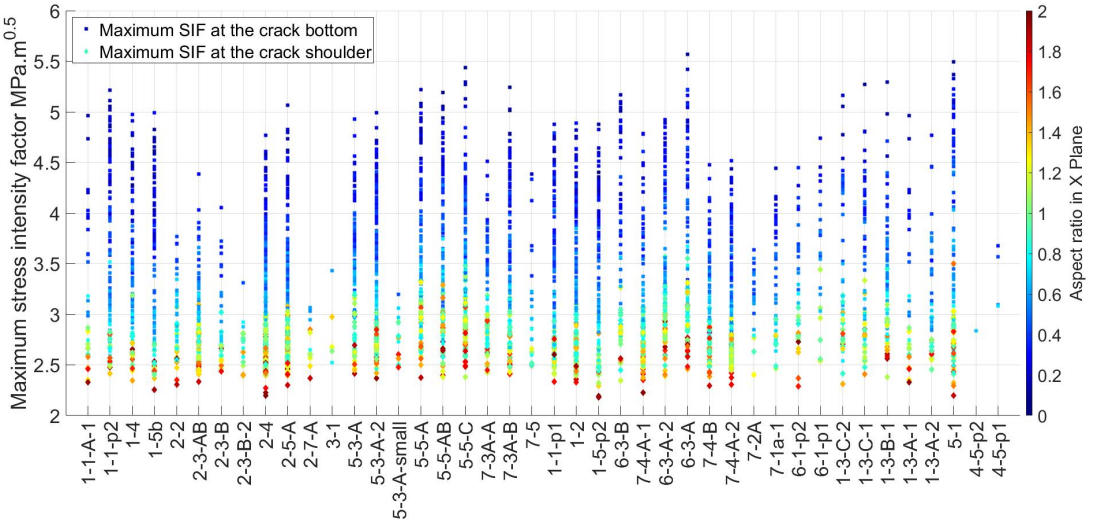

Figure 4.36: Maximum stress intensity values in the X plane of the crack analogy of pits using the maximum depth concept sorted by scan and coloured by aspect ratio (Only pits with an aspect ratio between zero and two)

Another factor to investigate was the influence of aspect ratio on the maximum value of the corrosion pit represented by the crack analogy. This can be seen with the colour scale in Figure 4.36 and Figure 4.37.

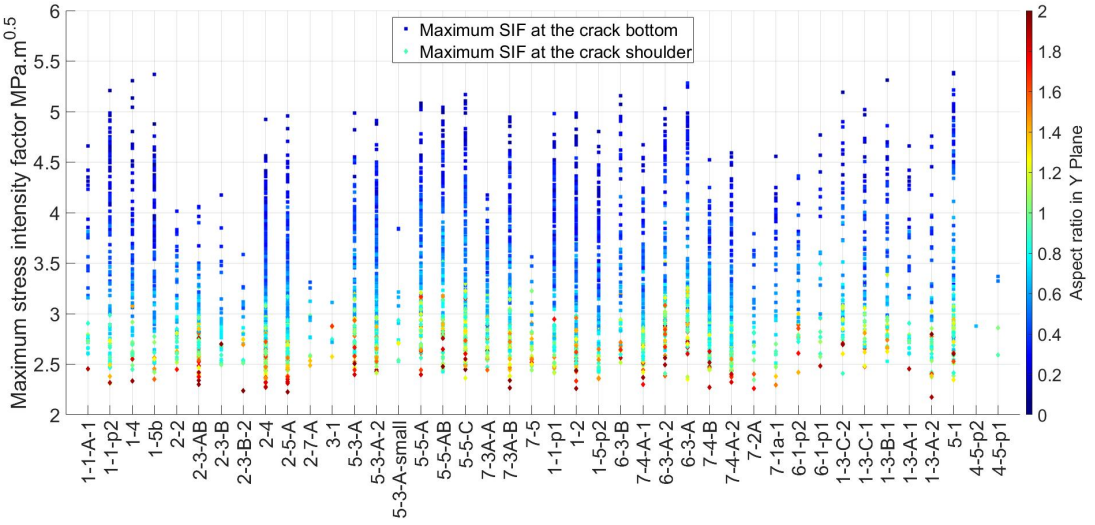

Figure 4.37: Maximum stress intensity values in the Y plane of the crack analogy of pits using the maximum depth concept sorted by scan and coloured by aspect ratio (Only pits with an aspect ratio between zero and two)

As can be seen from these graphs, the higher the aspect ratio the lower the maximum stress intensity factor detected. This was different to what would be expected, with the highest factors coming from the lowest aspect ratio pits.

This can be compared to the results when coloured by maximum depth, which can be seen in Figure 4.38 and Figure 4.39. In this case there was a relationship between the maximum depth and the maximum stress intensity factor, with deeper pits, in general having higher SIF values and being more likely to have the location of the highest SIF at the mouth of the pit.

Taking both sets of figures in combination, this suggests that the most worrying pits have high depth and low aspect ratio, meaning very high diameters. This suggests that the general trend is that the larger the defect, the higher the risk of crack initiation. It also suggests that the highest SIF values occur the the bottom of the pit.

These results would suggest that any surface cracking, such as that described by Hoddinott [37] and seen in experiments by Beretta [39, 104], are caused by shallow, high aspect ratio pits as the highest SIF is at the crack shoulder. Any cracking from the bottom of the pit would be caused by lower aspect ratio, deeper pits.

This tends to support the concept that this surface cracking occurs when very aggressive environmental conditions were present. The Hoddinott example occurred when a salt solution was trapped against the axle surface and the environmental conditions used by Beretta were far in excess of what might be expected. This would result in a highly aggressive, short term form of corrosion that would not favour the slower, more expansive pit formation and coalescence process that would be expected in less aggressive conditions.

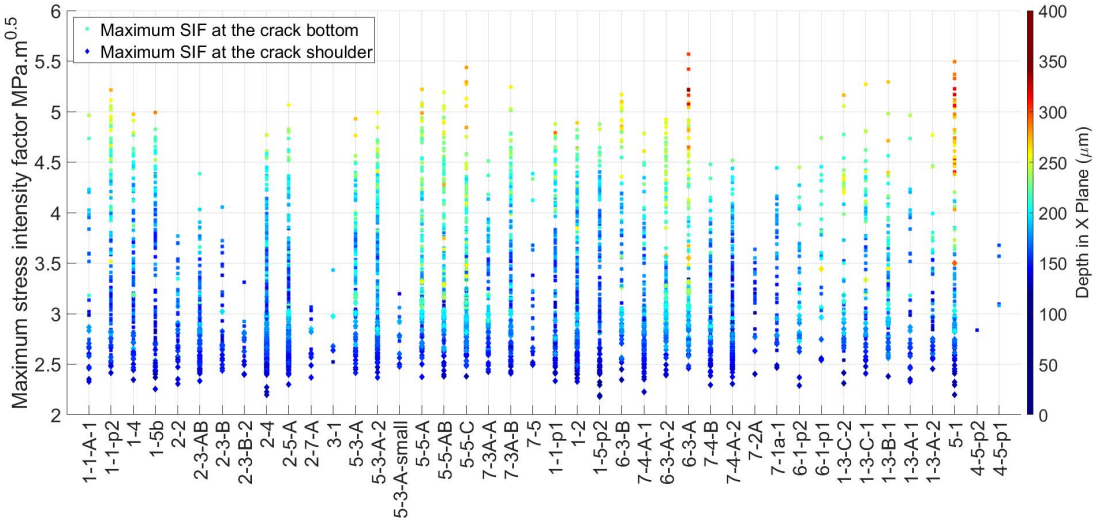

Figure 4.38: Maximum stress intensity values in the X plane of the crack analogy of pits using the maximum depth concept sorted by scan and coloured by depth (Only pits with an aspect ratio between zero and two)

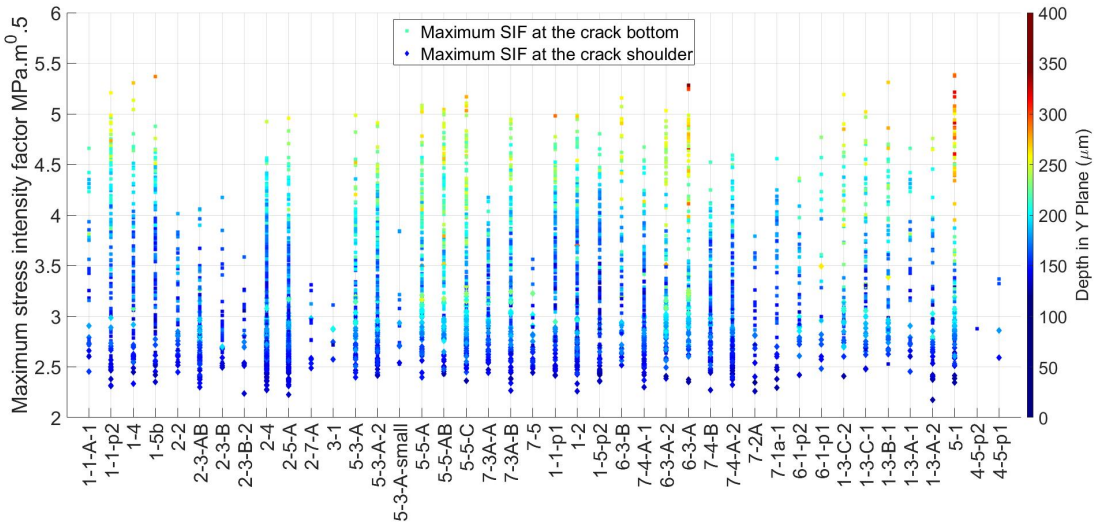

Figure 4.39: Maximum stress intensity values in the Y plane of the crack analogy of pits using the maximum depth concept sorted by scan and coloured by depth (Only pits with an aspect ratio between zero and two)

This would support the anecdotal responses from depot workers who did not report ever seeing surface cracking of this sort, and the lack of literature reporting this form of damage in axle surveys other than one instance reported by Hoddinott. This requires more investigation but may suggest that the use of aggressive accelerated testing of axles under environmental and stress loading leads to misleading crack formations.

Needing further investigation is the impact on time on the progression of corrosion pits, which will be covered in future work. How the pits develop overtime would be of great importance, with implications on possible methods of treatment.

If the corrosion pits are assumed to decrease in aspect ratio and increase in depth during their development, then the risky pits on corroded axles are ones with large apertures and high depths, whereas smaller, shallower and high aspect ratio pits can potentially be ignored as they do not risk any crack initiation and will take time to transform into the more risky type.

All of this work treats each pit as a single entity, and ignores the interplay of various pits in close proximity to each other, and the more complex geometry the actual pit, especially of coalescing pits. Action on these points will require additional investigation.

Fatigue approach

The $\sqrt{Area}$ parameter was used to estimate the value of the mode I stress intensity factor using Equation 4.38. Based on the assumptions, namely that the pit is assumed to be a surface crack, the geometry factor can be assumed and the equation becomes that seen in Equation 4.60. This equation will be used to estimate the stress intensity range.

$$\Delta K = 0.65\sigma_a\sqrt{\pi\sqrt{Area_{eff}}} \tag{4.60}$$

Initially the maximum allowable stress amplitude in an axle body, according to the standard [15], is 166MPa, although in reality most axles would experience values below this and undergo a more complex loading that this constant amplitude loading assumption. The stress intensity factor range, based on this assumption, can be seen in Figure 4.40 with the material threshold marked.

As can be seen in Figure 4.40, none of the identified pits break through the threshold value, so none would be expected to initiate a crack. The maximum calculated value was 6.22 $MPa.m^{0.5}$, less than half of the 13 $MPa.m^{0.5}$ limit of the material. This demonstrated the very large factors of safety that the detected pits operate under before crack initiation. This encouraged the idea that the procedures and standards could be changed without risk of crack initiation.

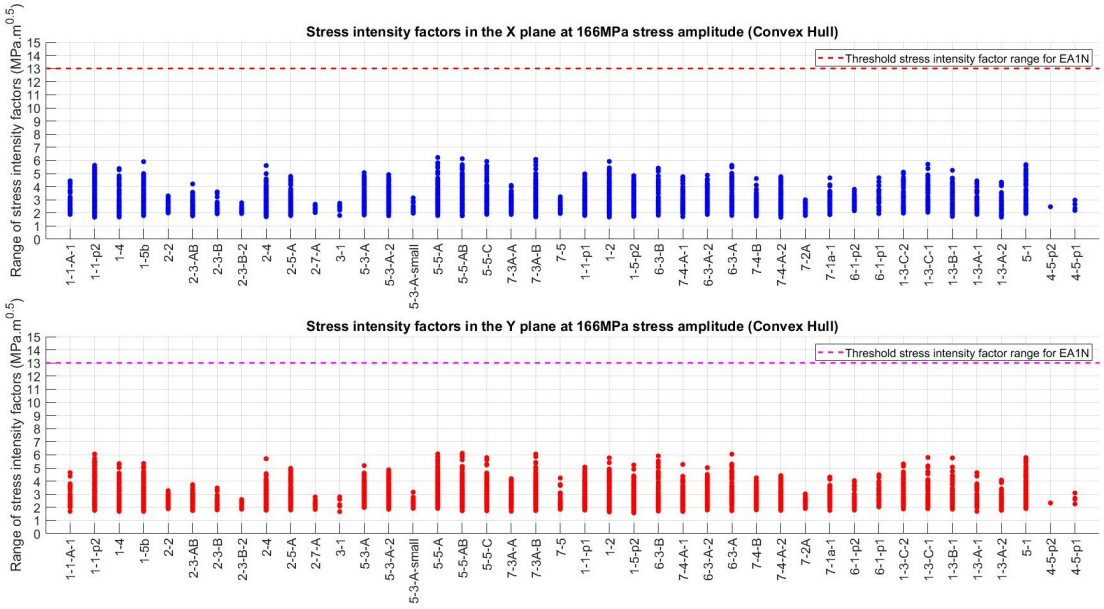

Figure 4.40: Stress intensity factor ranges for all pits, based on projected areas using a convex hull and with ΔK_{th} for EA1N marked. Using the maximum allowable surface stress.

Some of the values are for pits that appear to show evidence of coalescence between two or more pits, producing very large areas. When these pits are projected into a single plane, with a convex hull, this produces a significant $\sqrt{Area}$ that was not envisaged in the theory. The effect of this can be seen by comparing these results with the output from the compact boundary in Figure 4.41, where the maximum value drops to 5.55 $MPa.m^{0.5}$. This demonstrated the degree to which the convex hull approximation was a conservative estimate compared to the other areas definitions. The results with the highest calculated risks were used to ensure that the results complied with the primary concern of the rail industry, safety.

The values for stress intensity factor range in these examples use the maximum permissible surface stress range. The result will vary linearly with a change in the stress amplitude, as shown in Equation 4.60. As previously mentioned, many axles would never experience this maximum value as most axles are designed with significant spare material to allow for correction during their life and to ensure that they would remain compliant in all eventualities.

The correlation between the aspect ratio and depth of pits from these results was investigated. The results, coloured for aspect ratio, can be seen in Figure 4.42 and Figure 4.43 (the 99th percentile values were used as the maximums for aspect ratio as using the maximum depth concept skewed the results too significantly for interpretation). The results coloured for depth can be seen in Figure 4.44 and Figure 4.45.

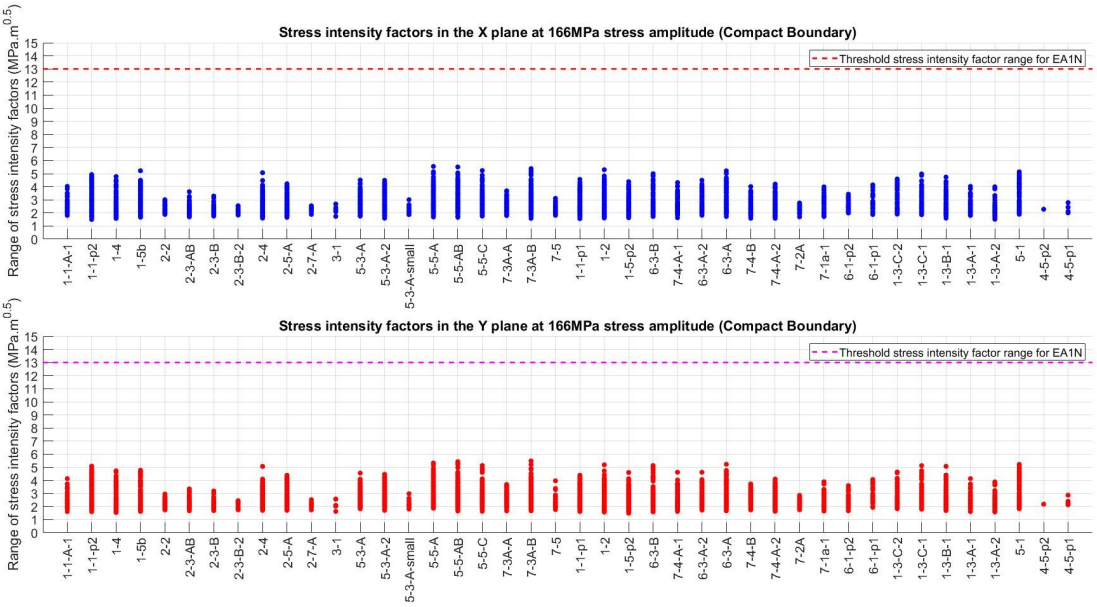

Figure 4.41: Stress intensity factor ranges for all pits, based on projected areas using a compact boundary and with ΔK_{th} for EA1N marked. Using the maximum allowable surface stress.

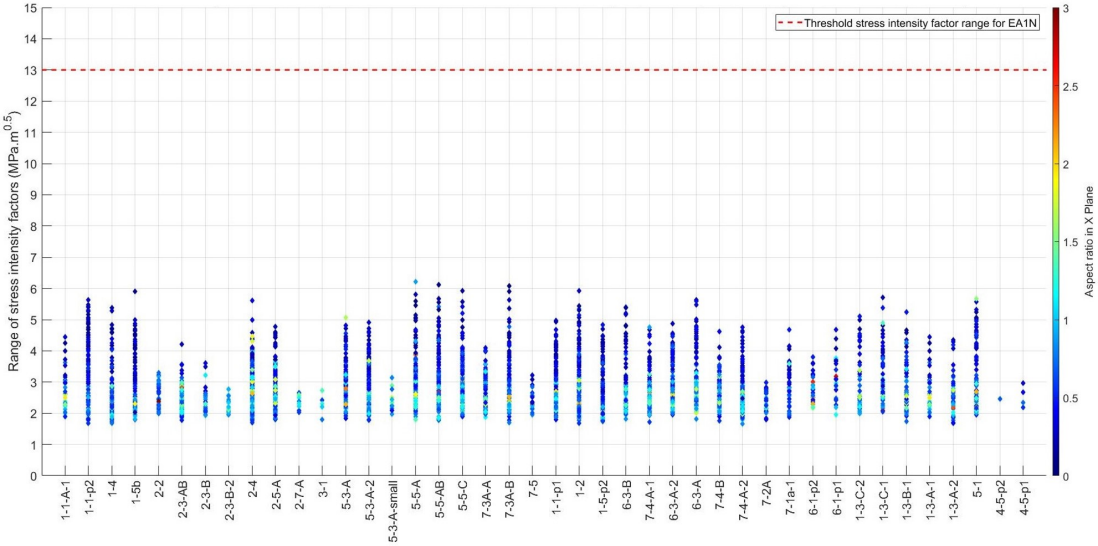

Figure 4.42: Stress intensity factor ranges for all pits, based on projected area in the X axis using a compact boundary at 166MPa stress amplitude and with ΔK_{th} for EA1N marked. Coloured based on the aspect ratio calculated from maximum depth concept

The relationships were similar to those discussed with the previous technique, although less pronounced. The higher the aspect ratio, the lower the maximum SIF although the division is less clear than before.

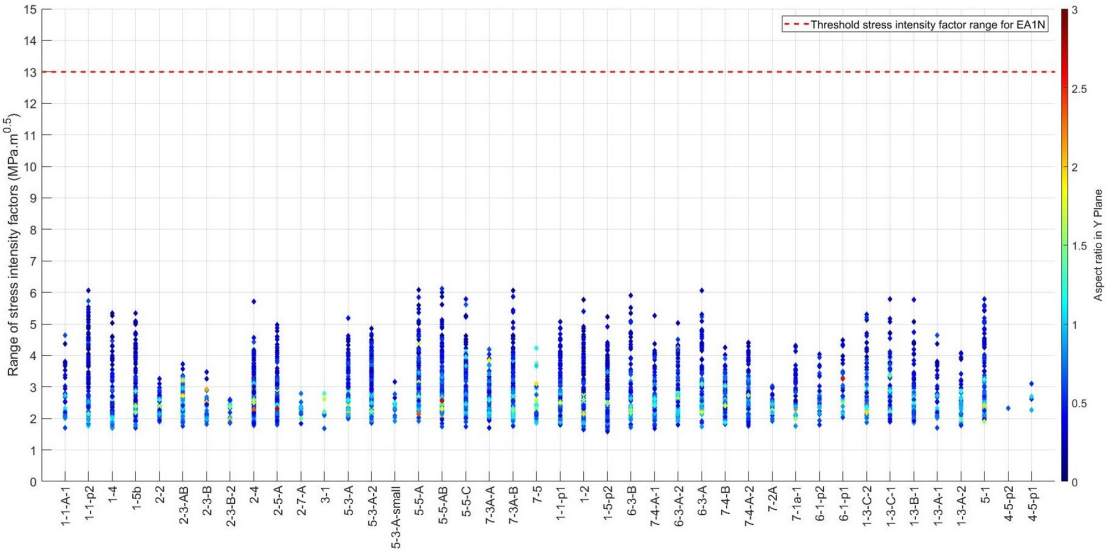

Figure 4.43: Stress intensity factor ranges for all pits, based on projected area in the Y axis using a compact boundary at 166MPa stress amplitude and with ΔK_{th} for EA1N marked. Coloured based on the aspect ratio calculated from maximum depth concept

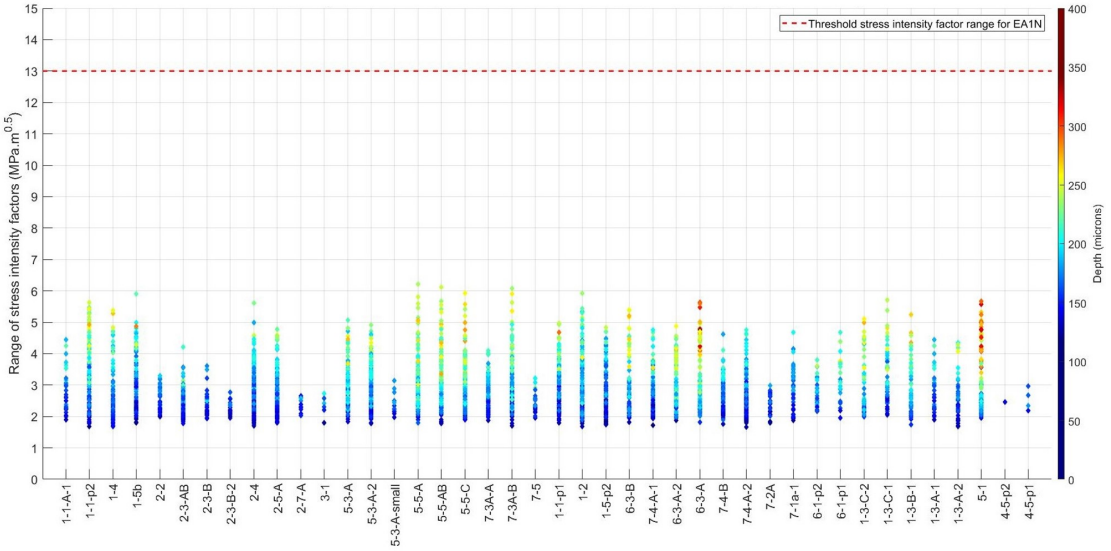

Figure 4.44: Stress intensity factor ranges for all pits, based on projected area in the X axis using a compact boundary at 166MPa stress amplitude and with ΔK_{th} for EA1N marked. Coloured based on the maximum depth

The depth parameter is more telling, with deeper pits having higher SIF values. As before this suggests that while shallow, high aspect ratio pits are an issue, it is not until they become larger and low aspect ratio that they become a problem. This outcome, using a different approach that is more dependent on pit shape, being the same as the analytical approach using larger shape assumptions, increases the confidence in the trend.

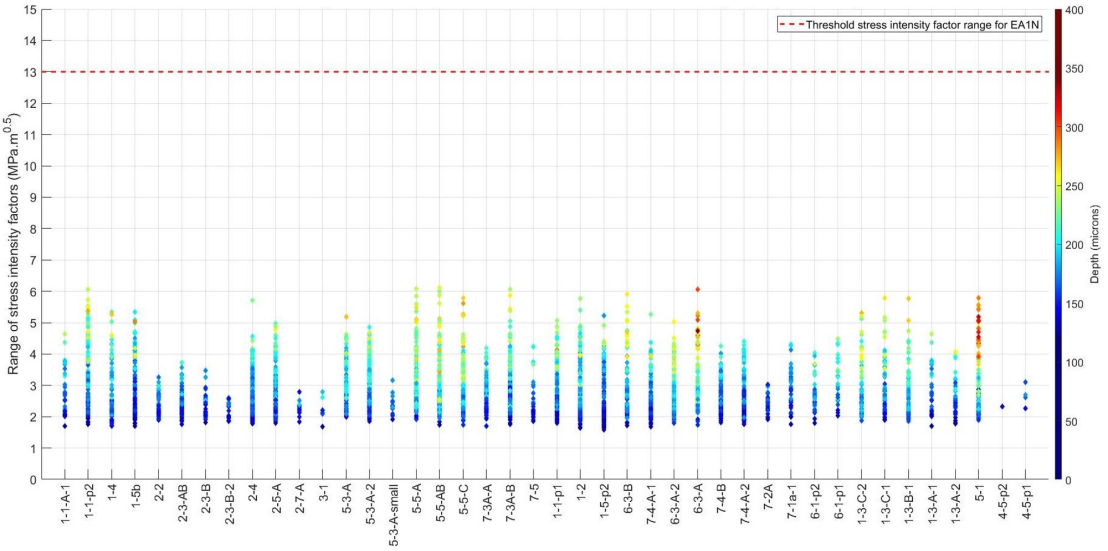

Figure 4.45: Stress intensity factor ranges for all pits, based on projected area in the Y axis using a compact boundary at 166MPa stress amplitude and with ΔK_{th} for EA1N marked. Coloured based on the depth

One of the downsides of this approach compared to analogous cracks, was that the location of the maximum SIF is not know. This means that it is not possible to consider the different locations of maximum SIF values, and the implications of that. In particular the damage observed in depots and from other experiments becomes harder to match to the outcomes of this work as a key comparator is neglected.

Values were based on several levels of simplification and assumption, so should be viewed with caution and more work is required to fully understand the implications of the results and added complications, such as the combined effects of multiple pits within a small area.

4.5.2 Comparison

Two techniques were presented for estimating the risk of a crack initiating from a corrosion pit. The first was based on mode I stress intensity factors calculated for a plate in tension. The pit was simplified to a two dimensional semi-elliptical crack, with the diameter of the crack at the surface being represented by the diameter of the pit in the plane that passes through the deepest point. The values for the X and Y plane were calculated separately. Two forms of the the equation were used depending on the aspect ratio of the analogous crack, up to a limit of two. The other technique was based on the work of by Murakami et al. [92, 93] using an El Haddad approach, where the $\sqrt{Area}$ parameter was linked to the ΔK value of the surface defect during fatigue. This technique required the projected area of the defect to be calculated in the X and Y plane. This was done using the convex hull, as opposed to a tighter boundary, due to the more conservative estimates that this technique produced that would produce results with a higher factor of safety.

The differences between these two techniques were fairly significant, with different input parameters being required. There was also a difference between the applicability of the two techniques. While there was no limit on the application of the $\sqrt{Area}$ approach, the aspect ratio approach was limited to aspect ratios below two. This means that some of the pits that were most interesting in terms of having outlying results were not able to be investigated using this technique.

On the other hand the aspect ratio equations were able to provide information that the $\sqrt{Area}$ technique was not. In particular it provided insight into the likely locations of crack initiation. This could provide significant outcomes around the conditions that corrosion initiated cracking occurs in, as well as critique of previous corrosion crack experiments on rail axles. When taken together both techniques were able to help provide a good overview of the crack initiation risk of a corrosion pit.

The maximum SIF values calculated using the aspect ratio technique were of the same order as the values calculated for the ΔK using the $\sqrt{Area}$ technique. Taking the ΔK of the tensile part of the cycle using the aspect ratio technique (assuming that the SIF drops to zero at zero stress) this appears to suggest that the compressive part of the cycle contributes a very small amount to the SIF values to the pit.

That being said, this is an assumption and the $\sqrt{Area}$ technique is more directly suited to this application. It requires lower levels of assumption as it considers the entire tensile compressive cycle, and was developed for this type of application. It also does not require the crack analogy to be used. Based on this the results from $\sqrt{Area}$ technique were judged to be more reliable and applicable than the results using the aspect ratio, although the locations of the maximum SIF are still an important outcome of this work and merit consideration.

The analysis carried out in the this Chapter is summarised in Figure 4.46.

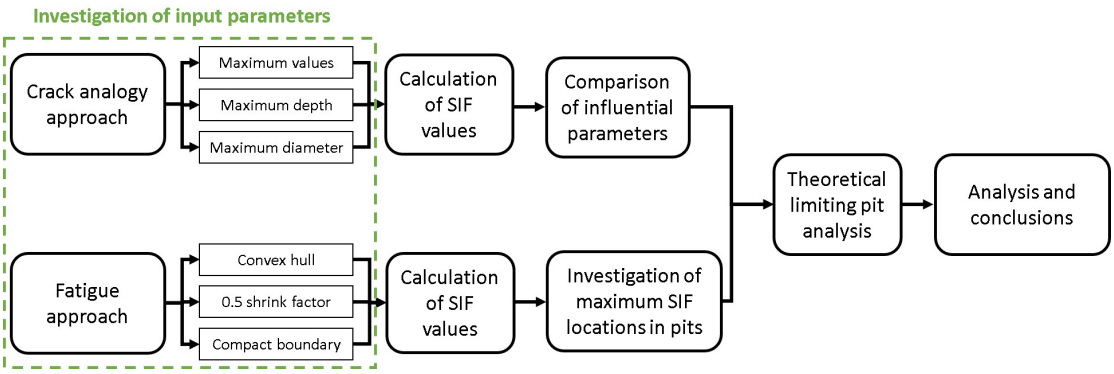

Figure 4.46: Summary of the analysis carried out in Chapter 4

4.6 Application to industry operations and standards

A key outcome of this work, and an aim of this project, was to consider the implications on the rail industry. In particular how this work interacted with the current standards and procedures. If changes to these could be made then potential financial savings or safety improvements could benefit the industry and customers.

4.6.1 Application of maximum standard pits

The work that had been carried out suggested that none of the pits identified in the survey would reach a level where a crack would be expected to initiate. However as previously seen from the corrosion survey none of the identified pits come close to the depth limit in the standard of 1000µm [5]. A key question, therefore is what is the risk of cracking if a pit was to be allowed to reach the depth limit of the standard?

To do this artificial pits were envisaged, based on the 1000µm depth limit and the average aspect ratios of pits in the survey based on the maximum values concept. This was chosen as it was the approach that was most similar to that used by the $\sqrt{Area}$ technique to calculate the area.

By assuming that the pit was a semi-elliptical bowl, the projected area could be calculated. This was then input into Equation 4.60, using the maximum allowable stress amplitude variation of 166MPa. The results can be seen in Table 4.3. Both of these SIF values were significantly lower than the threshold value of $13 MPa.m^{0.5}$ for crack initiation and propagation. This suggested that if a pit was allowed to meet the maximum allowable depth it would still be extremely unlikely to initiate a crack, the first step to the eventual failure of the component.

Table 4.3: ΔK values calculated based on the maximum allowable pit depth and average aspect ratio values

	Depth (m)	Aspect Ratio (Max Vals Mean)	Area (m^2)	ΔK ($MPa.m^{0.5}$)
X Plane	0.001	0.396	3.967E-6	8.54
Y Plane	0.001	0.405	3.879E-6	8.49

The locations of the maximum SIF value, using these assumptions, were also investigated using Equation 4.46. The result can be seen in Figure 4.47. The maximum value occurs in the centre of the pit, suggesting that surface cracking would not occur, making any crack from the pit more difficult to detect.

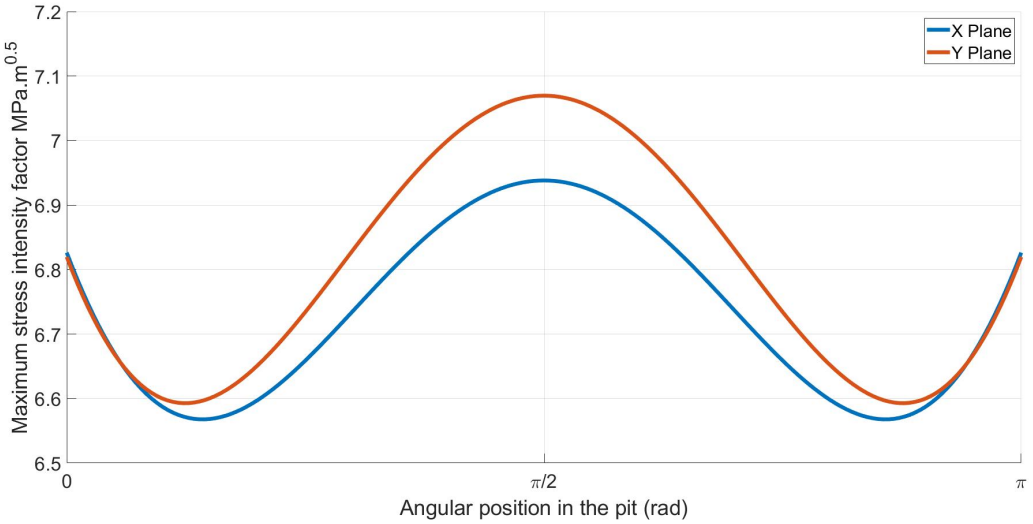

Figure 4.47: SIF values for a theoretical maximum depth pit at different angular positions within the pit

Using these results, the maximum allowable stress that an axle with this damage could withstand and remain below the $13MPa.m^{0.5}$ threshold would be 252.8MPa in the X plane and 254.3MPa in the Y plane compared to the current limit of 166MPa. This suggests that with current maximum depth limits the maximum designed surface stress could be increased by around 52% before the maximum permissible pit would risk crack initiation. This result was based on several layers of assumption and so should not be taken as an absolute value, however, it did demonstrate the extremely low risk that corrosion pits present to rail axles.

4.6.2 Implications and limitations

The standard was demonstrated to involve very high levels of safety within it, that contribute to the excess scrapping of rail axles. A hypothetical pit, based on the results of the axle survey, was assumed to reach the depth limit in the standard. It was demonstrated that the axle could have withstood a 50% increase in the stress amplitude before initiating a crack. This result was indicative rather than strictly accurate but still demonstrated the level of redundancy in the standards and provides a possible reason for the lack of axle failures in the last 20 years.

The axle survey from Chapter 3 found that pits generally did not exceed a third of the allowable depth, a finding that was supported by literature. These pits were shown to be at no risk of crack initiation. This finding showed that even if pits were allowed to reach the depth limit they would still have very large safety margins before becoming a risk. This demonstrates the scope within current standards and procedures to reduce the current scrapping of axles to corrosion damage.

Current practises appear to add extra levels of safety onto the levels in the standards. The standard appears to have a very large, up to 50%, margin of error which is then added to by depots as they cannot measure the depth of pits. This leads to them underestimating the depth of pits at around a third of the limit. This leads to over scrapping when it is not necessary. This outcome is based on the idea that depots scrap based on the depth limit. However, it has been demonstrated in Chapter 2 that the area limitation was more commonly invoked.

The area limit in the standard has its own issues, as the area of corrosion damage is dependent on the area of protective coating that had been removed from the axle, exposing the metal. It is less related to the severity of corrosion and risk of crack initiation from the damage to the paint layer. This made the relationship between area of corrosion and risk of cracking unclear.

There are several caveats to this work. These include the significantly simplified loading conditions assumed in this Chapter. While reasonable, this does reflect a deviation from the true loading of the axle. The other is that each pit is deemed to exist as a single incidence on an axle, with no accounting for interaction between them. It is not known to what effect these factors would influence the outcome, and should be the basis of further investigation.

There has also been no consideration of the competition model within this Chapter. The competition model is the idea that a crack will only propagate in a corrosive environment after the growth rate of the crack exceeds the corrosion depth increase of the pit. This means that below this threshold if a crack did initiate it would be overtaken and removed by the advance of the corrosion front.

The competition may have an effect on the threshold value of the crack initiation state if propagation after initiation is considered. As corrosion is a result of the system of the component's material and the environment it operates in, rather than being simply a material property, it is difficult to define the rate of competition accurately. For this work, the initiation of a crack, regardless of subsequent propagation, was viewed as a failure state.

4.7 Conclusion

As a follow on from the previous Chapter 3, containing the survey, this Chapter has some important outcomes.

Initially it has been shown how, when converting three dimensional corrosion pits into two dimensional features, there are several different concepts to do this. The results from these concepts can vary widely, and have significant impacts on the results of any further analysis. On the same point the difficulties with axle corrosion surveys that use a two dimensional approach are also shown to suffer from the same limitations with variations of up to 30% reported on an example pit. This questions the results of corrosion surveys that are conducted in this way, and demonstrate the benefits of a three dimensional approach.

The results of the fracture mechanics analysis of the pits suggested that current corrosion pitting damage found in the survey, would not result in crack initiation. Indeed, even if the standard was applied there would still be a significant margin before cracks would initiate. This demonstrated that there was a large amount of scope for current practices to change in judging permissible corrosion damage. This could result in a significant reduction in wastage of UK rail axles. However, the current practises were demonstrably safe.

The layering of safety margins at different levels of addressing corrosion damage was demonstrated. Due to the unsuitability of the standard to depots, multiple levels of conservative approximation are made resulting in extremely high factors of safety when axles are scrapped. This can be evidenced by the lack of any failures in the last 20 years. On the other hand this does lead to the near certainty that large numbers of axles are scrapped for corrosion damage that would be extremely unlikely to initiate cracking.

The results of the assessment of surveyed pits were that the parameter that had the strongest correlation to high stress intensity factors, and so risk of crack initiation, was pit depth, demonstrated in Figure 4.44 and Figure 4.45. This indicated that considerations of the pit depth were important to ensuring axle corrosion safety and should be included in any future standard. This outcome did, however, contradict the work of Cerit [35, 102] who suggested aspect ratio was a key factor. This was not borne out by the results of this survey.

The work also determined that the highest risk of cracking was coming from low aspect ratio pits with greater depths, with the highest SIF values being found at the bottom of the pits. The higher aspect ratio, and generally shallower pits were found to have lower SIF values and have their highest SIF values in the shoulders. This potentially calls into question the current methods of accelerated testing of corrosion crack initiation in rail axles, as surface cracking is often reported.

This does not appear, however to be the most risky crack location and neither has it been reported anecdotally from depots. Further investigation is required, but potentially too aggressive environments have been used in accelerated testing in the past, resulting in low depth, high aspect ratio pits that produce un-representative cracking at the pit shoulders.

Further work is required to make the results more specific to rail axle corrosion pits. In particular the assumptions made for the loading conditions and the interaction between multiple pits in close proximity.

The issue of changing nature of corrosion pits over time, in terms of geometric parameters and other features, is the topic of the other work stream and will complement the results of this thesis. The concept of the competition model will be returned to in a later Chapter.

4.8 Novelty

4.8.1 Industrial

In this Chapter an approach to quantify the risk from individual pits has been presented. The approach has been chosen with its appropriateness for use in a depot setting for practical application. This approach allows for the assessment of the risk of crack initiation from individual pits that was not previously available. Potential issues with the current standards, particularly in terms of depth and loading limits, have been presented. These could inform changes to the standards in future to ensure better outcomes for the industry.

4.8.2 Scientific

Within the work undertaken, the various concepts for parameter selection from pits has been demonstrated. By showing the variations that can arise from these different techniques the weaknesses of some previous methods has been demonstrated. This has called into question the veracity of some previous studies using sectioning inspection techniques.

The likely locations of crack initiation from corrosion pits on rail axles have also been explored. The outcome of this work suggests that the bottom of pits was the area of highest risk. This result suggests that previous accelerated corrosion testing to assess rail axle steels under stress, may have used too aggressive environments that lead to unrepresentative cracking. This can help to inform the design of corrosion experiments as well as possible inspection techniques in the future.

Chapter 5

Experimental Design and Procedure

5.1 Introduction

To be able to assess the risk of a pit causing a future failure in an axle, it was necessary to know how it would develop over time. To support this, an experiment was designed to investigate the changes in corrosion pit geometry over time, using an accelerated procedure.

As this experiment was of a new design, this Chapter details the design and manufacturing of the rig, as well as the justifications for the various cycles used in the experiment. The novelty of the design lay in its aims, design and the use of original axle surfaces as opposed to machined steel surfaces. The results from this rig filled a gap in the research of this area, regarding the progression of corrosion pits regardless of the cracking that may or may not occur.

There were several problems encountered during the operation of the experiment, requiring redesigning of the experiment and the construction and operation of additional rigs. The reasons for the changes and the reasoning behind the actions taken will also be discussed and explained.

The changes in the experiments had no significant effect on the outcomes so valuable results and conclusions were reached. These are presented in this Chapter and the experiments were shown to contribute significantly to informing UK standards and procedures going forward. The work flow of this Chapter is illustrated in Figure 5.1.

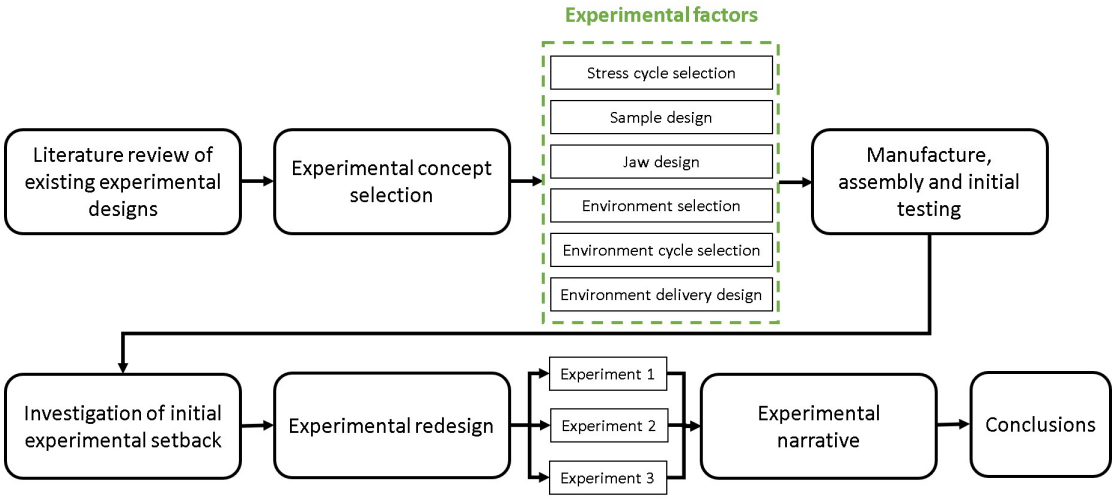

Figure 5.1: Work flow of Chapter 5

5.2 Previous rail axle experiments

5.2.1 Discussion of scope

There have been many experiments on rail axles. These have come in the form of crack growth tests, fatigue experiments and paint layer testing, to name a few examples. However, there does not appear to have been any testing of the growth and change in corrosion pit morphology over time on rail axles.

There have been experiments that contain elements that would directly contribute to the proposed experiment. These include the key parameter of applying corrosive mediums to samples undergoing stress cycles with special reference to the rail industry. The main issue with these experiments was the aims and outcomes that the work was attempting to produce that were not aligned with the aims of this experiment. Relevant examples and references will be given later in the Chapter.

A general exploration of experiments that cover rail axles that contained elements that would be useful to this experiment was performed to assess the approaches, techniques and rationale of previous work.

A way of separating the experiments into different sections was to divide them by scale. Experiments could generally be categorised as either large/full scale experiments or small/bench-top experiments.

5.2.2 Large scale experimentation

Large scale experimentation, in this case, was be defined as tests which involved the use of samples that were highly representative of real rail axles, being of comparative size. The easiest type of experiment to conceptualise, when trying to replicate the conditions of a rail axle, was one that used an actual axle or a sizeable portion of it.

Two examples of these types of experiment were resonance rigs and wheel-rail roller rigs, shown in Figure 5.2. These have often been used in industry and academia [19, 30, 105].

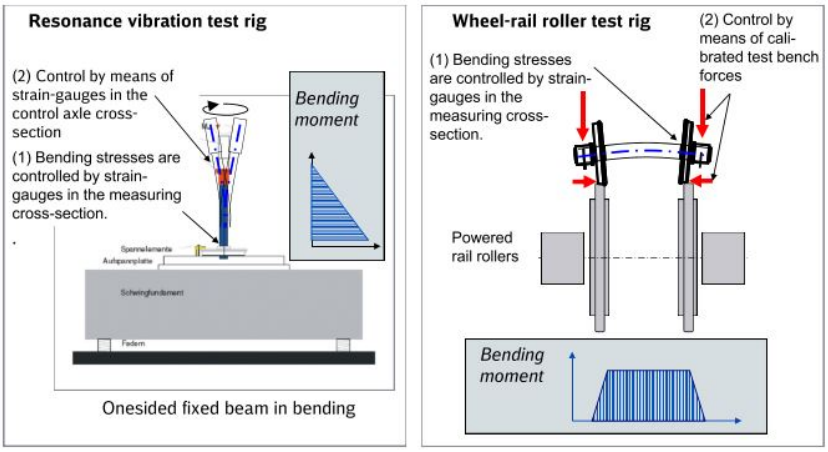

Figure 5.2: Resonance and wheel-rail roller test rigs [30]

The resonance test, an example can be seen in Figure 5.3, consists of an unbalanced rotor being placed on the end of a sample, often an axle with a wheel fitted. The wheel is clamped to the rig to provide a fixed base. When the unbalanced rotor is spun up, its forcing makes the end of the sample, which is unrestrained, describe a circle, creating a bending moment in the sample.

This produces a full $R = -1$ cycle in the sample, making it appropriate for crack propagation and fatigue testing. However, the bending moment produced is only constant in a single radial slice and changes throughout the sample, making replication of results problematic.

The wheel-rail roller rig is another piece of full scale testing equipment, popular as it is able to replicate many different types of conditions with a high degree of fidelity. By using a combination of hydraulic actuators and rollers, the loading, speed and other conditions of an active railway can be simulated in a laboratory setting to test the effects on vehicle components [107]. The components can then be attached to sensors and used to provide data on a wide range of conditions and circumstances that would be difficult to capture during day to day operations. Wheel-rail roller rigs can be used to test either single wheelsets or whole bogies depending on the size and complexity of the rig.

The advantage of this type of experiment over the resonance test, is that it produces a more realistic stress environment as the bending moment is the same across the entire axle body. This means more comparable testing sites are available per experiment [30].

Figure 5.3: Resonance test rig [106]

An example of a full scale rig can be seen in Figure 5.4. A key reason to use full scale roller rigs, rather than scaled samples, is the ability to test real standard components rather than special, one off, manufactured parts or samples.

Figure 5.4: Full scale wheel-rail roller rig [107]

A smaller scale experiment, although still using a full axle, can be seen in Figure 5.5. This rig uses a central actuator to cause bending in the sample as it rotates, producing a fully reversed stress environment.

This is very similar to the wheel-rail roller rig although it does not rotate through the movement of the wheels, but by direct drive to the axle. It is also actuated at the centre, rather than where the journals would sit as with the wheel-rail roller rig, to reduce the amount of force required to induce bending. This results in a more unrealistic bending moment as it is essentially a three point bending test as opposed to the four point seen in reality.

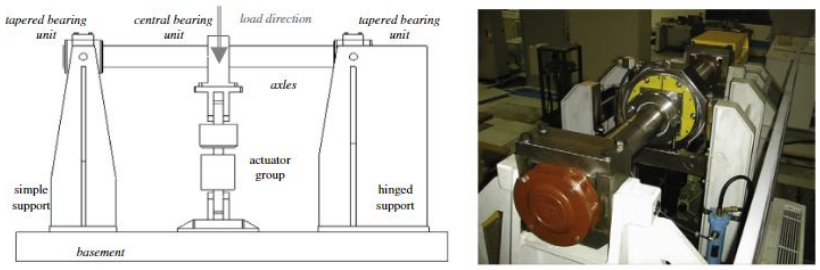

Figure 5.5: Bench test rig using a central actuator to cause bending. Diagram and image [108]

This last test has been used to conduct a corrosion fatigue experiment [109]. However the other tests do not appear to have been used in corrosive testing. This is likely due to the size of the rigs and the complication of including a corrosion facility.

While full scale rigs are useful and able to provide high fidelity results in terms of axle stress environments and simulation of real world conditions, they do come with downsides. Due to their size, weight, complexity and the forces required for such large samples, they are expensive and slow to develop and install. This limits the use of such rigs to facilities that have the time, space and resources. These restrictions ruled out the use of full scale rigs as part of this thesis.

5.2.3 Small scale experimentation

Another type of experiments is the small scale, or bench top, type. These are defined by samples that are significantly smaller than rail axles, and tend to be testing the material rather than direct axle replication.

The advantage of these smaller tests are the smaller size, cost and complexity, making them faster to produce and more adaptable to various experimental requirements. However, by using smaller samples there are significant trade-offs, particularly with the issues of stress replication and the effects of surface and subsurface features on the smaller samples compared to real world components.

An example such experiments is the small bench top rig developed at Politecnico di Milano and used in several similar papers investigating the fatigue life of axle steel [19, 24, 39, 110]. The experimental set up can be seen in Figure 5.6. The experiment consists of a rotating hourglass sample being exposed to a corrosive medium while undergoing stress loading. This appears to be based on a fatigue test described in the design methods of axles standards, EN13103 and EN13104, [15, 16], however with the addition of a corrosive chamber to allow for the application of the corrosive medium.

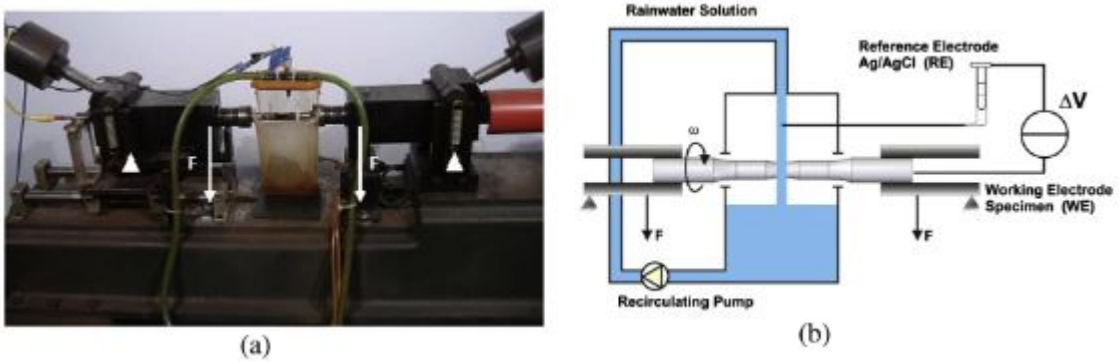

Figure 5.6: (a) Set up of Beretta et al. corrosion fatigue experiments. (b) Schematic drawing [39]

While this rig was not attempting to directly replicate the rail axle environment, the aim was to use factors that simulate the axle environment, such as stress frequency and the validation of crack formations. However, this particular technique while providing reasonable surface stress replication suffers from the issue of stress die off.

As bending consists of an equal compression and tensile element, with a central neutral axis, the bending stress will reduce towards the centre at a rate proportional to the diameter of the sample. While trying to replicate a 200mm diameter axle with a 10mm diameter sample with the same surface stress, a hypothetical pit that developed 1mm deep would experience 99% of the surface stress at the pit tip in the real axle, as opposed to 80% in the sample. This may call into question how the corrosion pits and cracking progress, given this disparity in experienced stress, within comparable features.

Other experiments that investigate the corrosion performance of axle steels, without the presence of stress cycles, are more simplistic in nature. These experiments consist of samples of the material, with polished surfaces, being suspended in a corrosive environment for set periods of time, with different wet/dry cycles [111]. These are more material engineering based tests, and try to provide the quantitative comparison of different materials performance in standardised environmental conditions rather than replicate the specifics of the rail axle environment.

5.2.4 Discussion

As previously mentioned, there did not appear to be a direct comparison of the experiment required for this project. However, there have been previous experiments that contained elements useful to this work.

Based on the literature a full scale test would be the best choice, with high fidelity of the axle environment. However, this was prohibited by the size, cost and time constraints of the project. This restriction means that a smaller scale test was required.

Having analysed the literature, it was clear that the stress and environmental conditions were complex to quantify, with a wide range used. This was due to the large range of conditions that rail axles experience. These different parameters will be discussed in following sections with more details of the selection process.

5.3 Aims of experiment

The aim of the proposed experiment was to produce information on the progression of rail axle corrosion over time. This would be achieved by comparing the before and after conditions of samples of rail axle steel being exposed to representative operational conditions.

The purpose was that this information would be particularly useful to maintenance depots, to have the largest effect on the industry, as this would be where any impact would be best realised. To be most useful to maintenance depots, the replicated conditions needed to be similar to conditions that axles would experience during operation across the UK.

It was also hoped that by designing an experiment that would replicate the rail axle environment accurately, the same design could be used in future studies that could investigate other issues relating to rail axles. Due to this, it was important when designing the experiment to include as many effects relevant to axles as possible, even if they were not strictly necessary for the current study, such as stress cycles.

5.4 Experimental requirements

To produce actionable information, the conditions the experiment replicated needed to represent a 'worst reasonable case' scenario. This was because the overriding focus of the rail industry is safety, so any experiment would need to assume a worst safety case so that anything less severe could be considered safe.

Initially the conditions that could be controlled were identified. These were identified as stress in the sample; environmental conditions; experimental cycle rates; sample surface condition and data collection procedures. These five factors were the focus of the experiment as they were controllable, had an potential effect on the corrosion of rail axles and influenced experimental design.

Outside of the technical aspects, the experiment must also meet more mundane restrictions. The designed experiment must be possible to build within budget and size limitations, as well as health and safety restrictions imposed by the University. Another significant deciding factor was the availability of equipment within the laboratories at the University, especially for the extended period that the experiment was required to run for by the nature of a corrosion experiment.

Stresses in the sample

The stress environment was relatively straightforward to define the limits for. In a simplified way a rail freight axle undergoes four point, fully reversed bending, at a frequency related to the train speed. There are other conditions, such as cornering, traction and braking forces and other aspects of operation that would effect the stress experienced by a particular section of a rail axle, however these would vary depending on factors such as the route being travelled.

The limit to the stress amplitude in EA1N steel, as defined by the RSSB standard [15, 16], is 166MPa. All axles should be designed to experience this stress level or less during operation, although this value is different for different steel types, defined by scale factors from 166MPa. As the proposed experiment aimed to produce a 'worst reasonable case' the sample should experience the limit use case, rather than a worst designed case.

Environmental conditions

Environmental factors are challenging to define and replicate in an accelerated corrosion experiment on rail axles. Due to the large geographical area that rail axles cover, it was problematic to identify a particular case that would be the basis of any replication. It was clear that, as corrosion is an aqueous process, rainwater would be the key medium of any corrosive process. Other factors, for example temperature, that may effect the corrosion process [112] would also need to be accounted for during decision making.

Any accelerated corrosion process would require a more severe form of corrosion medium to reduce the time required to replicate the natural process. The delivery method would also ideally replicate a worse case scenario, considering the location and specifics of rail axles in terms of shelter and movement.

Experimental cycle rates

The experimental cycle rates also required defining. This included both the cycle on which corrosive medium would be applied to the surface and the application of the stress cycle.

In an accelerated test there would need to be a trade off between different aspects of the cycles. For example, the experiment should seek to replicate around eight years of operation for the axle, as this represented an approximate time between overhauls. This would need to be compressed into a time that the experiment was able to be run over. The stress cycles applied would need to trade off between the frequency of the applied stresses and the total cycle count due to the time restrictions if one on these parameters was to be realistic.

Sample surface condition

As corrosion is primarily a surface effect, the condition of the surface would be of vital importance to the experiment. Due to the aim of the experiment to replicate the 'worst reasonable case' for rail freight axles, it was determined that pre-corroded rail axle surfaces would be used.

This would allow the highest fidelity possible at the start of the experiment, as the use of any 'perfect' metal samples would require the initiation of the corrosion, imparting bias depending on how it was achieved.

By using actual surfaces this starting phase could be assumed to be representative of axles on the whole. As the experiment was not researching the protective measures used in industry, no paint layers would be used.

In the analogy of a 'worst reasonable case' this would represent a scenario where the axle passed into a depot, was shot blasted to remove corrosion product and paint layers, then managed to pass through the rest of the process without inspection or repair. While this was extremely unlikely to happen, it represented the very worst case imaginable.

Data collection procedures

The experiment must also allow for the collection of the data. The experiment aims to assess the change in corrosion features over time. To do this the experiment should allow the collection of the state of the surface at the beginning of the experiment, and at the end. It was planned to use the same technique that had been developed previously in the project, and reported in Chapter 3, using replicating compounds and the Alicona machine.

5.5 Design concept proposal

Based on the requirements it was proposed that the experimental concept be based on a tensile test, using real axle surfaces. A basic diagram of the proposed concept can be seen in Figure 5.7. The equipment was able to produce both tensile and compressive force and so able to partially imitate the full bending cycle.

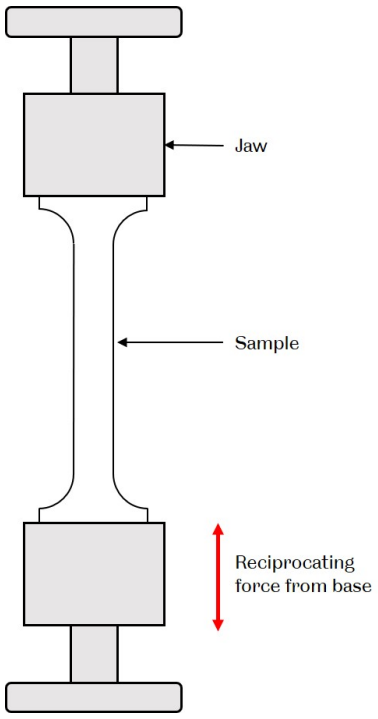

Figure 5.7: Basic diagram of proposed concept

The tensile test was selected for several reasons. Initially this was due to the availability of equipment. A large linear hydraulically actuated machine was available for uninterrupted use for long periods of time.

It was also more suitable than any bending equipment available, as corrosion is an effect confined to the surface layer. If the bending equipment available was used, then the samples would be so small that the stress die off towards the neutral axis would be extremely severe.

Using the linear equipment determined some other factors. As the samples would have to orientated vertically, any corrosive medium would need to be delivered to the surface through a spraying action, under pressure. Any dripping or other gravity fed techniques would have to be discounted. This was not a particular disadvantage as it would allow the corrosive medium to be spread more evenly over the sample surface.

The decision to use real axle surfaces also required project specific jaws to be made to allow the samples to be held in place. An additional complication was that by using real axle surfaces, this prevented flat samples being used, as would be standard in a fatigue test. This required the designing of rounded jaws to allow the use of the machine.

To support this experiment two axles were donated by an overhaul depot, and can be seen in Figure 5.8. Both of these axles were donated as they had failed inspection in the depot, due to corrosion damage that is visible in Figure 5.9. These axles were used to produce the samples for the experiment.

Figure 5.8: Axles donated to the project from overhaul depot

5.6 Stress replication and corresponding designs

Rail axles undergo four point bending during normal operation with added torsional and cornering effects. This would be highly problematic to replicate on a small scale, as applying force to a sample undergoing four point bending, while rotating, can be technically challenging. When using a small sample in bending, due to the reduced cross section, the stress reduction per unit distance into the sample, would be unrepresentative of a full axle.

If a larger sample were used to overcome this problem, then proportionately more force would be required to produce the stress at the surface. A linear test, using equal tensile and compressive cycles to replicate either side of the bending cycle, avoids the issue to a large degree. However, this lacks any torsional components in the stress profile, amongst other issues.

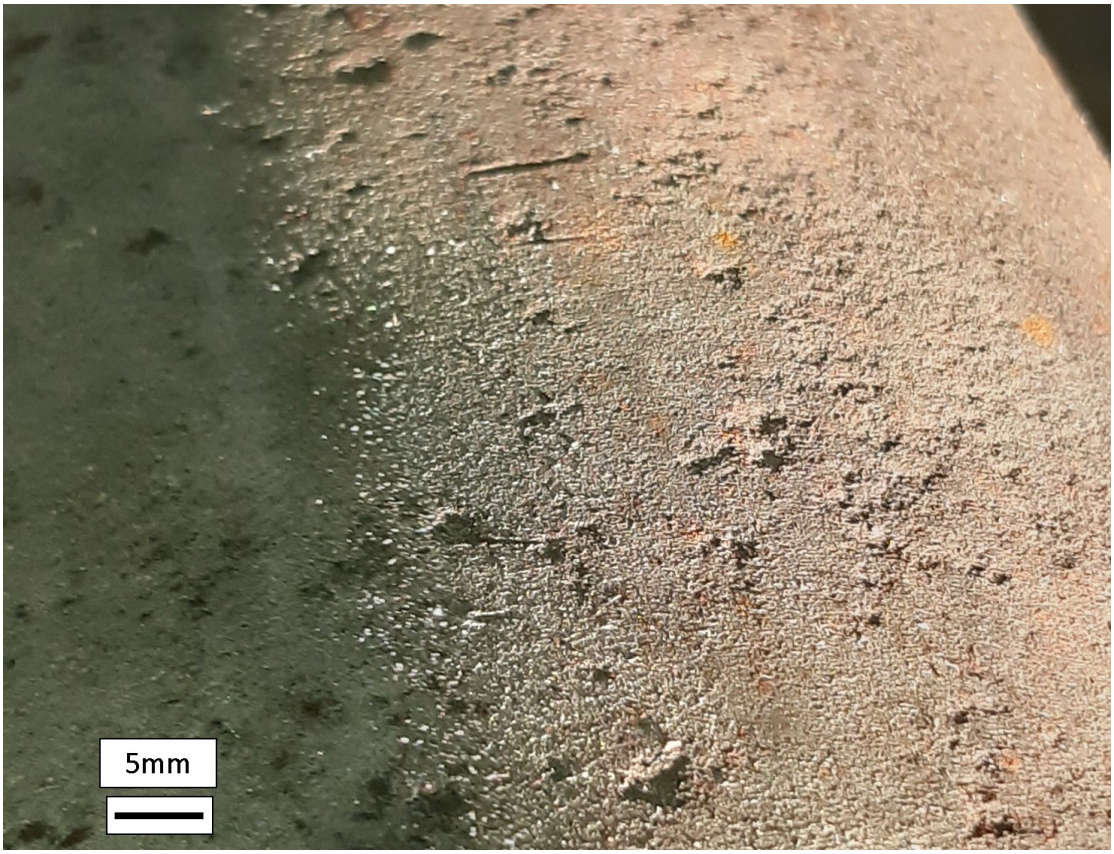

Figure 5.9: Image of the surface one of the donated axles, demonstrating visible corrosion damage

To assess the stress profile in axles a stress analysis was performed, based on the calculations used in industry from BS EN 13103 [15]. The values chosen were based on the axle donated to the project and other representative values. These values can be seen in Table 5.1. The axle was assumed to be a, non-guiding, solid axle with no breaking or drive train equipment attached to it.

Table 5.1: Values used in representative stress calculation

Parameter	Symbol	Unit	Value
Wheelset mass	m_2	kg	1100
Laden mass	m_L	kg	54000
Height of centre of gravity	h	mm	1780
Radius of wheel	R	mm	460
Distance between journal centres	2b	mm	1940
Distance between wheel rolling circles	2s	mm	1505

A free body diagram of the scenario can be seen in Figure 5.10. These calculations are used widely in industry to assess the acceptability of rail axle designs in terms of stress limits.

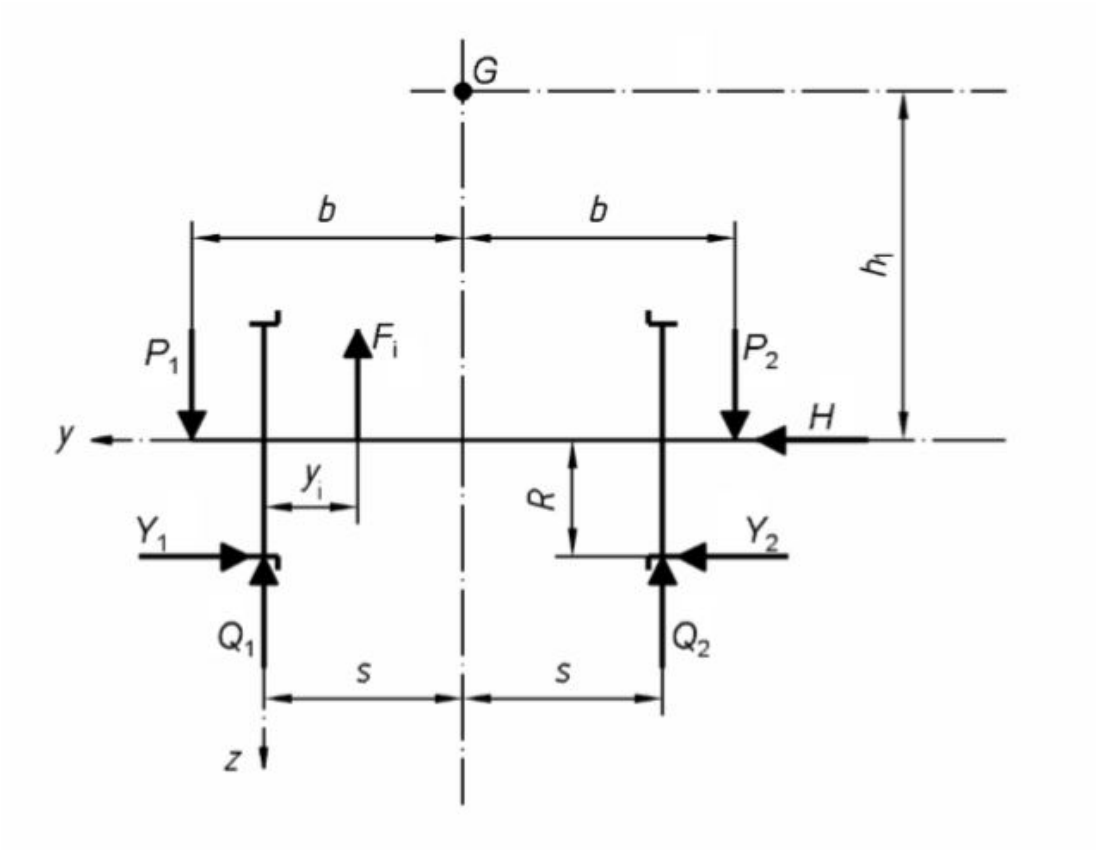

Figure 5.10: Free body diagram of axle scenario to assist with stress calculation [15]

All of the following equations used in the worked example were taken directly from the UK design standard [15]:

$$MPW = \frac{m_L}{4} \times g = 132.4kN \tag{5.1}$$

$$w = m_2 \times g = 10.8kN \tag{5.2}$$

$$m_1 = MPW - w = 121.6kN \tag{5.3}$$

$$H = Y_2 = 0.15 \times 121.6 = 18.24kN \tag{5.4}$$

$$h_1 = 1780 - 460 = 1320mm \tag{5.5}$$

$$P_1 = (0.625 + 0.075\frac{h_1}{b})m_1 \times g = 88.4kN \tag{5.6}$$

P_1 represents the the vertical force acting on the heavily loaded journal.

$$P_2 = (0.625 - 0.075\frac{h_1}{b})m_1 \times g = 63.58kN \tag{5.7}$$

P_2 represents the vertical force acting on the the less loaded journal.

$$Q_1 = \frac{1}{2s}[P_1(b+s) - P_2(b-s) + (Y_1 + Y_2)R - \sum_i F_i(2s - y_i)] \tag{5.8}$$

Q_1 represents the vertical force acting on the more heavily load wheel. The final term allows for any reaction due to braking or traction equipment, which is neglected in this scenario.

$$Q_2 = \frac{1}{2s}[P_2(b+s) - P_1(b-s) + (Y_1 + Y_2)R - \sum_i F_i y_i] \tag{5.9}$$

Q_2 represents the vertical force acting on the the less loaded journal. The final term allows for any reaction due to braking or traction equipment, which is neglected in this scenario.

$$Q_1 = 97.57kN \tag{5.10}$$

$$Q_2 = 54.41kN \tag{5.11}$$

$$M_x = P_1 y - Q_1(y - b + s) + Y_1 R - \sum_i F_i(y - b + s - y_i) \tag{5.12}$$

Let y be b so at the axle centre:

$$M_x = 29.1kN \tag{5.13}$$

$$M'_x = M'_z = 0 \tag{5.14}$$

$$M'_y = 0.2PR = 0.2\frac{(m_1 + m_2)gR}{2} = 6.09kN \tag{5.15}$$

$$MR = \sqrt{MX^2 + MY^2 + MZ^2} \tag{5.16}$$

$$MX = M_x + \sum M'_x = 29.1kN \tag{5.17}$$

$$MY = \sum M'_y = 6.09kN \tag{5.18}$$

$$MZ = \sum M'_z = 0 \tag{5.19}$$

$$MR = 29.73kN \tag{5.20}$$

$$\sigma_n = \frac{32\sqrt{MX^2 + MZ^2}}{\pi \times (2R^3)} = 60.33MPa \tag{5.21}$$

The normal stress uses bending of beams with a circular cross section.

$$\sigma_t = \frac{16MY}{\pi \times (2R^3)} = 6.313MPa \tag{5.22}$$

The torsion stress is calculated using torsion of beams with a circular cross section.

$$\sigma = \frac{32KMR}{\pi \times (2R^3)} = 61.64MPa \tag{5.23}$$

$$Stress\ limit = 166MPa \tag{5.24}$$

This calculation demonstrated, that the torsional component of the stress was around an order of magnitude lower than the normal stress. While this was still important, it demonstrated that using a tension and compression approach was capable of replicating the stress of an axle body with a reasonable level of fidelity.

A difference between the linear approach and a bending one, would be the lack of stress reduction away from the surface. In an ideal scenario a sample under tension or compression would experience the same stress level at every location within the sample. In a bending scenario the stress reduces from a peak at the surface to zero at the neutral axis.

In an axle body, which is a cylinder, this neutral axis would be at the centre. Using the donated axle as a guide, with a diameter of 169mm, for every 1mm away from the surface toward the neutral axis the stress would be expected to drop 1.18%. As 1mm represents the limit on corrosion pitting depth, this would be deepest into the axle that the experiment would be looking to replicate. A 1.18% error would be well within reasonable tolerances for an experiment for this sort.

5.6.1 Experienced stress cycles

A key factor in deciding on the appropriate stress cycle to use, was the stress cycles experienced by rail axles in operations. The design standard limits the surface stress to 166MPa in the body, but most rail axles will not be operating at this limit all the time, if at all. Loading information is often presented in the form of a stress histogram of the loading experienced by the axle.

In the literature there appears to be very little information about the stress cycles of freight wagons. Information exists as to the axle load limits of many types of wagon [113], however without the corresponding axle dimensions to calculate the maximum experienced stresses in the axle bodies.

Loading information has been collected for passenger vehicles previously, with axles having strain gauges attached and being monitored in normal service. An example of this was the T356 [114] study undertaken by Delta Rail, to determine the influence of track and train parameters on the stress environment of axles. There are also other examples of this work being performed, such as an investigation into German high speed trains [105] and as part of the WIDEM EU project [115].

This data was discounted for this project. This was due to the differences in loading between passenger and freight axles. For example, the variation between tare and loaded weight for passenger vehicles, is far lower than that of freight wagons [116] at 1.5:1 for passenger vehicles and 5:1 for freight wagons. Passenger services also run significantly faster than freight trains in most instances [116].

Other experiments have experienced the issue of estimating realistic stress cycles and have dealt with it in several ways. Watson performed a series of calculations, assuming that the axle working stress operated in the range of 80%-100% of the allowable maximum [117], giving an approximate range without basing the result on any particular data set.

A stress histogram of a freight axle was produced as part of the WIDEM project [103]. This can be seen in Figure 5.11. Based on this data, three other stress histograms were estimated, assuming the maximum allowable stress of 166MPa was used as the maximum stress in the histogram. These can be seen in Figure 5.12.

In both figures, the cycle axis is on a logarithmic base 10 scale. This means that the vast majority of a freight axle's life was at stress levels well below the maximum allowable, as would be expected.

The limited amount of data suggested that the selection of a stress level was ultimately a decision based on what conditions are being replicated, rather than any standardised testing level.

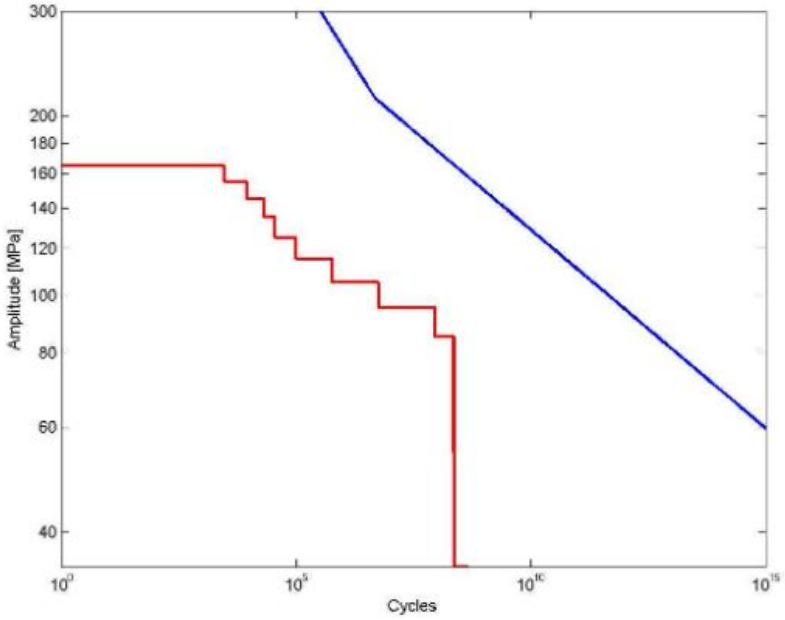

Figure 5.11: Freight axle stress histogram, compared to fatigue limit of A1N steel [103]

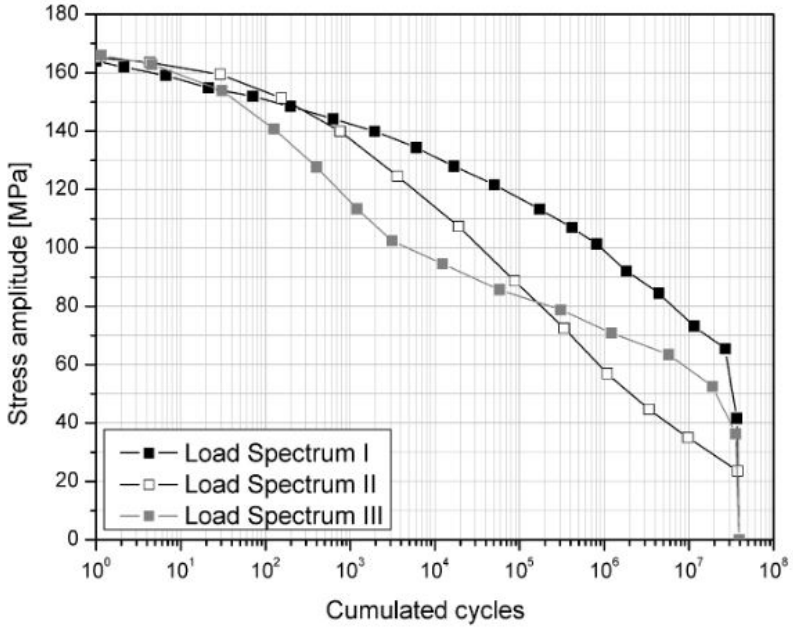

Figure 5.12: Three estimated stress histograms of a freight axle, used in work by the WIDEM project and based on extrapolation of measured data [103]

Stress cycles could also be applied in different ways, although they were almost always fully reversed (R=-1). The three methods were:

1. **Fixed amplitude loading**

This involves selecting a force that corresponds to a given stress level and applying it to the sample throughout the experiment [15, 16]. In a fully reversed test that seeks to replicate the axle environment this is most often in the form of a constant sine wave. This is the simplest form of stress loading, however may miss effects to do with variation in stress levels.

2. **Block loading**

   If a stress histogram has been produced, and several different stress levels of interest have been identified, a loading block sequence can be defined [41, 103]. A simple example would involve applying load level 1 for a set number of cycles, then load level 2 for a number of cycles then returning to level 1. This can be as complex as desired, and allows for the correct number of cycles at different stress levels to be applied.

3. **Data driven loading**

   This approach can be used if journey data is available [114]. The axle can be forced in such a way to replicate the actual loading it would go through on a given journey. This is not often used due to the problems of accelerating the testing process ahead of in service components, despite the high fidelity of results, as well as issues collecting the journey data.

5.6.2 Selection of stress in experiment

As was demonstrated by literature, there was no standard procedure for selecting the stress to be applied to replicate the rail axle environment. Based on the work undertaken in literature [103, 117], best displayed in Figure 5.11 and Figure 5.12, the limit of 166MPa is rarely reached and only for a few cycles, indicating a lower stress would better represent rail axle use cases.

A decision of the appropriate level would need to be based on the aim of the experiment. As the experiment was aiming to provide a cause to challenge the standard in terms of permissible corrosion damage, a scenario that tended towards a more severe case, rather than less severe, would be preferable to provide an upper limit on the damage.

It was decided that a maximum designed surface stress of 120MPa would be selected as it would represent a significant level of loading for the axle, that occurs for thousands of cycles based on the stress histograms. A higher value than this would only occur a small percentage of cycles, so could not be considered representative of the conditions as a whole.

Fixed amplitude loading was chosen as the method that the stress would be applied. This was due to a lack of data as to the actual distribution of cycles throughout a freight axles journey. This would also lower the complexity of the experiment.

Monitoring of stress cycles in operation

One of the difficulties of this experiment was the ability to measure the stress level in the sample. There were several ways of doing this, using strain gauges or extensometers being the most common.

These both worked by detecting the change in resistance in a wire under strain to infer the strain in the sample allowing the stress to be calculated. Strain gauges are stuck to the sample with adhesive, extensometers use blades to bite into the sample and measure the relative movement between the two blades.

While both forms of testing were available at the University, both were deemed to be unsuitable on advice from lab technicians. On the face of it the extensometers would be ideal, as they could provide the average strain over the entire sample. However, the extensometers are quite large pieces of sensitive electrical equipment that were difficult to make waterproof. Due to this is was decided that these would be unsuitable for use in the corrosion chamber, as the risk of damage would be high.

The strain gauge seemed to be a more practical solution, with the ability to be stuck onto the sample. However, due to the small size of these gauges, the strain in a localised area would be measured. Given the corroded geometry of the samples that are part of the experiment this could lead to a misleading view of the stress profile.

Due to the corroded surface of the samples, attaching the strain gauges would be difficult, as they required a smooth surface to be effective. On top of these issues, the use of the any electronics inside the corrosion chamber would be problematic with risks to the equipment and calibration issues.

It was decided that the best way to move forward would be to analytically calculate the load required to meet the desired stress and verify with Finite Element studies that the correct stress value was being reached.

The analytical and Finite Element approaches were used because there was no technique available to measure the stresses in the samples directly. However, the analytical and Finite Element approach was reliable for two reasons.

Firstly the material that the samples were made from, EA1N steel, was a well understood and predictable material. This meant that there were no complicating factors such as may have been the case with a composite material or a newer steel. Because the behaviour of the material was well understood, it was possible to use the results of the analytical and Finite Element studies with a high degree of confidence.

The second reason that analytical and Finite Element results were reliable was the regularity of the geometry of the dog-bone samples. Due to the regular sample geometry, to maximise the areas of the same stress levels in the gauge length, there was a low risk of complex stress conditions occurring. This increased the likelihood that the calculated results were similar to those experienced by the sample during the experiment.

One parameter that could be monitored during the experiment was the force applied by the hydraulic rig. This was done by using the load cell build into the machine that provided real-time feedback on the force exerted on the sample. Through monitoring of the applied force, as well the analytical and Finite Element analyses, the stress experienced by the sample would be known to a high degree of confidence.

5.6.3 Sample design

The following section details the design process for the samples that were used in the experiment.

5.6.4 Requirements

There were several requirements for the samples to allow them to provide useful information for the project.

- **Provide sufficient surface area to to allow a reasonable number of results**

  Given the long term nature of a corrosion experiment, it was not possible to run multiple repeats. Any experiment would have to provide enough pits, and by extension sufficient area, to allow useful conclusions to be drawn. This meant that the stress conditions should be materially the same over the entire area of interest, to allow like for like comparison.

- **Must be capable of reaching the desired stress, within the limit of the equipment available**

  The sample geometry must be chosen such that it was possible to reach the desired stress within the area of interest, given the limitations of the equipment available to provide forcing and the geometrical limitations.

- **Not fail through buckling**

  Given the requirements for a large investigative area, but limitations of applicable force, a thin sample was required. A risk of a thin sample was the possibility of buckling. The experiment was trying to produce a large area undergoing the same stress conditions. Buckling would produce significant stress variations throughout the sample. Any design should attempt to create conditions where crushing rather than buckling would occur.

- **Use the existing axle surface as the area of interest**

As a requirement from the design concept, the use of the existing axle surface was desirable, to provide a better replication of the corrosion conditions found in rail depots. This requirement necessitated the use of curved samples, complicating the design of both the samples and jaws.

5.6.5 Initial design and analytical checks

Using the requirements for the samples, an initial design concept based on a dog-bone sample was used. This would allow a large area for investigation and the same stress conditions throughout the area of interest.

The use of the original axle surface was problematic. Due to this requirement, and the limitations of applying the force to the samples, a non-regular shape was required. Any starting point would be based on a chord from an axle, with one curved and one flat side. This made centrally loading the sample difficult and meant only half the surface area was viable for experimentation.

To address this issue it was proposed that two samples would be produced and placed back to back in the rig. This created, in aggregate, a regular shape with an easily defined centre and double the surface area for the experiment to investigate. As long as the samples were securely clamped together with no relative movement, this was a viable strategy.

Using this concept, and the idea of a dog-bone sample, an initial design was developed and iterated through basic analytical calculations. This design can be seen in Figure 5.13.

Loading requirements

An initial calculation was the force required to produce the desired stress in the sample. Based on a desired stress of 120MPa and an area of 380mm^2 per sample, the required loading from the rig was 91.8kN in compression and tension, to produce an $R = -1$ loading scenario. This was well within the ability of the available laboratory equipment to provide.

Analytical buckling analysis

A draw back of this sample was its length, with the risk of buckling failure. To check this an analytical buckling analysis was under taken.

The first step was to calculate the slenderness ratio. A very long, thin beam would have a high slenderness ratio and would be likely to fail by buckling before crushing. A short, squat column would have a low slenderness ratio and would be likely to fail through crushing before buckling could occur.

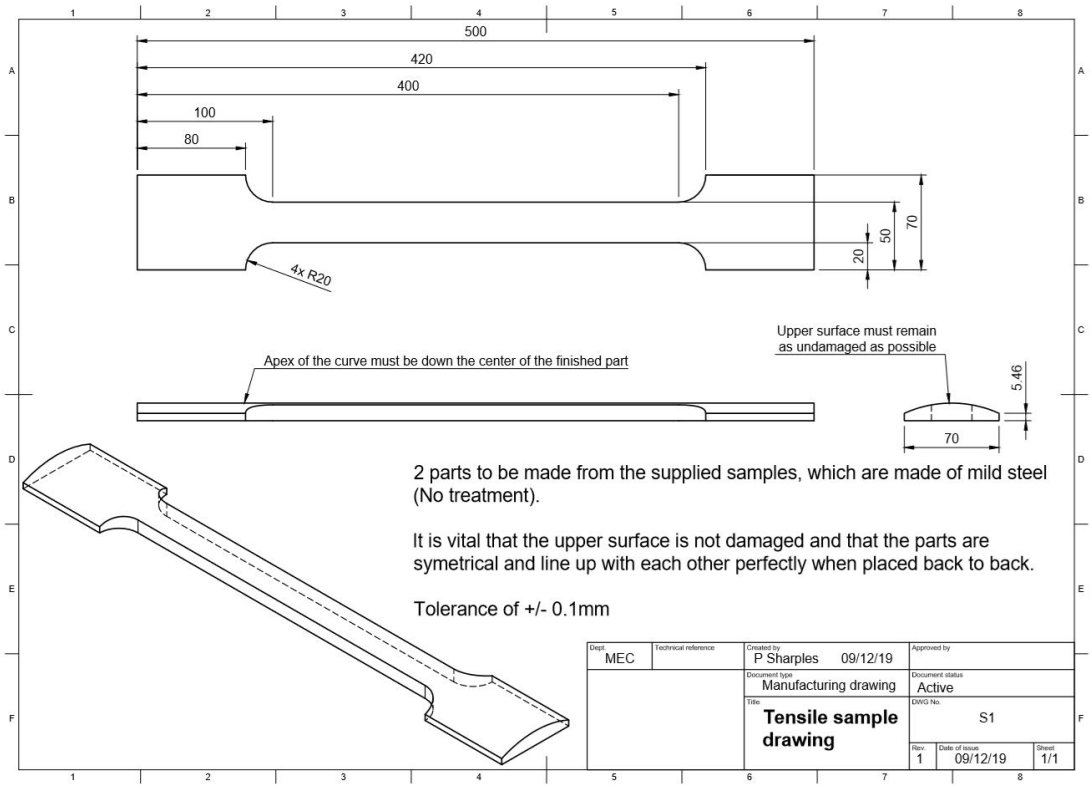

Figure 5.13: Production drawing of the samples produced

The equation for the slenderness ratio can be seen in Equation 5.25 and is the ratio of the effective length of the column and the radius of gyration, which is given in Equation 5.26.

$$S = \frac{l_e}{k} \tag{5.25}$$

$$k = \sqrt{\frac{I}{A}} \tag{5.26}$$

To determine if a column was a long column or a short column the critical slenderness ratio needed to be established. This value was based on the properties of the material. Above the critical value the column can be considered long and obey Euler's laws of buckling and below the column is considered short and obeys Johnson's parabolic formula [118].

Johnson's parabolic formula is an empirically defined formula that describes the critical buckling stress of short columns, as the Euler equations tend to infinity, as can be seen in Figure 5.14. The equation for the critical slenderness ratio is given and calculated in Equation 5.27. S_{cr} is the critical slenderness ratio, E is the Young's Modulus of the material and σ_y is the yield stress.

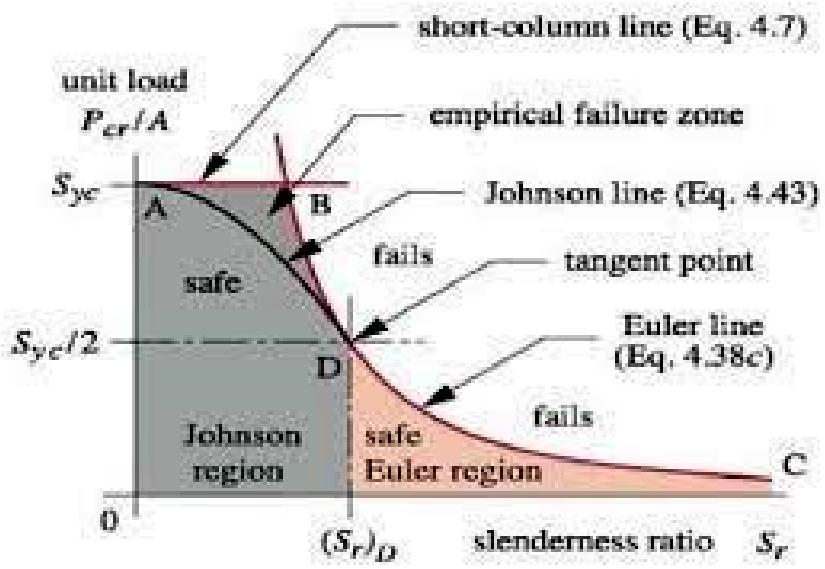

Figure 5.14: Figure of the relationship between Johnson's parabolic formula and Euler's buckling equation [119]

$$S_{cr} = \sqrt{\frac{2\pi^2 E}{\sigma_y}} = \sqrt{\frac{\pi^2 \times 206 \times 10^9}{370 \times 10^6}} = 104.83 \tag{5.27}$$

Based on the design shown in Figure 5.13, the area of the central section of each sample was $380mm^2$, the second moment of area was 5097mm^4 and the critical length of $350mm$. This lead to a slenderness ratio of 95.63 which was well below the critical slenderness ratio of 104.83, meaning the sample was categorised as a short column.

Using Johnson's parabolic formula, seen in Equation 5.28, the critical stress was calculated as 216MPa, which corresponded to a critical force of 82.1kN per sample, meaning the rig would have to exert a total force of 164.2kN to cause a buckling, well below the calculated requirement of 91.8kN.

$$\sigma_{cr} = \sigma_y - \frac{1}{E}\left(\frac{\sigma_y}{2\pi}\right)^2 \times \left(\frac{l_e}{k}\right)^2 \tag{5.28}$$

5.6.6 Finite Element Analysis

After arriving at an initial design, the samples were tested numerically using Finite Element techniques. This was a relatively straightforward way to double check that the analytically calculated results were accurate and that the samples would perform as expected.

The set up for this analysis can be seen in the Appendix B. This set up includes geometry creation, material properties, boundary and loading conditions and mesh independence analysis. The results presented here were the outcomes of the analysis after checking the validity of the set-up.

The analysis was separated into two cases, the tensile case and the compressive case. These were analysed separately to ensure that the sample would perform adequately throughout the entire tensile-compressive cycle.

Results and discussion

The main results that were analysed in each case were the equivalent stress (von-Mises) and displacement perpendicular to the axis of loading. The former was used as an assessment of the risk of failure of the sample. The displacement was used to check that no buckling, that would effect the stress environment of the sample, occurred.

The results of the tension case are presented first, and can be seen in Figure 5.15 and Figure 5.17. The maximum stress value in the sample, was calculated as 171MPa and occurred in the shoulder of the sample, as would be expected given the geometry. This can be seen in more detail in Figure 5.16. The 171MPa value was above the 166MPa maximum stress amplitude permitted on rail axles by the design standards [15, 16]. However, it was still below the fatigue limit of the EA1N steel of 200MPa defined in the same standards and away from the area of inspection. This suggested that no failure would occur during the experiment and the results would not be effected by the higher stress level.

Based on this simulation no failure in the sample was expected without secondary influences that were not accounted for in the simulation. The stress within the gauge length was consistent at 120MPa, with a maximum variation of $\pm$1.75MPa, representing a $\pm$1.5% variation in stress within the gauge length.

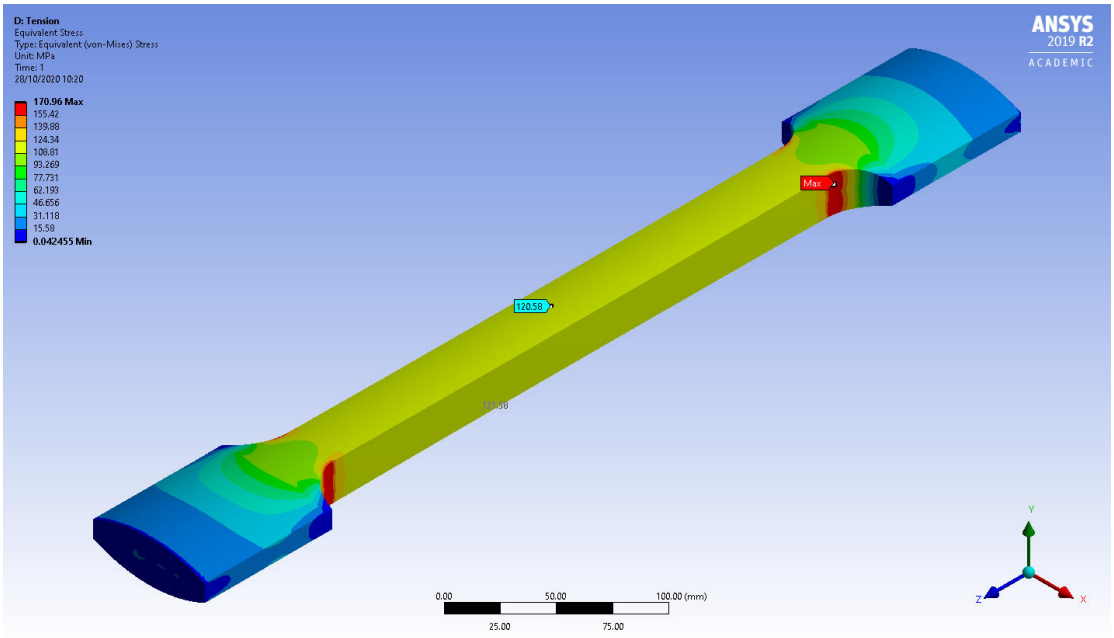

Figure 5.15: Von-Mises stresses of the samples under the tension load case

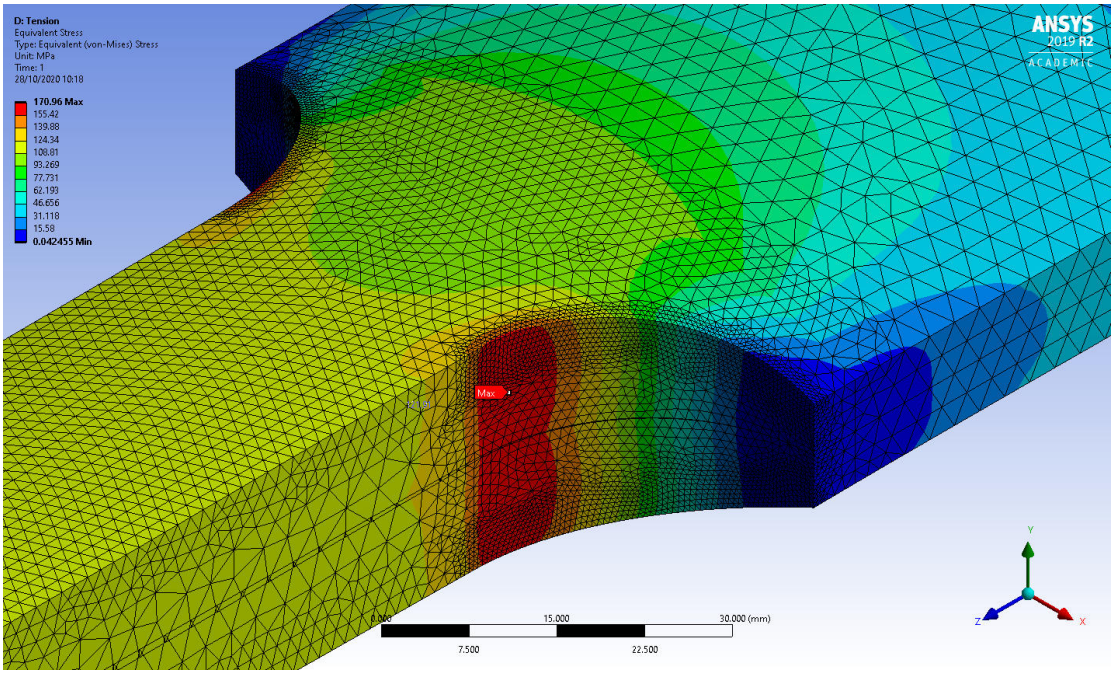

Figure 5.16: Von-Mises stresses of the samples under the tension load case, zoomed in on the location of the maximum stress

The displacement perpendicular to the axis of loading under tension, can be seen in Figure 5.17. This represented any gaps opening between the samples, that may have changed the stress environment. As would be expected in the tension case, no significant gap occurred, with the very small displacement being almost entirely down to contraction described by Poisson's ratio. The displacement toward the central axis displayed by both samples in Figure 5.17, demonstrated the effect of reduced cross section under tension.

The compression case was considered next. The same results, Von-Mises stress and perpendicular displacement, in the compression case can be seen in Figure 5.18 and Figure 5.20. The stress result again stood at 171MPa, within the fatigue limit of the steel. The location of maximum stress was also the same, as seen in Figure 5.19. This suggested that the samples were moving between a pure tension and pure compression case, with minimal buckling or other displacement that might lead to a change in the stress in the gauge length. The stress in the gauge length remained 120MPa throughout.

A difference between the tension and compression cases could be seen in the perpendicular displacement. As shown in Figure 5.20, a gap had appeared between the samples (Figure has increased scale to make gap visible). The maximum gap between the samples was 0.039mm, a similar value to the tension case, representing a very small movement in each sample. Due to the similarity in displacement values, but with a reversed direction, to the tension case, it was judged that the displacement in compression was also due to the effect of reduced cross section area under loading.

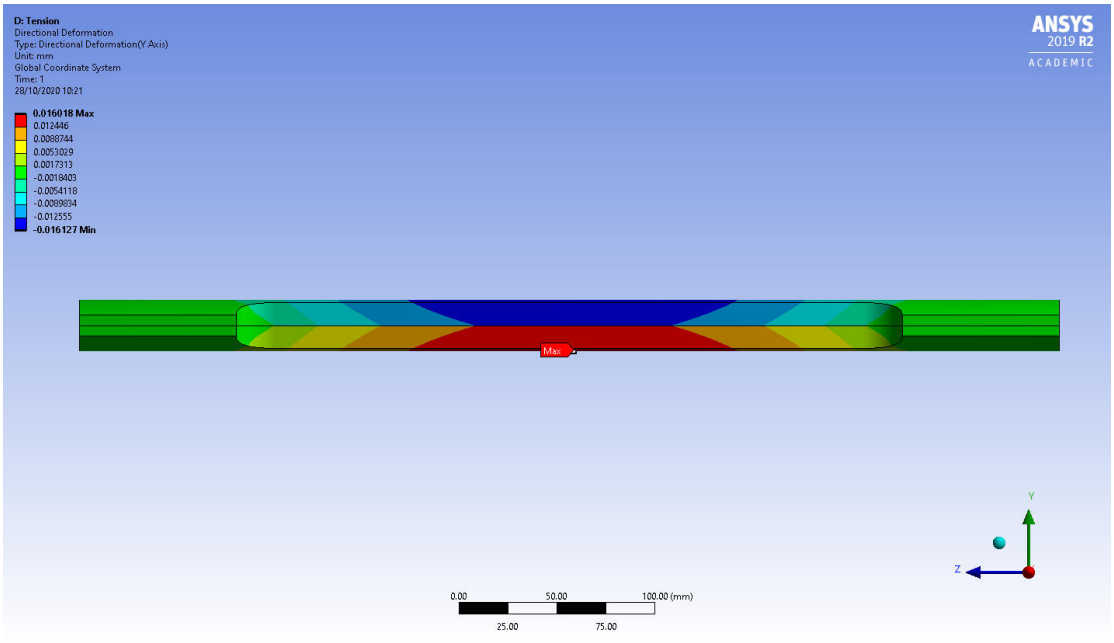

Figure 5.17: Displacement in the samples, due to tension, perpendicular to the axis of loading (Y-axis)

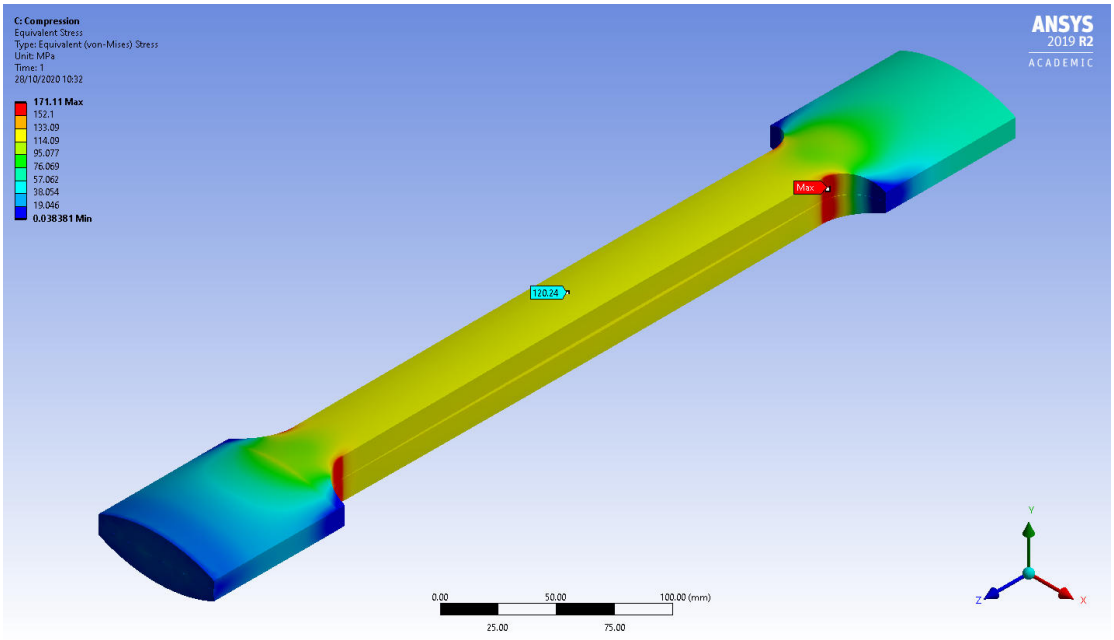

Figure 5.18: Von-Mises stresses of the samples under the compression load case

Based on the small value of displacement and the lack of a significant variation in the stress environment of the gauge length it was decided that this displacement was not significant enough to cause concern.

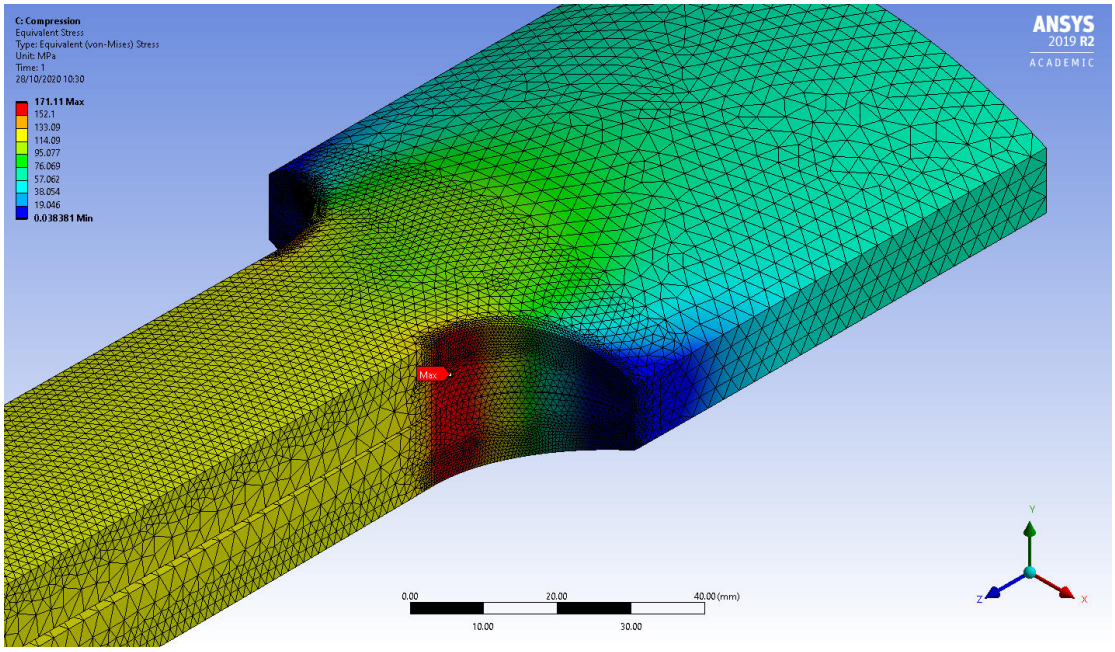

Figure 5.19: Von-Mises stresses of the samples under the compression load case, zoomed in on the location of the maximum stress

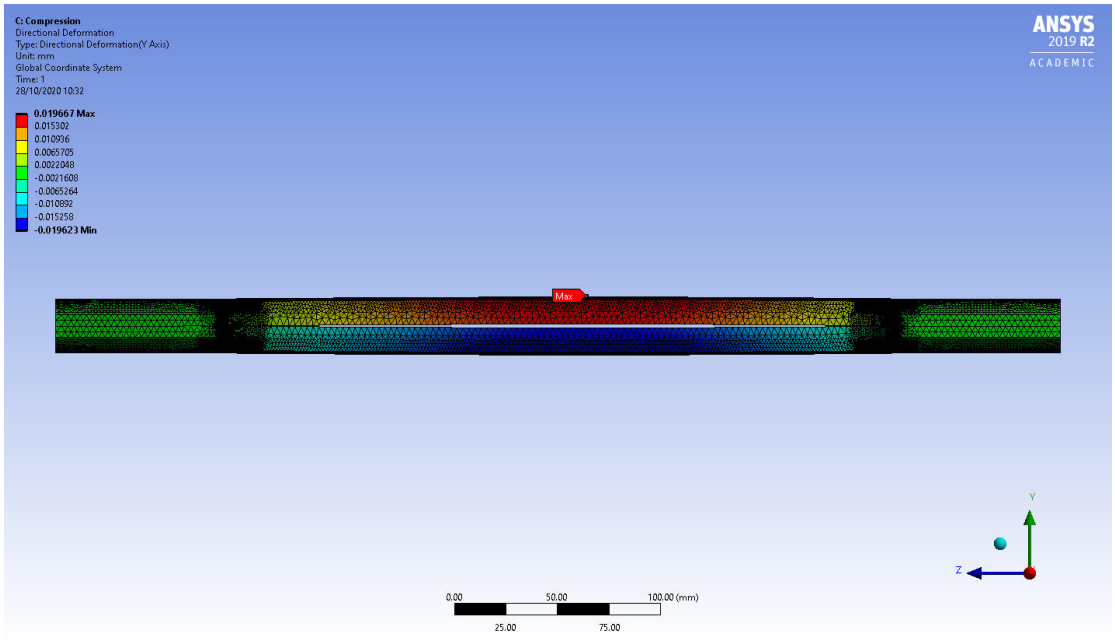

Figure 5.20: Displacement in the samples, due to compression, perpendicular to the axis of loading (Y-axis)

In conclusion, the results of the Finite Element analysis indicated that the samples were suitable for use in the experiment. The maximum stress values were within the fatigue limit of the material, suggesting it would not experience failure due to cyclic loading. No buckling behaviours were predicted, meaning that the inspection area would have the same stress environment along it's entire length. This meant that results collected at different locations on the sample would be comparable.

5.6.7 Manufacturing process

The samples were cut from the donated axles provided by a depot. They were scrapped for corrosion at overhaul, however the locations of the unacceptable corrosion were not known. The axles could be seen in Figure 5.8 shown previously.

The axles had been stripped of paint and corrosion product, as part of the inspection procedure at the rail depot. However, due to problems having the samples cut, creating a 12 month delay, some corrosion product would have reformed. It was ensured that they were stored inside in a dry location, so any corrosion would have been minimal.

The first stage was to cut a chord from an axle to make the samples, while retaining the corroded surface, shown in Figure 5.21. The samples were made by cutting a single, long chord from the axle, then dividing that in two to make two sample 'blanks'. This process was carried out by an external contractor due to the size and weight of the axles. A saw was used, despite the risk of residual stresses being produced, due to the impracticality of spark eroding, laser or water jet cutting from the size and geometry.

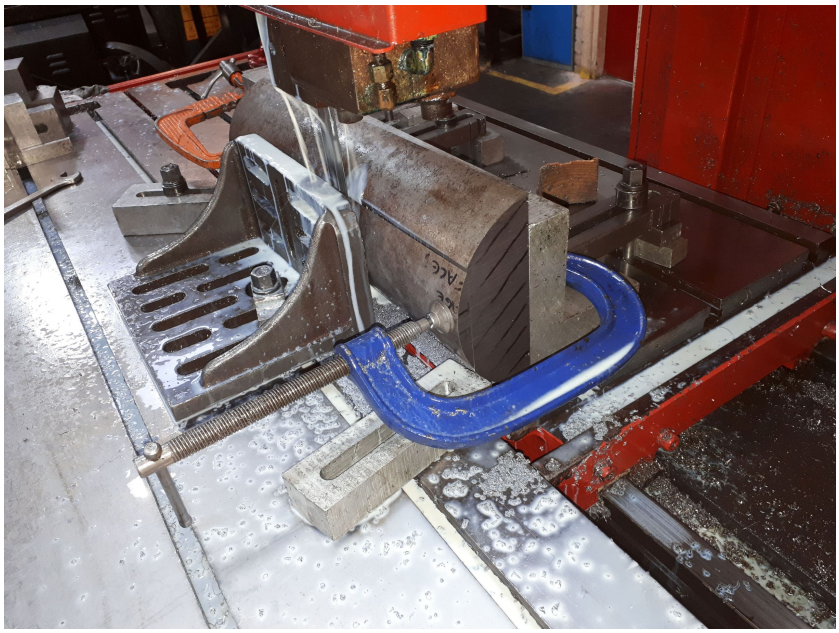

Figure 5.21: Cutting of the sample blanks from the original axle

The sample blanks can be seen in Figure 5.22. On inspection both samples displayed areas of the desired corrosion damage, which can be seen in Figure 5.23, although large areas of physical damage were also present. These included large areas of denting or scaring. Upon inspection, it was decided that these areas would be removed through the following machining steps, or would be located within the jaw clamping sections, and so have no impact on the samples.

Figure 5.22: Sample blanks as received from cutting service

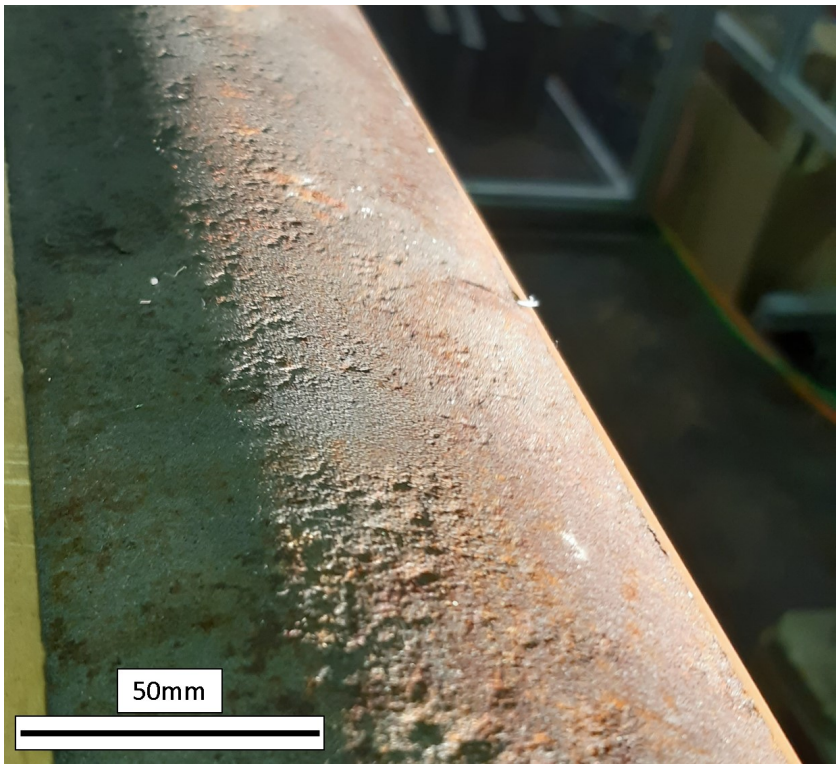

Figure 5.23: Close up of corroded surface of one of the sample blanks

The sample blanks were cut into the desired shape, shown in Figure 5.24. This was done using spark erosion, as this would not produce additional residual stresses. The samples were measured and compared to each other and were found to be, within the workshop tolerance of ± 0.1mm, identical to each other in terms of outline.

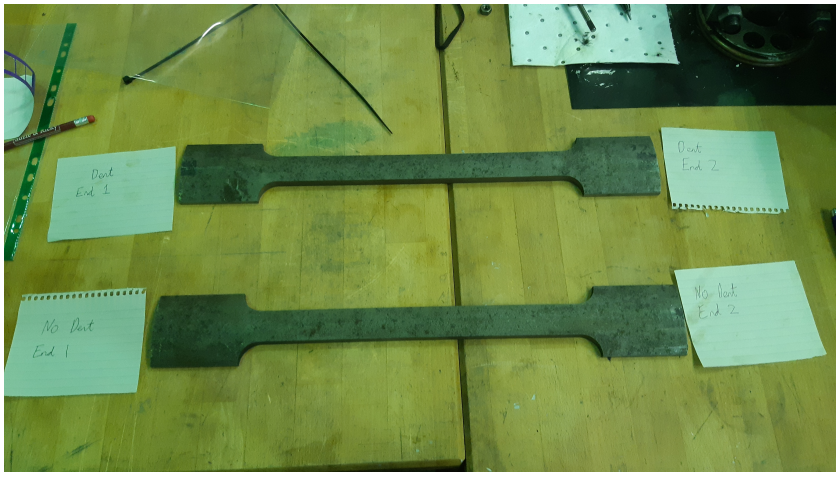

Figure 5.24: The two samples after being spark eroded into shape

The samples were cleaned to remove any debris from the machining process. After this a light phosphoric acid bath was used to remove any corrosion product that had built up on the surface during storage or handling. The aim was to produce a set of samples that were as close to what would be present in a rail depot.

5.6.8 Jaw assembly Design

The experiment called for the use of a tensile testing machine that was capable of applying the required load, at a defined frequency, for the time required for a long term test.

The equipment available for tensile testing fell into two categories, hydraulic and electrically driven machines. The electrical machine could be immediately discounted, as they were unsuitable for fatigue testing. This was due to their use of a screw thread to apply the forces. In a fatigue test this driving thread undergoes the same fatigue as the sample, causing rapid deterioration in the usefulness of the machine. This left a hydraulic actuated test rig.

The rig chosen was a Schenck 250kN hydraulic test rig, with a MOOG controller that can be seen in Figure 5.25. This machine had an upper section, which remained stationary when set, and a lower bench top, which contained the hydraulic ram head.

The experiment, by its nature, required an extended testing time, unusual for the lab it would be performed in. Because of the time requirement, this particular machine was offered as it was available for long term use. Project specific jaw assemblies would have to be produced for the test to be carried out.

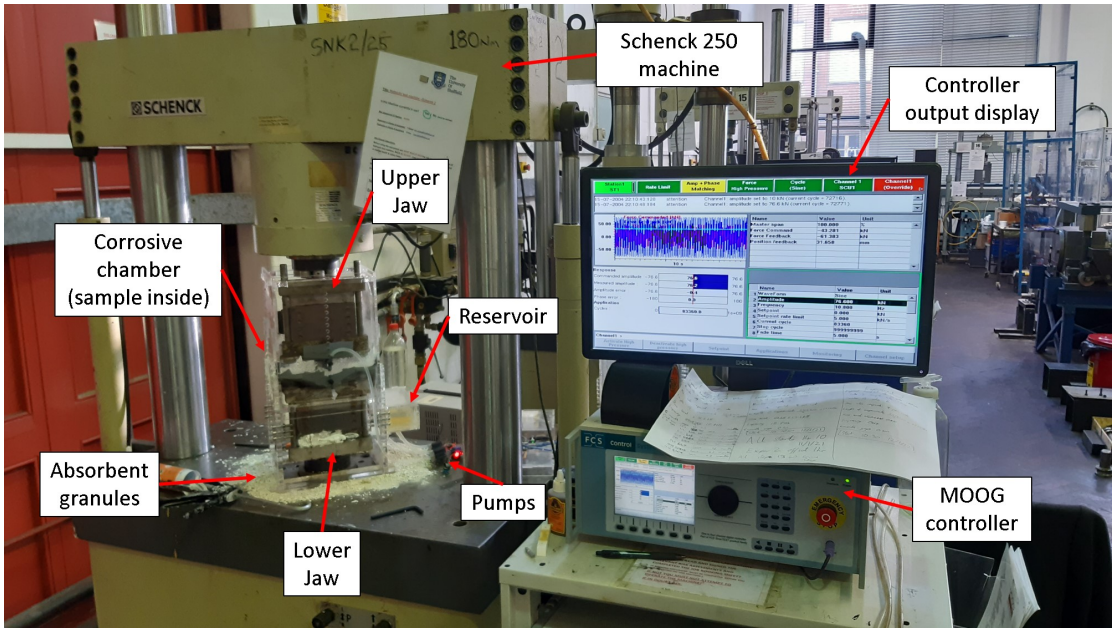

Figure 5.25: Image of Schenck 250kN hydraluic test rig with controller (Rig installed)

The design, manufacture and initial testing of the jaw assemblies can be seen in Appendix B. This includes the design methodology, analytical and Finite Element analysis of the jaw assembly under different loading conditions. The torquing values and process for the bolts to deliver the appropriate force are also calculated and justified. Initial snag testing was also undertaken, resulting in changes and additions to the design.

The outcome of this work was a new, bespoke, set of jaws that were capable of performing to the experimental requirements.

5.7 Environmental replication

In an experiment looking to replicate corrosion damage, the environment used was of great importance. The environment needed to be well defined to replicate conditions that the rail axle may experience, however it also needed to be more aggressive than actual conditions to allow for the acceleration of the corrosion damage into an experimental time scale. The increased aggressiveness would have to be balanced against being too extreme, as this could result in unrepresentative results seen in some previous experiments [37, 39, 109].

Rail axles can work in a large geographical area, with some freight journeys being over many thousands of miles, the Trans-Siberian railway being a famous example at over 5,700 miles. Even with a much smaller geographic area such as the UK, axles could be expected to operate over a large area with sometimes significantly varying environmental conditions in terms of corrosion of metal.

Atmospheric corrosion can be broadly defined in three categories: rural; urban; and marine, each with different corrosion rates of metals [18, 120]. Corrosivity maps have been produced broadly indicating areas with differences in corrosion effects due to environmental factors. One for the UK can be seen in Figure 5.26.

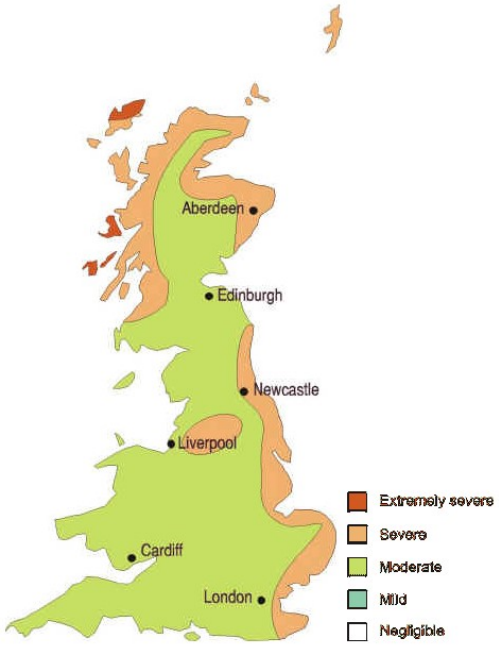

Figure 5.26: Corrosivity map of the UK [121]

A rail axle works in an environment under a locomotive where it may be exposed to dust, oil or any other contaminants including any leakage from the cargo being carried, which may effect the corrosivity of any corrosive medium that contacts the surface. An example of this can be seen in Hoddinott's paper [37] which mentions severe corrosion damage to a salt hopper wagon, which failed at Shields Junction in 1998.

In the 1998 accident it was suggested that the damage was severe due to salt water becoming trapped next to the surface of the axle. There is also evidence of increased corrosion on passenger train axles which are located underneath the toilet out flows [6]. No work was identified in literature which investigated any specifics of the rail axle environment beyond general environmental conditions.

Other considerations of the rail axle environment include the velocity effects and shielding. These involve the relative air velocity produced by the train moving at speed, as well as the rotation of the axle itself. Both of these could affect the wet/dry cycle and possibly prevent any droplets forming on the surface, effecting the corrosion development.

Rail axles are placed underneath trains and so experience a certain level of shielding from direct precipitation. This does not protect them from other forms of moisture such as dew or mist but will affect how the surface is wetted.

As corrosion requires an aqueous environment, the most obvious source for this for a rail axle was precipitation. This formed the basis of the replicated environment.

The corrosive medium used was based on that used in the experiments of Beretta et al. [24, 39, 110]. This in turn was based on the composition of rainwater in Manchester in 1986 as laid out in previous papers [122, 123].

The Manchester rainwater concentration was increased ten times for use in Beretta's experiments to accelerate the testing. However, this occasionally led to Hoddinott cracking, a type of failure that only appears to develop in extremely corrosive environments, such as saltwater trapped against a surface [37]. Hoddinott cracking is where a large number of cracks can be seen on the surface of a corroded axle. This was demonstrated in Figure 2.13.

Experiments by Beretta et al. using the corrosive medium detailed in the paper, resulted in a significantly reduced knee in the SN curve, dropping the fatigue limit to below the design limit laid out in EN13103 [15]. This was a result that did not seem to be borne out in reality, shown by the lack of axle failures in the fleet since the EN13103 standard was introduced. This was possibly due to the use of a severe corrosive medium in the experiment, which was not representative of normal axle experience.

It is undoubtedly true that the risks of environmental damage, such as acid rain, have dropped in the UK since 1986, due to de-industrialisation and increasing environmental measures. The original readings used to produce the artificial rainwater composition were unavailable. However, the data of the precipitation composition at a DEFRA weather station near Manchester was compared between 1986 and the period of 2009-2019 [124].

While not directly comparable to the composition of the rainwater used in the original paper, due to slight geographical differences, it demonstrated the significant change in the rainwater composition between these two periods. Many of the elements present in the rainwater were at between 25% and 75% of the values that were present in 1986, and the pH was 10% of the acidity, as seen in Table 5.2. The lower values of all contaminants suggested that the corrosiveness of the rainfall in the UK had fallen significantly compared to 1986.

Table 5.2: Rainwater composition near Manchester, UK, comparison between 1986 and 2009-2019 [124]

Parameter	Unit	1986 value	2009-2019 value	Current as % of 1986
Calcium	mg/l	2.28	0.80	35.1%
Chloride	mg/l	4.99	2.93	58.7%
Potassium	mg/l	0.30	0.16	53.3%
Magnesium	mg/l	0.29	0.19	65.5%
Sodium	mg/l	2.24	1.66	74.1%
Phosphate	mg/l	0.07	0.03	42.9%
Nitrate	mg/l	0.79	0.43	54.4%
Ammonium	mg/l	0.70	0.69	98.6%
Sulphate	mg/l	2.73	0.55	20.1%
Non-marine sulphate	mg/l	2.54	0.41	16.3%
Conductivity	µcm/l	49.36	22.14	44.9%
pH	N/A	5.00	6.02	9.6% (of acidity)
Rainfall	mm	21.58	32.48	150.5%

Based on the drop in pollutants that were known to increase corrosion potential, such as chloride and sulphate, and to avoid Hoddinott cracking [37] in the sample, the make-up of the solution was based on the 1986 sample but with the chemical concentrations halved.

The resulting solution was made up using the salts shown in Table 5.3 with ten litres of deionised water. The salts were measured out using calibrated scales as seen in Figure 5.27.

Table 5.3 details the salts added to the deionised water rather than the composition of the corrosive medium, such as that detailed in Table 5.2. The aim of the salt mix was to achieve an artificial rainwater composition with concentration values five times higher than the 1986 values detailed in Table 5.2.

Table 5.3: Salts mixed with ten litres of deionised water to form artificial rainwater

Parameter	Value	Unit
Ammonium sulphate	23.1	mg/dm^3
Sodium sulphate	15.98	mg/dm^3
Sodium nitrate	10.63	mg/dm^3
Sodium chloride	42.43	mg/dm^3

Figure 5.27: Equipment used to weigh out salts before being added to the artificial rainwater mixture

The pH of the artificial rainwater was tested using a pH meter, to allow comparison with other experimental solutions. First the meter was calibrated, using a buffer solution (pH 4) after which the probe was rinsed in de-ionized water. The probe was found to have a systematic error of 0.24pH, which was subtracted from the measured pH in the artificial rainwater.

The test indicated the pH of the solution to be 5.61pH with a resolution of 0.01pH, after the error had been removed. This value was 2.56 times lower than the pH of the rainwater between 2009-2019. This meant it was more acidic than the conditions that an operational axle would encounter today.

5.7.1 Environmental delivery

As the experiment called for the application of artificial rainwater to the samples, and no chamber existed that would be possible to use with the rig, a bespoke solution was required. This meant the assessment of the requirements of such a device, producing a concept and then designing and manufacturing the parts. This included the corrosion chamber and the delivery control system.

Requirements

The first stage in designing the chamber, was the identification of the requirements that it must fulfil. The experiment necessitated that artificial rain water be applied to the samples in a cycle, discussed later, over an extended period. From this general description, more detailed requirements were produced.

- **The chamber must be able to apply the corrosive medium in a controlled manner**

  The corrosive medium needed to be able be applied to the samples based on a cycle, discussed later in the Chapter. To do this it would need to be possible to control when the artificial rainwater was being applied to the surface. This require both control of the flow of the artificial rainwater and the ability to determine the appropriate time to do so.

- **The artificial rainwater needed to be applied under pressure**

  Due to the samples being held vertically, the artificial rainwater could not be dripped onto the samples under gravity, as was the case in some experiments. To achieve the desired wetting of the sample, some method of pressurising the water would be required.

- **The artificial rainwater needed to be kept away from the other equipment of the rig**

  A key factor in being allowed to use the rig was to ensure that it did not become damaged during the experiment. One of the most obvious ways that the hydraulic rig could become damaged was through the introduction of water into its internal systems. This was most likely to occur around the ram head, as a gap exists which could allow the water access. To prevent this it was vital that the rig did not leak.

- **The rig must be able to operate safely in the event of a water spillage**

  In the event that the corrosion chamber did leak and water escaped, it was important that this did not cause any danger to people in the area. For example, this would prevent the use of high voltage electronics.

- **The artificial rainwater needed to be applied evenly to the samples**

  In operation it was vital that the samples were evenly wetted, to prevent any variation between sites, that may impair comparison.

- **Data regarding the atmospheric conditions that the sample undergoes needed to be collected and stored**

A key part of corrosion are the conditions in which it takes place. To this end information that may be relevant to the experiment, such as the temperature of the local environment, needs to be collected and stored to allow for analysis.

Concept

Using the requirements listed, an initial concept was proposed that would cover the design requirements. A diagram of the basic concept can be seen in Figure 5.28.

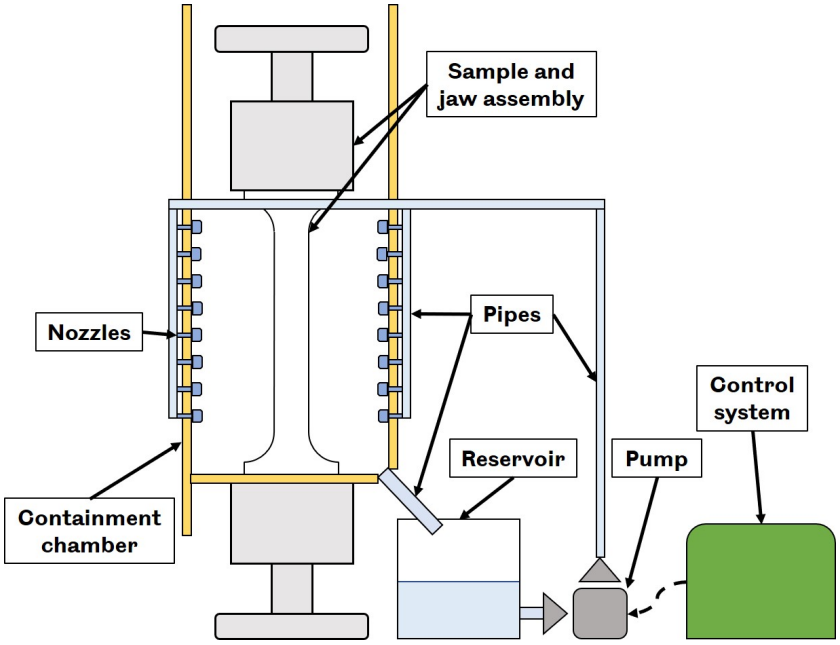

Figure 5.28: Basic concept of the environmental delivery system

The system consisted of a series of spray nozzles that sprayed the artificial rainwater onto the surface of the sample under pressure. The run off then flowed into a reservoir that supplied the pumps that created the pressure required for the nozzles to operate. The samples and nozzles were housed within a containment chamber that acted as both the physical support for the nozzles and prevented the spread of the water, directing it back toward the reservoir. The corrosion chamber sat separately from the sample and jaw assemblies supporting its own weight, to reduce the issue of movement induced by the hydraulic ram head.

Containment chamber

The containment chamber consisted of an aluminium frame, to provide stiffness and stability, with laser cut acrylic side panels to mount the nozzles and contain the artificial rainwater. This can be seen in Figure 5.29.

The design was divided into two halves, connected together around the sample and jaw assemblies. The acrylic side panels had holes cut into them to allow the nozzles to be push through and held in place.

Figure 5.29: Image of the corrosion chamber used to contain the corrosive medium during the experiment. Corrosion chamber has been assembled within larger rig (white material removed before testing)

The front and back panels were not attached rigidly to the aluminium frame to allow for any movement caused by the oscillation of the base in operation. Instead they were clamped in place allowing for their removal to access the samples.

The bottom of the chamber was formed of waterproof tape, laid to form a continuous flexible floor of the chamber. This was sloped so that the water, upon landing on the floor, would be directed toward the upper reservoir, that acted as a collection point for the artificial rainwater.

The upper reservoir had a waterproof tape top attached to it to prevent any loss of artificial rainwater. The pumps were connected to the lower reservoir and the nozzles by flexible hoses.

Clear acrylic was used to allow the operator to view the samples and assess if everything was working correctly. All the joints in the rig were sealed using silicone sealant.

Control system

The control system to deliver the corrosive medium to the samples was designed to be simple and cheap to produce. The system required design, physical manufacture and coding before testing and final assembly.

The system was controlled by an Arduino Uno, a commercially available micro controller, which helped keep costs low and allowed for easy use of existing peripherals and code snippets.

A real time clock was included to allow for accurate time keeping without the drift seen with processor clocks, due to variations in the demands on the processor. An LCD screen was included to allow for display of the cycle count and the time until a state change (from dry to wet or vice versa). When a state change was required a signal was sent to the 5V relay that switched to power the two 12V centrifugal pumps that pumped the water to the nozzles.

There was a temperature sensor attached to the outside of the box to measure the general temperature that the experiment was operating in. Data on all of the workings of the control system and the data measurements, were stored on a SD card attached to a breakout board. Finally a series of LEDs were used as error indicators to show problems with the code.

The decision to use 12V pumps was taken to decrease the risk if the electronics came into contact with any water. It was found that a single pump was insufficiently powerful to get good flow through all the nozzles, so two were used, each powering one side of the system.

An issue with the pumps selected, was that they needed to have water within them to work as they were unable to pump air alone. This required the reservoir level to remain above the pumps at all times, to prevent damage. Centrifugal pumps were used due to their ability to withstand particulates in the liquid being pumped compared to positive displacement pumps [125].

After prototyping on a breadboard to ensure the system worked the design was soldered onto strip board to make it more robust. The final control system can be seen in Figure 5.30.

5.8 Experimental cycles

There were three separate cycles that required defining for the experiment:

1. **Stress cycle**

   The frequency at which the stress was applied to the sample.

2. **Environmental application cycle**

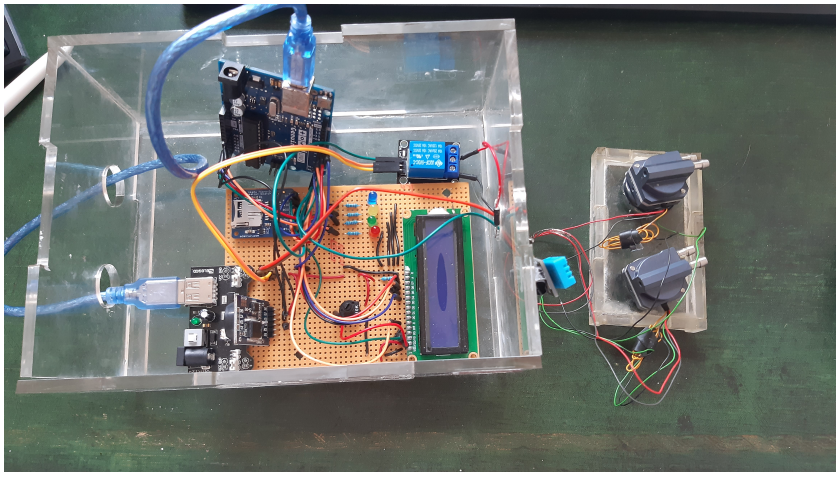

Figure 5.30: Final manufactured control system, before attachment to the rig or power

The time allowed for the sample to be fully wetted then allowed to fully dry

3. **Time for a single experiment cycle**

   The time taken for the experiment to simulate approximately eight years of axle corrosion damage

Stress cycle

The frequency of the stress cycles was defined based on a representative speed of trains in the UK. Assuming a speed of 70mph and a wheel diameter of 920mm, one full rotation would occur every 0.093 seconds, or a frequency of 10.8Hz. A similar assumption has been made in previous similar experiments [19]. This was the time taken to achieve a full compression and tension cycle.

Environmental cycle

Each wet/dry cycle of the experiment was required to fully wet and then dry the sample. This is often done with a one hour wet - two hour dry cycle. As most of the damage is done during the drying part of the process [24], it was not recommended to accelerate the drying part of the cycle with external heat sources (such as hairdryers), although this does happen in some experimental papers [24].

This experiment applied the corrosive medium in a two hour wet/dry cycle. This meant the sample was wetted by the nozzles for one hour, then dried naturally for the following hour. This was enough time to dry the samples without additional heat sources in the laboratory used, as has been confirmed by basic testing carried out in the lab.

The accelerated drying time was likely due to the slightly elevated temperature in the lab, as it contained significant amounts of hydraulics which raised the temperature through waste heat. As the sample would be dry in this time, there was no requirement to have a longer drying period, as there would be no water to aid the aqueous process.

Total experimental time

The total testing time was calculated at 2512 hours. This had been calculated by making the assumption that corrosion of rail axles in operation only took place during a 'rain day'. A rain day was defined by the Met Office as a day with at least 1mm of precipitation.

While it was not the case that no corrosion occured on days with less than this level of precipitation, it was assumed that the majority of corrosion occured on these days as there was more corrosive medium available at these times. The exact amount of precipitation was also not directly relevant as axles are underneath trains, so would be protected from direct exposure.

The Meteorological Office data available between 1961 and 2018 [124] showed that 43% of days in this period, across all weather stations in the UK, fell into the rain day category. There were some expected seasonal variations that were ignored, shown in Figure 5.31. Regional variation was also ignored.

Freight axles often go for eight years between overhauls, with differences between different fleets and operators. 43% of days for eight years, represented 1256 days where it was assumed, for the purpose of this experiment, that corrosion occured.

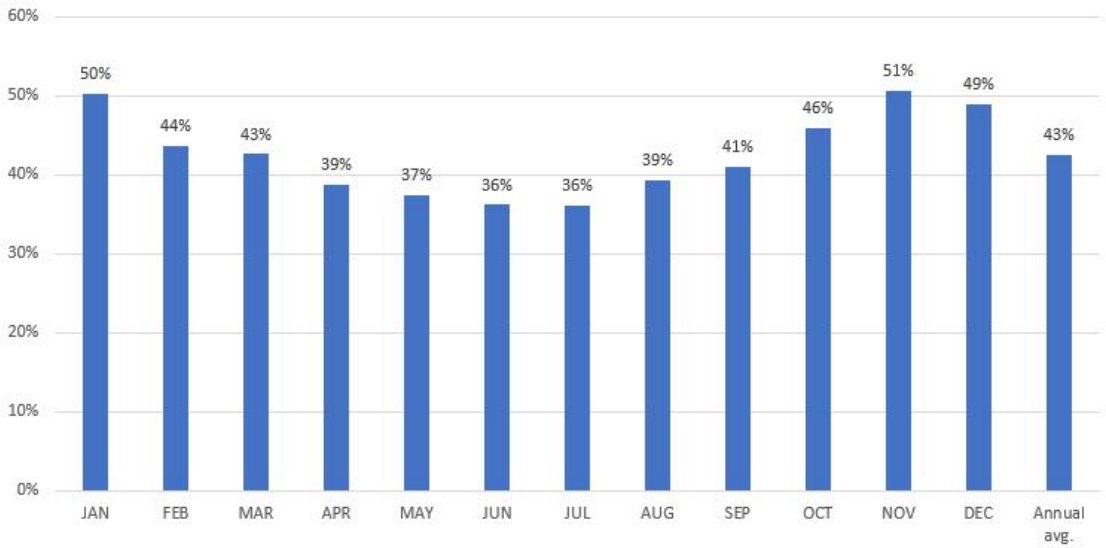

Figure 5.31: Percentage of days classified as 'rain days' in the UK between 1961 and 2018 by month (DEFRA data [124])

A further assumption was that the corrosion of a single day could be replicated by a single wet/dry cycle. This was a large simplification as there are possibly several wetting and drying processes during a rain day and over longer time periods, however there were several mitigating factors that would tend to support the assumption.

- The protection from the elements afforded by the location of the axle could be expected to prevent direct exposure to the majority of the precipitation.
- The higher corrosive potential of the artificial rainwater selected would result in more severe corrosion within a shorter time frame.
- The lack of centrifugal velocity on the sample, that would lead to drying on a real axle through water being projected away from the axle surface.
- The slightly elevated temperature in the lab, encouraging corrosion reactions to occur.

Based on these combined factors it was posited that this assumption, while not totally accurate, was sufficient for conclusions to be drawn. Based on these assumptions 1256 days could be replicated in 1256 cycles, or 2512 hours (roughly 3.5 months) based on a two hour wet/dry cycle. The experimental process can be seen in Figure 5.32.

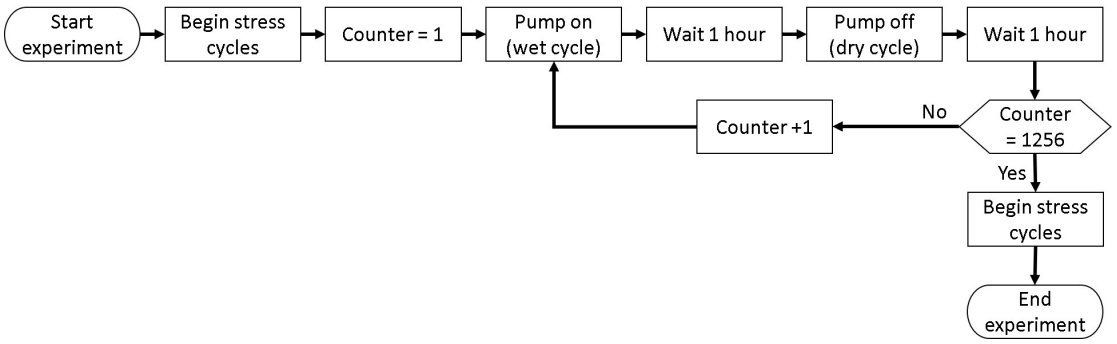

Figure 5.32: Summarised flow chart of the experimental process

Based on the total testing time and the testing frequency selected, the samples would experience 112,135,680 stress cycles during the experiment. This was a weakness in the accelerated testing procedure, as this was significantly lower than the number of cycles a real axle would experience during an eight year period.

A conservative estimate for the distance an axle might travel per year would be around 500,000km or 4,000,000km over eight years [126]. Based on an estimated wheel diameter of 920mm this would translate to around 1.384 billion stress cycles. This was 12.5 times higher than the number of stress cycles expected in the experiment, although to correct this the stress cycle frequency would have to increase proportionally to an unrealistic 'train speed'.

The decision was made to keep the train speed representative rather than the total cycle number, as the experiment was not a fatigue test, so the number of cycles was deemed less important than the frequency.

5.9 Data collection procedure

The data collection process used was proposed to be the same silicone replicating compound and Alicona scanning pairing used and validated in Chapter 3.

The usable section of each of the samples was 300mm x 30mm. If 5 mm was ignored from each long edge and 10mm from each short edge to discount edge effects, this left 280mm x 20mm to be analysed on each sample. A schematic diagram of the inspection areas can be seen in Figure 5.33. The scanner and lens combination on the Alicona was able to scan areas in multiples of 3.66mm x 3.66mm, defining a unit of scanning.

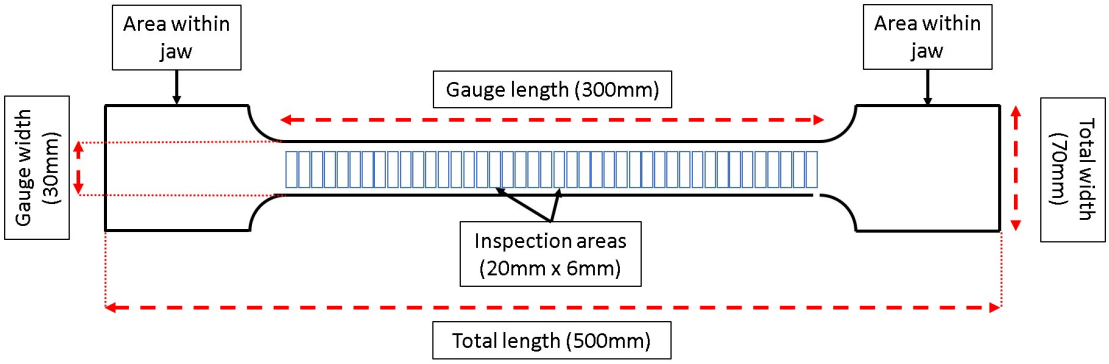

Figure 5.33: Schematic diagram of inspection areas in the gauge length of the samples

It was proposed that the samples are each divided into 6mm x 20mm sample areas (height by width), providing 46 sample sites per side and 92 overall, accounting for a 1mm separation between each site. All the sites had replicas and scans taken at the start of the experiment to provide a comparison point of the surface conditions to compare the changes after the completion of the experiment.

Using the wet/dry cycle analogy, five sites would need to be stopped from corroding every 'six months' over the 'eight year' investigation which equates to every 157 hours, or 6.5 days.

These areas could then be compared for changes over this time period, given the starting condition of each. This would provide five sample areas per 'six months' to allow tracking of the progress.

There were five sample areas that were left exposed to the atmosphere of the lab but with no corrosive medium. This would allow tracking of the effects of the stress-corrosion duopoly. A total of 12 sample areas experienced the full 'eight year' cycle allowing greater assessment of the long term effects of corrosion.

The samples would be heavily corroded after the experiment. As such they would require cleaning to remove the corrosion products from the surface before any casts were taken. This could not be easily done in situ, limiting the ability to collect data as the experiment progressed.

To avoid this issue, as an area reached the point that it needed to be removed from the experiment for inspection, during a dry cycle, it would be covered in waterproof tape. This rationale was based on corrosion being an aqueous process, preventing the artificial rainwater used in the experiment from reaching the surface would stop the corrosion from progressing.

A drawback of this solution was that the sample area would continue to experience the stress cycles, despite being insulated from the corrosive aspect. This was not an issue, as the samples would be stressed below the fatigue limit of the material [15] therefore no crack initiation was expected. This meant that once a corrosion pit was covered, preventing further development by removing the corrosive environment, the application of continued stress cycles would not effect the pit.

The use of a large number of areas that experienced the full experimental cycle, with smaller numbers of areas that were stopped over time, would provide a good tracking of the progress of individual pits and areas to allow generalised judgements to be made.

5.10 Assembly and testing

The experiment was assembled in the rig, with the jaw assemblies and the samples placed first, with the containment chamber built around the samples.

The lower jaw assembly was built first, with the samples in place. The upper jaw L-shaped base was then fixed in place, and the samples were raised until they came into contact with the upper base and experienced a compressive load of 3kN to ensure firm contact.

The jaw faces and backing plate were then added and the bolts torqued to the correct level to fully clamp the samples. The pre-load was then released to reset the sample to a neutral state, with only the weight of the lower jaw acting as a load in tension, when the rig was off. When turned on this load was countered by the control system. The use of feeler gauges demonstrated that the samples were well fitted into the jaw assemblies.

Initially a static test was carried out to confirm that the assembly was able to hold the required loads. This was performed incrementally up to the maximum calculated load of 91.8kN. No issues were encountered, either slipping of the jaws or any hinge like opening. This was confirmed through the use of feeler gauges.

The next stage was to test the full frequency cycle at different levels of loading. This was done in a similar way to the static test, with the force level being slowly increased at each step. It was discovered that, using the base sine wave control system setting, the error of the loading was over 100%. For example if using a $\pm$10kN load, it was found that the result would be an approximately $\pm$20kN force. To solve this issue, phase and amplitude matching was enabled, which reduced the error to around 0.1kN at the full 91.8kN load, or approximately 0.10% error.

The overshooting of the commanded force only occurred when the commanded load was met. The result of this was that if the command had been given to apply the whole load of 91.8kN, the loading would reach around twice this level before the amplitude matching started and reduced the value to that desired.

To solve this issue the loading was first set to 10kN and when this command value was reached the amplitude and phase matching took effect. Once this occurred the loading command value could be set to 91.8kN and this value would be reached without being breached.

The command screen of the rig can be seen in Figure 5.34, showing the level of error and the other control parameters used. The samples were assessed visually and with feeler gauges to assess if any gaps were opening between the samples and the L-shaped bases or between the samples and the jaw faces. Neither of these were detected.

Figure 5.34: Command screen of the rig, showing the error levels and other control parameters

With the stress cycle and jaw assemblies tested and shown to work for the required loading values and frequency, the corrosion chamber could be built. The completed rig can be seen in Figure 5.35.

When the electronics and corrosive medium application system was turned on it was found to work well, with the sample being wetted evenly across it's entire surface and experimental data being collected.

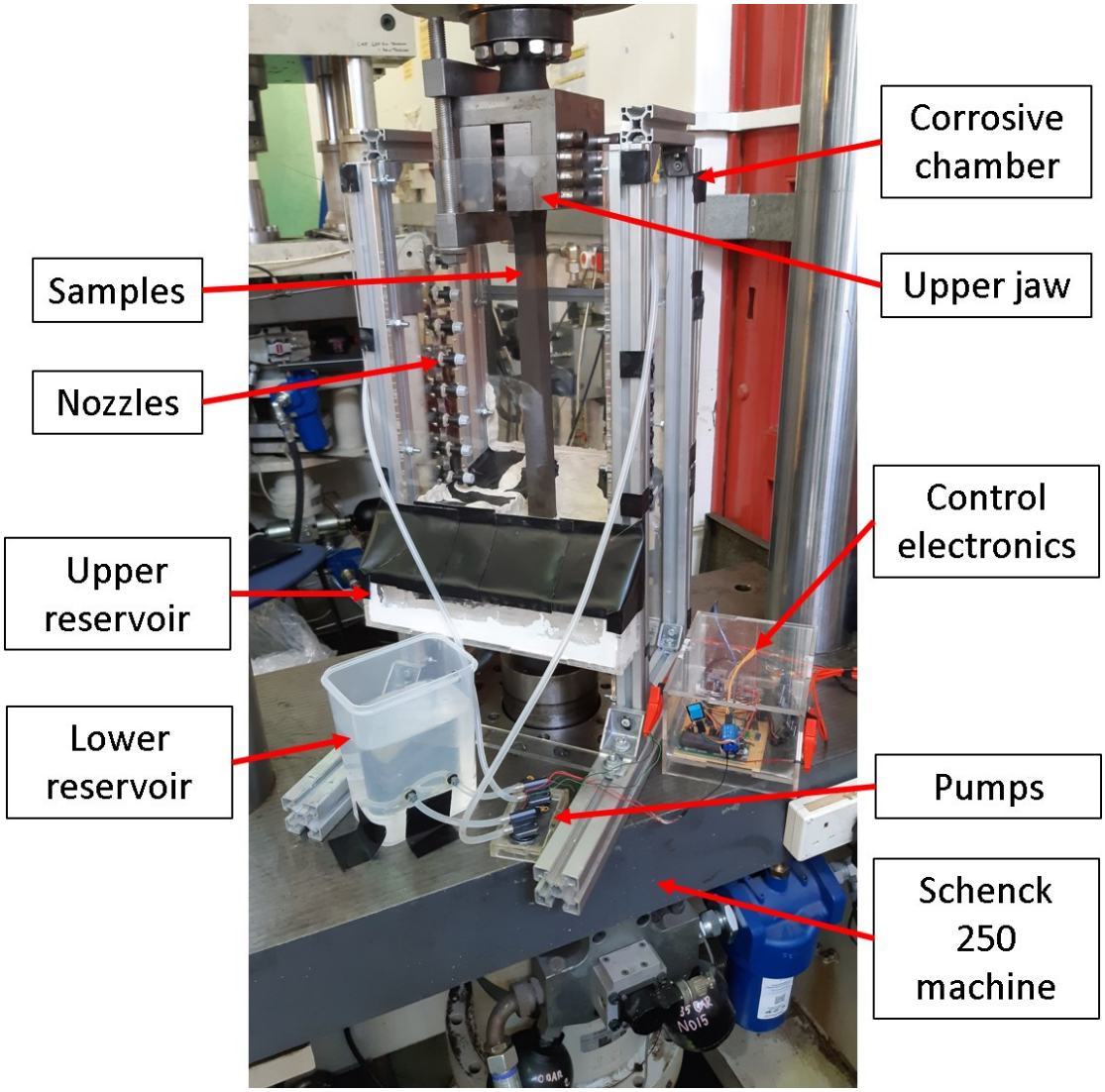

Figure 5.35: Image of rig before corrosion testing started (white material in the base was removed before testing)

5.11 Initial experimental setback

At this point the experiment had been designed, manufactured, assembled and tested. All issues that had been discovered had been addressed, and all components were thought to be designed to operate with significant factors of safety. The experiment was ready to begin.

As can be seen from the title of this section, this did not occur as planned. The issue that was encountered represented a significant set back to the project that required a rethink and a change of approach. The incident will be described first, followed by the steps taken to assess the issue and finally the changes that were made to carry the experiment forward. The results of the new approach are presented in Chapter 6.

5.11.1 Initial observations

The experiment began at 14:00 Monday. At 14:25 on Thursday of the same week a technician in the lab noticed a crack had appeared in one of the samples. This crack reportedly ran through the depth of the sample on one side. This was not present when the rig had last been inspected in detail on the previous day at 4pm. At 14:44 of the Thursday, it was noticed that both of the samples had failed, and the rig had stopped. This can be seen in Figures 5.36 and 5.37

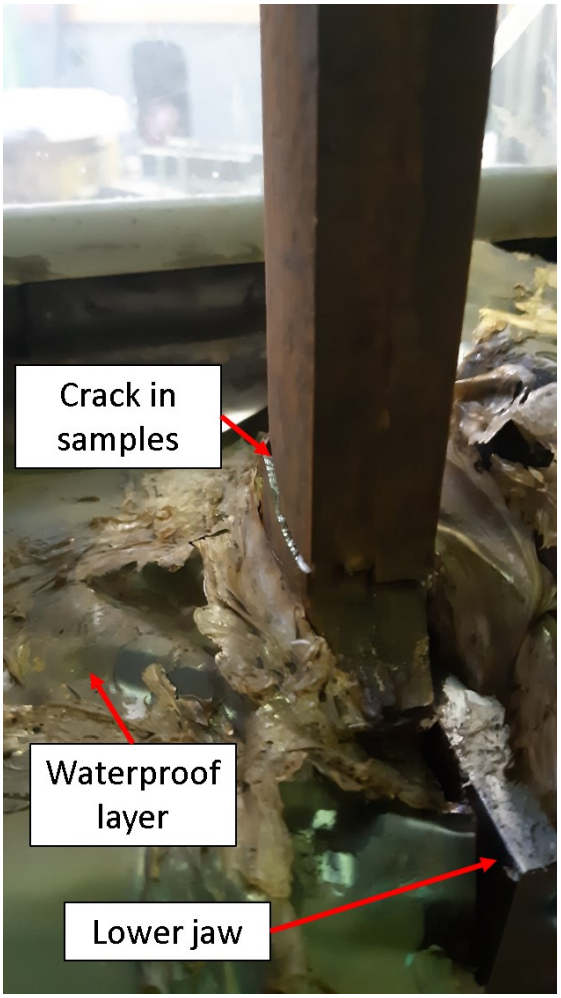

Figure 5.36: Image of the failure point of the samples

The length of time that the experiment ran for was three days, representing around "2.8 months" using the time analogy for the experiment. The number of stress cycles experienced was around 2.8 million cycles. This was significantly shorter than envisaged at the outset of the project and meant none of the 'six month' gateways had been reached.

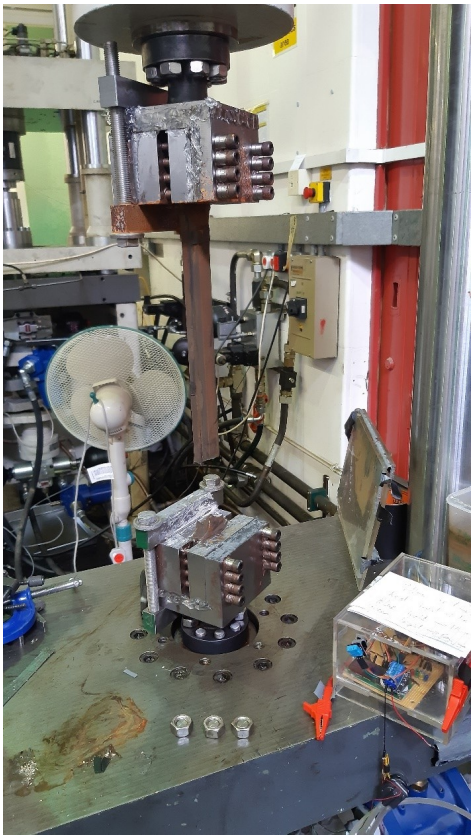

Figure 5.37: Image of the broken samples with the corrosion chamber removed

A fracture had developed at the top of the shoulders of both samples, at the lower driven end, as can be seen in Figure 5.38. A key difference was that one of the fracture surfaces was bright and the other dull. Debris was present within the dull surface. This debris seemed to have been compacted into the contact, suggesting that the experiment continued to run for some time after the failure of the sample, using the remaining sample to transmit the force.

The location of the failure was not unexpected, as the shoulder of the sample was the point of highest stress in a dog bone shaped sample. Finite Element analysis suggested that this stress should have still been well within the fatigue limit of the metal, 200MPa [15, 16], with the maximum stress at this point being 171MPa and a stress range of 342MPa.

Another result from initial observation was the failure of some of the threaded bar securing the jaw assembly to the machine. This can be seen in Figure 5.39. These sections of threaded bar were located under the sample that had a bright fracture surface, suggesting it did survive for a certain number of cycles after failure. These bolts would have borne the brunt of any asymmetrical loading.

Figure 5.38: View of lower fracture surface showing debris in the dull fracture surface

On initial inspection there were no other unexpected results. The samples exhibited 'red' corrosion product on the surface, with 'black' corrosion product inside the delivery system, suggesting oxygen rich and oxygen deficient corrosion respectively. This was in line with expectations and suggested that the system was working correctly.

5.11.2 Inspection of fracture surfaces

The fracture surfaces were divided between the bright and dull surface. They can be seen in Figures 5.40 and 5.41.

The dull surface was reported to be the sample that displayed the crack initially before failure. The crack was identified on one side, running across the depth of the sample (on the right-hand side of Figure 5.40). The fatigue interface was filled with detritus so the condition of the surface could not initially be assessed.

The surface appeared jagged and uneven on the side that the crack was reported on and flat and smooth on the other. After light cleaning with acetone the surface remained dull and it appeared that the surface may have been worn smooth by continued mechanical action. This suggested that the experiment had continued to run after the initial failure of one of the samples.

Figure 5.39: Fatigue failure of threaded bar machine assembly interface

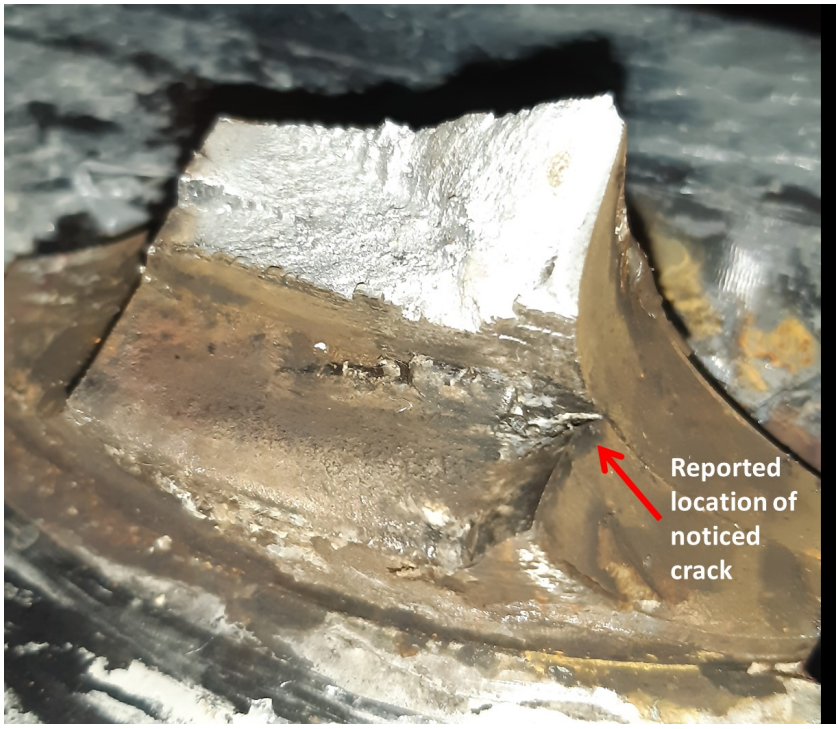

Figure 5.40: Close-up of lower fracture location (Witness unclear if crack initiated from inside face or outside)

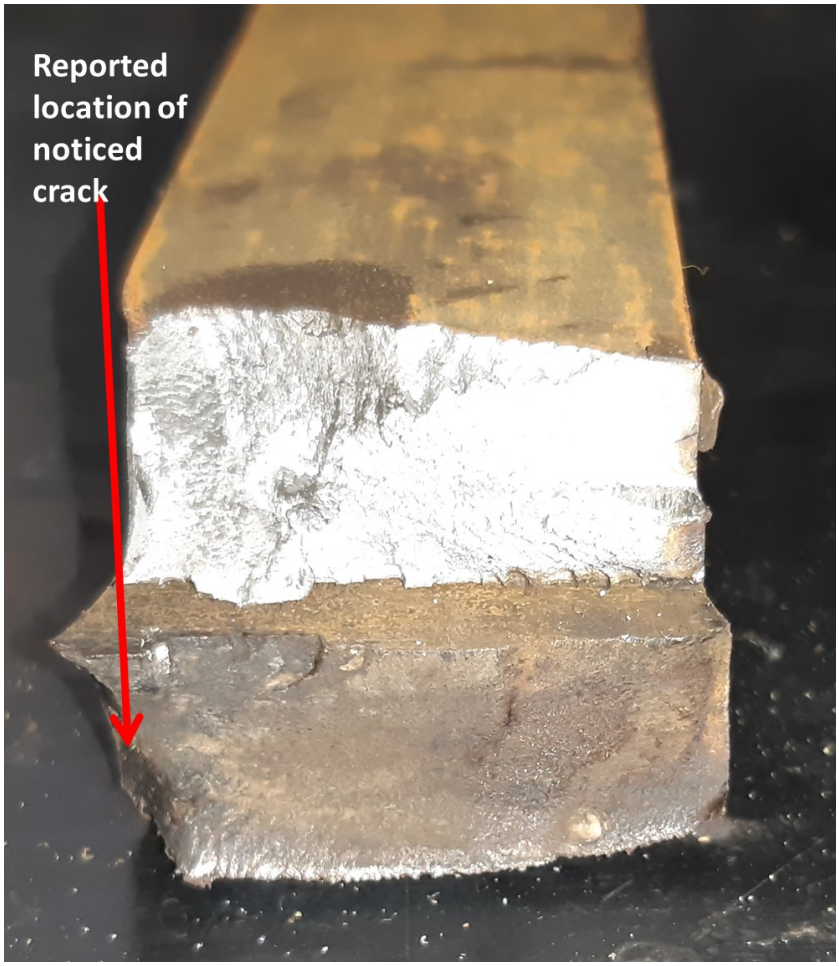

Figure 5.41: Close-up of upper fracture location

There was no evidence of a long-term fatigue fracture, as the expected 'beach marks' or a well-defined 'fast fracture' zone were not present [71], however the surface had been damaged during the continued operation so these may have been removed. The flatness of the failure surface did not suggest a ductile failure, with a lack of necking that would normally be seen.

The bright surface showed no evidence of continued application of force, suggesting that the experiment ended as soon as this sample broke. The surface appeared to show a classic case of moderately ductile fracture leaving a roughened surface and some evidence of limited necking.

5.11.3 Estimation of circumstances

Based on the evidence that could be gained from assessing the fracture surfaces, the broken threaded bar and the report from the lab technician, an assessment of the most likely progression of events was produced. While it was not possible to validate this interpretation, it did match the available evidence and was the most likely scenario based on a balance of evidence.

1. **Experiment began**

   One of the sample bars contained a small defect or crack. This could be due to either a manufacturing defect or a pre-existing crack from operations while it was still part of an axle. A corrosion pit was also a possibility, however previous work suggested that none of the pits on the sample should have been a risk for crack initiation.

2. **The crack propagated across the sample**

   This was noticed by the lab technician and reported at 14:25 on the 3rd day of operation.

3. **The crack reached a critical point and caused a sudden catastrophic failure across the sample**

   This was supported by the very flat, horizontal nature of the fractured surface, as well as the lack of a well-developed fatigue pattern in the material. This occurred at some point between 14:25 and 14:44.

4. **The experiment continued to run using the single surviving sample**

   This was supported by the detritus inside the fractured surface which would not be present if the experiment had stopped immediately. This may also have damaged the fracture surface, making it difficult to assess the failure mode.

5. **The axis of loading for experiment moved from the centre of the machine to one side, as only a single sample was transferring the load**

   This put increased stress on the threaded bars holding the jaw assembly to the machine on one side. This caused the threaded bars to fail on that side, leading to the breaking of the bars seen in Figure 5.39.

6. **The second sample failed after a further number of cycles, between 1 and 12,312, based on the stress frequency and the time between observations**

   The failure was due to a moderately ductile fracture, shown by the condition of the surface and the presence of slight necking on the sample. This failure finally brought the experiment to a stop.

7. **Some moments later, the corrosive medium application system was turned off by the technician**

   Upon noticing the failure of the sample, the technician turned off the system that supplied the corrosive medium. This prevented further corrosion to the samples.

The conclusion was that the initial fracture resulted from a defect in the sample, likely to be an existing crack, either from manufacturing or operation as a rail axle. There was a possibility that the sample became 'nicked' at some point during manufacture or handling, but this was not noticed on earlier visual inspections.

It was not considered likely that the failure was caused by the experiment itself, as the stress range being used was within the fatigue limit of the material. An existing corrosion pit was a possibility, however this was deemed unlikely as none of the corrosion pits were considered aggressive enough to cause a crack initiation.

5.12 Plan to proceed

Due to the fracture of the samples early in the testing cycle it was not possible to continue the experiment as planned. This required mitigation to ensure that important information could still be produced to advance the project.

It was proposed that the experimental concept was continued, but divided into three separate avenues. The original experiment was aiming to assess the change in corrosion geometries due to stress and corrosion, given the starting point of an original axle surface. The new experimental series divided the stress-corrosion dichotomy of corrosion development and the impact of using an original axle surface.

The first experiment, intended to continue where the failed experiment left off, required re-cutting smaller samples from the broken ones. The rest of the experiment would remain the same or undergo very minor updates.

The second experiment would be very similar to the original, applying a stress and corrosion environment to a new sample, machined from axle steel. Referred to as 'bright' samples due to the lack of corroded surface, these would be machined from a section of axle steel cut from the centre of the donated axle. This had originally been cut for a separate experimental concept that had not been built, and the use of the available blank would allow faster implementation of the new experiments.

The third would use the same bright sample design as the second experiment, but would not apply a stress cycle, only a corrosive medium.

The data from all these experiments would be gathered in the same way as was originally intended and described in Chapter 3. By comparing the results of the various experiments, the influence of stress and corrosion could be determined. This would ultimately still allow an assessment of the changes to corrosion pits over time, the same aim as the original experiment.

5.13 Experimental redesign

Due to the issues with the original experiment, new experiments were needed to allow useful results to be extracted. The three new experiments would require new parts to be designed and manufactured.

5.14 Experiment one

5.14.1 Concept

The first experiment in the new experimental series, was the closest to the original concept. Using the broken samples, new samples were cut to produce as close a replica of the original experiment as possible. These new samples were, by definition, smaller than the originals that they were cut from, but retained the same dog-bone concept and the curved geometry with a corroded surface. This would allow for the same, high fidelity, replication of an axle surface as the original experiment.

The experiment would use the same jaw assemblies and rig as the previous experiment. While not ideal, as the jaws were not designed for this sample, no other jaws were available that could accommodate the curved geometry. This also required the continued use of two back to back samples due to the design of the jaw assemblies. The target of 120MPa maximum static stress in the area of interest remained the same.

5.14.2 Sample design

The sample design followed the same process as the previous samples. First initial requirements were identified, then initial checks and calculations were preformed, finally a finite element study was undertaken to ensure that the samples were suitable for the experiment.

Requirements

The new samples had similar overall requirements to the original, such as:

- Provide sufficient surface area to to allow a reasonable number of results
- Be capable of reaching the desired stress, within the limit of the equipment available
- Not fail through buckling
- Use the existing axle surface as the area of interest

However, in this case the samples also needed to be possible to manufacture from the remains of the original samples. This limited the size of the samples considerably, given the location of the fractures in the old samples. In order to keep the largest possible area of investigation from the samples, it was decided that the least reduction of width possible would be targeted.

The new samples were designed as shown in Figure 5.42. The same dog-bone geometry of the original samples was used, with the same length of area in contact with the jaw faces. The width had to be reduced to allow for the samples to be manufactured from the broken samples. The 30mm maximum width, corresponds to the gauge length of the original samples.

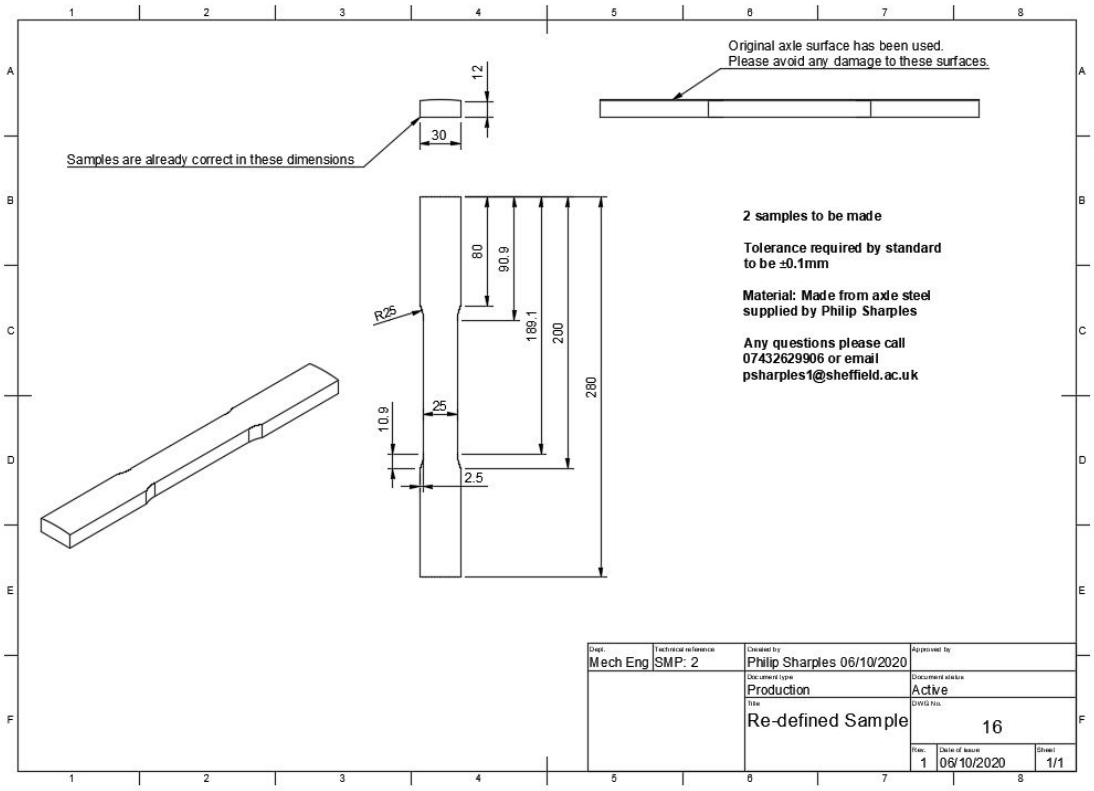

Figure 5.42: New samples cut from broken samples used previously

The radii of the shoulders was selected based on the smallest recommended in the ATSM E8/E8M standard [127] that controls the design of metallic tensile standards. This served to lower the risk of failure at this point, which was seen in the original samples.

The design of the samples was supported by analytical checks and finite element analysis. The analytical work to ensure there was no buckling can be seen in Appendix B.

Finite element analysis

The set up of the Finite Element analysis for the new samples can be seen in Appendix B. The approach used in terms of boundary conditions and demonstrating mesh independence was very similar to that used when investigating the original samples.

The Finite Element models were divided into the tension and compression cases. In both cases the loading was calculated to have a magnitude of 76.6kN, reduced from 91.8kN, due to the reduction in cross sectional area with the new design compared to the original. The design still consisted of the back to back concept used in the original experiment.

The results of the analysis in tension can be seen in Figure 5.43. Using the same approach as with the original samples, the Von-Mises stress and the displacement perpendicular to the axis of loading, were considered and assessed to judge the viability of the samples.

As can be seen in Figure 5.43, there was an area of higher stress along the line that defined the edge of the jaw faces. This was likely an area of high stress, due to the immobility of the material within the jaw faces, causing a build up at the boundary.

The maximum stresses in the samples were found to have a value of around 150MPa, as shown in Figure 5.43. This value was below the maximum in the original samples of around 171MPa, and below the maximum designed stress level of rail axles denoted in the standards of 166MPa [15, 16]. As the standard was designed to account for some level of secondary influence, such as a crack or other stress raiser, it was deemed that the sample should not experience failure.

The maximum stress was in the shoulder, the approximate area of the crack formation in the original sample, as seen in Figure 5.43. This value had a factor of safety of 1.3 compared to the 166MPa limit defined in the standard. This suggested that failure in the same area as the original sample was highly unlikely.

The gauge length was found to exhibit the desired 120MPa stress level to proceed with the design.

The stress results in the compression case can be seen in Figure 5.44. These results displayed the same maximum stress locations and approximate value as the tension case, 147MPa compared to 150MPa. The outcomes on the stress result were the same as for the tension case, and gave no cause for concern.

In both the tensile and compressive cases the maximum displacement perpendicular to the axis of loading results were found to be extremely low, at 0.002mm, as seen in Figure 5.45. They were also the same as each other to three decimal places. This suggested that there was no buckling occurring in either loading case.

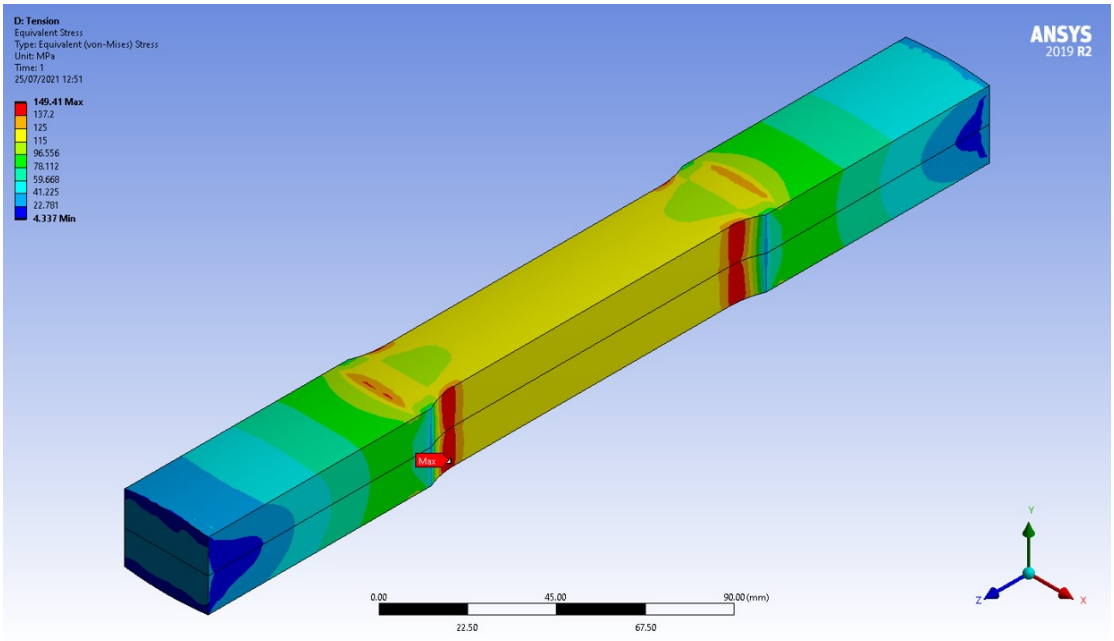

Figure 5.43: Von-Mises stress of the new samples in tension

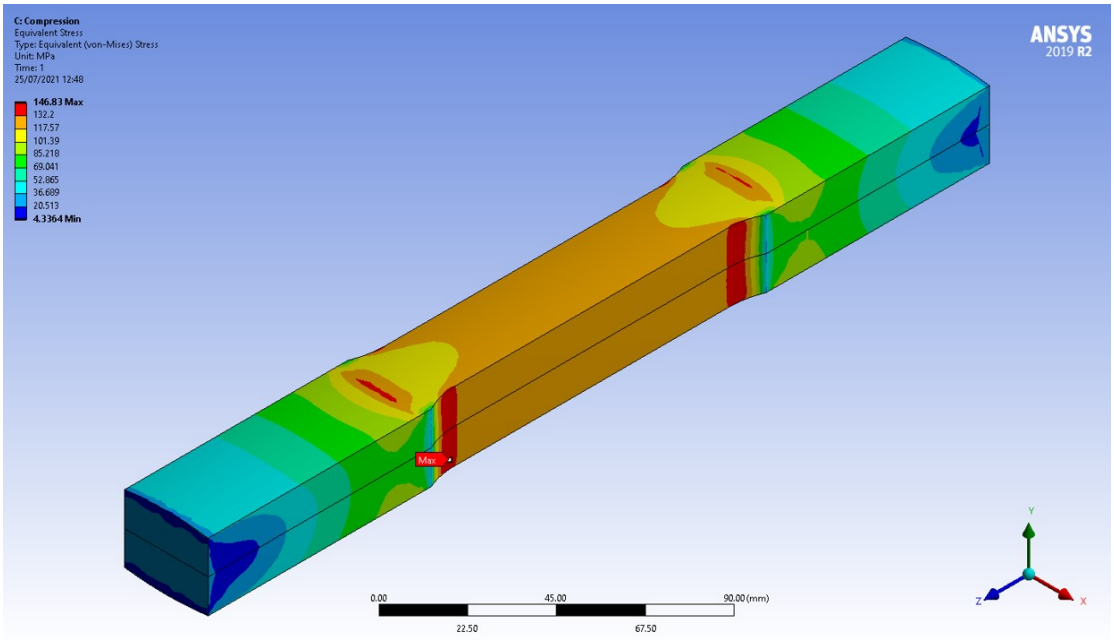

Figure 5.44: Von-Mises stress of the new samples in compression

In conclusion the Finite Element analysis of the new sample design indicated that the samples would operate within the maximum allowable stress amplitude, 166MPa, as defined by rail axle design standards [15, 16]. By operating within this limit, the chance of a failure in the samples was low. The displacement results also suggested that no buckling was occurring within the samples, concurring with the with the analytical analysis detailed in Appendix B. Based on these results the samples were shown to be suitable to meet the experimental requirements.

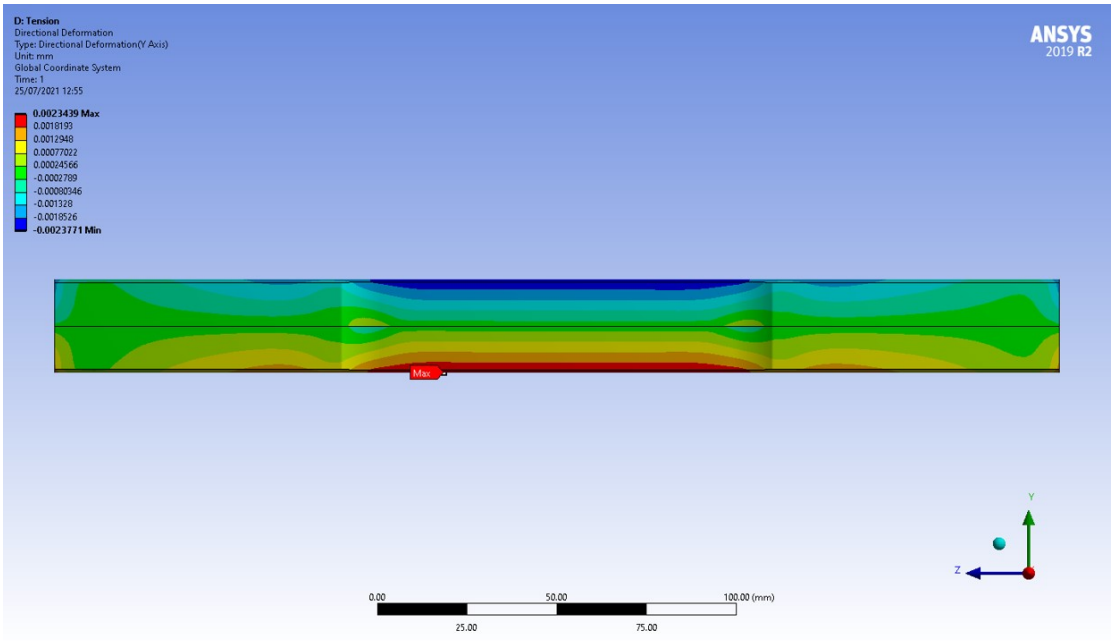

Figure 5.45: Displacement in the Y direction for the new curved samples under tension

5.14.3 Environmental delivery

The environmental delivery was fundamentally the same as previously, with the same electronic components and control system. Due to the change in the size of the samples, the number of nozzles per side was dropped from eight to four.

After issues with the original environmental delivery system, that mostly stemmed from manufacturing and assembly flaws, as well as design issues, an updated corrosion chamber was developed. The new chamber would be suitable for all three of the experiments.

The basic concept remained the same, with a central chamber that drained into an external reservoir. However, in the new design the reservoir fed directly into the pumps, rather than through a secondary holding tank. The new corrosion chamber was designed to be entirely made from laser cut clear acrylic parts and to be height adaptable to allow for variable sample lengths and jaw heights. The whole assembly was free standing and fitted around the existing jaws. Due to the tight tolerances, the chamber needed to be built around the jaws, limiting the ability to reuse it.

The use of laser cut parts allowed for tighter tolerances than were previously possible limiting the ability for the artificial rainwater to leak out of the rig. All the joints were sealed using silicone sealant to make the whole assembly water tight. The new large doors improved access to the samples during assembly and operation. This made operating the experiment far easier. The CAD render of the new corrosion chamber can be seen in Figure 5.46.

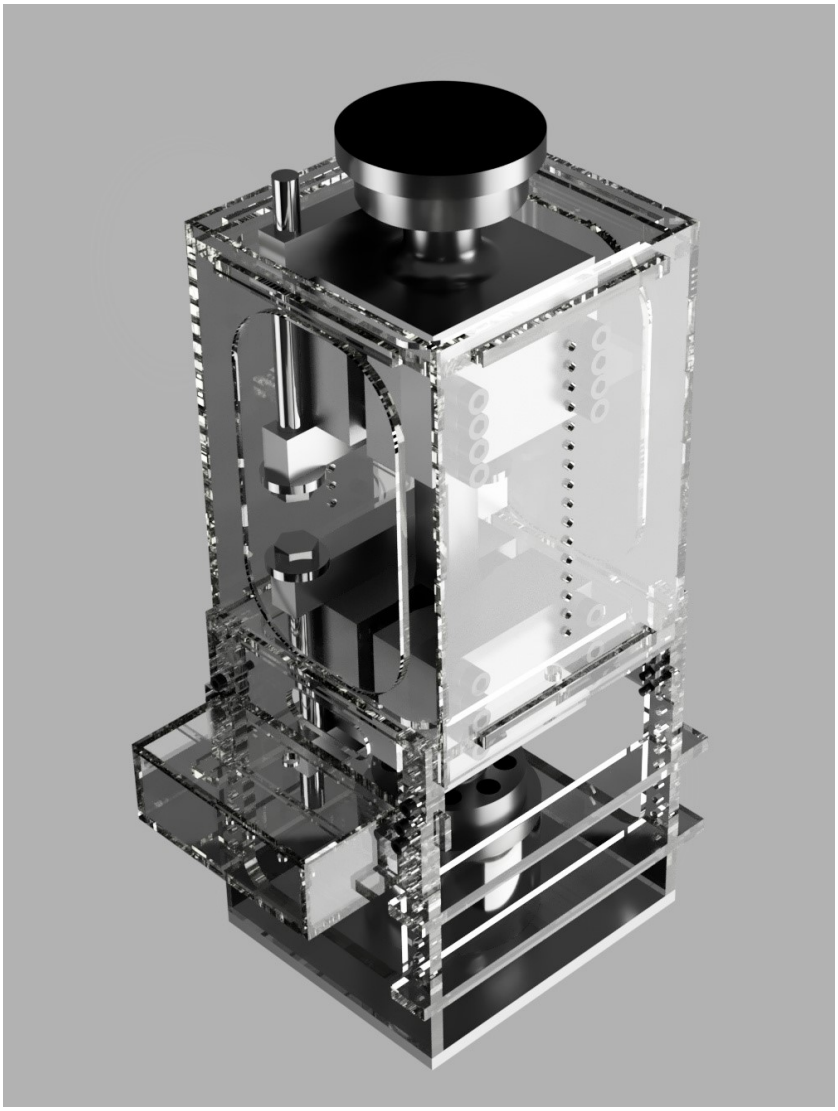

Figure 5.46: CAD model render the new corrosion chamber assembly, with the jaw assemblies and sample within

5.14.4 Experimental cycles

Due to the lack of time to run the experiment, from limitations on equipment availability, the original time frame needed to be reduced. Rather than running for the full 2512 hours, that represented eight years of corrosion damage, it was decided that running for the equivalent of four years, or 1256 hours (52.33 days) would provide an indication of changes over time.

The stress cycles and the environmental cycles remained the same as before, as these were selected independently of the length of time that the experiment ran.

5.14.5 Summary

The new experiment was very similar to the original experiment and had the same aims. The major changes were the change in the sample geometry, with the appropriate changes in loading, and the design and production of a more suitable corrosion chamber. The new experiment was capable of assessing the changes in axle corrosion pit geometry over time, given the starting point of a real corroded rail axle surface, negating the need to approximate the corrosion initiation stage.

All of the parts of this experiment were successfully manufactured and tested using very similar procedures to the checks carried out on the original samples. The final rig can be seen in Figure 5.47. It was shown to be capable of withstanding what was thought to be the required loading and the samples were wetted during the correct cycle to a satisfactory level.

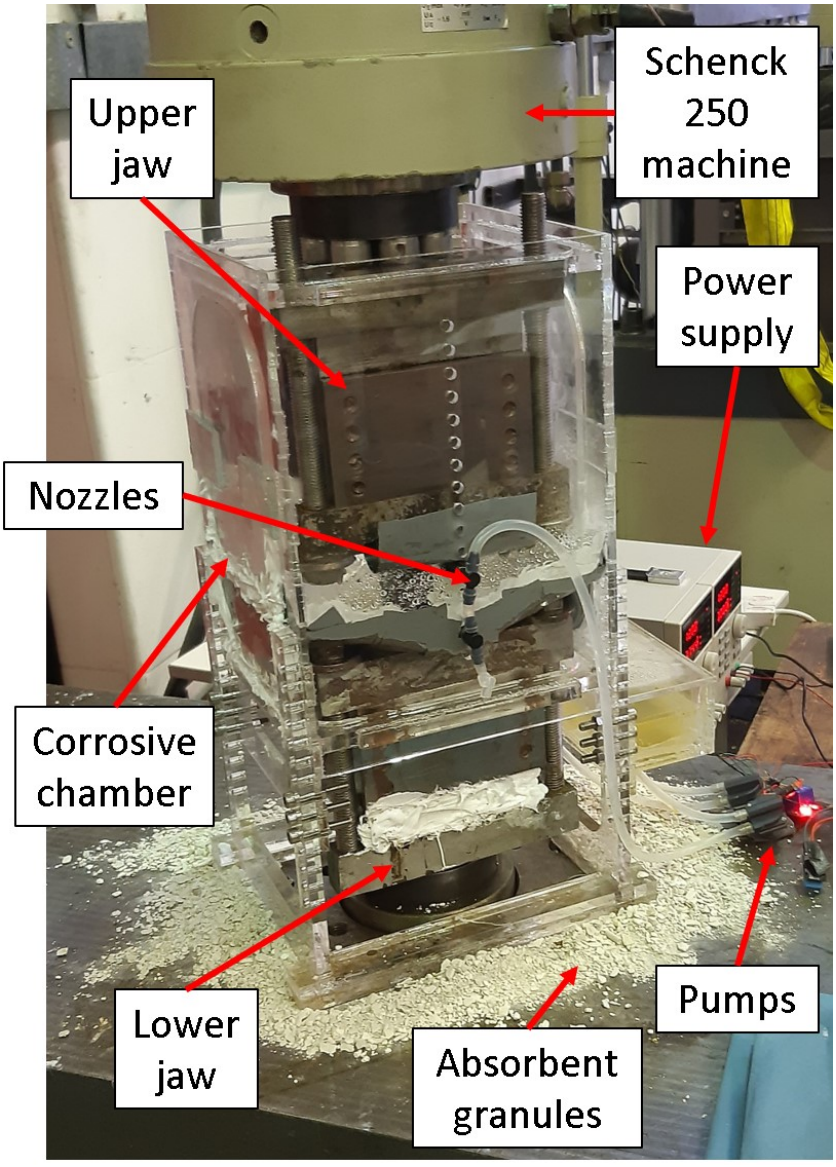

Figure 5.47: Experiment one assembled and ready for the beginning of operation

5.15 Experiment two

Experiments two and three were very similar to each other, both using a new 'bright steel' sample and the same corrosion chamber design. There was a large amount of overlap in the design work for these experiments which will only be presented once for experiment two.

5.15.1 Concept

The second experiment contained many of the same elements as the previous experiment. It did however contain a new sample design.

The new sample was designed to remove issues to do with the use of curved samples, principally the use of bespoke jaws. By using jaws that had been used previously, and were known to attach to the machine and be capable of holding the load, a large level of complexity and uncertainty could be removed, as well as reducing the cost. This would come at the expense of changing the geometry of the sample and so pivot the direction of the investigation.

By using a flat, un-corroded, sample the experiment would no longer be simulating an axle leaving a depot with corrosion present, and would instead be replicating the corrosion initiation phase as well.

Due to Covid-19, there was a lower demand for experimental rigs than in normal times. Due to this drop in demand, and after consulting the lab team, a different rig was identified that could be used for the reduced testing time. The new rig was also a hydraulic tensile testing machine and can be seen in Figure 5.48. The E.S.H. machine was rated to 100kN and used the same control system as the Schenck rig, meaning operating procedures could be directly replicated.

The existing jaw assembly, that was used as the inspiration for the bespoke set that were designed as part of this project, were available to be fitted to the rig by using an attachment plate. These jaws were known to work for the type of experiment proposed, yet could only take straight samples, requiring a redesign. Due to the geometry of the jaw assembly, to ensure the sample was positioned in the centre of the rig, the thickness of the sample was limited to 12mm.

The samples could not use the corroded axle surface as was the aim in the other experiments, due to geometric issues and the lack of available material. The only available material was axle steel that had been cut from the donated axles for another experimental design that had been abandoned earlier in the project. This steel came from the same section of the axle as the corroded samples, but originated in the centre of the axle rather than the edge. The cutting of these samples can be seen in Figure 5.49.

Figure 5.48: Image of the E.S.H. rig, with the jaws and sample fitted and the corrosion chamber under construction

The sample was exposed to the same stress and environmental cycles as the other experiments. The only significant differences were the change in sample geometry and the use of bright machined steel, rather than the corroded axle surface used previously.

5.15.2 Sample design

The sample design followed the same process as the previous samples. First broad requirements were identified, then initial checks and calculations were preformed, finally a finite element study was undertaken to ensure that the samples were suitable for the experiment.

Requirements

The requirements were similar to previous experiments, but with certain variations to account for the flat samples and the different jaws that were used. The requirements were identified as:

- Be capable of fitting into the jaws available
- Provide sufficient testing area to provide sufficient results

Figure 5.49: Cutting of the axle to produce the material used in the bright samples

- Not fail through buckling
- Provide the desired stress within the area of investigation, within the capability of the equipment used
- Use a single sample to reduce complexity

Design basis

The design of the new bright steel sample was as shown in Figure 5.50. The design was based on the tensile samples described by ATSM standard E8/E8M [127]. This was used rather than the samples used for fatigue testing [128] as those samples were of an unsuitable shape, due to variable gauge width along the sample. The standard provided a recommended gauge length and radii to be used in the shoulders, to prevent failure, increasing confidence in the design.

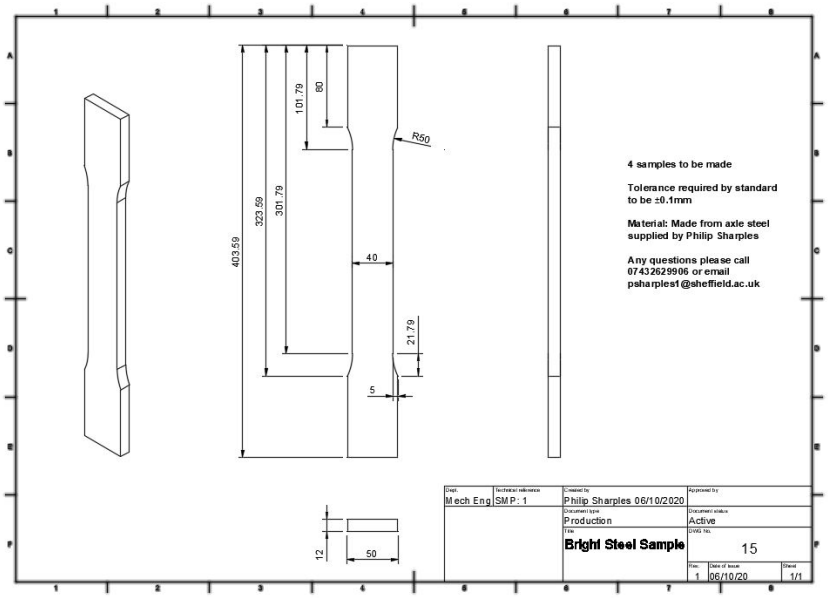

Figure 5.50: Drawing of the design for bright steel samples

Based on the cross sectional area of the gauge length of the sample, 480mm^2, and the targeted stress of 120MPa, the force used in the experiment varied between 57.6kN and -57.6kN. Analytical investigation to ensure the sample did not undergo buckling can be seen in Appendix A.

Finite Element analysis

The set up of the Finite Element studies can be seen in Appendix B. The boundary conditions, material properties and meshing approach remained similar to those used during the analysis of the original samples, apart from the absence of contact conditions as only a single sample was used in each of experiments two and three.

The Finite Element results were investigated for the maximum von-Mises stress levels, which can be seen in Figure 5.51 for the tension case and Figure 5.52 for the compression case, both using loading of 57.6kN to achieve the 120MPa stress in the gauge length. In both cases the results were almost identical, with maximum stress levels of 145.2MPa in both samples, below the 166MPa safe maximum allowable stress detailed in the design standards [15, 16]. The location was also as expected in the shoulders of the sample.

Both of these results displayed no evidence of buckling behaviours, and reported stress levels well within the fatigue limit of the sample. The stress level in the gauge length was also acceptable at 120MPa.

As the bright steel sample did not contain any corrosion damage and were taken directly from the machine shop, there was less chance of a stress raising factor being present in the design. This provided an added level of confidence that these samples would perform as intended.

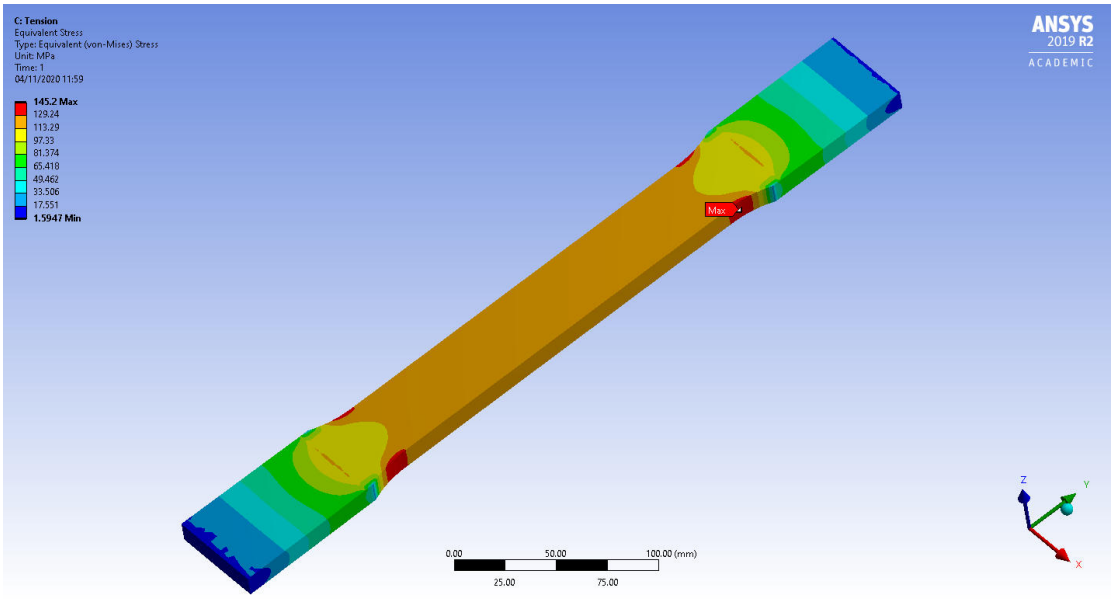

Figure 5.51: Von-Mises stress of the bright steel sample in tension

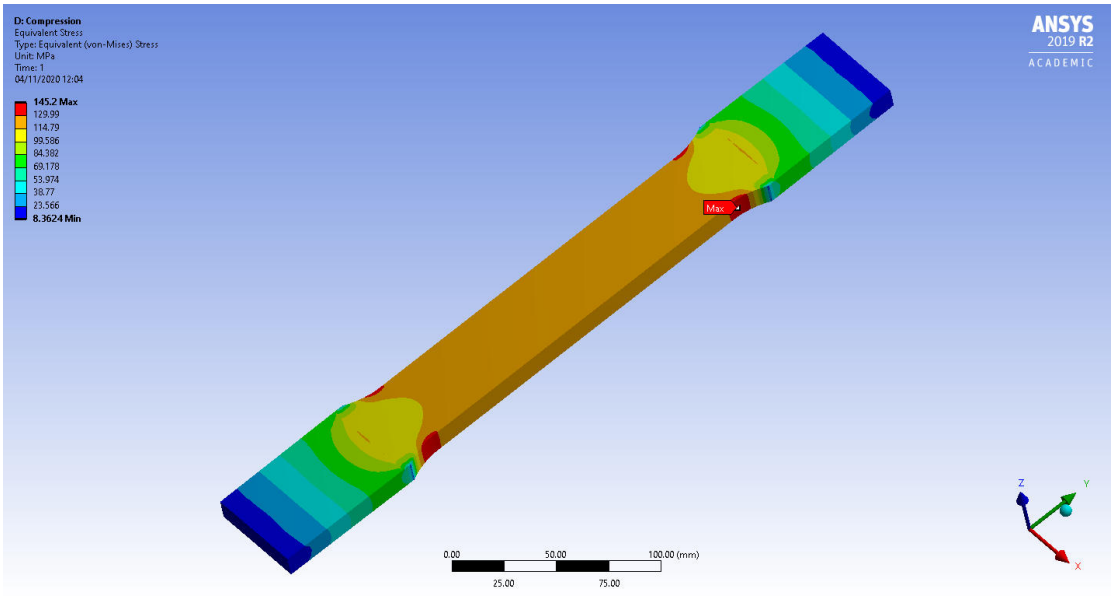

Figure 5.52: Von-Mises stress of the bright steel sample in compression

The conclusion of the Finite Element analysis was that the sample design would be capable of surviving the experiment. It would also provide suitable conditions to assess corrosion development on rail axles.

5.15.3 Experimental cycles

The cycles were the same as used before for both stress frequency and environmental cycles. The only variation was the use of new loading conditions to account for changes in sample geometry, which was changed to 57.6kN to -57.6kN.

5.15.4 Summary

The new experiment described above, used a similar idea to the original, but with a new sample design. Other changes, such as the use of pre-made jaws and a new rig, while important, have minimal impact on the experiment.

The new bright samples allowed the collection of data on the change in corrosion pit geometries through the six month gateways, using the starting point of a flat, smooth steel sample. The sample would still undergo the same stress and corrosion loading of experiment one, with this geometry and surface condition change being the only significant variation. By comparing the pit formation at each step to the pits that were found on pre-existing axles, the quality of the pit initiation replication can be assessed.

This experiment would provide more general information about the formation of pits, and their progression, especially when combined with the results of experiment three. The experimental set-up can be seen in Figure 5.53.

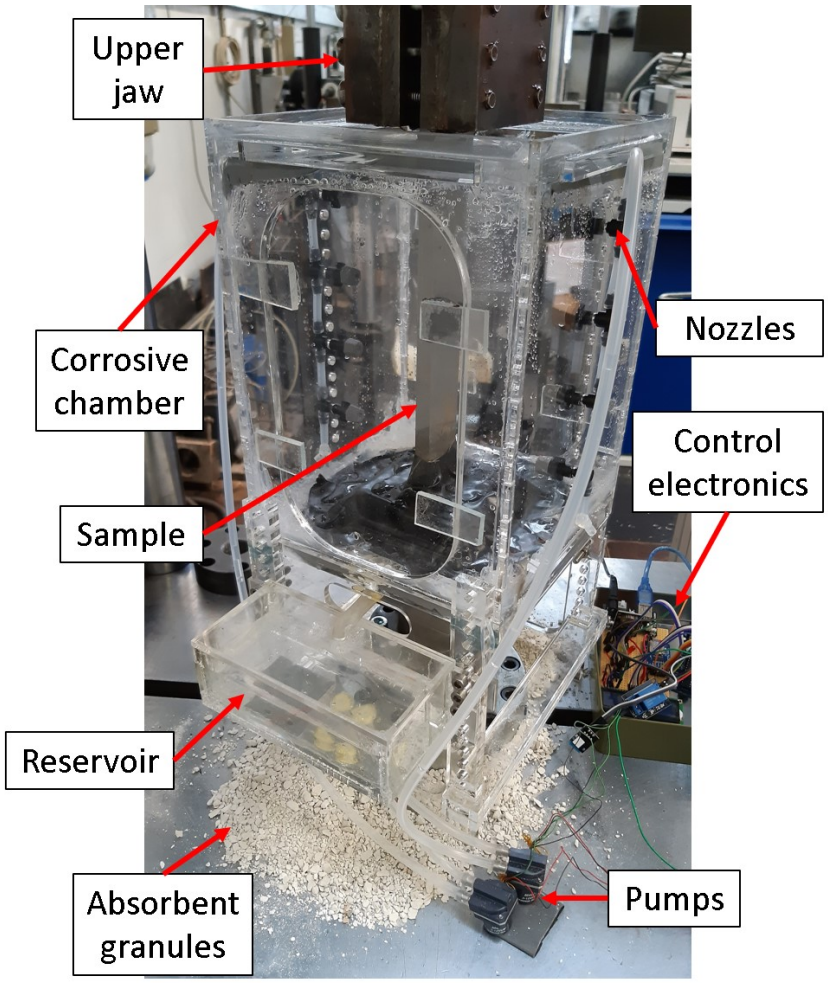

Figure 5.53: Experiment two built and beginning operation

5.16 Experiment three

5.16.1 Concept

Experiment three was the most simplistic experiment of the new set and the fastest to manufacture.

Very similar to experiment two, using the same sample and corrosion chamber as that test, this experiment considered only the corrosion environment, without any stress being applied. This would allow for assessment of the impact of stress on the formation of corrosion pits on rail axles when compared to the results of experiment two.

The rig consisted of the sample being held in the same orientation as the other experiments, with the same environmental cycle and corrosion chamber. The rig was placed in the same lab as the other experiments so experienced the same general temperature conditions as the others, allowing direct comparison of the results.

5.16.2 Rig assembly

The rig was assembled in a very similar way to experiment two as most of the components were identical. The only significant variation was that jaws capable of applying stress were not required. The sample was instead held vertical by the use of a simple clamp made of heavy tapped metal parts that were attached by bolts. These were tightened to grip the bottom of the sample and the top was left free. The rig can be seen in Figure 5.54.

All electronics and other peripherals were identical to the other two experiments.

5.16.3 Summary

Experiment three was an experiment that intended to investigate the degree to which the stress in rail axles contributes to the formation of corrosion pits, when compared to the results of experiment two. While not directly applicable to the question of rail axle maintenance in a depot setting, this provided valuable information on the future investigation of corrosion pitting on rail axles.

5.17 Experimental procedure - initial plan

In brief summary there were three separate experiments undertaken:

1. **Curved samples that consisted of the external surface of a scrapped axle were placed in a corrosion chamber and would undergo mechanical loading in a corrosive environment**

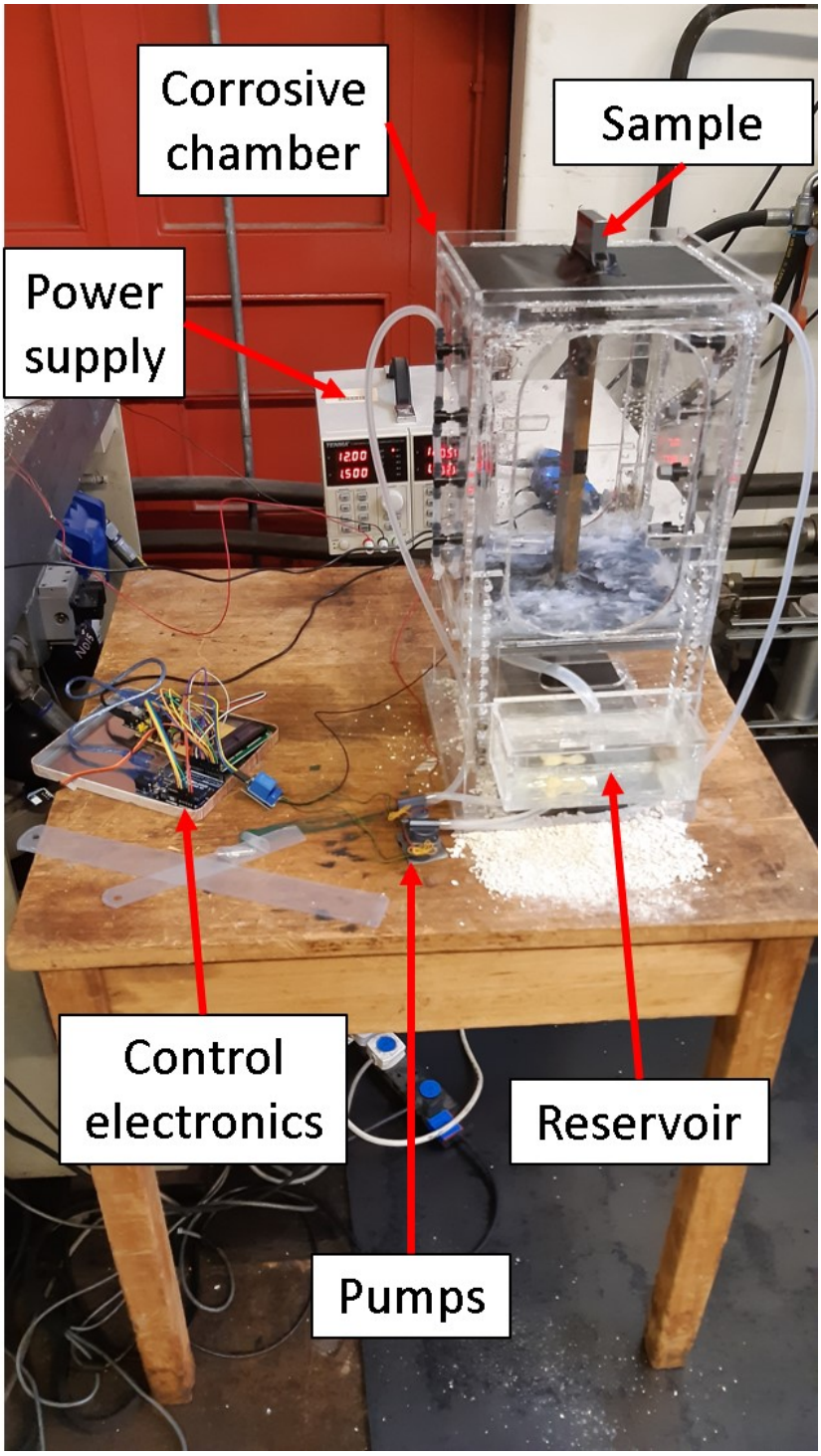

Figure 5.54: Experiment three built and beginning operation

2. **A dog bone style sample cut from the core of a scrapped axle was placed in a corrosion chamber and would undergo mechanical loading in a corrosive environment**

3. **A dog bone style sample cut from the core of a scrapped axle was placed in a corrosion chamber and only experience the corrosive environment with no mechanical loading**

The plan was for the two samples that underwent mechanical loading to experience a combined tensile-compressive loading cycle with a fully reversed fixed amplitude load, chosen to replicate a likely load that a rail axle would experience.

The chosen value was 120MPa, with a frequency of 10.8Hz chosen to simulate the speed of a locomotive. The actual value of the force applied to each sample was changed based on the geometries of the samples.

All the experiments would run for 1256 hours, which represented approximately four years of operation for a rail axle, within the assumptions of the experiment. During this time all samples would be sprayed with the corrosive medium of artificial rainwater on a one hour on, one hour off cycle.

5.17.1 Divisions of gauge length into gateway areas

The samples were divided into individual sites, with each site being covered one at a time every 'six months' in experimental time, to allow the study of the changes in corrosion pit geometry over time. For the curved samples, due to their smaller size, gateways were every '12 months'. Figure 5.55 and Figure 5.56 detail the locations of the gateway locations on the curved and bright samples.

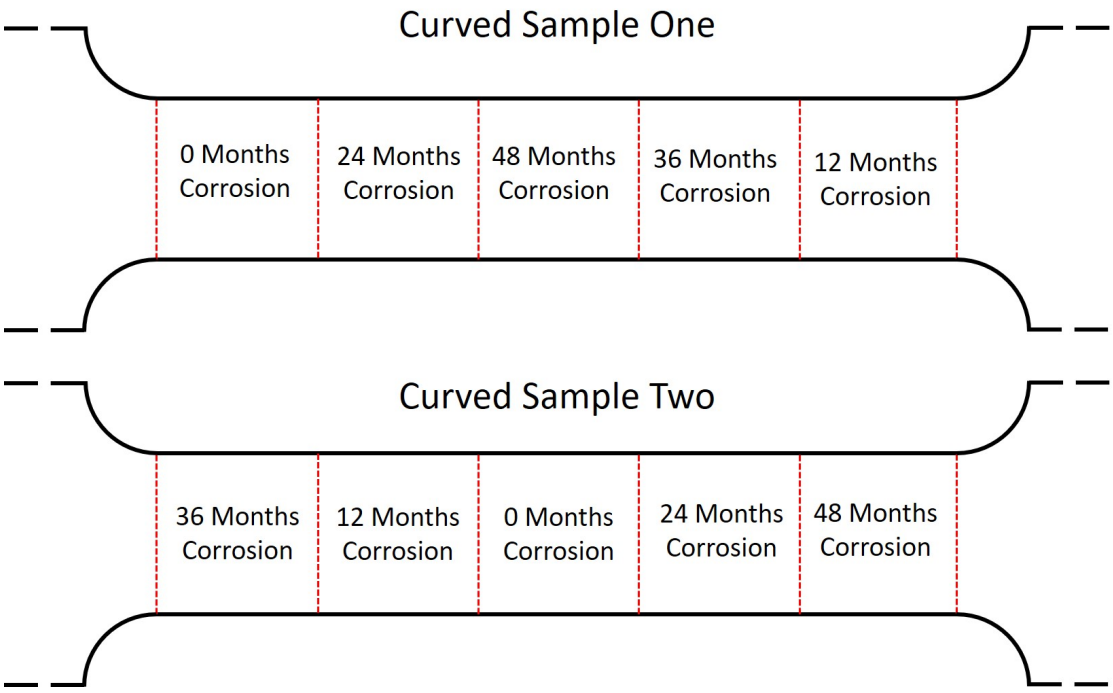

Figure 5.55: Layout of gateway areas for curved samples - Used in experiment One

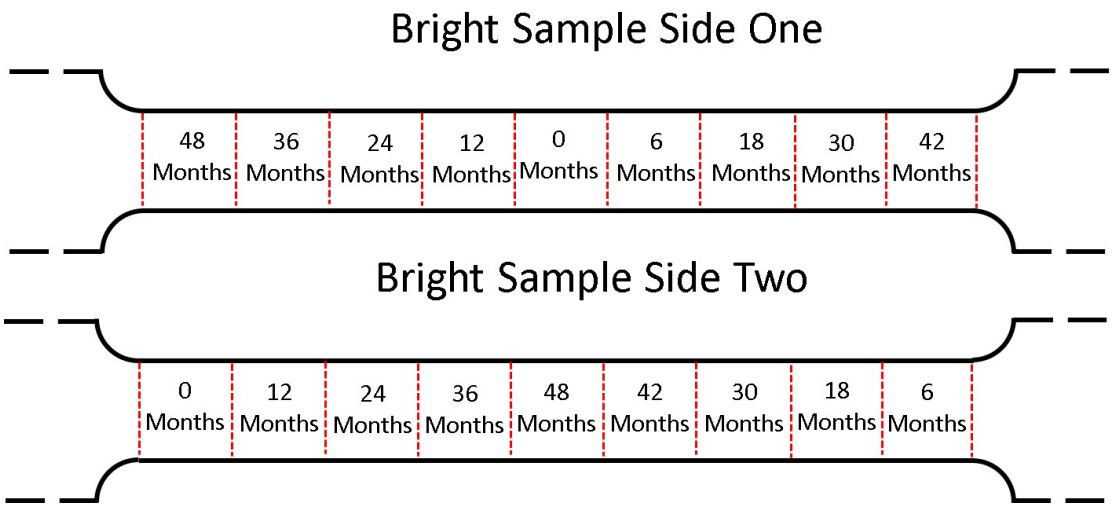

Figure 5.56: Layout of gateway areas for bright samples - Used in experiments Two and Three

The areas were covered using a waterproof patching tape to prevent any moisture contacting the surface, preventing the aqueous corrosion process from continuing. At the end of the experiment the patches would be removed and each location scanned using the Alicona and previously produced Matlab software to assess the changes over time.

The areas that represented each gateway were selected to ensure that the effect of any locational influences were mitigated. For example, if the 24 month areas were placed at the lowest point on all the samples then it would not be possible to determine if the flow of all the corrosive medium over these areas was having an influence on the results. To avoid this the sample sites were placed in different locations to discount this source of error.

5.17.2 Data outcomes

By combining the results of the various experiments the aim was that the following outcomes could be achieved:

1. By interpreting the changes in the original axle surface overtime, an understanding of how corrosion pits change geometry under realistic conditions.
2. By interpreting the developing pits in the bright samples, it would be possible to investigate the formation of pits at an early stage and how they change over time.
3. By comparing the results from the two bright samples, the influence of the stress cycle on the corrosion pit geometry compared to a corrosive medium only could be deduced.

4. By comparing the results of the bright corrosion and stress sample with the starting condition of the real axle surface, the suitability of the experimental set up to replicate the rail axle environment could be assessed.

Results would be extracted from the data collected by Alicona scans, and the pre-written Matlab software developed as part of this thesis. This range of outcomes would allow for a time dependent analysis of the risk of corrosion pits in rail axles, informing possible decisions around maintenance procedures, inspection intervals and the general approach to rail axle corrosion. This could lead to very significant savings, as leaving axles in service with less intervention would be of benefit to the industry and reduce wastage of serviceable axles.

The other advantage of the three experiment approach was to assess the influence of adding the stress element and if this was necessary at all. This could influence future experiments designed to look at the same topic.

5.18 Experimental narrative

Once all experiments had been assembled and prepared, they were all set running at the same time. Initial assessments were good with no noticeable issues apart from some small scale leaking from the under stress samples, which was easily dealt with.

After the first day of operation, the lead lab technician reported hearing a change in pitch from the machine that contained the original surface samples. The experiment was paused at this point and was investigated the next day.

On inspection it was discovered that one of the samples had fractured while the other remained intact. The fracture can be seen in Figure 5.57, which was taken after the equipment had been dismantled at the end of the experiment.

This crack occurred after 933,508 cycles, although these samples were cut from the original that has already undergone 2.8 million cycles.

The location of the crack was different to the previous failure in samples of a similar design, with the crack occurring much further into the gauge length of the sample and well away from the shoulders. The fracture surfaces were very similar to the surfaces of the original sample that failed, suggesting a similar failure mode.

The same existing flaw theory as attributed to the original sample failure was suggested. This was because the experiment was operating within the limitations of the material, suggesting that in the absence of other factors the sample should have survived. None of the corrosion pits on the surface were thought to be severe enough to initiate a crack (a conclusion later supported by work presented in Chapter 6) indicating that the corroded condition of the surface was unlikely to be a contributing factor.

Figure 5.57: Crack that developed in one of the samples that contained the original axle surface

In both cases of sample fracture only one of the samples failed, with the experiment continuing for some time after the initial break. This suggested that even when the tensile load in the other sample doubled, it did not break immediately. If both the samples had been identical and operating close to their limit in the absence of any flaws, it would be expected that the surviving sample would fail very quickly after the first. In both experiments it was demonstrated that this was not the case. The survival of one of the samples with much increased loading indicated that one was weaker than the other. This pointed toward an existing flaw or weakness in the fractured sample that made crack propagation to the point of component failure more likely than the other sample.

An un-related fate befell the experiment that used the bright sample under corrosion and mechanical loading. After three days of operation, a loud crack was heard. On inspection it was discovered that the commercially purchased jaws, that had been rated to operate within the limits of the experiment, had broken with the back separating from the bottom of the jaw. This can be seen in Figure 5.58.

It appears from Figure 5.58 that a fracture failure had occurred, evidenced by the smooth surface within the fracture services. This was disappointing, as the jaw was intended to operate within these conditions and had been originally introduced to the experiment because of the removal of risk from using bespoke jaws.

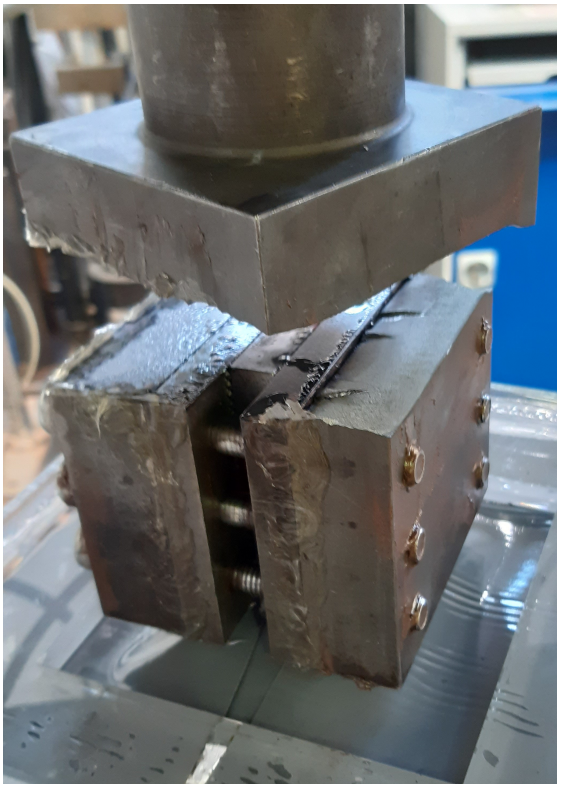

Figure 5.58: Failure of jaw on bright sample under stress rig

After conversations with the technician who controlled the jaw, it was suggested that the age of the component and the number of experiments that it had operated in could be contributing factors to their unexpected failure. The history of these jaws had not been tracked so analysis of previous use was not possible to assess the chance that this would have contributed to the failure.

The rig that did not involve any stress component continued to operate as expected.

5.18.1 Changes to experimental procedure in light of circumstances

The original set of three experiments had been changed significantly by the breaking of one sample and the failure of a set of jaws. This removed the stress component from both experiments, changing the situation from the original vision.

Options to restart the experiments with the stress cycles were investigated, however these were discounted due to issues with time, money and availability. The University's workshops were closed due to lock downs and a building move. There was not also enough budget to have the work done externally. There were additional problems with the time required to implement any further changes.

From this it was decided that the experiments would continue in all three cases, simply neglecting the stress cycle element. While this was not ideal in terms of the simulation of the rail axle environment, useful data could still be collected from this experiment.

5.18.2 Effect of stress on corrosion pit morphology

There was evidence that the influence of the stress cycle on the development of the corrosion pit was minor.

The two bright samples had been designed to allow the assessment of the influence of stress cycles on corrosion pit development, however literature was used to support the hypothesis that it had little to no influence.

While there was no literature assessing the influence of cyclic stress on rail axle steel corrosion pitting, it was an area of active research for other materials and steel grades. The information available suggested that the main factor deciding if the stress cycle had an influence on pit morphology was if the passivity layer was disrupted or broken. This was mainly based on the presence of plastic deformation as opposed to elastic deformation [129, 130]. Plastic deformation damages the passivity layer and exposes new areas of metal to the corrosive environment accelerating corrosion compared to the case where no stress was present.

If the cyclic stress being applied was below the yield stress, then the stress cycle would have little to no impact on the development of the pit [129, 131]. This suggested that the lack of the stress cycle in the experiment would have a minor effect on the development of the pits and so useful results could be gathered. This would be especially true of rail axles as the allowable designed stress cycle was significantly below the yield stress of the material.

There was an added complication to this outcome. The local stress at a pit could be raised to approaching or surpassing yield by the presence of the pit. This could mean that in general the development of corrosion pitting on an axle would be unaffected by the stress cycle. However, at a pit that reached a point where the local stress exceeded yield, the local passivity layer would become damaged and lead to accelerated corrosion in that case.

The effect of pits on the local stress field has been documented [35, 102] and has been shown to accelerate pit development in some cases [131, 132]. The increase multiplier in stress that Cerit calculated [35] would be up to 2.9 for corrosion pits with the aspect ratios detected during the axle survey in Chapter 3 using the maximum values concept. This suggested that very few, or none, of the pits identified had advanced to the state where the passivity layer would become damaged, increasing corrosion damage progression.

The yield stress of EA1N steel was 320MPa [17]. For a pit to raise the local stress value to this level the concentration factor would need to be around 3.6. Based on the results Cerit produced this would require pits of a much higher aspect ratio than were detected on rail axles, as can be seen in Figure 5.59.

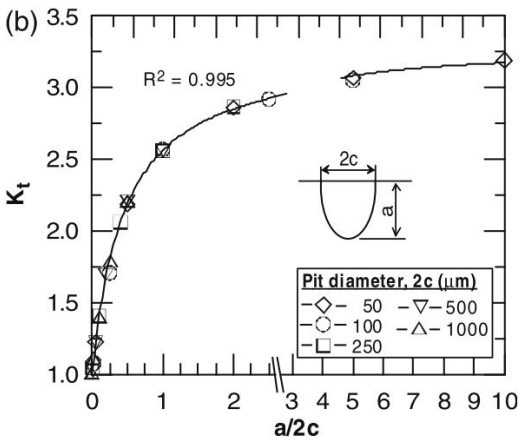

Figure 5.59: Stress concentration factors of smooth pits based on aspect ratio [35]

This is based on the assumption that pits could be generally described as smooth semi-elliptical pits. Cerit's work did suggest that higher stress concentration values could be achieved if secondary pits formed in the base of the primary pit. In this case it would be possible for the yield stress to be exceeded. However, such strong secondary pits were not identified during the axle survey, suggesting this was unlikely and in the overwhelming majority of pits the passivity layer would remain un-effected.

The overall outcome of the literature review was that the replication of the stress conditions of rail axles would not significantly impact the representative nature of the results of pit progression up to the point of crack initiation.

5.18.3 Data outcomes

Given the change in the operation of the experiments due to the lack of any ability to apply stress to the samples, the outcomes of the experiments had to be adjusted. The type of data collected and the techniques used to do this remained the same, however the implications of the data had been changed. The updated outcomes of the experiments were as follows.

1. By interpreting the changes in the original axle surface overtime, a broad understanding of how corrosion pits change geometry could be achieved. These pits could then be assessed to determine the change in risk of crack initiation.

2. By interpreting the developing pits in the bright samples, it would be possible to determine the early stages of pit development in axle steels.

3. By comparing the results of the bright samples with the starting condition of the real axle surface, the suitability of the experimental set up to replicate the rail axle environment could be assessed.

While the experiments did not represent the original experiment's intention, as it no longer contained the stress cycles that sought to closely replicate the real axle environment, the results of the experiments were still able to contribute significantly to the understanding of rail axle corrosion. In particular in terms of the changes in corrosion over time, allowing for the predictive nature of this work. Other outcomes included assessment of the suitability of the novel experimental approaches being used in simulating these conditions in the future.

From this point onward the problems with the experiment around applying stress became irrelevant. This was because the stress cycles were no longer part of the experiment and so would have no impact. It was also demonstrated that despite the absence of the stress cycles making the approach less of a direct representation of the axle environment, the results would still be representative due to the lack of influence cyclic stresses below yield on the development of corrosion pitting up to the point of crack initiation.

5.18.4 Events during experiment

Changes to inspection interval

The experiments continued with the changes above. The experiments were monitored during work hours by a technician to ensure that they were not leaking or otherwise performing poorly.

Due to Covid-19 enforced restrictions on the access to the equipment, which limited out of hours access, it was decided that the 157 hour interval between each ”six month” covering interval was not possible to maintain, as this equated to an interval of 6.54 days. This would mean that to access the lab at this interval would require access during inaccessible times, such as overnight. To address this issue the interval was extended to 168 hours, or 7 days, allowing the access to be arranged at the same time every week. This changes the ”six month” intervals into 6.42 month intervals or 6 months and 12 days. This would have a minor effect on the results due to the small change in time and the larger assumptions used in the interval definition in the first place.

Maintenance procedure and improvements during operation

Every 168 hours the corrosive environment equipment was checked to ensure it continued to operate as expected, the nozzles were cleaned to remove any corrosion product that could build up in them and the corrosive medium was changed. When changing the corrosive medium the pH and conductivity was measured using standard laboratory equipment of a hand-held pH meter of the type used to determine the pH during the original mixing of the artificial rainwater. The conductivity was measured using a hand-held meter that can be see in Figure 5.60. These values can be seen in Appendix C.

Figure 5.60: Use of the hand-held conductivity meter

Another interesting factor that was demonstrated by Figure 5.60 is the clear presence of corrosion product in the corrosive medium. This is what has changed the colour of the, previously clear, corrosive medium. This could also be seen building up on the surfaces of the containment chambers and the pipes used to connect the nozzles, pumps and reservoirs. This can be seen in Figure 5.61, with corrosion on the samples also being clear.

Figure 5.61: Demonstration of the build up of corrosion product within the corrosion chambers, with clear corrosion damage on the sample

Different evidence of the corrosion product being lost could also be seen in the bottom of the reservoirs. Instead of a fine layer of product, such as that being deposited on the surfaces of the corrosion chambers, larger bits of corrosion product were produced and settled in the reservoir. These can be seen in Figure 5.62. To address the potential issue of these larger bits of corrosion product entering the pumps and causing damage, a small piece of sponge was placed within the reservoir to separate the inlets and outlets, allowing the corrosive medium to pass between them with the largest sections of corrosion product filtered out.

During the maintenance intervals, the next area to have corrosion suspended was covered if applicable. This was done by applying the waterproof patch tape, as previously mentioned.

Figure 5.62: Larger sections of corrosion product that settled in the reservoirs, requiring the addition of a sponge to separate the outlets and inlets to prevent damaging the pumps

Issues encountered

During the first 840 hours of operation, no issues were encountered that caused a suspension of operations. The only problem was a one hour suspension of wetting of one side of the sample in the ESH machine due to the pump failing. This was solved by quickly replacing this pump with the spare that had been purchased for this purpose.

Unfortunately, over the course of the 48 hours leading to the end of the ”38.52 month” deadline four of the six pumps in use failed. The reason for the majority of the pumps to fail within a short interval was not known for certain, as they were operating within their recommended parameters and should have lasted significantly longer.

It was suggested that, due to the gradual build up of corrosion products within the pumps, particularly larger pieces of corrosion product, led to a gradual increase in the work the pumps were required to do, until they burnt out. This was possibly contributed to by the one hour on, one hour off, operation that allowed time for corrosion product to drop back out of the fluid and build up in the pumps, which were required to be at the lowest point of the design, to keep the pumps under water at all times.

The decision was made to end the experiment at that point. This was due to the difficulty in sourcing replacement parts for the experimental rigs and issues with the availability of the machines that the rigs were placed on.

840 hours of experimentation had been performed, compared to the 1256 hours planned. This represented 67% of the experiment, and around ”two years and eight months” in experimental time. While less than the four years intended, this would still be enough time to demonstrate the trend of the corrosion pit development and 33.3% of the inspection interval used at depots. This would be a useful period of time for informing any changes to inspection intervals of rail axles.

5.19 Conclusion

This section detailed the design process of a novel experiment to investigate the progression of corrosion pits on rail axles. The original experiment combined stress cycles and a corrosive environment to replicate the axle experience.

The design involved the selection of a realistic corrosive environment. This was done based on previous work using rainwater in Manchester in the 1980s but was updated to reflect the changes in environmental conditions in the UK since then and the unrepresentative results recorded in previous experiments. The environmental cycle was chosen based on the number of rain days in the UK and an assumption that most corrosion would take place on a day with precipitation. The length of the experiment to replicate the length of time that freight axles spend between overhauls was based on the rain day assumption and the selected wet/dry cycle.

The stress cycle was then simplified to a fully reversed tensile compressive cycle from the more complex cycle that a freight axle would undergo. This was due to the demonstrated dominance of the bending stress in the rail axle and the very small depths that corrosion pits exhibit, making replication with tensile loading possible. This was an advantage over previous work that used small scale bending experiments, due to the lack of stress die off towards the neutral axis.

The frequency of the stress cycle was also defined to replicate the speed of a train at the expense of total stress cycles. This was acceptable as the nature of the experiment was not a fatigue test and was focused on the development of corrosion pits that would be governed principally by the corrosion medium that was also used to help accelerate the corrosion testing.

The samples were designed using the corroded surface of a rail axle removed from service. This allowed for high fidelity experiments to assess the changes that would occur if corrosion damage from operation was returned to service. This was an advantage over previous work, as the initiation of the corrosion was not being replicated removing an element of uncertainty from the results.

The resulting curved samples required bespoke jaw assemblies to be designed that were capable of withstanding the applied loads and avoid slipping or unforeseen movement. This was performed using a combination of analytical and finite element studies and included the specification of bolts and bolt torques as well as other details. Other peripheral components such as electronic control and corrosion chambers were also designed to support the experiment.

All the parts were designed, sourced or manufactured, assembled and tested to iron out any issues that arose. This was achieved within budgetary, time and resource limitations.

Once the experiment began it quickly suffered from broken samples that resulted in cessation of the experiment. An investigation concluded that while the experimental concept was likely to be sound, an existing weakness in the designed sample had likely been missed. This weakness resulted in the failure of the sample, with no replacements available to continue testing, before meaningful results had been collected. In response to this the experiment was adapted and three new rigs were introduced to attempt to ensure useful data could be extracted.

A new set of curved samples were designed and manufactured from the broken samples to allow the experiment to continue. At the same time a new pair of bright samples were designed and manufactured support the goals of the experiment and mitigate against possible future incidents.

One of the bright sample experiments was very similar to the original, however the new bright samples did not exhibit existing corrosion damage. This meant that they were replicating the corrosion initiation stage of the process as well as the progression of the damage. This experiment exhibited both stress cycles and exposure to a corrosive environment while the other bright sample experiment was subjected to only the corrosive environment.

All three of the updated experiments were successfully designed, manufactured and tested. The experiments were then begun and the two that involved application of stress failed. The curved sample was judged most likely to have failed due to the same existing flaw problem as the original sample, while the bright sample failed due to the jaw fracturing. This removed the ability to apply stress to either sample.

The decision was made to continue the experiments without the stress elements. This decision was demonstrated to produce representative results as the stress cycle was not expected to have a significant influence on the development of corrosion pits. The experiments were successfully completed, although stopped early due to burn out of pumps, with 80% of the experimental time completed. The results of the experiments are analysed and presented in Chapter 6.

The concept provides a valuable starting point for future work in the field. Further work could add increased capabilities to the rig and allow for a wide range of high fidelity testing.

5.20 Novelty

5.20.1 Scientific

A novel experimental approach has been presented to assess the changes in corrosion pit morphology over time, under exposure to realistic accelerated corrosion conditions in a laboratory setting. The experiment made use of an existing corroded surface in a laboratory test to allow the use of a high fidelity starting point for corrosion pit development.

The rig not only fills a capability gap in the existing experimental repertoire, but also bridges a gap between large, expensive full scale testing and smaller bench testing that mostly test material properties rather than rail axle specifics. In combining the two ends of the spectrum, this concept would allow for faster, cheaper testing of a more specific rail axle environment, providing a platform for future work in this field.

5.20.2 Industrial

The new experimental design combines the testing specific axle conditions of large scale tests with the adaptability and replicable nature of bench top testing. This design provides a strong basis for increased testing of industry specific conditions to address industry questions.

Because of the relative ease of design and manufacture of the new experimental design, compared to previous full scale rigs, more could be produced. The increased number of available rigs could allow for more simultaneous testing, increasing the rate of research. The amount of possible research would no longer be coupled to the availability of a small number of large scale rigs.

Chapter 6

Experimental Results

6.1 Introduction

The experiments that were defined in Chapter 5 were run and the results are presented in this Chapter. The experiments aimed to assess the change in pit morphology over time and thereby calculate the risk of crack initiation from the pits. This process was successful and allowed conclusions to be drawn that suggested a change in current UK procedures.

A brief summary of the experiments is presented first, repeating the outcomes of Chapter 5. Then the data collection procedure is outlined, along with an assessment of the environmental data collected. The results of the experiments, as well as the processing of the data, are then presented and discussed, with the final implications and conclusions of the work at the end.

The work relied on replicating compounds to capture the surface conditions at a point in time and Alicona scanning to digitise the results. The results were then processed using bespoke MATLAB code and analysed using the El Haddad approach [70] to assess the risk of crack initiation.

The experimental set-up was found to be effective and representative of the operational axle conditions by comparing extrapolated results to the axle survey. This was despite the lack of stress cycles that had been originally intended.

The change in the risk of crack initiation was found to be sigbernificant when metal samples without protection from the corrosive environment were exposed. However, when a passivity layer had been produced, the rate of change of the corrosion pits dropped dramatically. This had implications on possible changes to the processes and procedures of how rail axle corrosion is currently addressed, that could lead to lower wastage in the fleet, with commensurate savings financially, environmentally and logistically. The work in this Chapter is summarised in Figure 6.1.

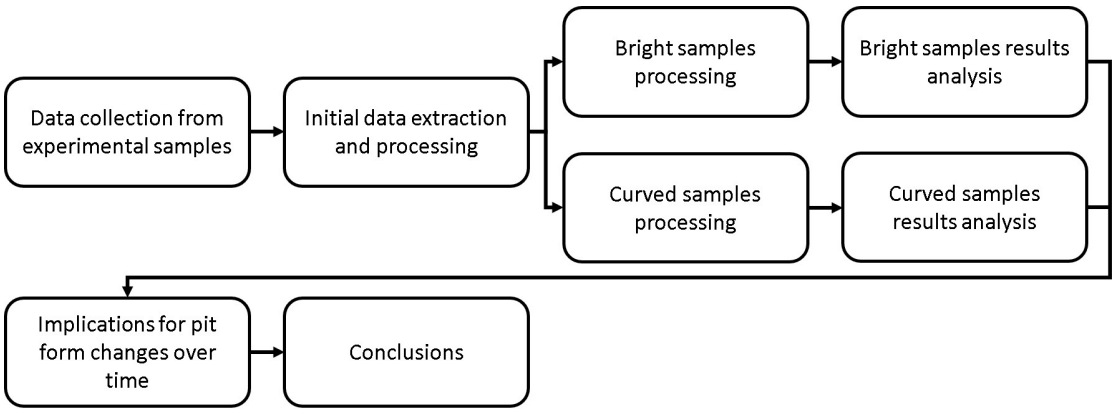

Figure 6.1: Work flow for Chapter 6

6.2 Summary of experiments

Three experiments were carried out to track the changes in corrosion pitting on rail axles over time. These were discussed in more detail in Chapter 5.

All three experiments were exposed to an artificial corrosive environment on a one hour wet, one hour dry cycle, with no stress loading. The artificial corrosive medium was based on a variation of rainwater in Manchester in 1986, equivalent to that used in previous experiments, but altered to reflect changes in the UK environment while still allowing accelerated testing. The experiments ran for a total of 840 hours which represented two years and eight months of corrosion using the analogy to the real time.

The first experiment involved two samples that were cut from the surface of an axle that had been scrapped for corrosive damage. This meant that the surface of interest for the axle had corrosive damage already present, of the kind that would be seen in an overhaul depot during operation. These were referred to as the curved samples.

The other two experiments used single samples cut from the core of the same axle. The samples were larger and possessed smooth machined surfaces without any pre existing damage. These were referred to as the bright samples.

All the samples used had casts taken of their surfaces before the experiment began. During the experiments areas of the samples were covered to prevent continued corrosion of the surfaces at pre-defined gateways. These gateways were set to take place every '6.42 months' in experimental time for the larger brighter samples and '12.84 months' for the smaller curved samples.

By comparing the condition of the surfaces before and after the experiment the changes induced by exposure to environmental factors could be assessed. From an assessment of the differences in changes between different gateways, it was possible to track the variations in pits state over the different time steps.

6.3 Data collection

The experiments ended, leaving four heavily corroded samples that required processing before having data collected from them. This included removing the samples from the rigs, cleaning the samples to remove corrosion product and expose the base metal and scanning to digitise the results. This process is detailed in this section and was materially the same as in Chapter 3 with some with minor adaptations.

6.3.1 Environmental and corrosive medium data

The temperature that the rigs operated in was monitored during the experiments. All of the equipment reported similar results, with minimal variation between each rig. This was as expected as all experiments performed were within the same lab. The consistent environment allowed for direct comparisons to take place between each rig.

The values for pH and conductivity of the corrosive medium at each time step were also recorded. The pH value indicated the concentration of hydrogen ions, representing the acidity of the solution. Conductivity is a measure of a solutions ability to carry an electrical current and indicates the amount of dissolved solids in the solution [133].

The results of the data collected can be seen in Appendix C.

6.3.2 Removing samples and observations

Once the experiments had ended the samples were removed from the rigs. This was achieved by dismantling the acrylic outer frame, cutting the tape and sealant away from the sample, and detaching the clamps.

A lot of care was taken to ensure that none of the tools used came into contact with any areas of interest. This prevented any scratches or dents from obscuring corrosion data from the surface. Once removed the samples were only handled by the areas that had been within the jaw faces.

On inspection it was clear that severe corrosion had occurred. Two of the surfaces from the bright samples can be seen in Figure 6.2, with the areas of corrosion clear especially when compared to the areas that had remained within the jaws.

The use of tape to prevent continued corrosion was also shown to have been effective upon removal of the tape from the surface. In Figure 6.3 it is easy to identify areas that were covered by tape, and identify areas with different amount of corrosion damage, with the area covered throughout being particularly easy to spot. The exposed areas can be compared to the gateway areas shown in Figure 6.4, the differences with Figure 5.56 were due to the changes in experimental run time and gateway intervals discussed in Section 5.18.4. The visibly different surface conditions between gateway areas suggested that the technique was effective and prevented the aqueous solution from coming into contact with the surface.

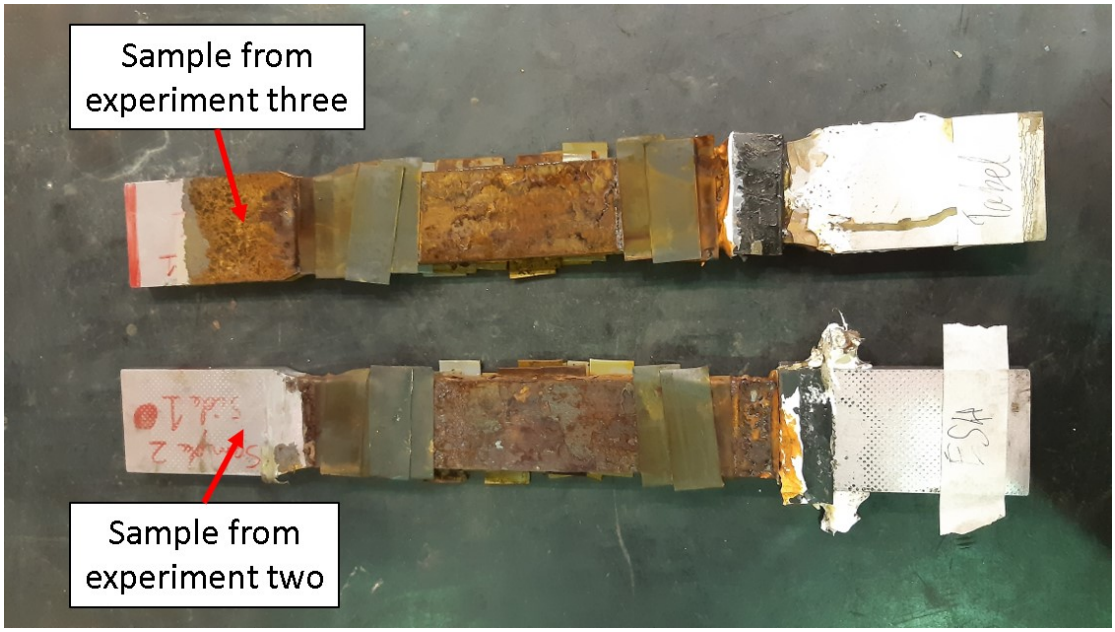

Figure 6.2: Condition of samples after removal from the rigs without removal of the tape or any cleaning. Extensive corrosion damage is visible

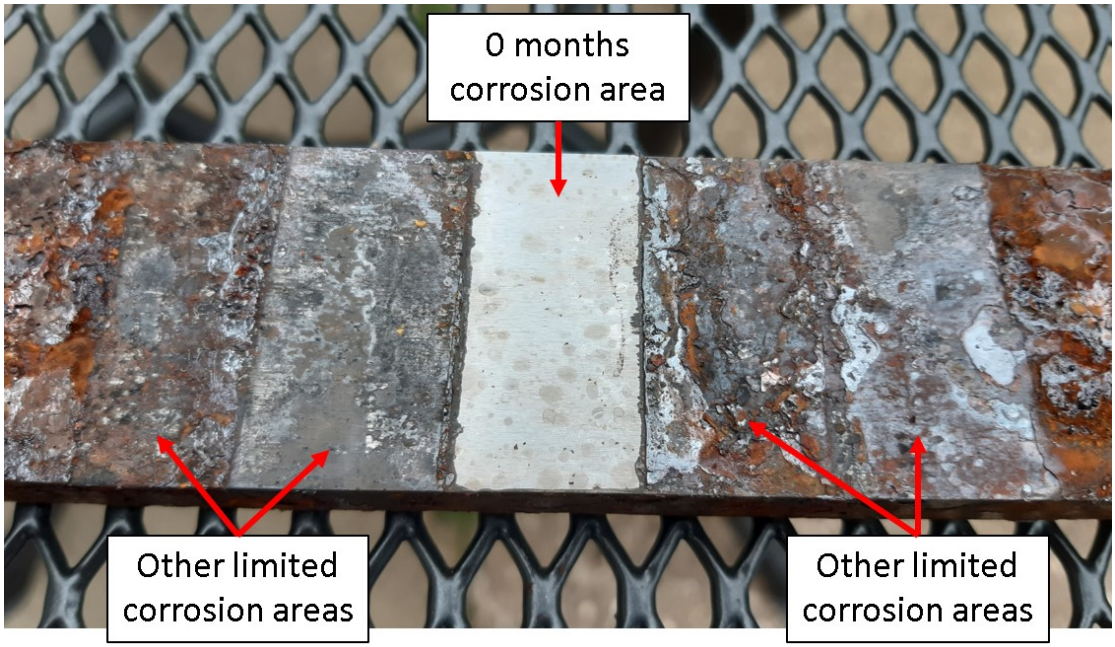

Figure 6.3: Example of side one of a bright sample with the tape covering the areas of interest removed, but before cleaning. The locations of areas covered by tape are identifiable

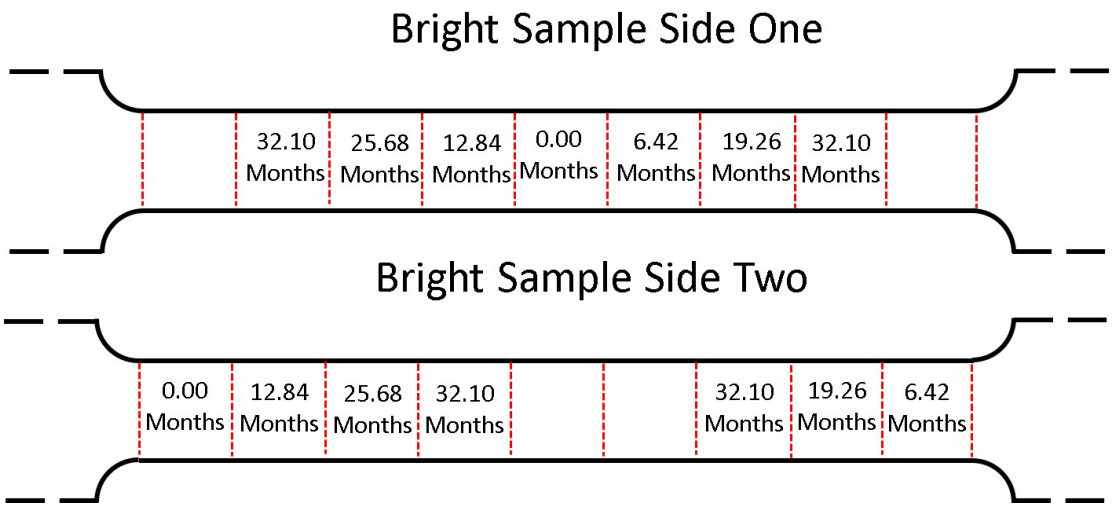

Figure 6.4: Layout of gateway areas for bright samples after change in experiment running time

To allow the samples to be scanned the corrosion product needed to be removed from the surface. This was done using a light acid bath and very light mechanical cleaning with a cloth. This was repeated until the bare metal had been revealed. An example of the results of this can be seen in Figure 6.5 where the cleaned sample has also been matched with the casts of the surface before the start of the experiment. By comparing the number and morphology of pits in each area over time, a pattern could be established.

Figure 6.5: An example of a sample (side one) after cleaning, that has been paired with the casts of the surface before the start of the experiment

The same process was used for the curved samples with similar results. The samples are shown in Figure 6.6 and the locations of each corrosion gateway compared to the schematic diagram in Figure 6.7.

It should be noted that for the curved samples there were a reduced number of sites due to the limited size of the samples. Because of this the gateways were separated by 12.84 months, rather than the 6.42 months used on the bright samples. As well as the increased time between gateways, as only two exposed sides were used, rather than the four across both bright samples, each gateway was represented by two areas. The exception to this was the 25.68 month gateway which had four areas, as demonstrated in Figure 6.7.

Figure 6.6: Image of the curved samples after having tape removed but before cleaning. Note the areas of reduced corrosion and the crack in the upper (”broken”) sample.

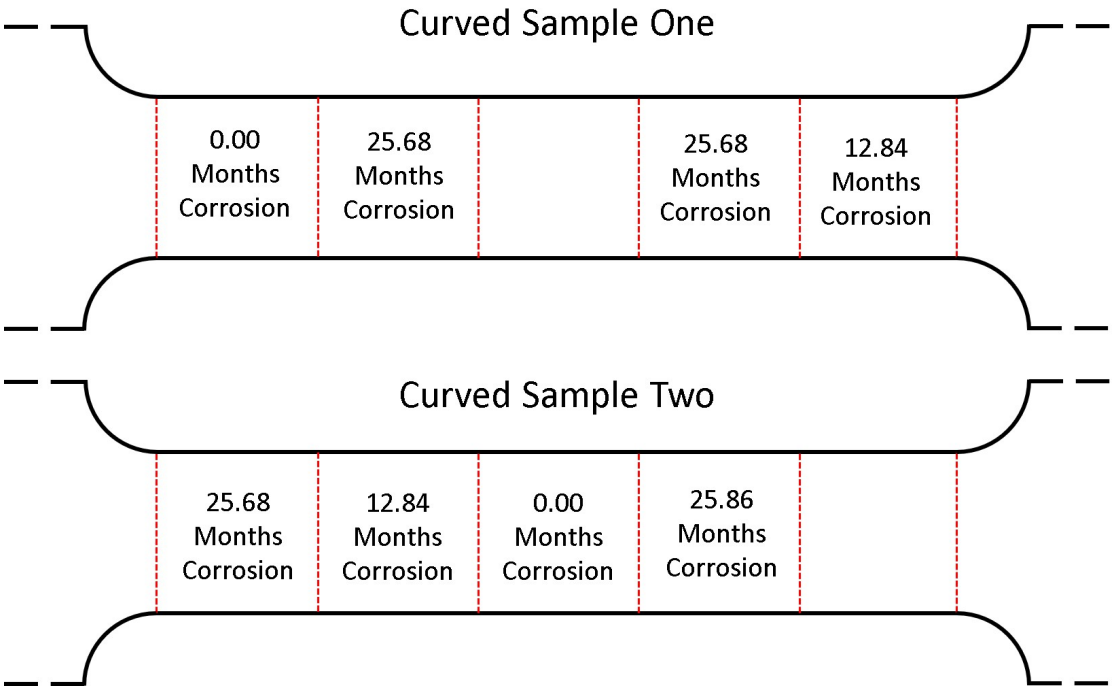

Figure 6.7: Layout of gateway areas for curved samples after change in experiment running time

The curved samples also had casts taken of the surfaces before the experiment began, in the same way as demonstrated in Figure 6.5. This meant that for each area there was a cast of the surface before the experiment began which could later be compared to the same area after the completion of the experiment. By comparing the changes between the two, conclusions could be drawn.

6.3.3 Scanning of samples to retrieve data

The samples and the original surface casts were taken to the Alicona machine for scanning to extract the data from the surfaces. As the metal samples in this case were small enough to be placed directly into the scanner, no casts were taken of the samples after the experiments and the metal was scanned directly.

The results were not sensitive to the minor change in technique. The condition of the surfaces when measured from the casts taken before the experiments began and from the metal at the end of the experiments, exhibited negligible changes as demonstrated in Section 6.4.2 and Section 6.4.3. As the zero month areas had been exposed to no corrosion, the surfaces were unchanged over the course of the experiments. The similarity in the scans taken from the casts and directly from the metal, therefore, demonstrated there was no impact due to adapting the technique.

Initial scanning demonstrated that the effect identified by visual inspection of the parts was also identifiable on the micro scale, as can be seen in Figure 6.8. This demonstrated that there was an identifiable variation between the amount of corrosion between each inspection interval.

The areas that were scanned were selected based on the visual markers found on the samples that identified the edges of each covered area. From these locations a point 5mm from the edge of the sample and 5mm from the edge of the covered area was chosen, to avoid edge effects that may have an impact on the results.

The locations were measured from a datum edge and the same locations were found on the casts to ensure the same area was scanned on both the sample and the cast. This allowed comparison between the original condition of the area and the condition after the experiment.

At this point it must be remembered that there were two types of samples. The first was the curved samples that were manufactured from the axle surface and there were the ”bright” samples manufactured for the central part of the axle. These two styles had different widths of the central section.

For the curved samples the area inspected was 10.2mm along the sample and 20mm across the sample for each gateway area. For the larger bright samples the area was 10.2mm along and 26.5mm across. The resolutions remained the same as with the previous scans for the axle survey at 460nm vertically and 4500nm laterally.

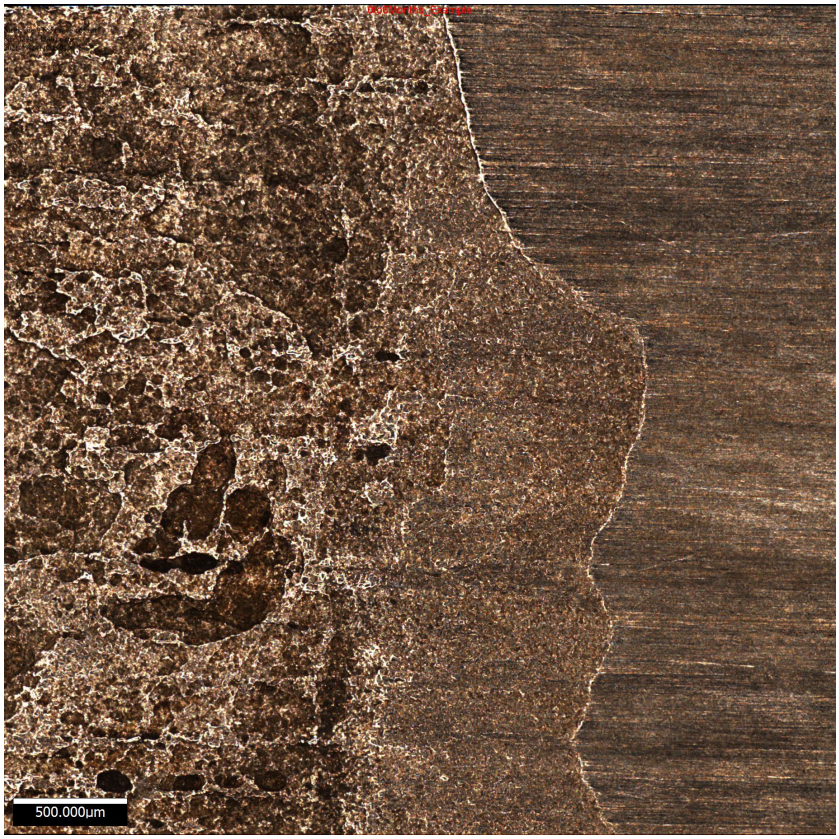

Figure 6.8: Optical image of the variation between a zero months of corrosion area (on the right) and a 6.4 months of corrosion area (on the left) through the Alicona

Cracked sample area

There was an issue with one of the curved samples that broke during the experiment. It developed a through crack during the experiment that meant the sample was in two pieces. This was potentially an issue, as the software used to analyse the pitting would potentially struggle to deal with significant voids in the data. Another possibility was that the Alicona mould misinterpret the surface and produce unrealistic data points, skewing the analysis. It also raised the possibility of misalignment issues between the two parts of the sample, leaving one half with a systematic error compared to the other.

The crack can be seen in the optical image in Figure 6.9 and lay within the 12 month of corrosion region of one of the curved samples. This crack extended all the way through the sample so the image was produced by pushing the two separate sections against each other.

Figure 6.9: Optical image of the crack in the 12 month section of the sample. Taken using the Alicona Machine

It was decided that the scan would be performed with the two sides of the sample pushed together, the results can be seen in Figure 6.10. This would allow the area to be scanned in an efficient way, although extra care was taken in ensuring that the crack did not affect the results of the corrosion development of the pits by producing unrepresentative results. It was found that the fears were unfounded and the results of the scan were of a high quality.

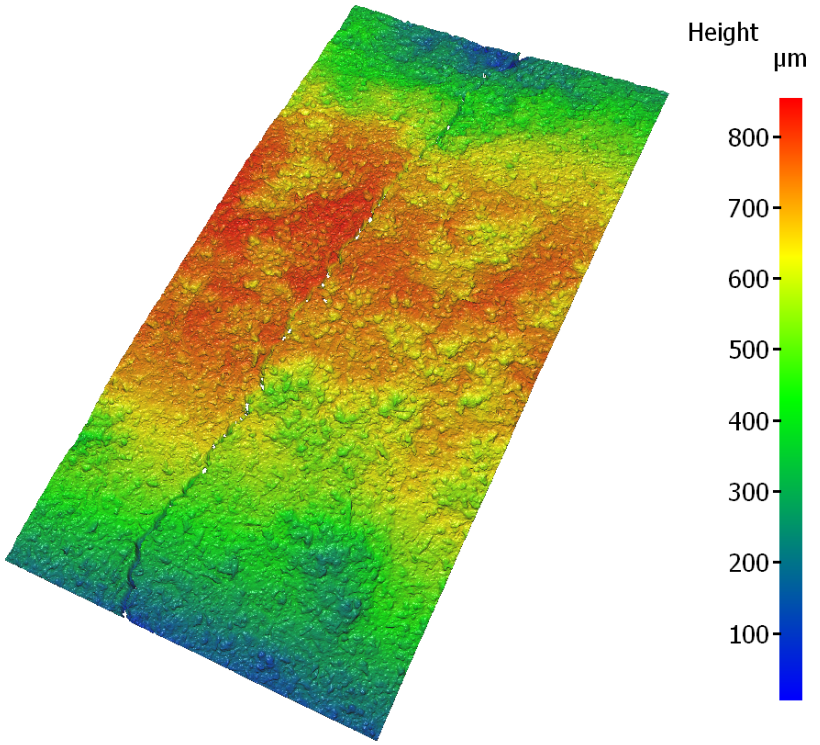

Figure 6.10: Scan of the cracked sample before processing (data has been decimated)

6.4 Results

This section details the results of the analysis of each sample type. It also contains details of the processing of the digital results to allow for results and conclusions to be drawn. The bright samples are presented first, with conclusions, followed by the curved samples. A summary of each experiment, its samples and gateways can be seen in Table 6.1.

Table 6.1: Summary of the three experiments, including the sample types, experimental time and gateway information

Experiments	**Sample type and number**	**Total experimental time (in analogous time)**	**Gateways and number of sample areas per experiment**
One	Curved samples - x2	25.68 months	0 months - x2 12.84 months - x2 25.68 months - x4
Two	Bright sample - x2	32.10 months	6.42 months - x2 12.84 months - x2 19.26 months - x2 25.68 months - x2 32.10 months - x 4
Three	Bright sample - x2	32.10 months	6.42 months - x2 12.84 months - x2 19.26 months - x2 25.68 months - x2 32.10 months - x4

6.4.1 General processing

The scan's and cast's results were converted to text files and loaded into Matlab. Pre-processing, similar to the one reported in in Chapter 3, was used resulting in continuous, filtered data was used. The filtering was still required for the curved scans and the casts due to the possibility of the replicating compound not having formed flat on the samples without bumps from areas of more compound settling in a single area. However, the bright samples didn't require filtering as the results were taken directly from a flat surface.

The Z axis was also reversed for the scans captured directly from the metal. This was to ensure the scans were in the same format as those taken from the replicating compound to allow the same code to be used for all scans.

6.4.2 Bright samples

The bright sample scans were analysed using the same image processing code as used on the axle survey results. No corrosion pits were identified in the study on any of the four surfaces before the experiments. This was as expected, as the samples had been manufactured from core steel of the axle and had been delivered immediately after manufacture. There were some tooling marks from the milling machine, however none of these were sufficiently deep enough to cause any false positives in the pit identification software. After the end of the experiments, the scan of each area was processed to identify and separate the corrosion pits on the surfaces.

Experiments two and three both used bright samples. As each sample had two sides, each corrosion gateway had four sample areas available for study, as can be inferred from Figure 6.4. The only exception was the ”32.10 months” corrosion gateway that had eight sample areas to increase resolution at the maximum exposure time. The use of multiple areas for each gateway was to increase the confidence of the results through replication and lower the risk of a single piece of experimental error skewing the results.

Each area had the number of identified pits recorded as well as the statistics of these pits calculated. This allowed for patterns to be formed of the progression of corrosion pits over time. These patterns could then be used to produce a predictive model of corrosion pit development.

It should be noted that the sample from experiment two, which was designed to experience a stress cycle that was abandoned, will be referred to as Sample two throughout. Experiment three’s sample will be referred to as Sample one. The naming convention was carried through from the manufacturing stage to allow consistent record keeping.

Initial results

Initial results indicated that corrosion had occurred broadly in line with expectations. These results were produced before pit identification and separation, so are merely indicative rather than final results.

In Figure 6.11 the maximum depth of each scan area for the bright samples is shown. As can be seen, there was a clear trend in the maximum depth reported increasing with time, however there are some major variations. The spread of the results also increases with more time for corrosion to occur, but did appear to plateau with extended exposure time.

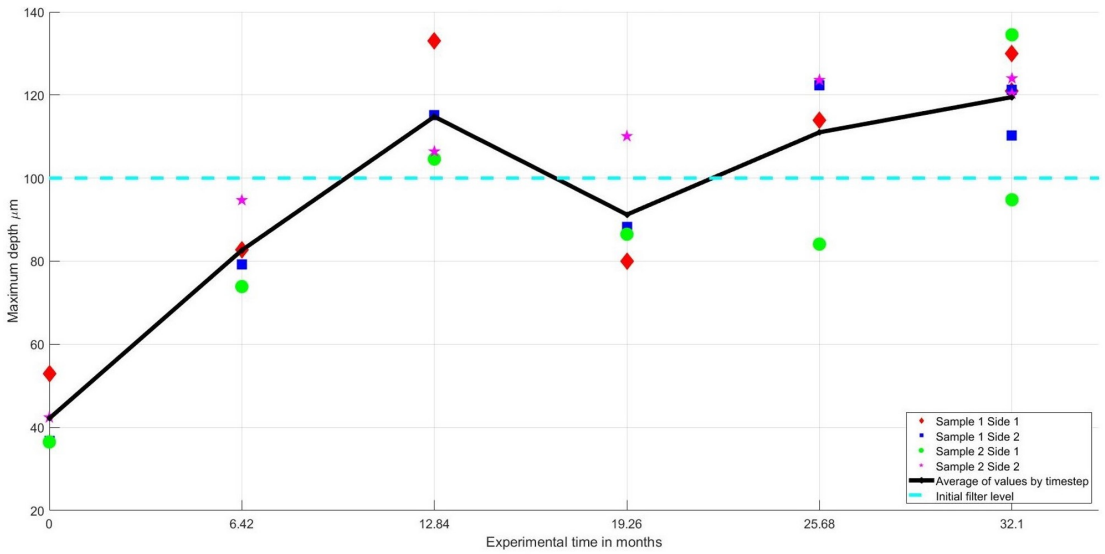

Figure 6.11: Maximum depth identified in each scan of the bright samples (without pit identification)

The use of the maximum depth value was vulnerable to experimental errors, for example if there was a single significantly higher point due to a measurement error then the conclusions drawn could be altered by this single error even if the rest of the results were representative. However, the same general trend can be seen in the average depth values of the entire scan, seen in Figure 6.12. This indicated that the general level of corrosion was increasing with time, as expected.

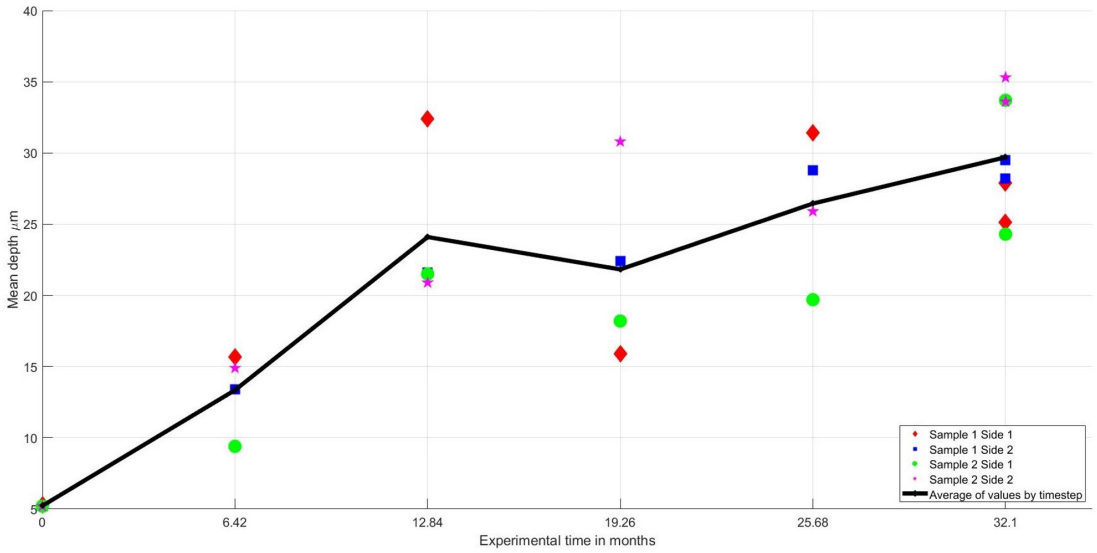

Figure 6.12: Mean depth identified in each scan of the bright samples (Without pit identification)

The plateauing effect seen in both Figure 6.11 and Figure 6.12 indicated that a change was occurring on the surface of the sample, that resulted in lower rates of corrosion damage increase. It was known this was occurring on the sample due to the controlled nature of the other parameters such as the corrosive environment, temperature, humidity, etc.

Pit identification parameters

With the analysis of the axle survey results, discussed in Chapter 3, the initial filter level was set to 100µm. This was due to the shot blasting procedure that the axles underwent which was shown to have affected the surface to a depth of around 100µm, meaning that any damage below this level could not be exclusively attributed to corrosion damage. However, with the analysis of the bright samples, this limit cannot be used. This was due to two factors, there was no shot blasting of the samples, removing the rationale for the limit and if the limit was used many samples would report no pits as no data points exist above this limit as shown in Figure 6.11. This was not unexpected as the early stages of corrosion were being replicated, rather than the end of the process corrosion that would be seen on axles being processed at depots.

An initial filter level was still required to allow the previously described approach to be used. This was a complex question to answer, due to the variations in time frame that each scan area had undergone.

If a flat filter level was chosen, it may result in either no pits being identified until the end of the experimental time frame, making trends difficult to spot or detecting pits at the lower levels but also detecting an unrealistic number of pits at the upper bounds of the time interval. This can be seen in Figure 6.12, with the large changes in the average data level between different scans.

Due to the difficulties of defining an flat initial filter level, to be applied across all gateway areas, a more adaptive filtering approach was used. The adaptive filter level chosen was based on the average depth over the entire scan with a multiplication factor applied to define a pit within the scan.

The multiplication factor was based on the concept, that, as corrosion became more severe, a higher mean scan depth would be expected, as well as higher variation in depth within the scan. This approach would also allow for pits to be identified earlier in the process, to indicate trends, without identifying unreasonable number of pits in the more corroded samples.

While this did represent a change in terms of the minimum depth of pits, compared to the work in Chapter 3, the area requirement remained constant throughout. This ensured that there was a consistent definition throughout the process allowing for comparisons to be drawn between the identified pits.

The definition of a pit for this part of the analysis was therefore changed to an area larger than a 300µm diameter circle, but less than a circle with a diameter of 4000µm. The area also consisted of data points with an minimum depth of more than 1.5 times the average depth of the sample. The filtering process occurred at ten intervals of 10µm, as testing indicated this was an appropriate level. The new filter level was different to the filter level used in Chapter 3 that used the same area definition but required the data points within the area to have a depth of greater than 100µm.

The exact filter level was decided based on testing of different multiplication factors and the number of pits identified at each. 1.5 was found to produce a reasonable number of pits, at all corrosion durations.

Using the 1.5 multiplication factor of the average depth as an initial filter level resulted in a number of pits being identified in each scan area. The number of these can be seen in Figure 6.13, with the averages at each time step also marked. As can be seen, there was an initial rise followed by a plateau, although this was subject to some quite large variations within each time step. This was not surprising, as a degree of pit consolidation was expected over time and the initial filter level varied with the average depth of the scans, so direct comparison became more difficult.

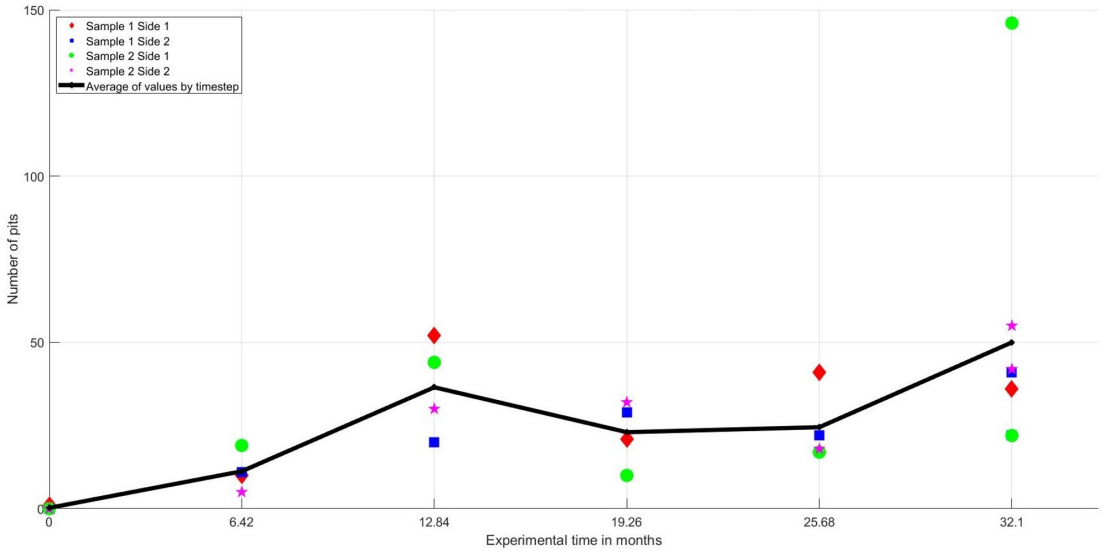

Figure 6.13: Number of pits identified in each scan area sorted by duration of corrosion and sample

Based on a visual inspection of pits identified on the scans the process had worked well, with an example of the results being shown in Figure 6.14. It should be noted that the pit numbers on each scan, as demonstrated in Figure 6.14, were assigned randomly based on the order they were separated, the number had no physical meaning but was a unique identifier, which allowed an individual pit to be tracked throughout the analysis. An inspection of all of the scans demonstrated that there were no major areas missed or included in error. This encouraged confidence in proceeding with the analysis.

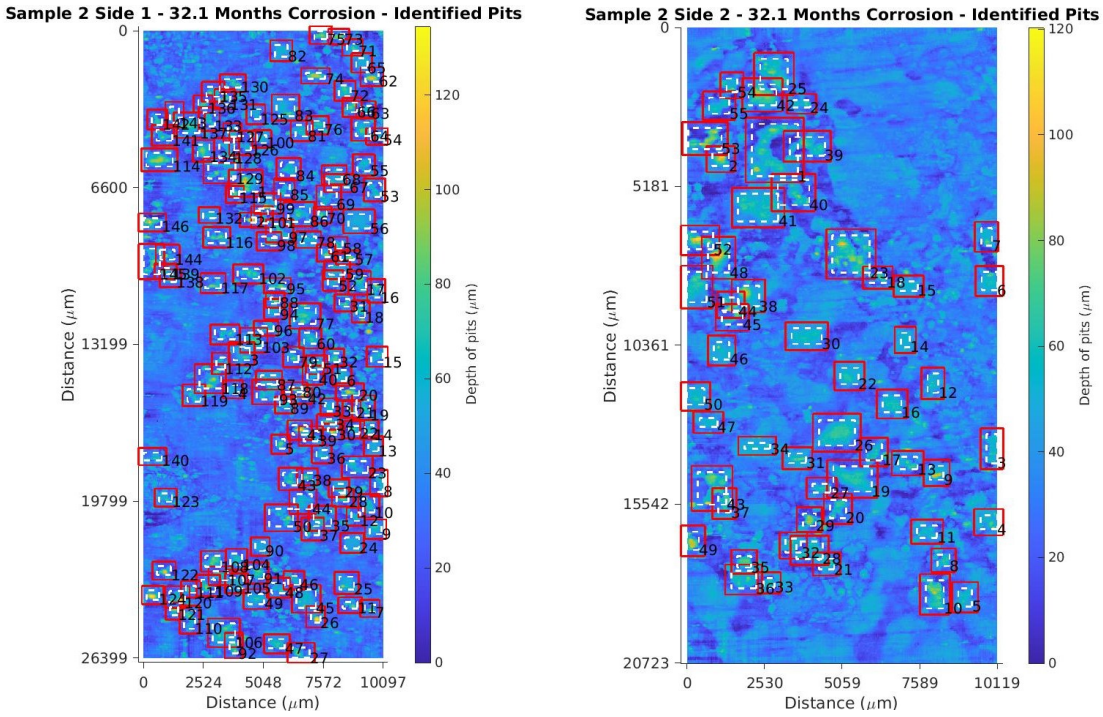

(a) Pits identified on Sample 2 Side 1 - 32.1 months of corrosion

(b) Pits identified on Sample 2 Side 2 - 32.1 months of corrosion

Figure 6.14: Examples of pit identification and separation on two areas that had undergone 32.1 months of corrosion

Once all the pits had been identified and separated using the same process as in Chapter 3, they were analysed to determine their depth and bounding box diameters which allowed calculations of aspect ratios. There was also analysis carried out to determine the influence of any shape factors. These were then compared to the results from the axle survey and analysed to determine if there were any patterns that could be determined.

Pit depth analysis

The depths of the separated pits are presented in Figure 6.15, sorted by time step. This means that all pits that underwent the same period of time exposed to corrosion were grouped together by colour, regardless of the sample or side that they were found on. It should be remembered that twice the area was scanned for the 32.10 months of corrosion time frame, because there were eight gateway areas compared to four for the other corrosion time frames, partially explaining the increased number of pits.

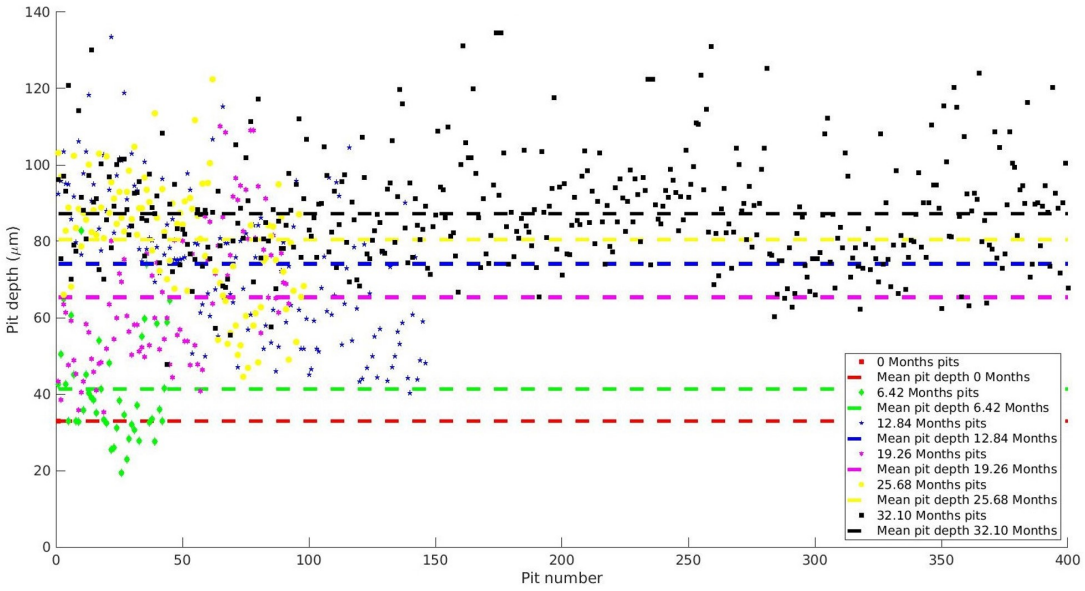

Figure 6.15: Depths of pits identified sorted by time step. Mean depth for each time step marked

As can be seen in Figure 6.15, the general trend was for the mean pit depth to increase as the amount of time exposed to corrosion increased. This supported the expected trend, and the values seen in Figure 6.12 where the pits had not yet been identified, including the 19.26 month areas being lower than expected based on the rest of the trend.

The increase in mean pit depth values could be partially accounted for by the adaptive filter level, based on 1.5 times the mean depth of the scan, shown in Figure 6.12. This would result in some of the smaller pits, that would be accepted in the shorter exposure time areas, not being accepted in the longer exposure time areas resulting in an inflated mean as shallower pits were excluded. However, it can be seen in Figure 6.15 that if the 100µm limit used in Chapter 3 were used, that very few pits would have been identified.

It can also be said that despite the adaptive filter level having a tendency to inflate the mean pit depth value through an increased threshold level, the number of pits that break through the threshold sufficiently to meet the minimum area definition generally increased with corrosion exposure time, as seen in Figure 6.13 despite effects such as pit consolidation that would have a downward pressure on pit numbers identified. The combination of higher mean depth values and increased numbers of pits identified, despite the changes in the threshold values, indicated that the trend of increasing mean pit depth with exposure time was valid.

As there was no stress applied to these samples for the majority of the experiments duration, the Godard corrosion model could be applied. This was given in Chapter 4 Equation 4.3, shown again here in Equation 6.1. It was suggested that the depth of corrosion of a given pit could be modelled based on the time of exposure, and two parameters, C and B that are dependent on the material-environmental combination. In previous work by Kawai et al. [75] it had been stated that the B term was almost always in the range of 0.3-0.5.

$$d = C(t)^B \tag{6.1}$$

Using the mean value of pit depth at each time step, Equation 6.1 was applied. The C and B terms were calculated by comparing the measured experimental values and the values calculated using Equation 6.1. C and B were the adjusted to minimise the sum of the square of the residuals.

The values were found to be 23.63 and 0.38 for C and B respectively. The calculated B term fell within the 0.3-0.5 reported range, increasing the confidence that the experiment had achieved its aim of measuring changes in corrosion over time. Figure 6.16, shows the mean pit depth data at each time step and the Godard model calculated from the measured data extrapolated over time.

Based on the extrapolated results, the mean pit depth after eight years of corrosion would be 132μ m, 154μ m after 12 years and 171μ m after 16 years. These time frames were chosen based on inspection intervals of rail freight axles shown in Figure 2.16 [42].

In Figure 6.17 mean values (green diamonds) can be compared to the mean pit depth values collected from the scans of operational axles in the axle survey (blue circles). These results are presented in Figure 6.17 and demonstrate that the mean values of pit depths extrapolated from the bright samples were of the same order of magnitude as the scans taken from real axles.

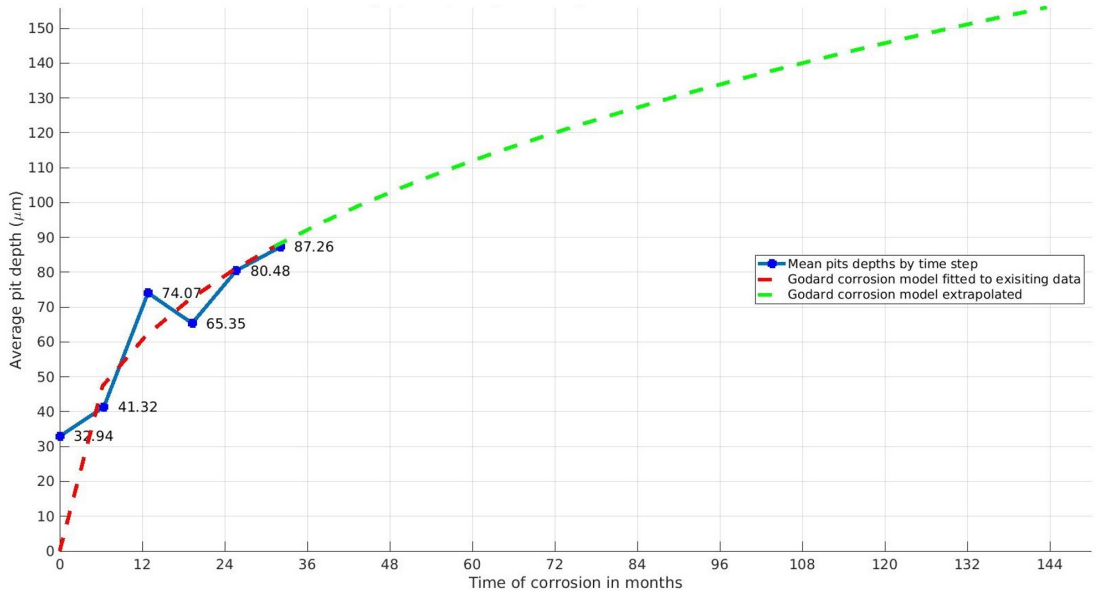

Figure 6.16: Godard model of corrosion extrapolated, based on measured mean pit depth data in each time step

The similarity between the extrapolated experimental mean pit depth and mean depth results from the axle survey, detailed in Chapter 3, suggested that the material and environment pairing in the experiment was similar to actual axle conditions. However, the extrapolated mean pit depth values were on the lower end of the group, suggesting that a slightly more aggressive environment could have been used. However, these results indicated a level of confidence in the experimental parameters chosen and the concept overall.

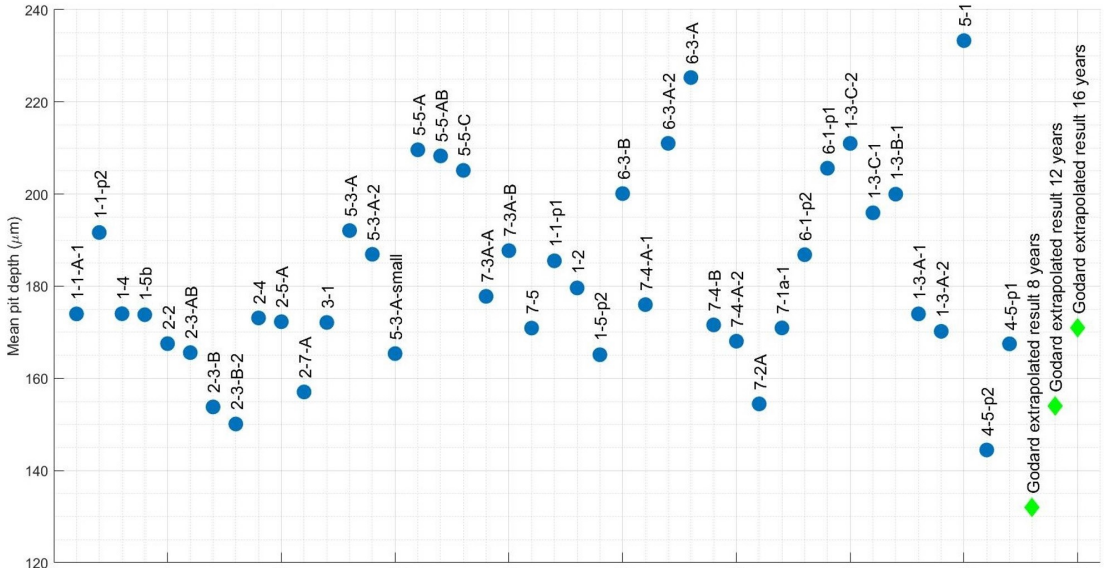

Figure 6.17: Mean pit depths of axle area scans compared to extrapolated Godard results

Taking the results of the areas that underwent the longest amount of corrosion, 32.10 months, and analysing the distribution of pit depths also produced results in line with those calculated from the real axle surfaces. This was demonstrated by Figure 6.18.

The 400 pits from the 32.10 month areas (all samples and sides included) were used to produce a normalised histogram of pit depths and the Gumbel distribution was calculated. The μ and β values of the distribution were 80.87 and 11.07 respectively. The results can be seen in Figure 6.18. These values were noticeably similar to many scans in Figure 3.43, with a similar shape factor, β, but with a lower location, μ, with the peak being at around 80μ m rather than the approximately 140μm of many of the original scans analysed in Chapter 3.

The difference in the location value, μ, of the distribution was as expected, with the trend of mean pit depth increasing with time of exposure and the operation axles having been in service for approximately three times as long (96 months compared to the experimental time of 32.10 months). The difference could also be partially explained by the threshold value to define a pit in Chapter 3 excluding pits below 100µm unlike the filter level used in this section that allowed shallower pits. However, as can be seen in Figure 6.18 even if pits below 100µm were excluded, the location of the distribution would still be lower than that reported for operational axles in Chapter 3.

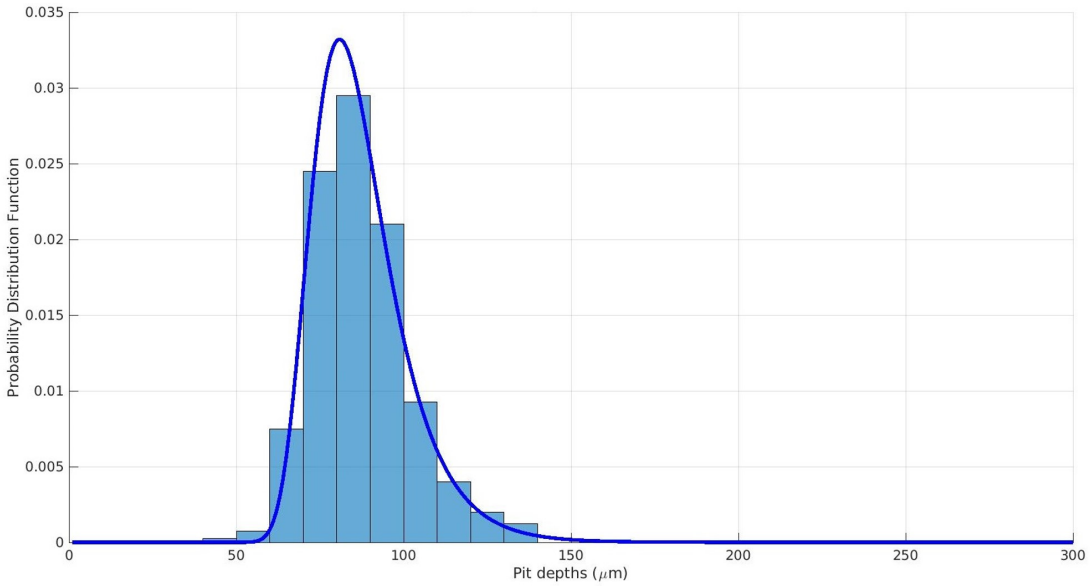

Figure 6.18: Normalised histogram of pits identified in 32.10 month areas, with the Gumbel distribution overlaid

Pit width analysis

The widths of the pits, calculated using the bounding box concept, were calculated next. The results of this can be seen in Figure 6.19 (representing the maximum dimension) and Figure 6.20 (representing the minimum dimension), with the pits sorted by time step and the mean value for each time step marked.

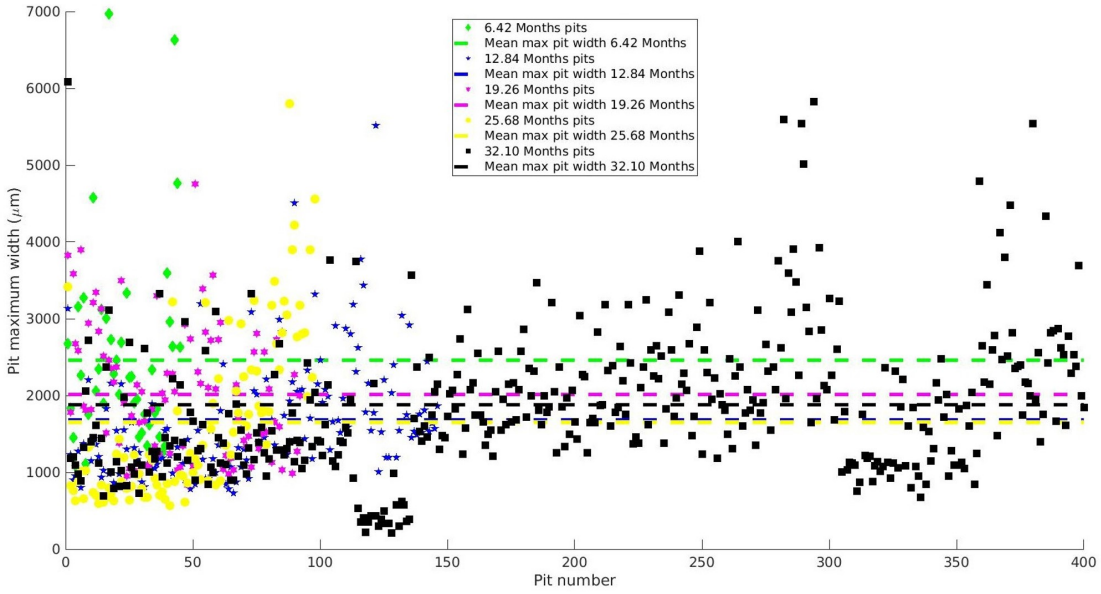

Figure 6.19: Maximum widths of pits calculated using the bounding box concept sorted by time step

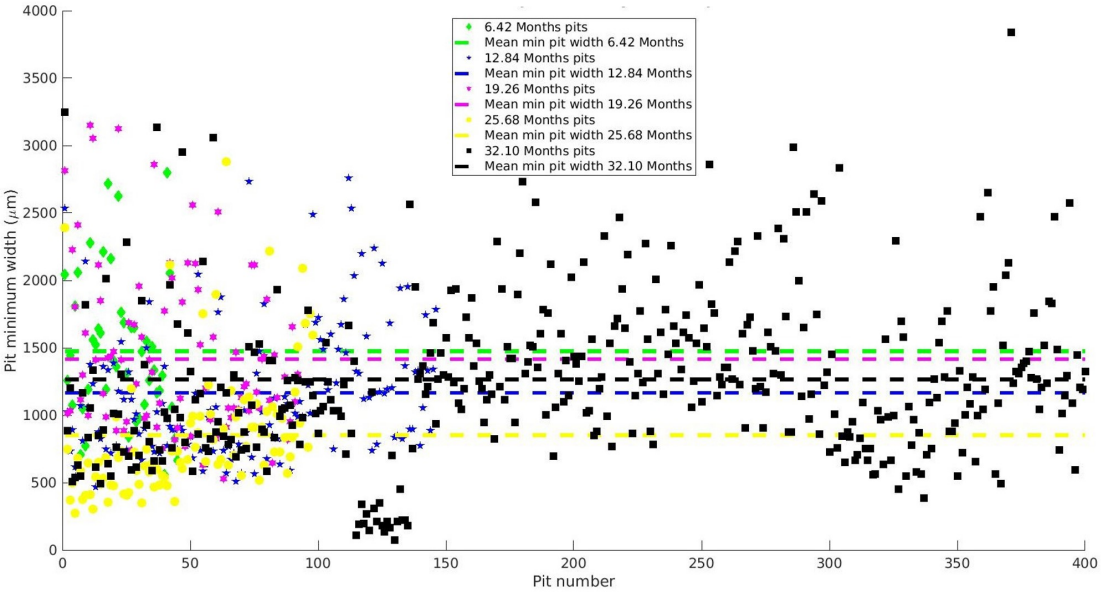

Figure 6.20: Minimum widths of pits calculated using the bounding box concept sorted by time step

By looking at these figures it can be seen that there is little pattern to the maximum and minimum diameter values, particularly if the zero month corrosion values were neglected as there was only a single pit in this time step, making drawing long term conclusions problematic.

There were certain groups of pits on the Figures, that appeared to be outliers compared to the rest of the data. The clearest examples of this can be seen in the 32.10 month time step, particularly with pits 117 to 132 and approximately 300 to 360. While these groups appear distinct in these, and later, Figures, this was a legacy of the way that the MATLAB function used to identify the pits worked. The grouping of these points had no physical meaning, and if they had been distributed more evenly across the data set their values would not appear so distinct.

As the X and Y axis values were known and consistent throughout the scans, an investigation of any directional influence or shape factor could be undertaken. If pits were being formed on a homogeneous surface and with equal application of the corrosive medium, it would seem sensible to suggest that the ratio between the diameter in the X axis and the Y axis would tend to one, as there would be no reason for the pits to tend to grow in one direction more than the other. A similar analysis was carried out for the axle scans, however due to a lack of data the use of the analysis was limited.

While a shape factor was detected in the axle survey in Chapter 3, with a statistically significant tendency for pits to grow more in one axis than the other, it was not possible to determine if this was axially or longitudinally to the axle. This was due to the relative orientation of the samples not being collected during the initial collection of data in the depot.

The values for the shape factor were calculated by dividing the X axis diameter by the Y axis diameter. The results of this can be seen in Figure 6.21, with the results separated by time step. Between each time step there was no detectable pattern to the mean value of the shape factor, but the mean shape factor of all pits was found to be 1.50. This was greater than the expected mean value of one and was statistically significant with a calculated p value of 9.70×10^{-40}. This suggested that there is an effect happening that means the pits develop with a bias towards the X axis, with pits being 150% longer in this axis on average.

In the experiment, the X axis of all the scans taken was the vertical orientation of the samples, running along the gauge length, as demonstrated in Figure 6.22. The bias towards this direction suggested that the running of the water down the samples contributed to the development of the pits in this direction.

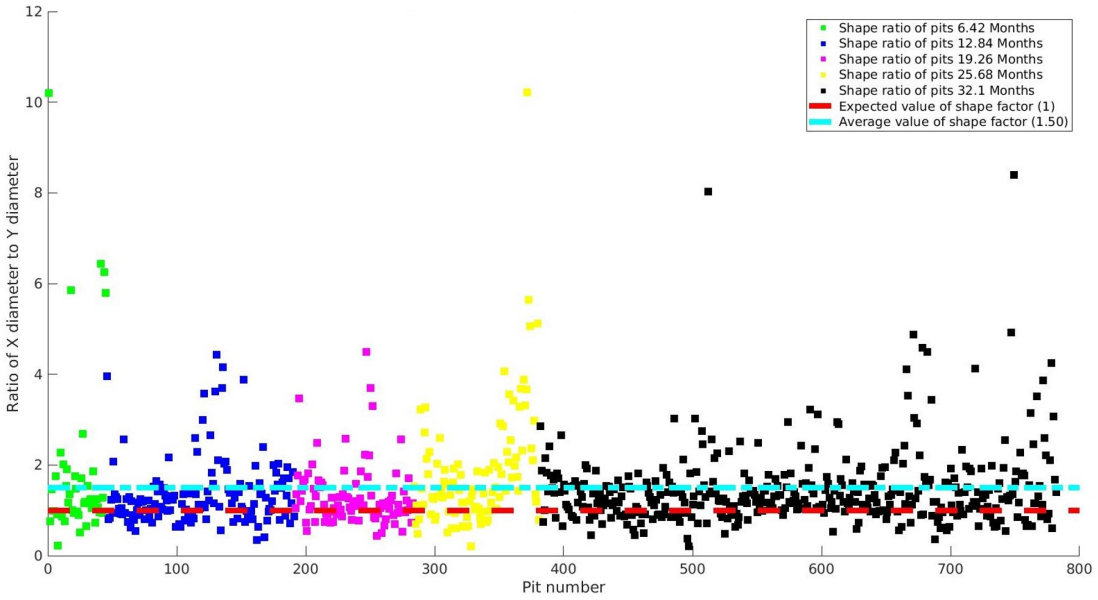

Figure 6.21: Shape factor of pits sorted by time step. Expected value and mean values marked.

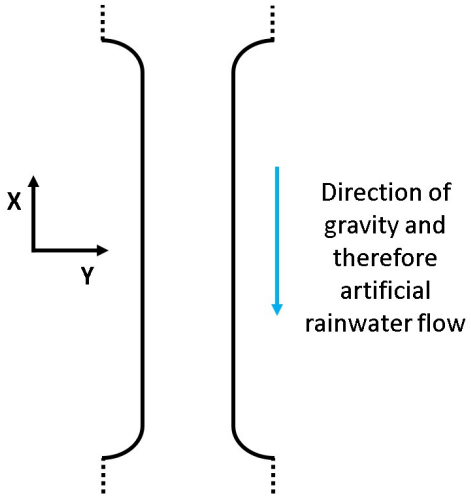

Figure 6.22: Orientation of samples when scans were taken with regards to X and Y axes and gravity

This shape factor was higher than the mean factor reported for the axle scans of 1.12, in Section 3.8.2, which itself was a statistically significant variation on the expected mean. The conclusion that could be drawn from this was that while the experimental results reported a shape factor variation, it was more pronounced than that found in the operational axles, and showed a bias towards the direction of flow of the running water. In this aspect the experimental results deviated in a minor way from the observed results on operational axles.

Aspect ratio analysis

The values of the aspect ratio between the depth and the radius of the pits was calculated for both the maximum and minimum bounding box diameter. The results can be seen in Figure 6.23 and Figure 6.24.

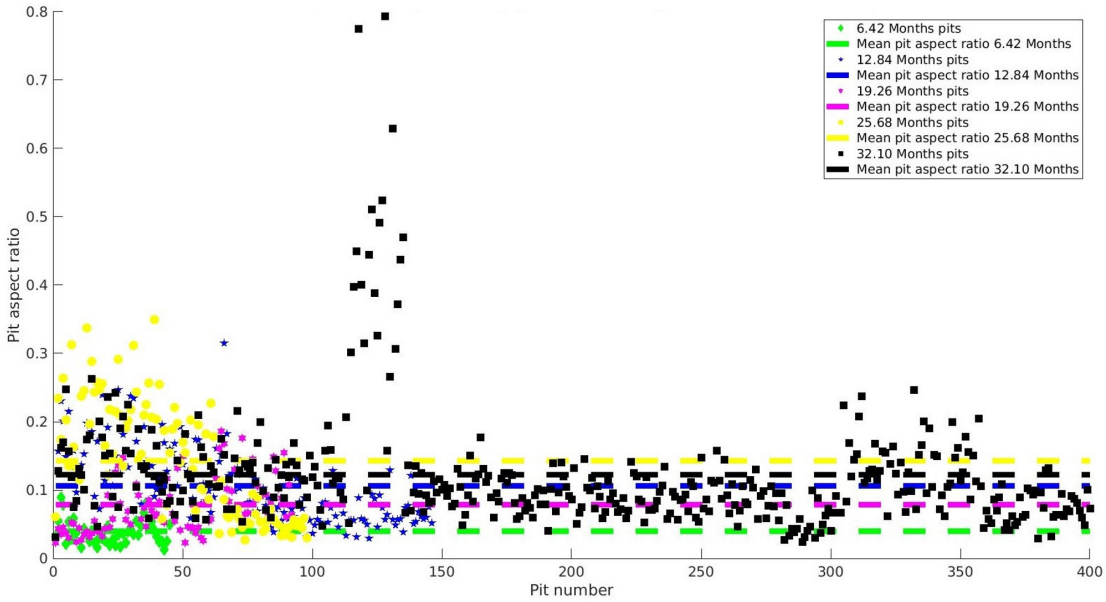

Figure 6.23: Aspect ratio of pits using the maximum diameter. Apparent peak is coincidental and has no physical meaning.

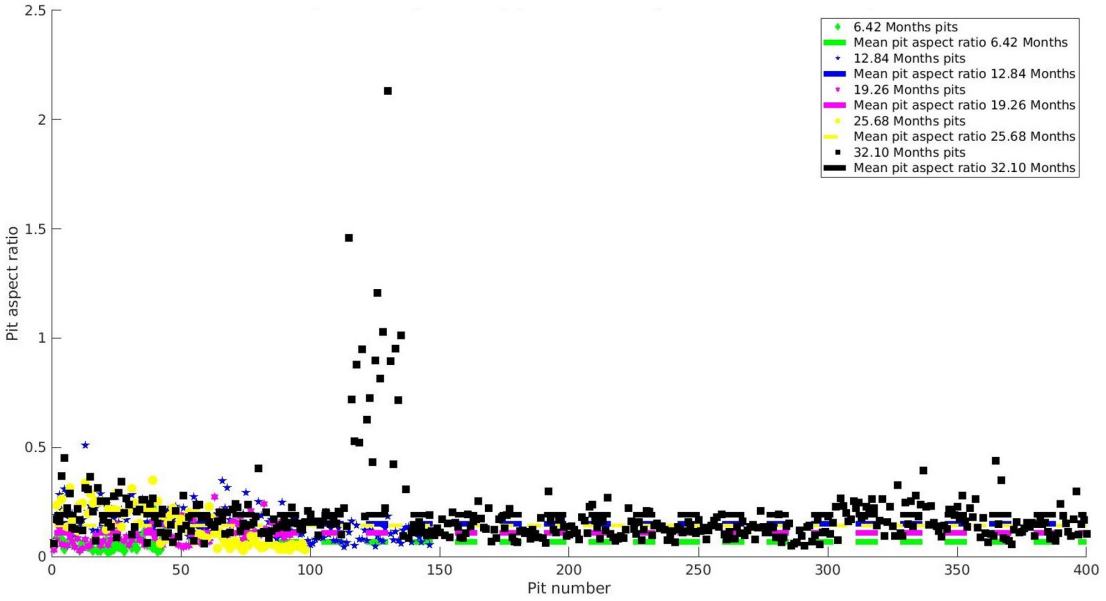

Figure 6.24: Aspect ratio of pits using the minimum diameter. Apparent peak is coincidental and has no physical meaning.

Using the maximum diameter, which produces by definition the lowest value for aspect ratio, the pits are all below an aspect ratio of one, with the vast majority of pits being below 0.2. However, there is a general trend that the mean aspect ratio increases with corrosion time, but there are variations within this. It can be seen that the highest aspect ratio values are present in the 25.68 and 32.10 month corrosion areas, suggesting that while more pits may be forming in the longer corrosion periods, keeping the mean low, some pits start to increase their aspect ratio rapidly.

The apparent peaks that can be seen in Figure 6.23 and Figure 6.24 have no meaning other than they occur in the 32.10 month gateway, suggesting higher aspect ratio values occurred after longer exposure times. The clustering of the results into what appears to be a spike in the data does not have any further meaning.

The same general trends can be seen in Figure 6.24, with a generally increasing aspect ratio and more high value aspect ratios with a longer corrosion exposure. The maximum aspect ratio values of around 2.2 were much higher than can be seen in Figure 6.23 but most pits still remained below around 0.25.

Comparing these results to the results from the axle survey, given in Figure 3.40, it can be seen that the average aspect ratios were significantly lower than that of the pits detected on operational axles. This was in line with expectations, as the initial aspect ratio of a corrosive pit would be very low as only the surface would be being attacked with minimal depth, then increase as the pit developed.

Square root of area parameter

The key parameter used to determine the risk of crack initiation from a corrosion pit in Chapter 4, was the $\sqrt{Area}$ parameter. The same parameter was calculated for the bright samples, as a direct estimation of the change in the risk of crack initiation from the developed pits.

As the planned axis of loading was known for the laboratory experiments it was possible to determine the correct projected area to use to calculate the risk of cracking. Due to experimental problems detailed in Chapter 5 the loading was not applied during the experiment, however calculations were carried out using the planned loading direction. It was not known which orientation the pits identified in the axle survey, reported in Chapter 3, were in so the projected area in both axes was calculated and presented in Chapter 4.

For the collected experimental data the X axis, defined in Figure 6.22, was known the be the axis of loading, so the projected area with a constant Y value was calculated. The projected area was produced using the convex hull approach detailed in Chapter 4.

The results of these calculations can be seen in Figure 6.25. Assuming that the sample underwent the maximum stress amplitude of 166MPa and the ΔK_{th} value for crack initiation was $13MPa.m^{0.5}$ (the same assumptions used in Chapter 4) the maximum allowable $\sqrt{Area}$ value was calculated to be 4620µm.

All of the pits identified from the bright samples were well below the threshold $\sqrt{Area}$ value, as shown by Figure 6.25. The low $\sqrt{Area}$ values indicated that none of the pits identified were likely to result in crack initiation, with significant factors of safety. The maximum ΔK calculated from the identified pits was $4.58MPa.m^{0.5}$, a factor of safety of 2.84 compared to the $13MPa.m^{0.5}$ threshold value. Assuming that loading remained at the same level the $\sqrt{Area}$ could increase by approximately eight times before risking crack initiation.

In the case where the experienced stress was lower than 166MPa the threshold would increase based on the terms of Equation 4.29. No clear trend can be observed although pits with higher square root of area values tend to occur more regularly after longer corrosion times. However, the rate of increase can be seen to plateau based on the mean value in Figure 6.25.

It should be noted that the calculated square root area parameters within these areas were very similar to those reported in the axle survey. This was evidenced by the mean $\sqrt{Area}$ value of pits in the axle survey being 236.9µm compared to a mean of 264.0µm for the 32.10 months corrosion pits of the bright samples. This indicated that the level of pitting in terms of projected area was not increasing significantly with time as the bright samples had achieved a similar level in around 'three years'. However, the maximum values were significantly lower for the bright samples compared to the operational axles.

The similarity in the averages compared to the differences in the maximum values could be explained by considering that the eight year time frame was between inspections rather than the length of time that corrosion had occurred over. If an area on an axle had had its protective coating removed after six years of operation, the corrosion time would be much lower than the eight years of service, with corrosion only occurring for only two years. This might explain both the similarities in the means as well as the presence of higher extreme values that may have been exposed for longer, up to the full eight years between overhauls.

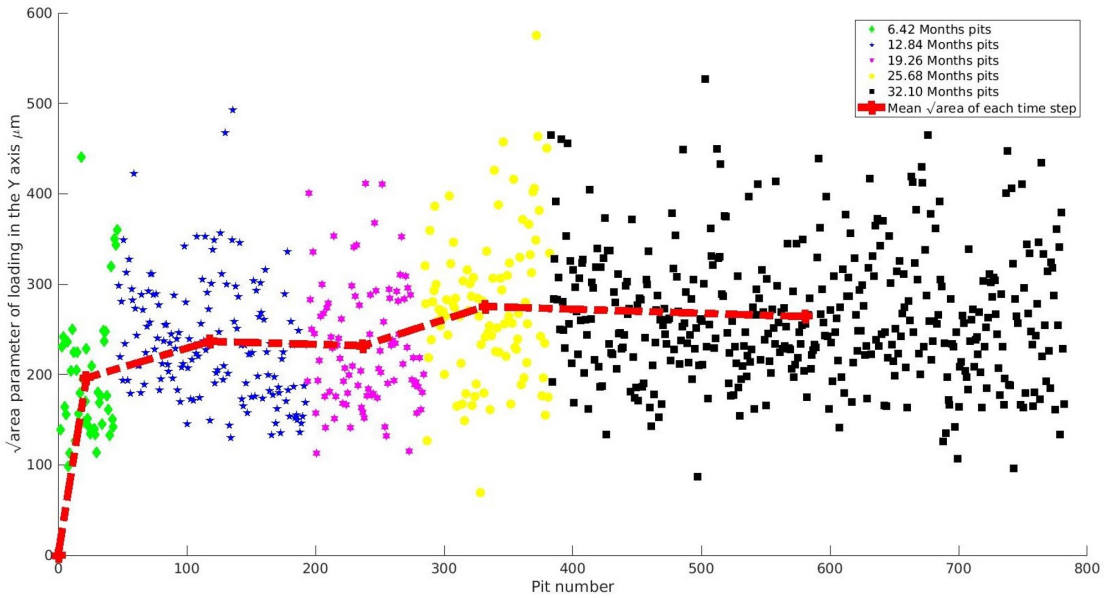

Figure 6.25: Square root area values of pits found in the bright samples by time step. Mean values placed at the centre of each time step and represent the mean of all pits in a time step rather than a rolling average.

Influence of stress on pit morphology

The experiment, as originally envisaged, consisted of samples undergoing both a stress and a corrosive loading cycle for the duration of the experiment. The aim of this was to as closely as possible match the conditions that rail axles experience during operation. Due to the circumstances around the experiment that have already been discussed, it was not possible to continue to provide the stress cycles. However, it was demonstrated by literature that the stress cycle would not have had a significant impact on the formation of corrosion pits before crack initiation.

It must be remembered that the point of the experiment was to investigate how the corrosion pits change over time, not the cracks that can initiate from them. The initiation and formation of the pit will be far more influenced by the electro-chemical environment than by the stress.

To investigate the potential impact of the stress cycles on the corrosion pit morphology, two approaches were taken. One was to consult the literature for any supporting evidence, this was performed in Chapter 5.

The other was to compare the results on the bright samples for the gateways where one had been undergoing stress loading, i.e. the 6.42 months gateway. By comparing the results between the areas that experienced the stress cycle and the areas that didn't, any variation should be identifiable. It should be remembered that the cyclic stress applied to this sample had an amplitude of 120MPa rather than the limit in the standard of 166MPa. However, the 120MPa value was representative of axle stresses while in standard operation.

Table 6.2: Comparison of the surface conditions of the 6.4 months of corrosion areas between the sample that underwent stress within the time period and the sample that did not

	Sample one (No stress)	**Sample two (Stressed)**	**Percentage difference**
Number of pits identified	22	24	9.1%
Mean pit depth (μm)	44.55	41.66	-6.4%
Mean $\sqrt{}$Area of pits (μm)	204.7	235.5	13.1%

These results can be seen in Table 6.2. As can be seen there did not appear to be a significant variation in the results, particularly considering the small number of pits identified in each area. The stressed sample exhibited slightly more pits, with a slightly higher average projected area. However, the unstressed sample had pits that were on average deeper.

Based on the relative lack of variation it was suggested that the stress cycle had had a very limited impact on the development of the corrosion pits.

Conclusion

There were several conclusions of the analysis of the bright samples. First the environment-material pairing was demonstrated to be representative of the environment that rail axles experience, based on the extrapolation of the experimental data. This suggested that the set-up of the experiment in terms of corrosive medium design, delivery system and experimental run time were broadly correct, with representative results being achieved. This increased confidence in the results and suggested that the analogy developed for the experimental series could be used in the future with minor corrections.

A second conclusion from the work was that the mechanical process for preventing corrosion was successful, as well as the data collection and processing techniques. This indicated that this procedure could be used in other scenarios looking to assess the development of corrosion pits in the absence of cyclic stresses. It also supports confidence in the outcomes of Chapter 3.

A separate conclusion that could be drawn was that there was no evidence of strong influence of stress on the development of corrosion pitting within the 6.42 month corrosion gateways. This increased confidence in the ability of the experiment to replicate realistic conditions despite missing the cyclic stress that axles would undergo in operation.

The final conclusion was that the pits in the bright samples appeared to be developing in the sample with a slight bias toward the direction that the corrosive medium would flow in. While it was not possible to link this directly to the shape bias detected in Chapter 4, it may suggest be an area of interest for future work. For example, if corrosion pits tended to develop with a bias radially around an axle, due to the natural flow of water off a rounded surface, then this could inform how corrosion damage was assessed and treated. This would be due to the implications on crack initiation of the largest projected area being perpendicular to the principle axis of loading.

6.4.3 Curved samples

Initial processing

The curved samples were processed differently to the bright samples, as the aim was to identify pits in the original casts and then match them with the same pits after the experiment had concluded. By comparing the conditions of these pits, conclusions could be reached about the changes that had occurred over the time frame. There were two samples in the experiment referred to as the ”broken” and ”whole” samples respectively, based on the crack that developed in the ”broken” sample.

Initial complications arose from ensuring that the same location could be identified on both the cast and the final sample, to allow comparison and draw conclusions around changes. During the experiment, this had been done by measuring to ensure that the scanning point was at the same location for both the cast and the final sample, however this was done using a ruler so has an tolerance of $\pm$0.5mm. Given the size of the scanned area this variation would have a minor effect, but did require correcting for.

Initially the correction of the positioning error was done with visual checking of the sample, to try and identify any clear visual locations that could be lined up with each other. An example can be seen in Figures 6.26a and Figure 6.26b (it should be noted that the two scans are mirror images of each other due to one scan being taken directly from the metal sample and converted to be in the same format as the results from the cast). In these figures matches can be made between different features to allow for comparisons to be made between the same pits over time. Some of these features have been highlighted by annotation.

Another outcome that could be identified from these Figures was that there was no significant variation between the two surfaces, which was encouraging as the surface should have undergone no corrosion.

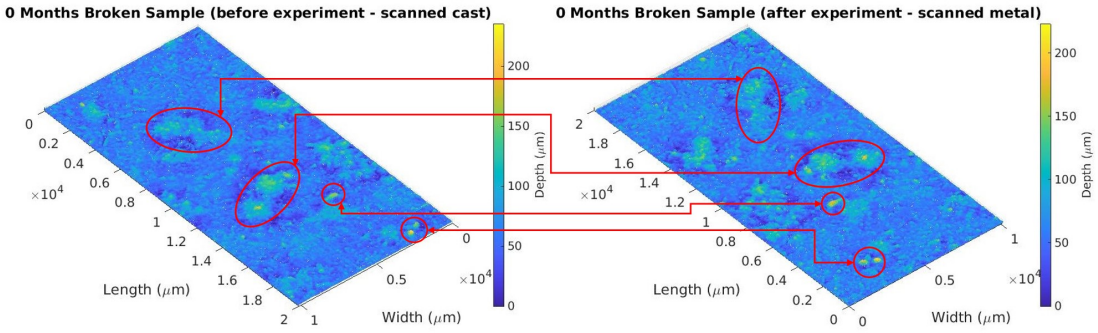

(a) Zero month corrosion areas - broken sample

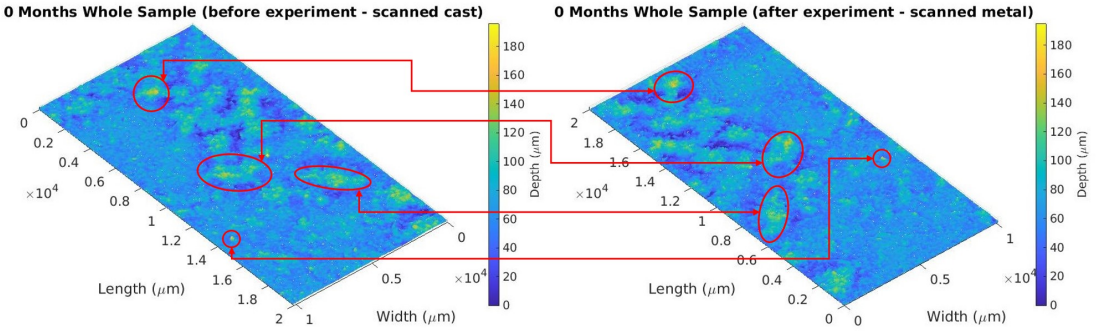

(b) Zero month corrosion areas - whole sample

Figure 6.26: Comparison of zero month corrosion areas on both the curved samples, between the cast of the surface before the experiment and the surface after the experiment. The same features on each scan are linked. Note that the before and after images are mirrored.

Table 6.3: Comparison of results between scans from casts and metal samples from 0 months corrosion areas

		Maximum Height (μm)	Average Height (μm)
Whole Sample	*Cast*	196.0	64.4
	Metal	195.0	62.3
Δ %		0.51	3.26
Broken Sample	*Cast*	222.8	58.6
	Metal	235.1	59.0
Δ %		5.52	0.68

The maximum and average heights of the zero months of corrosion areas for both samples were compared, with the results being presented in Table 6.3. These metrics were chosen as they would not be affected by the mirroring issue. With the variations being below 6% and the average of the data varying by less than 3.5%, confidence was high that the prevention of corrosion had been successful and that the data collection technique remained robust.

The lack of change in the scans in no corrosion areas could be contrasted with the changes for the areas that had undergone corrosion. As can be seen in Figure 6.27, with the 100µm limit applied, the difference between the scan that had undergone 12 months of corrosion and the scan of the cast of the surface before the experiment began were clear, with significantly more data points breaking through the limit floor, and a significantly higher maximum depth recorded. This suggested that corrosion had occurred that was sufficient to change the morphology of the surfaces.

The corrosion of the exposed areas was confirmed through initial analysis of the scans, comparing the number of pits detected using the 100µm limit, the maximum depth detected on each scan and the mean depth of each scan (this would be less affected by any single anomaly). The results can be seen in Table 6.4.

In the experiment, zero month corrosion areas reported results with negligible changes, contrasting the results of the areas exposed to corrosion where there was an increase in all the parameters. This suggested that the experiment, the data collection and the processing techniques were able to detect the expected changes to the condition of the surface, with increased numbers of pits, an increased maximum depth and an increased mean depth.

The first step to produce the final results from the dataset was to account for the misalignment of the samples. As mentioned previously, this was done visually by identifying key features and offsetting the images to ensure that these were located in the sample place on both images, once the mirroring had been corrected for.

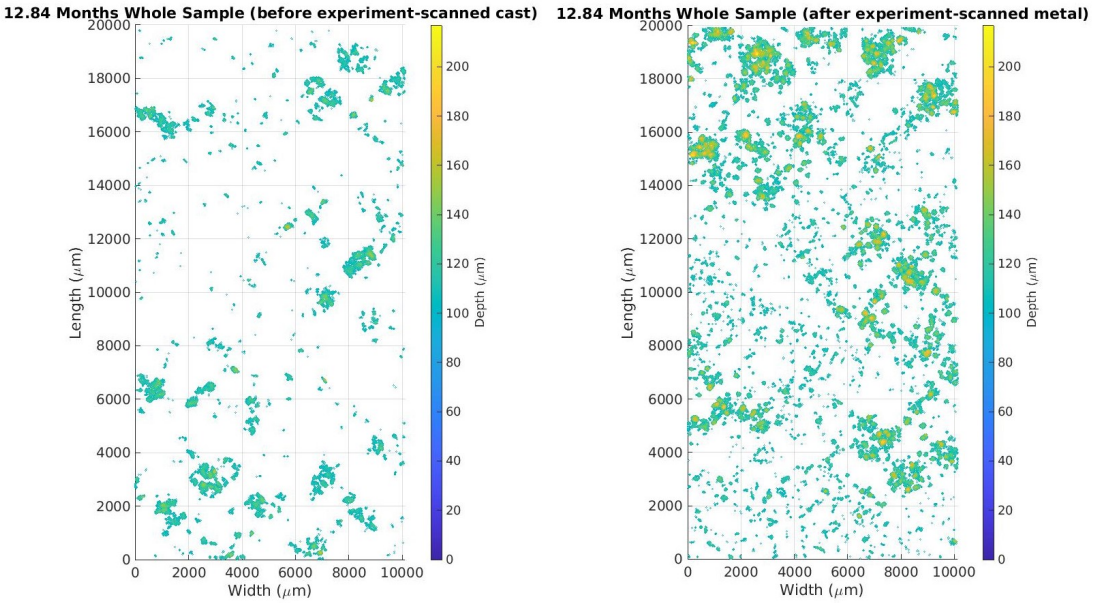

Figure 6.27: Comparison of the scan of 12 month corrosion area of sample 1 side 1 with a 100µm floor after the experiment and of the scan of the cast of the same area before the experiment

It was found that the angular alignment was near perfect for all the scans, however the lateral alignment needed correcting. The results of this can be seen Figure 6.28 and Figure 6.29 where key features can be identified, even after corrosion exposure, and can be seen to have been realigned to ensure spatial consistency.

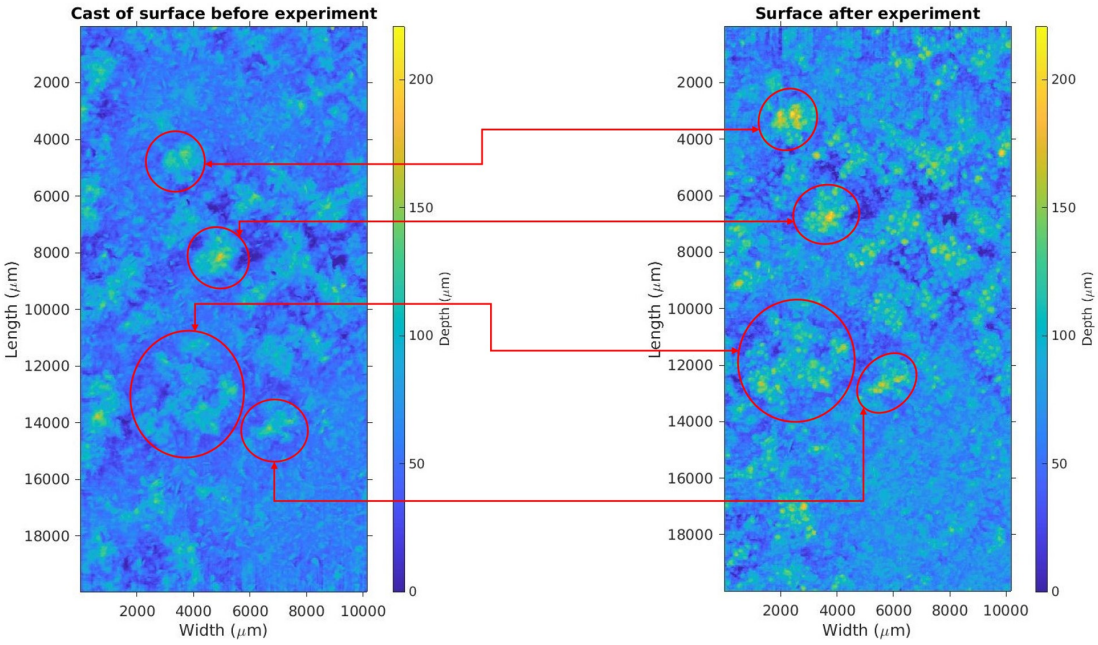

Figure 6.28: Images of Broken Sample 25.68 Months of corrosion before realignment

Table 6.4: Comparison of initial results for the curved samples

Whole Sample						
	Pits identified		**Max depth** μm		**Mean depth** μm	
	Cast	*Real*	*Cast*	*Real*	*Cast*	*Real*
0 Months	30	24	196.0	195.0	64.4	62.3
12.84 Months	21	49	167.1	217.0	58.8	70.9
25.68 Months (1)	2	17	157.1	187.8	43.0	54.5
25.68 Months (2)	32	67	190.3	221.0	61.5	72.7
Broken Sample						
	Pits identified		**Max depth** μm		**Mean depth** μm	
	Cast	*Real*	*Cast*	*Real*	*Cast*	*Real*
0 Months	22	23	222.8	235.1	58.6	59.0
12.84 Months	46	66	202.1	323.0	62.5	71.1
25.68 Months (1)	11	26	195.2	200.0	54.8	61.2
25.68 Months (2)	25	35	224.0	215.6	61.3	69.2

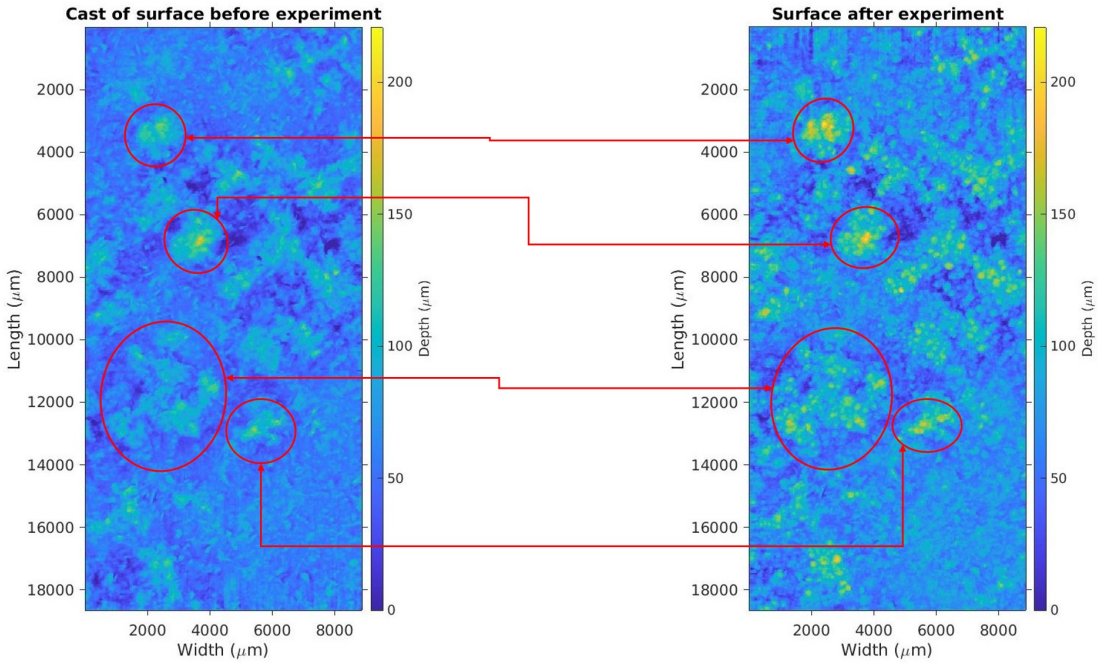

Figure 6.29: Images of Broken Sample 25.68 Months of corrosion after realignment (note the loss of width)

The downside of this alignment technique is demonstrated in Figure 6.30. For two scans of the same area, the measured misalignment in an axis results in twice that value lost in the final scan. This demonstrateed the importance of ensuring good alignment in the data collection phase.

Once all the scans had been corrected for misalignment, pits needed to be identified on the new, reduced, areas. This was done using the same pit identification software as had been used previously. The pits were again assigned numbers as unique identifiers to allow tracking during analysis.

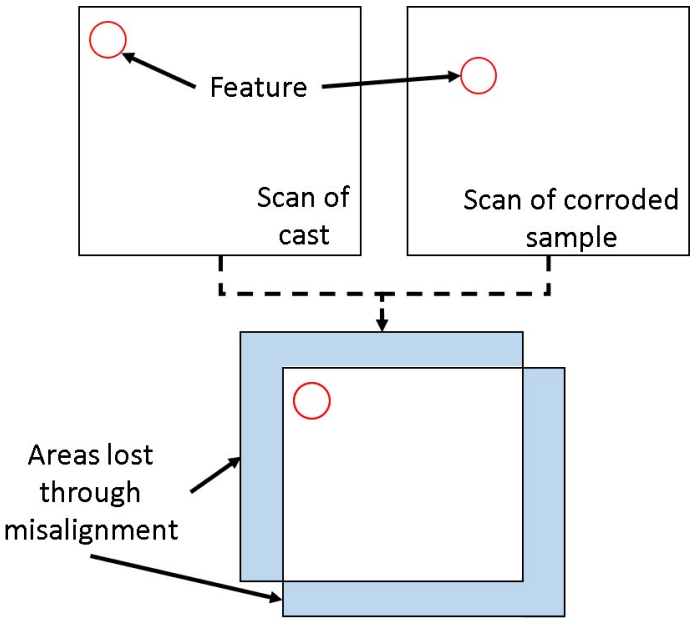

Figure 6.30: Demonstration of the loss of observed area through correction of alignment errors

In this instance the 100µm initial limit was used, as the sample had previously been shot blasted, meaning any corrosion damage below this level could not be separated from the shot blasting. All parameters were the same as those used on the samples collected from the depot.

The pits were identified on the more corroded samples and then the same areas were identified and separated on the casts, as demonstrated in Figure 6.31. These paired areas were analysed for the maximum depth recorded, the maximum depth diameters and the projected areas (convex hull) in both the X and Y planes. By comparing these results, it was possible to determine the changes over time, and to assess how the risk of crack initiation from the pits was changing.

The pits on the curved samples were identified, separated and paired up with the same locations taken from the scans of the casts of the surfaces before the experiment began. A pit identified on the scan taken after the experiment was paired with the same area on the scan of the cast of the surface taken before the experiment began, regardless whether or not a pit had been identified in that area on surface before the experiment began. The 100µm limit was then applied to both separated areas, hence the difference in shape and size in Figure 6.33, as any data points that dropped below the threshold were ignored. An example of this in practise can be seen in the following Figures.

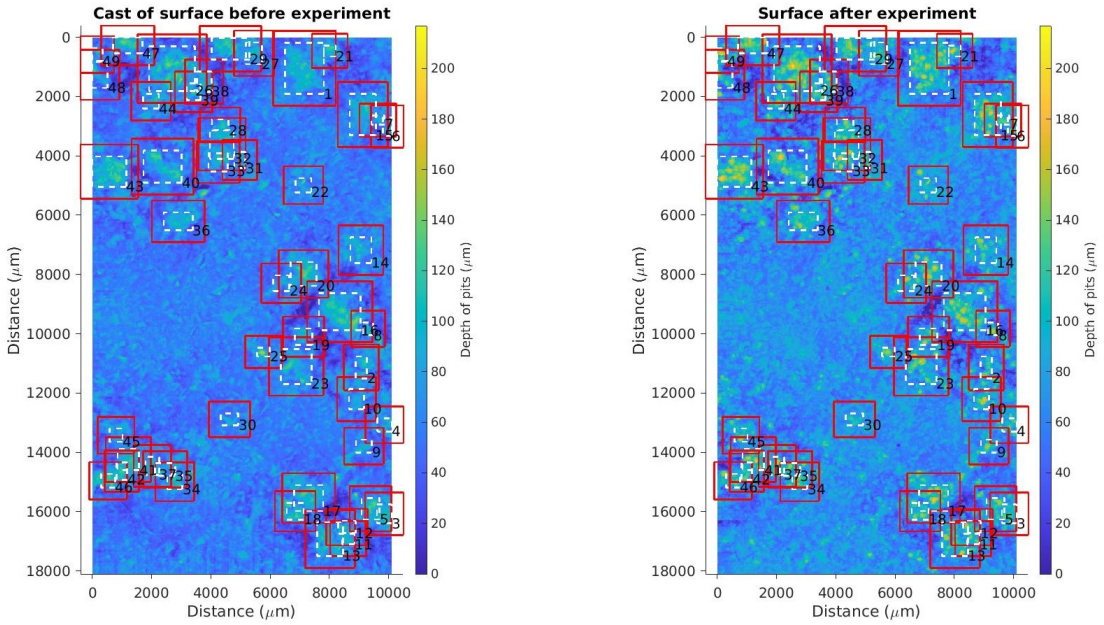

Figure 6.31: Comparison of pit identification between the cast and experimental area, with the areas of pits identified on the experimental sample also identified on the cast. Whole Sample, 12.84 months of corrosion.

In Figure 6.32 a pit had been identified on the sample after removal from the experimental rig. The same location had then been identified on the cast of the original surface (both have a margin included to provide context). As can be seen in Figure 6.32, while the features were identifiably the same, there had been a significant change in the morphology of the area. This included a noticeable increase in the maximum depth and increased isolated areas of attack.

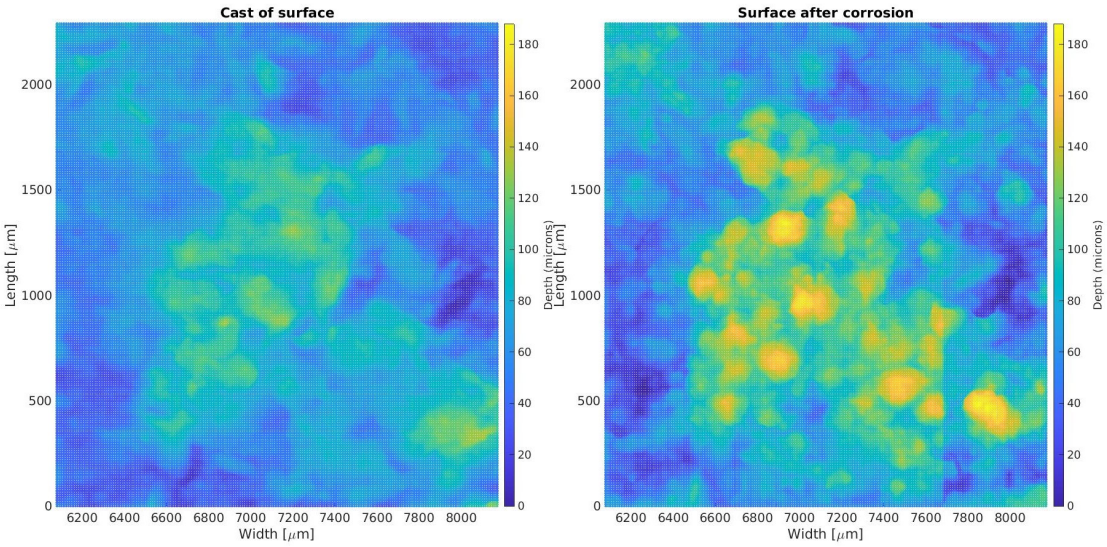

Figure 6.32: Comparison of an identified pit area between the cast of the surface before the experiment and after completion (Margin included). Whole Sample, 12.84 months of corrosion, pit 1.

The areas identified as making up part of the pit were then isolated in both the experimental sample and the cast. All of the areas from the experimental sample had a depth of greater than 100µm. Once the same threshold had been applied to the area observed before the experiment, the results can be seen in Figure 6.33. These results demonstrated the large change in the pit that had occurred during the corrosion process.

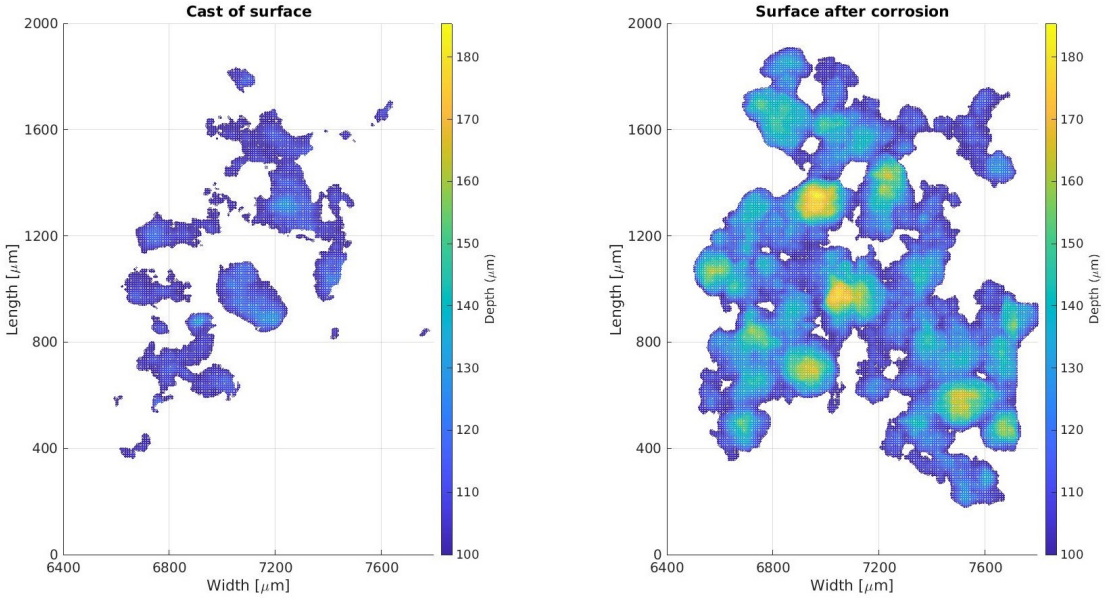

Figure 6.33: Comparison of an identified pit area between the cast of the surface before the experiment and after completion (Accepted area only, with 100µm limit applied). Whole Sample, 12.84 months of corrosion, pit 1.

The images seen in Figure 6.33 were then analysed. This allowed a direct comparison of the pits, with an easily defined edges. However, this approach did prevent the detection of any change in the surface below 100µm as this had been disregarded.

To correct for the issues that were caused by the crack in the 12.84 Month area of the broken sample, the pits that overlapped the crack were identified manually and excluded. This meant that the remaining pits identified in the scanned area could be used, despite the number of pits that had to be discounted due to the proximity of the crack.

Pit depth analysis

The depths of the pits analysed can be seen in Figure 6.34, for the whole sample, and Figure 6.35, for the broken sample. The maximum depths in each of the identified pits areas were recorded and compared to the maximum depth in the same area of the cast taken before the experiment began. Each of the sub-plots represents a different area that was exposed for a different amount of time. The blue squares represent the condition of the area before the experiment began. The red diamonds represent the condition of the area after the conclusion of the experiment. The green dots demonstrate the change in the surface over the experiment.

In the zero month areas of both the whole and broken samples, the difference in the depths was very small as expected. The mean of the difference was -0.03µm and 4.91µm for the whole and broken sample respectively. This result was reassuring as it demonstrated the level of experimental noise in the analysis of changes in pit depth, with an average variation of 2.44µm between the two samples. This produced a high level of confidence in the experimental results, as there should be no change in the condition of the surface.

It should be noted that there may be a source of possible error in the comparison of the samples. Due to the nature of the equipment used and the experimental process it was not possible to define a constant zero plane. The way this was dealt with was by using the highest point in the respective scans. It was hypothesised that this could not get higher, as material was not being added, and by using the highest point in each scan the movement should be minimised due to the cathodic protection offered by pitting corrosion. Due to this there may be minor movement in the definition of zero in the scans. This source of error would be very minor but it was not possible to quantify its effect.

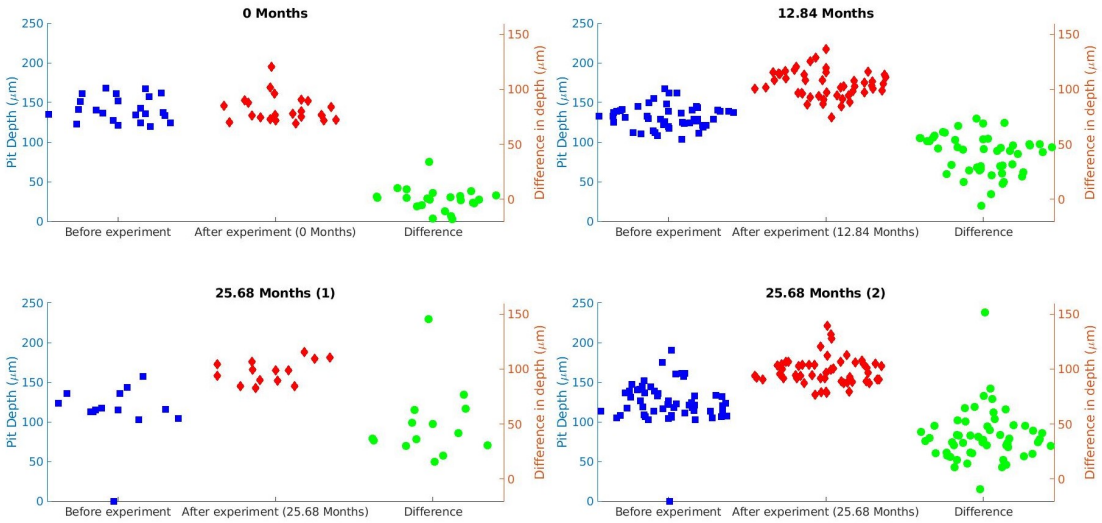

Figure 6.34: Depths of pits identified on the whole sample by time step, with the before, after and difference in depth calculated

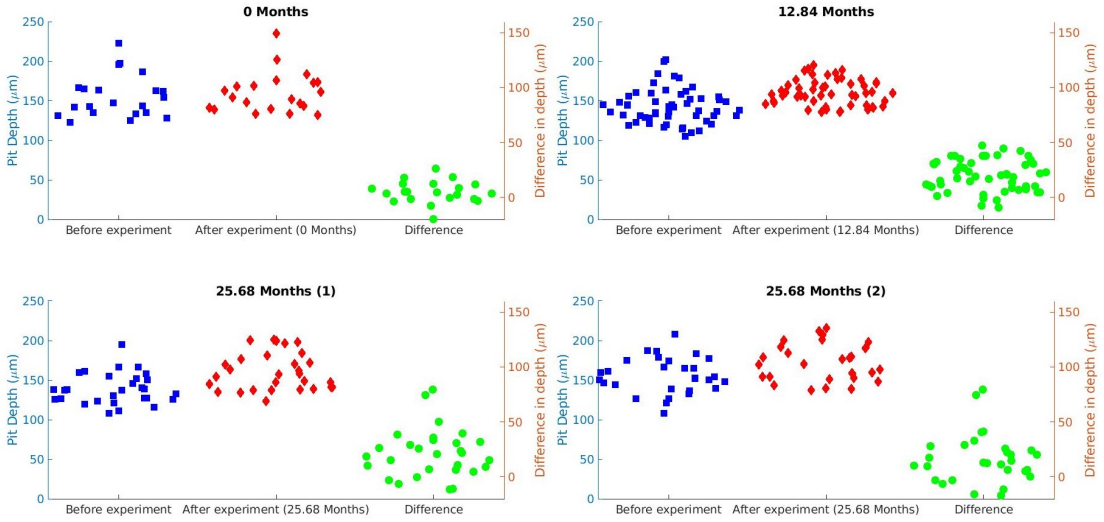

Figure 6.35: Depths of pits identified on the broken sample by time step, with the before, after and difference in depth calculated

In both of the samples, there was a noticeable increase in the difference in height between the cast and the corroded surface when corrosion occurred. This can be best seen in the mean of the variation between the time steps, shown in Table 6.5. As can be seen in the Table, after an initial significant change after 12.84 Months of corrosion, the rate of change dropped significantly.

After 12.84 months of corrosion the pits had gained a mean of 29µm of depth, with the maximum change being around 80µm. However, after 25.68 months, twice the time, the pits had only increased by 32µm on average, representing an increase in depth of 8.2% compared to 12.84 months. The maximums in this time, however were more pronounced, with two pits on the whole sample appearing to have not existed on the original cast and developing to depths of around 140-150µm over the course of the experiment. There were also more pits in the 80-90µm range for depth increase compared to 12.84 months areas, indicating corrosion was increasing generally but at a slow rate.

The two pits that appeared to exhibit very rapid growth were investigated. It was found that the two pits had only increased by 66µm and 72µm for the 25.68 months (1) and 25.68 months (2) areas respectively.

The much larger apparent increase was because when the locations of the pits identified on the surface after the experiment were separated on the cast of the surface before the experiment began, the cast area had no points that exceeded 100µm in depth. This meant that when the pits were compared to the surface before the experiment, no data points were detected, implying that the pit had developed entirely within the experimental time frame. This can be seen in the before experiment areas, where some pits were recorded with zero depth. When checked manually the increase was found to be more modest and within the range of the other experimental results.

Table 6.5: Mean differences in depth in each experimental area, with the average value by time step

	Mean difference in depth (µm)		
Corrosion Time	*Whole Sample*	*Broken Sample*	*Combined*
0 Months	-0.03	4.91	2.44
12.84 Months	40.94	17.44	29.19
25.68 Months	49.84	21.51	31.8
	39.03	16.81	

The hypothesis to explain this large variation in the mean depth gain between the single and double time step was to do with the condition of the surface. When the samples were placed into the experiment they had undergone the shot blasting that was part of the cleaning process. This left them with a surface that had lost the corrosion product that had made up its passivity layer, making them more vulnerable to corrosion until this could be recovered. A similar effect could be seen on the bright samples, where the average pit depth increased rapidly compared to the initial bright surface and then, as the passivity layer was built up, the rate of increase in pit depth dropped away. This also agrees with the power of a third law in Godards model.

This scenario would be similar to the protective paint layer of an axle being removed suddenly, such as with a ballast strike, exposing an area of bright, smooth metal. A large amount of corrosion damage would occur initially, until the passivity layer could be established. From this point on, the depth increase would be much lower, increasing steadily over time.

Pit width analysis

The widths of the pits were analysed to try and detect any changes. The pit width was analysed using the maximum depth plane approach, that was determined in Chapter 4 as being the most aggressive value for pit crack initiation risk. However, this technique does result in potentially high levels of variation in pits that only marginally break through the 100µm depth floor.

The changes in the pit widths in the X plane can be seen in Figure 6.36 for the whole sample, and Figure 6.37 for the broken sample. The widths in the X plane represent the dimension along the gauge length (perpendicular to the floor). In both these Figures it can be seen that there was a much higher level of change between the scans before and after the experiment in the samples that were exposed to corrosion compared to the zero month areas, suggesting that corrosion was taking place.

As with the depth data, there was minimal change between the pits after 12.84 months and 25.68 months, indicating that the rate of corrosion was significantly lower in the second time period. This was again assumed to be associated with the formation of a passivity layer.

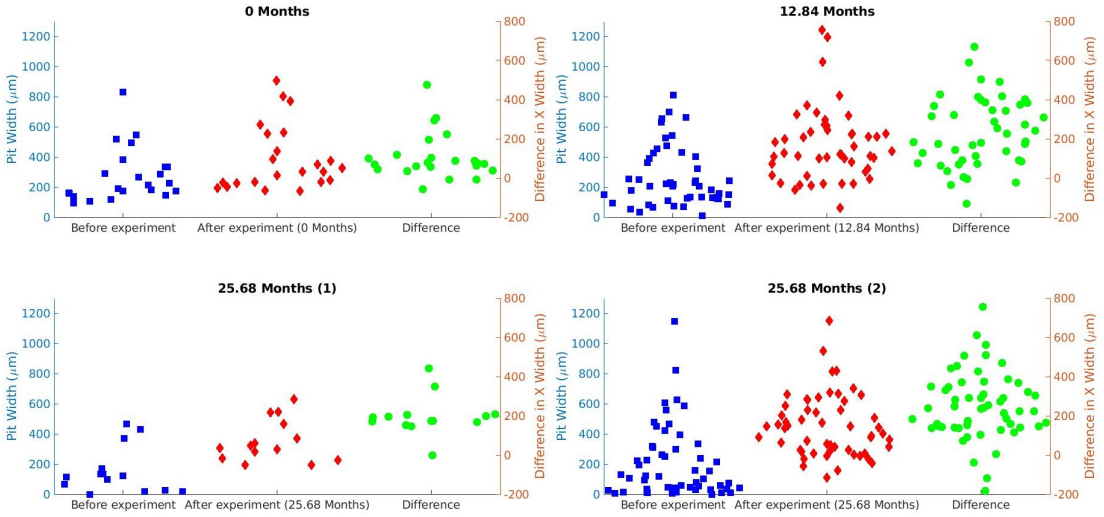

Figure 6.36: Widths in the X plane of pits identified on the whole sample by time step, with the before, after and difference in depth calculated

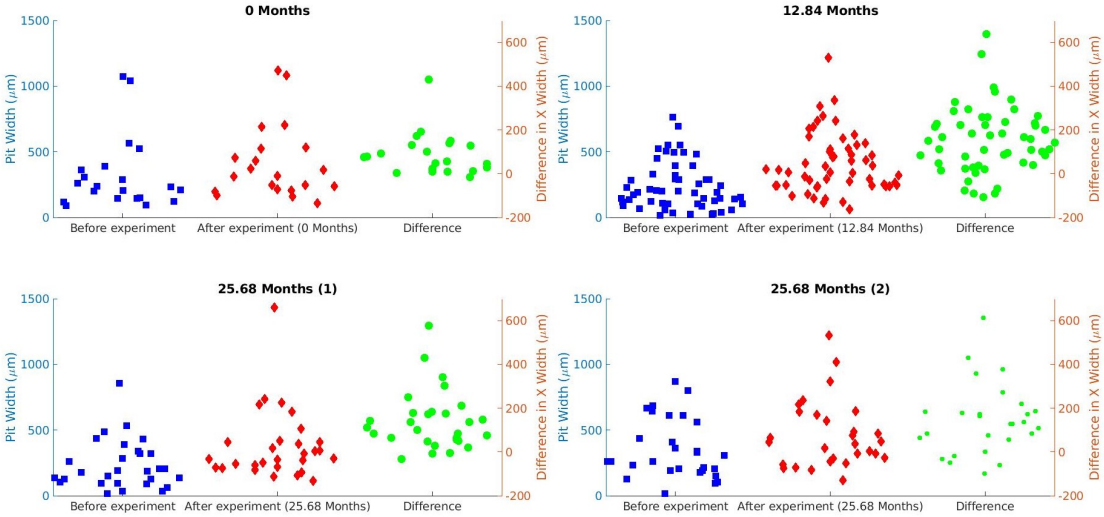

Figure 6.37: Widths in the X plane of pits identified on the broken sample by time step, with the before, after and difference in depth calculated

The Y axis widths for the whole and broken samples can be seen in Figure 6.38 and Figure 6.39 respectively. These values are the change in the width of pits across the sample gauge length (parallel to the floor). The rate of change in these values were more consistently increasing with time that the values for the X width, with a consistent, although dropping, increase in width after 25.68 months of corrosion compared to 12.84 months. This was an interesting result, as the increase is in the Y axis, rather than in the direction of the flow of the corrosive medium. This was a different result to that found on the bright samples, where there was a bias towards the X axis in pit development. Although it was not known precisely why this occurred, it was likely due to the variation in the starting geometry. This already corroded geometry was likely to result in more variation as to the flow of the corrosive medium.

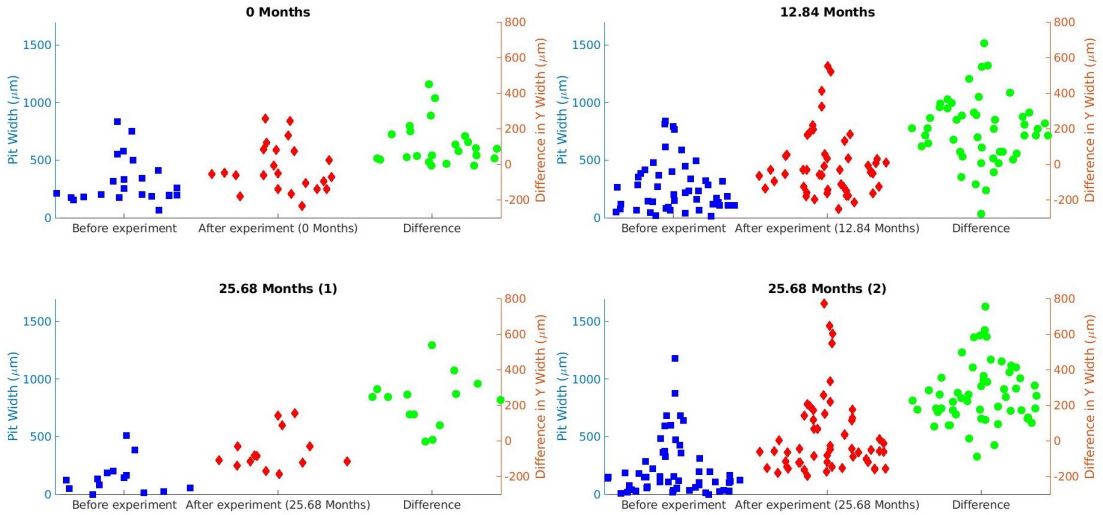

Figure 6.38: Widths in the Y plane of pits identified on the whole sample by time step, with the before, after and difference in depth calculated

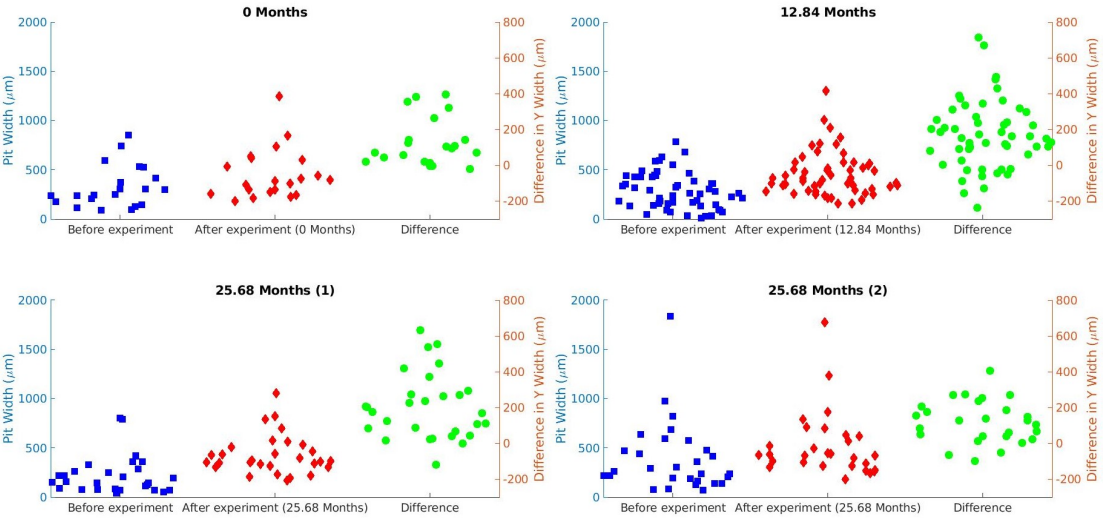

Figure 6.39: Widths in the Y plane of pits identified on the broken sample by time step, with the before, after and difference in depth calculated

Projected area analysis

The projected areas of the corrosion pits had been found to be a key parameter in determining the risk of corrosion pit crack initiation. These values were calculated using the convex hull approach detailed in Chapter 4, as this provided the most severe predictions. The advantage of this technique over the pit depth and width analysis was that it resulted in a more complete view of the changes, as it took account of both the depth and the widths and, to an extent, the geometry of the pits.

In the following Figures the square root of the projected area was used, as this was the direct value used in the key equation. However, this led to any pits, where the difference between the projected areas was negative, being plotted as zero due to the existence of an imaginary component. Manual checks on these values, however, found these negative values to be extremely small and most likely due to errors in the data collection and analysis process.

The values with a constant X plane can be seen in Figure 6.40 for the whole sample and Figure 6.41 for the broken sample. In these Figures there was a clear increase in the $\sqrt{Area}$ values between "before" and "after" corrosion conditions. This demonstrates that the increase in corrosion was increasing the risk of crack initiation, although it should be noted that all of these pits were well below the calculated threshold (approximately 4600µm). The same drop in the rate of corrosion increase can be seen in the second time period (12.84 to 25.68 months) as in the other results, supporting the view that the rate of corrosion lowered significantly as the passivity layer developed.

One result that could be seen in Figures 6.40 and Figure 6.41 was that within the area that underwent extended corrosion exposure there was an increase in the number of pits that underwent high levels of change. This was despite the mean value of increase between 12.84 and 25.68 months of corrosion being almost unchanged, at 123.47µm and 121.9µm respectively, after the initial corrosion damage. However, there were certain pits that experienced a higher rate of corrosion damage after longer exposure to a corrosive environment.

The increase in extreme pitting can be seen when considering the number of corrosion pits that have had an increase in $\sqrt{Area}$ values of over 200µm in the whole sample and over 150µm for the broken sample in Figures 6.40 and Figure 6.41. While not an absolute match it can be seen that there tended to be an increase in the number of pits that experienced higher increases in corrosion damage. What this suggested was a possibility that while on average the increase in damage after the initial exposure to the corrosive environment was minimal, there were certain pits that tended to experience a larger degree of damage.

As the catastrophic failure of an axle due to a corrosion pit initiated crack would most likely be due to an exceptional pit, the increased exposure to a corrosive environment was more likely to produce one of these pits.

It was not known from this experiment what might cause a particular pit to develop more quickly than another. This could be due to changes in geometry that might cause corrosive medium to become trapped against a surface encouraging more severe local corrosive conditions. Other explanations may be the attraction of aggressive ions or non-homogeneous aspects in the metallic structure that would encourage corrosive attacks or due to variations in anodic and cathodic conditions.

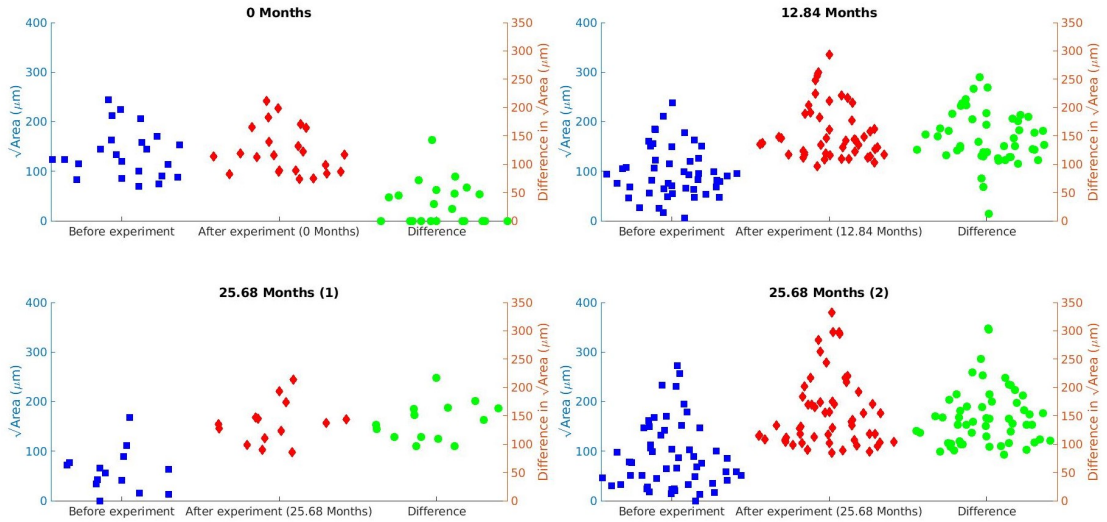

Figure 6.40: $\sqrt{Area}$ in the X plane of pits identified on the whole sample by time step, with the before, after and difference in depth calculated

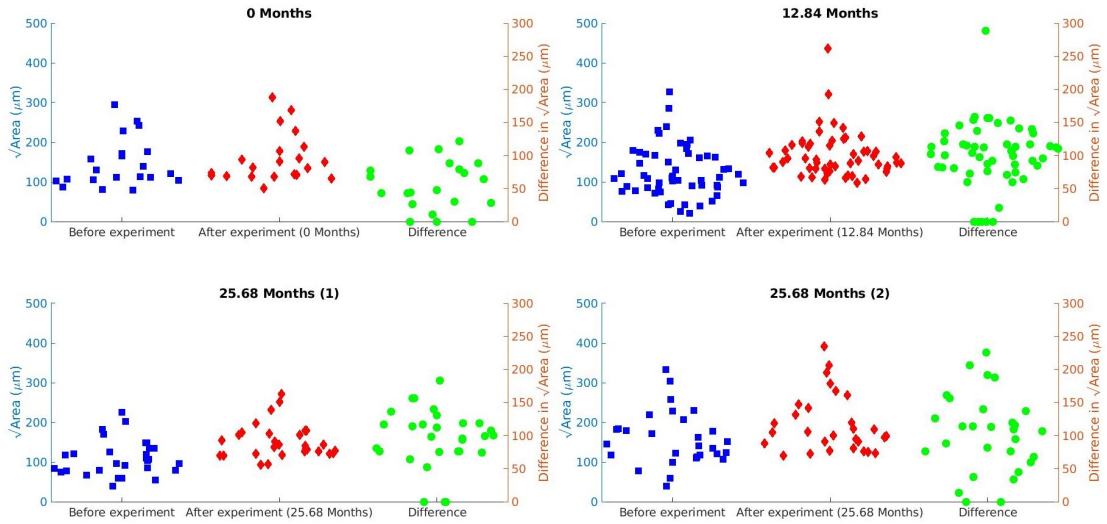

Figure 6.41: $\sqrt{Area}$ in the X plane of pits identified on the broken sample by time step, with the before, after and difference in depth calculated

The same approach was performed for the Y plane (Constant Y value) and can be seen in Figure 6.42 and Figure 6.43. The Y plane values would be the more relevant given the axis of loading in the original experimental plan. The results in this plane are nearly identical to those in the X plane.

The similarities can be most particularly seen when comparing the values between those of the same sample, i.e. whole sample in the X plane and whole sample in the Y plane. The values in all cases are very similar, with minimal variation between the two. This suggested that the increase in crack initiation risk was equal in both planes, despite indications from the bright samples that a bias was developing in the X axis.

In the values in the Y plane, there appeared to be less of an increase in exceptional pits that was seen in the X plane, with the 12.84 month corrosion periods appearing to have very similar results to the 25.68 months scan areas.

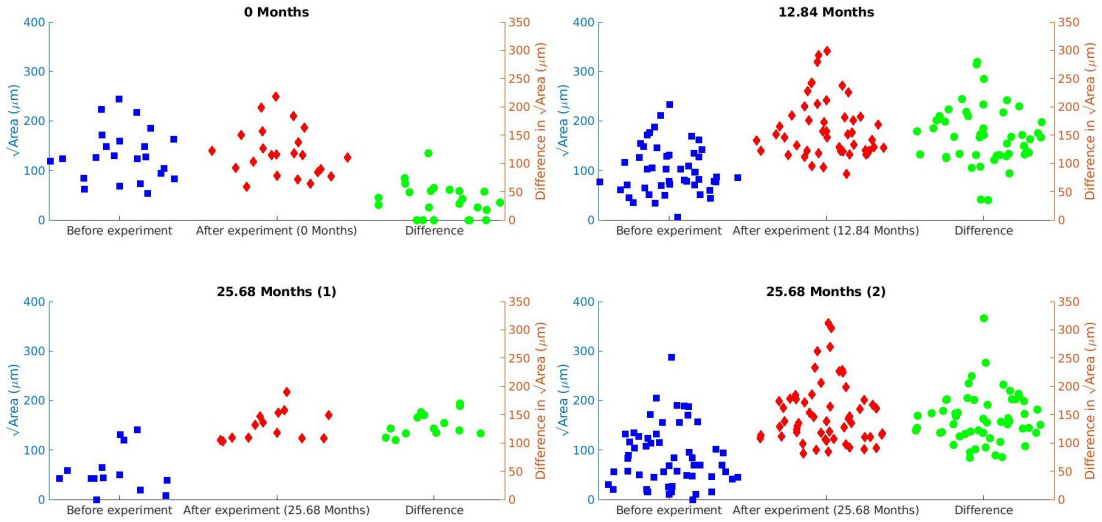

Figure 6.42: $\sqrt{Area}$ in the Y plane of pits identified on the whole sample by time step, with the before, after and difference in depth calculated

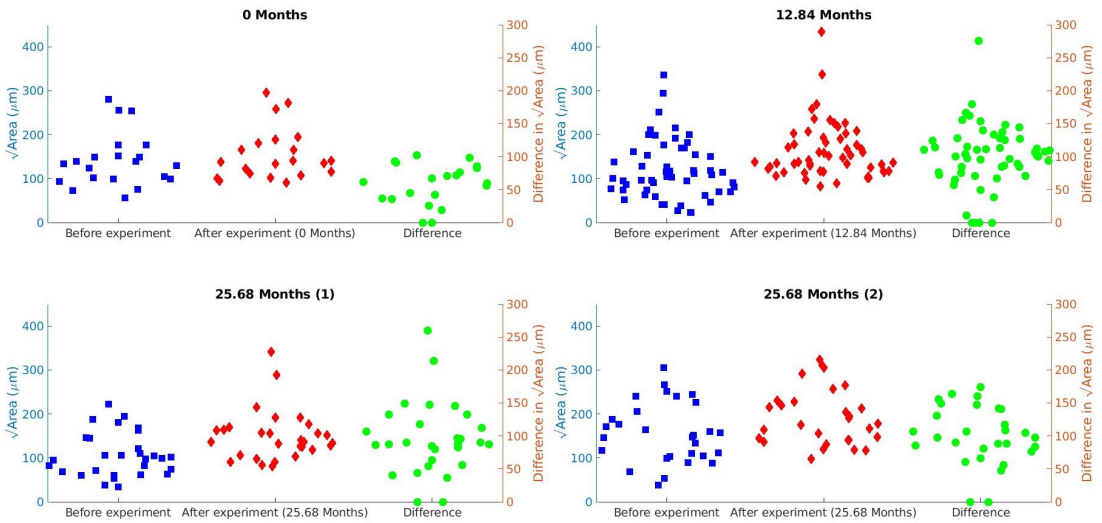

Figure 6.43: $\sqrt{Area}$ in the Y plane of pits identified on the broken sample by time step, with the before, after and difference in depth calculated

The values for $\sqrt{Area}$ in both planes experienced a large percentage change in the values after corrosion. Some pits experienced differences in projected $\sqrt{Area}$ of over 100% or even 150%. This suggested that the pits were made significantly more risky by the exposure to corrosion, doubling their risk or more in some cases. However, they remained significantly below the threshold values.

The generalised extreme value distributions of the projected $\sqrt{Area}$ changes can be seen in Figure 6.44 and Figure 6.45 for the X and Y planes respectively. As can be seen in the Figures, there was a significant variation in both planes after some corrosion compared to the zero corrosion condition. This can also be seen in the location parameter in Table 6.6 and Table 6.7. However, the variation was far more limited between the 12.84 and 25.68 month time steps.

Table 6.6: Generalised extreme value parameters for the gain in $\sqrt{Area}$ at each time step in the X plane

	Distribution parameters		
Corrosion time	**Shape**	**Scale**	**Location**
0 month	-0.38	60.41	7.08
12.84 month	-0.35	71.14	97.37
25.68 month	-0.14	48.11	104.92

Table 6.7: Generalised extreme value parameters for the gain in $\sqrt{Area}$ at each time step in the Y plane

	Distribution parameters		
Corrosion time	**Shape**	**Scale**	**Location**
0 month	-0.56	54.10	24.80
12.84 month	-0.34	69.87	99.23
25.68 month	-0.08	40.25	103.81

In both cases the location parameter had slightly increased between these time steps, however, the shape and scale parameters had reduced significantly. This resulted in a tighter distribution of projected area gains.

The overall outcome of these figures was that initially there is a significant increase in the gain of corrosion damage within the first 12.84 months of corrosion. After this the increase reduced significantly between 12.84 and 25.68 months, with only marginal gains, as the very small increase in the location factor suggested.

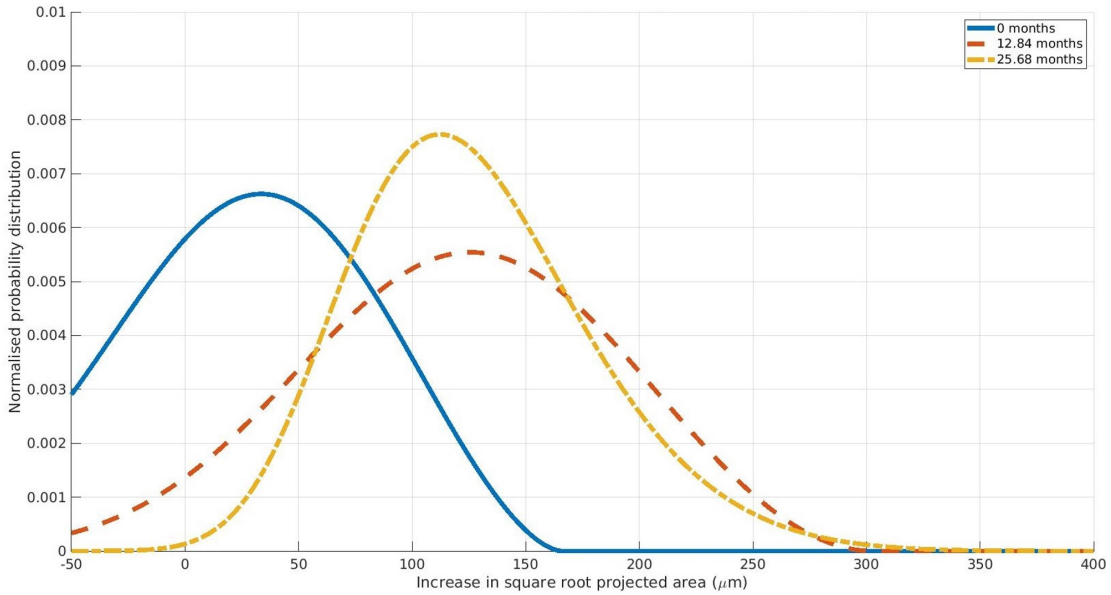

Figure 6.44: Generalised extreme value distributions for the gain in $\sqrt{Area}$ at each time step in the X plane

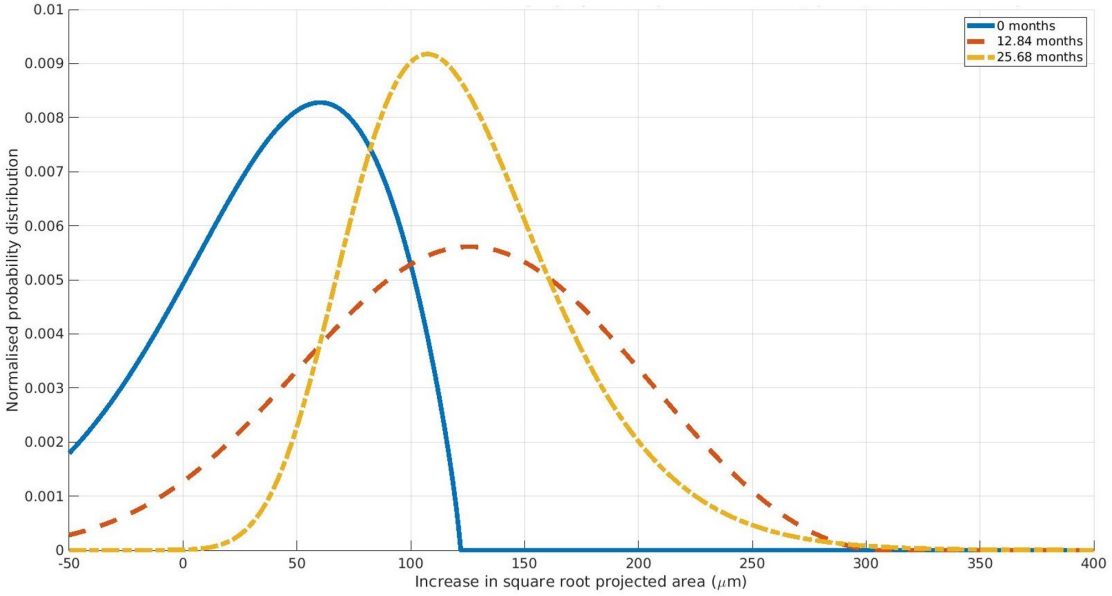

Figure 6.45: Generalised extreme value distributions for the gain in $\sqrt{Area}$ at each time step in the Y plane

The figures may appear misleading, with the 25.68 month distributions having tightened compared to the 12.84 month one. However, this was most likely due to the increased sample size resulting in a clustering around the true mean. This can be most easily demonstrated by the concept of standard error, with the equation given in Equation 6.2. This measures the discrepancy between the sample mean and the population mean, based on the standard deviation of the sample, σ and the number of samples, n.

Given that the populations for each time step increase, from 44 to 102 to 127, the standard error in X for each time step was 8.86, 6.38 and 4.66 and in Y 7.64, 6.38 and 4.13. This explained the tightening of the 25.68 month distribution rather than a significant change in the underlying data.

$$SE = \frac{\sigma}{\sqrt{n}} \tag{6.2}$$

Conclusion

The outcomes of the work on the curved samples proved useful in defining the importance of the passivity layer. The general evidence seen across all samples was that the majority of the damage occurred within the first period that the axle was exposed to the corrosive medium. This was seen by large increases in all of the investigated parameters during the first 12.84 months of corrosion, but very similar results were reported after 25.68 months. This suggested that once the passivity layer had formed the rate of increase dropped significantly.

All of the pits observed were well within the threshold values, even after being exposed to corrosive attack. However, the increases in parameters in particular cases could be significant. The $\sqrt{Area}$ values increased by even more significant amounts, with some increasing by over 100% in both planes. This demonstrated that the risk of crack initiation could be significantly raised through unprotected corrosive exposure.

The experimental process and analysis technique was quantified and validated by the lack of variation within the zero month corrosion sections, with small changes being observed and being well below those of the areas that underwent corrosion. This suggested that the results were robust and recorded the corrosive damage that was the target of the work.

6.5 Implications for pit form changes over time

The results of this experimental work provided a good basis to analyse the potential development of corrosion damage on rail axles and implications on how such damage could be dealt with in industry.

The main outcome of this work was that the loss of the protection of the axle surface, allowed rapid and destructive corrosion to occur. This corrosion could double, or more, the $\sqrt{Area}$ parameter that has been used in this project to assess the risk of corrosion crack initiation within 12 months. However, once a passivity layer had formed the rate of increase dropped very significantly. This could also be seen in the bright sample results, with initial corrosion making up the vast majority of the total damage. The rate of corrosion damage increase after this point was difficult to quantify, due to a lack of data points once the passivity layer had developed on the curved samples.

The average $\sqrt{Area}$ values appeared to be approximately consistent across the axle survey, curved and bright samples, once the initial corrosion had taken place. However, with increased corrosion exposure the number of exceptional pits that had a significantly higher risk of crack initiation increased. This may be due to issues with the measurement of the pits, using a variable zero plane, that was made necessary due to experimental limitations. However, it was more likely that this was due to the passivity layer, once formed, providing an effective barrier to further corrosion. In some cases this may have been broken or penetrated and certain pits developed significantly more aggressively. These pits were the only ones that represent any significant risk to the integrity of the component.

When considering the implications for rail axles, it was necessary to consider the conditions of the axles at each point in their journey, in terms of corrosion damage. Before the axle is taken into the depot it has an opening in the protective paint layer that allows corrosion access to the metal surface. However, assuming this has been present for a significant period of time, a passivity layer has developed. This passivity layer, based on this research, has effectively slowed the rate of corrosion and a significant amount of the corrosion damage present formed early in the process. If left without intervention, the corrosion would progress at a low rate, and likely remain within the calculated threshold.

Currently the axle would be taken into the depot at the appropriate time interval and inspected. If the initial inspection were passed, and the axle judged recoverable by the depot operator, it would be shot blasted in preparation for the second inspection. In this condition the protective paint layer and passivity layer have been removed, exposing the bare metal. This was the condition that the curved samples were in before being exposed to the experiment. If these axles were to be returned to service without any further work, then the results of this project would suggest that the pits might experience an increase in the $\sqrt{Area}$ value, and so the risk of crack initiation, of up to 150%. This could also happen in the scenario where no turning to remove material to correct the axle damage occurred and a new paint layer was applied, over the existing corrosion, that was then removed in later service, possibly through a ballast strike or some other event.

The outcome of this thought process was that once the passivity layer was removed from the axle, there was a significantly increased risk of corrosion damage, regardless of the initial surface geometry. However, if the passivity layer could remain undamaged then the damage would progress far more slowly and not necessarily require correction. In this case the process of inspecting the corrosion pitting was what made the damage require correction.

Based on this result it would suggest that axles could be left for longer without inspection or correction, due to corrosion, and remain safe. However, if they underwent inspection that removed this passivity layer they may require the correction that is currently being provided, as they would be at increased risk of corrosive attack. It should be noted however, that none of the pits in the experiment were ever close to reaching the calculated threshold and would have to become 1000% more severe to risk initiation. The other option would be to develop a process of inspecting the axles that did not require disruption to the passivity or paint layers. This could include drying out and painting over already corroded areas as a form of correction, as long as the paint layer would remain attached however, this would require further research.

6.6 Conclusion

This section detailed the analysis process and results of the experiment carried out as part of this project. This has been broadly separated into the ”bright samples”, where machined samples were used, and the ”curved samples” where the surface being inspected had been the external surface of an in service axle.

Both sets of results demonstrated the validity of the experimental and data collection technique, with corrosion being effectively prevented when desired. The analysis of the results fitted to existing theory, in particular the Godard model of corrosion.

Corrosion is a result of the system which it occurs in, rather than being a material property. The material in this case was defined, so the difficulty was in choosing and implementing environmental conditions that resulted in a system that produced similar results to that observed in industry, within an accelerated testing time frame. The results from the bright samples suggested that this had been achieved in this case, with extrapolated models resulting in outcomes similar to those observed in the axle survey. The results were slightly lower than desired, however similar enough to suggest that approach was successful and with further refinement could be made more aggressive to closer replicated conditions on in service axles.

The results from the bright sample also suggested a tendency for pits to develop in the same direction as the flow of the corrosive medium, however this was not obvious in the curved samples. This was an advantage of using samples that had already been corroded, as the simulation of the initiation phase in pit development is highly complex and subject to may factors.

The possibly controversial outcomes of this work were that it appeared that the act of inspecting the axles, removing the protective paint and passivity layers, potentially necessitated the correction of the corrosion damage. It could be suggested that axles could be left in service longer before inspection, as no pits identified at any stage of the project would have a significant risk of crack initiation. However, the risk of pit progression in metal that does not possess any protective layer, either natural or artificial, would mean that pits that had developed and then lost their protective layer might start to near the threshold through compounding corrosion damage. However, if these same pits were left without intervention, they would likely not become a risk for a significant period.

6.7 Novelty

6.7.1 Scientific

In this Chapter the conditions used in the experimental set-up have been validated and demonstrated to be representative. This included the corrosive environment and delivery mechanism as well as the run time of the experiment using a new analogy. This could provide a starting point for future experiments seeking to replicate the rail axle environment. The same can be said of the data collection and processing techniques that have produced representative results across all three experiments.

The work produced results for the development of corrosion pits in rail axles over time, adding to the understanding of the field and informing future decisions surrounding the treatment of corrosion in axle steels.

6.7.2 Industrial

Results from this Chapter suggested that the risk of crack initiation from corrosion pitting was very small and that the majority of the damage occurred within a short period of time before the passivity layer formed. The formation of a passivity layer has been demonstrated to be an effective way to slow the development of corrosion pits on rail axles.

The inspection of rail axles has also been challenged. The inspection of rail axles produces an environment where pitting could develop much more rapidly than if it had been left in its previous, corroded, state. The inspection of the axles makes the correction of the damage a necessity. This suggested that the inspection interval of rail axles could be increased, then the number of axles scrapped could be reduced without a significant increase in the risk of crack initiation.

Chapter 7

Prediction of Axle Failure After Corrosion Detection

7.1 Introduction

The work that has been carried out in this project has been part of two separate work streams. This is illustrated in Figure 7.1. This section aims to combine the two work streams and link the outcomes to produce a rounded assessment of current corrosion damage being observed in industry maintenance facilities, and the potential impacts of different strategies in addressing it.

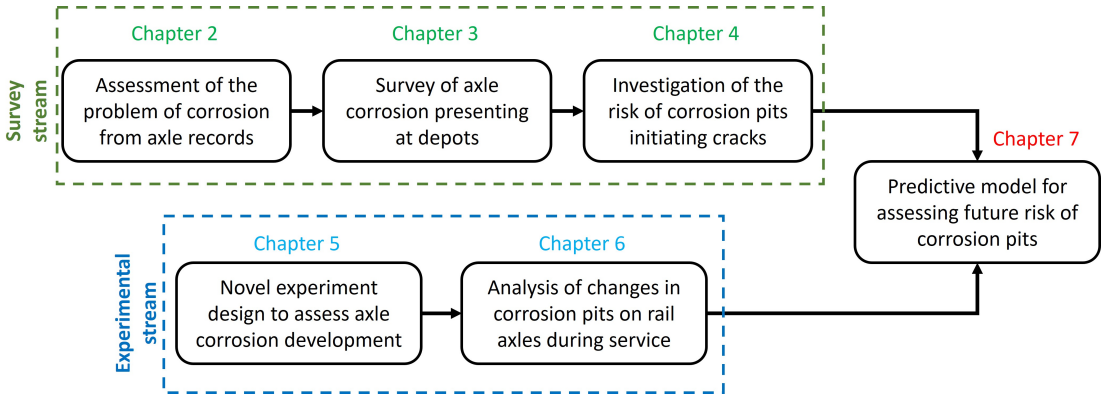

Figure 7.1: Work flow of the project

In this project several steps were undertaken to address the problem of corrosion on rail freight axles:

1. **Confirm that corrosion of rail axles was a problem that would benefit from addressing.**
2. **Identify pits on operational axles during an axle survey.**
3. **Estimate the risk of crack initiation from identified pits.**

4. **Replicate the conditions of operational axles in a laboratory setting and corrode samples in an accelerated time frame.**
5. **Study how the morphology of pits changed over different time steps.**

The results of the work done in the thesis so far will be used to estimate how long rail axle corrosion pits, and by extension the axles they occur on, could be left in service before a crack would initiate and propagate. This will be done in this Chapter with two final steps.

6. **Apply estimated changes in corrosion pitting damage over time to pits on operational axles.**
7. **Estimate the risk of crack initiation from pits if left in service under different treatment regimes.**

The completion of these steps, allowing recommendations to industry to be made regarding the approach to rail axle corrosion damage, represents the end of this thesis. Areas of further work to take forward and enhance the knowledge in the field are identified to assist future researchers in maximising potential value to industry.

7.2 Recap of previous results

The result of the work in Chapter 3, analysing the pits identified in an axle survey, concluded that no pits, identified as part of the survey, were close to approaching the limit set by the standard. The maximum depth recorded was 342.6µm, compared to the allowable limit of 1000µm, and a mean value of 184.7µm. This was supported by other literature in the field that reported similar depths.

Work in Chapter 4 then analysed the risk of a crack initiating from the pits identified. This was done by using both the projected area of the pits to calculate the range of stress intensity in fatigue, and by using a crack approximation to identify the location of the maximum stress intensity factor. The results of this analysis concluded that none of the pits breached the threshold for crack initiation, despite the conservative assumptions used throughout, and that the location of the highest stress intensity factors was at the bottom of the pits rather than the shoulders. It was also demonstrated that, based on assumptions around aspect ratios and shape, if a pit was produced that met the limits it would not be able to initiate a crack, with an approximate factor of safety of 1.5.

The results of Chapter 3 and Chapter 4 suggested that the current standard is unsuitable as no pits are approaching the permissible depth limit, with the maximum values recorded being around a third of allowable. This, added to the in built safety factor of the standard, suggested that axles were being scrapped with minimal risk of crack initiation. If the standard were written with limits that were quantifiable and verifiable in a depot setting, as depots currently cannot measure pit depth, then the rate of scrapping could be significantly lowered.

One conclusion of the pits being both less deep than the limit set by the standard, and shown to be safe as part of this project, was that the axles could be left in service longer before inspection and remain safe from crack initiation from corrosion pits. This has the potential to lower the costs and impact of maintaining axles as discussed in Chapter 2.

To investigate how the risk of crack initiation pits developed with time a second work stream was undertaken. This work stream consisted of the proposal of a novel experimental concept, described in Chapter 5, to simulate the progression of corrosion pits on rail axles over time. After addressing changes due to experimental difficulties surrounding Covid-19 and equipment availability, the results were analysed in Chapter 6. It was concluded that the accelerated testing procedure produced an accurate representation of the conditions of in service axles.

The outcome of the experimental data analysis was that the vast majority of damage occurred when bare metal was exposed, before the build up of the passivity layer. Based on the results of the curved samples, looking at the development of corrosion pits on pre-corroded axle surface, the mean increase in pit depth without the passivity layer was 29.19µm after 12.84 months. However, once this stage had passed, the rate of corrosion was significantly lower, with the difference in the mean depth value after 12.84 months compared to 25.68 months being only 2.61µm. This suggests that the rate of increase in pit depth after the passivity layer was formed was approximately a tenth of the value without it.

These results can be used to inform potential changes to the way that corrosion is dealt with by the industry. Such changes may lead to a decrease in the number of axles scrapped per year without a decrease in safety outside of published limits. This would result in lower cost to the industry in terms of financial, logistical and environmental impact.

7.3 Predicting corrosion risks of different axle treatment approaches

The results of the work previously carried out in this thesis led to a thought process that suggested several outcomes:

1. **No pits have been reported that approach the limit currently defined in the standard.**
2. **The pits identified on axles do not represent a crack initiation risk.**
3. **If the passivity layer remained in place, corrosion would develop slowly.**
4. **The inspection of the axles that remove the passivity layer exposes the axles to significant amount of corrosion damage, above what would have been experienced had the layer been left in place.**
5. **Based on the above, the inspection of the axles, in such a way that removes the passivity layer, means that the corrosion damage requires correction to prevent reaching the crack initiation threshold (if the axles were not repainted immediately).**
6. **Summarising the above: if the inspections did not take place, the axles could have safely remained in service for longer.**

This led to the conclusion that the best way to lower the rate of scrapping of UK freight axles, would be to extend the inspection intervals. Based on current results this would not run a significant risk of corrosion pitting that would break the limits in the standard and pose a crack initiation risk.

The issue with current inspection processes used is that it appeared that the act of carrying them out meant that the corrosion needed correcting. This limited the application of the original concept of the project, to allow the assessment of an area of pits and judge the correct next steps, as the act of investigating the pits causes increased risk of damage. However, this approach could still be taken based on the level of confidence in the paint system. The issue being that leaving corrosion damage in an area that then loses its paint layer would result in the corrosion starting from the more advanced stage than if the surface had been smooth. In this case the passivity layer was able to replace much of the role of the paint layer, albeit less effectively, in slowing the progressing of corrosion damage. This raised the question of designing axles with the formation of passivity layers as a key approach to mitigating corrosion damage.

The following sections will look at the results taken from the axle survey, of pits that have been found on rail axles, and predict the range of risk that these pits might represent after increased time in service. This will include two cases, where the pits were returned to service after shot blasting or if they had been left in service without intervention. It will be assumed that these pits had not undergone any turning or similar correction and that no protective paint layer had been applied or it had been damaged and removed immediately after entering service.

7.3.1 Technique for pit development prediction

The results of the increase in the projected $\sqrt{Area}$ in the X and Y planes were used to assess the increase in the risk of crack initiation from a pit after exposure to a corrosive environment. These can be seen in Chapter 6, but are presented again in Figure 7.2 and Figure 7.3. These Figures represent the extreme value distributions of the increase in the $\sqrt{Area}$ over different corrosion time steps.

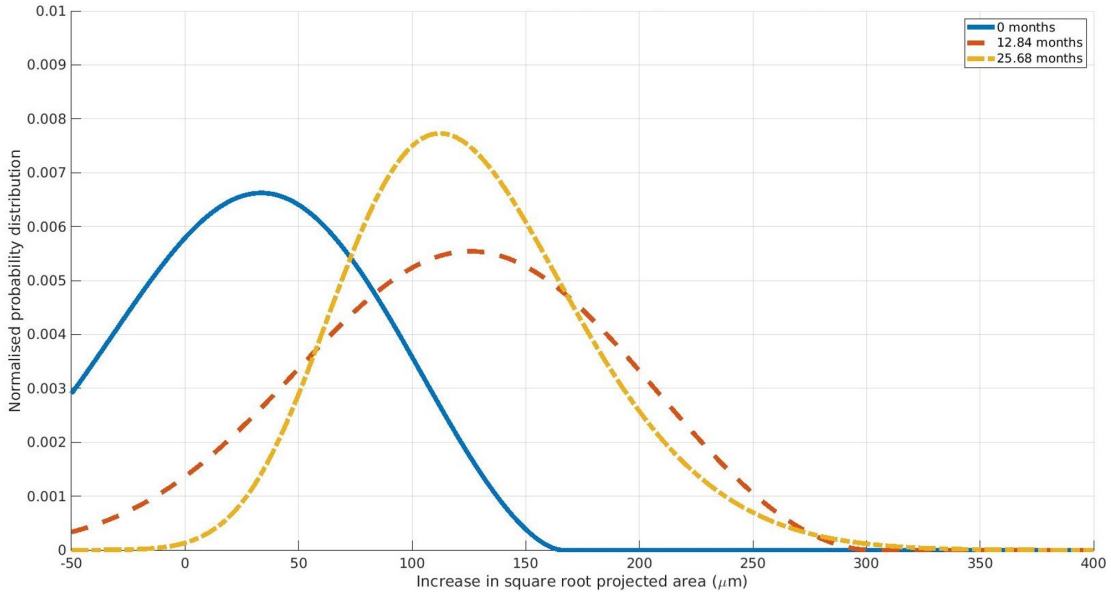

Figure 7.2: Generalised extreme value distributions for the gain in $\sqrt{Area}$ at each time step in the X plane

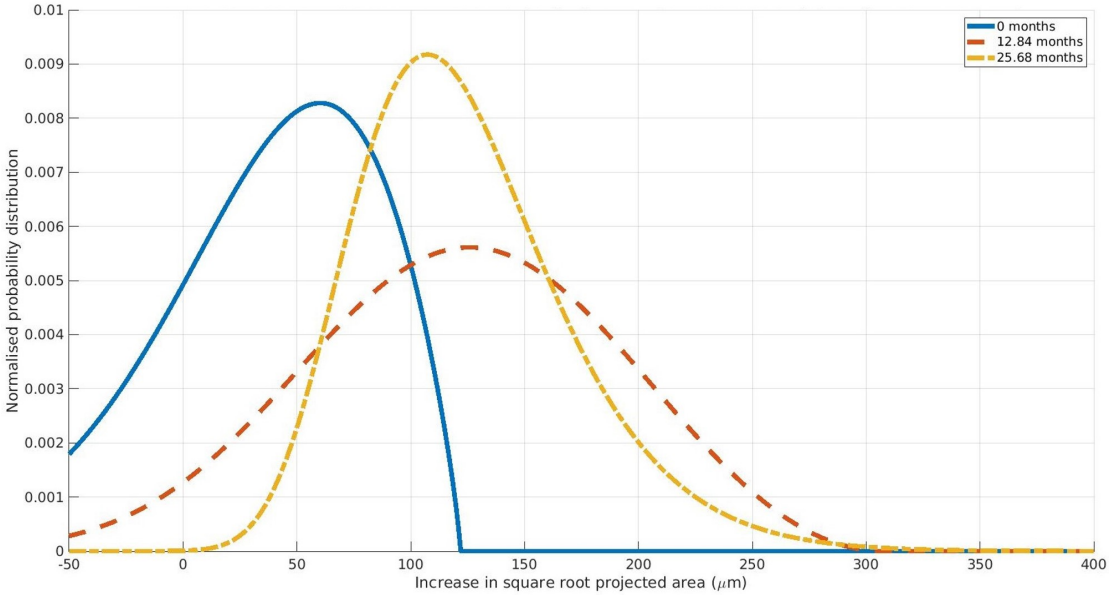

Figure 7.3: Generalised extreme value distributions for the gain in $\sqrt{Area}$ at each time step in the Y plane

As discussed in Chapter 6 the distributions generally state that there was a significant amount of corrosion damage within the 12.84 month time step compared to the un-corroded areas. However, the differences in the results between 12.84 months of corrosion and 25.68 months of corrosion were minimal, with an increase in the location factor of the distribution of only 7.55µm in X and 4.58µm in Y. This can be compared to the difference after 12.84 months of 90.00µm in X and 74.43µm, an order of magnitude higher.

The idea that the development of corrosion pits slows significantly after the initial damage was further supported by the bright sample results shown in Chapter 6, and shown again in Figure 7.4. The mean of each time step can be seen to rise rapidly initially, up to the 12.84 month exposure time, then appear to plateau significantly. This would agree with the results of the curved sample that most damage was done in the initial stages of corrosion, then the rate of increase dropped dramatically.

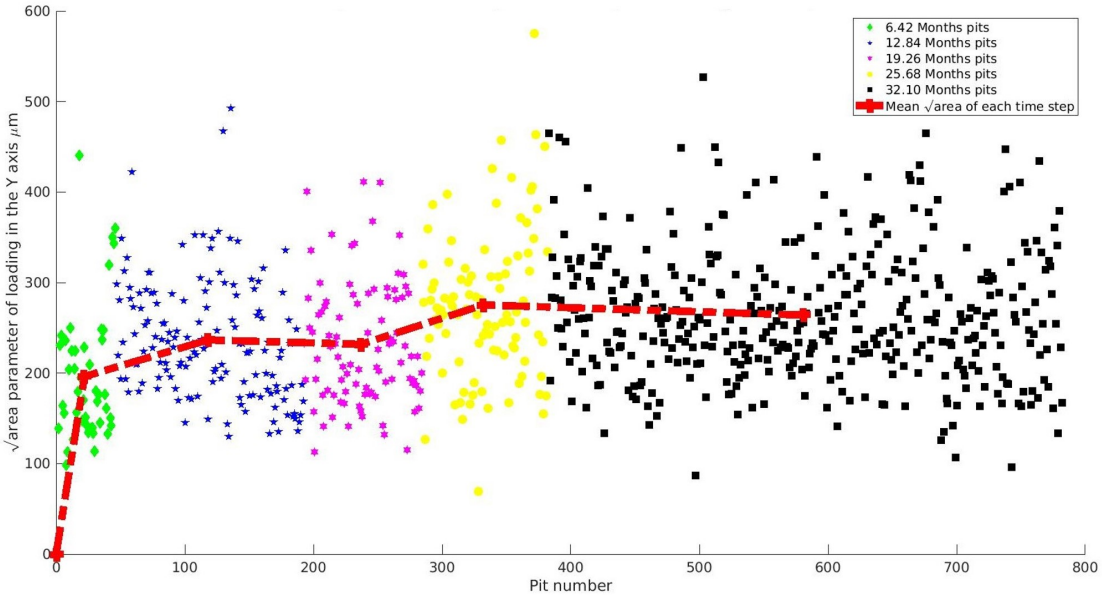

Figure 7.4: $\sqrt{Area}$ parameter of pits from bright samples in the Y plane sorted by time step

The fact that the same result was seen on both the curved and bright samples, suggests that the results, were not dependent on the starting geometry of the surface. This indicates that the passivity layer was the deciding factor in the rate of corrosion pit development. If a surface already had corrosion damage on it, had its passivity layer removed, and was then exposed again, it would still experience a rapid gain in corrosion damage.

Using the idea of the passivity layer being the key determinant in corrosion damage development, the overall concept that was used to assess the different treatment approaches can be seen in Figure 7.5. In this Figure all values were illustrative rather than representing a particular case. All progression lines were drawn obeying Godard's Law given in Chapter 4 to be representative of corrosion progression in general.

As shown in Figure 7.5, it was assumed an initial corrosion event occurred almost as soon as the axle left overhaul. This could be due to any scenario where the protective paint layer was not present, either due to misapplication in the depot or a result of a mechanical event such as a ballast strike.

The area of the axle where the paint layer was removed then begins to corrode rapidly until a passivity layer developed at around 12 months based on the results in Chapter 6. At this point the rate of progression drops to a much lower level of around a third power with time based on literature [75]. After eight years it returns to the depot and undergoes overhaul.

At the point of inspection there are two possible outcomes. If the axle was to pass through the inspection process without identifying the pit it could be expected to continue along the path of the initial rate of damage progression, represented by the green line in Figure 7.5. However, if the inspection were to be carried out removing the passivity layer and then the axle was returned to service without treatment, the second (red) line would occur. As can be seen between these two cases there would be an approximately 80% increase on the damage compared to the case where no inspection were carried out. In this case, despite this increase the axle could be returned to service as the damage would still not reach the threshold value. If this scenario was the case an inspecting depot could make the decision to return an axle to service without corrective measures, such as turning to remove the corroded material or even leaving the axle unpainted.

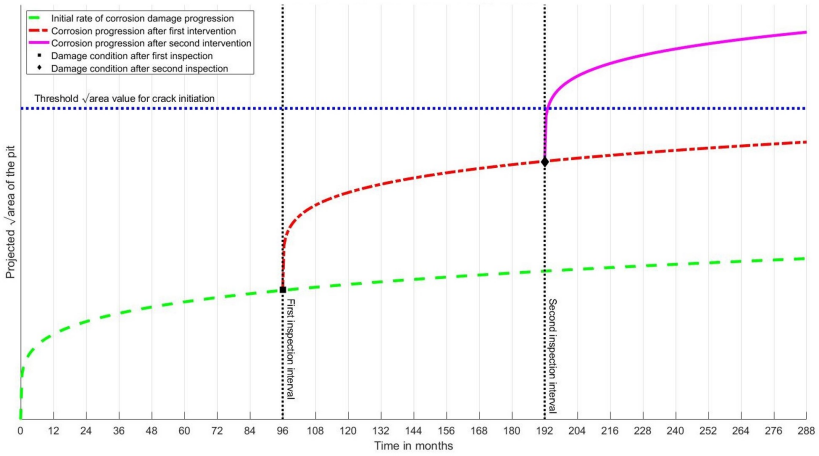

Figure 7.5: Concept of variation of outcomes based on different approaches to corrosion pitting damage. Based on an eight year inspection period with three inspections over 24 years.

The largest difference in outcome can be seen when comparing the difference after the second inspection interval. In the case where only a single inspection took place and the second inspection was neglected (the red line), the axle would have reached 288 months without exceeding the threshold value for crack initiation. However, if the inspection took place the axle would reach the threshold almost immediately (represented by the magenta line in Figure 7.5). In this instance carrying out of the inspection resulted in the axle being scrapped, but if the inspection had been neglected, the axle would have remained safely in service for another inspection interval period. This would have reduced the costs financially and logistically as well as environmentally.

This result was produced with many caveats:

1. Figure 7.5 was predicated on no corrective treatment taking place at each inspection

   However as treatment involves turning to remove the corroded material, this could be viewed as similarly reducing the life of the axle.

2. That no paint layer was applied to prevent corrosion or, if it was applied, it was removed almost immediately.

   This may not happen, as large areas of axles never have their paint layers removed, although it could be argued it was removed once it could happen again.

3. Progression of corrosion damage, as measured by projected area, increased smoothly approximately according to Godard's law.

   While this is a reasonable assumption, there was not enough evidence within this thesis to make that assertion confidently.

Another change that could affect the results seen in Figure 7.5 would be a change in the environment that the axle was operating in. This could be in terms of corrosive environment that would make the corrosion more aggressive, such as a change in the load of the wagon or a change of route to a more aggressive environment such as a marine or industrial area. The stress cycle that the axle experienced could also change, resulting in the shifting of the threshold value at which a crack would initiate.

It should also be remembered that axles do not only suffer from corrosion. The aim of an inspection could be to check for other damage that may risk the failure of the axle. This damage could include denting, scoring, cracks not initiated from pits or a wealth of other reasons, as mentioned in Chapter 2. In this case inspections may need to happen despite the possible detrimental impact on corrosion performance of the axles.

Inspections would also need to be carried out to assess the level of corrosion damage. Without knowledge of the state of corrosion damage on an axle it would not be possible to know what condition the axle was in in reference to Figure 7.5. Currently the only way to assess the state of corrosion damage is to shot blast it and remove the protective passivity layers. This limits the latitude depots may have to implement any changes. In the case where a method of inspection that could be carried out without impacting the passivity layer was developed, this would have a significant impact on the scope available to maintainers.

Despite the issues with the concept demonstrated by Figure 7.5, it highlighted the idea behind the investigation to quantify the different approaches carried out in this Chapter.

7.3.2 Axle returned to service after shot blasting

This scenario was based on the concept that the axles were put back into service in the condition they were in at the point at which they were surveyed, having had the passivity layer removed. This approach would be most easily applied in a depot setting, as it would allow the use of the existing axle cleaning process, but would require the implementation of a new inspection technique possibly based on the one developed as part of this project.

The outcomes of this approach were informed by the pit's condition in the axle survey in Chapter 3 and the changes in the curved samples after 12.84 and 25.68 months of corrosion in Chapter 6. The potential failure risk associated with the original pits could then be assessed.

The approximately two year prediction was the maximum possible, as this was the extent of the experimental results. However, this would increase the amount of time in service before a major axle inspection by around 27%, based on an eight year inspection interval.

There were two approaches that could be taken when considering how to apply the increases to corrosion damage with time. The damage could be applied as a percentage gain, or as a simple additional damage value.

It was not possible to assess the correct approach to use, due to the lack of time steps in the experiments carried out in Chapter 5, with the results in Chapter 6. For example, the pits from the curved samples, that consisted of corroded axle surfaces, generally increased their $\sqrt{Area}$ parameter by an average 97% once clear outliers were excluded. However, it was unclear if this was a percentage increase based on the size of the pit or a standard addition of around 100µm to 150µm of damage due to initial exposure to corrosion damage. There was some variation in percentage gain within the experimental results, however a large number of the outliers were found to be due to marginal pits on the cast becoming better formed in the scans of the samples. This meant that relatively small increases in the $\sqrt{Area}$ parameter resulted in very significant percentage increases. These pits were discounted to produce the mean increase.

The difference in the two approaches would have a significant impact when applied to the pits observed in the axle survey. If exposure of bare metal resulted in a known increase in corrosion damage then the number of inspections a pit could withstand would be simple to estimate. However, if the 97% value was used then the actual increase could be significantly more varied. It was not possible to determine this from the experimental results obtained due to a lack of data points and time steps.

It was assumed that the percentage increase value was correct, due to the higher severity that it represented. Using this assumption the $\sqrt{Area}$ parameters of the pits identified during the axle survey in Chapter 3, were increased by 97%. This simulated the scenario that the pits went through the inspection procedure and were returned to service without correction or protection for two additional years.

As can be seen in Figure 7.6, even in this scenario none of the pits identified on the corroded axles in service were predicted to reach the threshold at which crack initiation would take place.

The maximum range of stress intensity value calculated was $8.73 MPa.m^{0.5}$ compared to the previous maximum of $6.22 MPa.m^{0.5}$. This represented a 40% increase in the risk of crack initiation, although the new maximum value would still possess a 1.49 factor of safety. The average value also increased to $3.90 MPa.m^{0.5}$ compared to the previous mean value of $2.57 MPa.m^{0.5}$, a 52% increase.

The outcome of this work concluded that based on the pits that had been identified on the operational fleet, and the predicted increase in the $\sqrt{Area}$ parameter, all of the surveyed areas could have been returned to service without correction or protection for at least a two year period. It was possible that the period could have been longer than this, however, the lack of experimental data beyond this point made it impossible to validate this claim.

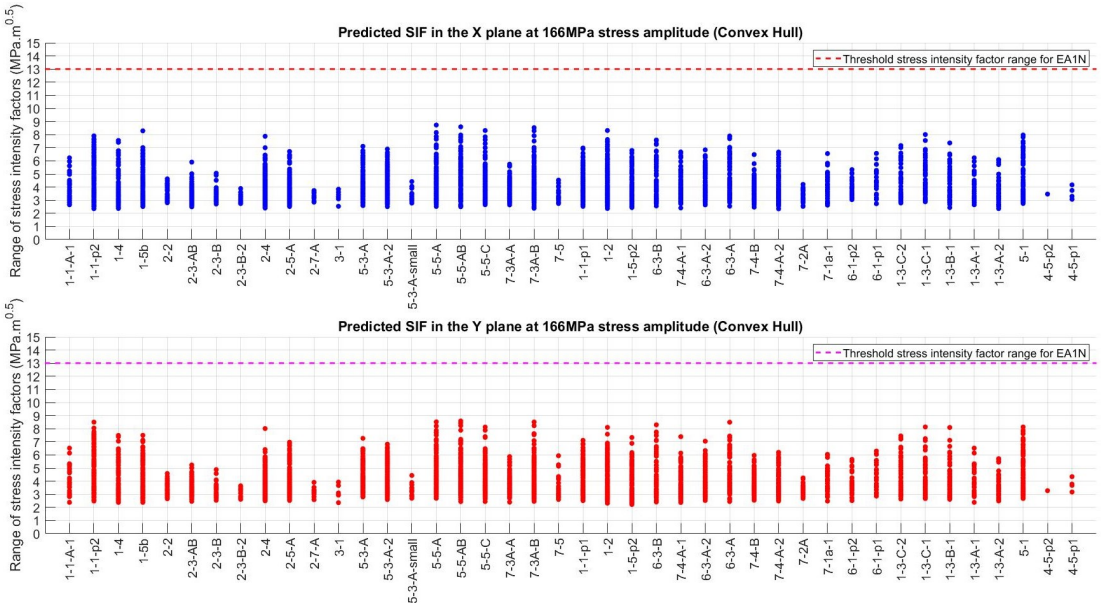

Figure 7.6: Predicted SIFs of corrosion pits identified during the axle survey after being cleaned for inspection and returned to service for two years

It should be noted that it was not intended to suggest that axles should return to service without painting to protect against corrosion damage. This scenario was used due to it being a 'worst possible case'. As it had been shown that even in this case the risk of corrosion cracking was low, using a paint layer to prevent any progression would be a significant additional safety measure.

A slight variation on this approach that may be of interest to maintainers, would be the possibility of addressing certain levels of corrosion damage through paint over it without correction. This would be cheaper than turning the axles, the current correction method, and would leave the axle with more metal when it returned to service. This could increase safety through lower stresses in the axle and, if corroded areas remained covered throughout the inspection interval, would allow other areas to corrode instead of removing untouched metal. The limit would have to be, however, the condition that the damage returned to service would not become critical if the paint layer was removed and it was once again exposed to the corrosive environment.

In the case of the surveyed axles, it was likely that they had been scrapped erroneously and could have safely remained in service. If they had done so then they would have represented a saving to the industry as a whole.

7.3.3 Axle remained in service without inspection

This concept was based on the idea that the corrosion damaged axle had been left in service for an extended period of time with no inspection or intervention. In this case the paint and passivity layers would have remained in place, slowing the rate of corrosion.

This approach was only capable of predicting the damage after a further 12.86 months of corrosion, approximately 13% longer in service, before inspection. This was based on the changes in the corrosion damage recorded on the curved samples between the 12.84 months and 25.68 months of corrosion results. This assumed that corrosion would continue at a proportional rate after the passivity layer had been produced, as the pit would have been undergoing corrosion over an extended period, possibly up to eight years.

The assumption made was that the rate of change in corrosion between the eighth and ninth year of corrosion would be the same as between the first and second. This was likely to be a conservative over estimate of the corrosion damage, as approaches such as Godard's [80] suggested that the rate of depth gain of a pit would be a third power relationship with time. However, it was unclear if this would also hold for the $\sqrt{Area}$ parameter that this project was using as an indicator of crack initiation from a corrosion pit.

Based on the same approach as was taken for the other scenario of axles being returned to service after inspection, the approximate percentage increase in the $\sqrt{Area}$ parameter was used. By comparing the location parameters of the generalised extreme value distributions between the 12.84 month and 25.68 month time steps, an estimate was produced of the percentage increase in $\sqrt{Area}$. It was calculated that, on average, the extra year of corrosion exposure after the passivity layer had formed produced a 7.7% increase in $\sqrt{Area}$.

Using the 7.7% increase value, the predicted change in the range of stress intensity values can be seen in Figure 7.7.

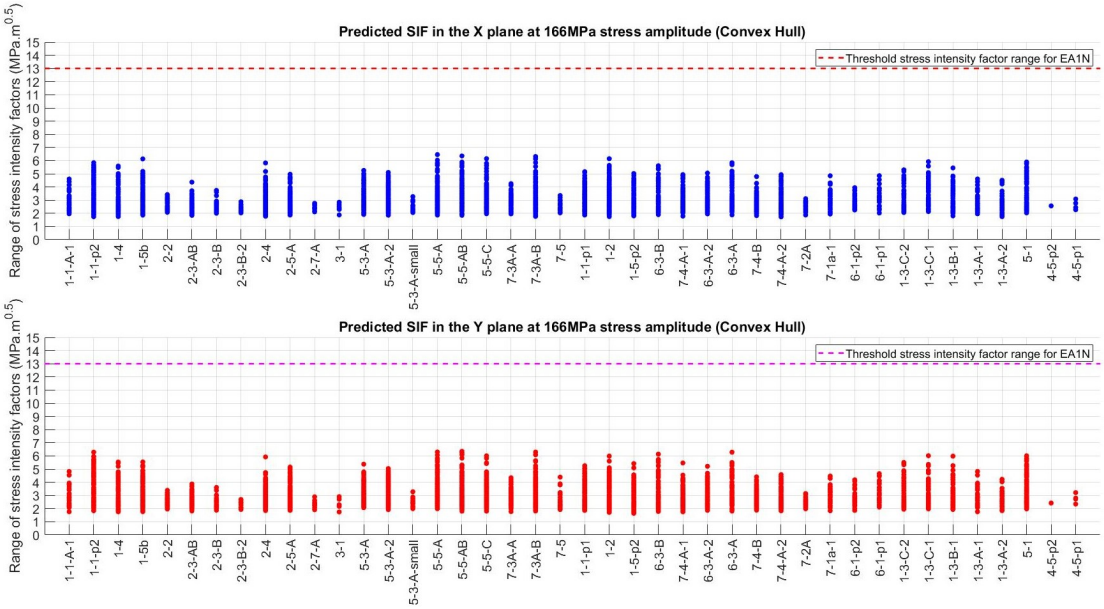

Figure 7.7: Predicted SIFs of corrosion pits identified during the axle survey without being cleaned for inspection and returned to service for one years

As expected the values in Figure 7.7 were significantly lower than the values in Figure 7.6. The maximum calculated range of stress intensity value was $6.46 MPa.m^{0.5}$ with a mean of $2.89 MPa.m^{0.5}$.

Due to the values in Figure 7.7 being significantly below the threshold it could be said that the inspected axles could have remained in service for an additional year without risk of failure through pit initiated cracking.

7.4 Outcomes and recommendations

The results of this Chapter suggested that the way rail axle corrosion of the freight fleet is treated could be changed to lower the rate of scrapping. By doing this, savings could be made that would have a direct benefit to the industry, financially, logistically and environmentally, helping to achieve larger strategic objectives such as potentially reducing the industry carbon footprint.

By combining the results of the axle survey performed in Chapter 3 and the results of the experiments undertaken, given in Chapter 6, two different changes to the procedure of addressing rail axle corrosion were presented.

The first approach was to inspect axles using current shot blasting methods to clean them. Once this had occurred the corrosion damage could be assessed and potentially returned to service without correction. This approach represented the highest level of risk, as the potential exposure of metal without a protection layer, either natural or artificial, had been shown in Chapter 6 to represent a risk of large increases in damage.

In this Chapter it was shown that based on the axles surveyed, all of the identified pits could have undergone an inspection and return to service without correction and have remained safe for a minimum of two extra years. This suggested that the axles had been scrapped erroneously as they would have remained safe.

The result of returning uncorrected axles to service and them remaining safe opened up a possibility for maintainers. If they were able to assess the level of corrosion damage in terms of the $\sqrt{Area}$ parameter used as part of this project then they could make more granular decisions on how to treat axles. This could allow operators to paint over damage without correcting it as long as the underlying damage was within a limit that would allow for a second period of exposure to corrosion damage. This would be a much faster maintenance procedure and would allow more metal to remain on the axle, potentially prolonging its life.

The issue with any proposed approach that relied on the measurement of pits in terms of the $\sqrt{Area}$ parameter, or any pit specific value, would be the limitations of collecting the information in depots. The techniques and processed used in this thesis could provide a strong starting point to allow this. However, more work would be required to make it practical in terms of both cost and speed before it could become widespread.

Another change in approach analysed in this Chapter was the possibility of extending the inspection intervals and leaving axles in service for one year longer. This would have the advantage of leaving the built up passivity layers intact on the axles, significantly slowing the rate of corrosion. The results showed that all of the axles surveyed would have also remained safe within this approach, suggesting a possible approach to reducing the cost of maintenance. The cost would be reduced through both lowering the number of inspections carried out, and reducing the number of axles scrapped, as the inspection of marginal axles may lead to the damage becoming critical and requiring correction or scrapping.

It should, however, be remembered that axles are inspected for many different forms of damage in addition to corrosion issues. While an increase in inspection intervals may make sense in terms of corrosion damage, it may not be sensible for other issues rail axles face such as ballast strikes or scoring, as detailed in Chapter 2. This may mean that continuing with the current interval periods makes more long term financial sense than having specific corrosion inspection intervals.

Overall the outcomes of this work were that there is a strong case for challenging both the current limits in the UK standards, and the procedures used by maintainers. This work could provide a strong platform for the industry to make significant savings without compromising safety. However, this would depend on depots acquiring the ability to quantitatively analyse pits, as well as being influenced by the other demands made on axle safety.

7.5 Summary

The work undertaken as part of this thesis was extensive and aimed to provide the basis for changes that could provide real value to the industry. In particular, care was taken to make sure that results would be useful in a depot setting and be applicable to everyday operation.

Initially the business case for addressing the problem was established. By gaining access to industry records, it was demonstrated that corrosion damage to rail freight axle bodies resulted in extensive costs to the industry financially, logistically and environmentally.

This was anecdotally attributed to the UK standards that placed severe limits on the amount of corrosion damage an axle could exhibit before scrapping. These standards have resulted in safe rail axles, with no failures having occurred in 20 years, but potentially high levels of waste.

An axle survey was undertaken to collect quantitative data about corrosion damage on rail axles. This involved the development and validation of a technique to collect the data in an operational depot, to a high degree of precision and without disrupting the depot's operation. The survey undertaken was the largest axle survey in terms of area analysed that had been found in literature. The outcome of the survey was digitised representation of corroded axle surfaces that allowed detailed analysis to take place.

Bespoke software, written in MATLAB, initially processed the digitised corroded axle surfaces to remove structural errors and allow systematic analysis. After initial processing, corrosion pits were identified and separated from the larger scans. This was done automatically and resulted in over 4000 pits being identified.

Pits were assessed in terms of their depth, widths and aspect ratios. The outcome of this survey was that none of the identified pits approached the depth limit set by the standard, with the maximum depth being around a third of the allowable limit.

The low pit depths compared to the standard indicated that the standard had been made irrelevant through the depot's own procedures or lack of capability to accurately assess pit depth.

The individual pits identified during the axle survey were assessed using fracture mechanics techniques. Using a crack analogy approach, the outcome was that the most likely location for cracks to initiate from corrosion pits was from the bottom of the pits. This called into question the results of some previous accelerated corrosion experiments, that had produced surface, Hoddinott, cracking.

Using an El Haddad approach to assess the risk of crack initiation, it was discovered that none of the pits identified were at risk of initiating cracks by a significant margin. The maximum pit size from the standard was also assessed and found to contain a factor of safety of around 1.5. When combined with the findings of the axle survey that pits were at most a third of the allowable depth, this demonstrated the very large margins of safety that current standards and procedures possessed.

During the fracture mechanics work, different definitions of pits were analysed based on previous axle surveys carried out in literature. It was demonstrated that these different approaches to measuring pits could result in large changes to the assessed risk of pits. This called into question the results of previous axle surveys and demonstrated some of the advantages of the approach developed in this thesis.

To produce the most value to industry, changes to the current standards or procedures would have to be made. To allow this, an understanding of the ways that corrosion pits changed over time was required.

Due to a lack of experiments in the literature that looked at this issue a novel experimental approach was proposed. Due to experimental problems the original concept had to change, however the final experiments were shown to produce representative results and avoid issues with previous designs.

The novel experiments also filled a gap in current experimental designs between full scale testing and bench top testing, providing a platform for increased research in this area.

The results of the experiment were analysed using the same approaches and techniques as were used in the axle survey. The same pit identification and separation software was also implemented. The experimental conditions were demonstrated to produce representative results in terms of both environmental condition replication and experimental time. The outcomes of the experiment were demonstrating the importance of the passivity layer in slowing corrosion development, and producing results that demonstrated the changes in corrosion pitting overtime on both machined samples and pre-corroded axle surfaces.

Finally an assessment of two different changes to the way that rail axle corrosion is currently dealt with were presented and evaluated. Both were shown to be safe and open up different avenues for maintainers to change how they treat rail axle corrosion. Either choice could have a significant impact in reducing waste in the industry without compromising safety. However, both were dependent on a depot's ability to quantitatively inspect axles and other factors that influence the inspection intervals of rail axles.

An additional consideration would be that while the work carried out in this thesis was focused on freight axles, there would be no clear reason while a similar outcome would not be true of passenger axles. However, this has not been tested and further work would be needed to verify this conclusion.

In conclusion this project has made significant advances in the understanding of the field of rail axle corrosion. It has quantified the problem faced by industry and has developed several tools and approaches to help advance further work. It is believed that the approaches and techniques developed as part of this thesis could eventually be made such that they could be applied in overhaul depots. Several changes to current standards and procedures have been suggested that could have a noticeable impact on the industry and improve efficiency. As ever though, more work would be needed to ensure the best possible outcomes had been reached.

Chapter 8

Conclusions, Further Work and Lessons Learned

8.1 Introduction

The following Chapter contains the main conclusions of the thesis and how they could influence the rail freight industry in the UK. This includes the effect both on the industry at large and in an individual depot setting.

After the conclusions are presented areas of further work are identified. The areas identified, if explored in the future, would either support and expand on the work in this thesis, or would investigate other areas of interest around rail axle corrosion.

Finally there is a lessons learned section. This contains some of the lessons that were learned during the work or advice that might help future researchers undertaking similar work.

8.2 Conclusions

The final conclusions of the work carried out as part of this thesis were as follows:

- **Large numbers of rail freight axles are scrapped at overhaul**

  Approximately 12% based on industry records, with 91% of these exhibiting corrosion. 65% of reported corrosion was found on axle bodies.

- **Most axles are scrapped based on a personal judgement rather than measurement**

  There is currently no way to effectively measure corrosion damage in overhaul depots, particularly pit depth.

- **No corrosion pits identified as part of this study approached the allowable limit, 1000µm**

  This finding agreed with finding of previous surveys. The deepest pits identified were approximately a third of the allowable depth, on axles that were scrapped for corrosion damage. This suggests that either the UK standards; the depot procedures; or both are not currently suitable for dealing with freight axle corrosion.

- **Previous surveys quantifying rail axle corrosion damage using two dimensional techniques may have suffered from large errors**

  Due to the limitations of the two dimensional techniques used to quantify three dimensional damage, previous corrosion surveys may have produced unrepresentative results.

- **None of the pits identified were likely to initiate a crack, and so risk catastrophic failure of the axle**

  Using a fracture mechanics based approach it was demonstrated that pits presenting on rail axles at overhaul depots were not a high risk for crack initiation.

- **Cracks are expected to initiate from the bottom of corrosion pits rather than the pit mouth**

  The fracture mechanics analysis of the identified corrosion pits, indicated that cracks were most likely to initiate from the bottom of corrosion pits. This stood contrary to the results of previous experiments in the field that displayed cracking from the pit mouth. This suggested that these previous experiments, seeking to replicate the rail axle environment, may have produced unrepresentative results.

- **Development of corrosion damage was effectively slowed by the development of a passivity layer**

  Experimental work in this thesis demonstrated the efficiency of the passivity layer in slowing the development of corrosion pitting. The corrosion damage develops aggressively without a passivity layer, regardless of the condition of the effected surface.

- **Inspection of rail axles increases the risk of corrosion damage**

  As previously mentioned, the removal of the passivity layer exposes the bare metal and leads to aggressive corrosion damage. Current techniques used to inspect rail axles, necessitates the removal of the passivity layer, exposing the metal. By this logic the inspection of rail axles increases the risk of corrosion damage, that may require mediation to prevent crack initiation, which may not have developed without the inspection.

- **The rail industry could increase inspection intervals without significantly increasing crack initiation risk from corrosion damage**

  No corrosion pits were identified that either approach the depth limit in the standard, or were shown to have a risk of crack initiation based on the fracture mechanics analysis. This suggests that the corrosion damage presented could have continued for sometime without representing an unacceptable risk.

  If the inspection interval were increased for corrosion damage, the risk has been shown to be minimal, especially if the passivity layer were left undamaged. This would result in savings due to decreased inspection costs, reduced logistical considerations and lowering the scrapping rate, as axles would be left with a passivity layer for longer. Further work would be required to determine the optimal interval. It should however be remembered that corrosion damage is not the sole reason for inspecting rail axles and other reasons for a shorter inspection interval may take priority.

- **Current UK limits and procedures surrounding rail freight axle corrosion should be re-examined**

  Currently the approach to rail axle corrosion suffers from a level of incoherence and lack of equipment to properly implement current standards. If the standard cannot be effectively implemented then there is a high risk of waste or inconsistent approaches, evidence of which has been found as part of this thesis. It would therefore be advisable that the responsible bodies re-examine this area and potentially change the advice given to better match actual conditions on the ground. Other areas where improvements could be made would be in the collection of relevant information in depots, through improved equipment and techniques.

8.3 Further work

Within this thesis there were several avenues that were either not able to be explored or discovered during the work that could provide real value and add to the understanding of the area. This was on top of other considerations based on the work undertaken that would benefit from further exploration.

These areas of further work have been categorised based on the Chapter that they occurred in. Hopefully this can provide a starting point for others to advance the knowledge of the field and help address this under appreciated application.

Chapter 2

The work carried out in Chapter 2 could be extended and added to. Access to more axle records and other fleets would improve the understanding of the business case for addressing the issue, potentially encouraging more work in the area.

Tracking axles through their operational lives would also be valuable. Currently when an axle enters a depot there appears to be no record of its age or operation history. Both these factors could in invaluable when assessing the impacts of different parameters on the complex, multifaceted, issue of rail axle corrosion.

Chapter 3

More and larger surveys of rail axles would improve confidence in the results of any individual survey, providing more data to validate against. With more data, other patterns and trends may come to light that are currently hidden within the noise of relatively small sample sizes. Using the technique developed in this thesis would be recommended, as it was demonstrated that other techniques can lead to significantly different outcomes to reality.

Tracking changes in corrosion damage on particular axles over time would provide an insight into the changes that axles undergo. While a long term project, it would allow assessment of many different factors that contribute to the eventual scrapping of axles. These could include corrosion pitting development but also the effects of ballast strikes and crack growth rates. A study of this sort could provide validation to a wide range of experiments and approaches currently used that can only compare against the end result, without being able to perform periodic checks.

Chapter 4

Final validation of the approach used in this thesis would be important. While this work relied on the work of others to increase the confidence in the results, the pairing of the way that pits were defined and the El Haddad approach was unique. If the conclusions of this combination could be experimentally confirmed, it mean that the approach used to identify and separate pits could be applied in overhaul depots, significantly enhancing the effectiveness of those facilities.

Chapter 5

Running the experiment as originally intended would allow the assertion of this thesis, that the stress cycles of rail axles do not contribute to the development of corrosion pits, to be validated. As it currently stands the experiment is valuable building block in continuing work in this area, however the addition of cyclic stress would make it more adaptable.

More repetitions of the experiment and for longer time periods could increase the confidence of the current results. It would also allow for a more long term view of corrosion development over the full inspection interval. An experiment that started with a smooth axle surface, ran it for "eight years", shot blasted it, then corroded it for another "eight years" would provide excellent results that would provide real value for industry. This could then be repeated for different inspection intervals. It would be a high fidelity exercise in the impacts of varying approaches to corrosion and inspection intervals.

A detailed study on the impact that the location of rail axles has on their environmental conditions would be useful. Current work assumes general atmospheric corrosion but the shelter and contaminants found beneath a train are likely to have some degree of impact.

Chapter 6

Analysis of the impacts of cyclic stresses on corrosion in general would be valuable. This is an active field of research but does not seem to be a focus of the rail industry.

A larger analysis of changes in corrosion pits overtime would be useful, as the work of this thesis was of a small sample size, making the generation of overall trends difficult.

Further work on the shape factor discussed in this thesis could provide interesting results that may allow an extremely granular approach to rail axle corrosion.

Chapter 7

The recommendations of the thesis require validation before implementation. Final proof of the different approaches would allow changes to operators procedures and have an immediate effect on scrap rates in industry.

General

A key piece of work would be to produce equipment that would allow quantitative assessment of corrosion of rail axles, ideally without damaging existing paint and passivity layers. This would result in a massive increase in the effectiveness and ability of depots to make correct decisions regarding rail axles. It could also open new avenues in other related fields, cascading the benefits to many different areas.

It would be an area of interest to investigate possible chemical treatments that could form a passivity layer on axles artificially. This would remove the requirement for painting of axles and may be more durable and adaptable to other shocks that axles experience in operation.

8.4 Lessons learned

While carrying out the work to produce this thesis, there were instances were certain aspects could have been carried out differently to prevent avoidable problems. With the benefit of hindsight, these changes could have resulted in more results and reduced work later in the project, improving the delivery speed of the project.

To aid future researchers who may take up the further work of this project, or undertake similar work in the future, this section contains some of the lessons learned during this project.

Chapter 2

- The industry is in general keen to learn and interested in finding areas of improvement. Time could have been saved by more confidently approaching industry stakeholders.
- The priority of the maintenance arm of the industry is to ensure that equipment is returned to industry in a safe condition as fast as possible. Most information collected is to support this aim rather than to produce research quality data. When analysing industry data this should be kept in mind.

Chapter 3

- Ensure that as mush information as possible is recorded when experiments are undertaken, even if it does not appear valuable at the time. If data is not collected, it can hamper future analysis if it is later required.
- Estimate the volume of data that will be collected and if sufficient processing power is available. This is especially true with large, data intensive, sample areas and techniques.

Chapter 4

- Define the amount of data required for a statistically significant survey. This would ensure the appropriate amount of work was carried out to arrive at valuable conclusions, without producing excess data.
- Determine the theoretical weaknesses of selected approaches before attempting to implement them. This would prevent going down dead ends and having to abandon large bodies of work, by identifying which approaches had fundamental weaknesses.

Chapter 5

- Do not try and do too much in a single step. When designing the experiment the minimal viable product was not defined, resulting in a needlessly complex design that caused a larger number of problems.
- Ensure that there are sufficient spare parts to account for component failures, where possible. This will minimise downtime in the event of predictable failures.

Chapter 6

- Ensure that the samples are marked with a known datum point to allow tracking across multiple measurements. This would have saved a significant amount of time and reduced alignment issues.
- Fully plan and test all the processes you will need to use. This will reduce the stress and uncertainty of the process significantly.

Bibliography

[1] J. M. West, *Basic Corrosion and Oxidation*, 2nd ed. Chichester: Ellis Horwood Limited, 1986.

[2] R. A. Smith and S. Hillmansen, "A brief historical overview of the fatigue of railway axles," *Proceedings of the Institution of Mechanical Engineers, Part F: Journal of Rail and Rapid Transit*, vol. 218, no. 4, pp. 267–277, jul 2004. [Online]. Available: http://journals.sagepub.com/doi/10.1243/0954409043125932

[3] Rail Accident Investigation Branch, "Accident at East Langton on 20th February 2010," Rail Accident Investigation Branch, Derby, Tech. Rep., 2012. [Online]. Available: https://www.railwaysarchive.co.uk/eventsummary.php?eventID=6644

[4] Rail Safety and Standards Board, "Rail Industry Standard for Wheelsets - RIS-2766-RST," London, 2017.

[5] ——, "GM/RC2496 - Recommendations for Railway Wheelset Maintenance," London, 2010.

[6] A. Watson, "T728 WP2: Effects of Corrosion on the Fatigue Performance of British Axles - Implications of Corrosion in Axles," Delta Rail, Derby, Tech. Rep., nov 2012.

[7] RailEngineer, "Wheels are turning," *RailEngineer*, jul 2012. [Online]. Available: https://www.railengineer.uk/2012/07/17/wheels-are-turning/

[8] HM Treasury, *The Green Book: appraisal and evaluation in central government*. London: The Stationery Office, 2018.

[9] J. Rudlin and R. Shipp, "Review of techniques for rail axle inspection," in *International Seminar on Railway Axles*. London: The Welding Institute, sep 2003.

[10] H. R. Inspectorate, "Railway Accident at Rickerscote: A report of the Investigation into the derailment of a freight train and the subsequent collision with a travelling post office train on 8 March 1996," Health & Safety Executive, London, Tech. Rep., 1996.

[11] D. Regazzi, "Advances in Life Prediction and Durability of Railway Axles," 2013.

[12] British Standards Institution, "BS EN 15313:2016 - Railway applications. In-service wheelset operation requirements. In-service and off-vehicle wheelset maintenance." London, 2017.

[13] P. J. Mistry, C. A. McRobie, M. S. Johnson, and I. A. Jones, "Design of A Lightweight Multifunctional Composite Railway Axle Utilising Coaxial Skins," *Research Square*, jul 2020. [Online]. Available: https://doi.org/10.21203/rs.3.rs-47622/v1

[14] M. Carboni and S. Beretta, "Effect of probability of detection upon the definition of inspection intervals for railway axles," *Proceedings of the Institution of Mechanical Engineers, Part F: Journal of Rail and Rapid Transit*, vol. 221, no. 3, pp. 409–417, may 2007.

[15] British Standards Institution, "BS EN 13103:2009+A1:2010 - Railway applications. Wheelsets and bogies. Non powered axles. Design method," London, 2010.

[16] ——, "BS EN 13104:2009+A1:2010 - Railway applications. Wheelsets and bogies. Powered axles. Design method," London, 2010.

[17] ——, "BS EN 13261:2009+A1:2010 - Railway applications. Wheelsets and bogies. Axles. Product requirements," London, 2009. [Online]. Available: https://bsol.bsigroup.com/Bibliographic/BibliographicInfoData/000000000030217346

[18] P. R. Roberge, *Handbook of Corrosion Engineering*, 2nd ed. New York: McGraw Hill, 2012.

[19] F. Moretti, S. Beretta, A. L. Conte, and D. Straub, "Corrosion-fatigue under Rainwater of a Q&T Steel: Experiments and Probabilistic Description," *Procedia Engineering*, vol. 74, pp. 12–17, jan 2014. [Online]. Available: https://www.sciencedirect.com/science/article/pii/S1877705814007851

[20] M. G. Fontana, *Corrosion Engineering*, 3rd ed., S. Rao, Ed. Singapore: McGraw Hill, 1987.

[21] Z. Szklarska-Smialowska, *Pitting Corrosion Of Metals*, 1st ed. Houston: National Association of Corrosion Engineers, 1986.

[22] Amarineblog, "What is Pitting Mechanism and Prevention?" 2020. [Online]. Available: https://amarineblog.com/2020/11/02/what-is-pitting-mechanism-and-prevention/

[23] J. Kruger, "Electrochemistry of corrosion," Baltimore, apr 2001. [Online]. Available: https://knowledge.electrochem.org/encycl/art-c02-corrosion.htm

[24] S. Beretta, M. Carboni, A. Lo Conte, and E. Palermo, "An investigation of the effects of corrosion on the fatigue strength of AlN axle steel," *Proceedings of the Institution of Mechanical Engineers, Part F: Journal of Rail and Rapid Transit*, vol. 222, no. 2, pp. 129–143, mar 2008. [Online]. Available: http://journals.sagepub.com/doi/10.1243/09544097JRRT157

[25] J. Rudlin, "WOLAXIM Report Summary," The Welding Institute, Cambridge, Tech. Rep., 2012.

[26] R. Smith, "Fatigue of railway axles: A classic problem revisited," *European Structural Integrity Society*, vol. 26, pp. 173–181, sep 2000. [Online]. Available: http://linkinghub.elsevier.com/retrieve/pii/S1566136900800497

[27] A. D. Quinn, M. Hayward, C. J. Baker, F. Schmid, J. A. Priest, and W. Powrie, "A full-scale experimental and modelling study of ballast flight under high-speed trains," *Proceedings of the Institution of Mechanical Engineers, Part F: Journal of Rail and Rapid Transit*, vol. 224, no. 2, pp. 61–74, mar 2010. [Online]. Available: http://journals.sagepub.com/doi/10.1243/09544097JRRT294

[28] U. Zerbst, C. Klinger, and D. Klingbeil, "Structural assessment of railway axles - A critical review," *Engineering Failure Analysis*, vol. 35, pp. 54–65, dec 2013. [Online]. Available: http://www.sciencedirect.com/science/article/pii/S1350630712002531

[29] Australian Transport Safety Bureau, "Investigation: 2006002 - Derailment of XPT Passenger Train, ST22; Harden, NSW; 9 February 2006," Australian Transport Safety Bureau, Canberra, Tech. Rep., jun 2007. [Online]. Available: https://www.atsb.gov.au/publications/investigation{_}reports/2006/rair/rair2006002/

[30] K. Madler, T. Geburtig, and D. Ullrich, "An experimental approach to determining the residual lifetimes of wheelset axles on a full-scale wheel-rail roller test rig," DB Systemtechnik, Berlin, Tech. Rep., 2013.

[31] P. Connor, "Train Maintenance," 2019. [Online]. Available: http://www.railway-technical.com/trains/train-maintenance/

[32] W. Kappes, D. Hentschel, and T. Oelschlägel, "Potential improvements of the presently applied in-service inspection of wheelset axles," *International Journal of Fatigue*, vol. 86, pp. 64–76, may 2016. [Online]. Available: http://www.sciencedirect.com/science/article/pii/S0142112315002662

[33] A. Turnbull, D. A. Horner, and B. J. Connolly, "Challenges in modelling the evolution of stress corrosion cracks from pits," *Engineering Fracture Mechanics*, vol. 76, no. 5, pp. 633–640, mar 2009. [Online]. Available: https://www.sciencedirect.com/science/article/pii/S0013794408002634

[34] D. A. Horner, B. J. Connolly, S. Zhou, L. Crocker, and A. Turnbull, "Novel images of the evolution of stress corrosion cracks from corrosion pits," *Corrosion Science*, vol. 53, no. 11, pp. 3466–3485, nov 2011. [Online]. Available: http://www.sciencedirect.com/science/article/pii/S0010938X11002721

[35] M. Cerit, K. Genel, and S. Eksi, "Numerical investigation on stress concentration of corrosion pit," *Engineering Failure Analysis*, vol. 16, no. 7, pp. 2467–2472, oct 2009. [Online]. Available: https://www.sciencedirect.com/science/article/pii/S1350630709001010

[36] S. Beretta, A. Lo Conte, J. Rudlin, and D. Panggabean, "From atmospheric corrosive attack to crack propagation for A1N railway axles steel under fatigue: Damage process and detection," *Engineering Failure Analysis*, vol. 47, no. PB, pp. 252–264, jan 2015. [Online]. Available: http://dx.doi.org/10.1016/j.engfailanal.2014.07.026

[37] D. S. Hoddinott, "Railway axle failure investigations and fatigue crack growth monitoring of an axle," *Proceedings of the Institution of Mechanical Engineers, Part F: Journal of Rail and Rapid Transit*, vol. 218, no. 4, pp. 283–292, jul 2004. [Online]. Available: http://journals.sagepub.com/doi/10.1243/0954409043125897

[38] M. Filippini, M. Luke, I. Varfolomeev, D. Regazzi, and S. Beretta, "Fatigue strength assessment of railway axles considering small-scale tests and damage calculations," *Procedia Structural Integrity*, vol. 4, pp. 11–18, jul 2017.

[39] S. Beretta, M. Carboni, G. Fiore, and A. Lo Conte, "Corrosion-fatigue of A1N railway axle steel exposed to rainwater," *International Journal of Fatigue*, vol. 32, no. 6, pp. 952–961, jun 2010. [Online]. Available: https://www.sciencedirect.com/science/article/pii/S0142112309002667

[40] J. I. Bluhm, "Fracture mechanics," Delft, jan 1963.

[41] European Steel Design Education Programme, "ESDEP Lecture notes - Lecture 12.13: Fracture Mechanics," 1998. [Online]. Available: http://fgg-web.fgg.uni-lj.si/{~}/pmoze/esdep/master/wg12/l1300.htm

[42] Vereinigung der Privatgüterwagen-Interessenten, "VPI European Maintenance Guide - Maintenance of Freight Wagons," Hamburg, 2012.

[43] R. Gallo, S. Cantini, and D. Minini, "A new wheelset maintenance concept," in *World Congress on Railway Research*. Sidney: Union Internationale des Chemins de fer (UIC), nov 2013.

[44] Health & Safety Executive, "RR617 Assessment of NDT in industry (PANI 3)," Health & Safety Executive, London, Tech. Rep., 2008. [Online]. Available: http://www.hse.gov.uk/research/rrhtm/rr617.htm

[45] A. Watson, "NDT Periodicity for Mk4 Coach and Mk4 DVT Axles," Great North Eastern Railway, Derby, Tech. Rep., 2006.

[46] U. V. John Rudlin, Antonietta Loconte, Angelique Raude, "New Methods of Rail Axle Inspection and Assessment," in *18th World Conference on Nondestructive Testing*, Durban, 2012.

[47] The Welding Institute, "Wolaxim - Inspection of railway axles." [Online]. Available: https://www.youtube.com/watch?v=4ZL95SJayEM

[48] ASTM International, "ASTM G46-94 Standard Guide for Examination and Evaluation of Pitting Corrosion," West Conshohocken, 2013. [Online]. Available: https://doi.org/10.1520/G0046-94R13

[49] S. Pottinger, "Freight rail usage 2017-18 Q4 Statistical release," London, jun 2018. [Online]. Available: https://dataportal.orr.gov.uk/statistics/usage/freight-rail-usage-and-performance/

[50] J. Rudlin, D. Panggabean, A. Loconte, and A. Raude, "Assessment of Corrosion on Rail Axles," in *51st Annual Conference of the British Institute of Non-Destructive Teststing*, The Welding Institute. Cambridge: NDT 2012, jan 2012, pp. 63–39.

[51] D. Müller, J. Nicolin, G. Peterhans, E. Feyen, F. Lombardo, L. Lochman, P. Tonon, E. Lehmann, M. Burkhardt, and M. Marianeschi, "Final report on the results of the Joint Sector Group activities linked to the action plan defined under the Task Force Freight Wagon Maintenance," Joint Sector Group, Tech. Rep., dec 2012.

[52] M. Broster, "An evaluation of replica methods used in roughness measurements," British Railways Research Department, Derby, Tech. Rep., 1972.

[53] A. M. Zimer, E. C. Rios, L. H. Mascaro, and E. C. Pereira, "Temporal series micrographs coupled with polarization curves to study pit formation under anodic polarization," *Electrochemistry Communications*, vol. 13, no. 12, pp. 1484–1487, dec 2011.

[54] A. M. Zimer, M. A. De Carra, E. C. Rios, E. C. Pereira, and L. H. Mascaro, "Initial stages of corrosion pits on AISI 1040 steel in sulfide solution analyzed by temporal series micrographs coupled with electrochemical techniques," *Corrosion Science*, vol. 76, pp. 27–34, nov 2013.

[55] Z. Xiong, Q. Li, Q. Mao, and Q. Zou, "A 3D laser profiling system for rail surface defect detection," *Sensors (Switzerland)*, vol. 17, no. 8, aug 2017. [Online]. Available: /pmc/articles/PMC5580074//pmc/articles/PMC5580074/?report=abstracthttps://www.ncbi.nlm.nih.gov/pmc/articles/PMC5580074/

[56] D. Coelho, O. A. Cuadros Linares, A. L. Oliveira, M. A. Andrade, L. H. Mascaro, J. E. Batista Neto, O. M. Bruno, and E. C. Pereira, "Introducing a low-cost tool for 3D characterization of pitting corrosion in stainless steel," *Journal of Solid State Electrochemistry*, vol. 24, no. 8, pp. 1909–1919, aug 2020. [Online]. Available: https://doi.org/10.1007/s10008-020-04586-2

[57] F. Tang, Z. Lin, G. Chen, and W. Yi, "Three-dimensional corrosion pit measurement and statistical mechanical degradation analysis of deformed steel bars subjected to accelerated corrosion," *Construction and Building Materials*, vol. 70, pp. 104–117, nov 2014.

[58] M. M. Kashani, A. J. Crewe, and N. A. Alexander, "Use of a 3D optical measurement technique for stochastic corrosion pattern analysis of reinforcing bars subjected to accelerated corrosion," *Corrosion Science*, vol. 73, pp. 208–221, aug 2013.

[59] Y. Wang and G. Cheng, "Quantitative evaluation of pit sizes for high strength steel: Electrochemical noise, 3-measurement, and image-recognition-based statistical analysis," *Materials and Design*, vol. 94, pp. 176–185, mar 2016.

[60] Y. Wang, G. Cheng, and Y. Li, "Observation of the pitting corrosion and uniform corrosion for X80 steel in 3.5 wt.% NaCl solutions using in-situ and 3-D measuring microscope," *Corrosion Science*, vol. 111, pp. 508–517, oct 2016.

[61] Olympus Corporation, "OLS 4100 LEXT," 2013. [Online]. Available: https://www.olympus-ims.com/en/metrology/ols4100/

[62] B. Holme and O. Lunder, "Characterisation of pitting corrosion by white light interferometry," *Corrosion Science*, vol. 49, no. 2, pp. 391–401, feb 2007.

[63] S. hua Xu and B. Qiu, "Experimental study on fatigue behavior of corroded steel," *Materials Science and Engineering A*, vol. 584, pp. 163–169, nov 2013.

[64] S. H. Xu and Y. D. Wang, "Estimating the effects of corrosion pits on the fatigue life of steel plate based on the 3D profile," *International Journal of Fatigue*, vol. 72, pp. 27–41, mar 2015.

[65] Microset, "Microset 101 Fluid — Technical Info — Replication — Moulding," 2019. [Online]. Available: https://www.microset.co.uk/technical-info/microset-101-fluid/index.html

[66] Bruker, "InfiniteFocusSL — 3D measurement system for form & finish — Alicona." [Online]. Available: https://www.alicona.com/products/infinitefocussl/

[67] N. Duboust, H. Ghadbeigi, C. Pinna, S. Ayvar-Soberanis, A. Collis, R. Scaife, and K. Kerrigan, "An optical method for measuring surface roughness of machined carbon fibre-reinforced plastic composites," *Journal of Composite Materials*, vol. 51, no. 3, pp. 289–302, feb 2017.

[68] L. de Haan and A. Ferreira, "Extreme Value Theory: An Introduction," in *Springer Series in Operations Research and Financial Engineering*, 1st ed., T. V. Mikosch, S. I. Resnick, and S. M. Robinson, Eds. New York: Springer Science & Business Media LLC, 2006, pp. 1–413.

[69] S. Kotz and S. Nadarajah, *Extreme Value Distributions*. PUBLISHED BY IMPERIAL COLLEGE PRESS AND DISTRIBUTED BY WORLD SCIENTIFIC PUBLISHING CO., oct 2000.

[70] M. H. El Haddad, T. H. Topper, and K. N. Smith, "Prediction of non propagating cracks," *Engineering Fracture Mechanics*, vol. 11, no. 3, pp. 573–584, jan 1979.

[71] R. W. Michael Janssen, Jan Zuidema, *Fracture Mechanics*, 2nd ed. Oxon: Spon Press, 2004.

[72] B. McGinty, "Fracture Mechanics: Loading Modes I, II, III," 2014. [Online]. Available: https://www.fracturemechanics.org/modes123.html

[73] MechaniCalc Inc., "Fracture Mechanics," 2020. [Online]. Available: https://mechanicalc.com/reference/fracture-mechanics

[74] N. O. Larrosa, R. Akid, and R. A. Ainsworth, "Corrosion-fatigue: a review of damage tolerance models," *International Materials Reviews*, vol. 63, no. 5, pp. 283–308, jul 2018.

[75] S. Kawai and K. Kasai, "Considerations of allowable stress of corrosion fatigue (focused on the influence of pitting)," *Fatigue & Fracture of Engineering Materials & Structures*, vol. 8, no. 2, pp. 115–127, 1985.

[76] Y. Kondo, "Prediction of fatigue crack initiation life based on pit growth," *Corrosion*, vol. 45, no. 1, pp. 7–11, jan 1989.

[77] T. Anderson, *Fracture Mechanics: Fundamentals and Applications*, 3rd ed. Taylor & Francis, 2005.

[78] L. Tudose and C. Popa, "Stress intensity factors analysis on cracks in the hertzian stresses field of teeth gears," in *The 10th International Conference on Tribology*, Bucharest, nov 2007.

[79] D. W. Hoeppner, "Model for predicition of fatigue lives based upon a pitting corrosion fatigue process," in *ASTM Special Technical Publication*, no. 675. Toronto: ASTM, jan 1979, pp. 841–870.

[80] H. P. Godard, "The corrosion behavior of aluminum in natural waters," *The Canadian Journal of Chemical Engineering*, vol. 38, no. 5, pp. 167–173, oct 1960. [Online]. Available: http://doi.wiley.com/10.1002/cjce.5450380507

[81] R. Baboian, W. France, L. Rowe, and J. Rynewicz, *Galvanic and Pitting Corrosion—Field and Laboratory Studies*. ASTM International, jan 1976.

[82] T. C. Lindley, P. McIntyre, and P. J. Trant, "Fatigue-crack initiation at corrosion pits," *Metals Technology*, vol. 9, no. 1, pp. 135–142, mar 1982. [Online]. Available: https://www.tandfonline.com/action/journalInformation?journalCode=ymst20

[83] S. Ishihara, S. Saka, Z. Y. Nan, T. Goshima, and S. Sunada, "Prediction of corrosion fatigue lives of aluminium alloy on the basis of corrosion pit growth law," *Fatigue and Fracture of Engineering Materials and Structures*, vol. 29, no. 6, pp. 472–480, jun 2006. [Online]. Available: http://doi.wiley.com/10.1111/j.1460-2695.2006.01018.x

[84] Q. Y. Wang, R. M. Pidaparti, and M. J. Palakal, "Comparative study of corrosion-fatigue in aircraft materials," *AIAA journal*, vol. 39, no. 2, pp. 325–330, may 2001. [Online]. Available: http://arc.aiaa.org

[85] D. Harlow and R. P. Wei, "Probability Approach for Prediction of Corrosion and Corrosion Fatigue Life," *American Institute of Aeronautics and Astronautics journal*, vol. 32, no. 10, pp. 2073–2079, oct 1994.

[86] R. S. Zhou, H. S. Cheng, and T. Mura, "Micropitting in Rolling and Sliding Contact Under Mixed Lubrication," *Journal of Tribology*, vol. 111, no. 4, pp. 605–613, oct 1989. [Online]. Available: https://asmedigitalcollection.asme.org/tribology/article/111/4/605/437368/Micropitting-in-Rolling-and-Sliding-Contact-Under

[87] M. R. Sriraman and R. M. Pidaparti, "Life prediction of aircraft aluminum subjected to pitting corrosion under fatigue conditions," *Journal of Aircraft*, vol. 46, no. 4, pp. 1253–1259, may 2009. [Online]. Available: http://arc.aiaa.org

[88] Y. Murakami, *Metal Fatigue: Effects of Small Defects and Nonmetallic Inclusions*, 1st ed. Kyushu: Elsevier Science Ltd, 2002.

[89] R. Salzman, D. Gandy, N. Rieger, B. Schönbauer, S. Tschegg, S. Zhou, and A. Turnbull, "Corrosion-fatigue prediction methodology for 12% Cr steam turbine blades," in *Proceedings of the ASME 2013 Power Conference. Volume 1: Fuels and Combustion, Material Handling, Emissions; Steam Generators; Heat Exchangers and Cooling Systems; Turbines, Generators and Auxiliaries; Plant Operations and Maintenance*, vol. 1. Boston: American Society of Mechanical Engineers, aug 2013.

[90] R. Salzman, N. Rieger, S. Stanzl-Tschegg, B. Schönbauer, A. Turnbull, S. Zhou, and D. Gandy, "(PDF) Corrosion-fatigue in steam turbine blades," in *6th International Conference on Advanced Materials for Fossil Power Plants*, jul 2010, pp. 450–469. [Online]. Available: https://www.researchgate.net/publication/286788721{_}Corrosion-fatigue{_}in{_}steam{_}turbine{_}blades

[91] S. I. Rokhlin, J. Y. Kim, H. Nagy, and B. Zoofan, "Effect of pitting corrosion on fatigue crack initiation and fatigue life," *Engineering Fracture Mechanics*, vol. 62, no. 4-5, pp. 425–444, mar 1999. [Online]. Available: http://www.sciencedirect.com/science/article/pii/S0013794498001015

[92] Y. Murakami and S. Nemat-Nasser, "Growth and stability of interacting surface flaws of arbitrary shape," *Engineering Fracture Mechanics*, vol. 17, no. 3, pp. 193–210, jan 1983.

[93] Y. Murakami, "Analysis of stress intensity factors of modes I, II and III for inclined surface cracks of arbitrary shape," *Engineering Fracture Mechanics*, vol. 22, no. 1, pp. 101–114, jan 1985.

[94] J. Tenkamp, M. Awd, S. Siddique, P. Starke, and F. Walther, "Fracture–mechanical assessment of the effect of defects on the fatigue lifetime and limit in cast and additively manufactured aluminum–silicon alloys from hcf to vhcf regime," *Metals*, vol. 10, no. 7, pp. 1–18, jul 2020. [Online]. Available: https://www.mdpi.com/2075-4701/10/7/943

[95] Efatigue.com, "Small Defect Technical Background." [Online]. Available: https://www.efatigue.com/smalldefect/background/smalldefect.html

[96] M. da Fonte, L. Reis, and M. de Freitas, "Fatigue crack growth under rotating bending loading on aluminium alloy 7075-T6 and the effect of a steady torsion," *Theoretical and Applied Fracture Mechanics*, vol. 80, pp. 57–64, dec 2015. [Online]. Available: http://dx.doi.org/10.1016/j.tafmec.2015.05.006

[97] S. Beretta, M. Carboni, S. Cantini, and A. Ghidini, "Application of fatigue crack growth algorithms to railway axles and comparison of two steel grades," in *Proceedings of the Institution of Mechanical Engineers, Part F: Journal of Rail and Rapid Transit*, vol. 218, no. 4, dec 2004, pp. 317–326.

[98] J. C. Newman and I. S. Raju, "An empirical stress-intensity factor equation for the surface crack," *Engineering Fracture Mechanics*, vol. 15, no. 1-2, pp. 185–192, jan 1981.

[99] M. Nagai, N. Miura, and M. Shiratori, "Stress intensity factor solution for a surface crack with high aspect ratio subjected to an arbitrary stress distribution using the influence function method," *International Journal of Pressure Vessels and Piping*, vol. 131, pp. 2–9, jul 2015. [Online]. Available: http://inis.iaea.org/Search/search.aspx?orig{_}q=RN:47019507

[100] G. Glinka, "Development of weight functions and computer integration procedures for calculating stress intensity factors around cracks - Progress report No.1 subjected to complex stress fields," Peterburg, Ontario, mar 1996.

[101] C. Q. Li and S. T. Yang, "Stress intensity factors for high aspect ratio semi-elliptical internal surface cracks in pipes," *International Journal of Pressure Vessels and Piping*, vol. 96-97, pp. 13–23, aug 2012.

[102] M. Cerit, "Numerical investigation on torsional stress concentration factor at the semi elliptical corrosion pit," *Corrosion Science*, vol. 67, pp. 225–232, feb 2013. [Online]. Available: https://www.sciencedirect.com/science/article/pii/S0010938X12005124

[103] D. Ongaro, M. Hoves, S. Beretta, and M. Carboni, "Wheelset integrated design and effective maintenance - D 5.1 – Endurance design procedure of wheelsets based on reliable load spectra and reliable Wohler curves," WIDEM Project, Tech. Rep., 2008.

[104] S. Beretta, M. Carboni, A. Lo Conte, D. Regazzi, S. Trasatti, and M. Rizzi, "Crack growth studies in railway axles under corrosion fatigue: Full-scale experiments and model validation," in *Procedia Engineering*, vol. 10. Elsevier, jan 2011, pp. 3650–3655. [Online]. Available: http://www.sciencedirect.com/science/article/pii/S1877705811007892

[105] M. Luke, I. Varfolomeev, K. Lütkepohl, and A. Esderts, "Fatigue crack growth in railway axles: Assessment concept and validation tests," *Engineering Fracture Mechanics*, vol. 78, no. 5, pp. 714–730, mar 2011.

[106] R. Fajkoš, R. Zima, and K. Karwala, "The new technologies for increase fatigue strength of railways wheelsets and methods for verification a quality proceedings," *Problemy eksploatacji*, vol. 1, no. 1, pp. 45–58, jan 2009.

[107] D. Shirres, "Huddersfield's rolling rig," *RailEngineer UK*, vol. 112, no. November 2016, pp. 1–12, 2016. [Online]. Available: https://www.railengineer.co.uk/huddersfields-rolling-rig/https://www.railengineer.uk/2016/11/22/huddersfields-rolling-rig/

[108] P. Rolek, S. Bruni, and M. Carboni, "Condition monitoring of railway axles based on low frequency vibrations," *International Journal of Fatigue*, vol. 86, pp. 88–97, may 2016.

[109] S. Beretta, M. Carboni, A. Lo Conte, D. Regazzi, S. Trasatti, and M. Rizzi, "Crack growth studies in railway axles under corrosion fatigue: Full-scale experiments and model validation," in *Procedia Engineering*, vol. 10. Elsevier Ltd, jan 2011, pp. 3650–3655.

[110] S. Beretta, A. L. Conte, J. Rudlin, and D. Panggabean, "From atmospheric corrosive attack to crack propagation for A1N railway axles steel under fatigue: Damage process and detection," *Engineering Failure Analysis*, vol. 47, pp. 252–264, jan 2015. [Online]. Available: http://www.sciencedirect.com/science/article/pii/S1350630714002544

[111] A. Moon, S. Sangal, and K. Mondal, "Corrosion behaviour of new railway axle steels," *Transactions of the Indian Institute of Metals*, vol. 66, no. 1, pp. 33–41, feb 2013. [Online]. Available: http://link.springer.com/10.1007/s12666-012-0167-0

[112] R. W. R. W. Revie and H. H. Uhlig, *Corrosion and corrosion control : an introduction to corrosion science and engineering*, 4th ed. John Wiley & Sons, 2008. [Online]. Available: https://books.google.co.uk/books?id=HJHMhOgrEiwC{&}dq=corrosion+definition{&}lr={&}source=gbs{_}navlinks{_}s

[113] DB Cargo, "The DB Cargo freight wagon catalogue — Deutsche Bahn AG," 2019. [Online]. Available: https://dk.dbcargo.com/rail-danmark-en/useful-links/freight-wagon-catalogue-3720536

[114] Delta Rail, "Optimising wheelset design and maintenance. Class 319 Axle strain measurements (T356 Report)," Derby, 2010.

[115] S. Beretta and M. Carboni, "Variable amplitude fatigue crack growth in a mild steel for railway axles: Experiments and predictive models," *Engineering Fracture Mechanics*, vol. 78, no. 5, pp. 848–862, mar 2011.

[116] S. D. Iwnicki, S. Stichel, A. Orlova, and M. Hecht, "Dynamics of railway freight vehicles," *Vehicle System Dynamics*, vol. 53, no. 7, pp. 995–1033, jul 2015. [Online]. Available: https://www.tandfonline.com/doi/abs/10.1080/00423114.2015.1037773

[117] A. S. Watson and K. Timmis, "A method of estimating railway axle stress spectra," *Engineering Fracture Mechanics*, vol. 78, no. 5, pp. 836–847, mar 2011.

[118] J. Shigley and L. Mitchell, *Shigley's Mechanical Engineering Design*, 4th ed. New York: McGraw-Hill, 1983.

[119] R. M. Bhoi and P. L. G. Kalurkar, "Study of Buckling Behavior of Beam and Column," *IOSR Journal of Mechanical and Civil Engineering*, vol. 11, no. 4, pp. 36–40, aug 2014.

[120] P. Schweitzer, *Fundamentals of Metallic Corrosion: Atmospheric and Media Corrosion of Metals*, 2nd ed. Boca Raton: CRC Press, 2006.

[121] Corrosion Doctors, "Corrosion and pollution in South Africa," 2016. [Online]. Available: https://corrosion-doctors.org/AtmCorros/mapUK.htm

[122] ASTM International, *Cyclic Cabinet Corrosion Testing*. ASTM International, jan 1995.

[123] G. Brunoro, A. Frignani, A. Colledan, and C. Chiavari, "Organic films for protection of copper and bronze against acid rain corrosion," *Corrosion Science*, vol. 45, no. 10, pp. 2219–2231, oct 2003. [Online]. Available: https://www.sciencedirect.com/science/article/pii/S0010938X03000659{#}!

[124] Department for Environment Food and Rural Affairs, "United Kingdom Eutrophying & Acidifying Network: Precip-Net," 2018. [Online]. Available: https://uk-air.defra.gov.uk/data/non-auto-data?uka{_}id=UKA00119{&}view=data{&}network=ukeap{&}year=2017{&}pollutant=681{#}view

[125] P. Walker, "Useful information on centrifugal pumps," 2021. [Online]. Available: https://www.michael-smith-engineers.co.uk/resources/useful-info/centrifugal-pumps

[126] C. Klinger and D. Bettge, "Axle fracture of an ICE3 high speed train," *Engineering Failure Analysis*, vol. 35, pp. 66–81, dec 2013. [Online]. Available: https://www.sciencedirect.com/science/article/pii/S1350630712002543

[127] ASTM International, "ATSM E8/E8M - Standard Test Methods for Tension Testing of Metallic Materials," West Conshohocken, 2020.

[128] British Standards Institution, "BS ISO 12106:2017 - Metallic materials. Fatigue testing. Axial-strain-controlled method," London, 2017. [Online]. Available: https://shop.bsigroup.com/ProductDetail?pid=000000000030323944

[129] L. Guan, B. Zhang, X. P. Yong, J. Q. Wang, E. H. Han, and W. Ke, "Effects of cyclic stress on the metastable pitting characteristic for 304 stainless steel under potentiostatic polarization," *Corrosion Science*, vol. 93, pp. 80–89, apr 2015.

[130] Y. F. Li, G. C. Farrington, and C. Laird, "Cyclic response-electrochemical interaction in mono- and polycrystalline AISI 316L stainless steel in H2SO4 solution - I. The influence of mechanical strain on the transient dissolution behavior during corrosion fatigue," *Acta Metallurgica Et Materialia*, vol. 41, no. 3, pp. 693–708, mar 1993.

[131] J. Ma, B. Zhang, J. Wang, G. Wang, E. H. Han, and W. Ke, "Anisotropic 3D growth of corrosion pits initiated at MnS inclusions for A537 steel during corrosion fatigue," *Corrosion Science*, vol. 52, no. 9, pp. 2867–2877, sep 2010.

[132] T. Zhang, Y. Yang, Y. Shao, G. Meng, and F. Wang, "A stochastic analysis of the effect of hydrostatic pressure on the pit corrosion of Fe-20Cr alloy," *Electrochimica Acta*, vol. 54, no. 15, pp. 3915–3922, jun 2009.

[133] R. D. Down and J. H. Lehr, *Environmental Instrumentation and Analysis Handbook*, 1st ed. John Wiley & Sons, 2005. [Online]. Available: https://books.google.com/books/about/Environmental{_}Instrumentation{_}and{_}Analys.html?id=6jhELyGJOm0C

[134] L. Mazzola, D. Regazzi, S. Beretta, and S. Bruni, "Fatigue assessment of old design axles: Service simulation and life extension," *Proceedings of the Institution of Mechanical Engineers, Part F: Journal of Rail and Rapid Transit*, vol. 230, no. 2, pp. 572–584, oct 2016. [Online]. Available: https://journals.sagepub.com/doi/10.1177/0954409714552699

[135] ANSYS Fluent, "ANSYS FLUENT 12.0 User's Guide - 6.2.2 Mesh Quality," 2015. [Online]. Available: https://www.afs.enea.it/project/neptunius/docs/fluent/html/ug/node167.htm

[136] S. Pashneh-Tala, A. Malins, R. Lewis, G. Heppell, and E. Rodriguez-Falcon, *The Little Book of Design*, 1st ed. Sheffield: Univeristy of Sheffield, 2011.

[137] BSI, "BS EN ISO 898-1:2013 - Mechanical properties of fasteners made of carbon steel and alloy steel Part 1: Bolts, screws and studs with specified property classes - Coarse thread and fine pitch thread," London, 2013. [Online]. Available: https://www.iso.org/standard/60610.html

[138] Wurth, "Dimensioning metric screw assemblies," Erith, 2020.

[139] Rocol, "Rocol J166 Copper Based Anti-Seize - Technical Data," Leeds, 2017. [Online]. Available: https://www.rocol.com/datasheets

[140] Sandvik Coromant, "Threading formulas and definitions," Birmingham, 2018. [Online]. Available: https://www.sandvik.coromant.com/en-gb/knowledge/machining-formulas-definitions/pages/threading.aspx

[141] D. Gupta, K. Phadatare, A. Shaikh, and M. Pawale, "Material Optimization of Gear and Pinion For Planetary Gearbox," Masters, University of Mumbai, 2015.

[142] Steel Express, "EN24T Steel Properties," Wolverhampton, pp. 17–19, 2014. [Online]. Available: https://www.steelexpress.co.uk/engineeringsteel/EN24T-properties.htmlhttp://www.steelexpress.co.uk/engineeringsteel/EN24T-properties.html

[143] Ed Vitz, John W. Moore, Justin Shorb, Xavier Prat-Resina, Tim Wendorff, and Adam Hahn, "22.7: Corrosion - Chemistry LibreTexts," 2020. [Online]. Available: https://chem.libretexts.org/Bookshelves/General{_}Chemistry/Book{%}3A{_}ChemPRIME{_}(Moore{_}et{_}al.)/22{%}3A{_}Metals/22.07{%}3A{_}Corrosionhttps://chem.libretexts.org/Bookshelves/General{_}Chemistry/Book{%}3A{_}ChemPRIME{_}(Moore{_}et{_}al.)/22{%}3A{_}Metals/22.07{%}3A{_}Corrosion{#}mjx-eqn-1

Appendix A

Appendix for Chapter 3

A.1 Corrosion Survey Methodology

The equipment and technique used to collect the samples in the depot were as follows. The aim of this section is to allow the repetition of the data collection in any future work.

A.1.1 Equipment used in collection of replicas

1. 50ml Microset gun
2. Microset 101 FF Black replicating compound
3. Microset mixing nozzles
4. Spreading nozzles (project design not Microset)
5. Compressed air can
6. Paint colour shaper - flat chisel
7. Backing paper
8. Plastic lock bags
9. DSLR camera
10. Small stickers

A.1.2 Technique used in collection of replicas

Steps used to collect axle corrosion sample data.

1. **Inspect axles to identify areas of interest**

Areas of interest are often identifiable because axles have already been inspected by professionals who have marked them. The identified areas are areas where the operators have found damage that is cause for concern.

2. **Label and photograph sample areas**

   Areas of interest and labelled and photographed for later analysis. Small stickers are placed near these areas to allow for a size reference in photo analysis. The diameter of the axle at the sample sites is measured. Any observations about the target areas are also noted at this point.

3. **Clean target areas**

   Areas have been shot blasted by this point. This leaves the area clear of any corrosion products or paint, however a layer of dust is present. After some experimentation compressed air was found to be the best way to clean without introducing debris into the target areas. Areas were sprayed until they became visibly shiner, indicating the removal of the dust.

4. **Assemble Microset gun parts** The parts of the Microset kit are assembled with the new nozzle design. It worth noting that if the replication fluid is left too long it hardens in the mixing nozzle, rendering it useless. If there are multiple sites to be assessed these should be prepared before hand to allow the reuse of the same nozzle on several sites.

5. **Application of the replicating compound and spreading**

   The compound is squirted onto the general area of interest. Then, using the flat chisel, it is spread onto the surface to ensure the elimination of air pockets and that all the geometries are filled with compound.

6. **Application of backing paper and curing time**

   The previous spreading process leaves a very thin layer of compound on the surface, which would rip if when removed. To avoid this more compound is added to the site to provide a thicker surface. Backing paper is then applied to the back of the sample and the sample is left to cure for 30mins.

7. **Final steps**

   The last steps are to label the samples to allow identification later. The axial direction is also recorded on the sample. The samples are then slowly peeled back off the surface to produce the replica. These are then stored before analysis with the Alicona machine.

The replicas collected are then analysed using the Alicona machine. The process and settings used to collect this are as follows.

1. **Samples glued to flat surface**

Due to the precise nature of the Alicona, there was significant variation present due to folding or crinkling of the backing paper effecting the samples. There was also an occasional problem where a draft, due to a door opening, would move a sample mid scan. This was accounted for by glueing the samples to a piece of plywood to provide a flat, stable surface for measurement.

2. **Settings on the Alicona**

   The Alicona machine was used with a 5x magnification lens attached and with a 5 micron lateral resolution and a 0.46 vertical resolution. Light settings were set manually and resulting data did not display errors due to high or low reflection.

Appendix B

Appendix for Chapter 5

B.1 Finite Element analysis of Samples

The Finite Element software used was ANSYS Workbench 2019 R2, a commonly used software in research and industry. The layout of the simulation can be seen in Figure B.1. The following section details the process used for the Finite Element study.

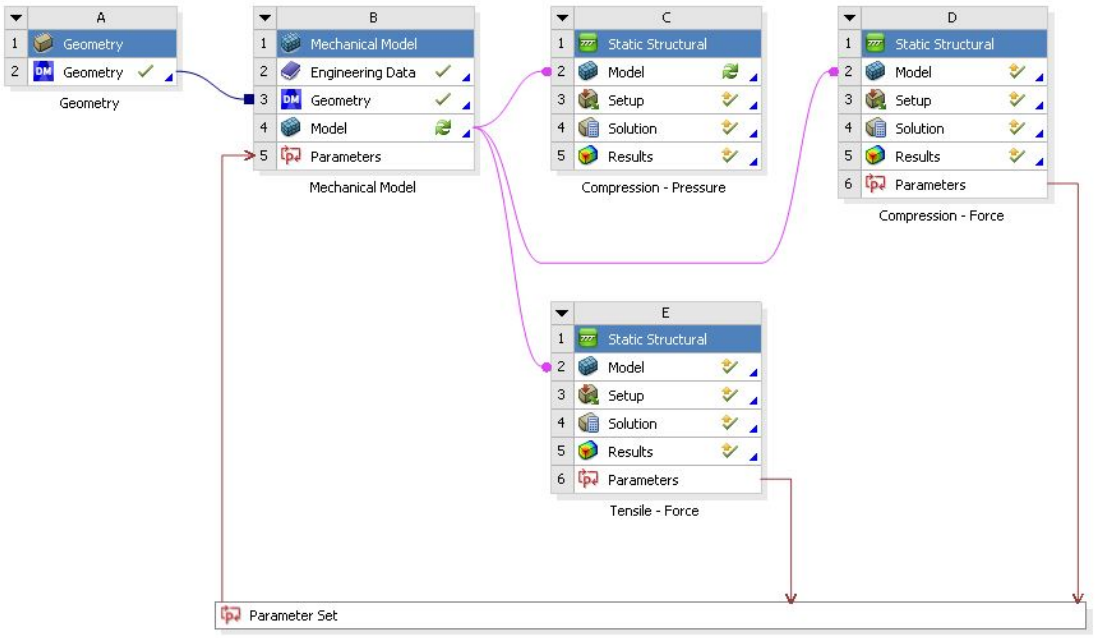

Figure B.1: Layout of ANSYS Workbench simulation carried out to verify sample suitability

B.1.1 Geometry and material properties

Initially the geometry was produced in the Design Modeler software package. The geometry was designed as shown in Figure B.2, based on the previous design work. This was a smooth sample that did not include any of the expected corrosion damage on the sample.

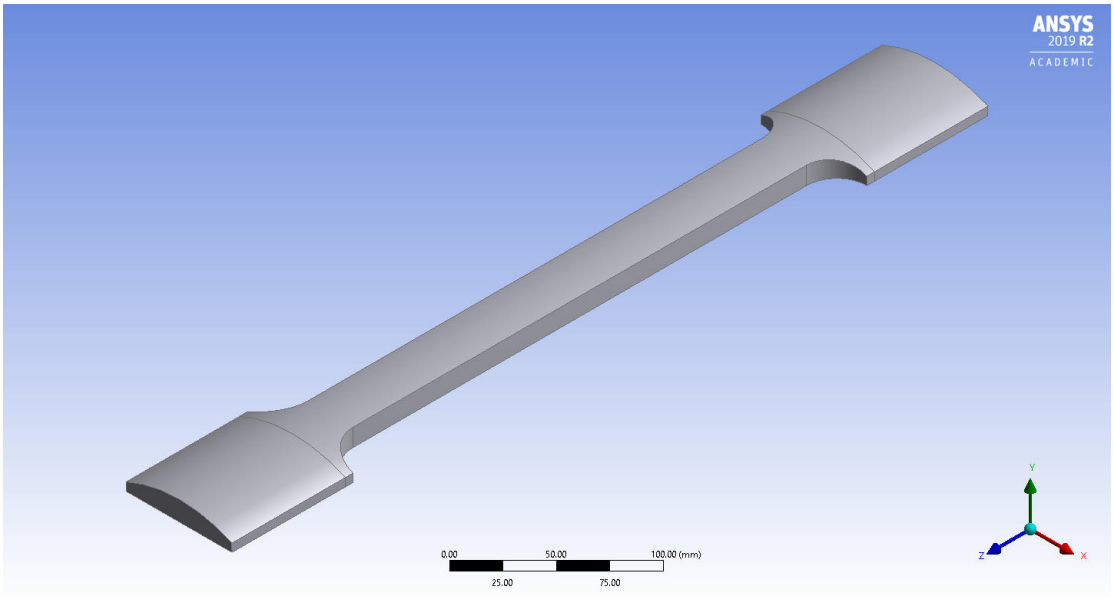

Figure B.2: Sample geometry produced in Design Modeller

After producing the geometry, two of the samples were imported into a workspace, as would be in the final rig. These were kept as two separate bodies, and not fused together. This improved the fidelity of the model to the real scenario, at the cost of increased complexity.

The material properties can be seen in Table B.1. These parameters were designed to replicate the properties of EA1N steel.

Table B.1: Mechanical properties of EA1N steel used in Finite Element analysis

Material property	**Unit**	**Value**	**Source**
Young's modulus	GPa	210	[134]
Poissons ratio	-	0.30	[134]
Yield strength	MPa	320	[17]
Fatigue limit	MPa	200	[15, 16]

B.1.2 Boundary conditions

Boundary conditions are a vital part of any finite element simulation. Without boundary conditions, no simulation can be performed, as they define the limitations and inputs of the simulation. Poorly defined conditions can lead to highly precise but misleading results.

Contacts

The contacts between the two back to back samples were defined as shown in Figure B.3. The areas of contact between the samples, that would be within the area of the jaw faces, were set to use a no separation conditions, these were the highlighted areas in Figure B.3b and Figure B.3c. The no separation contact definition would replicate the clamping force between the jaw faces, preventing any relative movement between the samples in these areas. The edges of these regions also had the same conditions applied.

The remaining area of contact, highlighted in Figure B.3a, was set as a frictionless contact. This contact was preferable, as the normal pressure would equal zero if separation occurred, as expected, and no sliding was predicted. This made the contact condition more appropriate than the others available that either included an unnecessary friction coefficient or prevented separation.

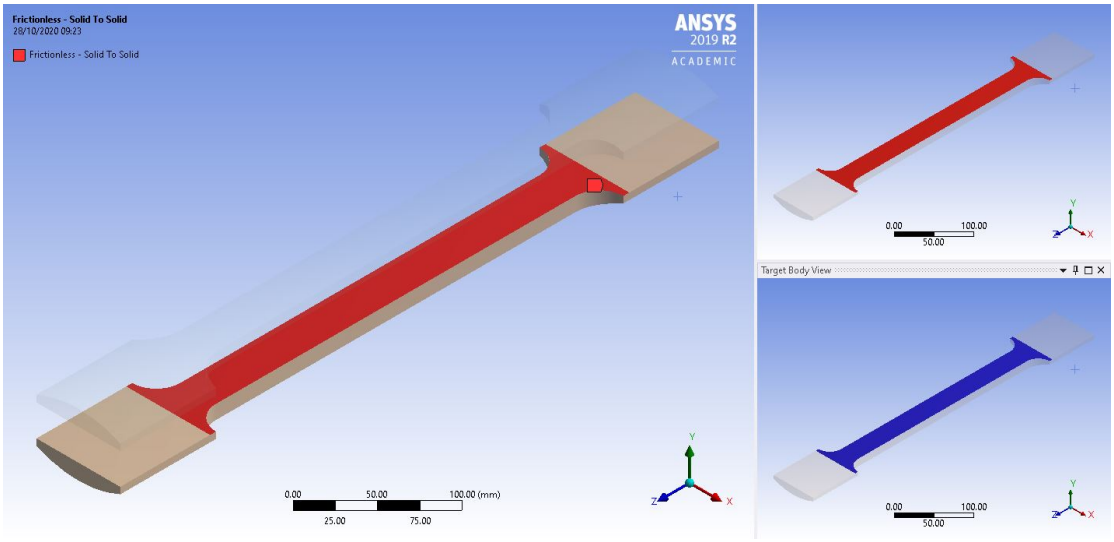

(a) Location of the frictionless contact condition

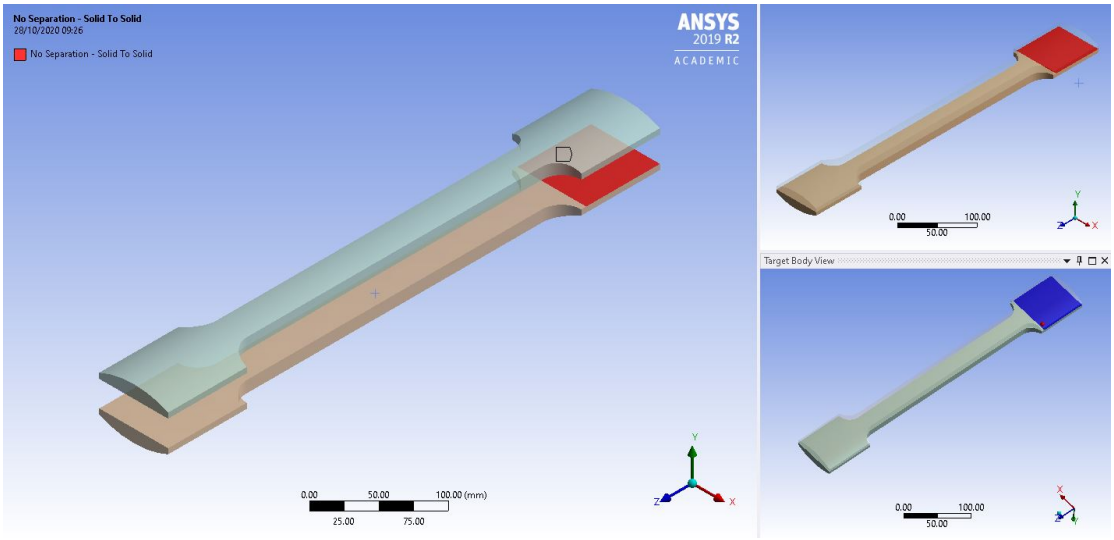

(b) Pair of faces with no-separation contact condition (top)

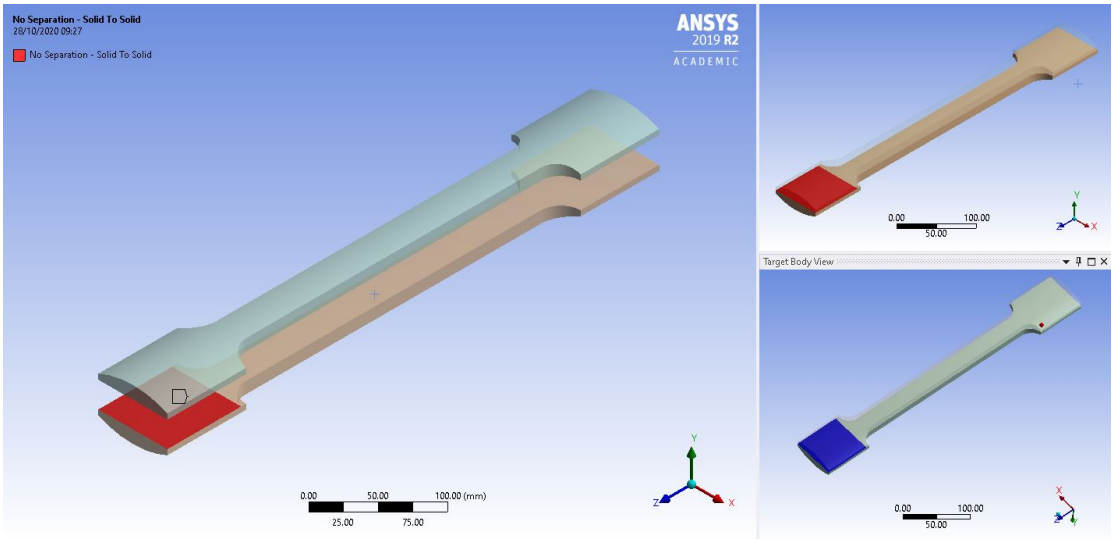

(c) Pair of faces with no-separation contact condition (bottom)

Figure B.3: Contact conditions between the two samples used in Finite Element analysis

Loading conditions

The tensile boundary conditions can be seen in Figure B.4. The aim of the conditions used was to simulate the situation that the samples would undergo during the experiment. In the case of the tensile part of the stress cycle, one end (fixed end) would be firmly clamped in place, preventing any movement. The other end (forced end) would have a force applied through the jaw faces clamped onto the sample. The jaws on the forced end would prevent any movement, other than in the direction of the applied load.

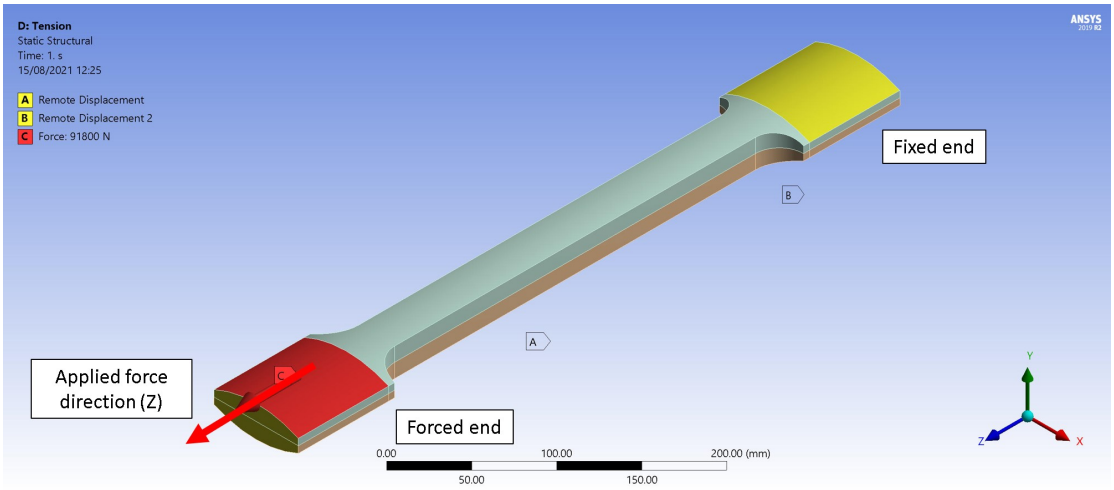

Figure B.4: Boundary conditions used during Finite Element analysis to replicate the moment of maximum tension during the stress cycle

To replicate the experimental conditions the boundary conditions were as follows, as can be seen in Figure B.4. The fixed end had the faces that would be in contact with the jaws, fixed by a remote displacement condition, preventing movement in the X, Y and Z directions as well as forbidding rotation. The faces the condition was applied to were the two curved faces that would be in contact with the jaw faces and the flat ends of the samples.

The forced end, shown in Figure B.4, had the tensile force applied in the direction of the arrow. The load was applied on the faces that would be gripped by the jaw, as this would be the mechanism by which the force was applied in the experiment. The same faces that had the load applied to them, and the flat ends of the samples, had a remote displacement condition applied, that prevented movement in the X and Y directions as well as any rotation. This was to simulate the fact that the jaw would prevent any movement in these planes.

The compression case can be seen in Figure B.5. The situation was very similar to that of the tensile case, although with the direction that the force was applied in reversed.

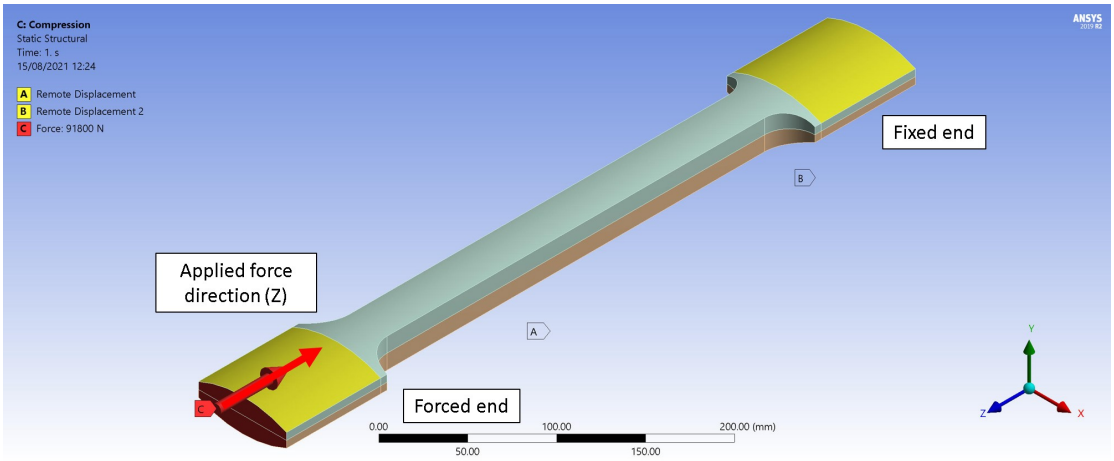

Figure B.5: Boundary conditions used during Finite Element analysis to replicate the moment of maximum compression during the stress cycle

At the fixed end the curved faces, that would be gripped by the jaws, and the flat ends of the samples, that would be in contact with the L-shaped jaw base, were fixed in all directions and with rotation forbidden. This was due to the lack of movement once the samples were firmly fixed into the jaws.

The forced end had the curved faces that would be within the jaws and the flat ends of the samples restricted to only move in the Z direction. The load was then applied as demonstrated in Figure B.5, with the load being applied on the flat ends of the samples. This was to replicate the L-shaped jaw base pressing on the sample during the compression part of the stress cycle.

The load applied in both directions was 91.8kN, to produce the same stress in the gauge length during the maximum amplitude points in the stress cycle, both in tension and compression. The 91.8kN value was calculated in Section 5.6.5.

B.1.3 Mesh settings and independence analysis

The mesh used in the analysis was designed iteratively, based on the quality metrics, and the expected locations of maximum stress. The primary defining parameter was the element size, varied as part of the independence study. The elements were of a quadratic order, and tetrahedral, to account for the curves inherent in the sample.

While the basis of the mesh was the element size, areas of expected high or interesting stress were refined to improve the resolution in these areas. The shoulders of the sample, an area where high stresses were expected, were refined by a factor of three meaning the the elements in these areas were an eighth the size of the standard element.

The surface of each sample, that would represent the corroded surface and therefore the area of interest, was refined by a factor of one, meaning the elements were half the size of standard.

The mesh independence study was required to ensure that the mesh was not having an unacceptable effect on the results of the analysis. The procedure employed was based on a factor of two being applied to the element size. When the variation in von-Mises stress was below 1% between mesh step, this was deemed an acceptable mesh variation. The results of the study can be seen in Figure B.6, with minimal variation regardless of the fineness of the mesh.

The equipment available was not able to solve the mesh for a 2mm element size, due to the number of elements. The 3mm size was the finest available, and the one used in the study as solutions had already been produced. The lack of any significant variation with element size, suggests an independent mesh throughout the analysis. The final mesh used was a 3mm element size, that can be seen in Figure B.7.

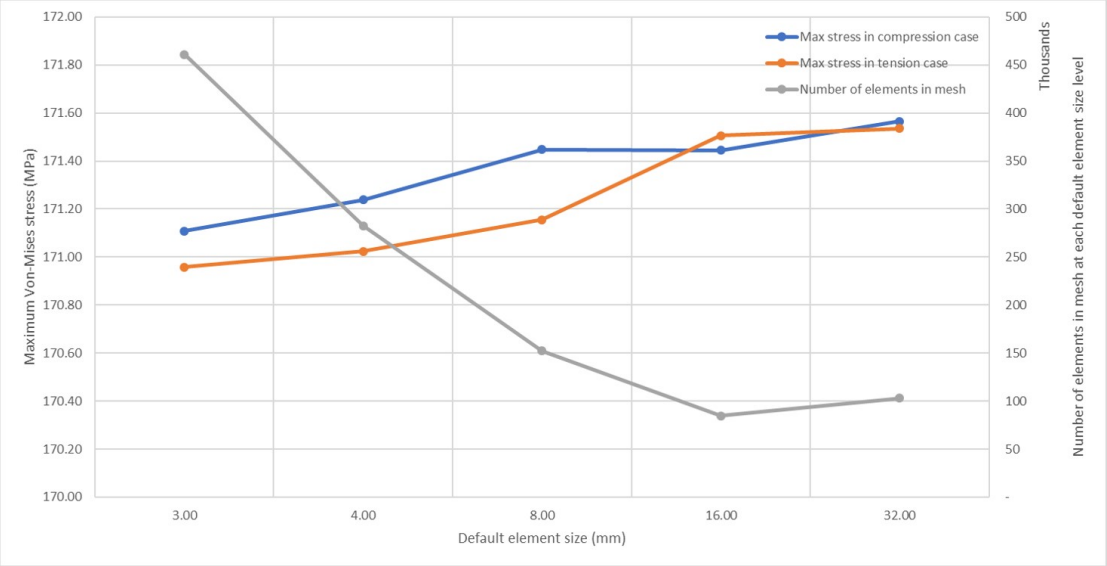

Figure B.6: Mesh independence study for the samples used in the experiment

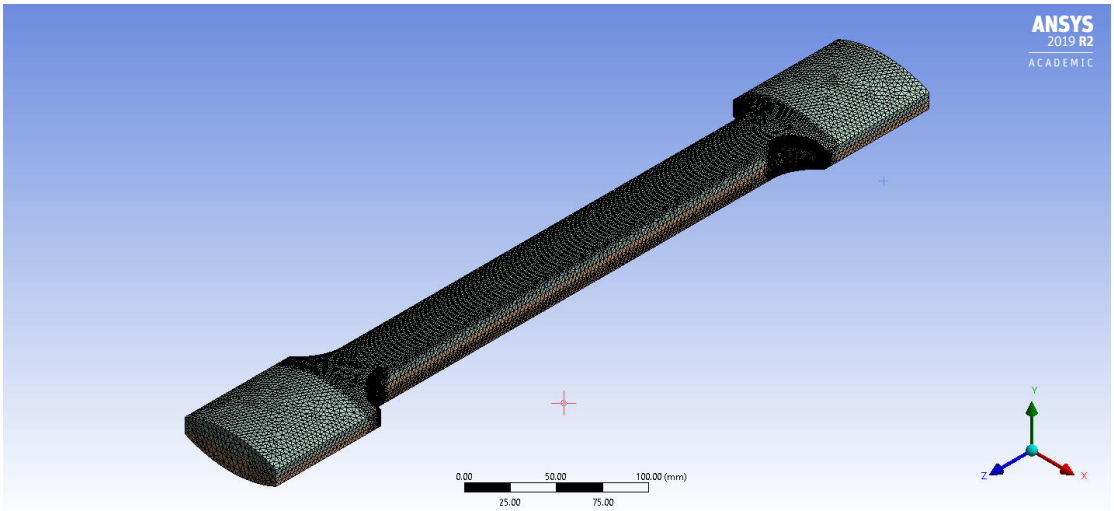

Figure B.7: Mesh independence study for the samples used in the experiment

The aspect ratios and skewness of the elements in the mesh, were also evaluated for any indication of poor quality elements. The results of this analsysis can be seen in Figure B.8, and were judged to be acceptable based on ANSYS documentation [135].

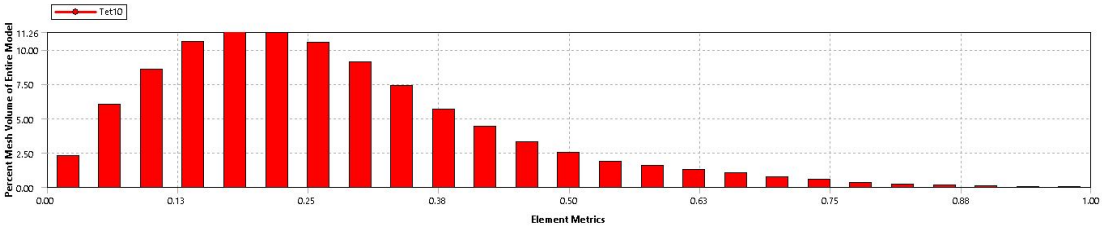

(a) Mesh skewness values by percentage of elements for mesh used

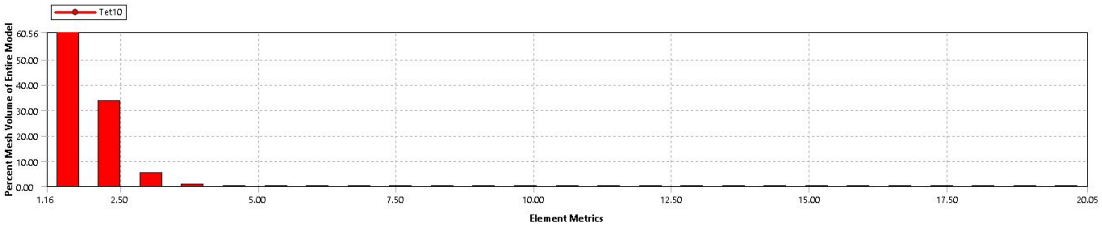

(b) Mesh aspect ratio values by percentage of elements for mesh used

Figure B.8: Mesh quality indicators produced by ANSYS program

B.2 Design and manufacture of jaw assembly

B.2.1 Design process

Requirements

The jaw assembly made as part of the experiment had several requirements:

- **Be able to withstand the forces without deflection**

  The aim of the experiment was to produce stress within the sample being tested. This would be made complex if there was significant deflection in the jaws, either making calculations complex or in a worst case moving the axis of loading. In an extreme case permanent damage to the jaw assembly or sample could occur.

- **Be able to apply sufficient gripping force to hold the samples with no relative movement**

  The samples needed to be held without slipping, to ensure the full force was applied. This also prevented fretting fatigue and the failure of the rig over time.

- **Attach to the existing rig by the set attachment points**

  The new jaw assembly had to be compatible with the existing connection points on the rig. It should not foul any other limitations, such as protrude from the ram head preventing full retraction.

- **Be re-usable for future tests**

As the cause of the rig being available was the lack of suitable jaws for many tests, the lab requested that the design be capable of adaptation and reuse for future experiments.

To reduce development time, it was decided to base the design on an existing jaw assembly. This can be seen in Figure B.9. Briefly, it consisted of an L-shaped steel section with a circular stem protruding from the bottom, then forming the attachment base. There was a boss on the bottom to assist with locating the assembly in the machine.

The jaws themselves consisted of removable faces that were knurled on the front to improve gripping force. A backing plate was used to spread the load that was applied by six M10 bolts that screwed into tapped holes in the L shaped base. These particular jaws were rated to use in a 100kN machine, with a maximum sample width of 12mm using the existing jaw faces.

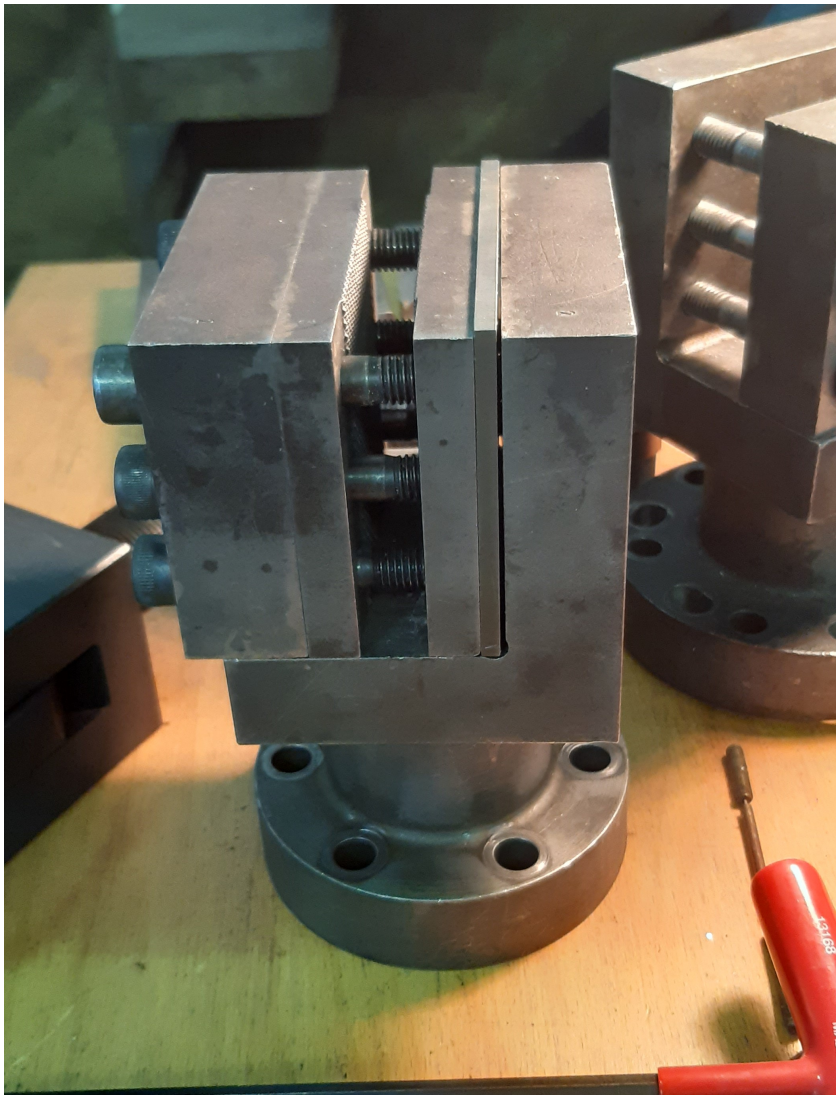

Figure B.9: Existing jaw assembly that formed the basis for the new design

A potential flaw in this design, was the lack of anything preventing the jaw assembly opening in a hinge like fashion during a tensile test. However, this was reported as not being an issue by previous users and lab technicians.

The reason that these jaws could not be used was that the connections on the bottom were designed for use on a electrically driven rig and were not compatible with the Schenck rig.

Design

After measuring the existing jaws and looking at the sample requirements, a new design was produced. This was achieved through an iterative mixture of analytical calculations and finite element techniques to arrive at the final design. The CAD model can be seen in Figure B.10. Similar to the original concept, the assembly consists of 4 parts:

1. **L-shaped base**

   The base was very similar to the original design, including the locating boss on the bottom. Changes included the addition of an extra pair of bolt holes to apply force and the change in the attachment points on the bottom.

   The locations of the threaded holes were also moved to the backing plate to allow improved access for tooling, given the positioning of the rig in the lab. The stress reliving feature in the corner was also removed to lower production costs.

2. **Two curved jaw faces**

   The jaw faces consisted of a bar of metal with the profile of the curved sample cut out of one side. The curved face was not knurled as originally intended, due to the lack of equipment to perform a rolling process on a concave face, but was milled with a cross hatch pattern to increase the friction between the jaw faces and the samples.

3. **Backing plate**

   The backing plate contained the tapped holes to accept the bolts that applied the force. The primary aim of this part was to spread the applied force across the sample. The use of a backing plate also meant that in future, other jaw faces could be produced and applied to the assembly to allow reuse without significant cost.

   The depth of the backing plate was selected to allow the maximum force from the bolts to be applied, exceeding the rule of thumb value of a tapped hole being 2.5 times as deep as the nominal diameter of the bolt it is accepting. Below this value the bolt would tear out of the plate before the maximum load from the bolt had been reached.

The force is created by eight M10, coarse thread, cap-head bolts, compared to 6 bolts in the original concept. The use of cap-head bolts was due to the ability to fit more bolts within the same area, increasing the potential force, due to the lack of requirement to fit a tool around the bolt head as is required with a hex head. The whole assembly was attached to the rig by eight M16 clearance holes, with threaded rod and nuts to attach it to the holes in the rig.

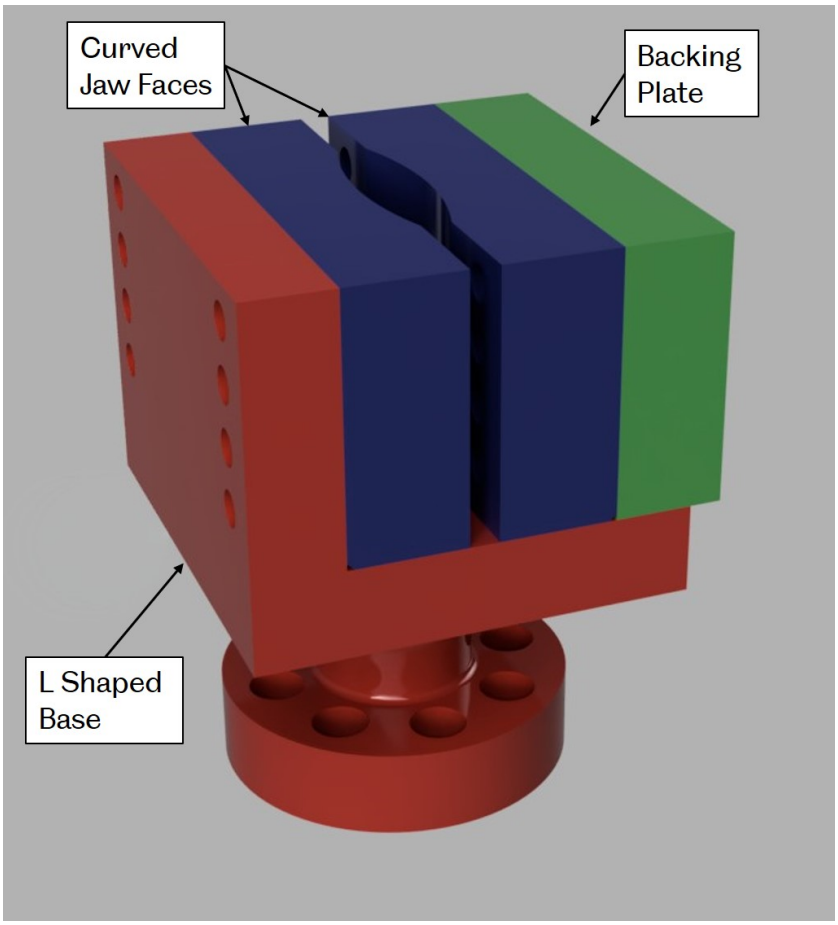

Figure B.10: Rendered CAD model of jaw assembly produced for the project

All of the parts were made of hardened steel, to increase strength and reduce the risk of deformation of the assembly during use.

Torquing of bolts

A key calculation of the rig was the amount of force that should be applied to the sample to prevent slipping. In the compressive cycle, the base would be able to apply the force to the samples, and the jaw faces prevent lateral movement. However, in the tensile cycle the force would be applied by the jaw faces, requiring friction between the faces sufficient to overcome the tensile force.

Bolt tightening force is described by Equation B.1 [136]. This relates the tightening torque T to the tightening force F_i, and the bolt diameter d. The other parameter, K, denotes the torque coefficient, this is the a value that takes account of the friction at both on the threads and underneath the cap head, and broadly accounts for the amount of force required to turn the bolt in the tapped hole and so is lost to friction. The torque coefficient can be calculated using Equation B.2 [118] where d_m is the major diameter, ψ is the thread helix diameter, μ is the coefficient of friction in the thread, α is the thread angle and μ_c is the friction coefficient under the bolt head. The torque coefficient is complex to calculate in most cases, however 0.2 is taken as standard estimate in most steel on steel fastening situations [118].

$$T = KF_i d \tag{B.1}$$

$$K = \left(\frac{d_m}{2d}\right) \frac{\tan\psi + \mu \sec\alpha}{1 - \mu \tan\psi \sec\alpha} + 0.625\mu_c \tag{B.2}$$

The force that was required to be applied was enough to produce a friction force that can overcome the tensile force of the rig. This tensile force had been established as 91.8kN.

The required resultant force can be estimated using the basic friction equation given in Equation B.3. The coefficient of friction between the samples and the jaws was not known, but the estimates from static friction between a dry, clean steel steel contact, ranges from 0.5-0.8. The friction between the clean but corroded geometry of the sample and the cross hatch pattern milled into the faces was likely to be at the upper end of this estimation. 0.5 was used as a conservative estimate, leading to a required pre-load force of 200kN.

$$F = \mu R \tag{B.3}$$

Based on this, the bolts selected would have to be capable of withstanding a pre-load of 25kN each. Metric bolts come in a variety of property classes based on the ISO 898/1 standard [137]. To determine the correct bolt class to use for a given pre-load, tightening torque tables [138] are produce with maximum pre-load, based on different coefficients of friction.

Due to this being a large unknown factor, and to prevent issues such as galling, an anti-seize compound was used to reduce the coefficient of friction to a known level. Rocol J166 [139] was used due to its low coefficient of friction of 0.15 when used with steel fasteners, and its resistance to water. The lower coefficient of friction would also increase the maximum force provided by the bolts.

From the torque tables with the known coefficient of friction, it was found that only 8.8, 10.9 and 12.9 grade bolts would be capable of providing this force. The 8.8 bolt would be able to provide the required force, but with a very slim safety of around 1.15, so was discounted leaving only 10.9 and 12.9 grade. Based on the availability and cost difference, it was decided to use 12.9 grade due to the increased force possible and so the increased margin for error.

Once the bolts had been specified, it was possible to calculate an estimate for the torque coefficient. The friction coefficient were both set to 0.15, due to the application of the lubricant. After contacting the manufactures, the thread mean diameter and thread angle were found to be 9.026mm and 60 deg respectively. The thread helix angle was calculated using Equation B.4 [140], with the number of starts, N, being given as one, the pitch, P, was known to be 1.5mm and the effective diameter, d_2, as 9.026mm. The angle was found to be 3 deg . Using these values in Equation B.2, gave a final result for the torque coefficient of 0.157.

$$\psi = \arctan\left(\frac{NP}{d_2\pi}\right) \tag{B.4}$$

Based on the torque tables, the maximum tightening torque for M10 12.9 grade bolts was 93Nm. Using this value and the the torque coefficient of 0.157 in Equation B.1, the force that could be provided by a single bolt was 59.2kN, 237% of the estimated required value of 25kN. This would produce a total clamping force on the samples of 473.9kN.

Based on this calculation the jaw would be more than capable of holding the samples stationary, and in future would be able to hold steel samples for tensile loads up to 237kN, close to the 250kN maximum capacity of the rig. The ability to over apply clamping force, allowed for a healthy factor of safety in this experiment, and increases the use of the rig, for following experiments.

Finite element checks

Finite Element checks were carried out using the same broad process as with the samples earlier. The aim was to check that the jaw assembly would not fail under loading, or produce any significant deflection that may prejudice the results of the experiment. The analysis was comprised of two static structural investigations, one looking at the highest force tensile case and one looking at the highest load compression case.

The material properties were set to those of EN24 hardened steel, shown in Table B.2. This was based on initial calculations of material property requirements conversations with workshop machinists to determine their capabilities in terms of materials that could meet the requirements.

Table B.2: Mechanical properties of EN24 hardened steel used in finite element analysis of jaw assembly

Material property	Unit	Value	Source
Young's modulus	GPa	205	[141]
Poisson's ratio	-	0.29	[141]
Yield strength	MPa	680	[142]

The boundary conditions were as follows. In both the compressive and tensile cases the lower faces of the of the jaw, that would come into contact with the main rig, were set to fixed displacement with no displacement of any sort.

The holes where the assembly would attach to the rig by the use of threaded bar were constrained to only displace vertically (Y direction), to replicate the force from the threaded bar resisting any twisting movement. The vertical face that contained the holes that would be used by the bolts applying the clamping force was constrained to not deflect in the horizontal (Z direction), or rotate, as this would be prevented by the bolts as the jaw faces and backing block pressed on the bed of the jaw. This can be seen in Figure B.11.

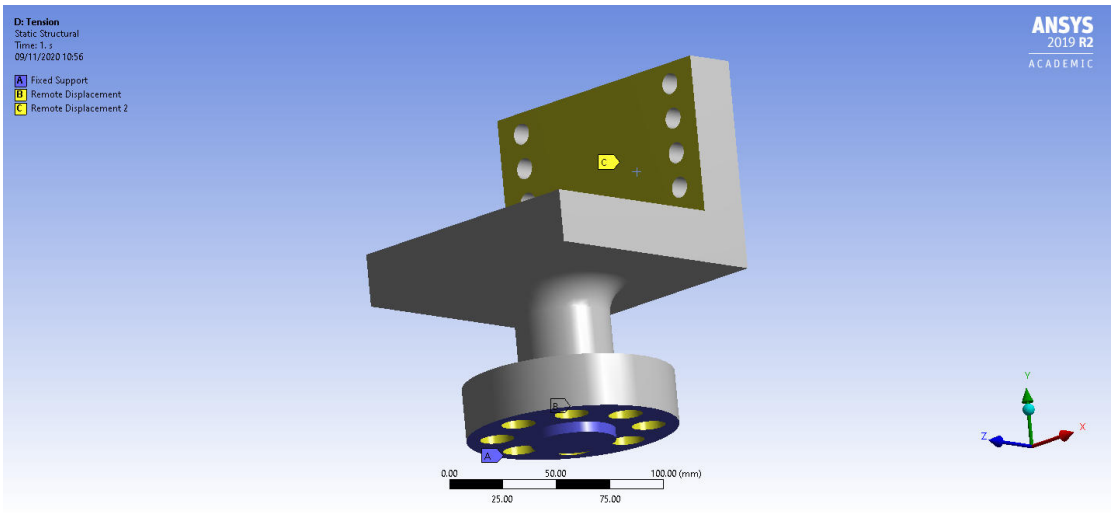

Figure B.11: Boundary conditions used on jaw base

The loading in each condition was different to reflect the two cases. In tension the load was applied to an area that represented the location and size of the end of the sample. While this would not be entirely accurate, as the clamping assembly would spread this load somewhat, it represented a worst case scenario allowing for a margin of error in the results.

In the tensile case, all the upward force was defined as acting within the bolt holes on the vertical plate. As would be the case in such a scenario, as it represents the only contact points between the clamping assembly and the jaw base.

The mesh conditions were set similar to the ones used on the samples, with areas of expected high stress being refined to increase the density of the mesh. The main variable was the default element size, that began at 32mm and reduced by a factor of two with each mesh step, representing a rough doubling in the number of elements in the mesh. After initial tests to identify areas of high stress, the two radii on the lower stalk were refined by a factor of three and the the corner between the base and vertical plate was refined by a factor of two. A mesh independence study was then performed, and can be seen in Figure B.12. 2mm was the lowest mesh performed as it was not possible, and unnecessary, to study a finer mesh.

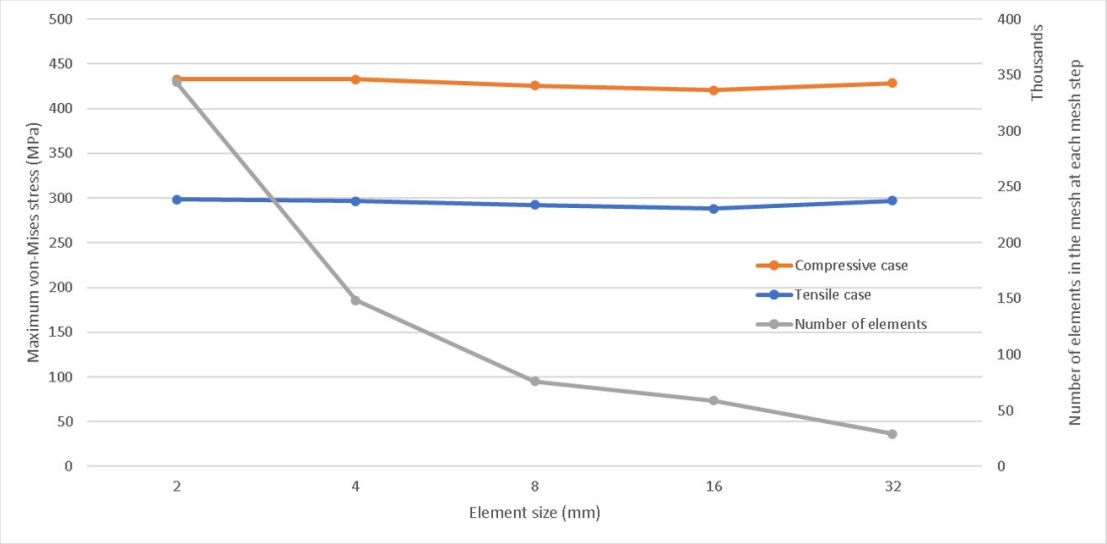

Figure B.12: Mesh independence study carried out for analysis of the jaw base

Based on these results shown in Figure B.12, the 2mm mesh was deemed acceptable due to the minimal change in stress after significant change in mesh density. The mesh was checked to ensure it's quality was acceptable, with the results for skewness and aspect ratio shown in Figure B.13 and Figure B.14.

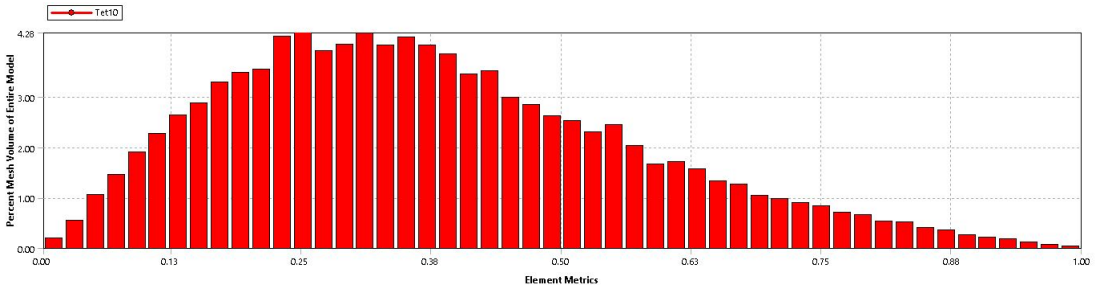

Figure B.13: Mesh skewness metrics for the jaw base using chosen mesh settings

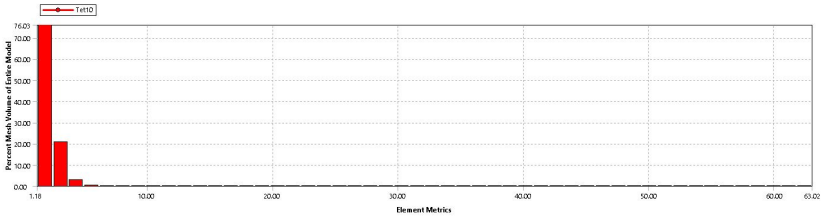

Figure B.14: Mesh aspect ratio metrics for the jaw base using chosen mesh settings

While the aspect skewness results were acceptable, the maximum value of the aspect ratio at 63.02 was concerning as this is much higher than would be desired [135]. However, investigations showed that these high aspect ratio values each represented a single element, away from areas of interest, while the vast majority of elements had acceptable aspect ratios.

The results of the compression study gave no cause for concern. The results can be seen in Figure B.15. The maximum stress occurs at the lower fillet, with a maximum value of 144.35MPa. This value is well within the limitations of the material, given in Table B.2, and so presented no issues to the rig in terms of failure. The displacement result was also acceptable with a maximum displacement of 0.02mm in the jaw, shown in Figure B.16, with the vast majority of this occurring in the vertical axis and only trace movement in any other axis. This was as expected due to the central loading parameters.

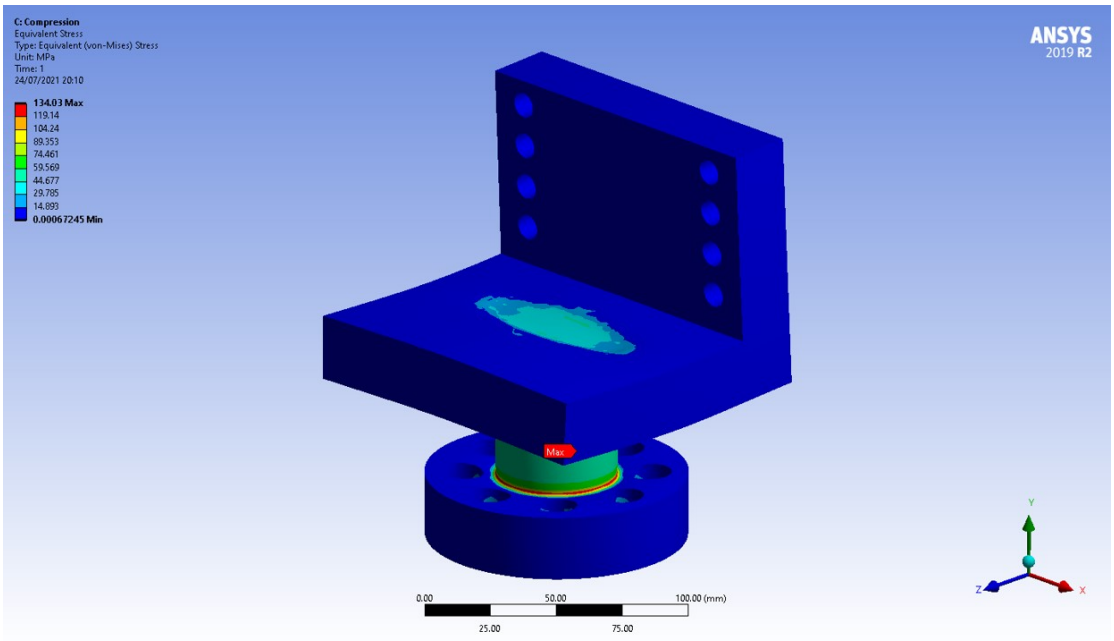

Figure B.15: Equivalent stress result for the jaw undergoing compression loading

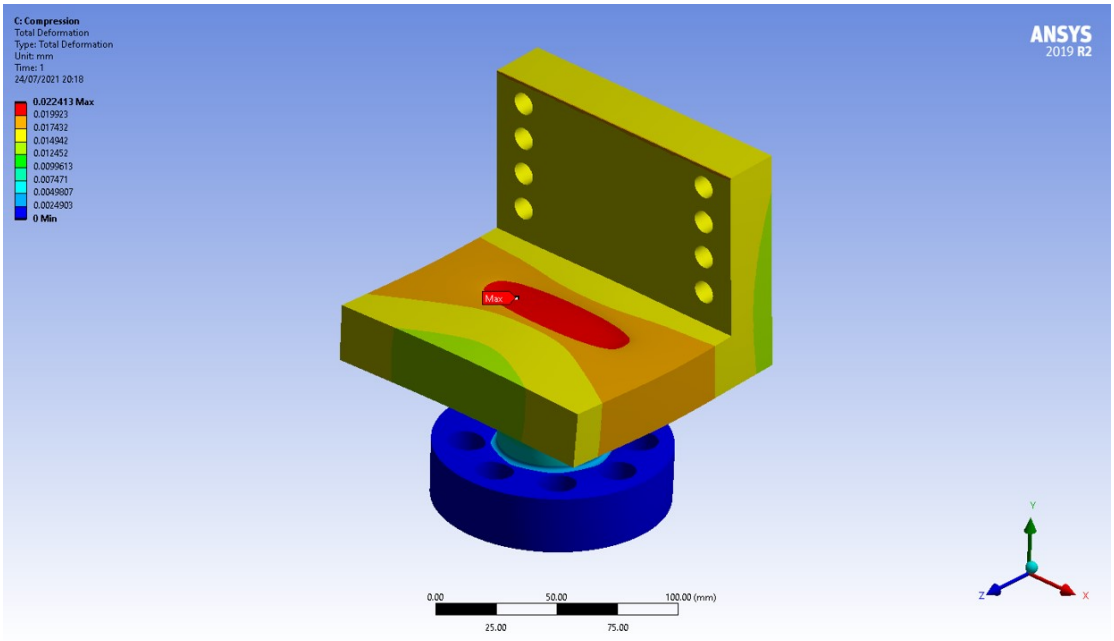

Figure B.16: Total displacement result for the jaw undergoing compression loading

The tension case was more of a cause for interpretation. Due to the off center loading environment cause by the bolts, the stress conditions were more complex than in the compression case. The results can be seen in Figure B.17. Slightly elevated stresses can be seen at the join in the L-shaped base and the lower radius, as would be expected given the location of the loading.

The maximum stress, 298.6MPa, in the upper radius beneath the vertical section, can be seen in Figure B.18. This value was slightly above twice that of of the compression case, but still well within the fatigue limits of the hardened steel used to manufacture the component, detailed in Table B.2. This suggests that the jaw would not experience failure during the operation of the experiment.

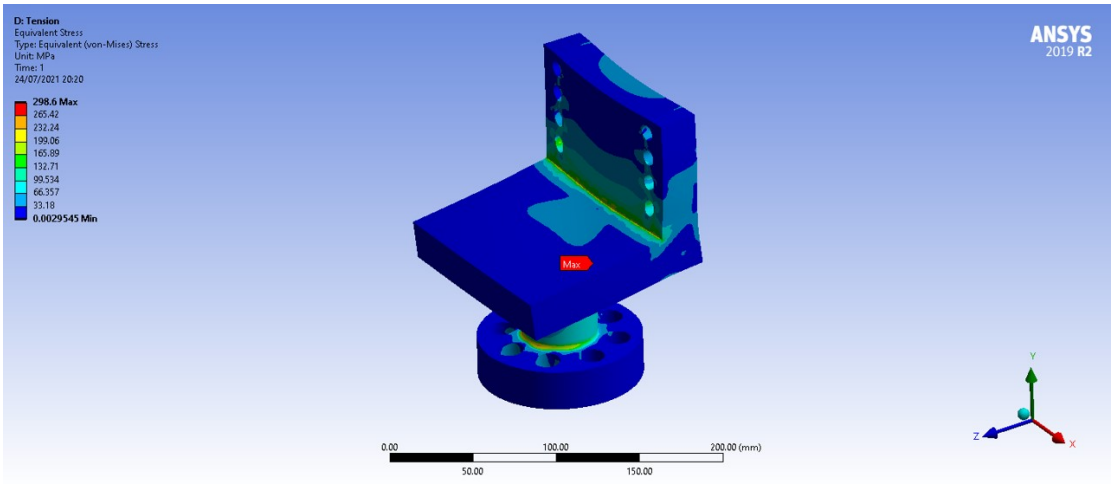

Figure B.17: Von-Mises stress of the jaw base in tension

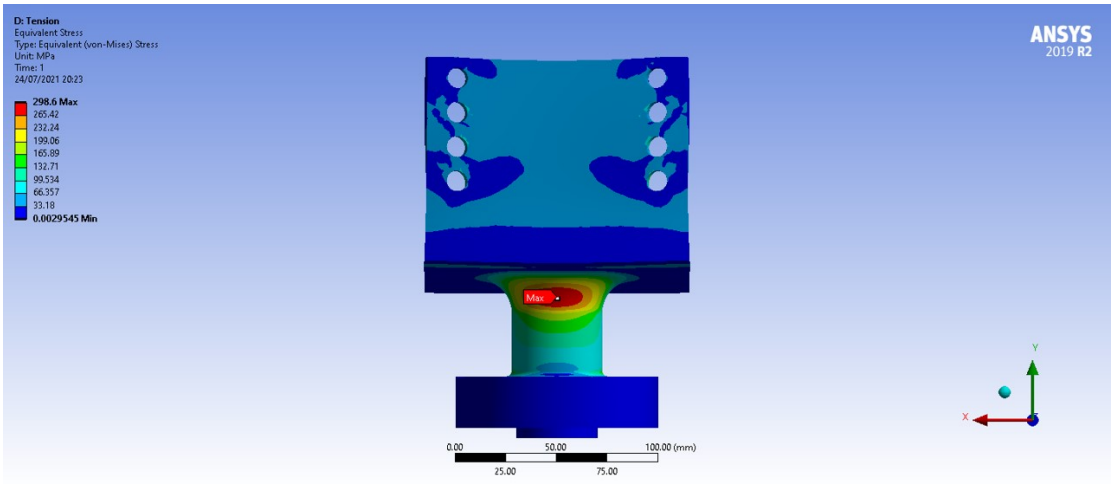

Figure B.18: Von-Mises stress of the jaw base in tension, with the area of maximum stress shown

The displacement in the tensile case was around 0.09mm. This can be seen in Figure B.19. A concern was the apparent angle that the L-shaped base takes on as the vertical section rises, potentially having and effect on the samples within the jaw. However, the displacements were very small and so unlikely to be problematic. A secondary reassurance was that the design was based on a previous jaw that was rated for higher stress levels, and demonstrated no issues or failures.

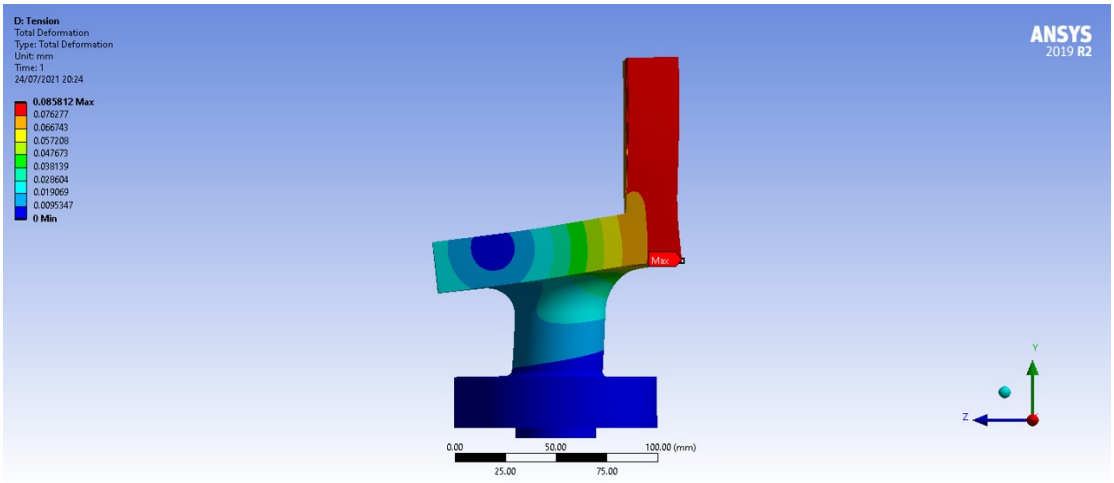

Figure B.19: Total displacement result for the jaw undergoing tension loading

In conclusion the results presented in this section indicated that the jaws would be capable of withstanding the loading required for the experiment without failure. Any displacement would also be negligible and not effect the experimental outcomes.

B.2.2 Manufacture and assembly

The jaw assembly parts were manufactured at the AMRC tool shop at Sheffield University. This was done using manual lathes, mills and drills. The hardening of the EN24 steel was done using the oil bath technique and annealing to increase the hardness of the steel. Due to this process potentially warping precise features such as holes, the drilling and tapping was performed after hardening.

Once the parts of the jaw assembly had been manufactured, the assembly of the rig could take place. This was performed easily, with the threaded bar and nuts, attaching the bases to the attachment points on the rig. This was done with no lubrication.

The samples were placed into the jaw faces and the bolts applied to hold the samples in place. The lower jaw was assembled first, then was raised until the top of the sample came into contact to the upper jaw. Contact was ensured by applying a 3kN compressive pre-load to the sample. Feeler gauges were then used at either end to check for gaps, with none detected down to 0.05mm between the jaw bases and the samples at either end. The top jaw faces were then assembled.

All the bolts that applied force to the sample through the jaw faces, were torqued to 93Nm. The order they were torqued in was also important, to avoid 'pinching' the sample at either the top or bottom, preventing clean contact between the two. The order of torquing can be seen in Figure B.20, with 5Nm being added each time until the torque wrench indicated the appropriate torque had been reached.

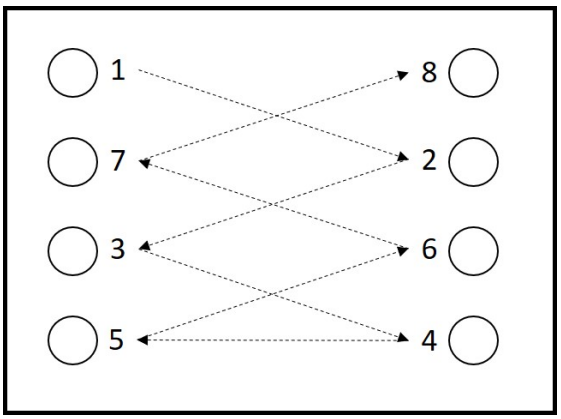

Figure B.20: Order of bolt torquing to avoid 'pinching' the samples

During initial loading testing, it was found that the samples were being pulled out of the jaws at 30kN of tensile loading, well below the calculated design estimates. On investigation it was discovered that this was due to the limited threaded length on the bolts.

Standard long bolts, are sold with only 34mm of thread at the end, the rest smooth. During the design phase this was found to be acceptable, with little margin but the tolerances of manufacture and the movement of the parts had been neglected.

At the highest levels of torque, the shaft of the bolts was being forced into the tapped holes, instead of the threaded section. This meant that the force used to tighten the bolts, was instead being used to tap the bolts.

To avoid this issue 8mm stainless steel shims were placed at the head end of the bolt, ensuring only the threaded part of the bolt came into contact with the tapped holes. This solved the issue, and the jaws held the samples, up to the required 91.8kN of force.

Addition of clamping bar

A second area of concern that was identified during initial testing was that during the tensile cycle, the jaw faces opened in a hinge like fashion with the jaw faces and backing plate moving away from the base. This was not an issue with the jaw assembly that was the basis of this design, however was one with the manufactured jaws, likely due to windage in the holes attaching the bolts to the base probably due to the smooth shaft. This was an unexpected drawback of moving the threaded holes from the base to the backing plate. To solve this issue, a locking bar was required to prevent the opening of the jaw assembly.

This was designed as a pair of bars connected by M16 bolts to clamp around the backing plate and the base, to prevent the movement. The restrictions on size, were determined by the available flat area on the base, due the the fillet that connected the L shaped section the the attachment plate. One of the bars would have clearance holes, with the other tapped.

The bolts selected were A4 stainless steel, with a maximum pre-load of approximately, 79kN when torqued to 225Nm, allowing resistance to the a maximum tensile force of 158kN. This bolt specification was sufficient for the current usage, and were in stock, but could easily be increased by using the 12.9 grade bolts used earlier in the design, increasing the maximum tensile load to 266kN, above the 250kN capacity of the rig.

The addition of the clamping bar would have an effect on the loading conditions in tension, as the load would be more central overall. The finite element model of the base in tension was updated to include the tensile force being equally spread between the contact point of the new bar and the bolt holes.

The results on the stress can be seen in Figure B.21, showing that the maximum stress dropped to 176.1MPa and the location changed to the other side of the part. This maximum stress level was 59% of the previous stress level under this loading, increasing the safety factor of the part significantly.

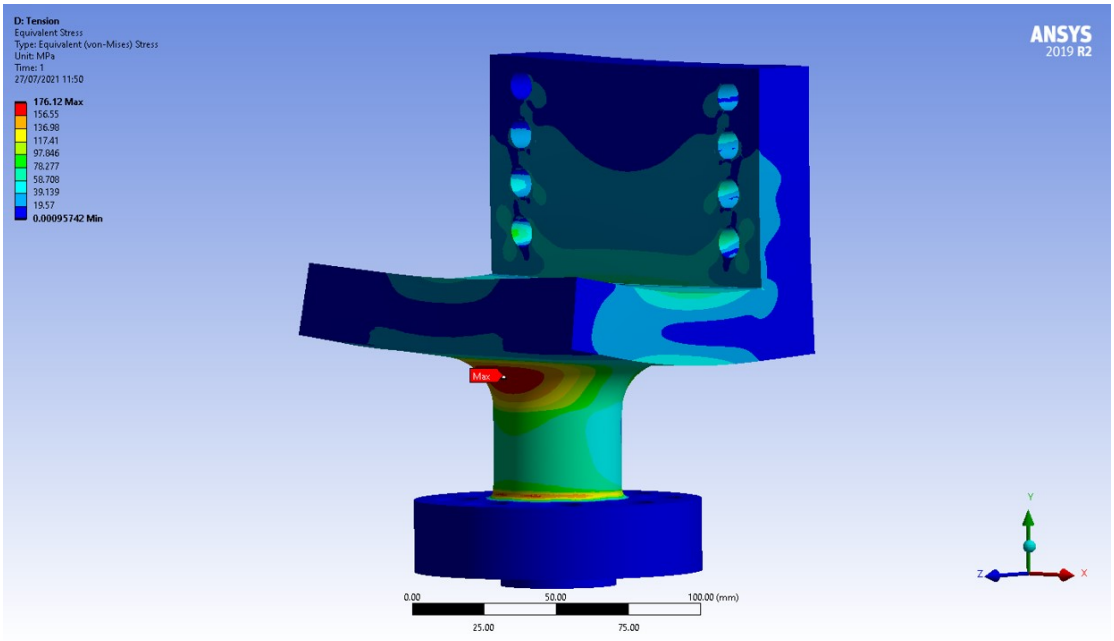

Figure B.21: Von-Mises stress result for the jaw undergoing tension loading, with the clamping bar added

The total displacement can be seen in Figure B.22. While the maximum displacement value remains at around 0.1mm, the total angle of the base remains more consistent. It was also possible that the boundary conditions were less realistic with this new loading condition, as the clamping assembly would have provided resistance to the lip of the base curving up as shown in Figure B.22. However, these results confirmed that the addition of the the clamping bar would also improve the stress environment of the jaw base and increase factors of safety.

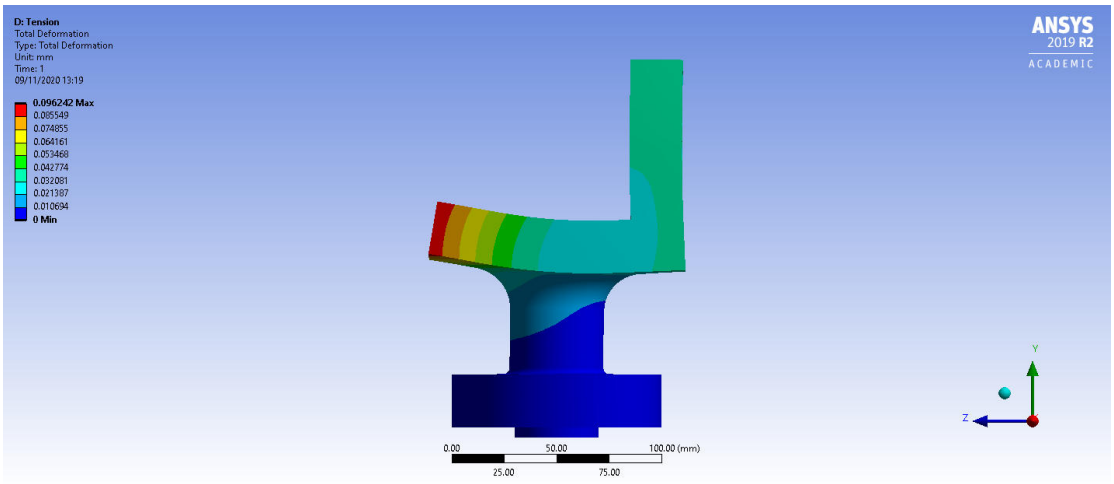

Figure B.22: Total displacement of the jaw undergoing tension loading, with the clamping bar added

The bars were made of tool steel. This was chosen due to its high hardness and strength compared to alloy steels. Initial simplistic finite element analysis had suggested that around the corners of the backing plate, when loading was applied to the locking bars, very high stresses would occur, that would cause standard steels to fail. The use of tool steel negated this problem due to the performance of the material. The jaw assemblies with the locking bars added, can be seen in Figure B.23.

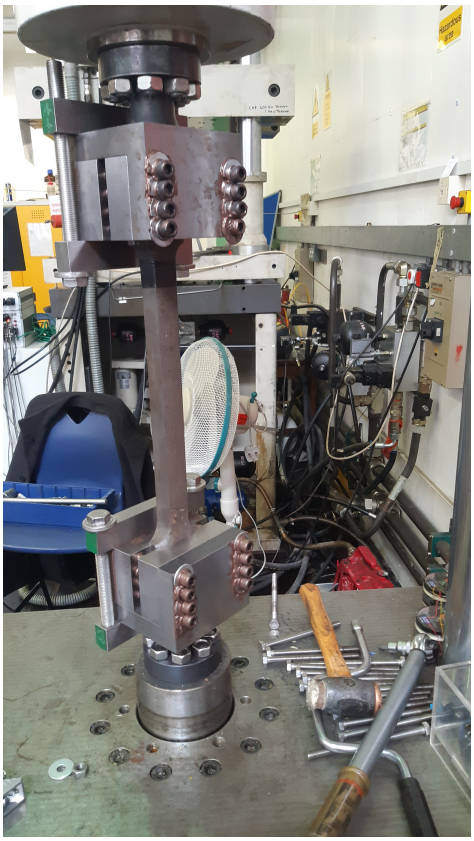

Figure B.23: Image of the jaw assemblies fitted to the rig, with the samples in place and locking bars applied

B.3 Design of new curved samples

Finite element checks

A Finite Element study was carried out to ensure the validity of the samples in terms of surviving the loading and not displaying buckling behaviours, for reasons discussed previously. The study was carried out in a vary similar way to the previous sample investigation, with the same boundary and contact conditions as well as mesh settings. These conditions, as well as the material properties, can be seen in Section B.1.

The loading was adapted to meet the same stress level in the area of interest of 120MPa, which was previously calculated as 76.6kN based on the cross section of the combined samples.

After the initial set up, a mesh independence study was again performed, using the same scale factor of two approach used previously. The results of this study can be seen in Figure B.24. The areas of interest and expected high stress, namely the faces that would be inspected and the shoulders of samples, were further refined by a factor of one and three respectively.

Despite Figure B.24 not showing a classic convergence curve, the small variation in stress given the large changes in mesh size, was deemed to be sufficient to conclude that the mesh was not having any significant effect on the results.

It was not possible to produce a finer mesh than 2mm and meshes over 32mm tended to distort due to the significant size of any single element compared to the total size of the sample. All results used the 2mm mesh as the results had already been calculated. The 2mm mesh can be seen in Figure B.25.

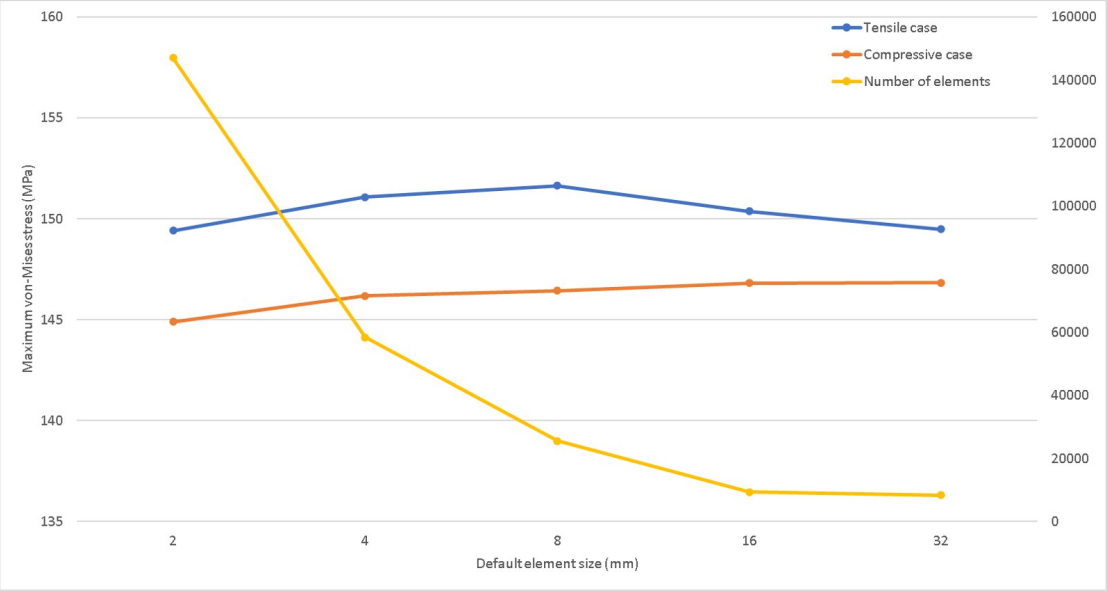

Figure B.24: Mesh independence study of new curved samples

B.4 Design of bright steel samples

Analytical checks and calculations

As the bright samples were developed from a design used only in tension [127], the slenderness calculations were performed to ensure it would be capable of working in compression without bending or buckling in the central span. Using the same approach as before, the slenderness ratio was found to be 75.61, lower than the original samples but higher than the new curved samples. This value was still below the critical slenderness ratio of 104.83. Using the Johnson parabola the critical stress to reach buckling failure was 273.8MPa, which is higher than the fatigue limit of the material so should not be a risk as the fatigue limit would not be breached.

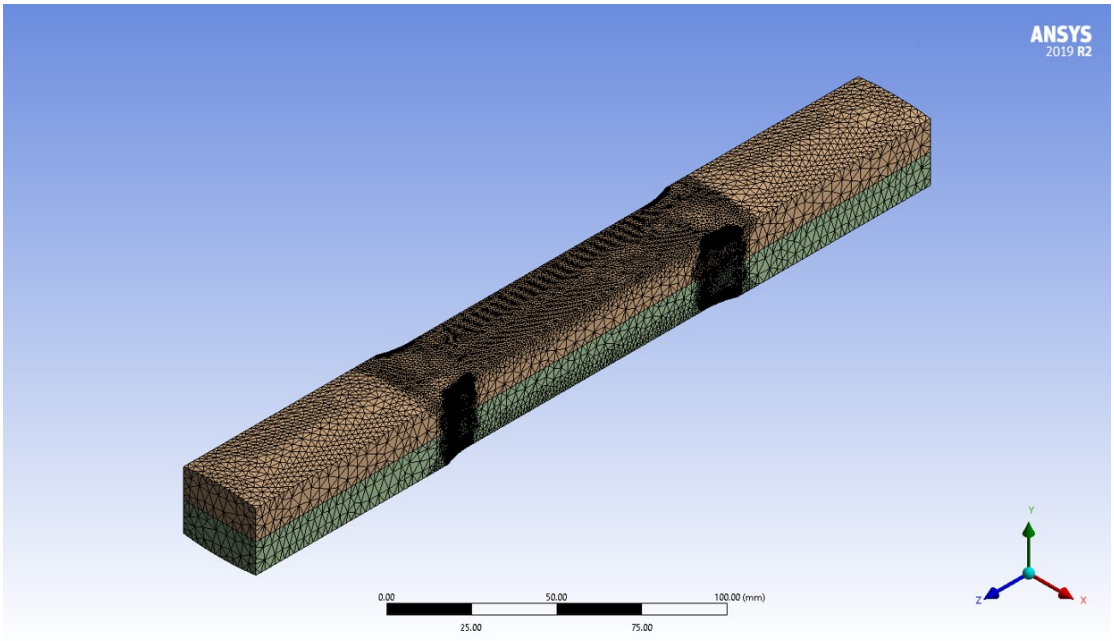

Figure B.25: Mesh of new curved samples, demonstrating areas of refinement

Finite element checks

As with the previous studies, the sample was interrogated using Finite Element techniques to test its stability for use. The boundary conditions were replicated as seen in Section B.1, although without the contacts as there was only a single sample in the experiment. The mesh settings and material properties also remained the same.

The mesh independence study can be seen in Figure B.26, showing that even with major changes in the mesh density there was no significant change in the reported stress level. This indicated that the mesh had been independent across all studied mesh sizes.

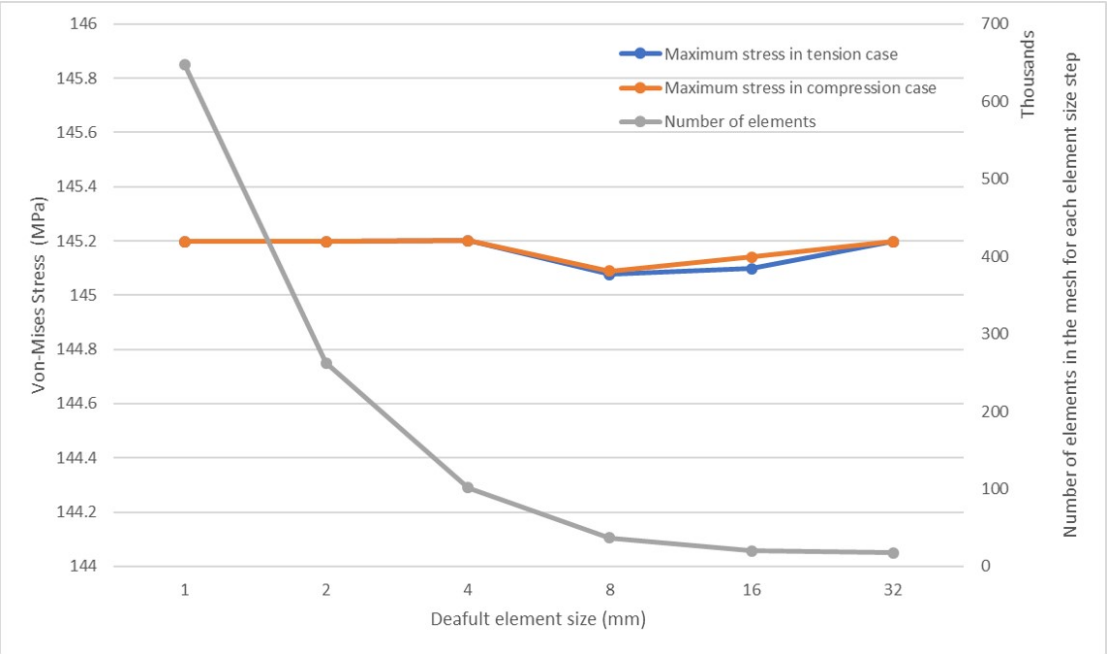

Figure B.26: Mesh independence study of bright samples

Appendix C

Appendix for Chapter 6

C.1 Temperature data from rigs

The measured temperature at each corrosion rig over the course of the experiment can be seen in Figure C.1. As can be seen, there was little variation, especially when considering absolute temperature. This was as expected as all of the rigs were in the same lab. Another factor of that contributed to the low temperature variation and lack of obvious day to night cycle was that, as a hydraulics lab, the equipment continually generated heat.

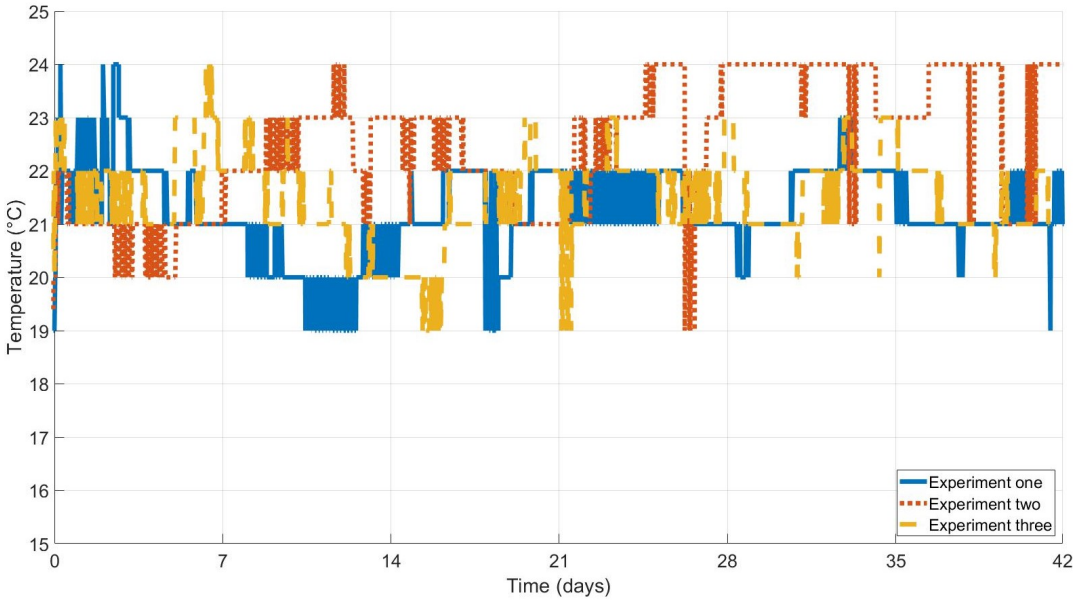

Figure C.1: Temperature at each experimental rig during the

The outcome of Figure C.1 was that the results of each experiment were comparable to each other.

C.2 Corrosive medium data

During the experiment, at 168 hour intervals, the corrosive medium was replaced. Before being replaced, however it was measured in terms of pH and conductivity. This was performed using hand held equipment detailed in Chapter 5. The pH is broadly a measure of the concentration of hydrogen ions in the solution and indicates the acidity. Conductivity is a measure of a solutions ability to carry an electrical current and indicates the amount of dissolved solids in the solution [133].

The pH values can be seen in Figure C.2. At each time step, the corrosive medium had begun with a pH value of 5.61, then reached the reported value after "6.42 months" of corrosion. The corrosive medium in every case after corrosion was more acidic than it had been at the beginning. This was principally due to the corrosive process for iron to form iron (III) oxide, seen in Equation C.1, that releases hydrogen ions [143]. The released hydrogen ions increase the acidity of the corrosive medium. The red colour of the corrosion product supports the conclusion that this chemical process was occurring rather than other oxides of iron.

$$4Fe(s) + O_2(g) + 7H_2O(l) \rightarrow 2Fe_2O_3 \cdot \frac{3}{2}H_2O(s) + 8H^+(aq) \tag{C.1}$$

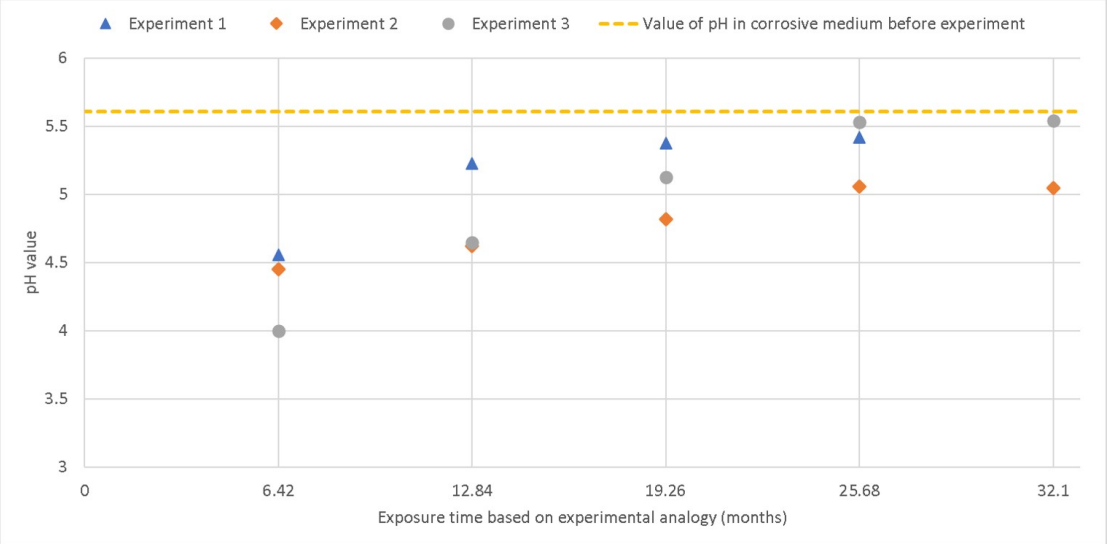

Figure C.2: Measured pH values in the corrosive medium at the point of medium replacement with each time step

It should be noted that the acidity increased more during the earlier phases of the experiment(indicated by a lower pH value). The longer the experiment progressed, the lower the increases in the acidity of the corrosive medium, despite the medium being exposed for the same amount of time at each time step. This supported the conclusion that the development of the passivity layer was reducing the rate of corrosion over time.

The same approach was taken, regarding conductivity values, shown in Figure C.3. Conductivity is broadly a representation of the concentration of ions within the corrosive medium. The results were very similar to those indicated by the pH values, with more ions being present in the medium after corrosive exposure, but with a reducing rate of increase over the life of the experiment. This suggested that the rate of corrosion was reducing over time.

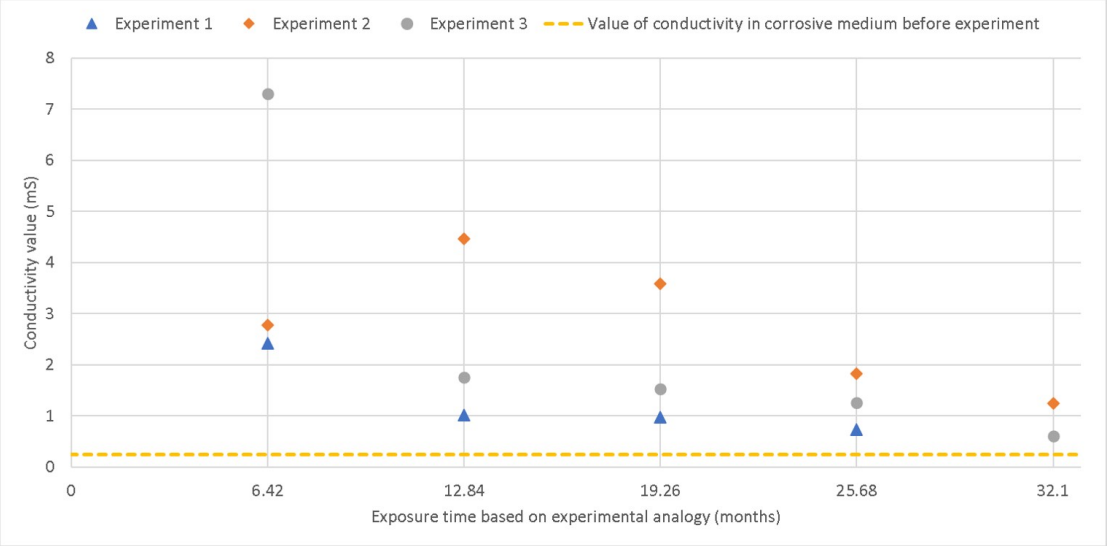

Figure C.3: Measured conductivity values in the corrosive medium at the point of medium replacement with each time step